

Jayvadan K. Patel
Yashwant V. Pathak *Editors*

Pharmacokinetics and Pharmacodynamics of Nanoparticulate Drug Delivery Systems

Pharmacokinetics
and Pharmacodynamics
of Nanoparticulate Drug Delivery
Systems

Jayvadan K. Patel • Yashwant V. Pathak
Editors

Pharmacokinetics and Pharmacodynamics of Nanoparticulate Drug Delivery Systems

 Springer

Editors

Jayvadan K. Patel
Nootan Pharmacy College
Faculty of Pharmacy
Sankalchand Patel University
Visnagar, Gujarat, India

Yashwant V. Pathak
College of Pharmacy
University of South Florida Health
Tampa, FL, USA

ISBN 978-3-030-83394-7 ISBN 978-3-030-83395-4 (eBook)
<https://doi.org/10.1007/978-3-030-83395-4>

© The Editor(s) (if applicable) and The Author(s), under exclusive license to Springer Nature Switzerland AG 2022, Corrected Publication 2022

This work is subject to copyright. All rights are solely and exclusively licensed by the Publisher, whether the whole or part of the material is concerned, specifically the rights of translation, reprinting, reuse of illustrations, recitation, broadcasting, reproduction on microfilms or in any other physical way, and transmission or information storage and retrieval, electronic adaptation, computer software, or by similar or dissimilar methodology now known or hereafter developed. The use of general descriptive names, registered names, trademarks, service marks, etc. in this publication does not imply, even in the absence of a specific statement, that such names are exempt from the relevant protective laws and regulations and therefore free for general use.

The publisher, the authors and the editors are safe to assume that the advice and information in this book are believed to be true and accurate at the date of publication. Neither the publisher nor the authors or the editors give a warranty, expressed or implied, with respect to the material contained herein or for any errors or omissions that may have been made. The publisher remains neutral with regard to jurisdictional claims in published maps and institutional affiliations.

This Springer imprint is published by the registered company Springer Nature Switzerland AG
The registered company address is: Gewerbestrasse 11, 6330 Cham, Switzerland

Foreword

It is indeed a pleasure and a privilege to write the foreword to this insightful and interesting book titled *Pharmacokinetic and Pharmacodynamic of Nanoparticulate Drug Delivery Systems*. I congratulate the editors and the contributors for their academic deliberation in the form of this book and hope that the book will be useful to the readers, academicians, industry professionals, scholars, and students working in the field.

There is paradigm shift in the innovation landscape across the world with a thrust on new drug development based on ideation research.

Nanoparticulate drug delivery systems are promising in providing modernized solutions to challenging diseases and disorders like cancer(s), CNS disorders, chronic infections, pulmonary diseases and in many other areas of therapeutic and diagnostic nature. Still, we find less drugs and treatments available in the market that are based on nanodrug delivery systems. The important challenges are stability, implementation path, and risk assessment along with other physicochemical, clinical, and ethical issues.

The chapters have been contributed by a well-curated team of scientists and expert professionals.

This book is a timely effort by the editors, Professor Jayvadan Patel and Yashwant Pathak, that provides deep insights about the pharmacokinetics and pharmacodynamics of nanoparticles. In this book, the editors have reviewed various aspects of PK/PD of nanoparticles, including pharmacokinetic evaluation of nanoparticles, preclinical animal models to study the PK/PD of nanoparticles, physiologically based pharmacokinetic modelling, clearance pathways for nano particles, and application of PK/PD to various nano-based drug delivery systems including PLGA nanoparticles, oral nanoparticle delivery, nanoparticles uptake in the pulmonary system and brain, liver diseases, and, finally, the pharmacokinetic modelling programs.

To overcome those challenges, it is vital to understand completely the pharmacokinetic and pharmacodynamic (PK/PD) aspects of the nanoparticulate drug delivery systems, and this becomes even more important when we talk about evidence-based medicine and personalized medicines.

With warm wishes,

Vice President, Pharmacy Council of India
New Delhi, India

Shailendra Saraf,

Preface

Nanoparticle drug delivery systems (NPDDS) are man made-engineered technologies using nanoparticles for the targeted delivery and/or controlled release of therapeutic agents. The modern form of a drug delivery system is expected to minimize side effects and reduce both the amount of dose and dosage frequency.

Nanomedicine and nanoparticulate delivery systems are comparatively new and rapidly developing drug delivery tools where materials in the nanoscale range are employed to serve as means of diagnostic tools or to deliver therapeutic agents to specific targeted sites in a controlled manner.

Pharmacology is the study of the interactions between drugs and the human and animal body. The two important aspects of pharmacology are pharmacokinetics (PK) and pharmacodynamics (PD). The difference between PK and PD is that pharmacokinetics (PK) is defined as the movement of drugs through the body, whereas pharmacodynamics (PD) is defined as the body's biological response to drugs.

PK describes a drug's exposure by characterizing absorption, distribution, bioavailability, metabolism, and excretion (ADME) as a function of time. PD describes drug response in terms of biochemical or molecular interactions.

Understanding the exposure response relationship (PK/PD) is key to the development and approval of every drug. PK and PD data contribute much of what is on a drug package insert. Strategic planning of the overall program for a drug and intelligent PK/PD study design can accelerate the development process (taken from <https://www.nuventra.com/services/pharmacokinetics-pharmacodynamics/>).

Some of the PK/PD analyses used:

1. Characterize drug exposure
2. Predict dosage requirements
3. Assess changes in dosage requirements
4. Estimate rate of elimination and rate of absorption
5. Assess relative bioavailability and bioequivalence
6. Characterize inter and intra subject variability
7. Understand concentration-effect relationships
8. Establish safety margins and efficacy characteristics

Since, 1995, over 60 products have received US FDA approvals, which are mostly used for cancer and other chronic diseases (<https://www.ncbi.nlm.nih.gov/pmc/articles/PMC5720487/>).

PK and PD studies are an important need for approvals of NPDDS. There is a need for a book to cover various aspects of PK/PD for NPDDS.

This book with over 20 chapters will fill the gap felt by scientists working in this field, and this book will be an excellent reference book for students, academicians, industry personnel, and all the concerned people who are working in NPDDS or PKPD areas.

The book has three main themes:

1. Modeling of PK/PD
2. PK/PD for specific nanocarriers
3. PK/PD in diseased conditions for NPDDS

Chapter 1 introduces NPDDS, while Chap. 2 discuss the properties of NPDDS affecting the PK/PD properties of NPDDS.

Chapters 3, 4, 5, 6, and 7 provide details about various models used for PK/PD studies of NPDDS, in vitro, in vivo, and in situ evaluations.

From Chaps. 8, 9, 10, 11, 12, 13, 14, 15, 16, 17, 18, 19, 20, 21, and 22, various nanocarrier-specific topics are discussed, such as liposomal nanoparticles (NP), polymer matrix NP, metallic NP, muco adhesive NP, solid lipid NP, and many different NP formulations.

We believe that this book will be very useful to the readers, and we have tried our best to cover all major aspects of NPDDS and its PK/PD aspects.

If there any lacuna, kindly do bring it to our notice and we will address it in the next edition of this book.

Our esteemed authors have made significant efforts to write and contribute their chapters on time and we have no words to express our gratefulness to them.

Our heartfelt thanks to Dr. Shailendra Saraf, Vice President, Pharmacy Council of India, for providing the foreword to this book.

We would like to express our sincere thanks to Springer for publishing this book; many people from Springer have been of great help to bring this book to the market.

Our families have been very supportive while we were working on this book project, their cooperation and support has always been an inspiration to us both.

Our institutions, the University of South Florida Taneja College of Pharmacy (USF TCOP for Yashwant Pathak) and Nootan Pharmacy College, Faculty of Pharmacy, Sankalchand Patel University, India (for Jayvadan Patel), have always been supportive of our ventures, and we are indebted to them for their support.

Last but not least, we owe a lot to our readers who hopefully will admire our efforts and will benefited from this book.

Visnagar, Gujarat, India
Tempa, FL, USA

Jayvadan K. Patel
Yashwant V. Pathak

Introduction

This book emphasizes and analyzes the evolution of nanoparticulate drug delivery systems from the laboratory to a commercially feasible sector.

This book consists of three subthemes addressing different aspects of pharmacokinetics and pharmacodynamics of nanoparticulate drug delivery system. Chapters 1, 2, 3, 4, 5, 6, and 7 discuss modeling of PK/PD for nanoparticulate drug delivery system, Chaps. 8, 9, 10, 11, 12, 13, 14, and 15 discuss PK/PD for specific nanocarriers, and Chaps. 16, 17, 18, 19, 20, 21, and 22 discuss PK/PD in diseased condition for nanoparticulate drug delivery system.

Contents

Part I Modelling of PK/PD for NPDDS

- 1 Introduction to Nanoparticulate Drug Delivery Systems 3**
Jayvadan Patel, Anita Patel, Mukesh Patel, and Govind Vyas
- 2 Nanoparticle Properties Affecting the Drug Release, Absorption, and Pharmacokinetics of Nanoparticulate Drug Delivery Systems 25**
Prachi Pandey, Jayvadan K. Patel, and Samarth Kumar
- 3 Models Used for Biopharmaceutical Evaluation of Nanoparticulate Drug Delivery System (NPDDS) 41**
Seema Kohli and Sumeet Dwivedi
- 4 Models Used for Pharmacokinetic Evaluation of Nanoparticulate Drug Delivery Systems (NPDDS) 53**
Nishtha Chaurawal and Kaisar Raza
- 5 Models Used in Pharmacodynamic Evaluation of Nanoparticulate Drug Delivery Systems (NPDDS) 69**
Megha Joshi, Chander Parkash Dora, Lokesh Kaushik, Jayvadan Patel, and Kaisar Raza
- 6 Preclinical Animal Models for the Experimental Design of Pharmacokinetic Studies with Nanoparticulate Drug Delivery Systems 79**
Aishwarya Deshmukh, Jayvadan K. Patel, and Yashwant V. Pathak
- 7 Pharmacokinetic Modeling Program (PKMP): A Software for PK/PD Data Analysis 101**
Ajit K. Shah

Part II PK/PD for Specific Nano Carriers

- 8 Pharmacokinetics and Pharmacodynamics of Liposomal Nanoparticles 143**
Prachi Pandey, Jayvadan Patel, Samarth Kumar, and Yashwant Pathak

- 9 Pharmacokinetics of Drug-in-Polymer Matrix-Based Nanoparticulate Drug Delivery System** 159
Sopan Nangare, Prashant Patil, Ashwini Patil,
Prashant Deshmukh, Trupti Powar, Jidnyasa Pantwalawalkar,
Zamir Khan, Rahul Tade, Jayvadan K. Patel,
and Pravin Patil
- 10 Pharmacokinetics of Long Circulating Inorganic Nanoparticulate Drug Delivery Systems.** 187
Namrata Gautam, Anushka Kulkarni, Debopriya Dutta,
and Sushama Talegaonkar
- 11 Metallic Gold Nanoparticles: In Vivo Pharmacokinetics and X-Ray Contrast Imaging Studies** 209
Nishith Patel, Sunita Chaudhary, and Jayvadan K. Patel
- 12 Mucoadhesive Nanoparticulate Drug Delivery System (NPDDS): In Vitro and Pharmacokinetic Studies.** 225
Sanjay Patil, Bhavin Choradiya, and Jayvadan Patel
- 13 Pharmacokinetic and Tissue Distribution Study of Solid Lipid Nanoparticles** 245
Himanshu Paliwal, Bhupendra G. Prajapati, Dignesh Khunt,
Chilakapalli Shirisha, Jayvadan K. Patel,
and Yashwant V. Pathak
- 14 Factors Affecting the Clearance and Biodistribution of Polymeric Nanoparticles** 261
Komal Parmar, Jayvadan Patel, and Yashwant Pathak
- 15 PKPD of PLGA-PEG-PLGA Copolymeric Micelles** 273
Shirleen Miriam Marques and Lalit Kumar

Part III PKPD in Diseased Conditions for NPDDS

- 16 Bridging Bio-Nanoscience and Cancer Nanomedicine** 295
Alka, Raquibun Nisha, Priya Singh, Ravi Raj Pal,
Neelu Singh, Nidhi Mishra, and Shubhini A. Saraf
- 17 Clearance Pathways and Tumor Targeting of Imaging Nanoparticles for Diagnostics.** 315
Palak K. Parikh, Nisha H. Parikh, Jayvadan K. Patel,
and Yashwant V. Pathak
- 18 PLGA Nanoparticles for Oral Delivery: Nephrotoxicity and Pharmacokinetic Studies.** 333
Neelu Singh, Nidhi Mishra, Kaiser Raza,
and Poonam Parashar
- 19 Pharmacokinetics of Nanoparticle Systems for Pulmonary Delivery** 347
Bhupendra Prajapati, Himanshu Paliwal, and Jayvadan Patel

20 In Vivo Biodistribution and Pharmacokinetic Studies of NPDDS for Brain Targeting	365
Aaishwarya Deshmukh, Jayvadan Patel, Govind Vyas, and Mukesh Patel	
21 Enhanced Bioavailability and Intestinal Uptake of Nanoparticles After Oral Delivery	385
Mitali Patel and Krutika Sawant	
22 Nanoparticle Pharmacokinetic Profiling In Vivo Using Magnetic Resonance Imaging	399
Bhupendra G. Prajapati, Himanshu Paliwal, and Jayvadan K. Patel	
Correction to: Pharmacokinetics and Pharmacodynamics of Nanoparticulate Drug Delivery Systems	C1
Index	417

Modelling of PK/PD for NPDDS

Nanotechnology is an upcoming and promising technology, offering pavement to a novel therapeutic field, that is, nanoparticulate drug delivery system. The interface of nanoparticles with biological system is dependent on the properties of nanoparticles, for example, size, superficial charge, and surface modification. Attributable to modification of physicochemical properties of nanoparticles the pharmacokinetics and effectiveness of the drugs at nanoscale are considerably transformed as a result nanoparticulate system get better the overall performance of drugs. The pharmacokinetic/pharmacodynamic (PK/PD) correlations and modeling connect the concentration-time profile as measured by pharmacokinetics to the intensity of experimental response as counted by pharmacodynamics. PK/PD modeling can illuminate the contributory correlation between drug exposure and response and present an enhanced understanding of the succession of events that result in the experimental drug effect. This information can be exploited to modernize the drug development process and dose optimization. This Part I of the book provides an update on the current state of PK/PD modeling for nanoparticulate drug delivery system from an academic, industrial, and regulatory perspective. Over the past 20 years, pharmacokinetic programs have been urbanized for clinical decision making and to support the clinician in the analysis, interpretation, and reporting of serum drug concentration data for a variety of medications.



Introduction to Nanoparticulate Drug Delivery Systems

1

Jayvadan Patel, Anita Patel, Mukesh Patel,
and Govind Vyas

Contents

1	Introduction	4
2	Nanomaterials	5
3	Why Are Nanoparticulate Materials So Special and Unique?	5
4	Classification of Nanoparticulate Materials	8
5	Properties: The Physics at the Nanoscale	11
6	Types of Nanomaterials	15
7	Conclusion	18
	References	18

Abstract

Nanotechnology is the innovatory technology of the twenty-first century, and nanoparticulates as drug delivery systems have created a considerable amount of attention from researchers. It is a promising interdisciplinary area of research wherever groups of atoms as well as molecules are handled at the nanometer levels. It can be defined as the systematic study of materials that have properties criti-

cally dependent on length scales on the order of nanometers. Such novel and improved properties make nanoparticulate materials promising candidates to provide the best scientific as well as technological progress in a number of fields in particular biology, communications, environment, energy, healthcare, information, medical care, and pharmacy. The use of nanotechnology in medicine and more explicitly drug delivery is set to spread speedily. The growing range of nanoparticulate-based drug delivery methods is assured of changing the formulation characteristics of new compounds and extending the lifecycle of existing compounds. In order to achieve this, the chapter deals with the definitions and classification of nanoparticulate materials, a fundamental understanding of their valuable properties, and different types of nanoparticulates employed as drug delivery systems.

J. Patel (✉) · A. Patel
Nootan Pharmacy College, Faculty of Pharmacy,
Sankalchand Patel University,
Visnagar, Gujarat, India

M. Patel
Experis, Edina, MN, USA

G. Vyas
Invahealth Inc., East Windsor, NJ, USA

Keywords

Nanoparticulates · Size-dependent characteristics · Distinctive properties · Superior performance · Drug delivery

1 Introduction

The first technical revolution, at the end of the eighteenth century, has sparked the progression of industrial research and the attainment of novel materials. At present, the obstacles are the miniaturization of devices as well as instruments: lesser volume and lesser power consumption but better performance. The progress relies upon searching out novel pleasing materials and the capacity to construct minute structures with high accuracy. The development of novel technology is not very smooth and effortless task. One of the best splendid techniques created to answer such a condition is nanotechnology [1, 2]. In recent times, the study engaging nanoparticulate materials has created a substantial amount of attention from researchers. They believe nanotechnology is the innovatory technology of the twenty-first century.

The word nanotechnology is taken from the Greek word “nano,” which stands for “dwarf” or “very small,” and so it relates to materials of minute size ranges [3, 4]. The interdisciplinary science of nanotechnology is a brilliant field wherever a group of atoms as well as molecules are handled at the nanometer scale. In actual fact, it is the design of components, devices, materials, and/or systems close to atomic or molecular levels. Generally, one of the dimensions of nanomaterials is between 1 and 100 nanometers (nm) length in scale. This promising technology implies the imaging, handling, manufacturing, measuring, modification, modeling, and reduction of matter at the nanoscale with characteristic properties, for example, cost-effective, definite, eco-friendly, good strength, lighter, and specific for a variety of purposes [5, 6].

The definition of nanotechnology has been divided into two parts: one is the part about man-

ufacturing at dimensions of 1–100 nm, and the other is about characteristics of materials at the nanometer scale that initiate their use for novel applications. The size range of particles that holds immense attention is characteristically from 100 nm down to the atomic level, for the reason that it is in this range that materials have fundamentally distinct properties from their bulk counterparts. The most important justifications for this revolutionize in performance are an increased significance of surface as well as the interfacial area [7]. At the same time, nanotechnology is a new-fangled paradigm in fundamental thoughts and understanding regarding the physical universe, where the bottom-up approach is the rule and not an exception. In this novel system, one has to imagine in terms of atoms and how they act together to create valuable materials, structures, devices, and systems [8–10].

Nanotechnology has been moving from the laboratory surroundings to applications and customer products for quite a while now [11]. Nanotechnology will create new perspectives for this world, and its promises have been noticed to provide the best scientific as well as technological progress in a number of fields in particular communications, electronics, energy, environment, information, health, and medical care [12]. Nanotechnology has also a wider perspective in the areas of biology, pharmacy, physics, and materials science which could merge to contribute to healthcare. The insight of nanotechnology has been investigated in healthcare research for the past three decades; it is still believed to be in the early stage of development as anticipated therapeutic advantages have not been totally understood [13, 14]. The educational as well as industrialized groups of people together are paying more attention along with money into the development of nanotherapeutics to conquer the superficial challenges and interpret the theoretically recognized benefits of nanoparticulate systems into clinical benefits. The exploit of nanotechnology in drug delivery is set to spread speedily. Although nanotechnology is at its early stages, however, it is expanding quickly, opening plentiful perspectives for the logical minds to uti-

lize this enhanced technology for human well-being [15].

This chapter addresses to fill up-to-date understanding of manufactured nanoparticulates, by providing an extensive review of current progress in the nanotechnology field. It draws attention to the different definitions, classifications, fundamental properties, and different types of nanoparticulate materials employed for drug delivery.

2 Nanomaterials

Nanomaterials, previously called by Paul Ehrlich as “magic bullets” [16], are one of the major investigated materials of the century that gave birth to a novel branch of science referred to as nanotechnology [17]. Nanomaterials are chemical materials that can be produced or employed at a minute scale. Indeed, the word material speaks about an infinite number of components, jointly showing an averaged statistical performance. As a result, the performance of nanomaterials is affected by specific interface effects and demonstrates characteristics affected by the size and the restricted number of constituents [18].

Nanomaterials are a diverse class of substances that have structural constituents lesser than 100 nm in a minimum of one dimension. Nanomaterials consist of nanoparticles, which are particles, with at least two dimensions between about 1 and 100 nm [19]. However, a single globally recognized definition for nanomaterials does not present. Diverse groups have dissimilarities in belief in defining nanomaterials [20]. To be classified as nanomaterials, the material must be less than 100 nm in size in a minimum of one direction. The International Organization for Standardization (ISO) has explained nanomaterials as a “material with any external nanoscale dimension or having the internal nanoscale surface structure” [21]. As per the European Union Commission, nanomaterials means “a manufactured or natural material that acquires unbound, aggregated or agglomerated particles where external dimensions are between 1–100 nm size ranges” [22].

The exploit of different definitions throughout diverse authorities is referred to as the most important obstacle to regulatory efforts as it shows the way to legal uncertainty in applying regulatory approaches for indistinguishable nanomaterials. So, the requirement to convince diverging considerations is the main confront in developing a single international definition for nanomaterials.

3 Why Are Nanoparticulate Materials So Special and Unique?

Nanoparticulate materials, which can be either stand-alone solids or subcomponents in other materials, are smaller than 100 nm in one or more dimensions. Putting this dimension in standpoint, a nanometer (nm) is one-billionth of a meter and one-millionth of a millimeter, approximately four times the diameter of an atom. For our macro-oriented brains, in fact, understanding the scale of the nanometer is not easy although real-life comparisons can help give us a good judgment. For example, the twinkling of an eye is to a year is what a nanometer is to a meter stick [23].

Nanoparticulate materials have a higher surface area-to-volume ratio in addition to the number of surface atoms, and their arrangement decides the size and properties of the nanoparticulate materials [24]. Size reduction of materials can bring about an entire range of novel physicochemical features and prosperity of prospective applications [25].

These features very much rely upon the size, shape, surface area, and structure of elements. Nanoparticulate materials can be present in single, compound, aggregated, or agglomerated structures with sphere-shaped, cylindrical, and asymmetrical shapes [26]. By the production of nanoparticulate structures, it is probable to manage the basic properties of materials, for instance, their charge capacity, magnetic properties, melting temperature, and even their color, without altering the chemical composition of the nanoparticulate structures. This will make possible novel,

highly efficient materials and nanotechnologies that were impracticable in the past. The most important benefits of nanoparticulate materials against bulk material consist of a reduction in melting point as well as surface area and an enhancement in dielectric constant in addition to mechanical strength [27–30]. Additionally, the size of nanoparticulate materials facilitates them to absorb remarkably onto other materials [29, 31, 32]. At the nanoscale, the power of gravity gives van der Waals forces, surface tension, and additional quantum forces.

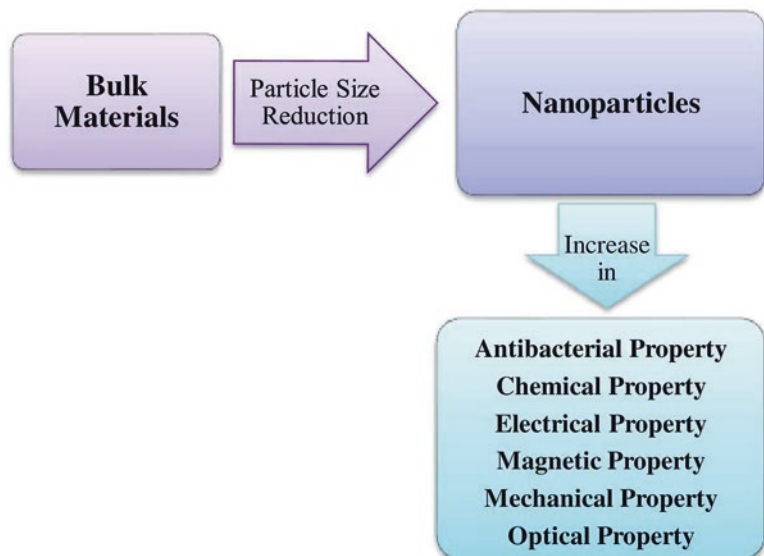
For differentiation of nanoparticulate materials from the bulk materials, it is essential to show the distinctive properties of nanoparticulate materials and their potential effects on science as well as technology. The size of the nanoparticulate materials has an enormous control on their properties (Fig. 1.1). When a particle is in its bulk state in comparison with its size in its microscale, there is not a large amount of dissimilarity in its properties. In contrast, when the particle achieves a size smaller than 100 nm, the properties revolutionize remarkably in comparison with its bulk state. In 1–100 nm, quantum size effects determine the properties of particles, like chemical, magnetic, optical, mechanical, electrical, and thermal properties [15, 23, 33].

Over the past few decades, the size-dependent properties of gold nanoparticles have been explicated well. Gold nanoparticles demonstrate the size-dependent color. At the nanoscale, the gold particle shows purple color diverse from the bulk, which was yellow-colored. This alteration in color is based on the alteration in their band type from continuous to discrete as a result of the confinement effect. These types of quantum effects in the nanometer scale are the elemental explanations behind the “tunability” of properties. By merely changing the particle size, we can alter the material property of our interest [15, 34].

Before talking about the properties of nanoscale substances, it may be beneficial to explain a case showing the basic effects of the minute size of nanoparticles [35]. The first and very important effect of smaller particle size is its huge surface area, and so as to get an idea of the significance of this geometric variable, the surface-over-volume ratio should be discussed. It is assumed that a particle is sphere-shaped, the surface a of one particle with diameter D is $a = \pi D^2$, and the corresponding volume v is $v = \frac{\pi D^3}{6}$. So, the surface/ volume ratio is

$$R = \frac{a}{v} = \frac{6}{D} \quad (1.1)$$

Fig. 1.1 Properties of nanoparticulate materials



This ratio is in opposite proportion to the particle size, and, accordingly, the surface enlarges with reducing particle size. Therefore, larger values of surface area are obtained for particles that are simply a few nanometers in diameter [36].

The distinctive properties and superior performance of nanoparticulate materials are established by their sizes, surface structures, and interparticle interactions. The role of particle size is incredibly analogous to the role of the particle's chemical composition, adding one more parameter for designing and managing the behavior of the particle. To entirely know the impacts of nanoparticulate materials in nanoscale science and technology, one requires to study why nanoparticulate materials are so special [36].

The excitement near nanoscale science as well as technology offers unique opportunities to build up innovatory materials. Nanoscale science and technology is a comparatively young field that includes almost all disciplines of science and engineering. Nanoparticulate structures are a novel branch of materials study drawing an immense deal of attention due to their impending application in chemical catalysis, computing, imaging, material synthesis, medicine, printing, and many other fields [36].

On account of all these inimitable behavior and properties, nanoparticulate materials have greater applications in cosmetics, electronics, and pharmaceutical industries. In addition, they are commonly employed for the advance of healthcare products and restoration of polluted environments [30]. Nanoparticulate materials stand for areas of scientific study and industrialized applications in the full expansion [37]. Nanoparticulate materials in addition play a very important role in drug delivery, imaging, and even in the surgical procedures as they have a size range comparable to that of biological molecules, for example, proteins, receptors, deoxyribonucleic acid, and ribonucleic acid (RNA) [38–42].

Nanoparticulate systems are moderately small in size in comparison with cells but are larger than the majority of “small molecule”-type drugs,

which could get better their residence time in circulation without any risk of clogging within the blood vessels, which sequentially can enhance the bioavailability and pharmacokinetic profile of a variety of drugs. Nanoparticles can make use of a natural process called endocytosis to go through cells, which offers a specific benefit in circumstances where normal penetration into cells would be difficult for a particular molecule [43]. This characteristic is also useful for the targeting of particular organelles within the cells like nuclei with gene knockdown by tiny interfering RNAs (siRNAs) [42, 44–46]. The higher surface-area-to-volume ratio is an additional interesting characteristic of nanoparticulate systems, which gives a huge substrate for adherence of definite moieties for active targeting [47]. Surface modification has been done to nanoparticles with specific antibodies or peptides to attain tissue targeting, which lessens the probability of distracted off-target toxicity [48, 49]. Consistent with therapeutic and diagnostic requirements, the surface features of nanotherapeutics can be customized with imparting stealth properties to avoid elimination by the reticuloendothelial system, which gets better the circulation time and raises drug concentration at the site of action [41, 50].

Nanoparticulate technology has opened up new opportunities in the early detection as well as management of different cancers, in biodetection of pathogens, and in the formulation of fluorescent biological labels as they receive both imaging and therapeutic aptitudes. Nanoparticulate technology is also beneficial in addressing solubility as well as stability problems of poorly soluble drugs and in modifying their pharmacokinetic profiles to get extended plasma half-life. Since the 1980s, the healthcare group of people has met clinical challenges where resistance has developed against antibiotics and chooses other conventional therapeutics. It is feasible that these problems can be tackled with nanoparticulate materials [40, 51]. As of 2014, more than 1800 consumer products containing nanoparticulate materials are on the market [52].

4 Classification of Nanoparticulate Materials

The manufacturing of traditional products at the nanoscale right now helps and will keep on helping the economic growth of various countries. To date, a variety of nanoparticulate products have been documented, and lots of other varieties of products are expected to come out in the future. Consequently, the requirement for their categorization has ripened. The first suggestion for nanoparticulate material classification was specified by Gleiter in 2000 [53]. A nanomaterial is a broad name given to every material existing at the nanometer scale. Numerous names have been presented to these novel materials like nanostructured, nanometer-sized, ultrafine-grained, etc. Nanoparticulate materials can be formed from one or more species of atoms or molecules and can demonstrate a broad range of size-dependent characteristics. In this range of size, nanoparticulate materials tie the gap among tiny molecules and bulk materials in terms of energy states [54, 55]. They can be found naturally or manufactured chemically, mechanically, physically, or biologically with a variety of structures [56]. Nanoparticulate materials can be categorized on the basis of special parameters including their origin, chemical composition, material-based, and their dimensions [57, 58].

4.1 Classification of Nanoparticulate Materials Based on Their Origin

Based on their origin, the nanoparticulate materials can be divided into two categories [59]:

Natural Nanoparticulate Materials

These types of materials speak about nanosized materials that belonged naturally to the environment (e.g., proteins, viruses, nanoparticles produced during volcanic eruptions, etc.) or that are formed by individual activity with no plan (e.g., nanoparticles produced from diesel combustion). These types of nanomaterials are formed in nature either by organic species or at

some stage in human-induced activities. Manufacturing of the simulated surfaces with the best micro- as well as nano-patterns and properties for industrialized application is effortlessly accessible from natural origins. Naturally generated nanoparticulate materials are present through the Earth's spheres – to be precise, in the atmosphere, hydrosphere, and lithosphere which are comprised of rocks, soils, magma, or lava at particular stages of evolution and even in the biosphere which covers microorganisms and higher organisms, including humans, apart from anthropogenic activities. Globe is made up of nanoparticulate materials that are naturally formed and are also present in the oceans, lakes, rivers, groundwater, and hydrothermal vents [60–62].

Synthetic (Engineered) Nanoparticulate Materials

These types of nanoparticulate materials are manufactured with intent by means of a defined production procedure like mechanical grinding, engine exhaust, and smoke or are synthesized by physical, chemical, biological, or hybrid techniques. Synthetic nanoparticulate covers a wide range of materials counting both inorganic (elemental metals, metal oxides, and metal salts) and organic (fullerenes, micelle-like amphiphilic polyurethane particles, and dendrimers) materials [63]. The issue of the risk assessment approach has come into existence recently as there is increased manufacturing and succeeding release of engineered nanoparticulate in addition to their utilization in consumer products and industrial application. This risk assessment approach is very much helpful in the prediction of the behavior and fate of engineered nanoparticulate materials in different environmental media. The most important confront among engineered nanoparticulate materials is whether existing information is ample to predict their behavior or if they show a distinctive environment-related performance, diverse from natural nanoparticulate materials. At present, different sources concerned with possible applications are employed for the fabrication of engineered nanoparticulate materials [64].

4.2 Classification of Nanoparticulate Materials Based on the Chemical Composition

According to their chemical composition, nanoparticulate materials can be categorized as metal-based materials that are mainly made up of metals, like silver, gold, and copper. And metal oxide nanoparticulate materials are made of metal and oxygen, for example, titanium, silica, and alumina [57].

4.3 Material-Based Classification of Nanoparticulate Materials

The most recent nanoparticulate materials can be classified into four material-based categories:

Carbon-Based Nanoparticulate Materials

Generally, these carbon-based nanoparticulate materials cover up a wide range of compounds, counting fullerenes, carbon nanotubes, carbon nanofibers, carbon black, graphene, and carbon onions [63]. For manufacturing these carbon-based nanoparticulate materials, different methods are used like laser ablation, arc discharge, and chemical vapor deposition (except carbon black) [26].

Inorganic-Based Nanoparticulate Materials

These inorganic-based nanoparticulate materials include metal and metal oxide nanoparticles. These nanoparticulate materials can be synthesized into metals like gold nanoparticles or silver nanoparticles, metal oxides like titanium dioxide and zinc oxide nanoparticles, and semiconductors such as silicon and ceramics [59].

Organic-Based Nanoparticulate Materials

Organic-based nanoparticulate materials consist of nanomaterials prepared generally from organic matter, exclusive of carbon-based or inorganic-based nanomaterials. The exploitation of non-

covalent interactions for the self-assembly and blueprint of molecules assists to renovate the organic nanoparticulate materials into most wanted structures, for instance, dendrimers, micelles, liposomes, and polymeric nanoparticles [59].

Composite-Based Nanoparticulate Materials

Composite nanoparticulate materials are multi-phase nanoparticles with one phase on the nanoscale dimension that can either join nanoparticles with other nanoparticles or nanoparticles attached with bigger or with bulk-type materials (e.g., hybrid nanofibers) or very complex structures, for example, metalorganic frameworks. The composites may be any combinations of carbon-based, metal-based, or organic-based nanoparticulate materials with any form of metal or polymer bulk materials. Nanoparticulate materials are fabricated in diverse morphologies contingent on the essential properties for the desired application [59].

4.4 Classification of Nanoparticulate Materials Based on Their Dimensions

Nanoparticulate materials with structural characteristics at the nanoscale can be created in various forms. In 2007, Pokropivny and Skorokhod formed a new idea of classification for nanoparticulate materials which listed the newly developed composites, for example, zero-dimensional (0-D), one-dimensional (1-D), two-dimensional (2-D), and three-dimensional (3-D) nanoparticulate materials [65]. This classification is greatly reliant on the electron association along the dimensions in the nanomaterials. For instance, electrons in 0-D nanoparticulate materials are captured in a dimensionless space, while 1-D nanoparticulate materials have electrons that can shift along the x -axis, which is less than 100 nm. Similarly, 2D and 3D nanoparticulate materials have electron associations along the x - and y -axis and x -, y -, and z -axis in that order. The ability to forecast the properties of nanoparticulate materi-

als decides the classification value of the nanoparticulate materials. The categorization of nanoparticulate materials given by researchers suggested that the features of nanoparticulate materials are ascribing to the particle shape as well as dimensionality, as per the “surface engineering” conception, and therefore class of nanomaterials [65, 66].

In accordance with this conception, nanoparticulate materials can be classified as follows:

Zero-Dimensional (0-D)

They are crystalline bunches of a few hundred to a few thousand atoms with sizes ranging from 2 to 100 nm [67]. All the dimensions of the materials present in the nanometer scale are called 0-D nanoparticulate materials. Nanoclusters are forms that are 1 to 100 nm in all space-based dimensions. These are in most cases sphere-shaped nanostructures, while their length, breadth, and heights are controlled at a single point. 0-D nanomaterials are either amorphous or crystalline in nature. In recent times, widespread investigation is in development to fabricate nanoparticles for a variety of applications [68].

One-Dimensional (1-D)

The second class of nanoparticulate materials, subjected as 1-D nanoparticulate materials, is held in reserve for those materials that have nanoscale dimensions that are equal in all but one direction [69]. The nanoparticulate materials have one of the dimensions, which are exterior, the nanoscale, and are called 1-D nanoparticulate materials. It has only a single parameter, either length or breadth or height. These are commonly needlelike nanostructures that include nanotubes, nanowire, nanofibers, and nanorods having a diameter between 1 and 100 nm and a length that could be much larger and are classified as 1-D nanostructures. These types of nanomaterials are either amorphous or crystalline in nature. These nanoparticulate materials present momentous benefits over bulk or thin-film planar devices [70]. Nanofibers are to some extent bigger in diameter than the characteristic nanomaterial definition, though still too small to see to the naked eye. They are generally manufactured by

electrospinning technique in the case of inorganic nanofibers or catalytic synthesis method for carbon nanotubes and exhibit size ranges between 50 and 300 nm in diameter. Nanofibers can be aligned biochemically and electrostatically [26]. Nanowires are similar to nanofibers. In these systems, one dimension surpasses by an order of magnitude the other two dimensions, which are in the nano-range [71].

Two-Dimensional (2-D)

In this class of nanoparticulate materials, only one dimension is in the nanometer scale, while another two are out of the nanoscale [71]. It has simply length and breadth. 2-D nanostructures display plate-like shapes [72]. Examples of 2-D nanostructures are nanotubes, dendrimers, nanowires, nanofibers, nanofilms, nanolayers, nanotextured surfaces or thin films, and nanocoatings. 2-D nanoparticulate materials can be amorphous or crystalline. They are fabricated from different chemical compositions. They are utilized as a single layer or multilayer structure [73]. The properties of 2-D systems are not as much understood, and their manufacturing capabilities are less advanced. 2-D systems are applied to structural bulk materials for the purpose of improving the desired properties of the surface, for example, corrosion resistance, wear resistance, friction, and holding the bulk properties of the material unchanged [74].

Three-Dimensional (3-D)

Three-dimensional (3-D) structures are materials having three random dimensions beyond the nanoscale [57]. 3-D nanostructures have all parameters like breadth, height, and length. These materials acquire a nanocrystalline nature [75]. Examples of these types of nanomaterials are quantum dots or nanocrystals, fullerenes, particles, precipitates, and colloids. A number of 3D systems, for example, natural nanomaterials, metallic oxides, and carbon black, are widely known, whereas others, for example, dendrimers, fullerenes, and quantum dots, portray the maximum confronts with regard to manufacturing and understanding of properties. 3-D nanoparticulate materials consist of the dispersion of nanoparti-

cles, bundles of nanowires, and nanotubes as well as multi-nanolayers [66, 76].

5 Properties: The Physics at the Nanoscale

Recently, the materials science investigation is paying attention to the discovery of novel materials with new-fangled and superior properties and novel synthesis methods to deal with the augmented technological requirement. Nanoparticulate materials are the center of interest attributable to their remarkable application and fascinating properties [77, 78].

In reality, the fundamental properties of matter transform at the nanoscale and nanoparticulate materials manifested fascinating and valuable properties. The chemical and physical properties of nanoparticulate materials can be quite diverse from those of larger particles of the same material. They are nearer in size to single atoms and particles over bulk materials, and to clarify their performance, it is essential to make use of quantum mechanics [26]. At the same time, practically all microstructured materials have identical properties to the corresponding bulk materials. This is mostly attributable to the nanometer size of the materials which make them (a) large fraction of surface atoms, (b) high surface-to-volume ratio and quantum confinement effects, (c) spatial confinement, and (d) reduced imperfections, which do not exist in the corresponding bulk materials [79]. Changed properties can comprise but are not restricted to color, solubility, material strength, electrical conductivity, magnetic performance, mobility, biological activity, and chemical reactivity (Fig. 1.2) [23, 80].

Size effects make up a peculiar and attractive aspect of nanoparticulate materials. The effects are taken into consideration by size pertaining to the advancement of chemical, electronic, electromagnetic, spectroscopic, structural, and thermodynamic properties of these predetermined systems with varying sizes [25]. The properties of material basically rely on the type of motion its electrons can execute, which depends on the gap available for them. Therefore, the properties

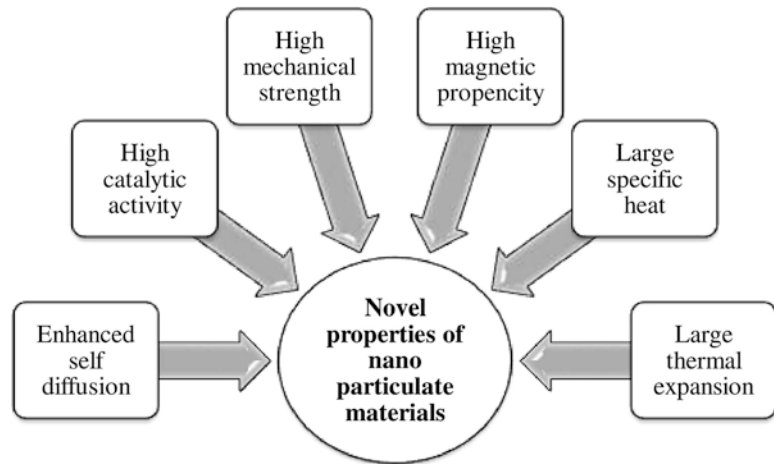
of a material are characterized by an explicit length scale, usually on the nanometer dimension. If the physical size of the matter is decreased below this length scale, subsequently there is a transformation of its properties that turn out to be susceptible to size along with shape. Attributable to our capacity of atom manipulation, we can formulate nanoparticulate materials suitable for specific applications [81].

In any matter, the considerable variation of basic electrical and optical properties with decreased size will be seen when the energy spacing between the electronic levels goes beyond the thermal energy. In tiny nanocrystals, the electronic energy levels are not constant as in the bulk but are discrete: on account of the captivity of the electronic gesture function to the physical lengths of the particles. This observable fact is called quantum confinement, and, consequently, nanocrystals are also referred to as quantum dots [82]. Furthermore, nanocrystals attain a higher surface area and a great fraction of the atoms present on their surface. Since, this fraction depends largely on the size of the particle (30% for a 1 nm crystal, 15% for a 10 nm crystal); it can give rise to size effects in chemical and physical properties of the nanocrystals.

5.1 Confinement Effect

Quantum size effects are correlated to the “dimensionality” of a system in the nanometer range [83]. The quantum effects are an outcome of quantum mechanics and of the particle-wave duality. These come about in cases where the size of the system is proportionate with the de Broglie wavelengths of the electrons, phonons, or excitons circulating in them [84]. In actual fact, electrons are active as particles and waves; seeing as waves, they voyage around the whole space in which they are free to move about. The nanograin acts similar to a type of box, in which a definite property may or may not be present. Below a specific critical size, characteristics of the matter straightforwardly and exactly rely upon the size of the grain. This is known as the confinement effect [85]. Quantum size effects play a fun-

Fig. 1.2 Size-dependent properties of nanoparticulate materials



damental role in deciding the physical and chemical properties, e.g., charge-transport mechanisms and electronic structure. Optical as well as electron-tunneling spectroscopies are crucial for learning these systems [79, 86].

5.2 Surface Effects

Atoms present at surfaces have fewer neighbors as compared to atoms in the bulk. As a consequence of this lesser coordination and unsatisfied bonds, surface atoms are little stabilized compared with bulk atoms [79]. If the particle is very small in size, it has a large fraction of atoms at the surface and a great average binding energy per atom. The surface-to-volume proportion scales with the contrary size, and, as a result, there are plentiful properties that comply with the identical scaling law. Edge and corner atoms have even lesser coordination and attach foreign atoms and molecules more strongly. The coordination number is also restricted in small pores [87].

The influence of size reduction is not exclusive of outcomes for the atomic arrangement and the physical properties of substances. In fact, if the structure of the superficial region of a particle is exaggerated over the range of the particle size, a surface layer cannot be specified precisely [88]. It is acknowledged that the composition or the structure of the crystal is customized at the free surface of the material. The volume of this sur-

face layer turns out to be noteworthy in nanoparticulate materials. The surface layer of nanoparticulate materials, in that case, can be specified as the outer region where the composition or the structure of the crystal is diverse from those of the particle interior [89].

5.3 Mechanical Properties

Nanostructures demonstrate advanced mechanical properties than the bulk materials, for example, mechanical hardness, elastic modulus, tensile stress, fatigue strength, scratch resistance, fracture toughness, etc. [90]. The aforementioned augmentation in the mechanical properties of nanoparticulate material is ascribing to the structural flawlessness of the material. The microscopic-sized matters get free of internal structural deficiencies like dislocations, microtwins, and impurity precipitations. Repeated mechanical failure is caused by multiplying imperfections in the nanoparticulate materials, which are more lively and move to the surface, under annealing, purifying the material. This repositioning of defects to the surface departs perfect material structures within the nanoparticulate materials. The exterior surface of nanostructure materials is incredibly small or free from imperfections in comparison to that of bulk materials. Materials with fewer defects will give out superior mechanical properties [91].

In a lot of nanoparticulate materials, hardness is noticed as the most common mechanical property. A variety of superhard nanocomposites manufactured using borides, carbides and nitrides [92]. Extraordinary production methods were employed to produce such nanocomposites, in particular plasma-induced chemical technique and physical vapor deposition technique [93]. The nanoparticulate materials are created containing excellent mechanical properties for impending applications in macro-, micro-, and nanoscales. Nanocrystalline copper is three times more resistant as compared to usual copper; they are also more flexible [94]. Carbon nanotubes and nanowires are employed to make high-frequency electromechanical resonators that can be utilized as nanoprobbers or nanotweezers to control nanomaterials on a nanometer scale [95, 96].

Elasticity conception deals with the small, continue and reversible deformations of isotropic elastic materials [97]. An elastic material exhibits the following three properties: It distorts under stress and comes back to its original shape when the stress withdraws. It is uniform, isotropic, and homogeneously distributed in its occupied volume. Materials are normally not isotropic as they are polycrystalline, with grains having diverse shapes and orientations. Conversely, as the lengths of the materials are very big to correspond to the mean grain, homogeneity and isotropy hypothesis are occasionally more or less satisfied. Therefore, the elasticity hypothesis is as well employed for polycrystalline materials [98].

5.4 Structural Properties

The reduction in particle size of material results in the transformation in interatomic spacing, and so surface and surface energy increase [33]. The structural alterations are noticed when the particle size reduces predominantly in the nanoscale range. Gold nanoparticles can accept a polyhedral shape, for example, cuboctahedral and multiply twinned decahedra [99]. Aforesaid shapes can be explored and understood by the enlargement of crystalline along with a variety of crys-

tallographic directions and energies of different crystallographic planes. Crystalline solid acquires long-range episodic structure of atoms and distinct prototypes. The fundamental factor of nanoparticulate materials is their shape, size, and morphological constitution. The surface morphology of nanoparticulate materials can be adjusted by means of a chemical agent named surfactant. The morphologies of nanoparticles are adjustable, and by scheming them, we can investigate their properties [100].

5.5 Thermal Properties

Several properties of materials can be customized by managing their nanoscale dimensions. Such customized nanostructures can be employed to meet the demands of various applications. The thermodynamics of nanosystem is different from the thermodynamics of macroscopic systems, where the number of particles has a tendency to perpetuate [101]. Higher surface energy will change monotonically with size and can be taken care of within the structure of thermodynamics [102]. Among them is the melting and other phase transition temperatures that exemplify the common experimental difference of melting point of gallium nitride spherical nanoparticles aligned with the size of the particles [103]. Its physical starting point is the raise of surface energy, the augment of the amplitude of atomic vibrations, and the supplementary surface growth of thermal vibration energy in the consequence [65]. It has been stated that the specific heat raised with the reduction in particle size, while the melting entropy, as well as enthalpy, diminished as the particle size reduces [104].

The exploit of nanofluid to improve the thermal transfer is a hopeful application of the thermal properties of nanoparticulate materials. Nanofluids are in general said to be solid-liquid composite materials, which contain nanoparticulate materials of size in the range 1–100 nm suspended in a liquid [105]. Nanofluids grasp greater than ever interests in both research and practical applications because of their very much superior thermal properties in comparison with their base

fluids. A great deal of nanoparticulate materials can be employed in nanofluids counting nanoparticles of oxides, nitrides, metals, metal carbides, and nanofibers such as single-wall and multiwall carbon nanotubes, which can be discrete into different base liquids dependent on the potential applications, for example, water, ethylene glycol, and oils [106].

The most significant attributes of nanofluids are the momentous increase of thermal conductivity proportionate to liquids exclusive of nanoparticulate materials, which have been proven by numerous investigational works [107]. Nanofluid-based devices will facilitate the expansion of real-time, plainly invasive medical diagnostic systems to observe astronaut health and assist in diagnosing and treating sickness [108]. As a result, investigators are facing problems for the hypothetical analysis of thermal transport in nanoparticulate materials [109]. The thermal properties of nanoparticulate materials can be tailored by numerous factors like the small size of particles, the shape of the particle, the huge interface area, etc. Hence, the thermal properties of nanoparticulate materials are fairly diverse in comparison to the bulk materials. As the length of the material lessens to the nanometer range, it is quite similar to the wavelength and means a free path of phonon, which results in the noteworthy transform in phonon transport in the material. As a consequence of the transform in phonon confinement and quantization of phonon transport, thermal properties without human intervention get customized [110].

5.6 Optical Properties

The optical properties are based on electronic structure, and an alteration in zone structure results in an alteration in absorption and luminescence spectra. Their distinctiveness, such as spectral width and position, and sensitivity to light polarization rely not only on the inherent properties of the nano-objects (e.g., composition, structure, size, shape) but also on their surroundings [85].

The diminution of material dimension as well has an effect on the optical properties of the materials. The optical properties of nanomaterials depend on the size of particles which can be clarified in two ways. One is due to the more confined structure, energy level spacing increases and another is related to surface plasmon resonance (SPR). The optical properties of metallic nanoparticles are measured by the SPR phenomenon [111]. The SPR is resultant from the steady motion of the conduction band electrons from one surface of the particle to the other, upon communication with an electromagnetic field. The reduction in size beneath the electron mean free path (distance the electron moves between scattering collisions with the lattice centers) brings about intense absorption in the UV-visible range. Optical excitation of the SPR causes surface plasmon absorption [112].

For semiconducting materials, the quantum size effect is most studied. By reduction of the particle size of semiconducting material, interband transition is shifted to the higher frequency, which results in the increase in bandgap. The bandgap of semiconducting materials is within a few electron volts, which rises quickly with reducing particle size. Quantum confinement results in a blue shift in the bandgap [113]. The optical properties of nanostructured semiconductors powerfully rely upon particle size. Hence, the optical properties of such materials are effortlessly adjustable by changing the size of particles. The nanostructured semiconducting materials acquire excellent transporter confinement and energy density states, which assemble it most appropriate and resourceful for laser devices [114]. When the particle size of metal nanostructures is lesser than the wavelength of incident radiation, a SPR is created. By commencing the above discussion, it is understandable that the optical properties of materials are very much affected by the particle dimension. By changing the dimension of materials in nanometer, we can modify sophisticated optical materials for devices [115].

5.7 Magnetic Properties

Nanomagnetism is a vibrant and very interesting topic of current solid-state magnetism and nanotechnology [116]. It is of foremost scientific attention and high technological importance. Ferromagnetic nanoparticulate materials encompass prospective benefits over present materials in various applications in hard magnets, soft magnets, magnetic recording, etc. It is well recognized that the coercivity of magnetic substances has an outstanding reliance on their size. Magnetic coercivity rises with the decrease in particle size in the nanometer range going through a highest at the solitary domain size and afterward reduces once more time for very tiny particles on account of thermal effects and turns into zero at the superparamagnetic particle size. An iron, which is a soft magnetic material with coercivity of about 20 Oersted (Oe) at room temperature, could be formed “hard” with a coercivity of 540 Oe [117]. An additional example is the amazing phenomenon of giant magnetoresistance of magnetic multilayers that has been developed to enhance the capability of hard discs by over a factor of a hundred in a few years [118].

The magnetic properties are exploited in drug delivery [119]. The magnetic characteristics of the nanoparticles can also be different from those of the related bulk material. Attributable to a smaller size of the particle, the surface area increases, and magnetic coupling with neighboring atoms also increases, which leads to the varied magnetic properties.

Ferromagnetism takes place even for the smallest dimensions. The magnetic torques are improved atom-like for clusters with not more than around 100–200 atoms. The magnetic torque diminishes and moves toward the bulk limit, as the size is raised up to 700 atoms, with vibrations probably resulting from surface-induced spin-density waves or structural alterations. Ferromagnetism is referred to a worldwide aspect of nanoparticles of the nonmagnetic oxides [120]. When the particle size diminishes beneath a definite size, ferromagnetic particles turn out to be unstable. Such instability is a result of the spontaneous polarization of domains and the adequately

elevated surface energy. Owing to this property, ferromagnetic grows to be paramagnetic at the nanometer scale, but it acts in a different way from the conventional paramagnetic, and therefore it is named superparamagnetism [121].

A bulk ferromagnetic substance generally includes multiple magnetic domains, while nanostructured ferromagnetic substances have minute magnetic nanoparticles and have simply one domain. These domains of different particles are arbitrarily dispersed as a result of thermal fluctuation and develop into aligned in the presence of an externally applied magnetic field [122].

6 Types of Nanomaterials

Nanomaterials are one of the key products of nanotechnology. Nanomaterials have a higher surface-to-volume ratio, and they preserve properties notably different from the bulk material as at this stage quantum effects might be noteworthy. Basically, we can say the electrical, electronic, magnetic, mechanical, optical, etc., properties of solids are considerably changed with a big decline in the particle size. Applications of nanotechnology in drug delivery take place through the use of designed nanomaterials as well as forming delivery systems from nanoscale molecules such as liposomes, polymeric micelles, polymeric nanoparticles, nanocapsules, nanocrystals, nanotubes, nanocages, dendrimers, quantum dots, etc. There are different types of nanomaterials utilized as drug delivery systems which are briefly discussed in this section.

6.1 Liposomes

Liposomes are concentric bilayer spherical-shaped vesicle systems in which an aqueous volume is totally enclosed by a lipidic bilayer membrane made up of phospholipids as well as steroids generally in the size range of 50–450 nm. The structure of the liposomal membrane is similar to that of cell membranes and for the reason that they make easy inclusion of drugs in them. Liposomes are employed as excellent drug deliv-

ery vehicles for biotechnological drugs because of various advantages like amphiphilic character, biocompatibility, and simplicity of surface modification. Due to their size, hydrophilic as well as hydrophobic features, and biocompatible and biodegradable character, liposomes are promising systems for drug delivery [123].

6.2 Polymeric Micelles

Polymeric micelles are nanoparticulate systems made of amphiphilic block copolymers that get together by themselves in the aqueous solution to create a nanoscale supramolecular core-shell arrangement under 100 nm sizes. Polymeric micelles because of their hydrophilic surface defend their nonspecific uptake by the reticuloendothelial system. The hydrophobic core of polymeric micelles can be laden with hydrophobic drugs like camptothecin and paclitaxel; however, the hydrophilic part makes the whole system soluble in water as well as stabilizes the core. Polymeric micelles have a strong potential for hydrophobic drug delivery seeing as their center core structure allows the incorporation of these kinds of drugs ensuing in the improvement of bioavailability as well as stability [124, 125].

Polymeric micelles have provided evidence as an excellent novel drug delivery system attributable to higher and adaptable loading capacity, steadiness in physiological circumstances, slow rate of dissolution, the higher buildup of drugs at the target site, and likelihood of end group functionalization for conjugation of targeting ligands [126].

6.3 Metallic Nanoparticles

Metallic nanoparticles are submicron size structures generally made of pure metals like cerium, gold, platinum, silver, titanium, and zinc or their compounds like chlorides, fluorides, hydroxides, oxides, and sulfides. Recently, the use of metallic nanoparticles has been growing in different medical applications, for instance, bioimaging, bio-

sensors, targeted drug delivery, and photoablation therapy [127, 128]. Additionally, the surface modification, as well as functionalization of metallic nanoparticles with definite functional groups, lets them attach to antibodies, drugs, and other ligands, rendering these systems more hopeful in biomedical applications [127–129].

6.4 Polymeric Nanoparticles

Polymeric nanoparticles are tiny particles within the size range from 1 to 1000 nm and can be laden with active pharmaceutical ingredients entrapped inside or surface-adsorbed onto the polymeric central part. The term “nanoparticle” includes both nanocapsules and nanospheres, which are different with regard to their morphology. Nanocapsules are made up of an oily interior portion in which the drug is dissolved, enclosed by a polymeric shell that manages the drug release from the core. On the other hand, nanospheres are continuous polymeric networks in which the drug is retained in the interior or adsorbed onto their surface [130–132]. Benefits of polymeric nanoparticles as drug carriers include their potential use for controlled release, the ability to guard drug and other molecules with biological activity against the environment, improve their bioavailability and therapeutic index. Polymeric nanoparticles have shown great potential for targeted delivery of drugs for the treatment of several diseases [133, 134].

6.5 Nanocapsules

Nanocapsules are nanoparticulate systems in which the drug is confined to a hollow space enclosed by a distinctive polymeric membrane which provides a unique nanostructure. A nanocapsule has magnetized enormous attention, owing to the protective coating, which is generally pyrophoric and simply oxidized and provides sustained release of active ingredients [135]. Nanocapsules as drug delivery systems can improve the bioavailability of drugs and also help

to attain targeted delivery. Similarly, by loading the drug within polymeric nanocapsules, it can defend the drug from breakdown or degradation done by the biological environment. Meanwhile, nanocapsules can successfully decrease the detrimental effects between drug and tissue environments [136].

6.6 Nanocrystals

Nanocrystal is a nanoparticulate carrier-free drug delivery system with at least one dimension ≤ 100 nm and that is solitary crystalline. However, even with the definition that points out nanocrystals as a “carrier-free” system, surfactants or polymeric steric stabilizers are indispensable to avert colloidal particle aggregation and as a consequence improve stability [137, 138]. Nanocrystals are of interest to researchers nowadays as they provide special features including enhancement of saturation solubility, dissolution velocity, and adhesiveness to surface/cell membranes, and so nanocrystals are employed as a means of achieving colloidal particles with customized biological properties that permit modifying the drug delivery as well as targeting [139].

6.7 Nanotube

Carbon nanotubes are tube-like cylindrical nanostructures having less than 100 nm diameter generally made up of carbon allotrope graphene with sp^2 hybridized carbon atoms. Nanotubes are categorized as single-wall nanotubes as well as multiwall nanotubes. Nanotubes show sparkling electrical, mechanical, optical, and synthetic characteristics, gaining widespread eagerness for their potential application in different fields like nanotechnology, electronics, optics, and other fields of materials science. Carbon nanotubes, has attracted incredible interest in the biomedical field due to their unique features like ability to deliver drugs at targeted sites, biocompatibility, higher drug loading capacity, higher surface area, great strength, and flexible interaction with pay-

load, excellent optical and electrical features [140–142].

6.8 Nanocages

Nanocages are nanoparticulate-based drug delivery systems that have a hollow structure that can put in a nutshell large amounts of drugs inside. The term “cage” means that it can be unlocked, and so nanocages are frequently intended to be stimulus-responsive, taking benefit of definite physical or chemical differences in the environment at their target to alter their molecular structure [143]. Nanocages have a higher loading capacity than other nanoparticles and so can be loaded with hundreds or even thousands of drug molecules. As a result, a lesser dose of nanoparticles is needed to deliver a therapeutically effective dose of the drug, and, therefore, the overall cytotoxicity of the nanocages is reduced. A different main feature of nanocages is the aptitude to encapsulate and defend the drugs from the environment fully so that nanocages can be utilized as carriers of highly lipophilic drugs and stay stable in hydrophilic environments like the bloodstream. As soon as the nanocages get to the target tissue, the more lipophilic environment facilitates drug release [144, 145].

6.9 Dendrimers

Dendrimers are highly bifurcated, monodisperse, symmetric molecules with well-defined and three-dimensional nanostructures whose size and shape can be accurately controlled. Dendrimers are highly defined nanoparticles with sizes ranging from 1 to 15 nm [146–148]. The well-defined globular-shaped nanostructure, which is hyperbranched, with high compatibility with a biological system and capability for surface functionalization without difficulty, makes dendrimers outstanding candidates for photodynamic therapy, gene delivery, small interfering RNA delivery, oligonucleotide delivery, medical and biomedical application, and vaccine delivery and as drug delivery agents [149].

6.10 Quantum Dots

Quantum dots are known as semiconductor nanocrystals with size ranging from 2 to 10 nm, and their optical properties, for example, absorbance and photoluminescence, are size-dependent. The quantum dots have achieved immense attention in the field of nanomedicine, since, unlike conventional organic dyes, the quantum dots give emission in the near-infrared region (<650 nm), an incredibly attractive characteristic in the field of biomedical images, thanks to the low absorption by the tissues and decline in the light scattering [150]. Additionally, quantum dots with diverse sizes and/or compositions can be excited by the same light source resultant in separate emission colors over a broad spectral range [151, 152]. In this sense, quantum dots are awfully interesting for multiplex imaging. Quantum dots have been widely studied as targeted drug delivery, sensors, and bioimaging in the medical field.

7 Conclusion

Nanotechnology can be characterized as the understanding, control, and manipulation of materials, having dimensions approximately within the 1–100 nm range, where conventional physics breaks down. Scientists consider nanotechnology as the innovatory technology of the twenty-first century. Nanomaterials refer to natural, incidental, or manufactured materials containing particles in unbound or agglomerated/aggregated states. It has been observed that nanomaterials are totally different from their bulk moieties and cannot be studied as same as bulk or small molecules because of their distinguishing properties in nanometer scale. These distinguishing properties of nanomaterials are dependent on the composition, chemistry, particle dimension, and interactions with other materials. The exploit of nanotechnology in developing nanoparticulate carriers for drug delivery is bringing lots of hope and eagerness in the field of drug delivery research. Nanoparticulate materials as a drug delivery present a number of benefits that demonstrate high intracellular uptake than the other

conventional form of drug delivery systems. Additionally, nanoparticulate materials can be coupled with a ligand-like antibody to help a targeted therapeutic strategy. Hence, nanoparticulate drug delivery systems may modernize the entire drug therapy approach and carry it to a new height in the nearest future.

References

1. Fajardo AR, Pereira AGB, Muniz EC. Hydrogels nanocomposites based on crystals, whiskers and fibrils derived from biopolymers. In: Thakur VK, Thakur MK, editors. Eco-friendly polymer nanocomposites, advanced structured materials. New Delhi: Springer; 2015. p. 43–71.
2. Huyen D. Carbon nanotubes and semiconducting polymer nanocomposites. In: Yellampalli S, editor. Carbon nanotubes-synthesis, characterization, applications. London: InTech; 2011.
3. Nikalje AP. Nanotechnology and its applications in medicine. *Med Chem.* 2015;5(2):81–9.
4. Rai M, Yadav A, Gade A. Current trends in phytosynthesis of metal nanoparticles. *Crit Rev Biotechnol.* 2008;28(4):277–84.
5. Asmatulu R, Asmatulu E, Zhang B. Nanotechnology and nanoethics in engineering education. In: Proceedings of the 2010 Midwest section conference of the American Society for Engineering Education. Lawrence, KS; 2010. p. 1–11.
6. Pradeep T. Nano: the essentials – understanding nanoscience and nanotechnology. New Delhi: Tata McGraw-Hill Publishing Company Limited; 2007. p. 3–15.
7. Wardak A, Gorman ME, Swami N, Deshpande S. Identification of risks in the life cycle of nanotechnology-based products. *J Ind Ecol.* 2008;12:435–48.
8. Raza H, Raza TZ. Introducing nanoengineering and nanotechnology to the first year students through an interactive seminar course. *J Nano Educ.* 2013;4:41–6.
9. Rocco MC. National nanotechnology initiative - past, present, future. In: Goddard WA, Brenner DW, Lyshevski SE, Iafrate GJ, editors. Handbook on nanoscience, engineering and technology. 2nd ed. Boca Raton: Taylor and Francis, CRC Press; 2007. p. 3.1–3.26.
10. Rocco MC, Mirkin CA, Hersam MC. Nanotechnology research directions for societal needs in 2020: retrospective and outlook. Dordrecht: Springer; 2011.
11. Barakat N, Jiao H. Nanotechnology integration to enhance undergraduate engineering education. In: Bernardino J, Quadrado JC, editors. Proceedings of the SEFI annual conference. 1st world engineering

- education flash week. Lisbon, Portugal; 2011. p. 623–30.
12. Daryoush B, Darvish A. A case study and review of nanotechnology and nanomaterials in green architecture. *Res J Environ Earth Sci.* 2013;5(2):78–84.
 13. Miyazaki K, Islam N. Nanotechnology systems of innovation – an analysis of industry and academia research activities. *Technovation.* 2007;27(11):661–75.
 14. Sandhiya S, Dkhar SA, Surendiran A. Emerging trends of nanomedicine – an overview. *Fundam Clin Pharmacol.* 2009;23(3):263–9.
 15. Daniel MC, Astruc D. Gold nanoparticles: assembly, supramolecular chemistry, quantum size related properties and applications towards biology catalysis and nanotechnology. *Chem Rev.* 2004;104(1):293–346.
 16. Kreuter J. Nanoparticles—a historical perspective. *Int J Pharm.* 2007;331(1):1–10.
 17. Khan MN, Mobin M, Abbas ZK, AlMutairi KA, Siddiqui ZH. Role of nanomaterials in plants under challenging environments. *Plant Physiol Biochem.* 2017;110:194–209.
 18. Guo D, Xie G, Luo J. Mechanical properties of nanoparticles: basics and applications. *J Phys D Appl Phys.* 2014;47(1):1–25.
 19. Klaine SJ, Alvarez PJJ, Batley GE, et al. Nanoparticles in the environment: behavior, fate, bioavailability and effects. *Environ Toxicol Chem.* 2008;27(9):1825–51.
 20. Boverhof DR, Bramante CM, Butala JH, et al. Comparative assessment of nanomaterial definitions and safety evaluation considerations. *Regul Toxicol Pharmacol.* 2015;73(1):137–50.
 21. ISO/TS 27687. Nanotechnologies – terminology and definitions for nano-objects – nanoparticle, nanofibre, nanoplate, 2008. <http://www.iso.org/standard/44278.html>.
 22. Potocnik J. Commission recommendation of 18 October 2011 on the definition of nanomaterials. *Off J Eur Communities Legis.* 2011;L275:38–40.
 23. Patel JK, Patel A, Bhatia D. Introduction to nanomaterials and nanotechnology. In: Patel JK, Pathak YV, editors. *Emerging technologies for nanoparticle manufacturing.* Cham: Springer; 2021. p. 3–23.
 24. Sarma S, Das R, Brar S, et al. Fundamental characteristics and their influence on fate and behavior of nanomaterials in environments. In: Brar SK, Verma M, Tyagi RD, Surampalli RY, Zhang TC, editors. *Nanomaterials in the environment.* 1st ed. Reston: American Society of Civil Engineers; 2015. p. 1–26.
 25. Henry C. Size effects on structure and morphology of free or supported nanoparticles. In: Brechignac CP, Houdy P, Lahmani M, editors. *Nanomaterials and nanochemistry.* Berlin/Heidelberg/New York: Springer; 2006. p. 3–34.
 26. Kumar N, Kumbhat S. Carbon-based nanomaterials. *Essentials in nanoscience and nanotechnology.* Hoboken: Wiley; 2016. p. 189–236.
 27. Maddinedi SB, Mandala BK, Ranjan S, Dasgupta N. Diastase assisted green synthesis of size controllable gold nanoparticles. *RSC Adv.* 2015;5:26727–33.
 28. Dasgupta N, Ranjan S, Chakraborty AR, Ramalingam C, Shanker R, Kumar A. Nanoagriculture and water quality management. In: Ranjan S, Dasgupta N, Lichfouste E, editors. *Nanoscience in food and agriculture 1, sustainable agriculture reviews 20.* Cham: Springer International Publishing; 2016. p. 1–42.
 29. Ranjan S, Nandita D, Bhavapriya R, Ganesh SA, Chidambaram R, Ashutosh K. Microwave irradiation-assisted hybrid chemical approach for titanium dioxide nanoparticle synthesis: microbial and cytotoxicological evaluation. *Environ Sci Pollut Res.* 2016;23(12):12287–302.
 30. Pulimi M, Subramanian S. Nanomaterials for soil fertilisation and contaminant removal. In: Ranjan N, Dasgupta N, Lichfouste E, editors. *Nanoscience in food and agriculture 1, sustainable agriculture reviews 20.* Cham: Springer International Publishing; 2016. p. 229–46.
 31. Dasgupta N, Ranjan S, Mundeekad D, Ramalingam C, Shanker R, Kumar A. Nanotechnology in agro-food: from field to plate. *Food Res Int.* 2015;69:381–400.
 32. Ranjan S, Nandita D, Sudandiradoss C, Ramalingam C, Ashutosh K. A novel approach to evaluate titanium dioxide nanoparticle-protein interaction through docking: an insight into the mechanism of action. *Proc Natl Acad Sci India Sect B Biol Sci.* 2017;87(3):937–43.
 33. Sun CQ. Size dependence of nanostructures: impact of bond order deficiency. *Prog Solid State Chem.* 2007;35(1):1–159.
 34. Junk A, Riess F. From an idea to a vision: there's plenty of room at the bottom. *Am J Phys.* 2006;74(9):825–30.
 35. Koo JH. Polymer nanocomposites – processing, characterization, and applications. New York: McGraw-Hill; 2006. p. 1–48.
 36. Koo JH. *Fundamentals, properties and applications of polymer nanocomposites.* New York: Cambridge University Press; 2016. p. 3–17.
 37. Gaffet E. Nanomaterials: a review of the definitions, applications, health effects. How to implement secure development, 2011. <https://hal.archives-ouvertes.fr/hal-00598817/file/E.Gaffet-GB.pdf>.
 38. Gendelman HE, Anantharam V, Bronich T, et al. Nanoneuromedicines for degenerative, inflammatory, and infectious nervous system diseases. *Nanomed: Nanotechnol Biol Med.* 2015;11(3):751–67.
 39. Pillai G. Nanomedicines for cancer therapy: an update of FDA approved and those under various stages of development. *SOJ Pharm Pharm Sci.* 2014;1(2):13–25.
 40. Wang R, Billone PS, Mullett WM. Nanomedicine in action: an overview of cancer nanomedicine on the market and in clinical trials. *J Nanomater.* 2013;2013:Article ID 629681.

41. Wang M, Thanou M. Targeting nanoparticles to cancer. *Pharmacol Res.* 2010;62(2):90–9.
42. Torchilin V. Tumor delivery of macromolecular drugs based on the EPR effect. *Adv Drug Deliv Rev.* 2011;63(3):131–5.
43. Liu S, Guo Y, Huang R, et al. Gene and doxorubicin co-delivery system for targeting therapy of glioma. *Biomaterials.* 2012;33(19):4907–16.
44. Huang R, Ke W, Han L, Li J, Liu S, Jiang C. Targeted delivery of chlorotoxin-modified DNA loaded nanoparticles to glioma via intravenous administration. *Biomaterials.* 2011a;32(9):2399–406.
45. Huang S, Li J, Han L, Liu S, Ma H, Huang R, et al. Dual targeting effect of Angiopep-2- modified, DNA-loaded nanoparticles for glioma. *Biomaterials.* 2011b;32(28):6832–8.
46. Vander Heiden MG. Targeting cancer metabolism: a therapeutic window opens. *Nat Rev Drug Discov.* 2011;10(9):671–84.
47. Moghimi SM, Hunter AC, Murray JC. Nanomedicine: current status and future prospects. *FASEB J.* 2005;19(3):311–30.
48. Yokoyama M. Drug targeting with nano-sized carrier systems. *J Artif Organs.* 2005;8(2):77–84.
49. Bae YH, Park K. Targeted drug delivery to tumors: myths, reality and possibility. *J Control Release.* 2011;153(3):198–205.
50. Gamucci O, Bertero A, Gagliardi M, Bardi G. Biomedical nanoparticles: overview of their surface immune-compatibility. *Coatings.* 2014;4(1):139–59.
51. Salata O. Applications of nanoparticles in biology and medicine. *J Nanobiotechnol.* 2004;2(3):1–6.
52. Vance ME, Kuiken T, Vejerano EP, et al. Nanotechnology in the real world: redeveloping the nanomaterial consumer products inventory. *Nanotechnology.* 2015;6:1769–80.
53. Gleiter H. Nanostructured materials: basic concepts and microstructure. *Acta Mater.* 2000;48(1):1–29.
54. Johnston RL, Wilcoxon JP. *Frontiers of nanoscience*, vol. 3. Oxford: Elsevier; 2012.
55. Smith AM, Nie S. Semiconductor nanocrystals: structure, properties, and band gap engineering. *Acc Chem Res.* 2010;43(2):190–200.
56. Saleh TA. Nanomaterials for pharmaceuticals determination. *Bioenergetics.* 2016;5(1):1000226.
57. Saleh TA, Gupta VK. *Nanomaterial and polymer membranes, synthesis, characterization, and applications.* 1st ed. Amsterdam: Elsevier; 2016. p. 1–284.
58. Buzea C, Pacheco-Blandino I, Robbie K. Nanomaterials and nanoparticles: sources and toxicity. *Biointerphases.* 2007;2(4):MR17–MR172.
59. Jeevanandam J, Barhoum A, Chan YS, Dufresne A, Danquah MK. Review on nanoparticles and nanostructured materials: history, sources, toxicity and regulations. *Beilstein J Nanotechnol.* 2018;9:1050–74.
60. Hochella MF Jr, Spencer MG, Jones KL. Nanotechnology: nature's gift or scientists' brainchild? *Environ Sci Nano.* 2015;2(2):114–9.
61. Sharma VK, Filip J, Zboril R, Varma RS. Natural inorganic nanoparticles-formation, fate, and toxicity in the environment. *Chem Soc Rev.* 2015;44(23):8410–23.
62. Jordan CC, Kaiser I, Moore VC. 2013 nanotechnology patent literature review: graphitic carbon-based nanotechnology and energy applications are on the rise. *Nanotechnol Law Business.* 2014;11(2):111–25.
63. Filella M. Nanomaterials. In: Pawliszyn J, editor. *Comprehensive sampling and sample preparation*, vol. 1. Amsterdam: Academic Press; 2012. p. 109–24.
64. Wagner S, Gondikas A, Neubauer E, Hofmann T, von der Kammer F. Spot the difference: engineered and natural nanoparticles in the environment-release, behavior, and fate. *Angew Chem Int Ed.* 2014;53(46):12398–419.
65. Pokropivny VV, Skorokhod VV. Classification of nanostructures by dimensionality and concept of surface forms engineering in nanomaterial science. *Mater Sci Eng C.* 2007;27(5–8):990–3.
66. Tiwari JN, Tiwari RN, Kim KS. Zero-dimensional, one-dimensional, two-dimensional and three-dimensional nanostructured materials for advanced electrochemical energy devices. *Prog Mater Sci.* 2012;57(4):724–803.
67. Wani IA. Nanomaterials, novel preparation routes, and characterizations. In: Shah MA, Bhat MA, Davim JP, editors. *Nanotechnology applications for improvements in energy efficiency and environmental management.* Hershey: IGI Global Publishers; 2015. p. 1–40.
68. Cao G. Nanostructures and nanomaterials: synthesis, properties and applications. *J Am Chem Soc.* 2004;126(44):14679.
69. Balaz P. From minerals to nanoparticles. In: Balaz P, editor. *Mechanochemistry in nanoscience and minerals engineering.* Berlin/Heidelberg: Springer; 2008. p. 177–256.
70. Abdelsalam HA, Abdelaziz AY. The smart grid state of the art and future trends. *Electr Power Components Syst.* 2014;42(3–4):306–14.
71. Gubin SP. Introduction. In: Gubin SP, editor. *Magnetic nanoparticles.* Weinheim: Wiley; 2009. p. 1–23.
72. Thomas S, Rafiei S, Maghsoodlou S, Afzali A. *Foundations of nanotechnology, volume two: nanoelements formation and interaction.* 1st ed. New York: Apple Academic Press; 2014.
73. Koski KJ, Cui Y. The new skinny in two-dimensional nanomaterials. *ACS Nano.* 2013;7(5):3739–43.
74. Koch CC, Ovidko IA, Seal S, Veprek S. *Structural nanocrystalline materials: fundamentals and applications.* New York: Cambridge University Press; 2007. p. 25–128.
75. Law M, Goldberger J, Yang P. Semiconductor nanowires and nanotubes. *Annu Rev Mater Res.* 2004;34:83–122.
76. Lin J, Zhang C, Yan Z, et al. 3-dimensional graphene carbon nanotube carpet-based microsupercapacitors

- with high electrochemical performance. *Nano Lett.* 2013;13(1):72–8.
77. West JL, Halas NJ. Engineered nanomaterials for biophotonics applications: improving sensing, imaging, and therapeutics. *Annu Rev Biomed Eng.* 2003;5:285–92.
78. Sozer N, Kokini JL. Nanotechnology and its applications in the food sector. *Trends Biotechnol.* 2009;27(2):82–9.
79. Roduner E. Size matters: why nanomaterials are different. *Chem Soc Rev.* 2006;35(7):583–92.
80. Blackwelder B. Nanotechnology jumps the gun: nanoparticles in consumer products. In: Cameron NM, Mitchell ME, editors. *Nanoscale: issues and perspectives for the nano century.* Hoboken: Wiley; 2007. p. 71–82.
81. Sugimoto Y, Pou P, Custance O, et al. Complex patterning by vertical interchange atom manipulation using atomic force microscopy. *Science.* 2008;322(5900):413–7.
82. Stucky GD, Mac Dougall JE. Quantum confinement and host/guest chemistry: probing a new dimension. *Science.* 1990;247(4943):669–78.
83. Richards R, Bonnemann H. Synthetic approaches to metallic nanomaterials. In: Kumar CSSR, Hormes J, Leuschner C, editors. *Nanofabrication towards biomedical applications: techniques, tools, applications, and impact.* Weinheim: Wiley; 2005. p. 3–32.
84. Naseri MG, Saion EB. Crystallization in spinel ferrite nanoparticles. In: Mastai Y, editor. *Advances in crystallization processes.* Croatia: InTech; 2012. p. 349–80.
85. Rezaie HR, Shokuhfar A, Arianpour F. Nanocomposite materials from theory to application. In: Andreas OA, Shokuhfar A, editors. *New frontiers of nanoparticles and nanocomposite materials.* Berlin/Heidelberg: Springer; 2013. p. 171–232.
86. Aznan NZK, Johan MR. Quantum size effect in ZnO nanoparticles via mechanical milling. *J Nanomater.* 2012;2012:Article ID 439010.
87. Lokhande J, Pathak Y. Concept, Definition and need for metallonutraceuticals. In: Lokhande J, Pathak Y, eds. *Handbook of metallonutraceuticals.* 1st ed. Boca Raton: CRC Press, Taylor & Francis Group 2014.
88. De Rogatis L, Montini T, Gombac V, Cargnelli M, Fornasiero P. Stabilized metal nanoparticles embedded into porous oxides: a challenging approach for robust catalysts. In: Prescott WV, Schwartz AI, editors. *Nanorods, nanotubes and nanomaterials research progress.* New York: Nova Science Publishers; 2008. p. 71–123.
89. Wang B, Xue D, Shi Y, Xue F. Titania 1D nanostructured materials: synthesis, properties and applications. In: Prescott WV, Schwartz AI, editors. *Nanorods, nanotubes and nanomaterials research progress.* New York: Nova Science Publishers; 2008. p. 163–201.
90. Meyers MA, Mishra A, Benson DJ. Mechanical properties of nanocrystalline materials. *Prog Mater Sci.* 2006;51:427–556.
91. Eletski AV. Mechanical properties of carbon nanostructures and related materials. *Phys Uspekhi.* 2007;50(3):225–61.
92. Zhang S, Sun D, Yongqing FU. Superhard nanocomposite coatings: review article. *J Mater Sci Technol.* 2002;18(6):485–91.
93. Chen Z, Dai XJ, Magniez K, et al. Improving the mechanical properties of epoxy using multi-walled carbon nanotubes functionalized by a novel plasma treatment. *Compos Part A Appl Sci Manuf.* 2013;45:145–52.
94. Lu L, Shen Y, Chen X, Qian L, Lu K. Ultrahigh strength and high electrical conductivity in copper. *Science.* 2004;304(5669):422–6.
95. Nguyen CV, Ye Q, Meyyappan M. Carbon nanotube tips for scanning probe microscopy: fabrication and high aspect ratio nanometrology. *Meas Sci Technol.* 2005;16(11):2138–46.
96. Dequesnes M, Rotkin S, Aluru N. Calculation of pull-in voltages for carbon-nanotube-based nanoelectromechanical switches. *Nanotechnology.* 2002;13(1):120–31.
97. Muskhelishvili NI. The fundamental law of the theory of elasticity. The basic equations. In: Muskhelishvili NI, editor. *Some basic problems of the mathematical theory of elasticity.* Dordrecht: Springer Science & Business Media; 2013. p. 52–84.
98. Juve V, Crut A, Maioli P, et al. Probing elasticity at the nanoscale: terahertz acoustic vibration of small metal nanoparticles. *Nano Lett.* 2010;10(5):1853–8.
99. Eguchi M, Mitsui D, Wu H-L, Sato R, Teranishi T. Simple reductant concentration-dependent shape control of polyhedral gold nanoparticles and their plasmonic properties. *Langmuir.* 2012;28(24):9021–6.
100. Ariga K, Li M, Richards GJ, Hill JP. Nanoarchitectonics: a conceptual paradigm for design and synthesis of dimension-controlled functional nanomaterials. *J Nanosci Nanotechnol.* 2011;11(1):1–13.
101. Labastie P, Calvo F. Thermodynamics and solid-liquid transitions. In: Brechignac C, Houdy P, Lahmani M, editors. *Nanomaterials and nanochemistry.* Berlin/Heidelberg: Springer; 2008. p. 55–87.
102. Niepce JC, Pizzagalli L. Structure and phase transitions in nanocrystals. In: Brechignac C, Houdy P, Lahmani M, editors. *Nanomaterials and nanochemistry.* Berlin/Heidelberg: Springer; 2008. p. 35–54.
103. Antoniammal P, Arivuoli D. Size and shape dependence on melting temperature of gallium nitride nanoparticles. *J Nanomater.* 2012;2012:415797.
104. Singh M, Lara S, Tlali S. Effects of size and shape on the specific heat, melting entropy and enthalpy of nanomaterials. *J Taibah Univ Sci.* 2017;11(6):922–9.
105. Obaid HN, Habeeb MA, Rashid FL, Hashim A. Thermal energy storage. *Nanofluids J Energy Technol Policy.* 2013;3(5):34–6.

106. Gorji TB, Ranjbar AA. A review on optical properties and application of nanofluids in direct absorption solar collectors (DASCs). *Renew Sust Energy Rev.* 2017;72:10–32.
107. Koblinski P, Eastman JA, Cahill DG. Nanofluids for thermal transport. *Mater Today.* 2005;8(6):36–44.
108. Patel J, Patel A. Nano drug delivery systems for space applications. In: Pathak Y, Araújo dos Santos M, Zea L, editors. *Handbook of space pharmaceuticals*. Cham: Springer; 2019. p. 1–22.
109. Cahill DG, Ford WK, Goodson KE, et al. Nanoscale thermal transport. *J Appl Phys.* 2003;93(2):793–818.
110. Balandin AA. Thermal properties of graphene and nanostructured carbon materials. *Nat Mater.* 2011;10(8):569–81.
111. Pattnaik P. Surface plasmon resonance. *Appl Biochem Biotechnol.* 2005;126(2):79–92.
112. Homola J, Yee SS, Gauglitz G. Surface plasmon resonance sensors: review. *Sensors Actuat B: Chem.* 1999;54(1–2):3–15.
113. Lin KF, Cheng HM, Hsu HC, Lin LJ, Hsieh WF. Band gap variation of size-controlled ZnO quantum dots synthesized by sol–gel method. *Chem Phys Lett.* 2005;409(4–6):208–11.
114. Huang MH, Mao S, Feick H, Yan H, Wu Y, Kind H, et al. Room-temperature ultraviolet nanowire nanolasers. *Science.* 2001;292(5523):1897–9.
115. Sanchez C, Belleville P, Popall M, Nicole L. Applications of advanced hybrid organic–inorganic nanomaterials: from laboratory to market. *Chem Soc Rev.* 2011;40(2):696–753.
116. Petravic O. Superparamagnetic nanoparticle ensembles. *Superlattice Microst.* 2010;47:569–78.
117. Schwarz JA, Contescu CI, Putyera K. *Dekker encyclopedia of nanoscience and nanotechnology*, vol. 4. Boca Raton: CRC Press; 2004.
118. Mills DL, Bland JAC, editors. *Nanomagnetism: ultrathin films, multilayers and nanostructures*, vol. 1. 1st ed. Netherlands: Elsevier Science; 2006. p. xi–xiii.
119. Wu H, Liu G, Wang X, et al. Solvothermal synthesis of cobalt ferrite nanoparticles loaded on multiwalled carbon nanotubes for magnetic resonance imaging and drug delivery. *Acta Biomater.* 2011;7(9):3496–504.
120. Sundaresan A, Bhargavi R, Rangarajan N, Siddesh U, Rao C. Ferromagnetism as a universal feature of nanoparticles of the otherwise nonmagnetic oxides. *Phys Rev B.* 2006;74(16):161306.
121. Sato K, Fukushima T, Katayama-Yoshida H. Superparamagnetic blocking phenomena and room-temperature ferromagnetism in wide band-gap dilute magnetic semiconductor (Ga, Mn) N. *Jpn J Appl Phys.* 2007;46(25–28):L682–4.
122. McHenry M, Laughlin D. Nano-scale materials development for future magnetic applications. *Acta Mater.* 2000;48(1):223–38.
123. Bozzuto G, Molinari A. Liposomes as nanomedical devices. *Int J Nanomedicine.* 2015;10:975.
124. Miyata K, Christie RJ, Kataoka K. Polymeric micelles for nano-scale drug delivery. *React Funct Polym.* 2011;71(3):227–34.
125. Xu W, Ling P, Zhang T. Polymeric micelles, a promising drug delivery system to enhance bioavailability of poorly water-soluble drugs. *J Drug Deliv.* 2013;2013:340315.
126. Panyam J, Labhasetwar V. Biodegradable nanoparticles for drug and gene delivery to cells and tissue. *Adv Drug Deliv Rev.* 2003;55(3):329–47.
127. Miele E, Spinelli GP, Miele E, et al. Nanoparticle-based delivery of small interfering RNA: challenges for cancer therapy. *Int J Nanomedicine.* 2012;7:3637–57.
128. McNamara K, Tofail SA. Nanoparticles in biomedical applications. *Adv Phys.* 2017;2(1):54–88.
129. Kudr J, Haddad Y, Richtera L, et al. Magnetic nanoparticles: from design and synthesis to real world applications. *Nano.* 2017;7(9):243.
130. Schaffazick SR, Pohlmann AR, Dalla-Costa T, Guterres SS. Freeze-drying polymeric colloidal suspensions: nanocapsules, nanospheres and nanodispersion. A comparative study. *Eur J Pharm Biopharm.* 2003;56(3):501–5.
131. Crucho CIC, Barros MT. Polymeric nanoparticles: a study on the preparation variables and characterization methods. *Mater Sci Eng C Mater Biol Appl.* 2017;80:771–84.
132. Guterres SS, Alves MP, Pohlmann AR. Polymeric nanoparticles, nanospheres and nanocapsules, for cutaneous applications. *Drug Target Insights.* 2007;2:147–57.
133. Soppimath KS, Aminabhavi TM, Kulkarni AR, Rudzinski WE. Biodegradable polymeric nanoparticles as drug delivery devices. *J Control Release.* 2001;70(1–2):1–20.
134. Owens DE III, Peppas NA. Opsonization, biodistribution, and pharmacokinetics of polymeric nanoparticles. *Int J Pharm.* 2006;307(1):93–102.
135. Kothamasu P, Kanumur H, Ravur N, Maddu C, Parasuramrajam R, Thangavel S. Nanocapsules: the weapons for novel drug delivery systems. *Bioimpacts.* 2012;2(2):71–81.
136. Deng S, Gigliobianco MR, Censi R, Di Martino P. Polymeric nanocapsules as nanotechnological alternative for drug delivery system: current status, challenges and opportunities. *Nanomaterials (Basel).* 2020;10(5):847.
137. Junyaprasert VB, Morakul B. Nanocrystals for enhancement of oral bioavailability of poorly water-soluble drugs. *Asian J Pharm Sci.* 2015;10(1):13–23.
138. Du J, Li X, Zhao H, et al. Nanosuspensions of poorly water-soluble drugs prepared by bottom-up technologies. *Int J Pharm.* 2015;495(2):738–49.
139. Patel AP, Patel JK, Patel K, Deshmukh A, Mishra B. Drug nanocrystal as a carrier free drug delivery. *Int J Res Ayurveda Pharm.* 2011;2(2):448–58.
140. Costa PM, Bourgognon M, Wang JTW, Al-Jamal KT. Functionalised carbon nanotubes: from intracellular uptake and cell-related toxicity

- to systemic brain delivery. *J Control Release*. 2016;241:200–19.
141. Alshehri R, Ilyas AM, Hasan A, Arnaout A, Ahmed F, Memic A. Carbon nanotubes in biomedical applications: factors, mechanisms, and remedies of toxicity. *J Med Chem*. 2016;59(18):8149–67.
 142. Singh B, Lohan S, Sandhu PS, Jain A, Mehta SK. Functionalized carbon nanotubes and their promising applications in therapeutics and diagnostics. In: Grumezescu AM, editor. *Nanobiomaterials in medical imaging*. Oxford, UK: William Andrew Publishing; 2016. p. 455–78.
 143. Karimi M, Zangabad PS, Mehdizadeh F, et al. Nanocaged platforms: modification, drug delivery and nanotoxicity. Opening synthetic cages to release the tiger. *Nanoscale*. 2017;9(4):1356–92.
 144. Uchida M, Terashima M, Cunningham CH, et al. A human ferritin iron oxide nano-composite magnetic resonance contrast agent. *Magn Reson Med*. 2008;60(5):1073–81.
 145. Corsi F, Mazzucchelli S. The potential of protein-based nanocages for imaging and drug delivery. *Ther Deliv*. 2016;7(3):149–51.
 146. Kesharwani P, Xie L, Banerjee S, et al. Hyaluronic acid-conjugated polyamidoamine dendrimers for targeted delivery of 3, 4-difluorobenzylidene curcumin to CD44 overexpressing pancreatic cancer cells. *Coll Surf B*. 2015;136:413–23.
 147. Zhu J, Shi X. Dendrimer-based nanodevices for targeted drug delivery applications. *J Mater Chem B*. 2013;1(34):4199–211.
 148. Madaan K, Kumar S, Poonia N, Lather V, Pandita D. Dendrimers in drug delivery and targeting: drug-dendrimer interactions and toxicity issues. *J Pharm Bioallied Sci*. 2014;6(3):139–50.
 149. Khopde AJ, Jain NK. Dendrimer as potential delivery system for bioactive. In: Jain NK, editor. *Advances in controlled and novel drug delivery*. New Delhi: CBS Publisher; 2001. p. 361–80.
 150. Volkov Y. Quantum dots in nanomedicine: recent trends, advances and unresolved issues. *Biochem Biophys Res Commun*. 2015;468(3):419–27.
 151. Liu J, Lau SK, Varma VA, et al. Molecular mapping of tumor heterogeneity on clinical tissue specimens with multiplexed quantum dots. *ACS Nano*. 2010;4(5):2755–65.
 152. Xu G, Zeng S, Zhang B, Swihart MT, Yong K-T, Prasad PN. New generation cadmium-free quantum dots for biophotonics and nanomedicine. *Chem Rev*. 2016;116(19):12234–327.



Nanoparticle Properties Affecting the Drug Release, Absorption, and Pharmacokinetics of Nanoparticulate Drug Delivery Systems

Prachi Pandey, Jayvadan K. Patel,
and Samarth Kumar

Contents

1	Introduction	26
2	Properties of NPs	29
3	Application of NPs	30
4	Characterization of NPs	32
5	Effects of NP Properties on Drug Release, Absorption, and Pharmacokinetics of Nanoparticulate Drug Delivery Systems	34
6	Future Prospects of Nanoparticulate Drug Delivery Systems	38
	References	39

Abstract

The nanotechnology-based drug delivery enhances the distribution and pharmacokinetic of the drug which in turn ultimately improves the efficacy of the drug. A particular advantage of nanotechnology is the ability to design and optimize the unique physiochemical properties of nanoscale materials and

structures. Nanoparticle (NP) drug delivery systems have the capability to improve current disease therapies due to their ability to overcome biological barriers and release a therapeutic drug quantity in the optimal dosage range. Altering the size, shape, and/or surface chemistry of NPs allows their functionalities to be tailored to meet various needs. These factors have been observed to significantly affect the distribution and blood circulation half-life of circulating NPs by reducing the level of nonspecific uptake, delaying opsonization, and enhancing the extent of tissue-specific accumulation. Modulation of the pharmacokinetics of NPs to prevent rapid clearance from blood has been attained by tuning their sizes, and successful temporary evasion of the RES postinjection has been demonstrated by measuring blood circulation

P. Pandey (✉)
Babaria Institute of Pharmacy, BITS Edu Campus,
Vadodara, Gujarat, India

J. K. Patel
Nootan Pharmacy College, Faculty of Pharmacy,
Sankalchand Patel University, Visnagar, Gujarat,
India

S. Kumar
Formulation- R & D, Sun Pharmaceutical Industries
Ltd, Vadodara, Gujarat, India

half-life and examining the biodistribution of NPs in the blood, RES organs, and targeted tissue.

Keywords

Nanoparticle properties · Drug release · Drug absorption · Pharmacokinetics

1 Introduction

Drugs are usually delivered by oral or parenteral route. But, in many cases, when drug is administered using various routes, it is distributed throughout the body which is not required and produces some undesirable side effect in other healthy organs or cells. So, pharmaceutical industries focus on developing different approaches for site-specific delivery. Nanotechnology is one of them. In nanotechnology drug delivery, drug is delivered either by dispersing drug in polymeric matrix, or drug is encapsulated in polymeric cell, etc., to prepare nanoparticles (NPs), nanospheres, and nanocapsules like drug carrier systems. Such drug carriers also protect drug from enzymatic degradation. NPs are colloidal particles ranging from 1 to 1000 Å [5].

The Major Benefits of Nanotechnology-Based Drug Delivery System Are as Follows:

- The nanotechnology-based drug delivery enhances the distribution and pharmacokinetic of the drug which in turn ultimately improves the efficacy of the drug.
- There are improvements in the stability of various drugs because of protection from degradation.
- It reduces the side effect of drugs as lesser quantity of drug is accumulated or reaches at nontarget sites.
- Biocompatible materials are usually utilized in nanotechnology, so toxicity is reduced [7].
- Without any chemical reaction, the drug is absorbed in the system by which it remains unaffected by surrounding atmosphere, and

the drug can be preserved for therapeutic action.

- It is easy to prepare and the release of the drug can be controlled, thereby avoiding wastage of drug.
- Nanotechnology-based drug delivery systems improve the solubility and half-life of the drug. Sustained drug delivery can be achieved, and because of this, the frequency of drug administration is less, making the formulation more patient compliant [4, 5].

Classification of NPs

Depending on their morphology, size, and chemical properties, nanoparticles are classified into different categories.

(i) *Carbon-Based NPs*

Two major classes of carbon-based NPs are fullerenes and carbon nanotubes. Fullerenes contain nanomaterial in the form of hollow cage such as allotropic forms of carbon. It creates remarkable commercial interest due to their electrical conductivity, high strength, structure, electron affinity, and versatility. These materials have arranged pentagonal and hexagonal carbon units, while each carbon is sp hybridized. Carbon nanotubes are elongated, tubular structure, and 1–2 nm in diameter. It is structurally similar to the graphite sheet rolling on itself. Rolled sheets can be single-, double-, or multi-walled, and therefore they are named as single-walled, double-walled, or multi-walled carbon nanotubes, respectively [2, 3].

(ii) *Metal NPs*

Metal NPs are made by using metal precursors. Because of well-known localized surface plasmon resonance characteristics, they carry unique optoelectrical properties. NPs prepared by using alkali and noble metals like Cu, Ag, and Au have a broad absorption band in the visible zone of the electromagnetic solar spectrum.

(iii) *Ceramic NPs*

These are inorganic nonmetallic solids, synthesized by heating and successive cooling. These are available in different forms like amorphous, polycrystalline, dense, porous, or hollow. These types of NPs are being used in catalysis, photocatalysis, photodegradation of dyes, and imaging applications; therefore, they receive great attention nowadays.

(iv) *Semiconductor NPs*

These types of materials have properties between metals and nonmetals. Semiconductor NPs comprise of wide bandgaps so they observe significant alteration in their properties with bandgap tuning. These are important material in photocatalysis, photo-optics, and electronic devices.

Semiconductor NPs show unique size-dependent material properties. These materials possess properties between metals and nonmetals, and therefore they have found various applications in the literature. With a change in the particle size, dramatic modifications to their electronic and optical properties take place [2–4].

(v) *Polymeric NPs*

These types of NPs are normally organic-based NPs. They are mostly nanosphere or nanocapsular shaped.

Types of NPs can be distinguished: (1) nanospheres, which are matrix systems where the drug is uniformly dispersed, and (2) nanocapsules, which are reservoir systems where the drug is located in the core surrounded by a polymer membrane.

(vi) *Lipid-Based NPs*

These types of NPs contain lipid moieties and are effectively used in biomedical application. It is spherical in shape with diameter ranging from 10 to 1000 nm. Lipid NPs have a solid core made of lipid, and a matrix contains soluble lipophilic molecules. External core of lipid NPs is stabilized by surfactants or emulsifiers.

are further classified as chemical, biological, and physical synthesis methods involving several techniques as illustrated in Fig. 2.1.

A. *Top-Down Synthesis*

Large API particles are broken down to small-drug NPs in a top-down method. As a result, these procedures are known as top-down technology. This sort of particle size reduction technology is now the most important and successful commercially [24].

The top-down technique is based on mechanical size reduction technologies that gradually break down bulk materials to nano-sized structures. This strategy employs a destructive approach. Starting with a bigger molecule, it is decomposed into smaller units, which are subsequently transformed into appropriate NPs. Grinding/milling, CVD, physical vapor deposition (PVD), and other decomposition processes are examples of this technology [1].

In top-down techniques, there will be imperfections in the surface structure of the product, which is a severe restriction, because the surface chemistry and other physical attributes of NPs are mostly dependent on the surface structure [23].

B. *Bottom-Up Synthesis*

Bottom-up techniques are based on the assembly of atoms or molecules to form molecular structures in the nanoscale range [1].

As NPs are generated from comparatively simpler compounds, this technique is used in reverse; this method is also known as the “building up” method. Sedimentation and reduction procedures are examples of this case. Solgel, green synthesis, spinning, and biological synthesis are all part of it.

NPs are created from smaller molecules in a bottom-up approach, for example, by combining atoms, molecules, and smaller structures. The building blocks of the NPs are first formulated in this nanostructure and then combined to make the finished particle [23].

Method of Preparation of NPs

The method of preparation of NPs is basically by bottom-up and top-down synthesis method which

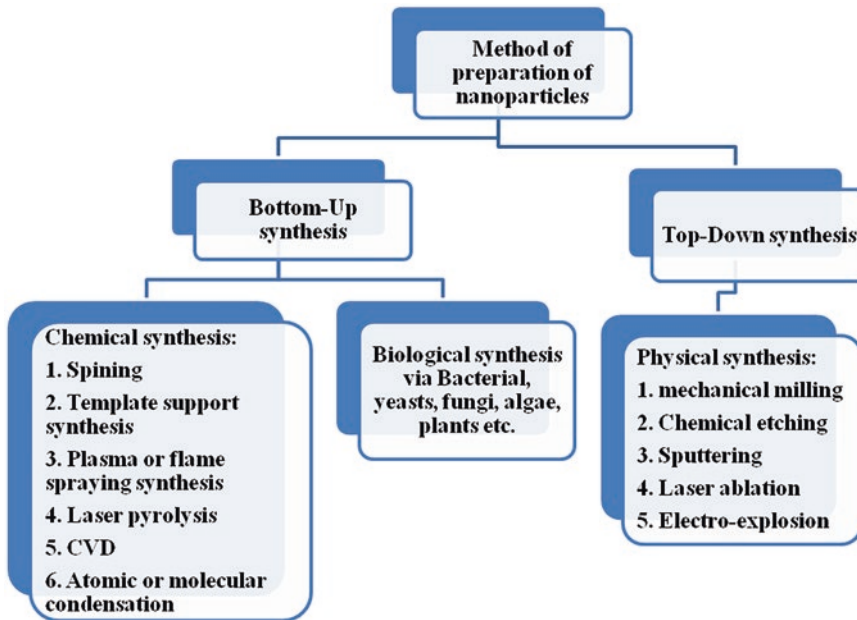


Fig. 2.1 Method of synthesis of NPs

(a) *Physical Method of NP Synthesis*

UV irradiation, sonochemistry, laser ablation, and radiolysis are some of the examples of physical methods for NP synthesis. Evaporation of metal atoms occurs during the physical synthesis process, followed by condensation on different supports, where the metallic atoms are reorganized and aggregated as small clusters of metallic NPs [25]. We can create NPs with great purity and defined shape using physical methods. However, these procedures typically necessitate extremely sophisticated instruments, chemicals, and radiant heating, as well as high power usage, resulting in high operating costs [23].

(b) *Chemical Method of NP Synthesis*

Another useful method for preparing NPs is to utilize chemicals to reduce metal ions in solution. Metal ions may support nucleation or aggregation to generate small clusters of metals depending on the conditions of the reaction mixture. The chemical agents such as hydrazine, sodium borohydride, and hydrogen are

common reducing agents [26]. Stabilizing agents such as cellulose, natural rubber, chitosan, and copolymer micelles are also employed. As such substances are hydrophobic, they must be mixed with organic solvents such as ethane, dimethyl, formaldehyde, toluene, and chloroform. These chemicals are hazardous in nature and nonbiodegradable, limiting the volume of manufacture [27]. Furthermore, some harmful compounds may contaminate the surface of NPs, thereby rendering them inappropriate for biomedical applications.

(c) *Biological Method of NP Synthesis*

The biogenic production of NPs has received a lot of attention in recent years. Microorganisms and plants are used in the biogenic synthesis process to produce NPs. When compared to other physicochemical methods of manufacturing, biosynthesis may produce NPs with better defined size and form. Although it has been discovered that the microbial-based synthesis process is easily scalable, environmentally friendly, and compatible with

the use of product for pharmaceutical purposes, manufacturing using microbes is frequently more expensive than production using plant-based materials. The fundamental benefit of plant-based synthesis methodologies over traditional chemical and physical methods is that these are more eco-friendly, cheaper, and easier to scale up for large-scale NP synthesis because they do not require high temperatures, pressures, or harmful chemicals [28].

A great number of research publications on the biological synthesis of NPs employing microbes such as bacteria, fungi, algae, and plants have been published. This is due to their reducing or antioxidant characteristics, which are responsible for the reduction of metal NPs, respectively. Furthermore, it has been discovered that microbe-mediated synthesis is not suitable for large-scale production because it necessitates strict aseptic conditions and special maintenance, so the use of plants for NP synthesis is preferable to microorganisms due to the ease of scale-up and the lack of the additional requirement of maintaining cell culture [21]. The use of plant extract for NP synthesis also minimizes the additional requirements of microbe isolation and culture medium preparation, increasing the cost-competitive practicability over microorganism-based NP synthesis. Plant-mediated synthesis is a one-step process, whereas microorganisms may lose their ability to create NPs over time due to mutation; hence, plant research is expanding quickly.

2 Properties of NPs

Different physicochemical properties like large surface area, mechanically strong, optically active, and chemically reactive make NPs unique and suitable applicant. Various properties of NPs are discussed in the following.

A. *Electronic and Optical Properties*

Optical and electronic properties are interdependent properties of NPs. Noble metal NPs possess size-dependent optical properties and express a strong UV-visible extension band, and it is generally absent in the spectrum of the bulk metal. When the incident photon frequency is constant with the collective excitation of the conduction electrons, excitation band results, and it is known as the localized surface plasma resonance (LSPR). LSPR excitation results in the wavelength selection absorption with extremely large molar excitation coefficient resonance with efficiency equivalent to that of ten fluorophores and enhanced local electromagnetic fields near the surface of NPs with enhanced spectroscopies. Size, shape, and interparticle spacing of NPs as well as its own dielectric properties and those of its local environment including the substrate, solvents, and adsorbates affect the LSPR spectrum. Gold colloidal NPs are responsible for the rusty colors seen in blemished glass door/windows, while Ag NPs are yellow in color. Free electrons on the surface of the NPs are freely transportable through the nanomaterial. The mean free path of Ag and gold is ~ 50 nm, and it is more than the NP size of these materials. Thus, upon light interaction, no scattering is expected from the bulk; instead, they set into a standing resonance conditions, which is responsible for LSPR in the NPs [5, 6].

B. *Magnetic Properties*

Magnetic NPs are of major interest for investigators from an electric range of disciplines; it contains heterogenous and homogenous catalysis, biomedicine, magnetic fluids, data storage magnetic resonance imaging, and environmental remediation like water decontamination. According to the literature, NPs perform best when the size is $<$ critical value like 10–20 nm. Magnetic properties of NPs dominated effectively at such low scale, and it makes these particles priceless and can be used in various applications. In NPs, uneven electronic distribution leads to magnetic property, and these properties are also

dependent on the synthetic protocol, and various synthetic methods such as solvothermal, coprecipitation, microemulsion, thermal decomposition, and flame spray synthesis can be used for their preparation [1–3].

C. Mechanical Properties

These types of properties of NPs incorporate researchers to look for novel application in different fields like tribology, surface engineering, nanofabrication, and nanomanufacturing. Exact mechanical natures of NPs can be determined by several mechanical properties like elastic modulus, hardness, stress and strain, adhesion, and friction. Other than these, surface coating, coagulation, and lubrication also assist in the mechanical properties of NPs. As compared to microparticles and their bulk materials, NPs show dissimilar mechanical properties. Furthermore, in a lubricated or greased contact, the contrast in the stiffness between NPs and the contacting external surface controls the phenomena, whether the NPs are indented to be on the plane surface or get deformed when the pressure is high. This significant information could reveal the fate of NPs in the contact situation. For determining the surface quality and material removal, a control over mechanical properties of NPs and their interactions with any kind of surface are necessary. Needful outcomes in these fields require a deep insight into basics of the mechanical properties of NPs like elastic modulus and hardness, movement law, friction and interfacial adhesion, and their size-dependent characteristics [1, 2].

D. Thermal Properties

Metal NPs possess thermal conductivity greater than those of fluids in solid form. One of the examples is the thermal conductivity of copper at room temperature is about 700 times greater than that of water and about 3000 times greater than that of engine oil. Oxides like alumina have thermal conductivity greater than that of water. So, the fluids containing suspended solid particles are expected to display significantly enhanced thermal conductivities as compared to those

of conventional heat transfer fluids. To produce nanofluids, disperse the nanometric scale solid particles into liquid like water, ethylene glycol, or oils. As compared to those of conventional heat transfer fluids and fluids containing microscopic sized particles, nanofluids are expected to exhibit superior properties. Heat transfer takes place at the surface of the particles, so it is desirable to use the particles with large total surface area. Suspension stability increases, when total surface area increases. Recently, it has been revealed that the nanofluids consisting of CuO or Al₂O₃ NPs in water or ethylene exhibit advanced thermal conductivity [1].

3 Application of NPs

A. NPs as Drug Delivery Systems

There are many drugs which are having a poor solubility and low bioavailability and can be cleared quickly in the body by the reticuloendothelial system. Efficacy of different drugs like chemotherapeutic agents is often limited by dose-dependent side effects [24]. There are several applications and routes of administration of NPs as illustrated in Fig. 2.2, which are further described as follows:

(a) Gastrointestinal Tract

Other portals for entry are basically GI tract and skin. Diffusion and accessibility through mucus initial contact with endocytosis, cellular trafficking, and post-translocation events affect the kinetics of particle uptake in GI tract. Particles having smaller diameter could diffuse faster through GI secretion to reach the colonic enterocytes. Following uptake by GI tract, NPs can translocate to the bloodstream and distribute through the overall body. Targeting strategies increase the interaction of NPs to the adsorptive sites in the GI tract that utilizes specific binding to ligands or receptors and nonspecific adsorptive mechanism. Surface of enterocytes and M cells possess cell-specific

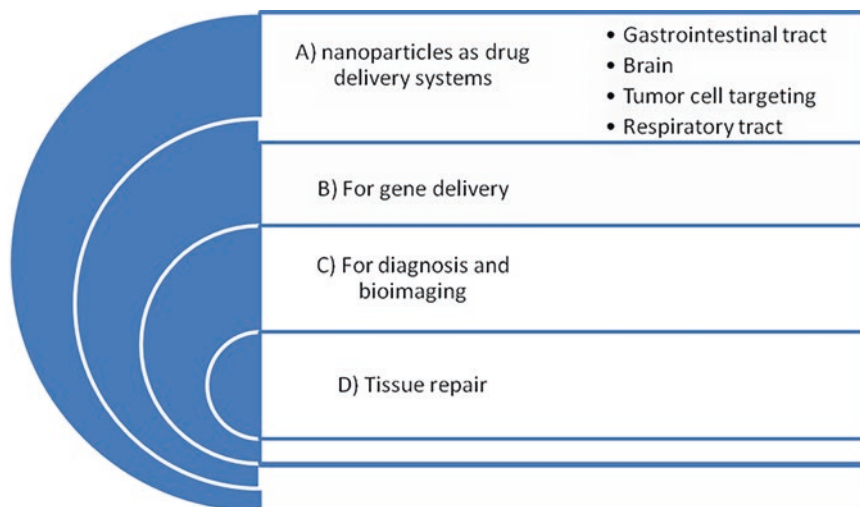


Fig. 2.2 Application of NPs

carbohydrates, which can serve as binding sites to NP drug carriers with appropriate ligands. By specific receptor-mediated mechanism, certain glycoproteins and lectins bind selectively to this type of surface structure [4, 5].

(b) *Brain*

Due to the presence of blood-brain barrier, the brain is probably one of the least accessible organs for delivery of drugs that controls the transport of endogenous and exogenous compounds, thus providing the neuroprotective function. Drugs that normally cannot cross the blood-brain barrier could be delivered to the brain after binding to the surface-modified poly(butyl cyanoacrylate) NPs.

(c) *Tumor Cell Targeting*

Anticancer drugs having a large volume of distribution are toxic to both normal and cancer cells. By using nanotechnology, targeting drug molecules to the site of action is becoming a reality resulting in a personalized medicine, which reduces the effect of the drug on other sites while maximizing the therapeutic effect. The small size of particles can penetrate across various barriers through small capillaries into individual cells. NPs can also be prepared to entrap,

encapsulate, or bind molecules to increase solubility, stability, and adsorption of several drugs and also avoid the reticuloendothelial system, thus protecting the drug from premature inactivation during its transport. NPs can also carry different therapeutic agents like DNA, proteins, peptides, and low molecular weight compounds. Liposome and polymer-based NPs are the most widely used NPs as a drug delivery system. These types of compounds are generally biodegradable, do not accumulate in the body, and are risk-free [4–6].

(d) *Respiratory Tract*

NPs could avoid normal phagocytic defenses therein respiratory tract as well as gain access to systemic circulation and reach to CNS. Aerosol therapy by using NPs as drug carrier is increasing importance for delivering therapeutic compounds. Lungs is an attractive target for delivery of drug because of noninvasive administration by inhalation aerosols, avoidance of first-pass metabolism, direct delivery to the site of action for the treatment of respiratory diseases, and the availability of a large surface area for local drug action as well as systemic absorption of drug.

B. *For Gene Delivery*

Major ingredients of polynucleotide vaccines, DNA, can be produced cheaply and has much better storage and handling properties as compared to the ingredients of the majority of protein-based vaccines. There are some issues related to the delivery of polynucleotides like efficient delivery of the polynucleotide to the target cell population and its localization to the nucleus of these cells and ensuring that the integrity of the polynucleotide is maintained during delivery to the target site which limit their application. NPs loaded with plasmid DNA could also provide as an efficient sustained release gene delivery system because of their rapid escape from the degradative endolysosomal compartment to the cytoplasmic compartment.

C. *For Diagnosis and Bioimaging*

There are various types of molecular imaging techniques that are available like optical imaging, magnetic resonance imaging, ultrasound imaging, positron emission tomography, and others that have been reported for imaging of in vitro and in vivo biological specimens. Nowadays, the development of luminescent and magnetic NPs advances bioimaging technologies. Two various types of NPs have been widely used for imaging: luminescent nanoprobe for optical imaging and magnetic NPs for MRI; other than this, there are also dual-mode NPs for simultaneous imaging by optical imaging and MRI. Gold NPs are used to detect cancer. It has been used as ultrasensitive fluorescent probes to detect cancer biomarkers in human blood. The method is very sensitive and is also employed in direct detection of viral or bacterial DNA. Gold NPs are promising probes for biomedical application because they can be easily prepared and, unlike other fluorescent probes like quantum dots or organic dyes, they do not burn out after long exposure to light.

D. *Tissue Repair*

By using iron oxide NPs, tissue repair is accomplished either via welding, apposing

two tissue surfaces and then heating the tissues sufficiently to join them, or via soldering, where protein or synthetic polymer-coated NPs are placed between two tissue surfaces to enhance joining of the tissues. To initiate tissue union induced by the denaturation of proteins and the subsequent entanglement of adjacent protein chains, temperatures more than 50 °C are known to be maintained. NPs which strongly absorb light corresponding to the output of a laser are useful for tissue repairing process. Gold- or silica-coated iron oxide NPs have been designed to strongly absorb light. Coat these NPs onto the surfaces of two pieces of tissue at the site where joining was desired. By using this technique, minimize tissue damage by using the least harmful wavelengths of light and lower powered light sources.

4 Characterization of NPs

NPs are studied using advanced microscopic techniques such as scanning electron microscopy (SEM), transmission electron microscopy (TEM), and atomic force microscopy (AFM) to determine their size, shape, and surface charge. The physical stability and in vivo distribution of NPs are influenced by their average particle diameter, size distribution, and charge. The overall morphology of polymeric NPs, which may impact their toxicity, can be determined using electron microscopy techniques. The physical stability and redispersibility of the polymer dispersion, as well as its in vivo performance, are determined by the surface charge [24, 29–31].

A. *Particle Size*

Electron microscopy is used to determine morphology and particle size. The most common uses of NPs are drug release and drug targeting. The size of the particles has been discovered to influence drug release. The surface area of smaller particles is greater. As a result, the majority of the drug put onto them will come into con-

tact with the particle surface, resulting in rapid drug release. Drugs, on the other hand, slowly diffuse among bigger particles. Smaller particles tend to aggregate during storage and transit of NP dispersion, which is a disadvantage. As a result, there is a compromise between NP size and maximum stability [6, 8, 12].

The particle size has an impact on polymer degradation. In vitro, for example, the degradation rate of poly(lactic-co-glycolic acid) was discovered to increase particle size.

As stated below, there are numerous tools for assessing NP size:

(i) *Dynamic Light Scattering (DLS)*

Photon correlation spectroscopy (PCS) or DLS is now the fastest and most commonly used process of detecting particle size. NPs in colloidal suspensions in the nano- and submicron ranges are commonly measured using DLS. When monochromatic light is shone on a solution of spherical particles moving in Brownian motion, the light undergoes a Doppler shift, changing the wavelength of the incoming light. This variation is proportional to the particle's size of NP. By monitoring the particle's diffusion coefficient and utilizing the autocorrelation function, it is possible to extract the size distribution and provide a description of the particle's motion in the medium [4, 6, 8].

(ii) *SEM*

A morphological evaluation with direct visibility is performed using SEM. Although electron microscopy techniques have significant advantages in terms of morphological and sizing studies, they only provide limited information on the size distribution and genuine population average. NP solution should first be converted to a dry powder, which is then mounted on a sample holder and coated with a conductive metal, such as gold, using a sputter coater for SEM characterization. The sample is further scanned with a finely focused electron beam. The secondary electrons emitted from the sample surface are

used to determine the sample's surface properties. The electron beam can damage the polymer; hence, the NP must be able to tolerate vacuum.

SEM yields a mean size that is comparable to the result of DLS. Moreover, these methods are time-consuming and expensive, and they typically require additional information about sizing distribution [6–8].

(iii) *TEM*

Although TEM works on a different principle than SEM, it frequently produces the same type of data. Because TEM samples must be superthin for electron transmission, sample preparation is complicated and time-intensive. The dispersion of NPs is deposited on support grids or films. NPs are fixed using either a negative staining substance, such as phosphotungstic acid or derivatives, uranyl acetate, etc., or plastic embedding, to make them withstand the instrument vacuum and enable handling. After immersing the sample in vitreous ice, expose it to liquid nitrogen temperatures as an alternative. When a beam of electrons is transmitted through an ultrathin sample and interacts with it as it passes through, the surface properties of the sample are obtained [6, 7].

(iv) *AFM*

AFM provides ultrahigh resolution in particle size assessment by physically scanning materials at the submicron level using an atomic scale probe tip. Based on forces between the tip and the sample surface, the instrument generates a topographical map of the sample. Depending on the qualities of the sample, it is commonly scanned in contact or noncontact mode. In contact mode, the topographical map is created by tapping the probe on the surface across the sample, while in noncontact mode, the probe hovers over the conducting surface.

The ability to topograph nonconducting objects without special preparation is AFM's main advantage, allowing imaging of delicate biological and polymeric nano- and microstructures [12, 13].

B. Surface Charge

The nature and strength of a NP's surface charge is critical since it dictates how it interacts with the biological environment as well as how it interacts electrostatically with bioactive chemicals. The zeta potential of NPs is used to assess colloidal stability. This potential is an indirect measure for the charge on the surface. It is the difference in potential between the outer Helmholtz plane and the shear surface. The measurement of zeta potential allows for predictions concerning colloidal dispersion storage stability.

To ensure particle stability and avoid aggregation, high zeta potential values, whether positive or negative, should be attained. The zeta potential readings can then be used to predict the level of surface hydrophobicity. The type of the material contained within the nanocapsules or coated on the surface can also be determined using the zeta potential.

C. Surface Hydrophobicity

Several approaches, such as hydrophobic interaction chromatography, biphasic partitioning, probe adsorption, and contact angle measurement, can be used to detect surface hydrophobicity. Several advanced analytical approaches for surface analysis of NPs have recently been disclosed in the literature. The detection of specific chemical groups on the surface of NPs is possible using X-ray PCS [12, 13].

D. Drug Loading

A successful nanoparticulate system should ideally have a high drug loading capacity, reducing the amount of matrix materials required for administration. There are two ways to administer drugs:

- Incorporation method (incorporating at the time of NP production)
- Adsorption/absorption technique (absorbing the drug after formation of NPs by incubating the C carrier with a concentrated drug solution)

The solid-state drug solubility in matrix material or polymer, which is connected to the polymer composition, molecular weight, drug polymer interaction, and the presence of end functional groups, heavily influences drug loading and entrapment efficiency (ester or carboxyl group) [7, 8].

E. Drug Release

Understanding the manner and extent to which drug molecules are released is important because one of the main reasons for studying nanotechnology is to deliver medications. Most release strategies necessitate the separation of the drug and its delivery vehicle in order to gather this information. The amount of drug bound per mass of polymer (typically moles of drug per mg polymer or mg drug per mg polymer) is the drug loading of NPs. It can also be expressed as a percentage relative to the polymer.

After ultracentrifugation, ultrafiltration, gel filtration, or centrifugal ultrafiltration, this examination was carried out using classic analytical methods such as ultraviolet spectroscopy (UV spectroscopy) or high-performance liquid chromatography (HPLC).

UV spectroscopy or HPLC are used for quantification. Drug release assays are comparable to drug loading assays, which are used to determine the mechanism of drug release over time [6–8].

5 Effects of NP Properties on Drug Release, Absorption, and Pharmacokinetics of Nanoparticulate Drug Delivery Systems

A typical advantage of nanotechnology is the ability to design and optimize the unique physicochemical properties of nanoscale materials and structures. Altering the size, shape, and/or surface chemistry of NPs allows their functionalities to be tailored to meet various needs. According to the specific location and type of targeted tissue, select optimal size of NPs. Modulation of the

pharmacokinetics of NPs to prevent rapid clearance from blood has been attained by tuning their sizes, and successful temporary evasion of the RES postinjection has been demonstrated by measuring blood circulation half-life and examining the biodistribution of NPs in the blood, RES organs, and targeted tissue. NPs affect the cellular uptake and tumor permeability [7, 11, 12].

There is substantial correlation between the NP properties and their effects on the pharmacokinetics of drug delivery and on the efficacy characteristics as illustrated in Fig. 2.3.

(i) *NP Size, Shape, and Core Composition*

A. *Cellular Uptake*

Size, shape, and core composition of NPs are strong determinants of cellular uptake. NPs created with a typical shape like spherical, cubic, rodlike, or wormlike will affect cellular uptake. When comparing the different gold NPs having a cubic, spherical, and rodlike shape, highest uptake is shown in spherical particles in terms of weight, but in terms of quantity, rodlike NPs show highest uptake. Similar trend is shown when polymeric NPs are loaded with DOX. In this also, higher cellular uptake is shown in rodlike and wormlike NPs than spherical NPs in MCF-7 cells.

NP size affects cellular uptake because of its influence on the enthalpic and entropic properties that govern the adhesion strength between NPs and cellular receptors. Researchers developed a thermodynamic model that describes optimal cellular uptake when ligand-coated NPs have a 50 nm diameter. When experiment is performed with HeLa cells, spherical mesoporous silica NPs with a 50 nm diameter showed the highest cellular uptake. Another study also conducted by using targeted gold NPs and reported that the highest cellular uptake shown in NPs having a size between 40 and 50 nm in SKBR-3 cells. Similar trend is observed when silver core is used instead of gold.

The surface of colloidal gold NPs of 2–100 nm was decorated with Herceptin molecules, and then their cellular uptake was compared with unmodified gold NPs.

Through binding to many receptors, large NPs drive the membrane-wrapping process however, receptor shortage showed when NPs are above 60 nm in diameter which decreases uptake due to the increasing entropic penalty. Although the actual optimal diameter varies between applications, a ligand-coated, spherical NP between 30 and 60 nm in diameter can recruit and bind to enough cellular receptors to drive the membrane-wrapping process without a receptor shortage affecting endocytosis. NPs within the size range of 10–60 nm showed maximum cellular uptake, regardless of core composition or surface charge according to the *in vitro* studies.

Surface charge and cell type are other parameters which affect cellular uptake. When comparing the cellular uptake of gold NPs having a size of 2, 4, and 6 nm in HeLa cells, the ligand coating (cationic, anionic, or zwitterionic) impacted the type of uptake. For sizes less than 6 nm, zwitterionic particles mainly entered the cell via membrane fusion. Other than this, 6 nm zwitterionic particles and all cationic and anionic particles entered the cell via multiple endocytic pathways [8].

B. *Active Targeting*

To avoid the RES system and increase blood circulation half-life, NPs are frequently coated with polyethylene glycol (PEG). This coating makes the NPs more hydrophilic as well as neutral, allowing them to bypass the immune system more easily; however, PEG poorly affects the cellular uptake and drug release.

Size-dependent cell binding is shown when gold NPs are targeted to the cancer cells. When comparing 15, 30, 90, and 150 nm targeted gold NPs, 13-fold

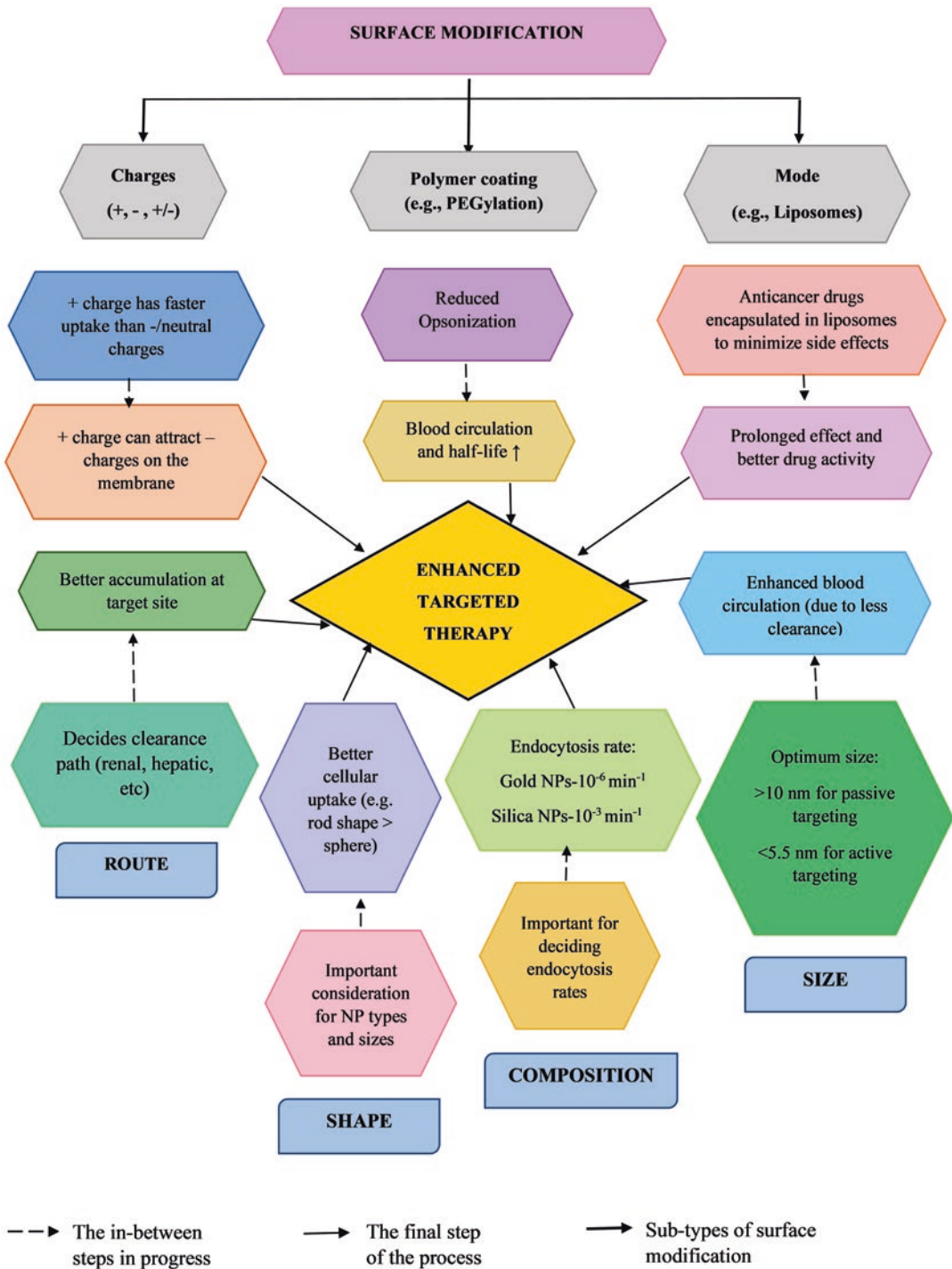


Fig. 2.3 NP properties affecting the pharmacokinetics of drug delivery

increase in cellular binding probability was shown in NPs having a 15 nm diameter as compared to 150 nm diameter NPs. Optimal targeting in terms of gold mass per cell and surface area per cell was shown in cells which have 90 nm diameter [15, 22].

(ii) *In Vivo NP Biodistribution and Pharmacokinetics*

In vitro studies focus on individual aspects of the delivery process, and in vivo studies focus on the effect of NP size within the context of the body. The NP size affects the blood circulation half-life, tumor permeability, and biodistribution [14, 15].

C. *Blood Circulation Half-Life*

Due to the rapid clearance of NPs, its use is limited because NPs do not have time to reach the targeted tissue. Problems with avoiding the MPS have moved NPs from the first generation of material design and biocompatibility to the second generation of stealth tactics and active targeting. By introduction of advancements so that circulation half-life increases, like coating with PEG, a closer look at the basic size of a NP shows significant, size-dependent changes in $t_{1/2}$.

To filter the blood and urine product, the kidney uses peritubular capillaries and renal corpuscles. Within a renal corpuscle is the glomerulus; it has three layers with different pore sizes. Ten nanometers is the effective size cutoff of the overall structure. According to the targeted cellular receptors, the upper size limit of NPs can vary, but a NP with a diameter greater than 200 nm will activate the complement system and be quickly removed from the bloodstream, accumulating in the liver and spleen [12–14]. Researchers suggest that, a maximum size limit of 150 nm for spherical NPs avoid filtration in the spleen. Further studies conducted and narrowed the range of sizes and gave information about the effects of size on $t_{1/2}$. When comparison occurred between 24 and 37 nm shell cross-linked NPs, the smaller particle

had a higher retention at 10 min and at 4 h postinjection. At 1 hr postinjection, 50% of the smaller NPs were found in circulation, compared with only 5% of the larger NPs [4].

D. *Biodistribution*

Quantitative biodistribution may be used to calculate the total quantity of NPs in the body at a particular period following injection or exposure. The distribution of NPs in organs and tissues of interest can be evaluated regardless of the mode of NP administration (inhalation, gavage to the GI tract, intravenous injection, or topical applications). Particle distribution is assessed at multiple time points following delivery using appropriate techniques. Analytical chemistry can be used to quantify nonradioactive NPs in the obtained specimens (e.g., inductively coupled plasma mass spectroscopy or atomic absorption mass spectroscopy) [9].

The biodistribution of NPs varies based on their characteristics and interactions with biological systems. NP size, in particular, has an impact on NP biodistribution throughout the body [10–13]. Micrometer-sized particles stay in the body for far longer than nanometer-sized ones [11].

NP accumulations are most common in the blood, liver, and spleen. Larger NPs tend to collect faster in the liver and spleen. The fast buildup is still being debated as to whether it is due to simple filtering or enhanced binding possibilities between the MPS cells and the NPs [14].

The size of NPs has an influence on biodistribution inside certain organs as well as across the body. Various filters inside organs or barriers between the organ and the surrounding fluid cause the size-dependent distribution of NPs [15].

E. *Tumor Permeability*

Although NPs can be tailored to target specific tumors, delivering them to tumor cells remains a challenge. Angiogenesis occurs during the development of a tumor

to supply blood and nutrients to the rapidly dividing cells. The levels of vascular endothelial growth factor-A (VEGF-A) in these new blood vessels are substantially higher than in most adult tissue. The major protein that helps to cause pathological angiogenesis is VEGF-A, which is extensively expressed in healing and developing tissues. The enhanced permeability and retention (EPR) effect occurs when VEGF enhances the vascular permeability of the endothelial cell layer, resulting in “leaky” blood vessels. The permeability of the blood vessels is determined by the size of the NPs as well as the pore size. Vascular permeability reduces as NP size increases [9]. Tumor vesicles have different pore sizes depending on the type of tumor and where it is growing. Cancers in the cranial window, for example, have much lower pore size than tumors in the dorsal chamber. As a result, NP size should be customized to the tumor’s nature and location [16].

When creating a NP to target a tumor cell, the half-life in circulation and the ability to reach the tumor must be balanced.

Some examples of NPs using different materials and its effects are discussed in Table 2.1.

6 Future Prospects of Nanoparticulate Drug Delivery Systems

NP drug delivery systems have the capability to improve current disease therapies due to their ability to overcome biological barriers and release a therapeutic drug quantity in the optimal dosage range. Rapid clearance of circulating NPs during systemic delivery is a critical issue for drug delivery systems and it is necessary to consider the factors affecting distribution and blood circulation half-life. It is important to study the factors which can influence NP blood residence

time and organ-specific accumulation. These factors include interactions with biological barriers and modifiable NP properties, such as composition, size, core properties, surface modifications (pegylation and surface charge), and also targeting ligand functionality. These factors have been observed to significantly affect the distribution and blood circulation half-life of circulating NPs by reducing the level of nonspecific uptake, delaying opsonization, and enhancing the extent of tissue-specific accumulation.

Table 2.1 Effects of characteristics of NPs on drug release Pharmacokinetics

Sr. No.	Types of NPs	Effect on drug release, absorption, and pharmacokinetics	References
1.	Lignin-based NPs	In this article, authors prepare three types of lignin NPs. Pure lignin NPs showed the capacity to efficiently load poorly water-soluble drugs and other cytotoxic agents. It also increases the release profile at pH 5.5 and 7.4 in a sustain manner	[17]
2.	Chitosan-based NPs	In this article, authors developed a drug delivery system based on chitosan NPs (CNs) to improve its bioavailability and anticancer activity. It was prepared by using convenient ionic gelation techniques between chitosan and tripolyphosphate. It is spherical particles with an average size of 200 nm. In vitro release kinetic study indicates that the drug was released from chitosan NPs in a sustain release manner. According to the result, chitosan NPs of MIF improve the anticancer activity as well as bioavailability	[18]

(continued)

Table 2.1 (continued)

Sr. No.	Types of NP s	Effect on drug release, absorption, and pharmacokinetics	References
3.	Chitosan-based NPs	In this article, authors prepared chitosan-based NPs for in vitro and in vivo drug and gene delivery. The effect of size on biodistribution was described, and according to that, smaller particles are considered to be more effective. Smaller particles can easily pass through gaps in tissue and membranes via nonspecific interactions and affect biodistribution and blood circulation time. Passive targeting of cancerous tissues through a phenomenon referred as EPR effect is achieved with chitosan-based NPs having an appropriate size	[19]
4.	Silver NPs	In this article, authors investigated the blood kinetics and tissue distribution of 20, 80, and 110 nm silver NPs in rats up to 16 days after intravenous administration once daily for 5 consecutive days. Silver NPs disappeared rapidly from the blood and are distributed to all organs like liver, lungs, spleen, brain, heart, kidneys, and testes, and it is evaluated. From all three types of NPs, 20 nm particles are distributed mainly to the liver, followed by kidneys and spleen, whereas the larger particles are distributed mainly to spleen, followed by liver and lung	[20]

(continued)

Table 2.1 (continued)

Sr. No.	Types of NP s	Effect on drug release, absorption, and pharmacokinetics	References
5.	Gold NPs	In this article, authors present a work regarding pharmacokinetics, biodistribution, and safety study of laser-ablated dextran-coated gold NPs under intravenous administration in small animal model. According to the results, authors conclude that gold NPs coated with dextran are rapidly eliminated from the blood circulation and accumulated preferentially in liver and spleen, without inducing liver or kidney toxicity. Certain residual accumulation in tissue did not show any sign of histological damage or inflammation in tissues	[22]

References

1. Khan I, Saeed K, Khan I. Nanoparticles: properties, applications and toxicities. *Arab J Chem.* 2019;12(7):908–13.
2. Christian P, Von der Kammer F, Baalousha M, Hofmann T. Nanoparticles: structure, properties, preparation and behaviour in environmental media. Springer. 2008;17(5):326–43.
3. Choi OH, Han H-K. Nanomedicines: current status and future perspectives in aspect of drug delivery and pharmacokinetics. *J Pharm Investig.* 2018;48:43–60.
4. Hoshyar N, Gray S, Han H, Bao G. The effect of nanoparticle size on in vivo pharmacokinetics and cellular interaction. *Nanomedicine (Lond).* 2016;11:673.
5. Singh S, Pandey VK, Tewari RP, Agarwal V. Nanoparticle based drug delivery system: advantages and applications. *Indian J Sci Technol.* 2011;4(3):177–80.
6. Li H-D, Huang L. Pharmacokinetics and biodistribution of nanoparticles. *Mol Pharm.* 2008;5(4):496–504.
7. de Barros AB, Tsourkas A, Saboury B, Cardoso VN, Alavi A. Emerging role of radiolabeled nanoparticles as an effective diagnostic technique. *EJNMMI Res.* 2012;2:39–53.

8. Albanese A, Tang PS, Chan WCW. The effect of nanoparticle size, shape, and surface chemistry on biological systems. *Ann Rev Biomed Eng.* 2012;14:1–16.
9. Geiser M, Kreyling WG. Deposition and biokinetics of inhaled nanoparticles. *Part Fibre Toxicol.* 2010;1–17
10. Dreaden EC, Austin LA, Mackey MA, El-Sayed MA. Size matters: gold nanoparticles in targeted cancer drug delivery. *Therapeut Deliv.* 2012;3:457–78.
11. Choi CHJ, Zuckerman JE, Webster P, Davis ME. Targeting kidney mesangium by nanoparticles of defined size. *Proc Natl Acad Sci U S A.* 2011;108:6656–61.
12. Faraji AH, Wipf P. Nanoparticles in cellular drug delivery. *Bioorg Med Chem.* 2009;17:2950–62.
13. Sonavane G, Tomoda K, Makino K. Biodistribution of colloidal gold nanoparticles after intravenous administration: effect of particle size. *Colloids Surf B Biointerfaces.* 2008;66:274–80.
14. Owens DE III, Peppas NA. Opsonization, biodistribution, and pharmacokinetics of polymeric nanoparticles. *Int J Pharm.* 2006;307:93–102.
15. Kulkarni SA, Feng SS. Effects of particle size and surface modification on cellular uptake and biodistribution of polymeric nanoparticles for drug delivery. *Pharm Res.* 2013;30:2512–22.
16. Jain RK, Stylianopoulos T. Delivering nanomedicine to solid tumors. *Nat Rev Clin Oncol.* 2010;7:653–64.
17. Figueiredo P, Lintinen K, Kiriazis A, Hynninen V, Liu Z, Bauleth-Ramos T, Rahikkala A, Correia A, Kohout T, Sarmiento B, Yli-Kauhahuoma J, Hirvonen J, Ikkala O, Kostiaainen MA, Santos HA. In vitro evaluation of biodegradable lignin-based nanoparticles for drug delivery and enhanced antiproliferation effect in cancer cells. *Biomaterials.* 2017;121:97–108.
18. Zhang H, Fuqiang W, Li Y, Yang X, Huang J, Lv T, Zhang Y, Chen J, Haijun Chen Y, Gao GL, Jia L. Chitosan-based nanoparticles for improved anticancer efficacy and bioavailability of mifepristone. *Beilstein J Nanotechnol.* 2016;7:1861–70.
19. Duceppe N, Tabrizian M. Advances in using chitosan-based nanoparticles for in vitro and in vivo drug and gene delivery. *Expert Opin Drug Deliv.* 2010;7:1191–207.
20. Lankveld DPK, Oomen AG, Krystek P, Neigh A, Jong A T-d, Noorlander CW, Van Eijkeren JCH, Geertsma RE, De Jong WH. The kinetics of the tissue distribution of silver nanoparticles of different sizes. *Biomaterials.* 2010;31:8350–61.
21. Dhuper S, Panda D, Nayak PL. Green synthesis and characterization of zero valent iron nanoparticles from the leaf extract of *Mangifera indica*. *Nano Trends J Nanotech.* 2012;13:16–22.
22. Bailly A-L, FlorianCorreard AP, GlebTselikov FC, RomainAppay AA-K, Kabashin AV, Braguer D, Esteve M-A. In vivo evaluation of safety, biodistribution and pharmacokinetics of laser synthesized gold nanoparticles. *Sci Rep.* 2019:9.
23. Khandel P, Yadaw RK, Soni DK, Kanwar L, Shahi SK. Biogenesis of metal nanoparticles and their pharmacological applications: present status and application prospects. *J Nanostruct Chem.* 2018;8:217–54.
24. Ranjit K, Baquee AA. Nanoparticles: an overview of preparation, characterization and application. *Int Res J Pharm.* 2013;4(4):47–57.
25. Hurst SJ, Lytton-Jean AKR, Mirkin CA. Maximizing DNA loading on a range of gold nanoparticle size. *Anal Chem.* 2006;78:8313–8.
26. Egorova EM, Revina AA. Synthesis of metallic nanoparticles in reverse micelles in the presence of quercetin. *Colloids Surf A Physicochem Eng Asp.* 2000;168:87–96.
27. Patel P, Agarwal P, Kanawaria S, Kachhwaha S, Kothari SL. Plant-based synthesis of silver nanoparticles and their characterization. In: *Nanotechnology and Plant Sciences.* Cham: Springer; 2015. p. 271–88.
28. Shankar SS, Rai A, Ahmad A, Sastry M. Rapid synthesis of Au, Ag, and bimetallic Au core–Ag shell nanoparticles using Neem (*Azadirachta indica*) leaf broth. *J Colloid Interface Sci.* 2004;275:496–502.
29. Molpeceres J, Aberturas MR, Guzman M. Biodegradable nanoparticles as a delivery system for cyclosporine: preparation and characterization. *J Microencapsul.* 2000;17(5):599–614.
30. Shi HG, Farber L, Michaels JN, Dickey A, Thompson KC, Shelukar SD, Hurter PN, Reynolds SD, Kaufman MJ. Characterization of crystalline drug nanoparticles using atomic force microscopy and complementary techniques. *Pharm Res.* 2003;20(3):479–84.
31. J & G Kreuter. Physicochemical research papers characterization of polyacrylic nanoparticle. *Int J Pharm.* 1983;14:43–58.



Models Used for Biopharmaceutical Evaluation of Nanoparticulate Drug Delivery System (NPDDS)

Seema Kohli and Sumeet Dwivedi

Contents

1	Introduction to Biopharmaceuticals.....	42
2	Nanoparticulate Drug Delivery System (NPDDS).....	42
3	Conclusion.....	50
	References.....	50

Abstract

Nanoparticle drug delivery systems are engineered technologies that use nanoparticles for the targeted delivery and controlled release of therapeutic agents. The modern form of a drug delivery system should minimize side effects and reduce both dosage and dosage frequency. Nanoparticle drug delivery focuses on maximizing drug efficacy and minimizing cytotoxicity. Fine-tuning nanoparticle properties for effective drug delivery involves addressing the following factors. The surface-area-to-volume ratio of nanoparticles can be altered to allow for more ligand binding to the surface. Model-based methods are increasingly used in almost every area of biopharmaceutical process technology. It can be applied in the field

of experimental design, process characterization, process design, monitoring, and control. Benefits of these methods are lower experimental effort, process transparency, clear rationality behind decisions, and increased process robustness. Biopharmaceutical modeling has become integral to the design and development of new drugs. Influencing key aspects of the development process, including drug substance design, formulation design, toxicological exposure assessment, and biopharmaceutical modeling, is now seen as the linchpin to a drug's future success. And while there are a number of commercially available software programs for drug modeling, there has not been a single resource guiding pharmaceutical. In the present chapter, these entire models used for biopharmaceutical evaluation of NPDDS have been highlighted.

S. Kohli (✉)
Kalanikaten Polytechnic College,
Jabalpur, Madhya Pradesh, India

S. Dwivedi
University Institute of Pharmacy, Oriental University,
Indore, Madhya Pradesh, India

Keywords

Nanoparticle · Biopharmaceutical · Models · Evaluation

1 Introduction to Biopharmaceuticals

Biopharmaceuticals are sophisticated medicines made from living cells or creatures and are frequently produced utilizing cutting-edge biotechnological techniques. A biopharmaceutical (biological or biologic) is a therapeutic product generated from biological sources such as humans, animals, or microorganisms and consists of carbohydrates, proteins, nucleic acids, living cells, or tissues. Unlike traditional pharmaceuticals, which are made through chemical methods, biopharmaceutical goods are made by biological processes such as the extraction of living systems or the synthesis of r-DNA technology. Transgenic species, such as plants, animals, or bacteria that have been genetically modified, could be used to create biopharmaceuticals [1].

Recombinant human insulin (trade name “Humulin”) was the first biopharmaceutical to be licensed for human medical purposes for marketing in 1982. Vaccines, entire blood (or blood components), immunosera, antigens, hormones, cytokines, enzymes, allergenics, cell treatments, gene therapies, tissues, and monoclonal antibodies are all examples of biopharmaceuticals in use today. Human treatments based on cells, genes, or tissue engineering are referred to as “advanced therapy medical products” (ATMPs) by the European Medicines Agency (EMA). CTPs are biomedicines that contain cells/tissues that have been modified to change their biological features and can be utilized to treat, prevent, or diagnose diseases. Gene therapy products (GTPs) are therapeutic agents used to enhance genetics by repairing, deleting, inserting, or replacing defective genes or making site-specific alterations for target therapies. Tissue engineering is the use of a combination of cell, engineering, and material approaches, as well as appropriate components, to improve, repair, or replace a portion or the entire biological system [2, 3].

Biosimilars, also known as “follow-on biologics,” are biologic medicinal products that are almost identical to copies of original products developed by various pharmaceutical companies. Despite small changes in therapeutically inactive

components, it is quite identical to a licensed reference product. In terms of safety, purity, and potency, there are no clinically relevant differences between biosimilars and reference products. In terms of dosage, safety, strength, administration, quality, performance, and intended uses, a generic medicine is identical to a brand name drug. To ensure that the generic drug can be used in place of the brand name drug, a series of stringent tests must be completed [4–6].

A generic drug must have the same active pharmaceutical ingredients (APIs) as the brand name product and must be proven to be bioequivalent to the brand name drug.

The scientific evaluation of generic drug substitutability or therapeutic equivalence is required. If a generic drug is determined to be therapeutically equivalent to a brand name product, it has the same effects and is less expensive. When the patent on the original “innovator” product expires, biosimilars, like generic medications, can be created and are formally approved replicas of the original products. A generic medicine and a biosimilar, on the other hand, have a lot of distinctions. Biosimilars have the same therapeutic impact as generic medications, but they are only comparable to the original “innovator” drugs because they have been validated. Unlike generic medications, where the APIs are same, biosimilars will not be identical to the reference pharmaceuticals. Despite this diversity, all generic pharmaceuticals and biosimilars must maintain a constant level of quality and efficacy throughout their life cycles [7].

2 Nanoparticulate Drug Delivery System (NPDDS)

Nanotechnology and nanoscience advancements have brought up new possibilities in medical science. Both the corporate and public sectors have increased their interest and investment in nanotechnology research and implementation for a variety of applications in the biological sciences. Nanoscience and nanotechnology have infiltrated the pharmacy industry, opening up new avenues

for enhanced drug delivery and therapy. Although nanotechnology holds a lot of promise, it also poses new concerns in terms of safety and ethics. Because traditional dose forms have a number of drawbacks, formulation pharmacists are constantly working on new medication delivery strategies [8].

Despite the fact that new-generation medications have potent activity, the majority of them have limitations such as poor water solubility, low gastrointestinal permeability, high first pass metabolism, poor stability, nonselective distribution, and others. As a result, in recent years, new particulate drug delivery systems (PDDS), either polymer- or lipid-based, have been explored as agents to treat a variety of diseases. Nanoparticulate systems (NS) have shown to be effective in overcoming these issues, with the potential to improve therapeutic outcomes. Traditional drug delivery techniques, particularly in cancer chemotherapy, are hampered by biological barriers. Drug NPs or NS, on the other hand, have shown enhanced membrane permeability, leading to improved therapy not just in cancer but also in the treatment of other diseases [9].

NPs are well known for increasing drug solubility and bioavailability, but they can also be utilized to target medications, especially peptide-based therapies, to specific areas or organs, as well as control drug release. Nasal delivery of nanoparticulate insulin was observed to result in increased insulin absorption. Within 10 years, it is estimated that 50% of all drug delivery and design will be automated. NPDDS' ultimate goal is to develop clinically relevant formulations that will improve therapy and patient quality of life. Chemotherapy is one area where NS has shown tremendous promise, as nonselective distribution of cytotoxic medicines in conventional dose forms resulted in severe adverse effects. According to the existing literature, the NPDDS are not only useful in chemotherapy but can also be used to deliver other types of medications to their sites of action via various routes of administration. Because NPs can be kept at the application site and prolong drug release to the eye, they may be a preferable alternative for oph-

thalmic administration. The TB treatments based on NPs are widely used [10, 11].

2.1 Types of Nanoparticles for Drug Delivery

NPs for drug delivery can be classified into solid lipid nanoparticles (SLNs), nanospheres, nanocapsules, liposomes, and polymersomes and micelles, based on the methods of preparation as shown in Fig. 3.1 [12]:

- Nanospheres are matrix systems in which the drug is incorporated throughout the solid polymers, whereas SLNs are solid nanoparticles made by integrating drug in lipid.
- Nanocapsules are vesicular systems in which a single polymeric membrane surrounds the drug alone or the drug restricted to an aqueous or oily drop. Lipophilic medications are generally encapsulated in nanocapsules.
- A polymersome is defined as a polymeric membrane with many layers. Various phospholipids (saturated and unsaturated) have been employed in nanosized liposomal systems, with promising results. To avoid buildup of the polymer matrix after repeated treatment, polymeric NPs are often made from biodegradable polymers.

2.2 Method of Preparation of Nanoparticles

In general, NPs are prepared by processes, such as solvent evaporation, solvent diffusion/displacement, reverse salting-out and droplet gelation, emulsification and polymerization, dispersion polymerization, interfacial condensation polymerization, and interfacial complexation [12, 13]:

- The SLN is prepared by emulsification and solvent evaporation techniques. The simplest method of NP preparation is nanoprecipitation. PLA, PLGA, and poly-ε-caprolactone (PCL) NPs can be prepared by emulsification

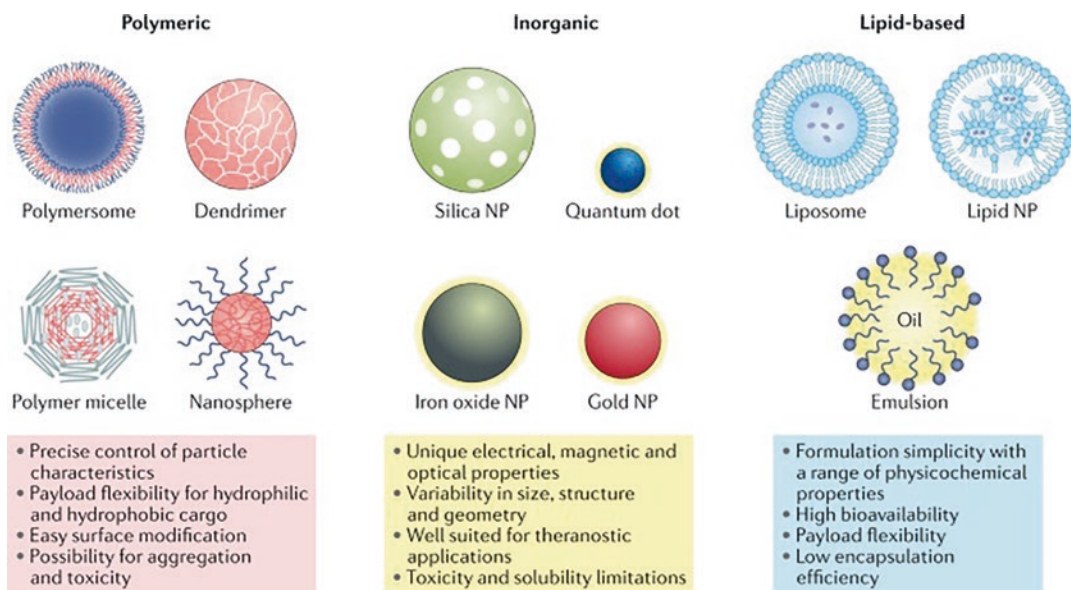


Fig. 3.1 Different types of nanoparticles for drug delivery

and solvent evaporation process, with average particle size of 250 nm and above. Amphiphilic block copolymer NPs can be prepared by using this method with polymers such as PEG-PCL, PEG-PLGA, PEG-PLA, and PEG-PACA. Though this method is used for preparing lipophilic drug-loaded NPs extensively, even hydrophilic drugs can also be encapsulated by this process. Solvents used for this method are methylene chloride, chloroform, ethyl acetate, etc.

- Another method used for preparation of NPs is emulsification and solvent diffusion/displacement process. As the name implies, diffusion of organic solvent into the aqueous phase is the key step in emulsion solvent displacement method. The organic solvent should be partially soluble in water and is selected from a wide range of solvents such as benzyl alcohol, 2-butanone, methyl acetate, propylene carbonate, ethyl acetate, isopropyl acetate, methyl acetate, methyl ethyl ketone, and isovaleric acid. This method can be used to prepare NPs of size around 150 nm for poorly water-soluble drugs.
- Nanocapsules can be prepared by the same method just by adding a small amount of oil into the organic phase.
- In emulsification-reverse salting-out method, water-miscible acetone is emulsified with aqueous phase containing high concentration of salts or sucrose. Magnesium chloride, calcium chloride, and magnesium acetate salts are preferably used, because of their high salting-out effect in aqueous phase. When acetone is added to aqueous phase, the miscibility of water to acetone decreases, due to the presence of the large quantity of electrolyte which holds water molecules, resulting in emulsion droplet formation. The precipitation of polymer from the emulsion is induced by adding excess water, which results in a sudden drop of the salt or sucrose concentration in the continuous phase of the emulsion, and hence inducing the organic solvent to migrate out of the emulsion droplets; this process is called reverse salting-out. The gelling property of the polymers is used to prepare the NPs from the emulsion, the polymers used being agarose, alginate, and pectin. This method of preparation is called emulsion droplet gelation.
- NPs prepared by in situ polymerization use monomer (alkylcyanoacrylates) to produce polymerization of alkylcyanoacrylate while forming NPs. The NPs are synthesized by an in situ spontaneous polymerization reaction.

This polymer can encapsulate both lipophilic and hydrophilic drugs and is used to prepare nanospheres and nanocapsules containing an aqueous or oily core. The NPs prepared by *in situ* method follow anionic polymerization reaction mechanism, and the reaction is spontaneously initiated by hydroxyl groups of water or any nucleophilic groups.

- Nanoprecipitation is the simplest, fastest, and most reproducible and economical method of preparing NPs especially for lipophilic drugs. In this method, the polymer, drug, and lipophilic surfactant are dissolved in a semipolar water-miscible solvent such as acetone, ethanol, dimethylformamide, and dimethylsulfoxide. The basic requirement of the selection of solvent is miscibility with aqueous phase, and the aqueous phase has to be a nonsolvent of the polymer. Once the organic solvent is added to aqueous phase, NPs form instantaneously because of the rapid diffusion of water-miscible solvent into the aqueous phase. Because of the instantaneous process, the nanoprecipitation method provides very fine particles (about 200 nm) with a narrow size distribution. This method can also be used to encapsulate hydrophilic drugs. The SLNs are composed of physiological lipid, dispersed in water or a solution of aqueous surfactant. The lipid matrices used in the preparation of SLNs are Acidan N 12, B-CD21C6, cetyl palmitate, Dynasan 114 (trimyristin), Dynasan 116 (tripalmitin), glyceryl behenate, glycerol monostearate, monostearin, stearic acid, tristearin, tricaprins, Witepsol E 85, and Precirol ATO 5. The proposed advantages of these polymeric NPs are increased drug stability, high drug payload (both hydrophilic and lipophilic drugs), no biotoxicity of the carrier, ease of scaleup, and sterilization.
- The nanoemulsion is prepared mainly by the spontaneous emulsification or titration method. In this method, the nanoemulsion is prepared by blending oil, water, surfactant, and cosurfactant in the appropriate proportions with mild agitation. Nanoemulsions are thermodynamically stable preparations with a particle size of less than 100 nm.

Nanoemulsions are mainly used to improve the transdermal and dermal delivery of drugs. The various approaches and methods of NP preparation are depicted in Fig. 3.2.

2.3 Methods of Concentrating NPs

The prepared NPs require concentrating to reduce the volume of administration; this reduces the systemic overexposure of excipients. The concentration process plays an important role in final particle size and its aggregation in the final formulations. There are several methods for concentrating NPs, such as centrifugation, lyophilization, evaporation, and dialysis. Concentrating to the desired volume by evaporation is usually performed by rotary evaporation. Based on the solvent and polymer, the temperature and vacuum are optimized. During this process, the polymer layer of the NPs is also solidified. Using lyophilization, the NPs are transformed into a free flowing dry powder, and this approach also helps to avoid microbiological degradation, premature polymer degradation, physicochemical instability, and loss of drug activity. To avoid damage to NPs during the freezing and lyophilization process, special excipients, for cryoprotectant (to overcome freezing stress) and lyoprotectant (to overcome drying stress) actions, are added to the nanosuspension before freezing. Some of the very frequently used cryo- or lyoprotectants are glucose, sucrose, lactose, mannitol, sorbitol, poly(vinyl pyrrolidone), glycerol, poly(vinyl alcohol), and dextran. Other methods of concentrating NPs are centrifugation and ultracentrifugation. Normal centrifugation, performed at low *g* forces, can remove aggregates and large particles from the polymeric nanoparticle suspension, but this method will not guarantee removal of all particles above the nanometer size in the formulation. Ultracentrifugations can sediment particles with slightly higher density than water. Ultracentrifugation is performed at 100,000–110,000 *g* for 30–45 min to form pellet of NPs. These pellets can be reconstituted to the desired volume of dispersion medium. NP concentration by dialysis can be performed using dif-

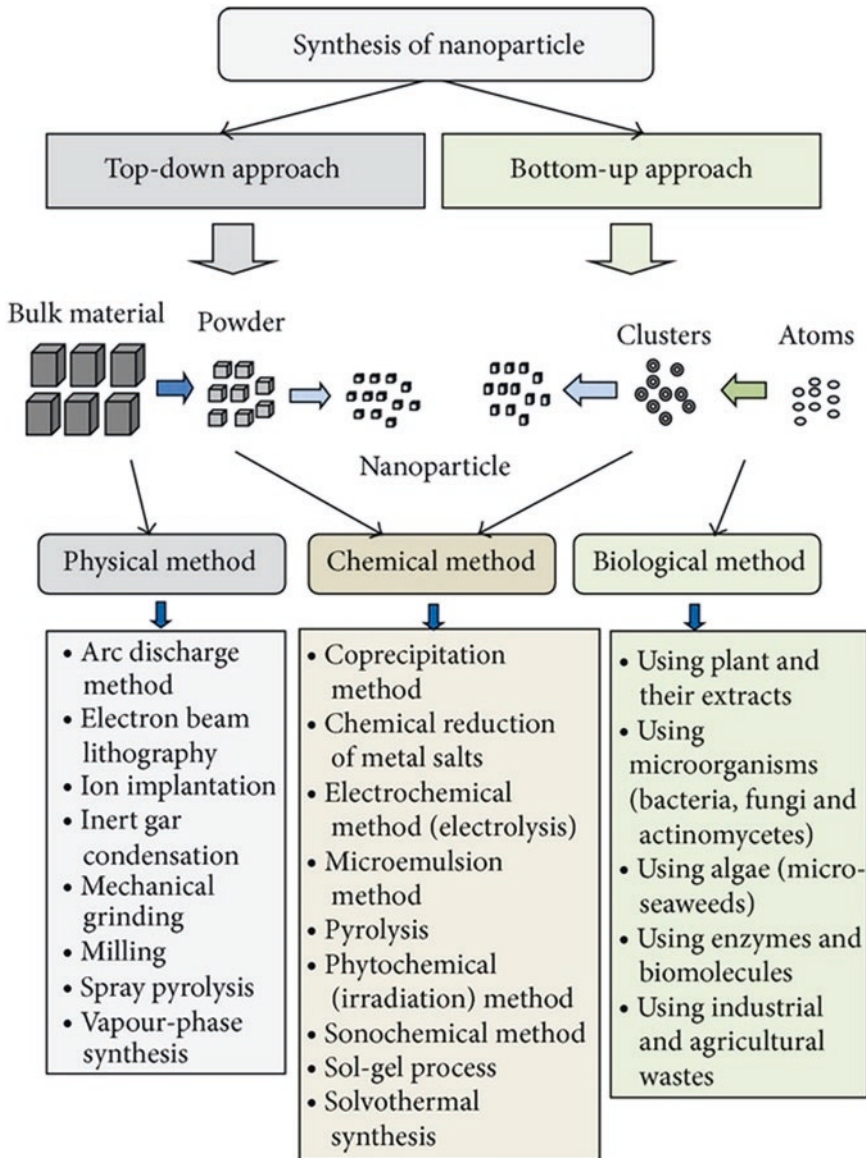


Fig. 3.2 Approaches and methods for nanoparticles

ferent cellulose membranes with various molecular weight cut-offs. In the simple dialysis method, the concentration of the suspension is performed against a polymer solution. This causes an osmotic stress producing a displacement of water from the nanosuspension toward the counter-dialysis solution. The dialysis method results showed that the amount of water removed can be controlled and the process is reproducible [12, 13].

2.4 Models for Biopharmaceutical Evaluation of NPDDS

Biopharmaceutical modeling has become integral to the design and development of new drugs. Influencing key aspects of the development process, including drug substance design, formulation design, and toxicological exposure assessment, biopharmaceutical modeling is now seen as the linchpin to a drug's future success.

And while there are a number of commercially available software programs for drug modeling, there has not been a single resource guiding pharmaceutical professionals to the actual tools and practices needed to design and test safe drugs.

2.5 Molecular Modeling

Molecular modeling can be seen as the sum of two components: a molecular model and a computational technique to properly characterize the behavior of the molecules.

Building a suitable molecular model, that is, how the system under investigation is rationalized and represented in the framework of a meaningful simulation, is the first fundamental step. In this framework, molecular models can be essentially divided into two categories; on the one hand, full atomistic models provide the highest level of detail since all atoms (considered as the smallest constitutive units of the model) are explicitly accounted for. On the other hand, coarse-grained (CG) models summarize the atomic detail by enclosing groups of atoms into beads that lump the main peculiarities (in terms of charge, polarity, etc.) of the atoms that they embed. This simplification is unavoidable for complex systems whose atomistic representation would be prohibitive from a computational point of view, in terms of the system size and/or time and length scales needed to investigate the phenomena of interest. Despite the loss of detail, a CG model that retains the main features of the system is able to provide meaningful insights at a reasonable computational cost (*vide infra*). For the sake of completeness, there exist more detailed representations where electrons are the smallest constitutive units and are explicitly included. Such models are treated with quantum chemistry methods, which are not considered or discussed here since their application in the field of nanomedicine is hindered by their computational inefficiency.

In a broader sense, a molecular model also includes unavoidable simplifications that allow for the simulation of complex systems, either at a full atomistic or CG level of detail, which could

not be treated otherwise. The simulation of protein adsorption on a microparticle surface, for example, is unfeasible because of the system size. Such a system is usually simplified by adopting a molecular model that involves the adsorption of a protein on a flat surface with a suitable thickness. This approach is reasonable since the phenomena of interest are restricted to the solvent/particle interface; in addition, since protein size is much smaller than microparticle radius, curvature effects can be reasonably neglected.

The second component of molecular modeling is constituted by suitable computational methods that allow the characterization of the dynamics, energetics, and conformational sampling of the system of interest. Full atomistic models are usually treated with molecular dynamics, while other techniques such as CG molecular dynamics and dissipative particle dynamics (DPD) are employed along with CG models [14–16].

2.6 Full Atomistic Models

In molecular dynamics simulations, atoms are represented as spheres that interact with each other by virtue of a potential energy function, usually called the force field (FF). Molecular coordinates and velocities as a function of simulation time can be evaluated by solving Newton's equation of motion with a suitable numerical integration scheme, as shown in Eq. 3.1:

$$m_i \frac{d^2 r_i}{dt^2} = F_i = -\nabla U(r) \quad (3.1)$$

where m_i is the mass of the i th atom, r_i are the spatial coordinates of the i th atom, t is time, F_i is the force acting on the i th atom, and $U(r)$ is the potential energy (i.e., the FF), which is a function of the coordinates of all atoms present in system r . Such an approach essentially implies a couple of assumptions, as follows. First, the motion of electrons can be reasonably described by the dynamics of the corresponding nuclei (Born–Oppenheimer approximation). Second, the motion of the atomic nuclei (which are heavier

than electrons) can be described as point particles that follow classical mechanics; this is an acceptable approximation when quantum effects are not important. Generally speaking, a FF takes into account both intramolecular and intermolecular interactions, in terms of bonds, angles, dihedrals, and long-range interactions, namely, van der Waals and electrostatic.

FFs contain several parameters that are computed in order to reproduce the conformational energies and minimum energy structures obtained from high-level quantum mechanics calculations and/or experimental data, such as hydration enthalpies or structural parameters from NMR experiments. There are “general-purpose” FFs, usually employed to describe small ligands, as well as FFs specifically tailored for given categories of molecules, like proteins, nucleic acids, carbohydrates, and lipids. The choice and the quality of the FF cannot be underestimated, since they strongly affect the reliability of the simulation outcome.

MD simulations do not explicitly consider electrons, so chemical reactions and excited states cannot be investigated; however, they constitute the ideal tool for those systems that are mainly governed by non-covalent interactions, like electrostatic and van der Waals forces. MD also allows environmental conditions to be included through the addition of explicit solvent molecules, ions, and other solute molecules into the system. The main outputs from an MD simulation are molecular trajectories, the post-processing of which can provide structural information (binding poses, protein conformation) as well as energetic information such as interaction energies [17–19].

2.7 Enhanced Sampling Methods

The characteristic time and length scales of MD simulations are in the tens to hundreds of nanoseconds (up to 1000 ns) and tens of nanometers (up to 20 nm), respectively. However, many phenomena of interest (e.g., molecular binding, protein unfolding) need large time scales to occur (up to minutes), and their investigation through

MD would be in principle unfeasible; this is due to the presence of metastable states separated by high free energy barriers. A way to overcome this issue is to use enhanced sampling methods, which allow enhancement of the transitions between different metastable states separated by energy barriers higher than the thermal energy $k_B T$, which would not be crossed in a standard simulation at temperature T (where k_B is the Boltzmann constant and T is absolute temperature). As recently reviewed, there are three different suitable approaches: (i) increasing the temperature T , (ii) changing the potential $U(r)$, and (iii) adding an external bias potential $V(r)$. Each approach has its own methods, the discussion of which (along with their theoretical basis) is well beyond the purpose of this review; the interested reader is referred to ad hoc reviews. Some of the popular enhanced sampling techniques are replica exchange (RE, first approach) and well-tempered metadynamics (WTM), which belongs to the third group. In particular, WTM and its variant forms allow the free energy of the system under investigation to be recovered by adding an external bias on a selected number of degrees of freedom, commonly referred to as collective variables (CVs). CVs are generally functions of atomic coordinates and can range from simple quantities, such as distances and dihedral angles, to more complicated variables, like the number of hydrogen bonds/hydrophobic contacts, alpha-helix content in a protein, or Debye–Hückel interaction energy. CVs must be chosen so that they can discriminate between metastable states and can be representative of the transition mechanism. Typical applications of WTM and WTM-based methods are the study of protein conformations (also in the presence of denaturants), the binding poses of small ligands to target proteins, and the conformation and self-assembly of polymeric and supramolecular systems. Some phenomena, such as protein folding, require a relevant number of CVs to perform meaningful simulations. Although conceptually feasible, running a WTM simulation with many CVs introduces some issues such as a drop in computational efficiency and a nontrivial analysis of the results obtained. In order to overcome this issue, some

WTM variants have been proposed, discussed, and validated in literature (mainly for protein folding), namely, parallel tempering metadynamics (PTMD), parallel tempering metadynamics in the well-tempered ensemble (PTMD-WTE), and bias exchange metadynamics (BEMD) [20–21].

2.8 CG Models

The aim of CG models is to perform meaningful simulations of systems whose analysis would be challenging or unfeasible with full atomistic MD methods by building simplified representations that allow the main physical/chemical features (like the interplay between hydrophobic and hydrophilic effects) to be retained.

In the coarse-graining procedure, groups of atoms are enclosed into “beads” or “interaction sites” that are representative of the embedded atoms in terms of charge, size, hydrophobicity/hydrophilicity, etc. Beads interact with each other by virtue of a potential energy function, which takes into account both bonded interactions (i.e., bond, angles, and dihedrals) and nonbonded interactions and which is parameterized in order to optimally reproduce some experimental properties (like water/octanol partition) or the behavior of more detailed full atomistic simulations [22, 23].

Trajectories can be computed by integrating Newton’s equation of motion and also adding other components to the force such as friction due to the solvent (if implicit solvent methods are used) (vide infra).

It is worth mentioning that the coarse-graining procedure can be performed to different extents, since a bead can enclose a group of atoms (three to four heavy atoms), a group of monomers (or amino acids), an entire protein, or an entire microparticle, according to the aim of the simulation. In this review, the term “CG models” is employed for all those approaches where there is a loss of degrees of freedom with respect to a full atomistic description.

A common drawback of CG models is that parameterization is strictly tailored for the system under investigation and in principle should

be repeated for every new system; in other words, parameters are not transferable. In this regard, the MARTINI FF (Marrink et al., 2007) attracted a lot of interest due to its reliability and straightforward coarse-graining procedure. Beads (which include groups of three to four heavy atoms) still interact with each other through a simple potential energy function, as described for MD (vide supra). MARTINI offers a library of parameterized beads, mainly divided into four categories: polar, nonpolar, apolar, and charged; in addition, each group includes subgroups representative of polarity and hydrogen bond capability. Parameters for bonded interactions (bonds, angle, dihedrals) must be determined from detailed MD simulations, while nonbonded interactions are tuned in order to reproduce thermodynamic properties like free energy of hydration, free energy of vaporization, and partitioning between water and different solvents. Explicit water and ions can also be added (a MARTINI water bead is representative of four water molecules) [24, 25].

Bead parameterization can be further refined by the user in order to improve agreement with full atomistic simulations. Even with simulations based on the MARTINI FF, some phenomena of interest can be still characterized at a time scale that is not accessible.

Another widely employed method with CG models is DPD. Bead trajectories are still obtained by means of Newton’s equation of motion, assuming that each i th particle is subjected to three pair-additive forces that arise from the interactions with the other j th particles: a conservative force, a dissipative force, and a random force.

$$m_i \frac{d^2 r_i}{dt^2} = f_i = \sum_{j \neq i} F_{ij}^c + F_{ij}^d + F_{ij}^r$$

The conservative force F^c is due to the interaction potential of particles and accounts for both bonded and long-range interactions through an elastic force and a soft repulsion force, respectively. F^d is a dissipative force that damps the relative motion between particles, and F^r is a random force directed along the line that connects bead centers. Dissipative and random forces are

momentum-conserving and represent the minimal model that takes into account viscous forces and thermal noise between particles [26–28].

3 Conclusion

Biopharmaceuticals' recent breakthrough success has transformed the treatment of a variety of disorders. However, there are still issues with formulation and administration. Colloidal nanocarriers may be a viable solution for overcoming these obstacles. Nanotechnology not only provides novel technologies for biopharmaceutical manufacturing but also suggests noninvasive, safe, and targeted decontamination solutions. Furthermore, the application of nanotechnology could improve the accessibility of biopharmaceuticals to target locations for the treatment of specific clinical disorders. Biological and technological obstacles make clinical translation and commercialization for biopharmaceutical delivery questionable, despite nanocarriers' great qualities. Scaling up nanocarrier formulations and conducting quality control to manage their physicochemical qualities takes a lot of work. The efficacy and short- and long-term toxicity of the nanocarrier-based biopharmaceuticals used in a given therapy must be determined. Overall, nanocarrier-based biopharmaceutical delivery has a lot of promise for successful treatment of diseases.

References

- Walsh G. Biopharmaceutical benchmarks 2018. *Nat Biotechnol.* 2018;36(12):1136–45.
- Chen YC, Cheng HF, Yeh MK. Cell therapy regulation in Taiwan. *Cell Transplant.* 2017;26(3):483–92.
- Gonçalves GAR, Paiva RMA. Gene therapy: advances, challenges and perspectives. *Einstein (Sao Paulo).* 2017;15(3):369–75.
- Calo-Fernández B, Martínez-Hurtado JL. Biosimilars: company strategies to capture value from the biologics market. *Pharmaceuticals.* 2012;5(12):1393–408.
- Nick C, The US. Biosimilars act: challenges facing regulatory approval. *Pharm Med.* 2012;26(3):145–52.
- Camacho LH, Frost CP, Abella E, Morrow PK, Whittaker S. Biosimilars 101: considerations for U.S. oncologists in clinical practice. *Cancer Med.* 2014;3(4):889–99.
- Declerck P, Farouk-Rezk M, Rudd PM. Biosimilarity versus manufacturing change: two distinct concepts. *Pharm Res.* 2016;33(2):261–8.
- Vert M, Doi Y, Hellwich KH, Hess M, Hodge P, Kubisa P, Rinaudo M, Schué FO. Terminology for biorelated polymers and applications (IUPAC recommendations 2012). *Pure Appl Chem.* 2012;84(2):377–410.
- Vert M, Doi Y, Hellwich K-H, Hess M, Hodge P, Kubisa P, Rinaudo M, Schué F. Terminology for biorelated polymers and applications (IUPAC recommendations 2012). *Pure Appl Chem.* 2012;84(2):377–410.
- Khan I, Saeed K, Khan I. Nanoparticles: Properties, applications and toxicities. *Arab J Chem.* 2019;12(7):908–31.
- Reiss G, Hutten A. Magnetic Nanoparticles. In: Sattler KD, editor. *Handbook of nanophysics: nanoparticles and quantum dots.* CRC Press; 2010. p. 2 1. ISBN 9781420075458.
- Crucho CIC, Barros MT. Polymeric nanoparticles: A study on the preparation variables and characterization methods. *Mater Sci Eng C.* 2017;80:771–84.
- Pal SL, Utpal Jana PK, Manna GP, Mohanta RM. Nanoparticle: an overview of preparation and characterization. *J Appl Pharm Sci.* 2011;01(06):228–34.
- Bochicchio D, Pavan GM. Molecular modelling of supramolecular polymers. *Adv Phys X.* 2018;3:315–37. <https://doi.org/10.1080/23746149.2018.1436408>.
- Bruno A, Scrima M, Novellino E, D'errico G, D'ursi, A. M., and Limongelli, V. The glycan role in the glycopeptide immunogenicity revealed by atomistic simulations and spectroscopic experiments on the multiple sclerosis biomarker CSF114(Glc). *Sci Rep.* 2015;5:9200. <https://doi.org/10.1038/srep09200>.
- Camilloni C, Pietrucci F. Advanced simulation techniques for the thermodynamic and kinetic characterization of biological systems. *Adv Phys X.* 2018;3:1477531. <https://doi.org/10.1080/23746149.2018.1477531>.
- Deighan M, Bonomi M, Pfaendtner J. Efficient simulation of explicitly solvated proteins in the well-tempered ensemble. *J Chem Theory Comput.* 2012;8:2189–92. <https://doi.org/10.1021/ct300297t>.
- Deighan M, Pfaendtner J. Exhaustively sampling peptide adsorption with metadynamics. *Langmuir.* 2013;29:7999–8009. <https://doi.org/10.1021/la4010664>.
- Dickson CJ, Hornak V, Pearlstein RA, Duca JS. Structure-kinetic relationships of passive membrane permeation from multiscale modeling. *J Am Chem Soc.* 2017;139:442–52. <https://doi.org/10.1021/jacs.6b11215>.
- Frenkel D, Smit B. *Understanding molecular simulation: from algorithms to applications.* San Diego: Academic Press; 2002.
- Bochicchio D, Pavan GM. Effect of concentration on the supramolecular polymerization mechanism via

- implicit-solvent coarse-grained simulations of water-soluble 1,3,5-benzenetricarboxamide. *J Phys Chem Lett.* 2017;8:3813–9. <https://doi.org/10.1021/acs.jpcllett.7b01649>.
22. Wei S, Ahlstrom LS, Brooks CL. Exploring protein-nanoparticle interactions with coarse-grained protein folding models. *Small.* 2017;13:1603748. <https://doi.org/10.1002/sml.201603748>.
23. Lopez H, Lobaskin V. Coarse-grained model of adsorption of blood plasma proteins onto nanoparticles. *J Chem Phys.* 2015;143:243138. <https://doi.org/10.1063/1.4936908>.
24. Yu GB, Zhou J. Understanding the curvature effect of silica nanoparticles on lysozyme adsorption orientation and conformation: a mesoscopic coarse-grained simulation study. *Phys Chem Chem Phys.* 2016;18:23500–7. <https://doi.org/10.1039/C6CP01478J>.
25. Marrink SJ, Risselada HJ, Yefimov S, Tieleman DP, De Vries AH. The MARTINI force field: coarse grained model for biomolecular simulations. *J Phys Chem B.* 2007;111:7812–24. <https://doi.org/10.1021/jp071097f>.
26. Marrink SJ, Tieleman DP. Perspective on the Martini model. *Chem Soc Rev.* 2013;42:6801–22. <https://doi.org/10.1039/c3cs60093a>.
27. Utesch T, Daminelli G, Mroginski MA. Molecular dynamics simulations of the adsorption of bone morphogenetic protein-2 on surfaces with medical relevance. *Langmuir.* 2011;27:13144–53. <https://doi.org/10.1021/la202489w>.
28. Valsson O, Tiwary P, Parrinello M. Enhancing important fluctuations: rare events and metadynamics from a conceptual viewpoint. *Annu Rev Phys Chem.* 2016;67:159–84. <https://doi.org/10.1146/annurev-physchem-040215-112229>.



Models Used for Pharmacokinetic Evaluation of Nanoparticulate Drug Delivery Systems (NPDDS)

Nishtha Chaurawal and Kaisar Raza

Contents

1	Introduction	53
2	Pharmacokinetic Approaches	54
3	Pharmacokinetic Evaluation of Nano-particulate Drug Delivery System	63
4	Future Prospects	65
5	Conclusion	65
	References	65

Abstract

Nanoparticulate drug delivery systems (NPDDS) are structured to refine the tissue distribution, pharmacokinetic profile and targeting characteristics of small molecules to prolong their systemic circulation. The nanoparticles serve several benefits in drug delivery but show complicated in vivo absorption and disposition properties compared to the conventional dosage forms. The pharmacokinetic compartment and non-compartment modelling has been a convenient tool for quantifying and characterization target exposure, the volume of distribution, safety and efficacy, bioavailability profile, clearance and systemic disposition of several kinds of drugs.

In this chapter, the models used to determine pharmacokinetic parameters of drugs and their evaluation in nanoparticulate systems have been described rigorously, along with their complications and future research necessity related to the clinical approach.

Keywords

Nanoparticulate drug delivery system · Pharmacokinetics · PBPK · Compartment models · Dendrimers · SLNs · Tissue distribution

N. Chaurawal · K. Raza (✉)
Department of Pharmacy, School of Chemical Sciences and Pharmacy, Central University of Rajasthan, Bandarsindri, Ajmer, Rajasthan, India
e-mail: drkaisar@curaj.ac.in

1 Introduction

Recent trends in the field of nanotechnology have gained special attention towards therapeutics and diagnosis [1]. Due to the size, shape and physico-chemical properties, these nanoscale materials are used for the targeted delivery approaches [2].

These targeted approaches relied on the cellular uptake and permeability of the nanoscale composite [3]. Based on the exposure to the human body, these nanoscale particles can be classified into two types: (a) unintentional and (b) intentional [4]. Intentional exposure of nanocomposites needs pharmacokinetic parameters to understand how these particles behave inside the body. The pharmacokinetic study depends on the nanoparticles' absorption, distribution, metabolism and excretion [5]. Various software has currently been explored to calculate multiple pharmacokinetic parameters like absorption rate constant, elimination rate constants, half-life, apparent volume of distribution and total clearance rate. These mathematical parameters were further valuable in the compartmental and non-compartmental models [6]. The non-compartmental model estimates the concentration-time graph by plotting the area under the curve (AUC) and the moment curve (AUMC).

In contrast, the compartmental model computes the graph between time and concentration using kinetic models [6]. Increased $T_{1/2}$, AUC, mean resident time (MRT) and reduced clearance are mainly observed if the nanomaterial exists for a prolonged time in the systemic circulation. At the same time, the vice versa occurs due to the faster elimination of nanomaterial. Thus, the insights of the pharmacokinetic models are essential for designing the dosage regimen, minimizing toxicity and providing better therapeutic efficacy [7].

The historical introduction to the pharmacokinetic model by Teorell was the most promising mathematical approach to calculate the absorption, distribution, metabolism and excretion parameters of a drug. However, this model is now known as a two-compartment open model with extra- or intravascular administration [8]. Later, Dominguez and Pomerene demonstrated the rate of absorption of creatinine from the plasma concentration by a one-compartment model [9]. Further, a two-compartmental open model with intravenous (IV) injection has been developed using the feathering technique [10]. With the aim of the two-compartmental model approaches, an introduction to nonlinear processes has shown to be promising. The nonlinear process is helpful

for the calculation of dosage schedule and mechanistic pathway. Nogami et al. applied a nonlinear least-squares method to study the pharmacokinetic behaviour of intravenously injected ethoxybenzamide [11]. Lowenthal and his co-author demonstrated some biological constants using the Fortran II computer program [12]. Later in 2008, the pharmacokinetic and toxicology studies of nanoparticle (quantum dot 705) were carried out by a physiologically based pharmacokinetic (PBPK) computer simulation model [13]. Further, Lee et al. compared the bio-distribution of a quantum dot with a blood-flow-limited PBPK model [14]. So, we require mathematical models to obtain a potential drug candidate or nanoparticle for a high therapeutic effect with a better pharmacokinetic profile and reduced toxicity.

2 Pharmacokinetic Approaches

The study of the pharmacokinetic parameter of a drug or nanoparticle is vital in drug discovery. These studies are helpful in the lead optimization of a drug by determining AUC, plasma concentration and threshold efficacy [15]. To understand the pharmacokinetic models, one has to understand some fundamental aspects of pharmacokinetics.

2.1 Basic Definitions

Some of the standard terms used in pharmacokinetic has been discussed in Table 4.1.

2.2 Compartmental Pharmacokinetics

Compartmental pharmacokinetics was first established by Gehlan (1933) and Beccari (1938) [21]. A compartment is a material of distinct amount which acts kinetically in a homogeneous way. However, some materials or drugs are treated as a compartment in clinical studies in a physiological

Table 4.1 Commonly used terms in pharmacokinetic studies

Terms	Description	References
Pharmacokinetic	It is the time duration of the drug and the concentration of metabolites in the body. It describes absorption, distribution, metabolism and excretion	[15]
Toxicokinetic	It is the removal or disposition of toxicants from the body. Similar to pharmacokinetic but in toxicokinetic, toxicants are used for the study	[16]
Toxicology	It is the study of hazardous substances when exposed to humans or the environment	[17]
Biopharmaceutics	It is the interrelation between the physiochemical properties of the drug with biological aspect	[18]
Clinical pharmacokinetic	It is a pharmacokinetic process through which the target concentration strategy is calculated	[19]
Chrono-pharmacokinetic	It is the correlation between the time of administration of a drug and the response of the organism	[20]

state. A finite number of parts have been used for analysing the compartmental system. A compartmental system has been consisted of two more compartments in which the exchange of materials takes place. This type of modelling has utilization in drug kinetics of pharmacology, the kinetics of the chemical reaction, analysis of ecosystems and studies of metabolic systems. The compartmental analysis is the mathematical model for detecting the behaviour of these systems of compartments. The compartment system is modelled with various types of differential equations illustrating the rate and time of change

of the amount of material in the specific compartment (dq/dt) that follows Fick's law of diffusion:

$$\frac{dq}{dt} = \text{inflow rate} - \text{outflow rate}$$

where

Inflow rate = rate of drug distribution to the GI tract

Outflow rate = rate of drug excretion from GI tract

In a demonstration of the compartmental system, the compartment has been denoted by a box, and the transfer of material into or out of the compartment has been signified by an arrow. There are also arrows indicating the outside environment (vertical arrows pointing towards the boxes), and there can be arrows showing the excretion of material from the compartment to the outside environment (vertical arrows pointing outside the boxes) [21]. It is assumed that the drug is homogeneously distributed throughout these compartments and the drug transfer between these compartments follows first-order kinetics. The compartmental systems are referred to as open and closed based on the exchange of material. If no material exchange occurs, the system is known as a closed compartmental system, otherwise called an open system. However, the compartmental system could be made up of two or more compartments, and blood is referred to as the central compartment, while other organs are the peripheral compartment. These compartment models are also known as elementary compartment models or linear models [22]. A three-compartment model has been shown in Fig. 4.1, K denotes the proportionality rate constant and A signifies the absorption of the drug. Compartment models are classified into mechanistic models and physiological models. The mechanistic models do not reflect all the entities and can only relate their parameters to the physiological processes, while, on the other hand, the PBPK models are the most extensive and contain structural compartments interconnected with lymph flow, blood flow and other biochemical fluxes [23].

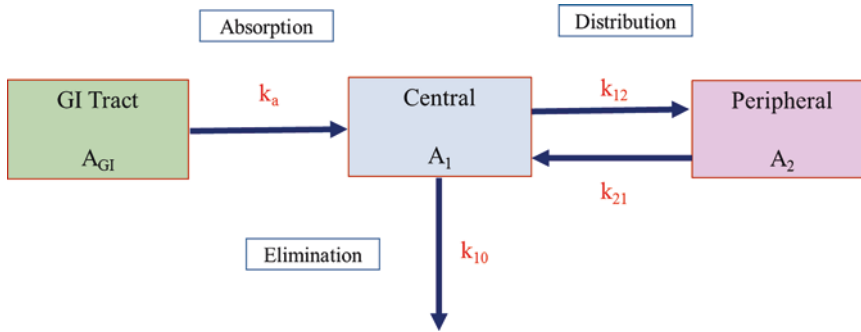


Fig. 4.1 A pictorial representation of three-compartment pharmacokinetic models

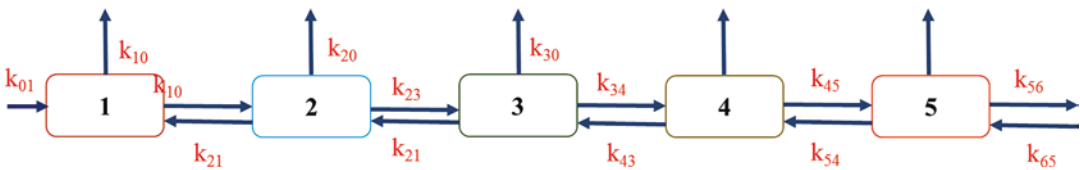


Fig. 4.2 Pictorial representation of catenary five-compartment pharmacokinetic model

Models Used in PK

A mechanistic model can be subdivided into the catenary model and mammillary model.

(a) Catenary Model

In a general catenary compartmental model (Fig. 4.2), it is supposed that each compartment is directly interconnected with a chain of compartments and the elimination occurs from any of the compartments. Let x_0 be the amount of drug injected into the compartments and time $t = 0$ and x_i be the amount of drug in the compartments at time t . Then, the equation for x_i becomes [24]

$$\frac{dx}{dt} = Kx$$

$$x(0) = x_0$$

(b) Mammillary Model

In a mammillary compartment model, all the peripheral compartments are connected directly

with the central compartment. The absorption of the drug takes place from the central compartment with elimination from any of the peripheral compartments (Fig. 4.3) [25].

(c) PBPK Models

Teorell, in 1937, introduced the PBPK model. For a long time, several attempts have been made to apply the PBPK models in drug development. PBPK models comprise the compartments that denote the different physiological organs of the body and the circulating system. The tissue volume and blood flow rate of specific species describe each compartment. Two rate-limited kinetics, i.e. perfusion rate-limited or permeability rate-limited, are used as assumptions for each tissue. The small lipophilic molecules containing tissues with blood flow as the limiting process of the absorption, the perfusion rate-limited kinetics tends to exist. In hydrophilic and larger molecules, the rate-limiting process of absorption is permeability across the cell membrane, implying the permeability rate-limiting kinetics in these tissues. A general PBPK model has been shown in Fig. 4.4 [26].

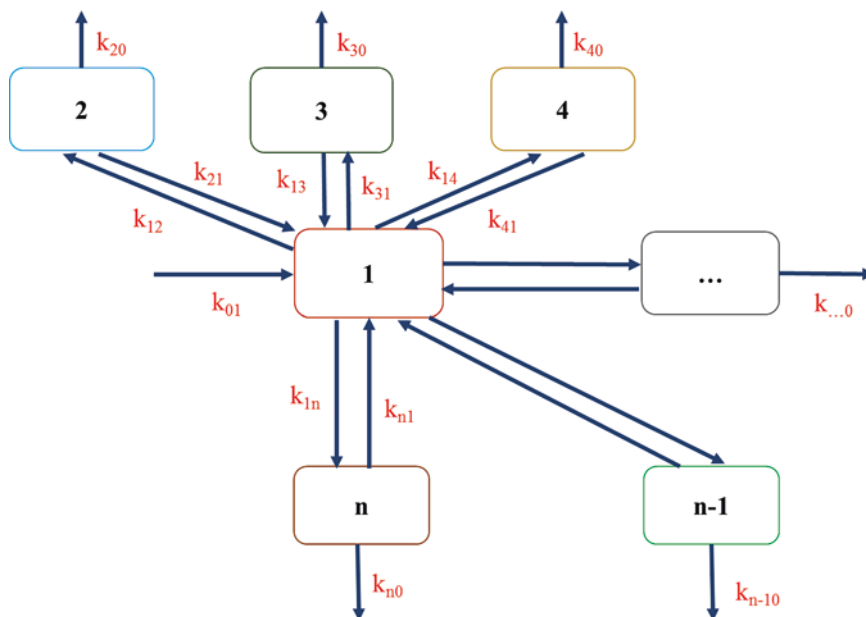


Fig. 4.3 Pictorial representation of a mammillary compartmental pharmacokinetic model

The PBPK modelling approach amalgamates various parameters on species physiology, drug-specific data and an understanding of all of the active processes affecting the drug's pharmacokinetics. There are various commercial PBPK modelling software such as GastroPlus (www.simulations-plus.com), Simcyp (www.simcyp.com), PKSIM (www.systemsnoiology.com/products/pk-sim.html), CLOEPK (<http://www.cyprotex.com/insilico/>), ADMEWORKS DDI Simulator (http://www.fqs.pl/chemistry_materials_life_science/products/ddi_simulator) and much more available for system-dependent parameters (e.g. blood flow, tissue volume, amount of microsomal protein per gram of liver, transporter abundance, enzyme and glomerular filtration) for the preclinical and the humans' species. One such example is PBPK models in humans specify ethnic population, which describes a system that accounts for covariation and variability between these parameters in the ethnic population. The physicochemical properties (basic or acidic nature of the drug, molecular weight, PK_a), permeability and solubility ($\log D$), drug deposition transporter, intrinsic clearance (CL_{int}) and blood cell and plasma protein binding

comprise the drug-dependent parameters. However, this approach may lack sufficient in vitro and in vivo data. The in silico models and in vitro assays determine all of these compound-specific parameters [26].

Structure of PBPK Models

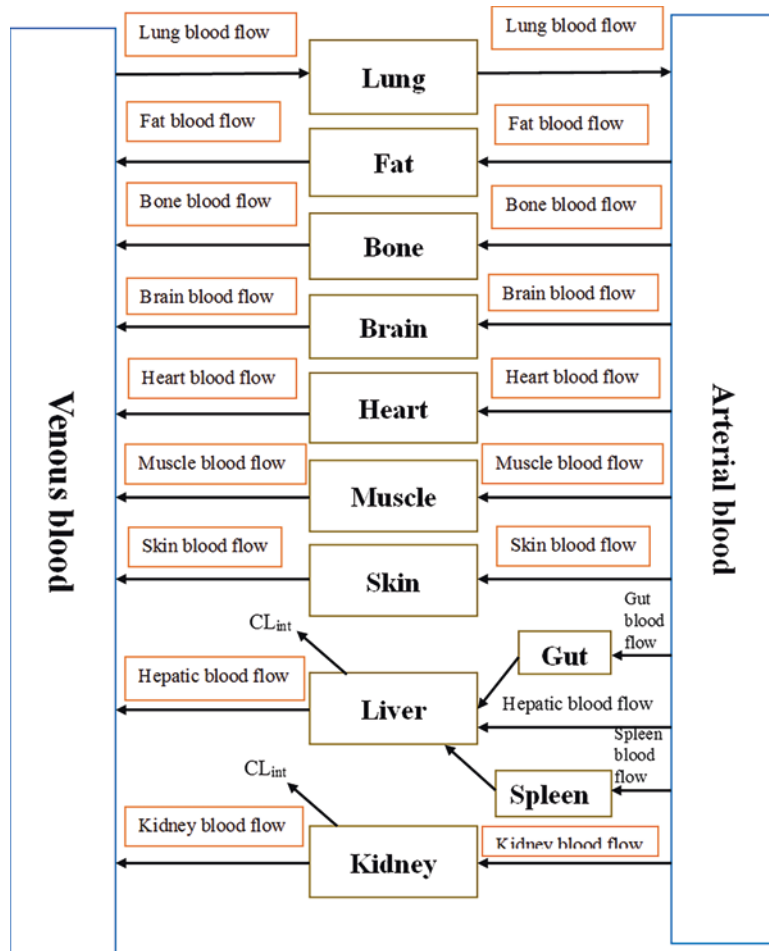
The PBPK modelling is ascribed as the mathematical model development for the drug uptake and disposition. It is dependent on the quantitative interrelations among the crucial biological parameters of these processes. The biological parameters are:

1. The partitioning of tissues due to the interaction of components of the tissue with the drug (P_{ka})
2. Rate of reactions due to enzymes
3. Physiological parameters (Q_i , V_i) [4]

A whole-body PBPK model has been developed by using four different steps, which are as follows:

1. The drug metabolic pathway and the compartment (organ) mathematical model description.

Fig. 4.4 Schematic structure of a PBPK model



2. The incorporation of various parameters, i.e. physicochemical, biological and physiological.
3. The simulation of a model involving the drug deposition and uptake by solving the equations of mass balance using numerical integration algorithm, i.e. the fourth-order Runge-Kutta method (analyse approximate solutions of an ordinary differential equation).
4. Finally, the model validation step includes the uncertainty analysis and parameter sensitivity analysis [27].

The first step in the model representation of whole-body PBPK is based on selecting admissible organs for the model. The blood compartment, kidney, adipose tissues or liver is

represented by the core tissues/organs, and the other drug-dependent tissues/organs include the skin, lung, brain or heart. Some organs are also anticipated in mass balance, such as the muscle, bone or skin [28]. However, appropriately modified PBPK models are derived if any compound is involved in enterohepatic cycling [29]. In the second step, every tissue compartment is subjected to mass balance differential equations incorporating parameters such as CL_{int} , permeability surface area product and biotransformation reaction (V_m/K_m). The following equation represents the principle of these equations:

$$\begin{aligned} \text{Rate of change of mass A in the system} = & \\ & \text{rate of gain of A} - \text{rate of loss of A} \pm \\ & \text{rate of gain or loss of A by reaction} \end{aligned}$$

In this step, each tissue or organ is denoted as perfusion rate-limiting tissue/organ or permeability rate-limiting tissue/organ (Fig. 4.5a, b) [30]. In perfusion rate limiting, the drug freely distributes in the physiological space. The movement of the drug in and out of the organ is controlled by the blood perfusion to the organ without any concentration gradient. In contrast, the latter limits the tissue or organ distribution, and the tissues are divided into two or three sub-compartments involving permeability as the rate-limiting steps between them. The blood drug concentration is not parallel with the tissue drug concentration (C_T), so the membrane-limited organ model is utilized.

Figure 4.5a shows the perfusion-limited uptake and illustrates that the tissue is considered homogeneous and C_T is in equilibrium with the drug concentration in venous blood leaving the

tissue; the following equation shows the rate of change of the drug in the whole tissue:

$$\frac{dAr}{dt} = V_r \frac{dcr}{dt} = Q_T (C_{a,bl} - C_{v,bl,T}) = Q_T [C_{a,bl} - C_T / Kp_{T:bl}]$$

where $C_{a,bl}$ and $C_{v,bl, T}$ are the concentration in arterial blood and venous blood leaving the tissue, respectively [32].

Figure 4.5b denotes the permeability rate-limited model or diffusion-limited uptake and expressed that the permeability surface area product (a mass transfer coefficient; PS_T) for the tissue is proportional to the movement of drug from tissue blood into the cellular matrix. Therefore, the rate of change of reaction is described by the following equation:

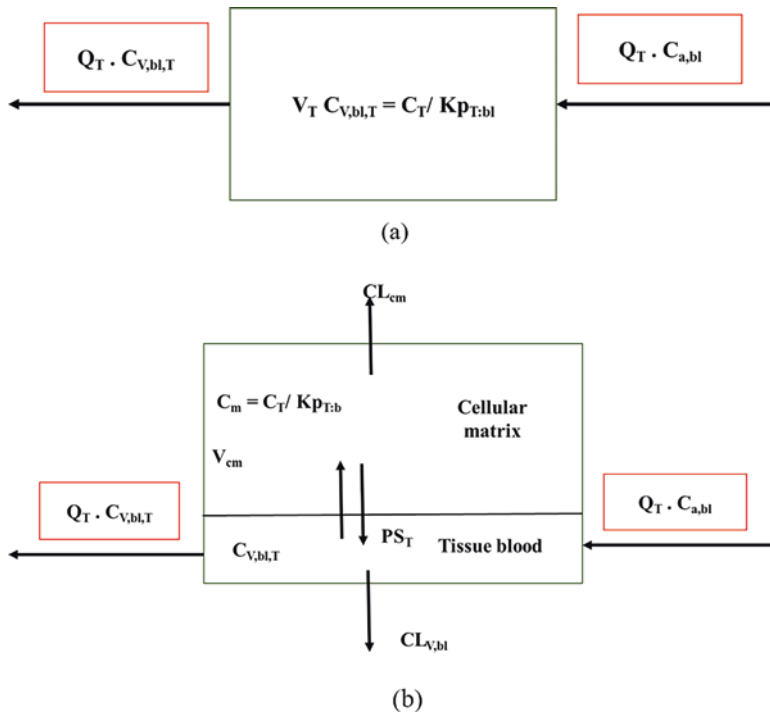


Fig. 4.5 (a) Schematic diagram of a perfusion rate-limited tissue or blood flow (Q_T)-limited organ. The concentration in venous blood leaving tissue ($C_{v,bl, T}$) is in equilibrium with the concentration in tissue (C_T). (b) Schematic diagram of a permeability rate-limited tissue or organ. The mass transfer coefficient (PS_T) is proportional to the movement of the drug from the tissue blood into a

cellular matrix. When $PS_T \ll Q_T$, the tissue uptake is diffusion-limited; A_T is the amount of tissue T ; $Kp_{T:bl}$ is the partition coefficient of drug between tissue and blood; $C_{a,bl}$ is the concentration in arterial blood; A_{cm} , C_{cm} and V_{cm} refer to the amount and concentration in cellular matrix; and $CL_{v,bl}$ and CL_{cm} are the clearance from tissue blood and cellular matrix [31]

$$dA_{cm} / C_T = V_{cm} \frac{dA_{cm}}{dt} = PS_T \cdot C_{v,bl,T} -$$

$$PS_T \cdot C_T / Kp_{T:bl} = PS_T \cdot \{C_{v,bl,T} - C_T / Kp_{T:bl}\}$$

where $\{C_{v,bl,T} - C_T / Kp_{T:bl}\}$ is the net flux from tissue blood [33].

IV Bolus Administration

One-Compartment Open Model IV Bolus

This is the easiest and simplest model by which drug distribution and elimination in the body can be explained thoroughly. In one-compartment IV bolus model, the body acts as a single compartment, and the entry and exit of drugs from the body becomes very facile. In this model, the whole drug enters into the blood directly, and the drug is also distributed through the blood circulation to all the tissues in the body. The blood flow to tissue and the drug's molecular weight are the dominant factors of drug concentration in several tissues or drug distribution in the body. The elimination of drugs occurs from the liver or the kidney after drug metabolism takes place. The apparent volume of distribution (V_d) plays a significant role in this model, which is described as the volume in which the drug is distributed within the body. Another parameter of this model is the elimination rate constant (k), which outlined the rate at which the drug concentration in the body reduces over time, and DB denotes the drug present in the body [34]. A one-compartment open model IV bolus has been illustrated in Fig. 4.6.

Henceforth, this model assumes that when the concentration of drug in plasma changes, drug concentration in the tissue will also change. The general equation of this model is as follows:

$$C = C_0 e^{-kt}$$

$$\text{or } \log C = \log C_0 - Kt / 2.303$$

where

C = plasma drug concentration of drug

C_0 = plasma drug concentration at $t = 0$

t = time

k = first-order elimination rate constant

However, to determine the volume of drug distribution in the body, it should be assumed that the drug present in the body depends on both concentration of drug in plasma and the fluid volume of the body in which the drug is distributed entirely.

Hence, drug in body = $V_d C$.

If the drug in the body is the IV dose, and AUC is area under the curve from $t = 0$ to $t = \infty$, then V_d becomes

$$V_d = C_0 / k [AUC]_0^\infty$$

Multicompartment IV Bolus

In two-compartment IV bolus, the plasma concentration-time curve of a drug indicates that the concentration of drug in plasma reduces as the sum of distribution and elimination. The administered drug is distributed between the peripheral and central compartments. The plasma concentration-time curve shows that the curve is split up into two phases: distribution and elimination. At the initial stage, $t = 0$, the drug distribution phase starts and shows the rapid decrease in the drug from the main to tissue compartment. After that, the drug enters the peripheral compartment and reaches a maximum level by maintaining equilibrium as the rate of the drug entered into tissues becomes uniform to the rate of exit from tissue. The decline of the drug in this phase follows a first-order process, which is called the elimination phase. The central com-



Fig. 4.6 Schematic diagram of one-compartment open model IV bolus administration

partment exhibits drug elimination in two-compartment models, and the binding sites of elimination are the kidney and liver, perfused with blood [35].

Intravenous (IV) Infusion Administration

IV infusion administration of drug is the slower administration into the blood through a vein at a constant rate (zero-order), which permits control of plasma drug concentration such as phenytoin, which is given slowly at a limit of 50 mg/min in adults. After drug administration via constant IV infusion, at $t = 0$, drug was not present in the body, but drug level increases until a constant or steady state has been reached. After the drug hit a steady state, the rate of absorption of drug into the body comes in equilibrium with the rate of elimination of drug from the body. The one-compartment IV infusion follows the zero-order absorption process and the first-order process [36]. The illustration of one-compartment IV infusion through a mathematical equation is as follows:

$$dD_B / dt = R - k C V_D$$

$$\text{or } C = [R / V_D k] (1 - e^{-kt})$$

where

R = rate of drug input

D_B = amount of drug in the body

At steady state, $C = C_{SS}$, and $t = \infty$, the equation becomes

$$C_{SS} = R / V_D k = R / \text{clearance}$$

Hence, for the two-compartment model of IV infusion, the drug in the tissue compartment is equal to the drug in plasma, and a steady-state concentration has been achieved. Then, the equation is expressed as

$$C = R / V_D k [1 - (k - b / a - b) e^{-kt} - (a - k / a - b) e^{-kt}]$$

At steady state, $t = \infty$, the equation becomes

$$C_{SS} = R / V_D k$$

Pharmacokinetics of Oral Absorption

The drug is also administered through the extravascular route, such as intramuscular, subcutaneous, oral or transdermal, besides the IV administration. In this route of administration, the drug is transferred from the absorption phase to the systemic circulation. The administration of drug via oral route is the most preferred route in recent times. The oral drug absorption would follow first-order kinetics unless it was verified using pharmacokinetic models that it is zero-order [36].

The plasma concentration -time curve of the oral route indicates an absorption phase with a first-order rate constant (K_a), and the rate of change in the drug amount is totally depends upon both the rate of absorption and rate of elimination of the drug. The plasma concentration of the drug that reaches a peak is denoted as C_{max} , and the time needed to reach that concentration is represented as T_{max} . The following equation expresses the change in the amount of drugs in the body:

$$dC / dt = dC_A / dt - dC_E / dt$$

Where, dC_A / dt = rate of drug absorption

dC_E / dt = rate of drug elimination from the body

The plasma-time curve of the drug via the oral route is divided into three parts:

- (i) The absorption phase, in which the rate of absorption of drug is greater than the rate of elimination of drug ($dC_A / dt > dC_E / dt$)
- (ii) The C_{max} phase, in which $dC_A / dt = dC_E / dt$
- (iii) The elimination phase, in which the rate of drug absorption of drug is less than the rate of elimination of drug ($dC_A / dt < dC_E / dt$) [37]

The pharmacokinetics of oral administration of the drug is based on two approaches:

1. Zero-order absorption model

It is already verified that the oral route of drug administration follows first-order kinetics, but the zero-order absorption model is also considered in some cases. The first case is if a carrier-mediated transport process is involved in the absorption of drug, and the second case is the absorption of controlled-release dosage forms.

The integrated mathematical equation for this model is described below:

$$C = K_A / \left[V_D \cdot k \left(1 - e^{-kt} \right) \right]$$

2. First-Order Absorption Model

The drugs administered through passive diffusion processes such as solutions and suspensions and the immediate release drugs like capsules and tablets follow first-order absorption kinetics. The integrated mathematical equation for the first-order absorption of the drug via the oral route is expressed as

$$C = \left[F \cdot K_A \cdot D_B / V_D \cdot (K_A - k) \right] \cdot \left(e^{-kt} - e^{-K_A t} \right)$$

where F = fraction of drug absorbed [37].

2.3 Non-compartmental Pharmacokinetics

The non-compartmental pharmacokinetics or the model-independent analysis is defined as the methods that are compiled from a kinetically homogeneous central compartment such as disposition decomposition analysis [38]. The non-compartmental approach is a pharmacokinetic analysis that involves identifying or assuming behavioural system properties rather than mechanistic ones, mathematic term expression of those behavioural properties and the exploitation of mathematical properties to label its applications.

The most crucial properties used in the non-compartmental analysis are as follows:

(a) Total clearance (CL_T), expressed as

$$CL_T = CL \cdot C_T$$

where CL = constant clearance concerning time

- (b) Linear time-invariant pharmacokinetics, which denotes the relationship between the input rate and systemic circulation has time invariance.
- (c) Existence of a terminal non-exponential phase in the systemic drug concentration-time course [38]

There are some other foremost properties involved in the non-compartmental approach, which are as follows:

- Mean residence time (MRT) = AUMC/AUC
- where AUMC is the area under the first moment curve
- Steady-state volume of distribution (V_{ss}) = MRT * CL
- Half-life ($t_{1/2}$) = slope of the natural log of the data [39]

There are various equations implied in the determination of various pharmacokinetic param-

Table 4.2 Equations employed for pharmacokinetic parameter determination

S. No.	Pharmacokinetic parameters	Formula
<i>Compartmental models</i>		
1.	1 CBM (IV bolus)	$C = C_0 e^{-kt}$
2.	1 CBM (IV infusion)	$C = k_0 / KV_D (1 - e^{-kt})$
3.	1 CBM oral	$C = K_A F X_0 / (K_A - k) V_D [e^{-kt} - e^{-K_A t}]$
<i>Non-compartmental models</i>		
4.	Area under curve	$[AUC]_0^t = 1/2 (C_1 + C_2) [t_2 - t_1]$
5.	The area under the first moment curve	$[AUMC]_0^t = 1/2 (C_1 t_1 + C_2 t_2) [t_2 - t_1]$
6.	Mean Residence Time (MRT)	$MRT = [AUMC]_0^\infty / [AUC]_0^\infty$
7.	Mean absorption time (MAT)	$MAT = [MRT]_{oral} - [MRT]_{iv}$
8.	Mean transit time (MTT)	$MTT = MAT + MRT$
9.	Mean residence number (MRN)	$MRN = MRT - MTT$

eters, which are summarized comprehensively in Table 4.2 [40].

3 Pharmacokinetic Evaluation of Nano-particulate Drug Delivery System

3.1 Solid Lipid Nanoparticles (SLNs)

There are various reports on the pharmacokinetic profile of SLNs having different routes of administration. The pharmacokinetics of SLNs is based on the discriminative quantification of free drug or the nanoparticle.

IV

The drug-loaded SLNs or free drug (IV administration) exhibits different pharmacokinetic profiles. The clearance reduces, plasma drug level increases and MRT of small-size SLNs enhances in comparison to the free drug due to the evading phagocytosis by reticuloendothelial system (RES) organs [41, 42]. Zara et al. reported that after the intake of doxorubicin-loaded SLNs, the plasma concentration of doxorubicin increases fivefold compared to the free doxorubicin and the high AUC, small V_D and low clearance rate [43, 44]. Chen et al. concluded that after the bolus administration of Brij 78-stabilized and F68-stabilized SLNs, the $t_{1/2}$ of paclitaxel was found to be 4.8 and 10.06 h, respectively, which indicated a slower elimination rate of paclitaxel from the body in comparison to free paclitaxel with a $t_{1/2}$ of 1.36 h [45]. The AUC of doxorubicin could be based on the number of stealth agents present in SLNs [43].

Oral

The oral administration of SLNs can improve various pharmacokinetic parameters of the drug, such as enhancement in bioavailability, improvement in lymphatic and transport and solubility of drugs [46, 47]. The oral administration of lovastatin-loaded SLNs leads to the increment in C_{max} and reduction in T_{max} of the drug compared to suspension of lovastatin

[48]. The pharmacokinetic profile of oral SLNs also showed that the emulsifying agent had a significant effect on the absorption of lovastatin [49].

Transdermal

The transdermal delivery of drug-loaded SLNs can prolong the action time of the drug. The nitrendipine-loaded SLNs were administered through transdermal route that exhibited a C_{max} similar to the oral administration of nitrendipine. However, a longer T_{max} (12 h) was observed compared to the oral administration of a drug (2 h). The transdermal administration of nitrendipine-loaded SLNs showed a sustained release profile with $t_{1/2}$ of 15.03 h compared to the oral administration (4.8 h) in rats [50].

3.2 Metallic Nanoparticles

The pharmacokinetics of these NPs is based on the size, surface charge, particle type, protein binding, dose, exposure route or surface coating. The dermal, oral or pulmonary absorption of metallic nanoparticles, i.e. gold nanoparticles (AuNPs), silver nanoparticles (AgNPs) or titanium oxide nanoparticles (TiO₂ NPs), is low. The smaller size and negative charge metallic NPs have high bioavailability. The AgNPs, AuNPs and TiO₂ NPs have oral absorption of about 0.01–5%, 1–4.2% and 0.01–0.05%, respectively. The blood-brain barrier penetration of AuNPs could be increased by coating with a neuropeptide. The metabolism of these metallic NPs is different from each other as AgNPs released Ag⁺ and reconstruct into AgNPs.

In contrast, in other metallic NPs, the peptide coating on the NP surface can be degraded in vitro. The metallic NPs tend to accumulate in the liver and spleen, which results in their low elimination from the urinary or biliary route. The $t_{1/2}$ of AgNPs via IV route was found to be threefold of the oral administration.

Most of the pharmacokinetic studies of metallic NPs do not reach the clinical phase and are only conducted in rodents. The plasma $t_{1/2}$ of AgNPs is threefold less in rats as compared to rabbits. Hence, the difference in species leads to

pharmacokinetic challenges in these NPs. Therefore, the pharmacokinetic studies of metallic NPs in larger animals or humans are necessary to improve results and reduce the concerned pharmacokinetic challenges [7].

3.3 Dendrimers

The dendrimers are branched molecules with nanodimensions, and some types of dendrimers are polyethyleneimine, poly-amidoamine (PAMAM), polypropyleneimine, etc. The administration route of dendrimers is IV or oral, and the surface charge is the most crucial parameter that affects the transepithelial permeability of oral drug-loaded dendrimers. Sadekar et al., in their study, concluded that PAMAM G4.0-NH₂ and G3.5-COONa contained an approximate two- to threefold which can enhance the oral absorption of camptothecin ($T_{max} = 2$ h) [51]. The use of permeability enhancers in the formation of dendrimers could also improve the pharmacokinetics of orally administered dendrimers. Yellepedi et al. prepared dendrimer-N-acetylcysteine (D-NAC) with Capmul MCM as a permeation enhancer. The study exhibited that 2% utilization of Capmul MCM improved the AUC of D-NAC by 1.5-fold. The Capmul also lowered the T_{max} of D-NAC by 2 h, which was 6 h without the permeation enhancer [52]. The pharmacokinetics of dendrimers has not been much widely discussed by experts till now. It needed more exposure in the future with analytical techniques for their

quantification and strategies for PBPK model establishment to understand the complexity of the GI absorption mechanism of dendrimers [53]. The types of nanoparticles with their pharmacokinetic consideration have been illustrated briefly in Table 4.3 [54].

3.4 Theranostic Nanoparticles

The theranostic nanoparticles belong to advanced nanotechnology and are utilized in drug delivery, disease diagnosis and disease biomarkers targeting at the molecular level. The theranostic nanoparticles emerged high surface area-to-volume ratio, which helps cross the biological barrier along with high permeability and minimum drug accumulation. The nanoparticles contain positive and negative charges on their surface. The positively charged nanoparticles indicate high uptake as compared to negatively charged surface NPs due to electrostatic interactions. The route of administration also affects the pharmacokinetics of theranostic nanoparticles. The oral administration of bovine insulin showed high bioavailability in comparison to the subcutaneously injected insulin in diabetics. It is needed to investigate the in vivo functionality of nanoparticles by biosample analysis with isolated toxic moieties or single cells. This can boost the pharmacokinetics and clinical benefits of theranostic nanoparticles [55].

Table 4.3 Types of drug-loaded nanoparticles with their pharmacokinetic considerations

Drug	Type of nanosystem	Route	Observed pharmacokinetics in vivo	References
Doxorubicin	Polylysine dendrimer	IV	Enhanced accumulation in tumour tissues	[30]
Piroxicam	Poly(amidoamine) dendrimer	IV	Prolonged systemic exposure	[32]
Curcumin	Nanocrystals	Oral	Improved oral bioavailability	[43]
Diclofenac	SoluMatrix™ technology	Oral	Faster absorption	[51]
Cyclosporin A	Self-emulsifying drug delivery system	Oral	Improved bioavailability	[58]
Amikacin	Liposomes	IV	Extended half-life	[29]
Clozapine	SLNs	IV	Decreased clearance	[59]
Lidocaine	SLNs	Dermal	Controlled dermal permeation and duration of action	[60]

3.5 Functionalized/Tailored Nanoparticles

Cheng et al. prepared polyacrylic acid and polyethylene glycol-incorporated functionalized nanoparticles and stated an increment in the blood circulation half-life of nanoparticles [56]. Guo et al. also reported high nanoparticle accumulation and improved pharmacokinetics of polyethylene glycol- and poly(lactic-co-glycolic acid)-loaded functionalized nanoparticles. Hence, the studies suggested that the tailoring of nanoparticles can alter the blood circulation, tissue targeting and drug loading of nanoparticles [57].

4 Future Prospects

The various pharmacokinetic models employed in the nanoparticulate drug delivery systems (NPDDS) serve various benefits in improving their physicochemical dynamics and possess several challenges related to a human health concern. There is a need for further research to identify all the factors related to pharmacokinetic consideration. Systematic clinical research based on different types of nanoparticles ranging from organic to inorganic is necessary. Until now, the research is only based on the preclinical level, which could not accurately justify the pharmacokinetics on humans due to differences in species morphology. Henceforth, the regulatory agencies have approved several kinds of nanoparticle-based drug delivery systems, which gives insight into the safety and efficacy of drugs compared to conventional dosage forms. The various pharmacokinetic models, especially the PBPK model, help in current treatment therapies to understand the drug safety profile in the body. Still, various challenges come with the benefits, i.e. cost-related factors, limited drug release and low drug targeting. The researchers are continuously working to overcome these utmost challenges related to the pharmacokinetics of nanoparticles, and there is an essential requirement of pharmacokinetic studies focused on the drug and nanoparticles. This approach might be given a better

understanding of the NPDDS and the fate of nanomedicine concerning human health.

5 Conclusion

This chapter has thoroughly described the basic theory and mathematical expressions of different pharmacokinetics using compartment and non-compartment modelling to evaluate NPDDS. The pharmacokinetic parameters play a pivotal role in the nanoparticle absorption, distribution, metabolism and elimination in the body. They help to identify the bioavailability and safety profile of a drug. However, pharmacokinetic modelling can improve the misconception of the concentration threshold of the nanoparticles. The new technology based on PBPK modelling illustrates the physicochemical properties of nano-drug delivery systems and their interactions with the physiological system. Hence, the research in pharmacokinetics is increasing daily and reporting a positive response about the understanding of what the body does to the nanoparticles after administering from different routes. Thus, there is still scope for immense research towards toxic material-loaded nanoparticles and their clinical development.

References

1. Mitragotri S, et al. Accelerating the translation of nanomaterials in biomedicine. *ACS Nano*. 2015;9(7):6644–54. <https://doi.org/10.1021/acsnano.5b03569>.
2. Elgrabli D, et al. Biodistribution and clearance of TiO₂ nanoparticles in rats after intravenous injection. *PLoS One*. 2015;10(4):1–13. <https://doi.org/10.1371/journal.pone.0124490>.
3. Peretz V, Motiei M, Sukenik CN, Popovtzer R. The effect of nanoparticle size on cellular binding probability. 2012;2012 <https://doi.org/10.1155/2012/404536>.
4. Li M, Al-jamal KT, Kostarelos K, Reineke J. Physiologically based pharmacokinetic modeling of nanoparticles. *ACS Nano*. 2010;4(11):6303–17.
5. Oliveira-nascimento L. Pharmacokinetic aspects of nanoparticle-in-matrix drug delivery systems for oral / Buccal delivery. 2019;10 <https://doi.org/10.3389/fphar.2019.01057>.
6. Yu R, Cao Y. A method to determine pharmacokinetic parameters based on andante constant-rate

- intravenous infusion. *Sci Rep.* 2017;1–8. <https://doi.org/10.1038/s41598-017-13437-6>.
7. Lin Z, Monteiro-Riviere NA, Riviere JE. Pharmacokinetics of metallic nanoparticles. *Wiley Interdiscip Rev Nanomedicine Nanobiotechnology.* 2015;7(2):189–217. <https://doi.org/10.1002/wnan.1304>.
 8. Yamaoka K, Nakagawa T, Uno T. Statistical moments in pharmacokinetics. *J Pharmacokinet Biopharm.* 1978;6(6):547–58. <https://doi.org/10.1007/BF01062109>.
 9. Dominguez R, Pomerene E. Calculation of the rate of absorption of exogenous creatinine. *Proc Soc Exp Biol Med.* 1945;60(2):173–81. <https://doi.org/10.3181/00379727-60-15130>.
 10. Xvii P. 4, 1967. 1967;(4):4–6.
 11. Takechi YTM, Uno C. NII-electronic library service. *Chem Pharm Bull.* 1994;17(11):1460–2. [Online]. Available: https://www.jstage.jst.go.jp/article/bpb1993/17/11/17_11_1460/_pdf-char/ja
 12. Lowenthal W, Vitsky BL. Computer program for a double exponential equation to determine biological constants. *J Pharm Sci.* 1967;56(2):169–73. <https://doi.org/10.1002/jps.2600560203>.
 13. Lin P, et al. Computational and ultrastructural toxicology of a nanoparticle, Quantum Dot 705, in mice. *Environ Sci Technol.* 2008;42(16):6264–70. <https://doi.org/10.1021/es800254a>.
 14. Lee HA, Leavens TL, Mason SE, Monteiro-Riviere NA, Riviere JE. Comparison of quantum dot biodistribution with a blood-flow-limited physiologically based pharmacokinetic model. *Nano Lett.* 2009;9(2):794–9. <https://doi.org/10.1021/nl803481q>.
 15. Pk S. Pharmacokinetics. 2016;(Iv) <https://doi.org/10.1016/B978-0-12-801076-1.00019-8>.
 16. VanDerMerwe D, Gehring R, Buur JL. Toxicokinetics. *Vet Toxicol.* 2012;37–47. <https://doi.org/10.1016/B978-0-12-385926-6.00003-X>.
 17. Costa S, Teixeira JP. Toxicology. *Encycl Toxicol Third Ed.* 2014;4:718–20. <https://doi.org/10.1016/B978-0-12-386454-3.00440-1>.
 18. Barbour NP, Lipper RA. Introduction to biopharmaceutics and its role in drug development. *Biopharm Appl Drug Dev.* 2008;1–25. https://doi.org/10.1007/978-0-387-72379-2_1.
 19. Atkinson AJ. *Clinical pharmacokinetics.* 3rd ed. Elsevier Inc.; 2007.
 20. Bruguerolle B. Clinical pharmacokinetics 35: 83-94, Aug 1998. *Clin Pharmacokinet.* 1998;35(2):83–94.
 21. Segre G. Pharmacokinetics-compartmental representation. *Pharmacol Ther.* 1982;17(1):111–27. [https://doi.org/10.1016/0163-7258\(82\)90049-3](https://doi.org/10.1016/0163-7258(82)90049-3).
 22. Fleishaker JC, Smith RB. Compartmental model analysis in pharmacokinetics. *J Clin Pharmacol.* 1987;27(12):922–6. <https://doi.org/10.1002/j.1552-4604.1987.tb05591.x>.
 23. Peng H, Cheung B. A review on pharmacokinetic modeling and the effects of environmental stressors on pharmacokinetics for operational medicine. *Def Res Dev Canada.* 2009;
 24. Chau NP. Linear n-compartment catenary models: formulas to describe tracer amount in any compartment and identification of parameters from a concentration-time curve. *Math Biosci.* 1985;76(2):185–206. [https://doi.org/10.1016/0025-5564\(85\)90004-5](https://doi.org/10.1016/0025-5564(85)90004-5).
 25. Holz M, Fahr A. Compartment modeling. *Adv Drug Deliv Rev.* 2001;48(2–3):249–64. [https://doi.org/10.1016/S0169-409X\(01\)00118-1](https://doi.org/10.1016/S0169-409X(01)00118-1).
 26. Zhuang X, Lu C. PBPK modeling and simulation in drug research and development. *Acta Pharm Sin B.* 2016;6(5):430–40. <https://doi.org/10.1016/j.apsb.2016.04.004>.
 27. Haddad S, Pelekis M, Krishnan K. A methodology for solving physiologically based pharmacokinetic models without the use of simulation softwares. *Toxicol Lett.* 1996;85(2):113–26. [https://doi.org/10.1016/0378-4274\(96\)03648-X](https://doi.org/10.1016/0378-4274(96)03648-X).
 28. Clewell HJ 3rd, Andersen ME, Wills RJ, Latriano L. A physiologically based pharmacokinetic model for retinoic acid and its metabolites. *J Am Acad Dermatol.* 1997;36(3 Pt 2):S77. [https://doi.org/10.1016/S0190-9622\(97\)70063-X](https://doi.org/10.1016/S0190-9622(97)70063-X).
 29. Ploeger B, Mensinga T, Sips A, Meulenbelt J, DeJongh J. A human physiologically-based model for glycyrrhizic acid, a compound subject to presystemic metabolism and enterohepatic cycling. *Pharm Res.* 2000;17(12):1516–25. <https://doi.org/10.1023/A:1007661209921>.
 30. Nasu R, Kumagai Y, Kogetsu H, Tsujimoto M, Ohtani H, Sawada Y. Physiologically based pharmacokinetic model for pralmorelin hydrochloride in rats. *Drug Metab Dispos.* 2005;33(10):1488–94. <https://doi.org/10.1124/DMD.104.001040>.
 31. Nestorov I. Whole body pharmacokinetic models. *Clin Pharmacokinet.* 2003;42(10):883–908. <https://doi.org/10.2165/00003088-200342100-00002>.
 32. Jones HM, Gardner IB, Watson KJ. Modelling and PBPK simulation in drug discovery. *AAPS J.* 2009;11(1):155. <https://doi.org/10.1208/S12248-009-9088-1>.
 33. Espié P, Tytgat D, Sargentini-Maier ML, Poggesi I, Watelet JB. Physiologically based pharmacokinetics (PBPK). *Drug Metab Rev.* 2009;41(3):391–407. <https://doi.org/10.1080/10837450902891360>.
 34. Ahmed TA. Pharmacokinetics of drugs following IV Bolus, IV infusion, and oral administration. *Basic Pharmacokinet Concepts Some Clin Appl.* 2015; <https://doi.org/10.5772/61573>.
 35. *An Introduction to Pharmacokinetics*, 2nd ed. Oxford: Blackwell Scientific. - Google Search. https://www.google.com/search?q=An+Introduction+to+Pharmacokinetics%2C+2nd+ed.+Oxford%3A+Blackwell+Scientific.&rlz=1C1CHBF_enIN882IN882&oq=An+Introduction+to+Pharmacokinetics%2C+2nd+ed.+Oxford%3A+Blackwell+Scientific.&aqs=chrome.69i57l1897j0j7&sourceid=chrome&ie=UTF-8. Accessed 20 Aug 2021.

36. Shargel L, Wu-Pong S, Yu A. Applied biopharmaceutics and pharmacokinetics, 5th edition, chapter 3, one compartment open model intravenous bolus. *Ann Intern Med.* 2004;94:826.
37. O. Access, We are IntechOpen, the world's leading publisher of Open Access books Built by scientists, for scientists TOP 1%.
38. Reidenberg MM. Trends in clinical pharmacokinetics. *Clin Pharmacokinet.* 1993;24(1):1–9. <https://doi.org/10.2165/00003088-199324010-00001>.
39. Noncompartmental Analysis. <https://cran.r-project.org/web/packages/ubiquity/vignettes/NCA.html>. Accessed 20 Aug 2021.
40. Raza K, Kumar P, Kumar N, Malik R. Pharmacokinetics and biodistribution of the nanoparticles. In: *Advances in nanomedicine for the delivery of therapeutic nucleic acids*. Elsevier Inc; 2017. p. 166–86.
41. Liu J, Zhu J, Du Z, Qin B. Preparation and pharmacokinetic evaluation of Tashinone IIA solid lipid nanoparticles. *Drug Dev Ind Pharm.* 2005;31(6):551–6. <https://doi.org/10.1080/03639040500214761>.
42. Li X, Wang D, Zhang J, Pan W. Preparation and pharmacokinetics of docetaxel based on nanostructured lipid carriers. *J Pharm Pharmacol.* 2010;61(11):1485–92. <https://doi.org/10.1211/JPP.61.11.0007>.
43. Zara GP, Cavalli R, Bargoni A, Fundarò A, Vighetto D, Gasco MR. Intravenous administration to rabbits of non-stealth and stealth doxorubicin-loaded solid lipid nanoparticles at increasing concentrations of stealth agent: pharmacokinetics and distribution of doxorubicin in brain and other tissues. *J Drug Target.* 2002;10(4):327–35. <https://doi.org/10.1080/10611860290031868>.
44. Zara GP, Cavalli R, Fundarò A, Bargoni A, Caputo O, Gasco MR. Pharmacokinetics of doxorubicin incorporated in solid lipid nanospheres (SLN). *Pharmacol Res.* 1999;40(3):281–6. <https://doi.org/10.1006/PHRS.1999.0509>.
45. Chen DB, Yang TZ, Lu WL, Zhang Q. In vitro and in vivo study of two types of long-circulating solid lipid nanoparticles containing paclitaxel. *Chem Pharm Bull (Tokyo).* 2001;49(11):1444–7. <https://doi.org/10.1248/CPB.49.1444>.
46. Varshosaz J, Tabbakhian M, Mohammadi MY. Formulation and optimization of solid lipid nanoparticles of buspirone HCl for enhancement of its oral bioavailability. *J Liposome Res.* 2010;20(4):286–96. <https://doi.org/10.3109/08982100903443065>.
47. Li HL, Zhao XB, Ma YK, Zhai GX, Li LB, Lou HX. Enhancement of gastrointestinal absorption of quercetin by solid lipid nanoparticles. *J Control Release.* 2009;133(3):238–44. <https://doi.org/10.1016/J.JCONREL.2008.10.002>.
48. Suresh G, Manjunath K, Venkateswarlu V, Satyanarayana V. Preparation, characterization, and in vitro and in vivo evaluation of lovastatin solid lipid nanoparticles. *AAPS PharmSciTech.* 2007;8(1):E162. <https://doi.org/10.1208/PT0801024>.
49. Chen C-C, Tsai T-H, Huang Z-R, Fang J-Y. Effects of lipophilic emulsifiers on the oral administration of lovastatin from nanostructured lipid carriers: physicochemical characterization and pharmacokinetics. *Eur J Pharm Biopharm.* 2010;74(3):474–82. <https://doi.org/10.1016/J.EJPB.2009.12.008>.
50. Bhaskar K, Mohan CK, Lingam M, Reddy VP, Venkateswarlu V, Rao YM. Development of Nitrendipine controlled release formulations based on SLN and NLC for topical delivery: in vitro and ex vivo characterization. *Drug Dev Ind Pharm.* 2008;34(7):719–25. <https://doi.org/10.1080/03639040701842485>.
51. Sadekar S, et al. Poly(amido amine) dendrimers as absorption enhancers for oral delivery of camptothecin. *Int J Pharm.* 2013;456(1):175–85. <https://doi.org/10.1016/J.IJPHARM.2013.07.071>.
52. Yellepeddi VK, et al. Pediatric oral formulation of dendrimer-N-acetyl-L-cysteine conjugates for the treatment of neuroinflammation. *Int J Pharm.* 2018;545(1–2):113–6. <https://doi.org/10.1016/J.IJPHARM.2018.04.040>.
53. Yellepeddi VK, Ghandehari H. Pharmacokinetics of oral therapeutics delivered by dendrimer-based carriers. *Expert Opin Drug Deliv.* 2019;16(10):1051–61. <https://doi.org/10.1080/17425247.2019.1656607>.
54. Onoue S, Yamada S, Chan HK. Nanodrugs: pharmacokinetics and safety. *Int J Nanomedicine.* 2014;9(1):1025–37. <https://doi.org/10.2147/IJN.S38378>.
55. Chen F, Ehlerding EB, Cai W. Theranostic nanoparticles. *J Nucl Med.* 2014;55(12):1919–22. <https://doi.org/10.2967/JNUMED.114.146019>.
56. Cheng L, Yang K, Shao M, Lu X, Liu Z. In vivo pharmacokinetics, long-term biodistribution and toxicology study of functionalized upconversion nanoparticles in mice. *Nanomedicine (Lond).* 2011;6(8):1327–41. <https://doi.org/10.2217/NNM.11.56>.
57. Guo J, et al. Aptamer-functionalized PEG-PLGA nanoparticles for enhanced anti-glioma drug delivery. *Biomaterials.* 2011;32(31):8010–20. <https://doi.org/10.1016/J.BIOMATERIALS.2011.07.004>.
58. Neslihan R, Benita GS. Self-emulsifying drug delivery systems (SEDDS) for improved oral delivery of lipophilic drugs. *Biomedicine & Pharmacotherapy* 2004;58(3):173–182. <https://doi.org/10.1016/j.biopha.2004.02.001>
59. Venkateswarlu V, Manjunath K. Preparation, characterization and in vitro release kinetics of clozapine solid lipid nanoparticles. *Journal of controlled release.* 2004;95(3):627–38.
60. Pathak P, Nagarsenker M. Formulation and evaluation of lidocaine lipid nanosystems for dermal delivery. *Aaps Pharmscitech.* 2009;(3):985–92.



Models Used in Pharmacodynamic Evaluation of Nanoparticulate Drug Delivery Systems (NPDDS)

5

Megha Joshi, Chander Parkash Dora,
Lokesh Kaushik, Jayvadan Patel, and Kaisar Raza

Contents

1	Introduction	70
2	Modeling Requirements	71
3	Pharmacodynamic Models	71
	References	76

Abstract

Pharmacodynamic models are an essential tool in clinical pharmacology for the prediction of safety and efficacy of drug molecule using the in vitro and in vivo data available from the previous studies. These models are based on the mathematical equations and are helpful in the development of new drugs and dosage forms as there were numerous difficulties associated with conducting the clinical trials like cost,

ethical issues, and adverse effects related to the study. The common types of pharmacodynamic models covered under this chapter are direct and indirect effect models. The direct model includes fixed effect model, linear model, log-linear model, E_{\max} model, and sigmoid E_{\max} model. The basic requirements for developing these models are the appropriate software and the expert analysts to develop and analyze the model. Currently, most of the drugs coming out of the pharmaceutical industry exhibit the issue of low solubility and insufficient bioavailability. Nanoparticulate drug delivery systems (NPDDS) are a newer approach for solving these problems of drug molecules. For speeding up the development of nanoformulations, pharmacodynamic models are also utilized. These models are utilized in the development of nanoparticles, liposomes, and nanogel. However, there is very less work done in utilizing the pharmacodynamic models in the development of NPDDS. Hence, there is a growing need in utilizing these models in the development of NPDDS to save the cost and time.

M. Joshi · C. P. Dora (✉)
M.M. College of Pharmacy, Maharishi
Markandeshwar (Deemed to be University), Mullana,
Ambala, Haryana, India

L. Kaushik (✉) · J. Patel
Nootan Pharmacy College, Faculty of Pharmacy,
Sankalchand Patel University, Visnagar, Mehsana,
Gujarat, India

K. Raza
Department of Pharmacy, School of Chemical
Sciences & Pharmacy, Central University of
Rajasthan,
Bandarsindri, Ajmer, Rajasthan, India

Keywords

Pharmacodynamic models · Nanoparticulate drug delivery system · PK/PD model

1 Introduction

Nowadays, Pharmacodynamic (PD) modeling and simulation are also an indispensable part of the drug development process along with Pharmacokinetic (PK) modeling. Using the modeling techniques, existing data can be utilized to provide the important information related to the safety and efficacy of the drug [1]. These models are based on the mathematical, numerical, and statistical techniques. Pharmacokinetics (PK) describes what the body does to the drug and mainly includes the study of absorption, distribution, metabolism, and excretion. Pharmacokinetic models are applied to predict the concentration of drug in the blood before its actual administration. PK model utilizes compartment and non-compartment modeling for the estimation of pharmacokinetic profile of drug. Different PK parameters are identified using this model, which include C_{max} , T_{max} , area under the curve, and clearance by plotting the concentration versus time graph [2]. To understand variation in data of different persons/patients due to their different physiological system, physiologically based pharmacokinetic models are introduced.

Physiologically based pharmacokinetic models are integral models in predicting the pharmacokinetic profile of a drug by incorporating the extensive information obtained from the in vitro/in silico data. Different information data values related to drug like molecular weight, partition coefficient, log partition coefficient, dissociation coefficient, distribution coefficient, plasma protein binding, and metabolism are required to initiate this modeling. Parameters related to the biological system were also added for adequate prediction which includes blood flow, organ composition, lymphatic flow, and organ volume [3]. Software used for the prediction of PBPK modeling and estimation of drug-

drug interactions are Simcyp[®], Gastroplus[®], PK-Sim[®] MoBi[®], and Cloe PK[®] [4].

On the other hand, pharmacodynamic models utilize the mathematical equations for the prediction of pharmacological effects [5]. These models can effectively predict the optimal dose regimen, safety, and efficacy of different drugs [6]. Moreover, they are also useful in the design and development of different drugs and their dosage forms as there are numerous difficulties in conducting the clinical trials due to the cost, ethical issues, reproducibility, and the adverse effects related to the study [7]. Serious implications and adverse effects are associated with the clinical trials of anticancer drugs because of their narrow therapeutic window [8]. Due to these reasons, there is a need for the prediction of effects by using the pharmacodynamic models. Pharmacodynamic and PK models are interrelated. As for the prediction of pharmacodynamic effects, firstly, we have to collect all the necessary information of pharmacokinetic profile of a drug. Only then we can predict the concentration versus pharmacological response [9]. The first step in the prediction of the pharmacological effects is the identification of the key parameters which can affect the in vivo profile. This helps in the easy prediction of the dose-response study by considering the different physiologic and pathologic conditions [10].

Pharmacodynamic modeling fastens the drug development process as it helps in the early decision-making. Prediction starts from the pre-clinical stage to the late phase III of clinical development [11]. The impact of the PD model depends on the availability of the quality data at every stage of the drug development [12]. Understanding of the mechanisms related to disease and identification of genetic polymorphism are very important as they affect the prediction of pharmacological response [13].

It was estimated that 70% of new drug candidates which are coming out of the pharmaceutical industries show poor aqueous solubility and belong to BCS class II [14], and the major obstacle involved is the permeation through the biological membrane which could be solved by formulating the nanoparticulate drug delivery

system (NPDDS). NPDDS is composed of the lipids or protein and has a size in the range of 10–1000 nm [15]. This helps in improvement of bioavailability of the drug. There are many drugs whose bioavailability issues are solved by formulating them into the NPDDS. Solid lipid nanoparticles of vinpocetine, micelles of paclitaxel-loaded Pluronic® P123/F127, nanoemulsion of ramipril, self-nanoemulsifying drug delivery system of rosuvastatin, polymeric nanoparticles of lorazepam, liposomes of ketoconazole, and nanocrystals of nitrendipine are the examples of NPDDS which are successfully utilized to solve the bioavailability issue of these drugs [16–22].

With the increase in the production of nanoformulations, there is a growing need to utilize the pharmacodynamic models to save the time by early prediction. Moreover, pharmacodynamic modeling system is applied to the formulation design of NPDDS like liposomes based on the preclinical data. Most of the drugs are modified by complexation and conjugation techniques by which the molecule becomes large in size and its prediction becomes difficult [23]. We have to collect the extensive data related to the drug profile and PK of the drug for correct prediction.

There is very less work done on the prediction of NPDDS by utilizing the pharmacodynamic models.

2 Modeling Requirements

Basic requirement in the development of pharmacodynamic models is the availability of the appropriate software, and there is a need of the analysts who have experience in the model development [24]. For developing the pharmacodynamic model, we require suitable pharmacokinetic data and molecular and cellular mechanisms related to the pharmacological/toxicological responses. There is a requirement of the quantitative measurements of the biomarkers that can describe the drug target interaction and the pharmacological effects. Data must cover the wide concentration range of dose and study duration [25].

3 Pharmacodynamic Models

Pharmacodynamic model is the quantitative relationship between the drug concentration and the pharmacological effect. PD models are broadly classified as simple direct effect model and indirect effect (non-steady-state) model. In direct effect model, the pharmacological effect is directly related to the drug concentration. This can be explained by taking the example of moxifloxacin. As the moxifloxacin concentration increases, there is correspondence increase in the QT interval [26]. In indirect effect model, drug does not have a direct impact on the pharmacodynamic response. In pharmacodynamic study of warfarin, with increase in the concentration of warfarin, firstly, there is inhibition of the prothrombin synthesis which further produces anticoagulant effect [27].

Simple direct effect model mainly involves five types of model, i.e., fixed effect, linear, log-linear, E_{\max} model, and sigmoid E_{\max} model as described in Fig. 5.1.

3.1 Fixed Effect Model

This model is also known as a quantal effect model. The drug response may vary from person to person, and this model is helpful in describing whether the response for a particular drug concentration is present or not. In that case, logistic regression analysis has been utilized to derive the concentration versus response or no response. It is not based on the intensity of the dose and response study but on the frequency in which response is present [28]. Minimum alveolar concentration was determined by utilizing this method. Clinical dose was given to the large number of subjects and quantal response was noted and linear regression was applied to note the relationship between dose and response [29].

3.2 Linear Model

The linear model explains the direct relationship between the drug concentration and the pharma-

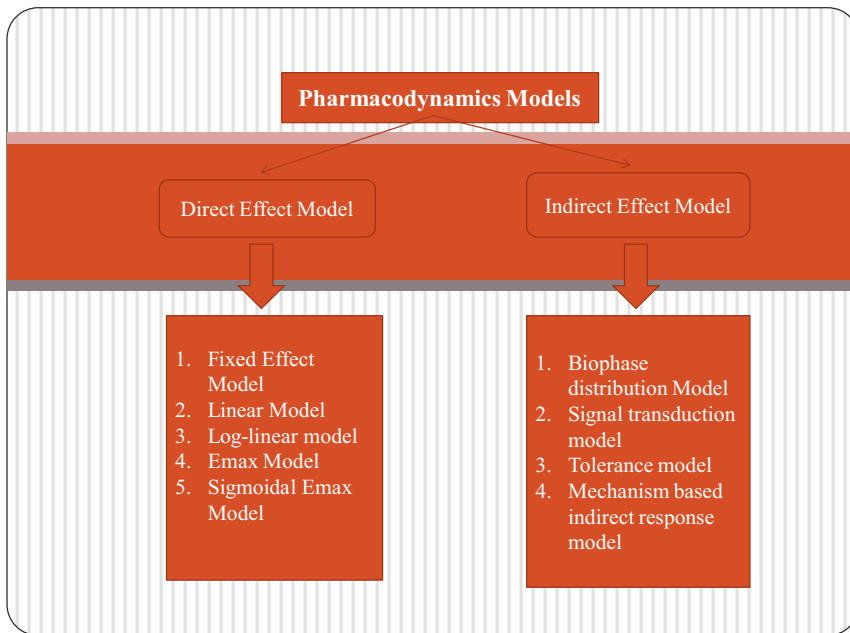


Fig. 5.1 Different types of pharmacodynamic mode

cological effect of the drug [30]. This is expressed in Eq. (5.1):

$$E \propto C \quad (5.1)$$

$$E = S \times C \quad (5.2)$$

where E is the effect of drug, C is the drug concentration, and S is the slope obtained from the effect vs. concentration graph shown in Fig. 5.2a.

In case of the baseline effect, model may be represented as

$$E = E_0 + S * C \quad (5.3)$$

where E_0 = effect when the concentration is zero.

This is a simple model, and parameters can be easily estimated by linear regression. However, this model does not predict the maximum effect. In the pharmacodynamic study of rivaroxaban, a direct factor Xa inhibitor shows linear relationship of dose versus response with the increase in concentration. Prothrombin time increases with increase in the concentration of the rivaroxaban [31].

3.3 Log-Linear Model

Log-linear model can be considered as a special case of the E_{\max} model because it shows linearity only in a certain concentration range from 20% to 80%. Because of the logarithmic function, the pharmacological effect cannot be estimated when the drug concentration is zero or when the concentration is maximum [32]. This model can be used for the interpolation but not for the extrapolation of data. As compared to linear model, it is applicable over the large concentration range. This model is shown in Fig. 5.2b:

$$E = E_0 + S * \log C \quad (5.4)$$

where

E = pharmacological effect of drug

E_0 = baseline effect (when no drug is present)

C = drug concentration

S = slope of the relationship

In the study of bosutinib for the treatment of chronic myeloid leukemia, it was found there is a

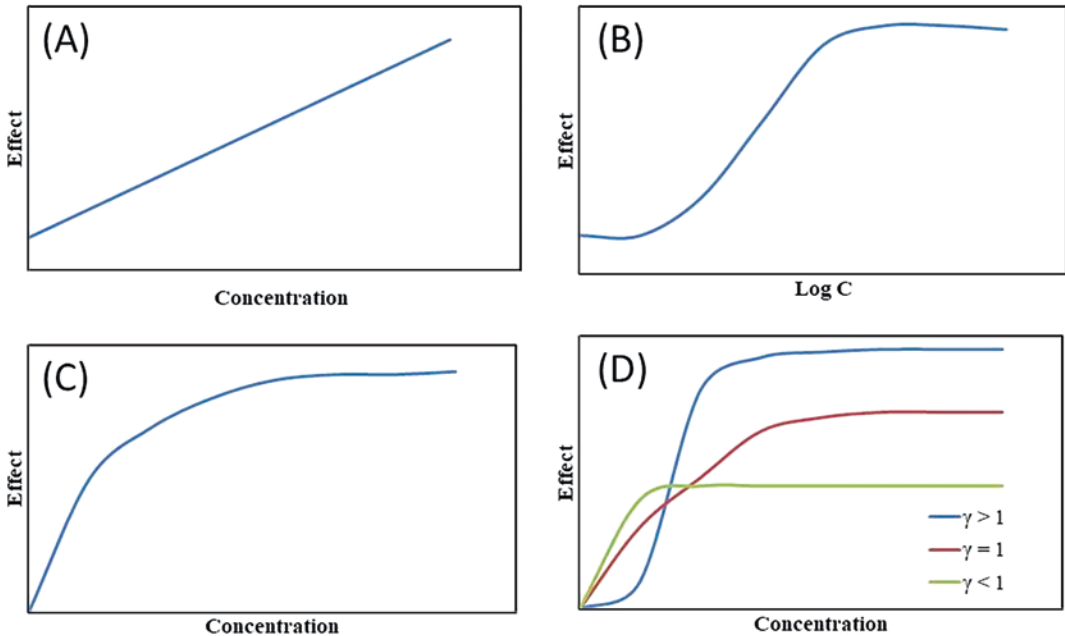


Fig. 5.2 Pharmacodynamic models: (a) Linear model, (b) log-linear model, (c) E_{\max} model, and (d) sigmoidal E_{\max} model

log-linear relationship between the concentration and response [33].

$$E = \frac{E_{\max} C}{EC_{50} + C} \quad (5.5)$$

3.4 E_{\max} Model

This model was derived from the drug-receptor interaction. It explains the interaction of the drug with the receptor site to produce the pharmacological effect [34]. This model carries two important properties: firstly, it predicts the maximum effect a drug can have, i.e., E_{\max} , and it also predicts the zero-order effect when there is no drug present. The effect depends on the number of receptor sites occupied by the drug molecules. It shows maximum effect when all the receptor sites are occupied and when half of the receptor sites are occupied; then, it produces half of the maximum effect (E_{50}). The curve obtained between pharmacological response and drug concentration is hyperbolic in shape. The software used in the prediction is GraphPad Prism [35]:

where E_{\max} is the maximum effect, C is the concentration, and EC_{50} is the concentration necessary to produce 50% of maximum effect. This is described in Fig. 5.2c.

For further improvement in the equation, baseline effect, i.e., E_0 , was added in the equation which is required for baseline physiological conditions:

$$E = E_0 + \frac{E_{\max} C}{EC_{50} + C} \quad (5.6)$$

In the formulation of nanoparticles of paclitaxel for tumor-targeted drug delivery for the treatment of lung cancer, the tumor inhibition was explained by the E_{\max} model. There is complex mechanism involved in the nano-mesenchymal stem cells which make it difficult to translate an effective pharmacodynamic response [36].

3.5 Sigmoidal E_{\max} Model

This model was given by Hill which describes the pharmacodynamics of many drugs by plotting the curve between the pharmacological response and drug concentration. The curve obtained was sigmoidal in shape rather than the hyperbolic curve as seen in case of simple E_{\max} model [37]. Model was based on the ligand binding theory in which receptor has a multiple drug binding sites. For that, Hill coefficient factor was introduced.

The equation for sigmoid E_{\max} model is generalized from E_{\max} model and described in Eq. (5.6):

$$E = \frac{E_{\max} \cdot C^\gamma}{EC_{50}^\gamma + C^\gamma} + E_0 \quad (5.7)$$

where γ value represents the steepness of the curve and its value affects the slope of the curve.

$\gamma = 1$ represents the hyperbolic curve.

$\gamma > 1$ represents the steeper curve.

$\gamma < 1$ represents the smoother curve.

This is explained by the graph in Fig. 5.2d.

PK/PD modeling helps in the selection of the opioids for clinical use because of the advanced understanding of the time and effect relationship after using different dosage regimens. Different EEG-derived parameters like pupil size and pain are utilized to assess the opioids. Analgesic effect of the opioids can be described by the sigmoidal model. Pain relief depends on the concentration of the opioids at the site of action. Effect on pupil diameter after consuming R-methadone was also described using this model [38].

Mohammed and his coworkers used pharmacodynamic model for the estimation of skin absorption of tenoxicam through transdermal delivery of nanogel formulation. They use pure tenoxicam and solid lipid nanoparticles of tenoxicam, and pharmacodynamic model was applied to the rat paw model by converting concentration into the mathematical expressions. It was found that the concentration absorption from the solid lipid nanoparticles was much more than the plain

drug. This was described by the sigmoidal model of pharmacodynamics [39].

3.6 Essential Indirect Response Models

An essential physiologic representation for drugs that construct pharmacological effects by indirect process is shown in Fig. 5.3. In this model, the starting material is converted into or showed as the rejoinder unpredictable or mediator which, in order, is then aloof from the system. Drugs by indirect actions can construct their special effects by the action on one or more of the indicated process shown in this model. The agent can be responsible for inhibition or stimulation of the secretion or synthesis of the response results or of its removal or of processes leading to the production of starter.

Four basic indirect pharmacodynamic response (IDR) models were planned and described to characterize the pharmacodynamic responses of drug molecule with no direct mechanisms of action [40, 41]. The basic premise of these IDR models is that the measured response (R) to a drug is produced by an indirect mechanism. The rate of change of the response over time with no drug present can be described as

$$\frac{dr}{dt} = K_{in} - K_{out} \cdot R \quad (5.8)$$

k_{in} is zero-order reaction rate constant of the production of response.

k_{out} is first-order reaction rate constant of the loss of response.

R is a response variable.

It is tacit that k_{in} , k_{out} is completely responsible for the loss and production of the responses. Equation (5.8) cannot be completely unified exactly and thus must use another equation to solve the integration algorithms.

Models I and II are showing the parameters and factors controlling drug response. Inhibition responses are calculated by Eq. (5.9):



Fig. 5.3 Representation of indirect pharmacodynamic responses

<p>I Inhibition- k_{in}^0</p> $\frac{dR}{dt} = k_{in}^0 \cdot \left(1 - \frac{I_{max} \cdot C_p}{IC_{50} + C_p} \right) - K_{out} \cdot R$ <p>$0 < I_{max} \leq 1$</p>	<p>III Stimulation- k_{in}^0</p> $\frac{dR}{dt} = k_{in}^0 \cdot \left(1 + \frac{S_{max} \cdot C_p}{SC_{50} + C_p} \right) - K_{out} \cdot R$ <p>$S_{max} > 0$</p>
<p>II Inhibition- K_{out}</p> $\frac{dR}{dt} = k_{in}^0 - K_{out} \cdot \left(1 - \frac{I_{max} \cdot C_p}{IC_{50} + C_p} \right) \cdot R$ <p>$0 < I_{max} \leq 1$</p>	<p>IV Stimulation- K_{out}</p> $\frac{dR}{dt} = k_{in}^0 - K_{out} \cdot \left(1 + \frac{S_{max} \cdot C_p}{SC_{50} + C_p} \right) \cdot R$ <p>$S_{max} > 0$</p>

Inhibition function $I(t) = 1 - \frac{I_{max} \cdot C_p}{IC_{50} + C_p}$ (5.9)

I_{max} , plasma drug concentration C_p , and IC_{50} values control the dynamic responses or functions. I_{max} is the maximum partial capability of the drug to affect the zero-order and first-order response reaction; this is always equal or less than one unit. Half-maximal inhibitory concentration (IC_{50}) is the most widely used and informative measure of a drug’s efficacy. It indicates how much drug is needed to inhibit a biological process by half, thus providing a measure of potency of an antagonist drug in pharmacological research. C_p value is representing the pharmacokinetic of the drug.

Model I is showing drug response by the inhibition of the production response variable factor (k_{in}). Inhibition in the form of I_{max} and IC_{50} value is

$$\frac{dr}{dt} = K_{in} \cdot I(t) - K_{out} \cdot R$$
 (5.10)

In model I, plasma drug concentration is more (i.e., $C_p \gg \gg IC_{50}$), IC_{50} value turns into the insignificant value, and C_p value is very less, and if $I_{max} = 1$, then $I(t) = 0$. At high plasma drug concentration, the zero-order reaction constant is zero; hence, there is full obstruction of the making of the response variable. When plasma con-

centrations turn down to low values, C_p would be below IC_{50} ($C_p \ll \ll IC_{50}$). When that happens, drug effect would be zero and $I(t) = 1$, meaning k_{in} would be converted in full value.

The whole system converts in its baseline by the rate constant refilling the pharmacodynamic section by the drug response variables.

Model II reports drug response ensuing from inhibition of the factors overriding the indulgence of response variable (k_{out}). Inhibition with an IC_{50} is measured to act on k_{out} according to:

$$\frac{dr}{dt} = K_{in} - K_{out} \cdot I(t) R$$
 (5.11)

$I(t)$ is the function shown as Eq. (5.9).

Models III and IV characterize processes that stimulate the variables or factors controlling drug response, where stimulation processes function according to

$$S(t) = 1 + \frac{S_{max} \cdot C_p}{SC_{50} + C_p}$$
 (5.12)

SC_{50} = the drug concentration showing 50% of the maximum stimulation target at the effect site.

S_{max} can be any number greater than zero. All these parameters are described in Table 5.1.

Model III describes drug response resulting from stimulation of the factors regulating the pro-

Table 5.1 Estimation of indirect response model parameter profile

Parameter	Model I	Model II	Model III	Model IV
I_{\max} or S_{\max}	$(R_0 - R_{\max})/R_0$	$(R_{\max} - R_0)/R_{\max}$	$(R_{\max} - R_0)/R_0$	$(R_0 - R_{\max})/R_{\max}$
k_{in}	$-S_f/I_{\max}$	S_f/I_{\max}	S_f/S_{\max}	$-S_f/S_{\max}$
k_{out}	k_{in}/R_0	k_{in}/R_0	k_{in}/R_0	k_{in}/R_0
IC ₅₀ or SC ₅₀	$C_{R_{\max}} \cdot (R_{\max} - (1 - I_{\max}) \cdot R_0) / (R_0 - R_{\max})$	$C_{R_{\max}} \cdot (R_0 - (1 - I_{\max}) \cdot R_{\max}) / (R_{\max} - R_0)$	$C_{R_{\max}} \cdot (R_0 \cdot (1 - S_{\max}) - R_{\max}) / (R_{\max} - R_0)$	$C_{R_{\max}} \cdot (R_{\max} \cdot (1 + S_{\max}) - R_0) / (R_0 - R_{\max})$

Measured characteristics [42]

duction of the response variable. Stimulation with SC₅₀ is considered to act on k_{in} according to:

$$\frac{dr}{dt} = K_{in} \cdot S(t) - K_{out} \cdot R \quad (5.13)$$

Model IV describes drug response ensuing from stimulation of the factors calculating or controlling the indulgence of the response variable. Stimulation with SC₅₀ is measured to act on k_{out} according to

$$\frac{dr}{dt} = K_{in} - K_{out} S(t) \cdot R \quad (5.14)$$

The area between the baseline and effect curve (ABEC) can be considered as a summing up parameter to differentiate the overall outcome of drug:

$$ABEC = R_0 \cdot t_T - AUEC_0 - t_r \quad (5.15)$$

R_0 = baseline value, AUEC = area under or over the response vs. time plot (time interval 0 to t), value of t assumed ∞

References

- Sheiner LB, Steimer JL. Pharmacokinetic/pharmacodynamic modeling in drug development. *Annu Rev Pharmacol Toxicol.* 2000;40(1):67–95.
- Urso R, Blardi P, Giorgi G. A short introduction to pharmacokinetics. *Eur Rev Med Pharmacol Sci.* 2002;6:33–44.
- Zhuang X, Lu C. PBPK modeling and simulation in drug research and development. *Acta Pharm Sin B.* 2016;6(5):430–40.
- Min JS, Bae SK. Prediction of drug–drug interaction potential using physiologically based pharmacokinetic modeling. *Arch Pharm Res.* 2017;40(12):1356–79.
- Gambús PL, Trocóniz IF. Pharmacokinetic–pharmacodynamic modelling in anaesthesia. *Br J Clin Pharmacol.* 2015;79(1):72–84.
- Derendorf H, Lesko LJ, Chaikin P, Colburn WA, Lee P, Miller R, Powell R, Rhodes G, Stanski D, Venitz J. Pharmacokinetic/pharmacodynamic modeling in drug research and development. *Curr Rev Clin Exp Pharmacol.* 2000;40(12):1399–418.
- Singh VP, Pratap K, Sinha J, Desiraju K, Bahal D, Kukreti R. Critical evaluation of challenges and future use of animals in experimentation for biomedical research. *Int J Immunopathol Pharmacol.* 2016;29(4):551–61.
- Byun JH, Han DG, Cho HJ, Yoon IS, Jung IH. Recent advances in physiologically based pharmacokinetic and pharmacodynamic models for anticancer nanomedicines. *Arch Pharm Res.* 2020;43(1):80–99.
- Yassen A, Olofson E, Romberg R, et al. Mechanism-based PK/PD modeling of the respiratory depressant effect of buprenorphine and fentanyl in healthy volunteers. *Clin Pharmacol Ther.* 2007;81(1):50–8.
- Zou H, Banerjee P, Leung SS, Yan X. Application of pharmacokinetic-pharmacodynamic modeling in drug delivery: development and challenges. *Front Pharmacol.* 2020;11:997.
- Rajman I. PK/PD modelling and simulations: utility in drug development. *Drug Discov Today.* 2008;13(7–8):341–6.
- Chien JY, Friedrich S, Heathman MA, de Alwis DP, Sinha V. Pharmacokinetics/pharmacodynamics and the stages of drug development: role of modeling and simulation. *AAPS J.* 2005;7(3):E544–59.
- Chaikin P, Rhodes GR, Bruno R, Rohatagi S, Natarajan C. Pharmacokinetics/pharmacodynamics in drug development: an industrial perspective. *J Clin Pharmacol.* 2000;40(12):1428–38.
- Khadka P, Ro J, Kim H, et al. Pharmaceutical particle technologies: an approach to improve drug solubility, dissolution and bioavailability. *Asian J Pharm Sci.* 2014;9(6):304–16.
- Saha RN, Vasanthakumar S, Bende G, Snehalatha M. Nanoparticulate drug delivery systems for cancer chemotherapy. *Mol Membr Biol.* 2010;27(7):215–31.
- Luo Y, Chen D, Ren L, Zhao X, Qin J. Solid lipid nanoparticles for enhancing vinpocetine's oral bioavailability. *J Control Release.* 2006;114(1):53–9.
- Wei Z, Hao J, Yuan S, et al. Paclitaxel-loaded Pluronic P123/F127 mixed polymeric micelles: formulation, optimization and in vitro characterization. *Int J Pharm.* 2009;376(1–2):176–85.

18. Shafiq S, Shakeel F, Talegaonkar S, Ahmad FJ, Khar RK, Ali M. Development and bioavailability assessment of ramipril nanoemulsion formulation. *Eur J Pharm Biopharm.* 2007;66(2):227–43.
19. Sharma D, Maheshwari D, Philip G, et al. Formulation and optimization of polymeric nanoparticles for intranasal delivery of lorazepam using Box-Behnken design: in vitro and in vivo evaluation. *Biomed Res Int.* 2014;2014:156010.
20. Ahsan MN, Prasad Verma PR. Solidified self-nano-emulsifying drug delivery system of rosuvastatin calcium to treat diet-induced hyperlipidemia in rat: in vitro and in vivo evaluations. *Ther Deliv.* 2017;8(3):125–36.
21. Patel R, Patel H, Baria A. Formulation and evaluation of liposomes of ketoconazole. *Int J Drug Deliv Technol.* 2009;1(1):16–23.
22. Quan P, Xia D, Piao H, et al. Nitrendipine nanocrystals: its preparation, characterization, and in vitro–in vivo evaluation. *AAPS PharmSciTech.* 2011;12(4):1136–43.
23. Burman CF, Hamrén B, Olsson P. Modelling and simulation to improve decision-making in clinical development. *Pharm Stat.* 2005;4(1):47–58.
24. He H, Yuan D, Wu Y, Cao Y. Pharmacokinetics and pharmacodynamics modeling and simulation systems to support the development and regulation of liposomal drugs. *Pharmaceutics.* 2019;11(3):110.
25. Felmler MA, Morris ME, Mager DE. Mechanism-based pharmacodynamic modeling. In: *Computational toxicology*. Totowa: Humana Press; 2012. p. 583–600.
26. Grosjean P, Urien S. Reevaluation of moxifloxacin pharmacokinetics and their direct effect on the QT interval. *J Clin Pharmacol.* 2012;52(3):329–38.
27. Kim S, Gaweda AE, Wu D, Li L, Rai SN, Brier ME. Simplified warfarin dose–response pharmacodynamic models. *Biomed Eng.* 2015;27(01):1550001.
28. Meibohm B, Derendorf H. Basic concepts of pharmacokinetic/pharmacodynamic (PK/PD) modelling. *Int J Clin Pharmacol Ther.* 1997;35(10):401–13.
29. Hannam JA, Anderson BJ. Pharmacodynamic interaction models in pediatric anesthesia. *Paediatr Anaesth.* 2015;10:970–80.
30. Derendorf H, Lesko LJ, Chaikin P, et al. Pharmacokinetic/pharmacodynamic modeling in drug research and development. *J Clin Pharmacol.* 2000;40(12):1399–418.
31. Mueck W, Eriksson BI, Bauer KA, et al. Population pharmacokinetics and pharmacodynamics of rivaroxaban—an oral, direct factor Xa inhibitor—in patients undergoing major orthopaedic surgery. *Clin Pharmacokinet.* 2008;47(3):203–16.
32. Pérez-Urizar J, Granados-Soto V, Flores-Murrieta FJ, Castañeda-Hernández G. Pharmacokinetic-pharmacodynamic modeling: why? *Arch Med Res.* 2000;31(6):539–45.
33. Hsyu PH, Mould DR, Upton RN, Amantea M. Pharmacokinetic–pharmacodynamic relationship of bosutinib in patients with chronic phase chronic myeloid leukemia. *Cancer Chemother Pharmacol.* 2013;71(1):209–18.
34. Ploeger BA, van der Graaf PH, Danhof M. Incorporating receptor theory in mechanism-based pharmacokinetic-pharmacodynamic (PK-PD) modeling. *Drug Metab Pharmacokinet.* 2009;24(1):3–15.
35. Finlay DB, Duffull SB, Glass M. 100 years of modeling ligand–receptor binding and response: a focus on GPCRs. *Br J Pharmacol.* 2020;177(7):1472–84.
36. Cheng S, Nethi SK, Al-Kofahi M, Prabha S. Pharmacokinetic—pharmacodynamic modeling of tumor targeted drug delivery using nano-engineered mesenchymal stem cells. *Pharmaceutics.* 2021;13(1):92.
37. Thomas N. Hypothesis testing and Bayesian estimation using a sigmoid E max model applied to sparse dose-response designs. *J Biopharm Stat.* 2006;16(5):657–77.
38. Lötsch J. Pharmacokinetic–pharmacodynamic modeling of opioids. *J Pain Symptom Manag.* 2005;29(5):90–103.
39. Elkomy MH, El Menshawe SF, Eid HM, Ali AM. Development of a nanogel formulation for transdermal delivery of tenoxicam: a pharmacokinetic–pharmacodynamic modeling approach for quantitative prediction of skin absorption. *Drug Dev Ind Pharm.* 2017;43(4):531–44.
40. Dayneka NL, Garg V, Jusko WJ. Comparison of four basic models of indirect pharmacodynamic responses. *J Pharmacokinet Biopharm.* 1993;21(4):457–78.
41. Sharma A, Jusko WJ. Characterization of four basic models of indirect pharmacodynamic responses. *J Pharmacokinet Biopharm.* 1996;24(6):611–35.
42. Sharma A, Jusko WJ. Characteristics of indirect pharmacodynamic models and applications to clinical drug responses. *Br J Clin Pharmacol.* 1998;45(3):229–39.



Preclinical Animal Models for the Experimental Design of Pharmacokinetic Studies with Nanoparticulate Drug Delivery Systems

Aishwarya Deshmukh, Jayvadan K. Patel, and Yashwant V. Pathak

Contents

1	Introduction	80
2	Nanotechnology in Drug Delivery	82
3	PK Aspects	83
4	The PK Profile of the Drug	86
5	PK Models	88
6	Modelling Drug Release	96
7	IVIVC	96
8	Summary	97
	References	97

Abstract

A comprehensive investigation of disposition and pharmacokinetic (PK) behaviours is a dire step in the translation of nanomaterial studies from preclinical animal studies to humans. Disposition and PK data are exploited to eval-

uate the systemic exposure and effects of nanomaterials which are principal contributing factor of the potential toxicity and therapeutic efficacy of nanoparticulate drug delivery systems (NPDDS). NPDDS exhibits an exceptional challenge for investigations pertaining to disposition and PK due to their extended circulation times, nonlinear PK profiles and broad distribution patterns. Studies are lacking for predicting and extrapolating associations between nanomaterial physicochemical properties and their in vivo behaviours and further are bewildered by various differences in the context to anatomy, physiology and immunology amongst preclinical animal models and clinical settings. Imprecise assumptions of disposition, PK and toxicoki-

A. Deshmukh (✉)

Smt. Kashibai Navale College of Pharmacy,
Pune, Maharashtra, India

J. K. Patel

Nootan Pharmacy College, Faculty of Pharmacy,
Sankalchand Patel University,
Visnagar, Gujarat, India

Y. V. Pathak

College of Pharmacy, University of South Florida
Health, Tampa, FL, USA

netic profile through species can impact non-clinical toxicity studies as well as clinical phase 1 trials detrimentally, if these encounters are implicated appropriately. Thus, experimental design of PK studies with NPDDS should be explored and highlighted. Providentially, with the extensive progress in NPDDS, much consideration is given by researchers for PK evaluations as a dominant part of the study of these systems. Since absorption, distribution, metabolism and excretion (ADME) is required to be considered from the early stages of the system design to the final clinical evaluations for the accomplishment of any therapeutic goal(s) by a novel drug delivery system, broad acquaintance of the PK aspects related to ADME becomes vital measure of research in this field.

Keywords

NPDDS · ADME · In vitro/in vivo correlation · PBPK · IVIVC

1 Introduction

The use of pharmacologically active agents systemically, though, provides beneficial outcomes but can display unsolicited adverse reactions. The pharmacology of a drug is exhibited in two phases: a pharmacokinetic (PK) phase, also known as the biophase, a process in which the dose is administered to reach a certain concentration in tissues, more importantly the site of action, and a pharmacodynamic (PD) phase, where the drug concentration translates into a drug effect

(Fig. 6.1). The pharmacologic response reaches a maximum as the drug concentration at the receptor site increases; hence, developing therapeutic carrier systems, which would direct the drugs to the site(s) of the intended action within the body selectively, has been explored and worked on in the field of drug delivery research globally. There are numerous examples of efficacy and safety considerations, the most common being novel drug targeting methods in cancer chemotherapy, which has comprehensively endeavoured an equilibrium between anticancer and cytotoxic effects. This strategy is highly essential for planning and management of the treatment protocols for different types of cancer in various stages of disease. There are a number of drug candidate probed for delivering the drug at the right target within the body at the right concentration range and in the right time [1–3]. Sustained drug delivery system, which works on the basic principle of maintaining the drug concentration within the therapeutic window with minimum fluctuation possible, is yet another vital prerequisite for efficacious, time-controlled drug therapy practices. Thus, irrespective of the strategy whether spatial- or time-controlled release, PK profile modification of the parent drug is the principal mode in attaining the anticipated effect from a drug. Looking at the fact that drug molecules and bioactive agents are exceedingly variable in their physicochemical properties, and hence their therapeutic applications, novel drug delivery systems (NDDSs) are developed to reach an ideal PK profile from a drug of interest [4]. Nanoparticulate systems hold vast prospective as therapeutic and/or diagnostic agents and a major potential for the future development of therapeutic regimens. Unquestionably, a wide-ranging evaluation of the PK information

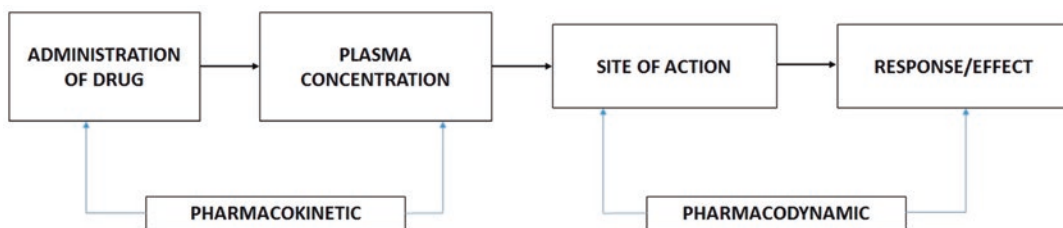


Fig. 6.1 Interrelation between PD and PK phenomenon

of these delivery systems has an important role in design, evaluation and use of NDDSs in clinical applications [5]. From a PK perspective, the key intents of the nanoparticulate drug delivery systems (NPDDS) are (1) improvement in drug-release profile in vivo, (2) enhancement of drug absorption, (3) drug distribution in a site-directed fashion, (4) modification in drug metabolism pattern, (5) prolongation of drug residence time in the body (e.g. in blood circulation) and (6) delay and/or reduction of renal excretion of the drug [6].

A methodical and detailed quantitative analysis of the PK, i.e. ADME profile of drug-associated nanostructure, is essential and can lead to the following:

1. A better understanding of the basic PK profile of the drug of interest, particularly in the disease matrix of the patient population of interest.
2. A more realistic design of the nanocarrier tailored for specific diagnostic and therapeutic applications.

3. An improved comprehension of the likely specific and nonspecific interactions between nanostructures and tissue/cell type.
4. Assessments of the possible ways to change the basic ADME scenarios to optimise safety and efficacy profiles of the drug and to predict future investigation trends (Fig. 6.2) [7]. PK delivers a quantitative depiction of the in vivo conditions under which a drug dose can lead to observed therapeutic or toxic effects by the drug concentrations in the biophase and/or toxic phase.

The basis for PK study is drug concentration–time curves and estimating the PK parameters with the proper mathematical models, which, in turn, can be used to quantitatively relate the effect to the equivalent biological concentrations. Since nanoparticulates are “drug PK modifiers,” the PK profiling of the drug and the developed nanostructures turn out to be an instrumental tool for evaluating novel or improved delivery systems [8].

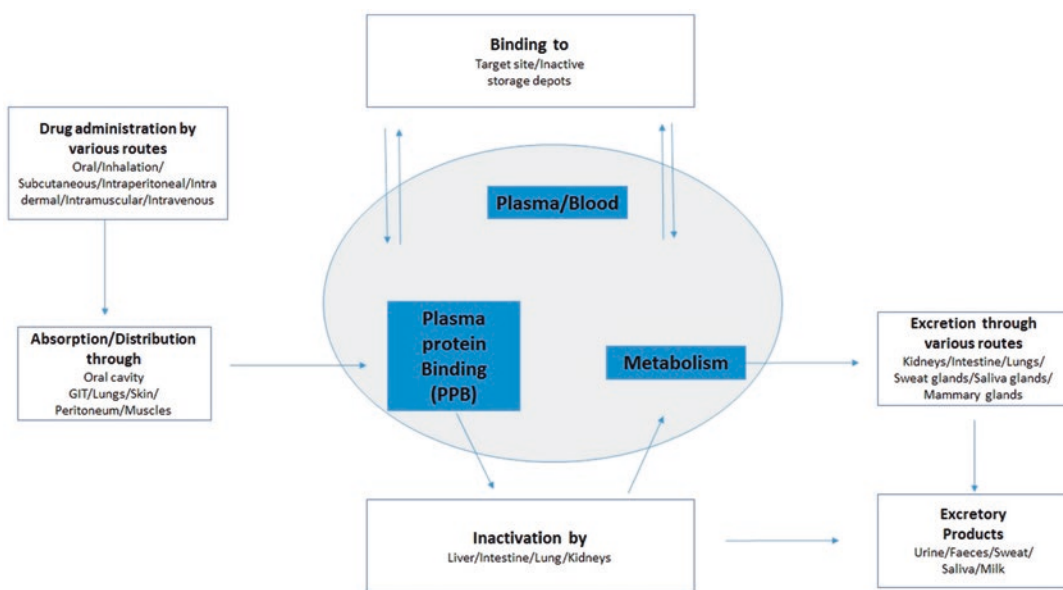


Fig. 6.2 A graphical representation of PK phenomena of a drug molecule within the host body

2 Nanotechnology in Drug Delivery

Nanotechnology has unlocked new vistas in drug delivery by offering delivery of a vast range of agents from small molecule drug to macromolecules such as proteins, peptides or genetic materials, for both localised and systemic purposes [9].

Nanotechnology acts as a connection of biological and physical sciences by relating nanostructures and nanophases at several fields of science, especially in nanomedicine and nano-based drug delivery systems. Nanomaterials, materials with size ranging between 1 and 100 nm, impact the frontiers of nanomedicine right from biosensors, microfluidics and drug delivery to microarray tests in tissue engineering, providing curative agents at the nanoscale level to develop nanomedicines. Nanomedicines have been valued in current time, since the nanostructures can be exploited as delivery agents via encapsulating or attaching therapeutic drugs and precisely delivering them to target cells with a controlled release [10].

Furthermore, nanoparticulate allegedly helps in averting gastrointestinal (GI) degradation of drugs and the delivery of sparingly water-soluble drugs to their target location. Thus, nanoparticulate has greater oral bioavailability by the virtue of their being exhibiting typical uptake mechanisms of absorptive endocytosis. They also remain in systemic blood for an extended period and enable the release of incorporated drugs as per the specified dose, causing less plasma fluctuations and in turn decreased adverse effects. Moreover, NPDDS makes the penetration of drug in the tissue system possible, facilitates ready cellular uptake of the drug, permits a proficient drug delivery and, thus, guarantees action at the targeted location, eventually exhibiting direct interactions with cells in the disease with enhanced efficiency and abridged or insignificant side effects.

The major advantage of nanoparticles is that various proteins can be affixed to the surface; gold nanoparticles used as biomarkers and tumour labels in biomolecule detection procedural assays can be the best suited example. In

case of drug delivery, the nanoparticle is selected on the basis of physicochemical features of drugs [11], and properties of drug like bioavailability, targeting and controlled release are modulated; a bioactive compound in *Nigella sativa*, thymoquinone, has been studied post-encapsulation in lipid nanocarrier and displayed sixfold increase in bioavailability in contrast to free thymoquinone and consequently defends the GI materials [12]. Many constituents such as metallic, organic, inorganic and polymeric nanostructures, like dendrimers, micelles and liposomes, are normally deliberated in the design of target-specific drug delivery systems. The drugs having poor solubility and less absorption are attached with these nanostructures, though the efficacy of these nanoparticulates as drug delivery vehicles differs conditional to the size, shape and additional inherent biophysical/chemical characteristics; for example, polymeric nanomaterials, such as alginate, chitosan as well as polyvinyl alcohol, poly-L-lactic acid, polyethylene glycol (PEG) and poly(lactic-co-glycolic acid) (natural and synthetic, respectively) having diameters between 10 and 1000 nm, because of their properties like higher biocompatibility and biodegradability, are ideal for a competent delivery vehicle and thus are used comprehensively in the nanofabrication of nanoparticles [13–15]. In addition to polymeric nanoparticles, compact lipid nanostructures and phospholipids like liposomes and micelles are also highly valuable in targeted drug delivery as well.

However, the complications related to the use of nanoparticles in the drug delivery system such as toxicity cannot be ignored and needs to be fixed for a successful application in the pharmaceuticals. There are recent studies, where nanoparticles have mostly been employed in amalgamation with natural products to counter the toxicity problems. New techniques like that of the green chemistry route for designing drug-loaded nanoparticles are extensively employed to minimise the perilous constituents in the biosynthetic process; hence, green nanoparticles for drug delivery have shown to reduce the side effects of the medications [16]. An array of characterisation tests are characteristically executed

on the developed nanocarriers, mainly as *in vitro* and *in vivo* tests for optimisation of drug delivery properties of nanotechnology-based drug delivery systems. On the one hand, *in vitro* tests, via a series of physicochemical characteristics – particle size, shape, chemical composition, surface hydrophilicity, polarity and drug-release profile – deliver an indirect measure of the drug delivery properties of the nanoparticles; *in vivo* tests, on the other hand, are performed to assess the drug carriers directly within the living organism or in parts of its organs or tissues and its performance successive to *in vitro* tests [1].

3 PK Aspects

3.1 PK/Biodistribution

PK and biodistribution are incorporated in pre-clinical trials of nanomedicines. PK parameters, for instance, area under the curve, clearance rate, distribution volume and elimination half-time, offer significant understanding concerning stability in circulation, renal clearance, mononuclear phagocyte system clearance and the predisposition for uptake in normal tissue. For broad appraisal of various drug delivery approaches, an exhaustive data concerning the PK, biodistribution and tissue accumulation is indispensable, but these are relatively laborious and expensive experiments, thus making them unrealistic for benchmarking [17].

Many factors hinder the acceptable PK of drugs, *viz.* poor absorption, low penetration into target tissues, high clearance and/or insolubility of drugs, with the resulting low bioavailability, and have a serious concern for drug development in the pharmaceutical industry. More than 60% of new drug candidates are estimated to be poorly soluble in water, impeding development programmes and eventually the realisation of new treatments [18]. Furthermore, the inability of drug penetration in target tissues, where the maximum exposure is needed, has a damaging influence on therapy efficacy and toxicity. Thus, currently, several nanomedicine strategies are considered to increase drug delivery.

Nanomedicines include nanoparticles (solid sub-micron particles consisting of polymers or inorganic material) and liquid-based drug nanocarriers, e.g. nanoemulsions (NEs). Nanoformulations may comprise a drug (or drugs), antibody, detection probe and several other substances associated with the particle in different ways. There are nanoformulations which have the capacity to get effectively absorbed and consequently get concentrated in tissues via passive targeting, manipulating the physicochemical characteristics of the nanocarriers as well as the specific properties of the tissues of interest. Likewise, diverse approaches can be applied for active targeting of tissues and pathogens besides cancer cells, which affirms a wide range of nanoformulation designs as well as availability of a great range of delivery strategies for research and application. Polymers, either by forming solid polymer matrix nanoparticles for encapsulating drugs or by the construction of vehicles like block copolymer liposomes/vesicles, micelles and NE, act as containers for drug molecules. Moreover, direct covalent or non-covalent conjugation of drugs to polymers has been effectively employed to augment circulatory times and delivery of drugs through triggered/controlled release. There are extensive inorganic oxides that have been explored for creating nanoparticles, such as gold, silver, silica and iron. Nevertheless, the impact of these formulations on drug PK is only partially implicated. Physiologically based pharmacokinetic (PBPK) modelling is an effective pharmacological tool to appraise the design of nanoformulations and optimise their PK, which has been efficaciously explored for traditional formulations in drug development programmes as well as simulations of appropriate clinical scenarios [19, 20]. In addition, PBPK modelling can also be considered as a bottom-up technique that has goals to mimic distribution of drug by coalescing system data relating a population of interest (e.g. demographics, physiology, anatomy and genetics) with *in vitro* drug data (e.g. Caco-2 permeability, protein binding, intrinsic clearance, lipophilicity) by the means of a mathematical depiction of ADME. With the use of this model-

ling technique, a complete overview of all the physiological and anatomical processes involved in drug distribution, posing the opportunity to categorise important determinants of PK, is possible. Absorption can be simulated allowing for the vibrant interaction between dissolution, passive permeability and the affinity/activity of metabolic enzymes and transporters for traditional formulations. Drug distribution is replicated by assessing tissue volumes and the diffusion of drugs into tissues, under the influence of physico-chemical properties, while tissues and organs are connected by virtual blood and lymphatic flows. For simulating clearance, *in vitro* metabolism data is exploited and assimilated into the model using scaling factors. Furthermore, inter-patient variability is perceived in all of the above processes, and virtual human and animal populations can be replicated apprehending interindividual variability by considering anatomical and physiological characteristics and their covariance. As far as development of PBPK models for nanomedicine is concerned, numerous challenges are noted, primarily since currently there is only a partial understanding of the molecular processes regulating nanoparticle distribution.

3.2 Importance of Nanoformulation PK

Although nanoformulation delivery systems have the prospective of improving drug PK profoundly, drug efficacy and toxicity can also be adversely impacted by nanoformulation distribution, for instance, insufficient absorption and diffusion into tissues leading to change in drug activity or unwarranted accumulation of nanoformulation leading to tissue-specific toxicity (related to the drug, the nanoformulation or potentially both). Subsequently, comprehending the interfaces between the human body and nanoformulations is of vital relevance for the designing future treatment approaches, and an exhaustive investigation of regulation of nanoformulation disposition processes is indispensable to improve effective and safe nanoformulations for drug delivery. There are many processes mediating the distribution of nanoformulations in the human body, and the ADME properties can fluctuate markedly from conventional formulations (Fig. 6.3). In addition, ADME of nanoformulation is not entirely characterised and differs depending on the class of the nanoformulations. The preferred routes of

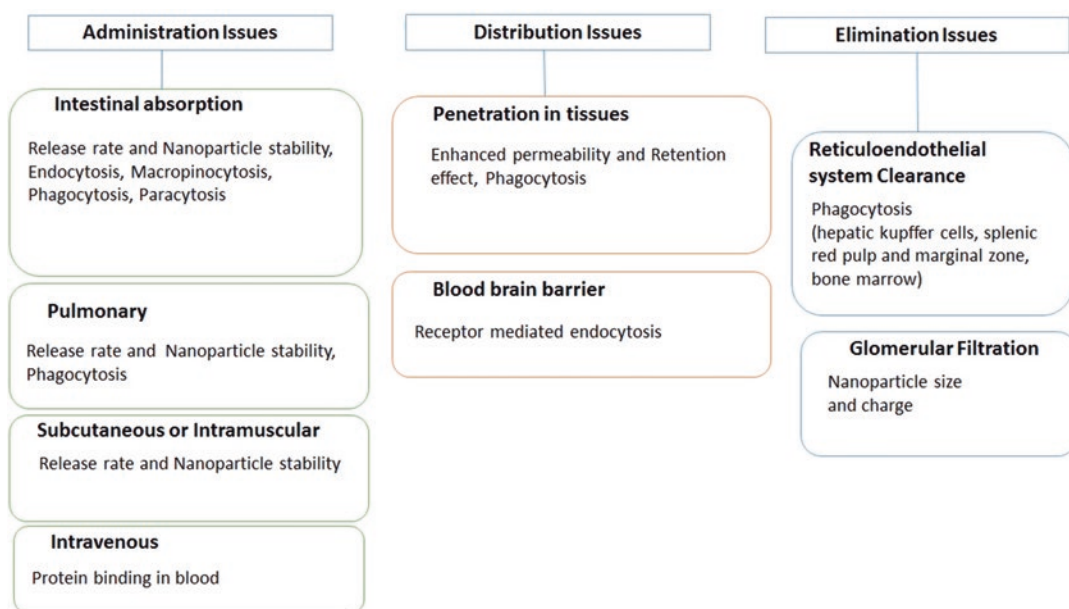


Fig. 6.3 Issues related to the administration, distribution and elimination of nanomedicines

administration for nanoformulations being oral, transdermal, ocular, nasal, pulmonary and i.v., it is important to understand the ADME pattern according to the route of administration.

Oral Administration

The intestinal wall architecture is in such a way as to absorb nutrients and act as a barrier to pathogens and macromolecules. Various nanoformulations improve the drug absorption by releasing drug into the lumen in an organised manner and in turn reduce the solubility issues. Many small amphipathic and lipophilic molecules are absorbed through passive diffusion by separating into the lipid bilayers and crossing the intestinal epithelial cells, while nanoformulation absorption is more complicated due to the intrinsic nature of the intestinal wall, the foremost being the physical obstacle to nanoparticle oral absorption due to mucus barrier covering the luminal surface of the intestine and colon [21, 22]. The mucus barrier, which comprises of distinct layers, is composed mainly of heavily glycosylated proteins called mucins having the prospective to block the absorption of certain nanoformulations. Thus, nanoformulations can be produced by modifying which would give increased mucus-penetrating properties [23]. Moreover, after traversing the mucus coating, transportation of nanoformulations across intestinal epithelial cells can be controlled by several steps, like cell surface binding, endocytosis, intracellular trafficking and exocytosis, causing transcytosis (transport across the interior of a cell) with the impending engrossment of several subcellular structures. Besides, nanoformulations may move between cells by paracytosis (opened tight junctions). Non-phagocytic pathways, including clathrin-mediated and caveolae-mediated endocytosis and macropinocytosis, are considered as the most common mechanisms for absorption by oral route of nanoformulation, even though heterogeneity in process efficiencies has been designated for diverse types of nanoformulations, thus making the identification of a predominant process determining transcytosis of nanoformulations quite tough [24].

Alternative Administration Routes

The use of administration route other than oral affords supplementary benefits, one of the most important being direct targeting to the desired site of action and a protracted period of drug action. The skin can be considered as a desired route of nanomedicine administration, since it evades the risks associated with intravenous (i.v.) therapy and the problems related with varying gastric pH, emptying time and first-pass hepatic metabolism. Though it is hard to administer drugs through skin because of the impermeable nature of the skin [25], nevertheless, nanoformulations, such as solid lipid nanoparticles (SLNs) and NEs characterised by good biocompatibility, lower cytotoxicity and desirable drug-release modulation, has been optimised for transdermal administration. Many nanotechnologies have been exploited to flabbergast the ocular barriers and help the drug reach to the target conjunctival epithelial cells, for example, successful administration of nanoformulated intraocular pressure-lowering drugs and anti-apoptotic drugs. Certain nanoformulations for nasal administration have been assessed where nanoformulations have shown to cross the membrane by a transmucosal route via endocytosis or carrier- or receptor-mediated transport process, for instance, nasal administration of chitosan nanoparticles of tizanidine for improving brain penetration and drug efficacy in mice [26]. Moreover, few nanoformulations are preferred by i.v. administration to obtain an efficient distribution in the body, due to their insignificant biological membrane penetration in sites of absorption.

3.3 Distribution in Tissues and Organs

After the absorption of nanoformulations, the distribution initiates, which differs extensively depending on the delivery system used, the characteristics of the nanoformulation and the possible inconsistency between individuals (organ size, body fat index, etc.). Moreover, it is also to be noted that the rate of drug loss from the nanoformulations will differ, due to differences in the distribution characteristics of both the free drug and

nanoformulated drug. Nanoformulations, once in systemic circulation, come in contact with several proteins, which forms a dynamic nanoformulation–protein coronas with environment-specific stability and characteristics, which in turn impact the nanoformulation size and physicochemical characteristics, subsequently affecting nanoformulation degradation, cellular uptake, accumulation and clearance processes. The nanoformulation–protein coronas likewise affect the body, by causing pathologies such as inflammation and haemolysis [27]. In human blood, serum albumin, immunoglobulin, fibrinogen and apolipoproteins constitute a protein corona; in some nanoformulations, abundant proteins like albumin and/or fibrinogen may initially bind non-specifically to nanoformulations and later get substituted by proteins having higher binding affinity. Hence, the theoretical determination of the distribution of these nanoformulations is complex, and additional studies are needed in this area. Moreover, nanoformulations of a specific size and composition can diffuse in tissues by processes, like the enhanced permeability and retention (EPR) effect, whereas some accumulates in specific cell populations. Thus, high molecular weight drugs, prodrugs and nanoparticles exploit this improved permeability and retention effect to accumulate in sites of inflammation or cancer the tissues with increased vascular permeability. Deliberation of these factors would be critical when constructing models for investigating drug tissue penetration. Studies correlating particle properties with nanoformulation entry pathways and processing in the human blood–brain barrier (BBB) endothelial barrier have shown limited penetration through the BBB of uncoated nanoparticles and that the efficiency and mechanisms of endocytosis can be influenced by surface modification. Low tissue penetration of nanoformulations is considered to be a chief obstacle for the treatment of diseases and the usage of ligands to augment this process of uptake into tissue, thus signifying a favourable solution [28]. The most appropriate example can be use of tumour-penetrating peptides which activates bulk tissue-specific transport pathways, targeting receptors present in the tumour vasculature such as annexin I, plectin-1 and neuropilin-1. Moreover, the ability

of monocytes to migrate in numerous tissues and in sites of inflammation, infection and tissue degeneration offers an exclusive mechanism for exhibiting drug delivery improvements. Certainly, macrophages as well as monocytes have a fundamental role in the pathogenesis of diseases like cancer, HIV, tuberculosis, leishmaniasis, inflammatory bowel disease, rheumatoid arthritis, diabetes and chronic obstructive pulmonary disease, affirming these cells to be drug targets [29].

3.4 Elimination and Clearance

A number of processes are involved in the regulation of the nanoformulation clearance, ranging from chemical and enzymatic degradation to renal and biliary elimination. Degradation in penetrated tissues or circulating blood leads to gradual release of nanoformulation content, thus making degradation kinetics a significant variable controlling the drug release, and might confound designing of optimal drug delivery systems with anticipated drug-release properties. In addition, the immune system removes foreign entities from the body, such as pathogens, debris and nanoformulations. A phenomenon known as accelerated blood clearance (ABC) is occasionally perceived, where a delayed immune response causes a rapid clearance of specific nanoformulations [30], thus requiring a thorough understanding of the interaction of nanoformulations with immune cells as well as all related consequences. There are instances where the nanoformulations with PEG exhibit a prolonged presence in the systemic circulation by preventing receptor interactions and so the phagocytosis by the mononuclear phagocytic system. Apart from this, renal clearance is a chief mechanism mediating nanoformulation excretion.

4 The PK Profile of the Drug

Many biological factors related to the anatomy and physiology of the host organism impacts the circulation time and tissue distribution pattern of a nanoparticulate drug carrier system, thus defining the PK profile of the drug being delivered.

The factors regulating the biological performance of nanoparticles are the physicochemical properties of the bioactive agent to be delivered, the nanostructure used for delivery, the interactions between drug and the nanostructure and the actions enacted by the host body upon the nanoparticles. The physicochemical factors of nanoparticles, viz. particle size distribution, shape, density, chemical composition, mechanical properties (e.g. rigidity/deformability and strength) and surface characteristics (e.g. hydrophilicity/hydrophobicity, conformation of surface adsorbed or grafted polymers/ligands, surface electric charge, surface density, etc.), control the residence time of nanoparticles within the systemic circulation and regulate tissue distribution pattern, mode of cell internalisation, intracellular trafficking, content release and toxicity, e.g. spherical particles are shown to adhere less efficiently to biological substrates in comparison to their equal-sized oblate ellipsoidal counterparts [1]. Thus, these factors affect different components of the ADME system resulting in a new drug concentration vs. time profile with respect to different biological compartments. Therefore, to achieve improved design and preparation of nano-based drug delivery systems or diagnostic and/or therapeutic objectives, a thorough understanding of the basic PK profile of the therapeutic agent in study, along with specific and/or nonspecific interaction(s) with diverse tissues and cell types of nanostructure including the biodistribution pattern, is necessary. Generally, chronological events occur to drug-associated nanoparticulate inside the host body post-administration, viz. nanocarriers enter the body, followed by its absorption (in the case of extravascularly administered nanostructures) and distribution in systemic circulation to multiple organ or tissues. Additionally, they might undergo modifications or remain unaltered in structure, enter the cell for a specific period of time and eventually get degraded or exocytosed and eliminated from the body via different routes (major being hepatic and renal elimination) [31]. There is also a scope where a deviation in typical sequence may occur, depending on the nanostructure and the drug being delivered; however, the drug-release kinetics outside the nanocarrier may play

a crucial role in the drug-carrier interface. If the drug molecule vacates the carrier instantly upon administration, PK characteristic of drug will govern the final behaviour; on the contrary, outcome will be determined by the carrier disintegration/clearance in the body that will decide the behaviour, if the drug does not leave the carrier. The actual circumstances, yet, replicate a combination between these extremes.

Extensive studies are required to recognise and designate diverse aspects and study biofate of both the nanocarrier and the drug delivered, in addition to conventional *in vivo* evaluation for nanotechnology-based drug delivery systems. Important carrier-related determinants of the nanocarrier biofate are average particle size and size distribution, particle charge (i.e. positive, negative or neutral), particle polarity (hydrophilicity/hydrophobicity of the particle surface) and the chemical composition of the carrier. The drug-release kinetics must be deliberated sensibly prior to *in vivo* testing, since it is of immense importance in site-directed drug delivery. Moreover, validated *in vitro* models are perilous to back the early screening of novel nanocarrier systems in order to evade laborious and expensive *in vivo* studies. At the same time, it is in fact true that there is still necessity of complete experimental studies using *in vivo* models, viz.:

- The molecular mechanism of a nano-associated drug's absorption and its access into systemic circulation
- The probable interfaces between nanocarriers and mucosal surfaces
- Membrane transporters in ADME with each nanocarrier
- The comparative involvement of the released and entrapped drug in the appearance and perseverance of a given effect from a drug at the biophase
- The interface between the metabolising the nano-loaded and drug enzyme
- The micro-equilibriums taking place in micro-environments during the distribution of the nano-loaded drug
- The mechanisms of excretion of nano-loaded drug from the kidney [1]

5 PK Models

Evaluation of the changed drug disposition is highly critical to understand the exposure–efficacy interactions and discourse the safety concerns, since nanodrugs might swift novel toxicity apprehensions due to altered disposition of the active pharmaceutical ingredients (APIs). Perhaps, Doxil® upsurges doxorubicin deposition in the skin, which results in a lower single-dose maximal tolerable dose as compared to doxorubicin (50 mg/m² every 4 weeks or 12.5 mg/m²/wk. vs. 60 mg/m² every 3 weeks or 20 mg/m²/wk) [32]. Furthermore, the non-anticipated biological effects of the nanoparticle compositions should also be studied. For instance, safety concerns due to chronic exposure to nonbiodegradable materials and augmented penetration of biological barriers, like blood–brain barrier or placenta, have already been raised in the FDA Guidance for Industry “Drug Products, Including Biological Products, that Contain Nanomaterials” (December 2017) [33].

5.1 PBPK Modelling

PBPK modelling is a quantitative support tool recommended by the Organisation for Economic Co-operation and Development and the new European Union regulatory framework, Registration, Evaluation, Authorisation and Restriction of Chemicals, for evaluating nanoparticle hazards. PBPK has been well acknowledged by the pharmaceutical industry as well as regulatory agencies in PK modelling and simulation experiments for many types of drugs. With its distinguishing separation of physiology- and drug-dependent information, this tool has proven a feasible option for providing a mechanistic understanding of the influential factors and sources of PK variability that further helps in envisaging drug exposure at numerous clinically pertinent scenarios. Moreover, by combining it with pharmacodynamic (PD) models which relates the exposure at target tissues to pharmacological effects, efficacy and toxicity can be predicted well. PBPK models have been exploited

for numerous types of nanoparticles, comprising liposomes, silver nanoparticles, carbon nanoparticles, polymeric nanoparticles, nanocrystals, gold–dendrimer composite nanoparticles and others. Certainly, structural and functional complexity and various particle properties, such as composition, size, shape, charge and surface chemistry, affect particle interaction with the biological system that seems to be a major challenge for the study of the nanodrug disposition.

The PBPK modelling concept was first introduced by Teorell in 1937. Figure 6.4a PBPK models utilise discrete tissues (the main tissues like brain, gut, heart, kidney, liver, lung, spleen, muscle and adipose tissues) in the body as building blocks or compartments dissimilar to how it is in mammillary models [34], remaining tissues usually being grouped into a remainder or carcass compartment if they aren't from the organ of interest and few tissues being ignored if not significant in terms of mass balance. Apart from this, tissues having similar kinetics can also be endured together for simplification of the model (e.g. minimal PBPK model) [35]. All tissue compartments in PBPK models are connected by the circulating blood system and occasionally the lymphatic system as well, mimicking the physiological systems. Drug clearance is defined in the liver and kidney, with them being drug-metabolising tissue compartments of the body. As shown in Fig. 6.4b, for description of each tissue compartment, either a perfusion-limited or permeability-limited model is utilised [34]. Perfusion-limited models adopt the setup that the drug present in the tissue can reach rapid distribution equilibrium with the drug in the blood system, representative of the drug being easily penetrable into tissue cell membranes with blood perfusion as a limiting step. Permeability-limited models, on the other hand, assume that the tissue cell membranes act as diffusional barriers to the studied drug and thus divide the tissue into intracellular space and extracellular space. Active drug transporters on the cell membranes can likewise be modelled by integrating uptake and efflux transporting mechanisms. Other parameters like affinity and capacity, which are associated with uptake and efflux transporters, are

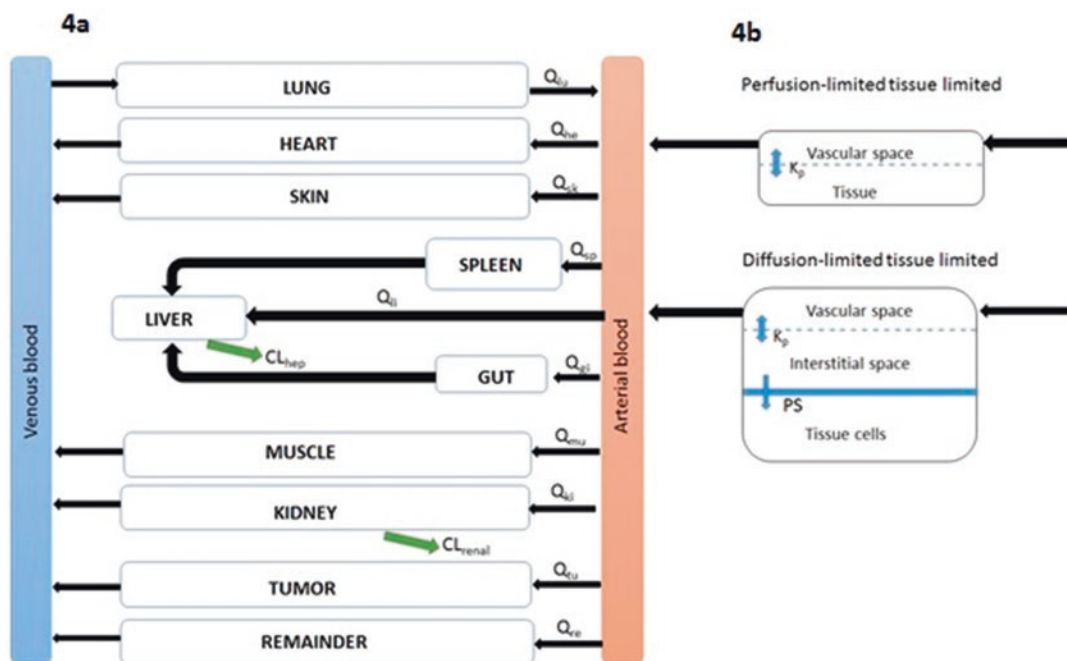


Fig. 6.4 (a) General PBPK model, (b) type of tissue model structure. Q_i , blood or plasma flow; CL_{hep} , hepatic clearance; CL_{renal} , renal clearance; k_p , tissue partitioning

coefficient, i.e. concentration ratio between tissue and blood at steady state; PS, membrane permeability coefficient

typically derivative of cell-based assays, adjusted by using empirical in vitro/in vivo extrapolation (IVIVE) approaches.

PBPK models usually employ both physiological parameters (tissue volume, tissue blood flow and abundance of metabolising enzymes and transporters) and drug-specific parameters (clearance and tissue partition coefficient k_p), essential for defining the drug disposition within the physiological system. Additionally, the drug-specific parameters are recurrently ascended from a range of in vitro systems, e.g. hepatic drug clearance can be scaled on the basis of in vitro measurements using recombinant enzymes, liver microsomes or hepatocytes, or k_p , defined as the tissue/blood concentration ratios at a steady state, can be assessed using *in silico* methods grounded on both tissue composition and drug physicochemical characteristics, like lipophilicity, charge and protein binding [34, 36]. Thus, IVIVE acts as an integral part of PBPK modelling, permitting prediction of the plasma and tissue concentration time profiles

without in vivo studies [34]. IVIVE also plays a pivotal role in the early stage of drug discovery when a huge number of drug candidates are required to be screened. An important advantage of PBPK modelling is that by extricating drug-specific parameters from physiological parameters, the PK variability sources can be identified efficiently, therefore simulating PK variability across subpopulations on the basis of the distribution of patients' physiological parameters. Moreover, the mechanistic nature of PBPK models permits to infer the PKs to different disease states (like liver and kidney dysfunction and obesity), various special populations (e.g. the elderly, the paediatric population, pregnant women, carriers of genetic polymorphisms) and different species, thus making PBPK models popular as a powerful tool for drug development from lead screening to late clinical evaluations. Moreover, as far as the implementation of PBPK models is concerned, they are stereotypically expressed as differential equations relating the mass balance based on fitting conventions or

interpretations of drug disposition processes. The initial parameter values can be obtained from various sources, viz. literature reports, in vitro measurements and/or initial estimates based on simulations. Stereotypically, physiological parameters are fixed to a set of commonly used values, and drug-specific parameters are to be adjusted by fitting the model with entire available experimental data. The mass transfer conventions and adjusted parameter values might be substantiated against an independent data set which was not used for parameter optimisation. The development of PBPK models is an iterative process, with ample scope of further update once a new set of data becomes available, and such type of corroborated PBPK model can then be utilised for drug PK and tissue distribution predictions at varied scenarios, like that of different dosing regimens, special populations or across species [33].

5.2 The Application of PK–PD Modelling and Simulation Systems in Liposomal Drug Delivery

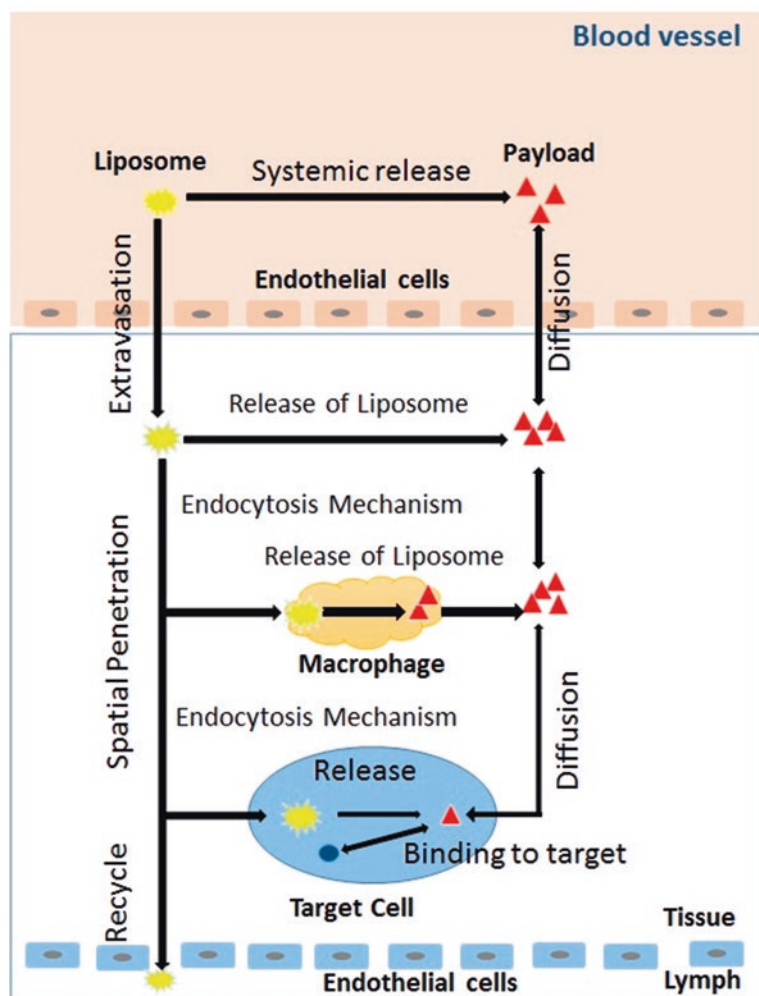
PBPK Modelling and Simulation

Multiple mechanisms of liposomal drug disposition are predisposed by various physiological factors. A study by Zamboni et al. designated that various physiological factors like age, gender, body composition, monocytes and status of hepatic disease outline the disposition of liposomal drugs [37, 38]. Whole-body PBPK model and a mechanism-based model for tumour (Fig. 6.5) can be projected to apprehend the comprehensive disposition of both liposomes and payload in the biological system using a “bottom-up” approach. This PBPK model could also be employed for exploring the impact of drug-associated factors and physiological factors (such as the MPS) on the multiscale mechanisms of liposomal disposition. Presently, PBPK models are commonly used in small molecular drug development and regulatory reviews [39] and have developed as a dominant tool to delineate the PK and tissue distribution profiles of liposomal drugs.

Simplified PBPK Model

There are certain hybrid models developed by researchers. Harashima et al. correlated the systemic disposition of liposomes with the targeted exposure of the free API by using the hybrid model [40, 41], where a compartmental model described the systemic PK profiles of encapsulated and released doxorubicin. The target tissue, i.e. tumour, was listed as an individual compartment, which consisted of capillary, interstitial and tumour cell sub-compartments, which was associated with the systemic compartment by blood flow to the tumour by the capillary sub-compartments and was used to designate the disposition of encapsulated and released doxorubicin in tumours. The systemic PK profiles of the liposomes were measured to estimate the tumour distribution profile of free doxorubicin to establish the PK–PD relationship. The influence of the physicochemical and physiological properties of the liposomes on the exposure of the tumour to free doxorubicin and the antitumour effect were assessed by this PK–PD framework [40]. The result showed that the local release rate and liposomal retention in tumours had a crucial impact on the antitumour effect of liposomal drugs; likewise, BPK models can be utilised for approximating the influence of other physiological variations on liposomal disposition properties. In yet another hybrid PBPK model by Hendriks et al., the impact of tumour physiology on the cellular and subcellular transport of doxorubicin inside tumour was successfully assessed [42], and this study set an example for using PBPK modelling and simulation for identification of critical physiological factors to develop treatment outcomes and assist trans-species or population translation. A systems model for liposomal RNA disposition quantification and study of its effect on serum bilirubin was developed by Apgar et al. [43]. In the study by Apgar et al., RNA delivery to the hepatocytes was computed by a simplified PBPK model of the kinetics of liposomal RNA degradation, biodistribution, hepatocyte attachment, endocytosis-induced uptake and hepatic intracellular degradation processes. The effect of the delivered RNA on glucuronidation regulation and bilirubin clearance was analytically investi-

Fig. 6.5 Tumour tissue compartment model for liposomes. The distribution of liposome from blood to the drug target includes many processes like liposome extravasation, diffusion of the released payload between blood and interstitial fluid, macrophage-mediated release of the payload (direct or tissue-associated), endocytosis of liposomes into tumour cell, intracellular release of the payload in tumour cells, binding to target and salvaging intact liposomes through lymph back into the systemic circulation



gated. This model was applied to link preclinical and clinical studies and predict the first human dose.

Whole-Body PBPK Model

A dual-layer, whole-body PBPK model was developed by Kagan et al. to evaluate and describe the disposition of intact liposomes and free amphotericin B (Ambisome®) [44], and the two PBPK layers were connected via the drug-release kinetics. Parameters of model were adjusted to link the plasma and tissue concentrations with the time profiles; it constituted the first whole-body PBPK model to be developed which has a proficiency to simultaneously quantify the tissue disposition profiles of the encapsulated in addi-

tion to free drugs. Moreover, key factors and processes can be assimilated using a PBPK model for successful assessment of the PK–PD relationship [45].

PBPK Modelling of Nanoparticles

Nanoparticles and the biological system interaction are complex and particularly grim to replicate in vitro, e.g. minor deviations in particle properties or the biological system can considerably modify the systemic disposition of nanoparticles [46]. But, by conjointly integrating the significant biological factors and the nanoparticle-specific properties, PBPK modelling can be very beneficial in envisaging the PK, tissue exposure, efficacy and toxicity of nanoparticles.

Predicting the Dose–Effect Relationship

A PBPK model to check and optimise the therapeutic benefit of anionic, PEGylated liposomes with amitriptyline (AMI) and bupivacaine (BUP) overdoses in humans with 15 compartments, perfusion-limited tissue distribution and clearance from the liver and kidneys was developed by Howell and Chauhan [47]. The study showed that liposomes were capable of sequestering serum AMI and BUP and thus reduced the distribution of the drugs to the tissues like the heart and brain, which has toxicity concerns. This model was developed for drugs instead of the liposomes, as the researchers presumed liposomes to be remaining within the blood compartments until elimination, and thus was engaged to mimic the variations in AMI and BUP exposure and the efficiency of the liposome therapy. AMI and BUP's time-varying sequestration by the liposomes in systemic circulation was modelled by an empirical equation which described the clearance of liposomes from blood as well as a linear relationship established *in vitro* linking the drug liposome/blood partition coefficients and liposome concentrations. Additionally, the model simulated the decrease in AMI and BUP exposure (area under the concentration curve and C_{max}) in plasma and the heart and brain tissue upon liposome administration. The anticipated heart concentration was pooled with a PD model relating the drug concentrations with the variation in heart functions to foresee the reversal of heart functions after liposome administration. The effects of liposome dose and the time lapse between overdosing besides liposome administration on therapeutic efficacy were also studied. It was further demonstrated by the study that ignoring the tissue distribution of liposomes (especially in the liver) may lead to underrating the hepatic clearance of bound AMI and BUP, though the prejudice could be partly abridged by considering the total drug plasma concentration in calculating hepatic extraction.

Interspecies and Population Translation

Another study by Lu et al. compared the alterations in the disposition of docetaxel between a small molecule formulation and a folate-modified

liposomal formulation in rats post-intravenous administration and to envisage mouse and human PKs [48]. This PBPK model involved arterial blood, venous blood, lung, brain, heart, spleen, liver, intestine, kidney and muscle tissues, along with a remainder compartment, and clearance via liver and intestines and presumed a perfusion-limited structure model for each compartment. Nonlinear mixed effect modelling was applied, and the effect of sex and formulation, categorical covariates on k_p and clearance were studied. Results showed higher k_p for lung, kidney and muscle tissues and lower k_p for brain, spleen and liver tissues that were found in liposomal formulation as compared to the small molecule formulation. The higher kidney k_p was attributed to the expression of folate receptors in the kidneys. Furthermore, higher k_p for heart tissues and lower intestinal clearance were observed in female rats; however, the interface between formulation and sex was not studied. Moreover, the model previously developed for rats was efficaciously used to predict mouse and human data by means of species-specific physiological parameters and allometric scaling for clearance.

Formulation Development of Nanodrugs

Poor patient compliance seriously hampers the efficacy of present oral formulations of antiretroviral, which demands daily dosing. Rajoli et al. [49] used PBPK model to evaluate the viability of developing monthly parenteral (intramuscular injection) nanodrugs (solid drug nanoparticles) for antiretrovirals, which would be expected to enhance patient compliance and treatment efficacy. At the same time, it is still elusive to find if the long-acting formulations could preserve effective antiretroviral concentrations between dosing intervals. The PBPK model, which was developed on the basis of oral formulation clinical data for each antiretroviral by a compartmental absorption and transit model [50], was then protracted with an intramuscular depot compartment to mimic the drug-release and absorption pattern. The model was later substantiated against an existing antiretroviral nanodrug. This model made optimisation of the combination of dose and release rate for each of eight antiretrovirals to

maintain therapeutic plasma concentrations for the entire dosing interval possible. The sustainability of a monthly nanodrug for each antiretroviral was recognised when the optimised dose was within the dose limits for intramuscular injections, though that of the optimised nanodrugs necessitated experimental confirmation.

In Vitro/In Vivo Correlation (IVIVC)

In a PBPK modelling, Jung et al. [51] correlated in vitro drug release with plasma concentrations post-oral administration of nanocrystal flurbiprofen. The model employed a two-compartment model (plasma and peripheral) to define the distribution and elimination processes post-absorption; absorption process was studied by a more mechanistic PBPK model. The GI tract divided into two compartments, stomach and intestine, which was employed to estimate the fraction of drugs released in the stomach and the intestine separately via in vitro biorelevant release tests. The design was structured in a way such that the drug released from the formulation during the GI transition diffused into the unstirred water layer and then permeated the intestinal barrier to reach the plasma. For optimising the drug diffusion rate across the unstirred water layer and the intestinal barrier as well as the systemic distribution and elimination parameters, PK data of a reference tablet formulation were considered. The model thus validated was further used to mimic the PKs of a nanocrystal formulation by apprising the model with the in vitro release profiles. Furthermore, two in vitro dissolution methods, a filter method and a dispersion releaser technology, were compared, to find that plasma PK was extra sensitive to the drug-release variations that was predicted by the dispersion releaser method than by the filter method, which further established that the dispersion releaser technology and PBPK model combination can be exploited to screen drug formulations. In yet another study, Shono et al. [52] employed a combination of PBPK model and biorelevant release tests to examine the size effect of nanocrystals on absorption and plasma PK. Besides, the model also envisaged the effect of food on drug absorption and plasma PKs, since the model considered the

difference in the GI emptying rate and fluid volume with and without food. Another study by Kumar and Singh [53] interrelated the Weibull in vitro release profile of a carvedilol-loaded silk fibroin-casein nanoparticle with the plasma PKs post-oral administration in rats with the help of built-in advanced compartmental absorption transit model and PBPK model in GastroPlus™. This validated IVIVC was then employed in simulation study of plasma PKs based on different in vitro release profiles [54].

Current Models of Oral Drug Bioavailability

Oral administration being the most common route of administration for pharmaceuticals, with high levels of drug stability and dosage accuracy, and economic is widely used. But orally administered drugs have varying bioavailability based on many factors like solubility, stability in the GI tract, absorption by intestinal epithelia, first-pass metabolism and reabsorption rates. Thus, the models used to assess the PK of drugs administered orally as a proxy for in vivo bioavailability are explored widely [55]. Caco-2 monolayers are a modest model of the intestinal epithelial cell layer derived from a human colon carcinoma line and are largely used for evaluating bidirectional absorption/reabsorption across the monolayer, as well as efflux mechanisms studied by using P-glycoprotein (P-gp) and breast cancer resistance protein (BCRP) inhibitors. This system can also be developed to evaluate the effects of alterations in the intestinal fluid properties (e.g. pH). Absorption systems have also exploited Caco-2 monolayer to appraise the impact of viscosity of food on dissolution and permeation of the active pharmaceutical ingredient.

Excised tissue assays preserve many physiological parameters like pH, enzymes, mucus layer, etc., and have physiological tissue architecture. In addition, ex vivo skin and corneal models also have the capacity to assess the kinetics of both dermal and ocular topically applied drugs, where they are used by absorption systems for estimating drug accumulation in specific corneal and skin layers and skin dryness. Intestinal perfusion, an in situ assay is engaged to evaluate

uptake of drug along well-defined GI tract sections in an anaesthetised animal models along with endpoints of drug absorption, transporter-specific uptake/efflux and formulation efficacies of simpler systems in a physiological setting.

Benefits of In Vivo Systems

In vivo models are essential for considering how a drug functions in a living organism prior to clinical trials and thus are the gold standard for evaluating safety and bioavailability for NDDS. These models afford an accurate assessment of PK of drug besides integrating first-pass metabolism by the liver, drug–drug interactions and drug excretion processes. Whereas in vitro toxicology screens are expedient in lead selection in the process of drug discovery, suitable assessment of toxicology, tolerability and dosing regimens does necessitate entirely integral biological systems. In vivo system is the precise representation of organism-level states and can integrate systemic changes altering the drug behaviour – e.g. compensatory functions of the tumour microenvironment responsible for poor translation of in vitro drug discovery for tumour metabolism in clinical trials. Moreover, animal models can assess the effect of fasting, circadian or behavioural states on drug response [56].

5.3 PK–PD Modelling System with Spatiotemporal Characterisation

PK–PD modelling and simulation are extensively explored in drug development and regulation systems in which mainstay includes the translation of preclinical observations to the clinical setting, dosing regimen selection in special populations and clinical trial optimisation [57]. This systems-based approach empowers the combined analysis of system- and drug-specific factors and has revealed substantial prospective in the identification of multiscale mechanisms of liposomal disposition, quantification and optimisation of delivery systems and correlation of the physicochemical properties with systemic performance [33, 58]. In tumour, increased permeability of

blood vessels and dysfunction of the lymphatic system are hallmark characteristics which allow the buildup of liposomal drugs in the tumour. This EPR concept is applied to liposomes for targeted delivery of cytotoxic drugs to solid tumours. In the tumour tissues, liposomes are generally positioned far from the tumour cells in the perivascular areas and roots of the capillary sprouts and represent a spatial biodistribution pattern that is highly heterogeneous, which in turn describes the moderate improvement in survival of patient [59]. The same pattern of biodistribution of liposomes is related to irregular blood vessels in the tumours, elevated interstitial fluid pressure (IFP) and dense extracellular matrix cell packing; the said properties can thus limit the extravasation and penetration of the liposomes. Thus, many system-based models are projected to investigate the impact of tumour vasculature and physical properties on heterogeneity in spatial distribution [60, 61].

Macklin et al. designed a mathematical model for describing solid tumour growth and tumour-induced angiogenesis [62], based on which another researcher Frieboes et al. replicated tumour growth and the progression of the tumour microenvironment over a specific period of time-point. The influence of the tumour microenvironment properties, particle size, ligand density and ligand–receptor binding affinity were analysed on the spatiotemporal distribution of nanoparticles in tumours [60], along with the assessment of the effects of drug-loading methods, release rates and diffusivity on treatment efficacy [63]. The studies explicated the relationship between physiological and physicochemical properties or liposomal disposition and antitumor efficacy. The extravasation of nanocarriers into the tumour is accelerated by the impaired blood vessels, though the augmented permeability of the fluid raises IFP in the tumour, obstructing the extravasation of nanoparticles, postulating that normalisation of the vasculature can improve extravasation by decreasing IFP in the tumour. Further, the effect of vascular normalisation on the delivery of nanomedicines to tumours was studied by a mathematical model designed by Chauhan et al. [64], where a two-dimensional

percolation network was fabricated with an inlet and an outlet to simulate the tumour microvasculature structure, taking into consideration the blood flow, fluid flow (transvascular), interstitial fluid transport and drug transport, besides permeability in tumour vessel wall. It was observed that vascular normalisation upgraded delivery of the smaller nanoparticles to the tumour; however, it delayed transport of the larger ones [64]. Nonetheless, this model was applied to assess the effect of the particle surface charge on the distribution of nanoparticles in the tumour, once electrostatic interactions between the particles and pores in the blood vessel wall were taken into account.

In context to particle engineering, this model investigated the effect of particle size, drug-release rate and targeted binding affinity on intratumour distribution [65, 66], which disclosed small particles (≤ 10 nm) being more effective in tumour distribution and deep penetration. Thus, a two-stage methodology was projected to encapsulate the 5-nm secondary particles into a 20-nm primary particle to avert the fast clearance of small particles and their extravasation to normal tissues. Moreover, antitumor efficacy of nanoparticles relates positively to the release rate; thus, a fairly high value of release rate will be desirable for liposomes. For augmenting the efficacy, suitable targeted binding affinity is obligatory, since relatively high binding rate can trap the drug. The simulation data, thus, recommended a binding rate constant of around $1000 \text{ (M}^{-1} \text{ s}^{-1}\text{)}$ to be optimal rate for killing tumour cells.

5.4 Combination of In Vitro Study and the PK–PD Modelling System

The physicochemical properties of liposomes and the biological system decide the systemic disposition profile of liposomal drugs; the extravasation rate of liposomes is determined by varied factors like particle size, surface charges, shapes, vascular endothelial structures and the permeability of the targeted tissue. Kirtane et al. established a system-based model for predicting the

targeted exposure of nanoparticles based on particle and vascular pore sizes [67] and showed that a particle size that was entirely optimal for all types of tumours could not be identified and that the optimal particle properties were dependent on the type and features of the tumour. Moreover, the inconsistency of experimental animals misperceives the identification of influential particle parameters on each process of particle disposition. For identifying the effect of particle properties on particle disposition, an *in vitro* assay under well-controlled biological conditions is a much anticipated tool in comparison to the *in vivo* study. Yet, translation of result of *in vitro* assay to *in vivo* liposome disposition prosperities remains a major obstacle. The IVIVC is defined as a predictive mathematical model used to describe the relationship between the *in vitro* property of a dosage form and a relevant *in vivo* response [68]. As soon as IVIVC is established and validated, the results of *in vitro* studies can be exploited to envisage drug performance *in vivo*. Thus, a combination of well-controlled high-throughput *in vitro* assays and IVIVC methodologies between particle properties and the *in vivo* disposition (e.g. clearance, extravasation) of the liposomes has potential in liposome optimisation. Besides, IVIVC could be assimilated with PK–PD modelling system to foresee the targeted exposure of API and the efficacy of the liposome based on the *in vitro* measurable particle properties.

Mayer et al. established an IVIVC method to foresee liposome *in vivo* release [69], wherein multilamellar vesicles were used as “acceptors” to simulate the *in vivo* membrane and in turn calculate drug release *in vivo*. The *in vitro* release testing method specifically prophesied the *in vivo* release characteristics of liposomal drugs in comparison to dialysis membrane method. Another study employed a two-stage reverse dialysis method (i.e. dialysis in pH 7.4 HEPES buffer solution [stage 1] and dialysis in 1% TX100 solution in HEPES buffer solution [stage 2]) to imitate the drug release into the circulation and targeted tissue [70]. Furthermore, premature drug release could be persuaded by plasma protein adsorption and the consequent

identification of liposomes by the MPS. Researcher Crielaard et al. used surface plasmon resonance and single-molecule tracking fluorescence microscopy to categorise liposome–protein interactions and liposome aggregations to predict systemic clearance [71]. The study showed no aggregation and clearance of the liposomes positively related to interactions between the liposomes and proteins, signifying that liposome–protein interactions could be used to envisage the systemic clearance of liposomes. This IVIVC approach when combined into a PBPK model was able to measure the effect of liposomal properties on the multiscale mechanisms of liposomal disposition [72]. Thus, integrated modelling framework enhances the capacity to recognise serious or inconsequential physicochemical properties, which would possibly help the regulatory reviews that are steered to evaluate generic liposomal drugs.

6 Modelling Drug Release

Due to complexity of nano-sized dosage forms and difficulty in drug release evaluations, few studies have deliberated to describe drug release profiles from nanoparticulate dosage forms by employing mathematical models. Conversely, Barzegar-Jalali et al. endorsed the usage of reciprocal powered time (RPT) as general model to analyse multifaceted characteristic of drug release from nanoparticles, together with substitute method being the Weibull and log-probability models [73]. In an additional study, Zeng et al. exploited a three-parameter model reflecting reversible drug–carrier interactions as well as diffusional drug release from liposomes [74, 75]. Clearly, utilisation of mathematical models to designate drug-release profiles has numerous advantages; namely, the elucidation of drug-release mechanisms becomes possible, and it can be used to guide formulation development efforts. Moreover, model parameters can help in representation and comparison of in vitro release profiles. Nevertheless, attention must be used when applying mathematical models to complex drug-release mechanisms.

7 IVIVC

IVIVC is a predictive mathematical model which describes the relationship between an in vitro property of an extended release dosage form (usually the rate or extent of drug in vitro release or release) and a relevant in vivo response (plasma drug concentration or amount of drug absorbed). IVIVC, designated as a link between in vitro release and in vivo behaviour, augments the efficacy of an in vitro study. As per the 1997 FDA guidance document, an IVIVC will decrease the regulatory burden by paring the number of in vivo studies needed for product approval as well as endorses the setting of clinically relevant in vitro release specifications [76]. IVIVCs can be categorised into three levels: Level A signifies a linear or nonlinear point-to-point association between the in vitro and in vivo release profiles and designates the highest correlation and is most commonly used to obtain a biowaiver. In case of nonlinear relationship, appropriate modelling or scaling is required. Level B signifies a comparison of summary parameters such as the mean in vitro dissolution time with mean in vivo dissolution time or mean residence time (MRT). Level B relationships are not as prejudiced as level A, because numerous in vivo curves will produce a similar MRT value or mean in vitro dissolution time. Level C correlation designates a relationship between an in vitro release parameter like % dissolved at a particular time and a PK parameter like C_{max} , though a level C correlation does not describe the complete shape of the in vivo release profile and is rarely used. Per se, the FDA guidance is projected for oral extended release products but had been used to establish an IVIVC from several non-oral dosage forms, including nano-sized preparations as well. In most studies, in vitro release behaviour is compared with the in vivo absorption profile in IVIVC [76, 77], and after computing the fraction absorbed, an association is obtained by relating it with the in vitro release profile followed by determination of the type of IVIVC (level A, level B, etc.).

In a study by Kumar et al., the relationship between in vitro and in vivo release from indomethacin gelatin nanoparticles was explored

post-oral administration in Wistar albino rats [78]. Results showed a good correlation when the fraction absorbed in vivo (Wagner–Nelson method) was plotted against the fraction released (performed using regular dialysis (dialysis bags)). In yet another study, the Wagner–Nelson method was also employed where the in vivo absorption from silybin meglumine hollow sphere mesoporous silica nanoparticles was compared with in vitro results obtained using a combination USP I (paddle) dialysis bag setup in beagle dogs treated with oral dose with nanoparticles [79]. Results of this study demonstrated that a level A IVIVC ($R^2 > 0.97$) was obtained with 0.06M Na₂CO₃ and 0.08M Na₂CO₃ solutions in comparison with five different release media employed in the study [80]. In addition, many studies have compared in vivo release from beagle dogs with in vitro release assessed using a combination USP I (paddle) dialysis bag setup [81].

8 Summary

The anticipated progress in ADME and PK profiles of the encapsulated drug being delivered is mainstay characteristic in the value proposition of any nanomaterial-based drug delivery system. Noteworthy evolution has been initiated to comprehend the intricate and multifactorial associations between various factors like nanomaterial physicochemical properties, species physiology, biological interactions, etc., with the PK profiles which has powered the coherent strategy for numerous nanomaterials with long circulation times and enhanced tissue accumulation. However, the fundamental shortcomings in these research efforts are the unpredictable and inadequate categorisation of the PK profiles of nanomaterials in scientific reporting. Consequently, a transformed attention in establishing reliable and wide-ranging approaches for designing pre-clinical experiments to evaluate the nanomaterial PK with assorted physicochemical properties has thrived in recent times. The projected and implemented strategies for the experimental design of PK studies with NPDDS are sum-

marised to deliver nanomaterial researchers with concrete information and realistic commendations for choosing the paramount design and procedures for PK profile evaluation and optimistically capitalise on the probabilities of translational success of these innovative products into human use.

References

1. Celia C, Cosco D, Paolino D, Fresta M. Gemcitabine-loaded innovative nanocarriers vs GEMZAR: biodistribution, pharmacokinetic features and in vivo antitumor activity. *Expert Opin Drug Deliv.* 2011;8(12):1609–29.
2. Florence AT. “Targeting” nanoparticles: the constraints of physical laws and physical barriers. *J Control Release.* 2012;164(2):115–24.
3. Mahapatro A, Singh DK. Biodegradable nanoparticles are excellent vehicle for site directed in-vivo delivery of drugs and vaccines. *J Nanobiotechnology.* 2011;9(1):55–65.
4. Musthaba SM, Ahmad S, Ahuja A, Ali J, Baboota S. Nano approaches to enhance pharmacokinetic and pharmacodynamic activity of plant origin drugs. *Curr Nanosci.* 2009;5(3):344–52.
5. Li M, Al-Jamal KT, Kostarelos K, Reineke J. Physiologically based pharmacokinetic modeling of nanoparticles. *ACS Nano.* 2010;4(11):6303–17.
6. Hamidi M, Azadi A, Rafiei P, Ashrafi H. A pharmacokinetic overview of nanotechnology-based drug delivery systems: an ADME-oriented approach. *Crit Rev Ther Drug Carrier Syst.* 2013;30(5):435–67.
7. Oberdörster G. Safety assessment for nanotechnology and nanomedicine: concepts of nanotoxicology. *J Intern Med.* 2010;267(1):89–105.
8. Yang RSH, Chang LW, Yang CS, Lin P. Pharmacokinetics and physiologically-based pharmacokinetic modeling of nanoparticles. *J Nanosci Nanotechnol.* 2010;10(12):8482–90.
9. Moghimi SM, Hunter AC, Murray JC. Long-circulating and target-specific nanoparticles: theory to practice. *Pharmacol Rev.* 2001;53(2):283–318.
10. Patra JK, Das G, Fraceto LF, Campos EVR, Rodriguez-Torres MDP, Acosta-Torres LS, et al. Nano based drug delivery systems: recent developments and future prospects. *Nanobiotechnology.* 2018;16:71–103.
11. Wang N, Feng Y. Elaborating the role of natural products-induced autophagy in cancer treatment: achievements and artifacts in the state of the art. *Biomed Res Int.* 2015;2015(934207):14.
12. Abdelwahab SI, Sheikh BY, Taha MME, How CW, Abdullah R, Yagoub U, El-Sunousi R, Eid EE. Thymoquinone-loaded nanostructured lipid carriers: preparation, gastroprotection, in vitro toxicity,

- and pharmacokinetic properties after extravascular administration. *Int J Nanomedicine*. 2013;8:2163–72.
13. Tan Q, Liu W, Guo C, Zhai G. Preparation and evaluation of quercetin loaded lecithin-chitosan nanoparticles for topical delivery. *Int J Nanomedicine*. 2011;6:1621–30.
 14. Sanna V, Roggio AM, Siliani S, Piccinini M, Marceddu S, Mariani A, Sechi M. Development of novel cationic chitosan-and anionic alginate-coated poly (d, l-lactide-co-glycolide) nanoparticles for controlled release and light protection of resveratrol. *Int J Nanomedicine*. 2012;7:5501–16.
 15. Casettari L, Illum L. Chitosan in nasal delivery systems for therapeutic drugs. *J Control Release*. 2014;190:189–200.
 16. Lam P-L, Wong W-Y, Bian Z, Chui C-H, Gambari R. Recent advances in green nanoparticulate systems for drug delivery: efficient delivery and safety concern. *Nanomedicine*. 2017;12:357–85.
 17. Dawidczyk CM, Kim C, Park JH, Russell LM, Lee KH, Pomper MG, et al. State-of-the-art in design rules for drug delivery platforms: lessons learned from FDA-approved nanomedicines. *J Control Release*. 2014;187:133–44.
 18. Sikarra D, Shukla VAA, Kharia AA, Chatterjee DP. Techniques for solubility enhancement of poorly soluble drugs: an overview. *JMPAS*. 2012;1:1–22.
 19. Siccardi M, Rajoli RKR, Curley P, Olagunju A, Moss D, Owen A. Physiologically based pharmacokinetic models for the optimization of antiretroviral therapy: recent progress and future perspective. *Future Virol*. 2013;8:871–90.
 20. Karlsson FH, Bouchene S, Hilgendorf C, Dolgos H, Peters SA. Utility of in vitro systems and preclinical data for the prediction of human intestinal first-pass metabolism during drug discovery and preclinical development. *Drug Metab Dispos*. 2013;41:2033–46.
 21. Corazzari ES. Intestinal mucus barrier in normal and inflamed colon. *J Pediatr Gastroenterol Nutr*. 2009;48(Suppl. 2):S54–5.
 22. Johansson ME, Ambort D, Pelaseyed T, Schutte A, Gustafsson JK, Ermund A, et al. Composition and functional role of the mucus layers in the intestine. *Cell Mol Life Sci*. 2011;68:3635–41.
 23. Ensign LM, Schneider C, Suk JS, Cone R, Hanes J. Mucus penetrating nanoparticles: biophysical tool and method of drug and gene delivery. *Adv Mater*. 2012;24:3887–94.
 24. He B, Lin P, Jia ZR, Du WW, Qu W, Yuan L, et al. The transport mechanisms of polymer nanoparticles in Caco-2 epithelial cells. *Biomaterials*. 2013;34:6082–98.
 25. Rehman K, Zulfakar MH. Recent advances in gel technologies for topical and transdermal drug delivery. *Drug Dev Ind Pharm*. 2013;40:433–40.
 26. Patel D, Naik S, Misra A. Improved transnasal transport and brain uptake of tizanidine HCl-loaded thiolated chitosan nanoparticles for alleviation of pain. *J Pharm Sci*. 2012;101:690–706.
 27. Tenzer S, Docter D, Kuharev J, Musyanovych A, Fetz V, Hecht R, et al. Rapid formation of plasma protein corona critically affects nanoparticle pathophysiology. *Nat Nanotechnol*. 2013;8:772–81.
 28. Ruoslahti E. Peptides as targeting elements and tissue penetration devices for nanoparticles. *Adv Mater*. 2012;24:3747–56.
 29. Moss DM, Siccardi M. Optimizing nanomedicine pharmacokinetics using physiologically based pharmacokinetics modelling. *Br J Pharmacol*. 2014;171:3963–79.
 30. Abu Lila AS, Kiwada H, Ishida T. The accelerated blood clearance (ABC) phenomenon: clinical challenge and approaches to manage. *J Control Release*. 2013;172:38–47.
 31. Fischer HC, Chan WCW. Nanotoxicity: the growing need for in vivo study. *Curr Opin Biotechnol*. 2007;18(6):565–71.
 32. Gabizon A, Shmeeda H, Barenholz Y. Pharmacokinetics of pegylated liposomal doxorubicin. *Clin Pharmacokinet*. 2003;42(5):419–36.
 33. Yuan D, He H, Wu Y, Fan J, Cao Y. Physiologically based pharmacokinetic modeling of nanoparticles. *J Pharm Sci*. 2019;108:58–72.
 34. Jones H, Rowland-Yeo K. Basic concepts in physiologically based pharmacokinetic modeling in drug discovery and development. *CPT Pharmacometrics Syst Pharmacol*. 2013;2(8):e63.
 35. Cao Y, Balthasar JP, Jusko WJ. Second-generation minimal physiologically based pharmacokinetic model for monoclonal antibodies. *J Pharmacokin Pharmacodyn*. 2013;40(5):597–607.
 36. Quignot N. Modeling bioavailability to organs protected by biological barriers. In *Silico Pharmacol*. 2013;1:8.
 37. Wu H, Infante JR, Keedy VL, Jones SF, Chan E, Bendell JC, et al. Population pharmacokinetics of PEGylated liposomal CPT-11 (IHL-305) in patients with advanced solid tumors. *Eur J Clin Pharmacol*. 2013;69:2073–81.
 38. Wu H, Infante JR, Keedy VL, Jones SF, Chan E, Bendell JC, et al. Factors affecting the pharmacokinetics and pharmacodynamics of PEGylated liposomal irinotecan (IHL-305) in patients with advanced solid tumors. *Int J Nanomedicine*. 2015;10:1201–9.
 39. Sinha V, Zhao P, Huang SM, Zineh I. Physiologically based pharmacokinetic modeling: from regulatory science to regulatory policy. *Clin Pharmacol Ther*. 2014;95:478–80.
 40. Harashima H, Tsuchihashi M, Iida S, Doi H, Kiwada H. Pharmacokinetic/pharmacodynamic modelling of antitumor agents encapsulated into liposomes. *Adv Drug Deliv Rev*. 1999;40:39–61.
 41. Harashima H, Iida S, Urakami Y, Tsuchihashi M, Kiwada H. Optimization of antitumor effect of liposomally encapsulated doxorubicin based on simulations by pharmacokinetic/pharmacodynamics modeling. *J Control Release*. 1999;61:93–106.
 42. Hendriks BS, Reynolds JG, Klinz SG, Geretti E, Lee H, Leonard SC, et al. Multiscale kinetic modeling of

- liposomal Doxorubicin delivery quantifies the role of tumor and drug-specific parameters in local delivery to tumors. *CPT Pharmacometrics Syst Pharmacol*. 2012;1:e15–25.
43. Apgar JF, Tang JP, Singh P, Balasubramanian N, Burke J, Hodges MR, et al. Quantitative systems pharmacology model of hUGT1A1-modRNA encoding for the UGT1A1 enzyme to treat crigler-najjar syndrome type 1. *CPT Pharmacometrics Syst Pharmacol*. 2018;7:404–12.
 44. Kagan L, Gershkovich P, Wasan KM, Mager DE. Dual physiologically based pharmacokinetic model of liposomal and nonliposomal amphotericin B disposition. *Pharm Res*. 2014;31:35–45.
 45. D'Souza S. Pharmacokinetics and pharmacodynamics modeling and simulation systems to support the development and regulation of liposomal drugs. *Adv Pharm*. 2019;2014:12.
 46. La-Beck NM, Zamboni BA, Gabizon A, Schmeeda H, Amantea M, Gehrig PA, et al. Factors affecting the pharmacokinetics of pegylated liposomal doxorubicin in patients. *Cancer Chemother Pharmacol*. 2012;69(1):43–50.
 47. Howell BA, Chauhan A. A physiologically based pharmacokinetic (PBPK) model for predicting the efficacy of drug overdose treatment with liposomes in man. *J Pharm Sci*. 2010;99(8):3601–19.
 48. Lu XF, Bi K, Chen X. Physiologically based pharmacokinetic model of docetaxel and interspecies scaling: comparison of simple injection with folate receptor targeting amphiphilic copolymer-modified liposomes. *Xenobiotica*. 2016;46(12):1093–104.
 49. Rajoli RK, Back DJ, Rannard S, Freel Meyers CL, Flexner C, Owen A, et al. Physiologically based pharmacokinetic modelling to inform development of intramuscular long-acting nanoformulations for HIV. *Clin Pharmacokinet*. 2015;54(6):639–50.
 50. Yu LX, Amidon GL. A compartmental absorption and transit model for estimating oral drug absorption. *Int J Pharm*. 1999;186(2):119–25.
 51. Jung F, Nothnagel L, Gao F, Thurn M, Vogel V, Wacker MG. A comparison of two biorelevant in vitro drug release methods for nanotherapeutics based on advanced physiologically-based pharmacokinetic modelling. *Eur J Pharm Biopharm*. 2018;127:462–70.
 52. Shono Y, Jantravid E, Kesisoglou F, Reppas C, Dressman JB. Forecasting in vivo oral absorption and food effect of micronized and nanosized aprepitant formulations in humans. *Eur J Pharm Biopharm*. 2010;76(1):95–104.
 53. Kumar S, Singh SK. In silico-in vitro-in vivo studies of experimentally designed carvedilol loaded silk fibroin-casein nanoparticles using physiological based pharmacokinetic model. *Int J Biol Macromol*. 2017;96:403–20.
 54. Siccardi M, Martin P, Smith D, Curley P, McDonald T, Giardiello M, et al. Towards a rational design of solid drug nanoparticles with optimised pharmacological properties. *J Interdiscip Nanomed*. 2016;1(3):110–23.
 55. Waechter BSJ, Martin D. Pharmacokinetics. In: *Applied pharmacology*. Saunders; 2011. p. 17–34.
 56. Lyulkin M. The route less travelled: utilizing pre-clinical models to address challenges with novel drug delivery systems. <https://www.pharmoutsourcing.com/Featured-Articles/564960-The-Route-Less-Travelled-Utilizing-Pre-Clinical-Models-to-Address-Challenges-with-Novel-Drug-Delivery-Systems/>
 57. Garralda E, Dienstmann R, Tabernero J. Pharmacokinetic/pharmacodynamic modeling for drug development in oncology. *Am Soc Clin Oncol Educ Book*. 2017;37:210–5.
 58. Li M, Zou P, Tyner K, Lee S. Physiologically based pharmacokinetic (PBPK) modeling of pharmaceutical nanoparticles. *AAPS J*. 2017;19:26–42.
 59. Khawar IA, Kim JH, Kuh HJ. Improving drug delivery to solid tumors: priming the tumor microenvironment. *J Control Release*. 2015;201:78–89.
 60. Frieboes HB, Wu M, Lowengrub J, Decuzzi P, Cristini V. A computational model for predicting nanoparticle accumulation in tumor vasculature. *PLoS One*. 2013;8(2):e56876.
 61. Troendle EP, Khan A, Searson PC, Ulmschneider MB. Predicting drug delivery efficiency into tumor tissues through molecular simulation of transport in complex vascular networks. *J Control Release*. 2018;292:221–34.
 62. Macklin P, McDougall S, Anderson AR, Chaplain MA, Cristini V, Lowengrub J. Multiscale modelling and nonlinear simulation of vascular tumour growth. *J Math Biol*. 2009;58:765–98.
 63. Curtis LT, Wu M, Lowengrub J, Decuzzi P, Frieboes HB. Computational modeling of tumor response to drug release from vasculature-bound nanoparticles. *PLoS One*. 2015;10:e0144888.
 64. Chauhan VP, Stylianopoulos T, Martin JD, Popovic Z, Chen O, Kamoun WS, et al. Normalization of tumour blood vessels improves the delivery of nanomedicines in a size-dependent manner. *Nat Nanotechnol*. 2012;7:383–8. PMID: 22484912; PMCID: PMC3370066. <https://doi.org/10.1038/nnano.2012.45>.
 65. Stylianopoulos T, Economides EA, Baish JW, Fukumura D, Jain RK. Towards optimal design of cancer nanomedicines: multi-stage nanoparticles for the treatment of solid tumors. *Ann Biomed Eng*. 2015;43:2291–300.
 66. Stylianopoulos T, Jain RK. Combining two strategies to improve perfusion and drug delivery in solid tumors. *Proc Natl Acad Sci U S A*. 2013;110:18632–7.
 67. Kirtane AR, Siegel RA, Panyam J. A pharmacokinetic model for quantifying the effect of vascular permeability on the choice of drug carrier: a framework for personalized nanomedicine. *J Pharm Sci*. 2015;104:1174–86.
 68. FDA. Guidance for industry: extended release oral dosage forms: development, evaluation and application of in vitro/in vivo correlations. Available online: <https://www.fda.gov/downloads/drugs/guidances/ucm070239.pdf>. Accessed 15 Jan 2019.

69. Shabbits JA, Chiu GN, Mayer LD. Development of an in vitro drug release assay that accurately predicts in vivo drug retention for liposome-based delivery systems. *J Control Release*. 2002;84:161–70.
70. Xu X, Khan MA, Burgess DJ. A two-stage reverse dialysis in vitro dissolution testing method for passive targeted liposomes. *Int J Pharm*. 2012;426:211–8.
71. Crielaard BJ, Yousefi A, Schillemans JP, Vermehren C, Buyens K, Braeckmans K, et al. An in vitro assay based on surface plasmon resonance to predict the in vivo circulation kinetics of liposomes. *J Control Release*. 2011;156:307–14.
72. Stylianopoulos T, Soteriou K, Fukumura D, Jain RK. Cationic nanoparticles have superior transvascular flux into solid tumors: insights from a mathematical model. *Ann Biomed Eng*. 2013;41:68–77.
73. Barzegar-Jalali M, Adibkia K, Valizadeh H, Shadbad MR, Nokhodchi A, Omid Y, et al. Kinetic analysis of drug release from nanoparticles. *J Pharm Pharm Sci*. 2008;11(1):167–77.
74. Zeng L, An L, Wu X. Modeling drug-carrier interaction in the drug release from nanocarriers. *J Drug Delivery*. 2011;2011:D370308.
75. Zeng L, Wu X. Modeling the sustained release of lipophilic drugs from liposomes. *Appl Phys Lett*. 2010;97(7):073701.
76. FDA guidance for industry, extended release oral dosage forms: development, evaluation and application of in vitro/in vivo correlations. 1997 <https://www.fda.gov/regulatory-information/search-fda-guidance-documents/extended-release-oral-dosage-forms-development-evaluation-and-application-vitro-in-vivo-correlations>
77. Wagner JG, Nelson E. Per cent absorbed time plots derived from blood level and/or urinary excretion data. *J Pharm Sci*. 1963;52:610–1.
78. Kumar R, Nagarwal RC, Dhanawat M, Pandit JK. In-vitro and in-vivo study of indomethacin loaded gelatin nanoparticles. *J Biomed Nanotechnol*. 2011;7(3):325–33.
79. Cao X, Deng WW, Fu M, et al. In vitro release and in vitro in vivo correlation for silybin meglumine incorporated into Hollow-type mesoporous silica nanoparticles. *Int J Nanomedicine*. 2012;7:753–62.
80. Cao X, Deng W, Fu M, et al. Seventy-two-hour release formulation of the poorly soluble drug silybin based on porous silica nanoparticles: in vitro release kinetics and in vitro/in vivo correlations in beagle dogs. *Eur J Pharm Sci*. 2013;48(1–2):64–71.
81. D'Souza S. A review of in vitro drug release test methods for nano-sized dosage forms. *Adv Pharm*. 2014;2014:12.



Pharmacokinetic Modeling Program (PKMP): A Software for PK/PD Data Analysis

7

Ajit K. Shah

Contents

1	Introduction	102
2	Organization of PKMP	103
3	Analysis Modules	103
4	Bioequivalency (BE) Analysis (Two-Way Crossover Study)	106
5	Repeated BE Analysis	106
6	Analysis of Variance (ANOVA)	108
7	Dose Proportionality Analysis	108
8	Urine Data Analysis	109
9	Superposition Analysis	110
10	Toxicokinetics	110
11	Interspecies Scaling	112
12	Method 1: NCA	114
13	Method 2: PK Parameters	114
14	Method 3: Human Equivalent Dose (HED) (Table 7.12)	115
15	Dose Escalation	115
16	Compartmental Pharmacokinetics (CA-PK)	117
17	Pharmacodynamics (PD) Analysis	117
18	Dissolution Data Analysis	118
19	Dissolution Profile Comparison	120
20	Difference Factor	121
21	Similarity Factor	121
22	Multivariate Statistical Difference (MSD) Determination	121

A. K. Shah (✉)
APL, Eden Prairie, MN, USA
e-mail: shah.ajit@aplanalytics.com

23	IVIVC Model	121
24	Level A Correlation	122
25	Correlations	125
26	Simulation	127
27	IVIVC	130
28	Bioequivalence (BE)	130
29	Sample Size	131
30	Differential Equation-Based Analysis (dEq)	132
31	Conclusions	135
	References	138

Abstract

In drug research and development, pharmacokinetics, which characterizes absorption, distribution, metabolism, and elimination of the drug from the body after its administration in animals and humans, plays an important role in delineating the dose-response relationship, either for toxicity in animal studies or safety and efficacy analysis in human clinical trials. The following is an overview of the pharmacokinetic modeling program (PKMP) developed to perform data analysis to support drug research and development. PKMP is a web-based commercial program created using the open source codes for Java coding language and R libraries. The web-based platform allows easy and secure access to the program using any Internet browser, and the program is independent of operating systems, such as MacOS or Windows. The program has been extensively tested for validation and verification of every module for its quality and functionality. Pharmacokinetic, pharmacodynamic, statistical analysis, dissolution, IVIVC, simulation, modeling, and reporting are some of its main functionalities, allowing for a wide range of data analyses to support drug product evaluation and development during different phases of drug development.

Keywords

Pharmacokinetics · Pharmacodynamics · Dissolution · IVIVC · Modeling · Simulation · Toxicokinetics · Interspecies scaling · Biopharmaceutics · Bioequivalence

1 Introduction

The drug development process involves discovery phase, preclinical research, clinical research, and regulatory approval for marketing. From start to finish, the drug development takes 10–15 years, and the average research and development cost is estimated to be \$2.6 billion [1]. In each phase of drug research and development, pharmacokinetics, which characterizes absorption, distribution, metabolism, and elimination of the drug from the body after its administration in animals and humans, plays an important role in delineating the dose-response relationship, either for toxicity in animal studies or safety and efficacy analysis in human clinical trials. Therefore, pharmacokinetic data analysis has become an essential part in the following key areas of drug development, including, but not limited to, lead identification/optimization, dose-response analysis, bioequivalence analysis of drug products, in vitro–in vivo correlations for formulations, dissolution data analysis, modeling, and simulations. These analyses are critical in drug development for cost and time savings. The generic drug products are created to provide medicines at a reduced cost and involve drug development based on demonstrating pharmacokinetic equivalence of systemic drug concentrations of generic and innovator products. The pharmacokinetic data analysis nowadays is performed using commercial software packages having a wide range of capabilities for data analysis, visual display, and simulations. The following is an overview of the pharmacokinetic modeling program (PKMP) developed to perform these types of data analysis

to support drug research and development. Theoretical aspects of each analysis and functionalities of PKMP are extensively published elsewhere [2–4]. The computational algorithms in PKMP are based on the pharmacokinetic and statistical theories from textbooks [2–4], published literature [5], and regulatory guidance documents from the Food and Drug Administration (FDA) of the United States.

2 Organization of PKMP

The organization of PKMP data analysis modules, file upload functionalities, sample files for data analysis, and the last file analyzed are displayed on the dashboard of program as shown in Fig. 7.1. The user is required to have a user ID and password to access the dashboard and analysis modules. The typical file format for upload is Excel data types, such as XLS, XLSX, or CSV. Once the file is selected for upload, its association for the type of analysis is required using the radio buttons provided on the dashboard. Sample data files for different types of analysis are provided to get used to the data format needed for an analysis module. Previously performed analyses and their reports are stored and can easily be accessed from the dashboard.

3 Analysis Modules

The data analysis modules are displayed on the left side of the dashboard. Each module has sub-modules for appropriate data analysis and is described below.

3.1 NCA-PK

Noncompartmental methods (NCA-PK) for pharmacokinetic parameters are based on estimation of the area under a curve of drug concentration vs. time data following the drug administration by either extravascular (oral, intramuscular, topical, etc.) or vascular routes (intravenous, intra-arterial, etc.).

Noncompartmental methods do not require the assumption of specific compartmental model for either drug or metabolite. The methods assume input, elimination, and sampling from the central compartment [2, 3, 5].

3.2 Extravascular/IV Bolus/IV Infusion

The plasma concentration time profiles following oral administration of a drug are shown in Fig. 7.2.

To compute noncompartmental pharmacokinetic parameters for a plasma concentration vs. time profile, as shown in Fig. 7.3, the curve is divided into a number of trapezoids by drawing a vertical line for each concentration corresponding with time point on x-axis.

The following methods [2] are used to compute area under each trapezoid:

Linear Trapezoidal Rule

$$\text{AUC} = \sum_{i=0}^{i=n} \frac{C_i + C_{i+1}}{2} \cdot t \quad (7.1)$$

C_i and C_{i+1} are the plasma concentrations at time t_i and t_{i+1} , respectively, and Δt is the sampling time interval. After a single oral dose of a drug, C_i at time 0 is typically zero. C_i at time 0 has a positive value following a single intravenous bolus dose of drug. Therefore, the concentration at time 0 can be extrapolated back using either linear back extrapolation, a user-defined value, or a compartmental back extrapolation for one, two, or three compartment body models for an IV dose. The area under the curve is summation of individual area under each trapezoid up to last time of sampling t .

Log-Linear Trapezoidal Rule

In cases where concentrations are more curved between the sampling time points, area estimates are obtained using the log-linear trapezoidal rule:

$$\text{AUC} = \sum_{i=0}^{i=n} \frac{(C_i - C_{i+1})}{(\ln C_i - \ln C_{i+1})} \cdot t \quad (7.2)$$

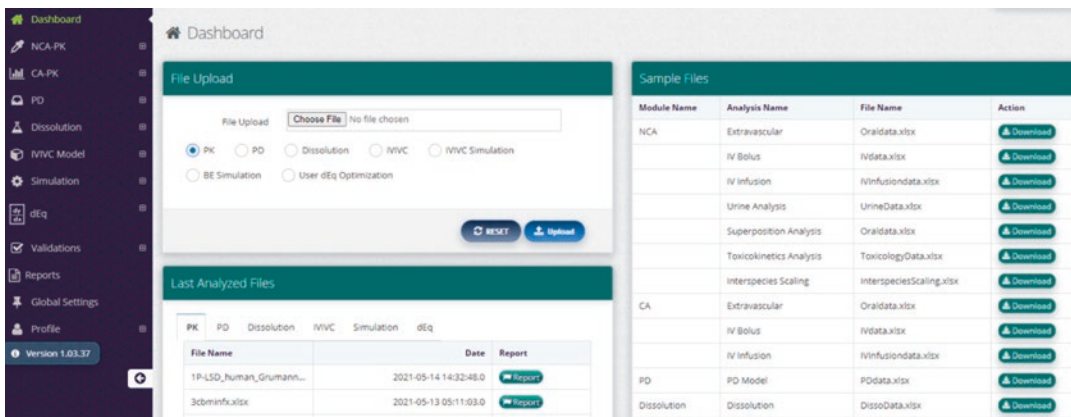


Fig. 7.1 The organization of PKMP

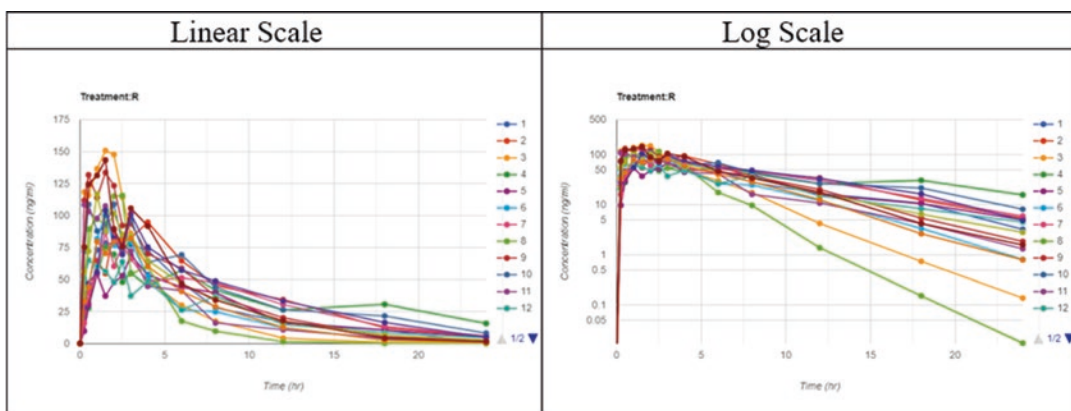


Fig. 7.2 Plasma concentration vs. time profiles in subjects following oral administration of a single dose of a drug

3.3 Mixed Log-Linear

This method is a combination of above linear and log-linear trapezoidal methods applied to up and down parts of a concentration time profile.

Maximum drug concentration (C_{max}) and time to C_{max} (T_{max}) are estimated based on observed data as shown in Fig. 7.3. The terminal phase elimination rate constant, K_{el} , is estimated from the slope of the concentration-time data during the log-linear terminal phase using least squares regression analysis. For the K_{el} calculation, PKMP uses the last four data points by default (Fig. 7.4). The calculated regression parameters (slope and intercept), their statistics for R^2 and R^2 -adjusted, and number of data points used are displayed. The user can modify this, as

appropriate, by clicking and selecting other data points. The updated calculations are saved and retained by the program.

The terminal phase elimination half-life ($T_{1/2}$) is calculated as

$$T_{1/2} = \frac{0.693}{K_{el}} \tag{7.3}$$

The area under the concentration-time curve (AUC_{0-t}) from time 0 to the last measurable concentration (C_t) at time t is calculated using the trapezoidal method and extrapolated to $AUC_{0-\infty}$ using

$$AUC_{(0-\infty)} = AUC_{(0-t)} + \frac{C_t}{K_{el}} \tag{7.4}$$

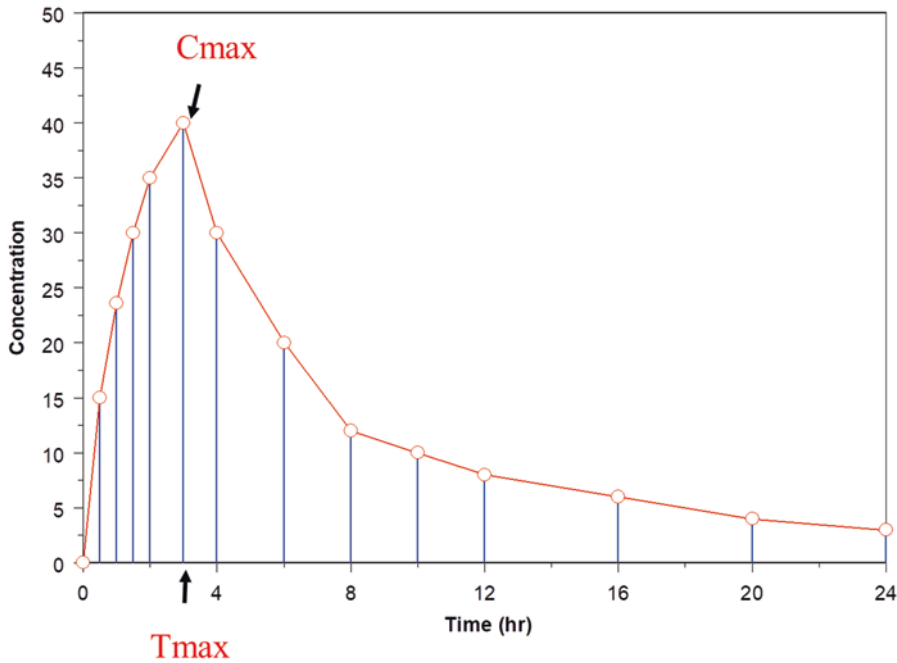


Fig. 7.3 Representation of plasma concentration vs. time profile divided into trapezoids for the noncompartmental method calculations

Partial areas under the curve also can be computed as per the selection of time points such as 0–2 hours, 4–8 hours, etc., and analysis can be repeated for all subjects.

The apparent total body clearance for oral administration is calculated as

$$CL / F = \frac{D_{\text{oral}}}{AUC_{(0-\infty)}} \quad (7.5)$$

For an intravenous dose, the term F for bioavailability is considered 1.

The apparent volume of distribution during the terminal phase after oral administration is calculated as

$$V_d / F = \frac{CL_{\text{oral}}}{K_{el}} \quad (7.6)$$

The apparent volume of distribution at steady state (V_{ss}) or equilibrium after intravenous administration is calculated as

$$V_{ss} = CL \cdot MRT \quad (7.7)$$

where

MRT is the mean residence time and is calculated as

$$MRT = \frac{\int_0^{\infty} t \cdot C dt}{\int_0^{\infty} C dt} = \frac{AUMC}{AUC} \quad (7.8)$$

For infusion administration, the duration of infusion is included in computation.

AUMC is area under the moment curve calculated by means of trapezoidal rule and extrapolated to infinity using the following equations:

$$AUMC = \sum_{i=n}^{i=0} \frac{t_i \cdot C_i + t_{i+1} \cdot C_{i+1}}{2} \cdot t \quad (7.9)$$

and

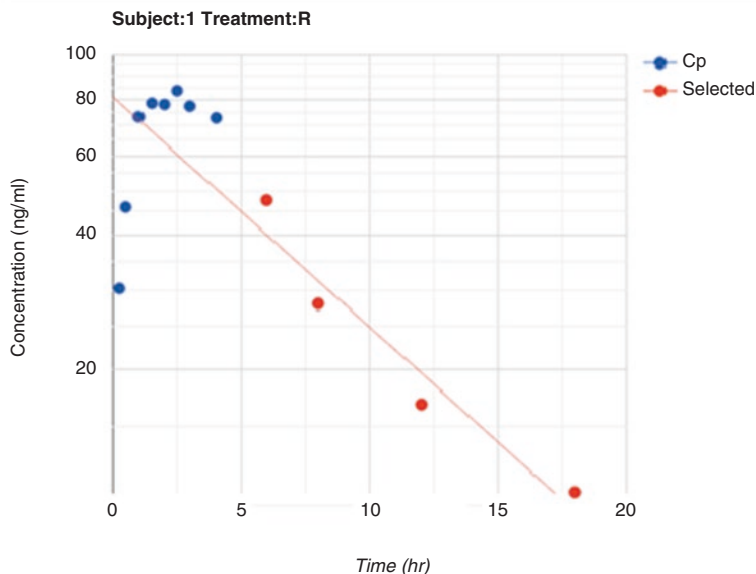
$$AUMC_{(0-\infty)} = AUMC + \frac{t_{\text{last}} \cdot C_{\text{last}}}{K_{el}} + \frac{C_{\text{last}}}{K_{el}^2} \quad (7.10)$$

The computation of NCA PK parameters is shown in Table 7.1:

The following statistical analysis can be performed after completion of NCA [6].

Fig. 7.4 Calculation of K_{el} using concentration-time data during the log-linear terminal elimination phase. Default last four points are used in the calculation which can be changed as appropriate by selecting other data points

Kel	Slope	Intercept	R ²	R ² _Adj	No. of Points
0.1295	-0.1295	83.9906	0.9590	0.9385	4



4 Bioequivalency (BE) Analysis (Two-Way Crossover Study)

Bioequivalency for two orally administered drug products is required to demonstrate the same rate and extent of absorption between the active drug ingredient or moiety in the test (T) product and the reference (R) drug product to ensure therapeutic equivalence. Bioequivalency assessment between formulations is needed during different clinical stages of drug development. Additionally, it is required for the generic product abbreviated new drug application submission. The study is conducted as a two-formulation, two-period, and two-sequence crossover design in a group of subjects administered test and reference treatments. Blood samples are obtained after administration of products to quantitate drug or metabolite concentrations and pharmacokinetic parameters [6].

For the average bioequivalence calculations, AUC and C_{max} of T and R products are log transformed. A 90% confidence interval for the T to R parameter ratio of the averages (population geometric means) is computed using an analysis of variance (ANOVA) model including sequence, period, and treatment as fixed effects and subject

within the sequence as random effect. To establish BE, the calculated confidence interval should fall within a BE limit, usually 80–125% for the T to R ratio of the parameter averages (Table 7.2).

5 Repeated BE Analysis

Repeated bioequivalence studies in which test (T) and reference (R) treatments are administered repeatedly over three or four periods. The analysis is performed as per the FDA guidance [6], using a restricted or residual maximum likelihood (REML) procedure.

The following is a model for the replicated BE studies as described in the FDA guidance document [6] that assumes a four-period design with equal replication of T and R in each of sequences, with an assumption of no (or equal) carryover effects (equal carryovers go into the period effects):

$$Y_{ijkl} = \mu_k + \gamma_{ikl} + \delta_{ijk} + \varepsilon_{ijkl} \quad (7.11)$$

where

$i = 1, \dots, s$ indicates sequence

Table 7.1 Computation of noncompartmental analysis pharmacokinetic parameters

Subject	Treatment	Period	Sequence	Dose	Kel	R ²	T _{1/2}	T _{max}	C _{max}	Time Reg Start	Time Reg End	T _{lag}	C _{last} /C _{max}	AUC _{0-t}	AUC _{All}	AUC _{0-inf}	AUC _{0-∞0-inf}	AUMC _{0-t}	AUMC _{0-inf}	MRT _{0-t}	MRT _{0-inf}	V _d /F	Cl/F
Units				mg	l/hr		hr	hr	ng/ml	hr	hr	hr		ng/ml ² hr	ng/ml ² hr	ng/ml ² hr		ng/ml ² hr ²	ng/ml ² hr ²	hr	hr	L	L/hr
1	R	1	RT	100	0.12	0.94	5.88	2.5	83.72	6	18	0	0.13	644.16	676.34	735.21	0.88	3731.24	6142.84	5.79	8.36	1154.4	136.0
2	R	2	TR	100	0.14	0.99	4.99	4	94.75	8	24	0	0.06	889.12	889.12	927.93	0.96	6664	7875.09	7.5	8.49	776.2	107.8
3	R	1	RT	100	0.30	1.00	2.31	1.5	150.86	8	24	0	0	625.14	625.14	625.6	1	2115.29	2127.8	3.38	3.4	532.2	159.8

Table 7.2 Bioequivalence analysis for a two-way crossover study

Parameter name: AUC _(0-t)						
Source	df	SS type I	SS type III	MSE	F-value	Pr >/i
Sequence	1	0.002	0.002	0.002	0.014	0.9068
Subj(Sequence)	10	1.594	1.594	0.159	29.431	4.32E-06
Period	1	0.021	0.021	0.021	3.784	0.0804
Trt	1	0.000397	0.000397	0.000	0.073	0.7921
Model	13		1.618	0.124	22.969	
Error	10		0.054	0.005		
90% confidence interval						
Trt difference log scale			Lower	Upper		
0.00813			-0.0463	0.0626		
Original scale%			T/R ratio lower%	T/R ratio upper%		
100.82			95.47	106.46		

Similar analysis for C_{max} or other parameters can be performed

$j = 1, \dots, n$ indicates subject within sequence i

$k = R, T$ indicates treatment

$l = 1, 2$ indicates replicate on treatment k for subjects within sequence i

Y_{ijkl} = the response of replicate l on treatment k for subject j in sequence i

γ_{ikl} = the fixed effect of replicate l on treatment k in sequence i

δ_{ijk} = the random subject effect for subject j in the sequence i on treatment k

ε_{ijkl} = the random error for subject j within sequence i on replicate l of treatment k

The ε_{ijkl} 's are assumed to be mutually independent and identically distributed as

$$\varepsilon_{ijkl} \sim N(0, \sigma^2 W_k^2)$$

for $i = 1 \dots s, j = 1 \dots n, k = R, T,$ and $l = 1, 2.$

In addition, the random subject effects are assumed to be mutually independent.

An example of four-period crossover study design is shown in Table 7.3.

The BE analysis for the four-period crossover repeated study for log transformed AUC for T and R treatments is displayed in Table 7.4. Similar analysis for the C_{max} can also be computed. Additional statistical results for summary, ANOVA, LSMEAN, LSMDIFF, confidence

where

y = PK parameter

intervals, correlation coefficients, residuals, and ratio test are also computed.

6 Analysis of Variance (ANOVA)

ANOVA models for parallel or repeated groups with equal or unequal sample sizes (using Welch's correction) for comparison between the means can be performed. An example of ANOVA for parallel groups is shown in Table 7.5.

7 Dose Proportionality Analysis

Dose proportionality between the pharmacokinetic exposure parameters, such as C_{max} and AUC, and administered dose is assessed to evaluate the linearity in the pharmacokinetic of a drug. This ensures predictability in increase in drug exposure as measured by C_{max} and AUC, meaning twofold increase in dose results in a proportional twofold increase in exposure. Dose proportionality is evaluated by the following analysis:

7.1 Linear Model

$$y = m \cdot x + b \tag{7.12}$$

m = slope

Table 7.3 Example of a four-period repeated crossover plasma concentration data

Subject	Time (hr)	Dose(mg)	Sequence	Treatment	Period	C_p (ng/mL)
1	0.00	100	RRTT	R	1	0.00
1	0.25		RRTT	R	1	30.36
1	1.00		RRTT	R	1	73.08
1	0.00	100	RRTT	R	2	0.00
1	0.25		RRTT	R	2	41.93
1	1.00		RRTT	R	2	132.30
1	0.00	100	RRTT	T	3	0.00
1	0.25		RRTT	T	3	30.36
1	1.00		RRTT	T	3	73.08
1	0.00	100	RRTT	T	4	0.00
1	0.25		RRTT	T	4	41.93
1	1.00		RRTT	T	4	132.30

Data for additional time points and subjects

x = dose

b = intercept

An example of dose proportionality for a PK parameter, $AUC_{(0-t)}$, is shown in Fig. 7.5. where

y = PK parameter

b = coefficient

m = exponent

x = dose

An example of dose proportionality using the power model for a PK parameter, $AUC_{(0-t)}$, is shown in Fig. 7.6.

7.3 Dose Normalization

Pharmacokinetic parameter is normalized to the lowest dose as shown in Table 7.6 and analyzed to assess dose proportionality.

Normalized C_{max} is obtained as $C_{max}/\text{dose}/\text{lowest dose}$ (Fig. 7.7).

8 Urine Data Analysis

Urinary excretion is important in understanding the routes of elimination of a drug from the body to account for the mass balance. Urinary excretion rate [2] involves measurement of drug con-

7.2 Power Model

$$y = b \cdot x^m \quad (7.13)$$

$$\log y = \log b + m \log x \quad (7.14)$$

centration in the urine over the urine collection interval and is calculated as

$$\frac{dXu}{dt} = \frac{Cu \cdot Vu}{t} \quad (7.15)$$

where

dXu/dt = urinary excretion rate

Vu = urine volume

Δt = urine collection interval

The renal clearance of a drug is calculated as

$$CL_r = \frac{Xu}{AUC} \quad (7.16)$$

where

CL_r = renal clearance

Xu = amount of drug in urine over the interval t

AUC = area under the plasma concentration-time curve over time t

The computation of urinary data from the PKMP analysis is shown in Table 7.7, and graphical output for a selected plot is shown in Fig. 7.8.

Table 7.4 Bioequivalence analysis of AUC for the four-period crossover repeated study for test (*T*) and reference (*R*) treatments

Treatment	LS means estimate	Standard error	DF	<i>T</i> -value	Lower CI	Upper CI	
T	6.64	0.047	22.9	141.258	6.55	6.74	
R	6.64	0.047	22.9	141.258	6.55	6.74	
LS means difference				90% CI		95% CI	
Treatment	Estimate	Standard error	DF	Lower	Upper	Lower	Upper
T–R	0.0	0.0509	44	–0.0855	0.0855	–0.1026	0.1026
Original scale ratio (%)				90% CI		95% CI	
Estimate				Lower	Upper	Lower	Upper
100.0				91.8	108.9	90.3	110.8

Table 7.5 Analysis of variance of AUC_(0–t) comparison for a parallel group study

ANOVA					
Effect source	Sum of squares	Degree of freedom	Mean square	<i>F</i> -value	Prob > <i>F</i>
Treatment	0.308	1	0.308	6.857	0.014
Error	1.346	30	0.045		
Total	1.653	31			

Confidence interval						
Source	Group 1 vs. Group 2					
Difference	Standard error	Degree of freedom	<i>T</i> -value	CI.low	CI.high	<i>P</i> -value
–0.196	0.075	30	1.697	–0.323	–0.069	0.014

Group comparison						90% CI		
Group	<i>N</i>	Geo. mean	%CV	Ratio	Point est.(%)	Low	High	<i>P</i> -value
Group 1	16	694.71	21.97	GP1/GP2	82.19	72.38	93.33	0.01
Group 2	16	845.21	19.97					

Similar analysis for C_{\max} and other PK parameters can be performed

9 Superposition Analysis

The principle of superposition [2] allows for the prediction of concentration-time curve after multiple consecutive doses based on the drug concentration-time data obtained after a single dose. The basic assumptions are that the drug is eliminated by first-order pharmacokinetics and the pharmacokinetics of the drug is linear. Based on the calculations of terminal elimination rate constant, dose, and intervals (equal or unequal) and number of doses, superposition analysis for data in Table 7.8 is performed as shown in Fig. 7.9.

10 Toxicokinetics

In toxicokinetic studies, mainly in mice, rats, and other rodents, the generation of a complete concentration-time profile for each animal is difficult due to the limited blood volume that can be drawn. In such a scenario, a single blood sample is obtained from each animal, and several animals are used to generate the complete concentration-time profile over a sampling time period. As the animals are sacrificed after the sampling, this is also called “destructive sampling” method [7]. An example of such a data is shown in Table 7.9.

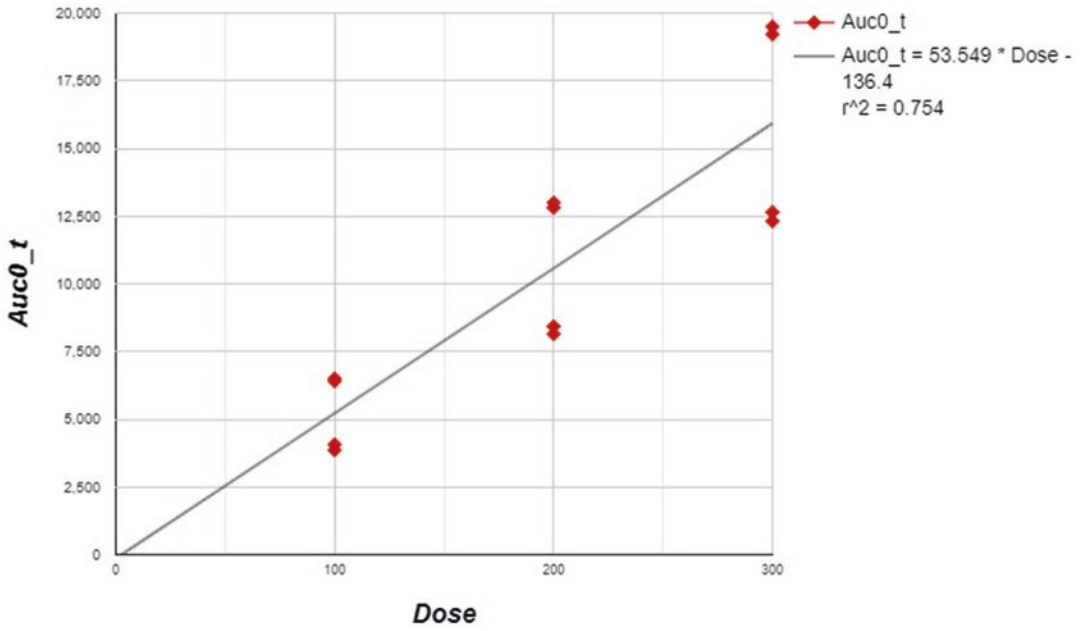


Fig. 7.5 Dose proportionality analysis using the linear model for $AUC_{(0-t)}$

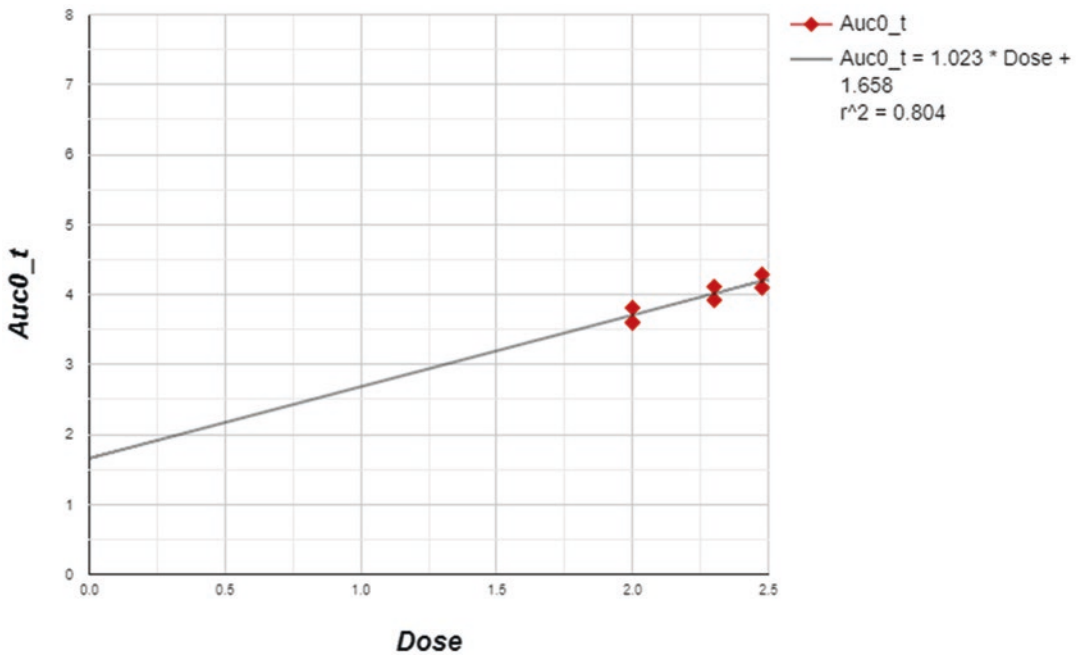


Fig. 7.6 Dose proportionality analysis using the power model for $AUC_{(0-t)}$

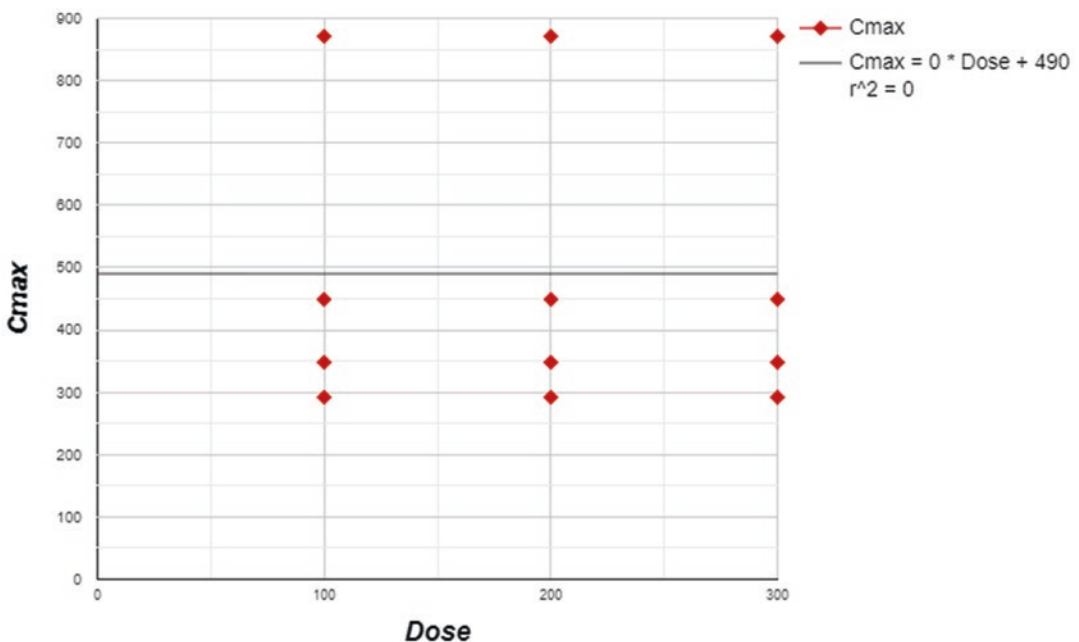
Table 7.6 Dose normalization of a PK parameter

Dose (mg)	C_{max} (mcg/ml)	Normalized C_{max}
100	449	449
100	292	292
100	871	871
100	348	348
200	898	449
200	584	292
200	1742	871
200	696	348
300	1347	449
300	876	292
300	2613	871

Normalized C_{max} is obtained as $C_{max}/\text{Dose}/\text{lowest dose}$

11 Interspecies Scaling

Interspecies scaling in pharmacokinetics allows for the prediction of in vivo drug disposition behavior in humans from the experimental observations made in one or more species. Interspecies scaling of the pharmacokinetic processes of absorption, distribution, and clearance of drugs can be performed by allometry [9, 10]. The allometric approach involves estimation of the pharmacokinetic parameters – clearance, half-life, volume of distribution, etc. – in humans based on their relationship to body mass in several test ani-

**Fig. 7.7** Dose proportionality of C_{max} using the dose normalization method

The analysis of this type of toxicokinetic data can be performed as follows using the toxicokinetic module of PKMP as shown in Table 7.10.

An ANOVA can be performed to determine the differences in the treatments administered as well as the bootstrap analysis [8] to simulate the data.

mal species. PKMP interspecies scaling module includes the following methods for prediction of human pharmacokinetics and estimation of a maximum safe starting dose (MSSD) in initial clinical trials for drugs in human subjects as per FDA guidance [11].

Table 7.7 Urine concentration data analysis

Subject	Treatment	Time (hr)	Concentration (mg/ml)	Volume (ml)	Dt (hr)	Tm (hr)	Xu_Int (mg)	CUM_Xu (mg)	Dxu_Dt (mg/hr)	Xu_Inf_Xu (mg)	%Dose	AUC (mg/ml*hr)	CL _R (ml/hr)
1	A	0	0	1	0	0	0	0	0	59.58	0	50	0.02
1	A	1	4.02	1	1	0.5	4.02	4.02	4.02	55.56	6.7	50	0.02
1	A	2	3.75	1	1	1.5	3.75	7.77	3.75	51.81	12.95	50	0.02
1	A	3	3.49	1	1	2.5	3.49	11.26	3.49	48.32	18.77	50	0.02
1	A	6	9.15	1	3	4.5	9.15	20.41	3.05	39.17	34.02	50	0.02
1	A	12	13.47	1	6	9	13.47	33.88	2.25	25.7	56.47	50	0.02
1	A	24	14.75	1	12	18	14.75	48.63	1.23	10.95	81.05	50	0.02
1	A	36	6.42	1	12	30	6.42	55.05	0.54	4.53	91.75	50	0.02
1	A	48	2.79	1	12	42	2.79	57.84	0.23	1.74	96.4	50	0.02
1	A	60	1.22	1	12	54	1.22	59.06	0.1	0.52	98.43	50	0.02
1	A	72	0.52	1	12	66	0.52	59.58	0.04	0	99.3	50	0.02

Dt collection interval, Tm midpoint of collection interval, Xu_Int amount excreted over a collection interval, CUM_Xu cumulative amount excreted, Dxu_Dt excretion rate, Xu_Inf_Xu amount at infinity-Xu_int, CL_R renal clearance

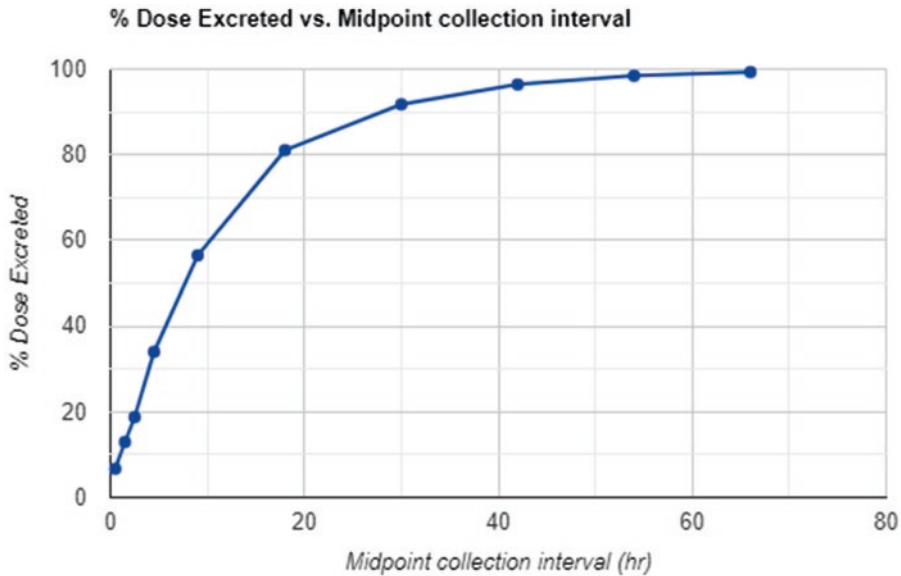


Fig. 7.8 Urinary excretion plot for the % dose excreted and the midpoint of urine collection interval for a drug

Table 7.8 Example of a plasma concentration-time data for a subject for the superposition analysis

Subject	Time (hr)	Concentration (ng/mL)	Dose (mg)
1	0	0	100
1	1	255	
1	2	447	
1	3	449	
1	4	410	
1	6	226	

$$Y = a \cdot W^b \quad (7.17)$$

or its logarithmic transformation.

$$\log Y = \log a + b \log W \quad (7.18)$$

where

Y = pharmacokinetic parameter

W = body weight

a = allometric coefficient

b = allometric exponent

Similar analysis is done for a V_d parameter for human prediction as shown in Table 7.11.

12 Method 1: NCA

In order to perform analysis using this method, pharmacokinetic data after an intravenous administration of a drug in three or more animal species, such as mice, rats, and dogs, are needed. Intravenous data is preferred for the complete bioavailability of a drug, although extravascular route PK data can be used with consideration to differences in bioavailability across the species. In this method, the pharmacokinetic parameters, CL and V_d , among animal species are correlated as exponential functions of body weight or body surface area (BSA) using the simple allometric equation below, as shown in Fig. 7.10:

13 Method 2: PK Parameters

In this method, PK parameters from animal species are converted to human parameters or animal parameters using the BSA ratio extrapolation. For example, human and mouse BSA are 1.8 and 0.007 m², respectively, and the human-to-mouse BSA ratio is 257. For a mouse CL value of 5 mL/hr, the human CL can be predicted as product of

Fig. 7.9 Superposition analysis of a data in Table 7.8 based on K_{el} , 0.057 (/hr); dosing interval (τ), 6.0 hour; and number of steps, 4

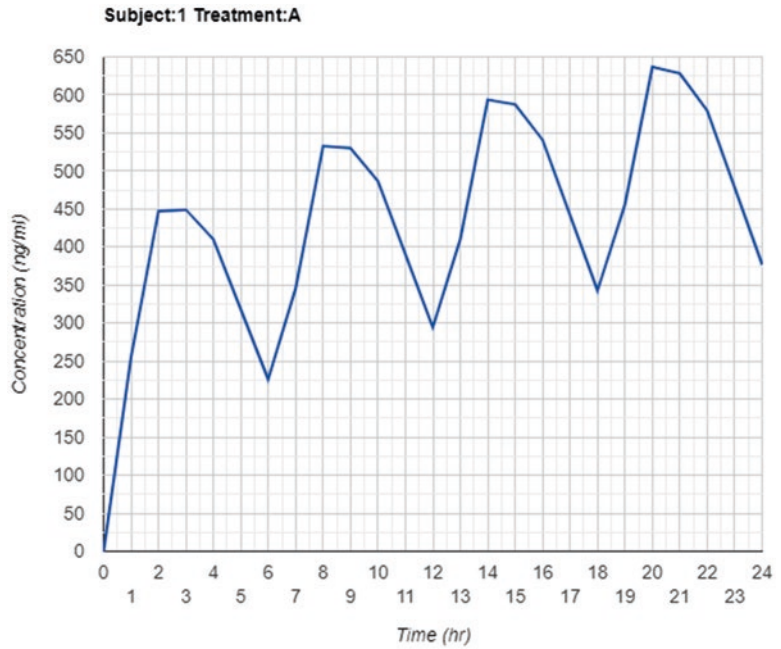


Table 7.9 Example of a toxicokinetic data collected in a limited sampling method with each animal providing one blood sample

Mouse#	Treatment	Dose (mg/kg)	Time (hr)	C_p (mcg/mL)
1	A	50	0	0.66
6	A		0	0.32
11	A		0	0.34
16	A		0	0.44
2	A		1.5	0.059
7	A		1.5	0.031
12	A		1.5	0.084
17	A		1.5	0.082
...

or

$$HED = \text{animal NOAEL} \times \left(\frac{W_{\text{animal}}}{W_{\text{human}}} \right)^{(1-b)} \tag{7.19}$$

where

W = body weight

b = allometric exponent (typically = 0.67)

257 and 5 equal to 1285 mL/hr. A similar approach can be used for prediction of V_d .

14 Method 3: Human Equivalent Dose (HED) (Table 7.12)

HED from an animal’s no observed adverse effect level (NOAEL) is calculated as per the FDA guidance [11] using

$$HED = \text{animal NOAEL} / \text{HED factor} \tag{7.18}$$

15 Dose Escalation

The phase 1 clinical trials are conducted in a dose escalation manner to determine an optimal recommended dose or maximum tolerated dose for a new compound for further testing in phase 2 trials. The dose escalation scheme in phase 1 trials is based on the careful evaluation of safety consideration both to study subjects and to attain the goals of trial [12]. Typically, the starting dose for the phase 1 clinical studies is selected using NOAEL from animals and escalated using either empiric, modified Fibonacci, or logarithmic increments. The PKMP computes and provides these dose escalation schemes as shown in Table 7.13, and these dose escalation schemes

Table 7.10 Toxicokinetic analysis of a limited sampling data

Treatment	Dose	Kel	R^2	$T_{1/2}$	T_{max}	C_{max}	T_{lig}	C_{list}/C_{max}	AUC_{0-t}	AUC_{All}	AUC_{0-inf}	$AUC_{0-#0-}$	$AUMC_{0-t}$	$AUMC_{0-}$	MRT_{0-t}	MRT_{0-}	V_d/F	Cl/F	AUC_{VAR}	AUC_{SEM}
Units	mg/ kg	1/hr		hr	hr	mg/ ml	hr		mg/ ml*hr	mg/ ml*hr	mg/ ml*hr		mg/ ml*hr ²	mg/ ml*hr ²	hr	hr	L/kg	L/hr/ kg		
A	50	0.747	0.943	0.927	0	0.043	0	0.021	0.047	0.049	0.048	0.974	0.031	0.039	0.67	0.814	1368	1022	2.48	0.007
B	150	0.646	0.812	1.072	0	0.272	0	0.047	0.342	0.361	0.362	0.944	0.28	0.412	0.819	1.137	640	414	0.011	0.047
C	600	0.975	0.996	0.71	0	0.464	0	0.007	0.563	0.568	0.566	0.993	0.415	0.435	0.737	0.768	1085	1059	0.032	0.08

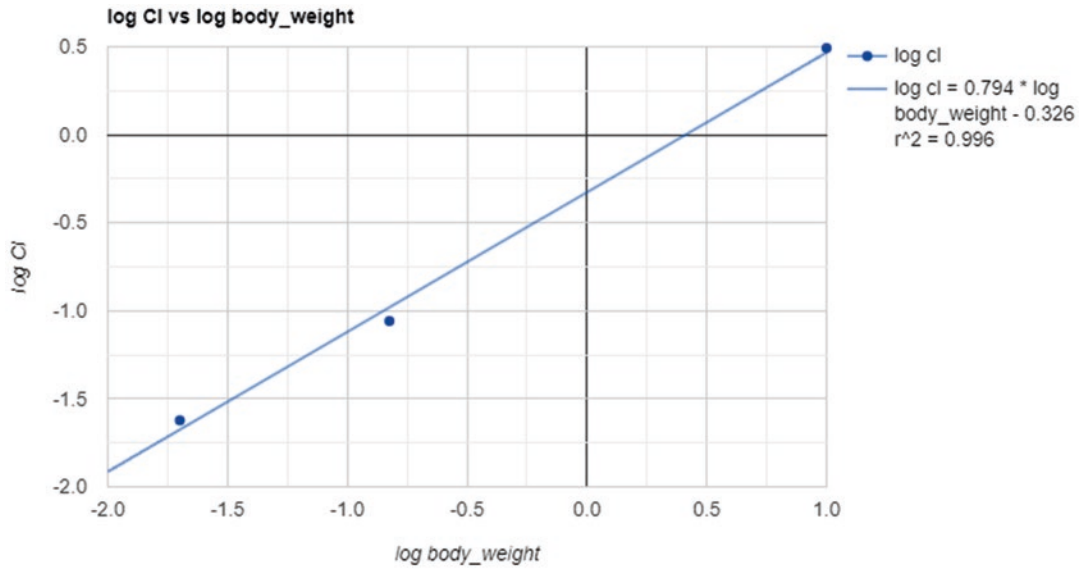


Fig. 7.10 Interspecies scaling using pharmacokinetic data obtained after an intravenous administration of a drug in the mouse, rat, and dog

Table 7.11 Human predicted parameters based on interspecies scaling using the body weight analysis

Dose (mg/kg)	Kel (1/hr)	Body weight (kg)	Body surface area (m ²)	$T_{1/2}$ (hr)	AUC _{0-∞} (mg/L·hr)	Cl/F (L/hr)	V_d/F (L)	C_{max} (mg/L)	T (hr)	C_{avg} (mg/L)
1	0.156	60	1.62	4.45	4.93	12.17	78.1	0.77	12	0.41

Table 7.12 HED based on the animal NOAEL

Species	NOAEL (mg/kg)	HED factor	HED (mg/kg)
Mouse	100	12.3	8.1
Rat	75	6.2	16.1
Dog	50	1.8	55.6

can be customized by changing a factor. Using the maximum safe recommended dose (MSRD) of 10 mg/kg and using the eight steps, the dose escalation is computed. The initial dose value can be selected as 1/10 of MSRD or other as appropriate.

16 Compartmental Pharmacokinetics (CA-PK)

The plasma concentration vs. time data after administration of a drug can be fitted to the appropriate pharmacokinetic model depending on the route of administration to the following compartmental body models (CBM) [2] as shown in Table 7.14:

The concentration and time data is fitted to a selected model, and the convergence of parameters is achieved by Levenberg-Marquardt method [13], with selected weighting options (1, $1/C_{obs}$, $1/C_{obs}^2$, $1/C_{pred}$, and $1/C_{pred}^2$). The parameters, their standard errors, secondary parameters, and model selection criteria are computed (Table 7.15), and the observed and predicted concentration plots are shown in Fig. 7.11.

17 Pharmacodynamics (PD) Analysis

Pharmacodynamics is a relationship between the plasma concentration of a drug and a given response [2]. The response can be the drug interaction with the receptor both directly and reversibly (e.g., anti-arrhythmic and neuromuscular blocking agents), indirectly (e.g., coumarin anticoagulants), or irreversibly binding to the receptors (e.g., anticancer agents and bactericidal antibiotics).

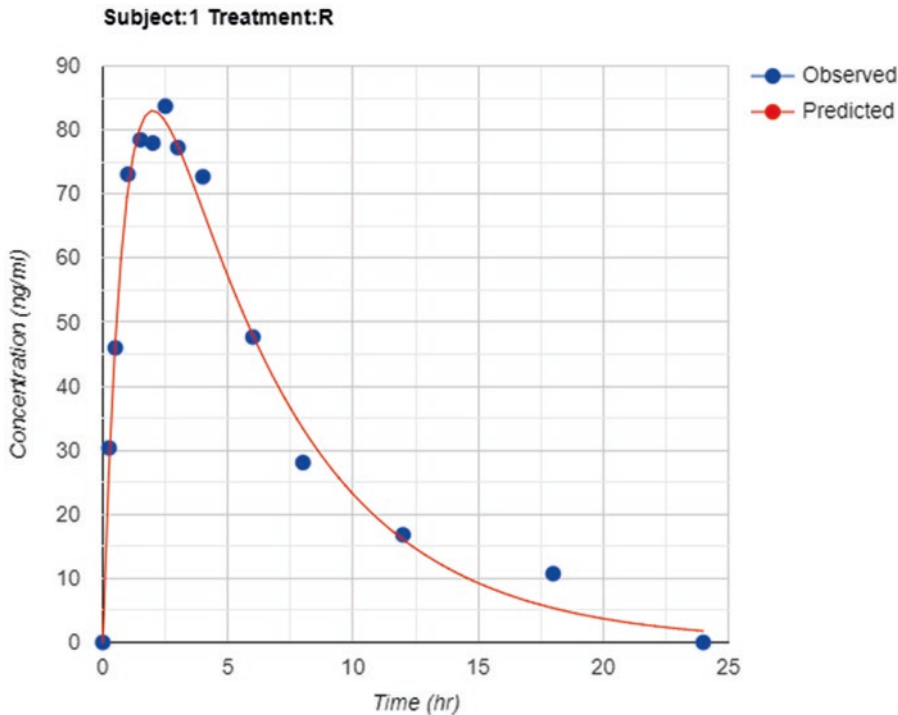


Fig. 7.11 Plot of the observed and predicted concentrations for a 1-CBM oral absorption model

Table 7.13 Dose escalation scheme based on the NOAEL and MSRD

Dose no.	Empiric		Modified-Fibonacci		Logarithmic	
	Factor	Dose value	Factor	Dose value	Factor	Dose value
1	1	1	1	1	0	1
2	2	2	0.65	1.7	0.5	1.6
3	1.5	3	0.52	2.5	1	2.7
4	1.3	3.9	0.4	3.5	1.5	4.5
5	1.3	5.1	0.29	4.5	2	7.4
6	1.3	6.6	0.33	6	2.5	12.2
7	1.2	7.9	0.33	8	3	20.1
8	1.1	8.7	0.33	10.7	3.5	33.1

Using a 10 mg/kg MSRD and the eight steps, the dose escalation is computed. The initial dose value is selected as 1/10 of MSRD

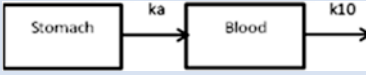
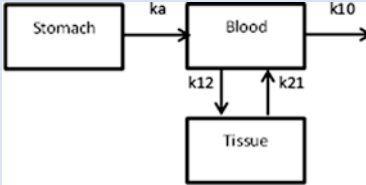

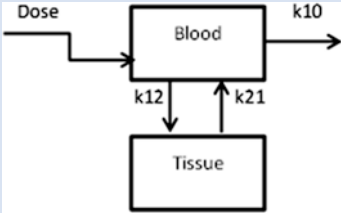
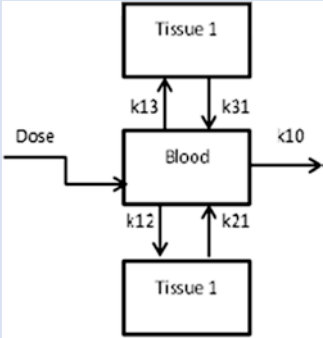
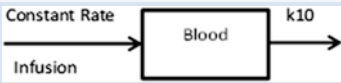
The following pharmacodynamic models are available for evaluation of concentration-effect relationship after a drug administration (Table 7.16). The effect vs. concentration data is optimized using Levenberg-Marquardt or Nelder-Mead [14] methods, and the parameter estimate, standard error, percent coefficient of error, and

model diagnostics are computed. An example of a model fit for the sigmoidal E_{\max} model is presented in Table 7.17 and Fig. 7.12.

18 Dissolution Data Analysis

Dissolution is the process of dissolving a drug substance from the solid state. Drug absorption from a solid dosage form after oral administration depends on the release of the drug substance from the drug product, the dissolution of the drug under physiological conditions, and the absorption across the gastrointestinal tract. Because of the critical nature of the first two of these steps, in vitro dissolution may be relevant to the prediction of in vivo performance of drug product. Therefore, in vitro dissolution for immediate release solid oral dosage forms, such as tablets and capsules, is used to assess the lot-to-lot quality of a drug product, guide development of new formulations, and ensure continuing product quality and performance after certain changes,

Table 7.14 Compartmental analysis models and equations

Route of administration	PK model	Equation
Extravascular 1-CBM (with and without lag time)		$C = \frac{FDka}{V(ka - k10)} \left[e^{-(k10,t)} - e^{-(ka,t)} \right]$ <p><i>C</i> concentration, <i>F</i> bioavailability, <i>D</i> dose, <i>V/F</i> apparent oral volume of distribution, <i>ka</i> first-order absorption rate constant, <i>k10</i> first-order elimination rate constant</p>
2-CBM (with and without lag time)		$Cp = Ae^{-\alpha t} + Be^{-\beta t} + Ce^{-kat}$ $A = \frac{kaFD(k21 - \alpha)}{V(ka - \alpha)(\beta - \alpha)}$ $B = \frac{kaFD(k21 - \beta)}{V(ka - \beta)(\alpha - \beta)}$ $C = \frac{kaFD(k21 - ka)}{V(\alpha - ka)(\beta - ka)}$
IV bolus 1-CBM		$C = \frac{D}{V} e^{-k10,t}$
2-CBM		$C = Ae^{-\alpha t} + Be^{-\beta t}$ $A = \frac{D(\alpha - k21)}{V(\alpha - \beta)}$ $\alpha + \beta = k12 + k21 + k10$ $\alpha\beta = k21k10$ $B = \frac{D(k21 - \beta)}{V(\alpha - \beta)}$
3-CBM		$Cp = Ae^{-\alpha t} + Be^{-\beta t} + Ce^{-\gamma t}$ $A = \frac{D(k21 - \alpha)(\alpha - k31)}{V(\gamma - \alpha)(\alpha - \beta)}$ $Co = A + B + C$ $B = \frac{D(k21 - \beta)(k31 - \beta)}{V(\gamma - \beta)(\alpha - \beta)}$ $C = \frac{D(k21 - \gamma)(k31 - \gamma)}{V(\gamma - \alpha)(\gamma - \beta)}$
IV infusion 1-CBM		$C = \frac{ko}{Vk10} (1 - e^{-k10t}) e^{-k10t}$

(continued)

Table 7.14 (continued)

Route of administration	PK model	Equation
2-CBM		$C = \frac{ko(k21 - \alpha)(e^{-\alpha T} - 1)}{V\alpha(\alpha - \beta)} e^{-\alpha t^*} + \frac{ko(\beta - k21)(e^{-\beta T} - 1)}{V\beta(\alpha - \beta)} e^{-\beta t^*}$
3-CBM		$Cp = A[e^{(\alpha t^*)} - e^{(-\alpha T)}] + B[e^{(-\beta t^*)} - e^{(-\beta T)}] + C[e^{(-\gamma t^*)} - e^{(-\gamma T)}]$

Table 7.15 Parameters of a 1-CBM oral absorption model

Parameter	Unit	Estimate	Standard error	CV%
Subject 1				
A	ng/ml	144.532	3.715	2.57
ka	1/hr	164	031	2.946
k10	1/hr	0.183	005	2.63
t _{1/2} ka	hr	0.651		
t _{1/2} k10	hr	3.787		
V/F	(mg)/(ng/ml)	0.836		
CL/F	(mg)/(ng/ml)hr	0.153		
T _{max}	hr	1.997		
C _{max}	ng/ml	8329		
AUC _{0-t}	ng/ml*hr	64448		
AUC _{0-inf}	ng/ml*hr	653.81		
AUMC	ng/ml*hr ²	418666		
MRT	hr	6.403		
R _{obs-pre}	-	0.995		
SS	-	14128		
WSS	-	14228		
R ²	-	0.997		
WR ²	-	0.997		
SE	-	3.593		
AIC	-	75.384		
SC	-	77.301		

such as changes in the formulation, the manufacturing process, the site of manufacture, and the scale-up of the manufacturing process [15, 16]. The mathematical models for describing dissolution models [17–20] for drugs are shown in Table 7.18.

An example of a dissolution data fitted to the Weibull₄ model is shown in Table 7.19 and Fig. 7.13.

19 Dissolution Profile Comparison

Dissolution profile comparison is done to accept product sameness under scale-up and post-approval-related changes, to waive bioequivalence requirements for lower strengths of a dosage form, and to support waivers for other bioequivalence requirements [15, 16, 19]. The following are dissolution profile comparison using model-independent methods.

20 Difference Factor

The difference factor calculates the percent difference between the two curves at each time point and is a measurement of the relative error between the two curves:

$$f1 = \frac{\left[\sum_{t=1}^n \| Rt - Tt \| \right]}{\left[\sum_{t=1}^n Rt \right]} * 100 \quad (7.20)$$

where

Rt = reference assay at time point t

Tt = test assay at time point t

n = the number of dissolution time points

The dissolution data is displayed in Fig. 7.14, and the $f1$ comparison analysis is shown in Table 7.20.

21 Similarity Factor

The similarity factor is a logarithmic reciprocal square root transformation of the sum squared error and is a measurement of the similarity in the percent dissolution between the two curves:

$$f2 = 50 * \log \left\{ \left[1 + \left(\frac{1}{n} \right) \sum_{t=1}^n (Rt - Tt)^2 \right]^{-0.5} * 100 \right\} \quad (7.21)$$

where

Rt = reference assay at time point t

Tt = test assay at time point t

n = the number of dissolution time points

The dissolution data is displayed in Fig. 7.14, and the $f2$ comparison analysis is shown in Table 7.21. A bootstrap analysis for the $f2$ comparison can also be performed, and the results are displayed in Table 7.21.

22 Multivariate Statistical Difference (MSD) Determination

In instances where dissolution is measured at multiple time points and within batch variation is more than 15% CV, a multivariate model-independent procedure is more suitable for dissolution profile comparison [21]. The statistic of Mahalanobis distance is used to assess the difference between the means of test and reference data with adjustments for differences in measurement variation at different time points and the correlation among the measurements at multiple time points. The variance-covariance matrix and inverse of variance-covariance matrix for the pooled data is computed to calculate overall statistics as shown in Table 7.22.

23 IVIVC Model

The objective of developing an in vitro–in vivo correlation (IVIVC) is to establish a predictive mathematical model describing the relationship between an in vitro property and a relevant in vivo response [22]. The IVIVC for modified release dosage forms has often been used during pharmaceutical development in order to reduce development time and optimize the formulation. A good correlation is a tool for predicting in vivo results based on in vitro data. IVIVC allows dosage form optimization with the fewest possible trials in human, fixes dissolution acceptance criteria, and can be used as a surrogate for further bioequivalence studies; furthermore, it is also recommended by regulatory authorities. The schematic of the process to develop an IVIVC is shown in Fig. 7.15. It involves in vitro dissolution data for formulations under evaluation and in vivo bioavailability data for formulations, as well as a reference formulation such as intravenous, solution, or immediate release formulation [20, 23–30]. The correlations are established between in vivo parameters and in vitro data.

Table 7.16 Pharmacodynamics models and equations

Model	Equation
E_{\max}	$E = \frac{E_{\max} \cdot C}{C + EC_{50}}$
E_{\max} with baseline effect	$E = E_0 + \frac{(E_{\max} - E_0) \cdot C}{C + EC_{50}}$
Sigmoid E_{\max}	$E = \frac{E_{\max} \cdot C^\gamma}{C^\gamma + EC_{50}^\gamma}$
Sigmoid E_{\max} with baseline effect	$E = E_0 + \frac{(E_{\max} - E_0) \cdot C^\gamma}{C^\gamma + EC_{50}^\gamma}$
Inhibition E_{\max}	$E = E_{\max} \left[1 - \left(\frac{C}{C + EC_{50}} \right) \right]$
Inhibition E_{\max} with baseline effect	$E = E_{\max} - (E_{\max} - E_0) \left(\frac{C}{C + EC_{50}} \right)$
Inhibition sigmoid E_{\max}	$E = E_{\max} \left[1 - \left(\frac{C^\gamma}{C^\gamma + EC_{50}^\gamma} \right) \right]$
Inhibition sigmoid E_{\max} with baseline effect	$E = E_{\max} - (E_{\max} - E_0) \left(\frac{C^\gamma}{C^\gamma + EC_{50}^\gamma} \right)$

E effect, E_{\max} maximum effect, E_0 baseline, C concentration, EC_{50} concentration producing 50% of maximum effect, γ sigmoidicity factor

24 Level A Correlation

A level A correlation is a predictive mathematical model for the relationship between the entire in vitro dissolution-time course and the entire in vivo response-time course of drug absorbed. A level A IVIVC is considered to be the most informative and is recommended [22]. It involves

Table 7.17 PD parameter estimates for a sigmoidal E_{\max} model

Parameter	Estimate	Standard error	CV%
Subject 1			
E_{\max}	99.995	3.948	3.948
EC_{50}	11.424	0.846	7.406
Gamma	1.371	0.125	9.127
Diagnostics	Values		
$r_{\text{obs-pre}}$	0.998		
SS	14.719		
WSS	14.719		
R^2	1		
WR ²	1		
SE	1.918		
AIC	24.824		
SC	24.662		

obtaining in vitro dissolution profiles and in vivo plasma concentration profiles for the formulations under evaluation. The estimate of the in vivo absorption, or dissolution time course, using a deconvolution technique described below for each formulation and subject is obtained. The linear correlation, as shown in Fig. 7.15d, between the % absorbed and the % dissolved to predict plasma concentrations is achieved using the convolution methods. The predictability in the model is determined by estimation of the prediction error in AUC and C_{\max} for internal and/or external batches of formulations based on observed and predicted plasma concentration-time data [22]:

$$\%PE = \left(\frac{\text{observed} - \text{predicted}}{\text{observed}} \right) * 100 \quad (7.22)$$

Average absolute percent prediction error (%PE) of 10% or less for C_{\max} and AUC establishes the predictability of the IVIVC. In addition, the %PE for each formulation should not exceed 15%.

The following models are included for deconvolution of in vivo data in PKMP for analysis:

24.1 Deconvolution: Wagner-Nelson Method

For a drug with one-compartment body model characteristics, the fraction of drug absorbed to time t is given by [2]:

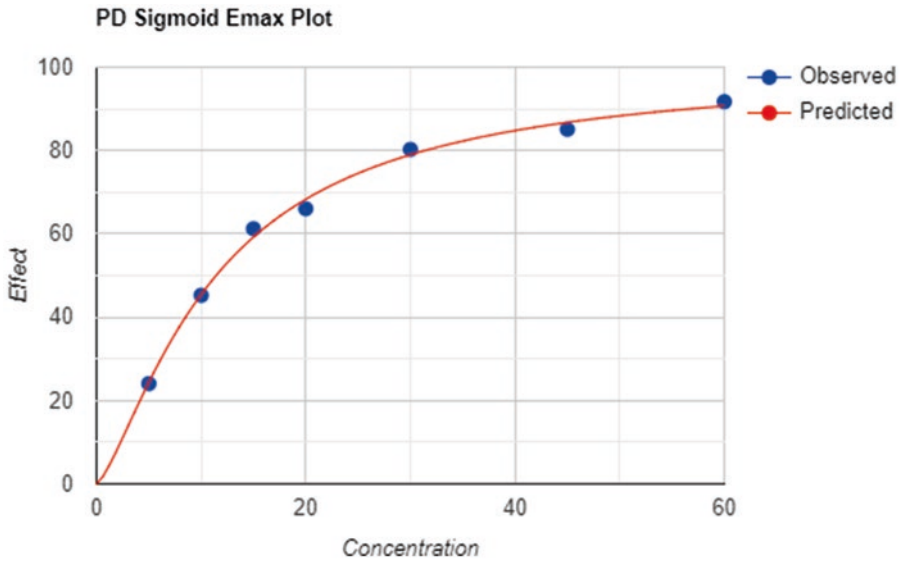


Fig. 7.12 Plot of the observed and predicted effect vs. concentration plots for a sigmoid E_{max} model

$$\frac{(X_A)_t}{(X_A)_\infty} = \frac{C_t + K \int_0^t C dt}{K \int_0^\infty C dt} \quad (7.23) \qquad C p_{pred} = \frac{X}{V_d \text{ or } S_F} \quad (7.25)$$

X_A = amount of drug absorbed to time t or ∞
 C_t = plasma concentration of drug at time t
 K = apparent first-order elimination rate constant

V_d = apparent volume of distribution
 S_F = scaling factor

24.2 Convolution

Using the superposition principle and following equation for 1-CBM [25], the amount of a drug in the body is predicted from the amount dissolved at each time and K and summed over all the individual dissolution times:

$$X = X0e^{-Kt} \quad (7.24)$$

$X0$ = amount in at each dissolution time
 K = apparent first-order elimination rate constant

Predicted concentrations (Cp) are obtained as X :

24.3 Deconvolution: Loo-Riegelman Method

For a drug with two-compartment body model characteristics, the fraction of drug absorbed to time t is given by [2]:

$$\frac{(X_A)_t}{(X_A)_\infty} = \frac{C_t + k10 \int_0^t C dt + \left(\frac{1}{V_c}\right)(X_p)_t}{k10 \int_0^\infty C dt} \quad (7.26)$$

X_A = amount of drug absorbed to time t or ∞
 C_t = plasma concentration of drug at time t
 $k10$ = apparent first-order elimination rate constant from the central compartment
 V_c = the apparent volume of the central compartment

Table 7.18 Dissolution models

Model	Definition	Equation
Zero order	F = amount of drug dissolved in time t k_0 = zero-order release constant	$F = k_0 \cdot t$
Zero order with T_{lag}	T_{lag} = lag time in dissolution	$F = k_0 \cdot (t - T_{lag})$
Zero order with F_0	F_0 = initial amount of drug in the solution	$F = F_0 + k_0 \cdot t$
Baker-Lonsdale	k_{BL} = release rate constant	$\frac{3}{2} \left[1 - \left(1 - \frac{F}{100} \right)^{\frac{2}{3}} \right] - \frac{F}{100} = k_{BL} \cdot t$
Baker-Lonsdale with T_{lag}		$\frac{3}{2} \left[1 - \left(1 - \frac{F}{100} \right)^{\frac{2}{3}} \right] - \frac{F}{100} = k_{BL} \cdot (t - T_{lag})$
First order	k = first-order rate constant	$F = 100 \cdot (1 - e^{-k \cdot t})$
First order with T_{lag}		$F = 100 \cdot \left[1 - e^{-k \cdot (t - T_{lag})} \right]$
First-order with T_{lag} F_{max}	F_{max} = maximum amount of drug dissolved in time t	$F = F_{max} \cdot \left[1 - e^{-k \cdot (t - T_{lag})} \right]$
First-order with F_{max}		$F = F_{max} \cdot [1 - e^{-k \cdot t}]$
Higuchi	K_H = Higuchi dissolution constant	$F = K_H \cdot t^{0.5}$
Higuchi F_0		$F = F_0 + K_H \cdot t^{0.5}$
Higuchi with T_{lag}		$F = K_H \cdot (t - T_{lag})^{0.5}$
Hixson-Crowell	K_{HC} = constant	$F = 100 \cdot [1 - (1 - K_{HC} \cdot t)^3]$
Hixson-Crowell with T_{lag}		$F = 100 \cdot [1 - (1 - K_{HC} \cdot (t - T_{lag}))^3]$
Hopfenberg	K_{HB} = constant	$F = 100 \cdot [1 - (1 - K_{HB} \cdot t)^n]$
Hopfenberg with T_{lag}		$F = 100 \cdot [1 - [1 - K_{HB} \cdot (t - T_{lag})]^n]$
Korsmeyer-Peppas	F = fraction drug released at time t K_{KP} = release rate constant n = release exponent	$F = K_{KP} \cdot t^n$
Korsmeyer-Peppas with F_0		$F = F_0 + K_{KP} \cdot t^n$
Korsmeyer-Peppas with T_{lag}		$F = K_{KP} \cdot (t - T_{lag})^n$
Weibull_1	α = scale parameter T_i = location of parameter β = shape parameter	$F = 100 \cdot \left[1 - e^{-\frac{(t - T_i)^\beta}{\alpha}} \right]$
Weibull_2		$F = 100 \cdot \left[1 - e^{-\frac{t^\beta}{\alpha}} \right]$
Weibull_3		$F = F_{max} \cdot \left[1 - e^{-\frac{t^\beta}{\alpha}} \right]$
Weibull_4		$F = F_{max} \cdot \left[1 - e^{-\frac{(t - T_i)^\beta}{\alpha}} \right]$

Table 7.19 Weibull_4 parameters for a dissolution data shown in Fig. 7.13

$F = F_{\max} \cdot \{1 - \text{Exp}[-((t - T_i)^{\beta}) / \alpha]\}$	
Parameter	Value
Alpha	188.547
Beta	1.212
T_i	119.829
F_{\max}	2.547
Parameter	Value
(time for % dissolved)	
T25	25.323
T50	47.97
T75	7881
T80	7733
T90	84.354
Parameter	Value
N_observed	8
DF	4
R_obs-pre	0.996
Rsqr	0.991
Rsqr_adj	0.991
MSE	19.878
MSE_root	4.458
Weighting	1
SS	79.511
WSS	79.511
AIC	3707
MSC	4.476

X_p = amount of drug in the peripheral compartment

24.4 Convolution

Using the superposition principle, drug amounts in the body are predicted from the dissolution amount at each time and using the following 2-CBM equation:

$$X = \frac{X0(\alpha - k21)}{(\alpha - \beta)} e^{-\alpha t} + \frac{X0(k21 - \beta)}{(\alpha - \beta)} e^{-\beta t} \tag{7.27}$$

Predicted concentrations (C_p) are obtained as

$$C_{p_{\text{pred}}} = \frac{X}{V_c \text{ or } S_F} \tag{7.28}$$

V_c = apparent volume of distribution of central compartment
 S_F = scaling factor

24.5 Numeric Deconvolution

The absorption rate (r_{abs}) that results in plasma concentration $c(t)$ can be estimated by solving the following equation:

$$c(t) = \int_0^t c_{\delta}(t-u) r_{\text{abs}}(u) du \tag{7.29}$$

where

$c(t)$ = plasma concentration versus time profiles of tested formulation
 C_{δ} = concentration time profile resulting from instantaneous input of a unit amount of drug
 r_{abs} = input rate of the oral solid dosage form into the body
 u = variable of integration

25 Correlations

25.1 Level A Correlation

Using an Interpolation Method

Slope and intercept between two successive time points for mean %dissolution vs. time and mean % in vivo fraction absorbed (FA) vs. time are computed. Times of 10%, 20%, and up to 100% dissolution are determined, and the %FA corresponding to these times is computed. Based on the %FA vs. %dissolved data, level A linear regression with parameters slope, intercept, and correlation coefficient is obtained.

Using the Hill Equation

$$D = \frac{D_{\max} [C]^{\gamma}}{[D_{50}]^{\gamma} + [C]^{\gamma}} \tag{7.30}$$

D = rate of dissolution
 D_{\max} = maximum dissolution rate
 C = %dissolved

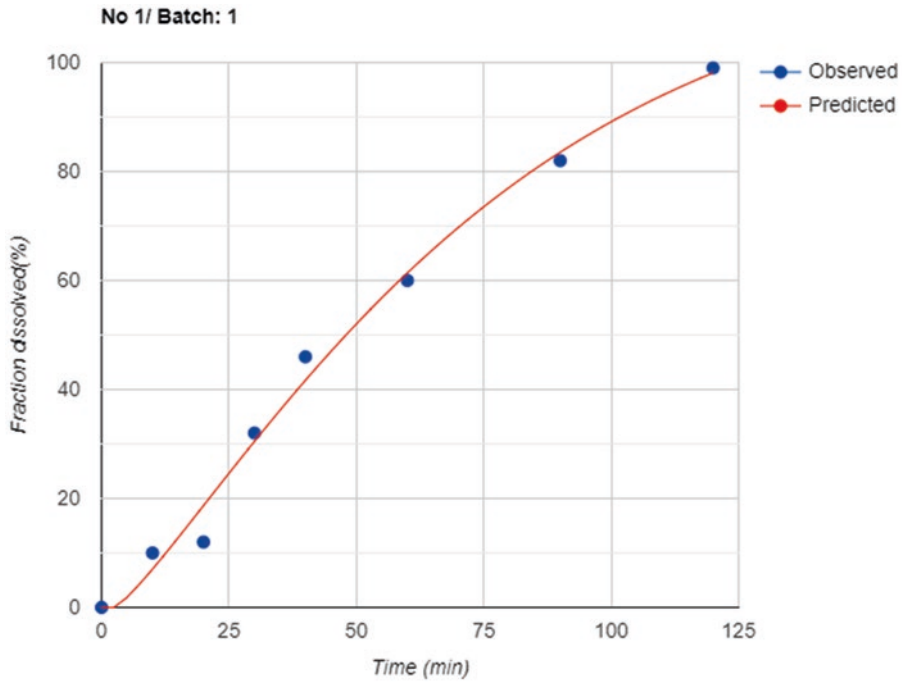


Fig. 7.13 Plot of the observed and predicted dissolution data fitted to a Weibull_4 model

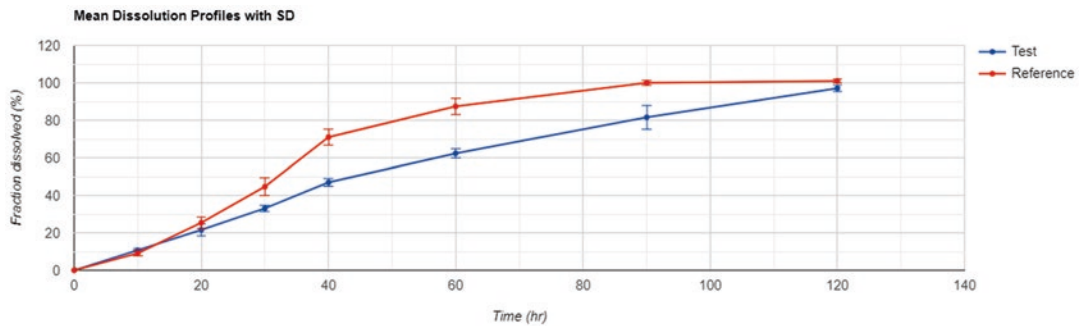


Fig. 7.14 Mean (\pm SD) dissolution profiles for test and reference oral products

D_{50} = time of 50% dissolved
 γ = shape factor

Both %dissolution-time and %FA-time data are fitted to the Hill equation. Additional computations are done in the same way, as indicated in the interpolation method above.

Using Weibull Equation

$$D = D_{\max} * \left\{ 1 - e^{-\left[\frac{(t-Ti)^\beta}{\alpha} \right]} \right\} \quad (7.31)$$

D = cumulative % dissolved
 t = time
 α = scale parameter
 Ti = lag time

Table 7.20 f_1 difference factor in dissolution comparison

	Mean_R vs Individual_T		Mean_Test vs Mean_Reference
	Mean	SE	
Overall statistics			
f_1	25.2	0.93	25.1
Is f_1 between [0,15] for Mean_Test and Mean_Reference?	No		
Similarity of test and reference	Reject		

Table 7.21 f_2 difference factor in dissolution comparison and the bootstrap simulation

	Mean_R vs Individual_T		Mean_Test vs Mean_Reference
	Mean	SE	
Overall statistics			
f_2	41.5	0.73	41.7
Is f_2 between [50,100] for Mean_Test and Mean_Reference?	No		
Similarity of test and reference	Reject		
Bootstrap analysis statistics for f_2	Value		
Observed f_2	41.7		
Number of bootstrap	5000		
Bootstrap mean	41.7		
Bootstrap median	41.7		
5% percentile	40.1		
95% percentile	43.3		
Skewness	0.1		
Kurtosis	0		

B = shape parameter

For further computations, a similar process, as described above under using Hill equation, is applied.

25.2 Level B Correlation

The level B correlation is a predictive mathematical model for the relationship between summary parameters characterizing the in vitro and in vivo time courses, such as the mean in vitro dissolution time to the mean in vivo dissolution time, the mean in vitro dissolution time to the mean residence time in vivo, or the in vitro dissolution rate constant to the absorption rate constant [22]. An example of mean dissolution time in vivo and mean dissolution time analysis is shown in Fig. 7.16.

25.3 Level C Correlation

The level C correlation is a predictive mathematical model of the relationship between the amounts dissolved in vitro at a particular time ($t_{50\%}$, $t_{90\%}$, etc.) and a summary parameter characterizing the in vivo time course (AUC, T_{\max} , or C_{\max}) [22]. An example of level C correlation for the C_{\max} for three formulations and % dissolved at time is shown in Fig. 7.17.

26 Simulation

Simulation analysis allows predicting dose-concentration, as well as concentration-response relationships, based on mathematical models. Pharmacokinetic simulations allow predicting multiple-dose drug concentrations based on a single-dose data which can be used to evaluate safe margins during drug development. In formulation development,

Table 7.22 Overall statistics for a MSD analysis

Statistics	Value
P (sampling points)	8
K (scaling factor)	0.511
$F(p, n1 + n2 - p - 1, 0.95)$	2.641
Hotelling's T^2	1533.549
Mahalanobis distance (MSD)	15.987
Relative distance (RD)	23.717
Lower 95% CR MSD	13.715
Upper 95% CR MSD	18.26
Upper 95% CI less than RD	Yes
Reference and test global similarity	Reject

IVIVC simulations aid in modified release product optimization. Pharmacodynamic simulations allow examining the relationship between the drug concentration and the response. These techniques assist in optimizing the formulation development and predicting the dose-response relationship to design better clinical trials.

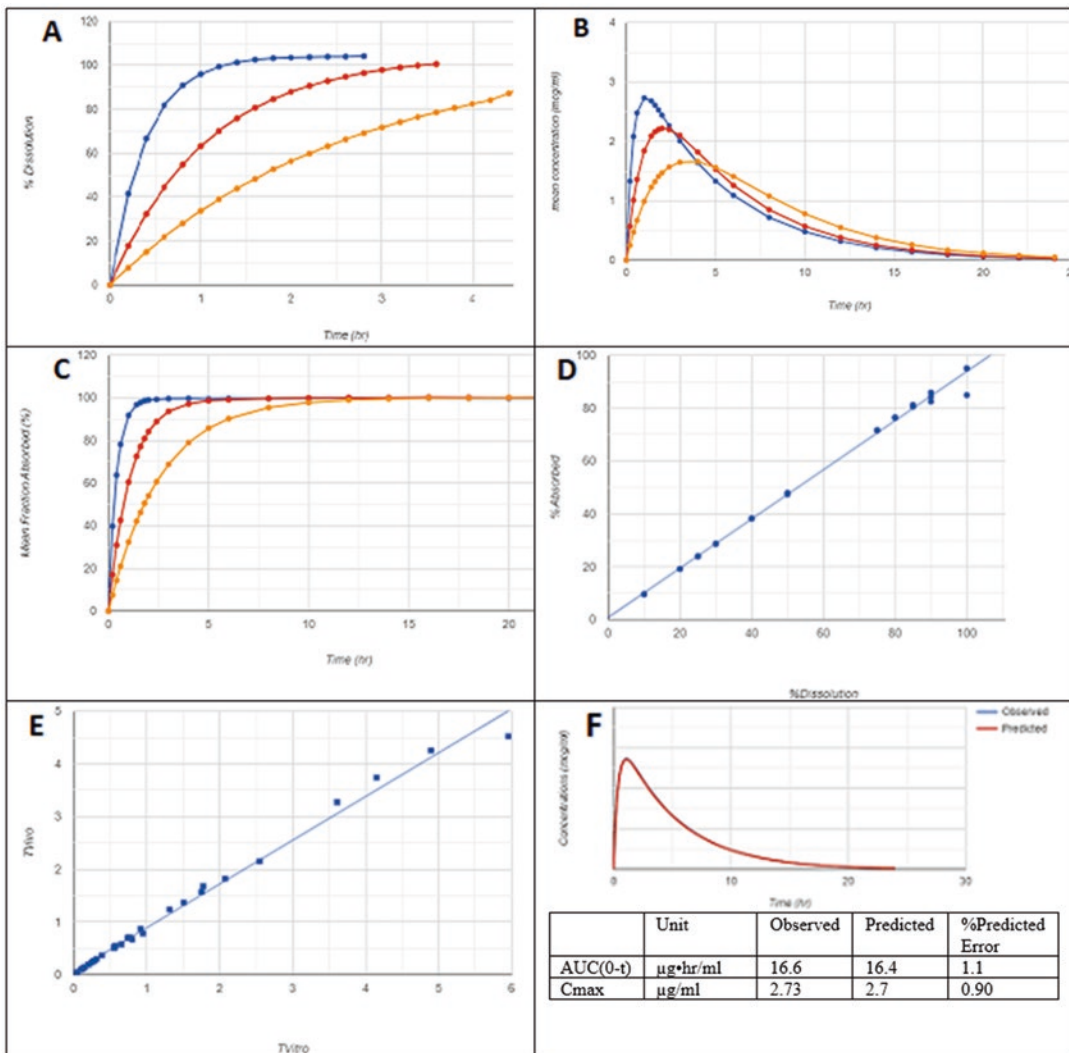


Fig. 7.15 Schematic representation of the process to develop an IVIVC involving (a) dissolution, (b) in vivo concentration data, (c) computation of in vivo dissolution or fraction absorbed, (d) level A correlation for in vivo

dissolution and in vitro dissolution, (e) Levy plot related to time for in vivo dissolution and time for in vitro dissolution, and (f) prediction error for convolution

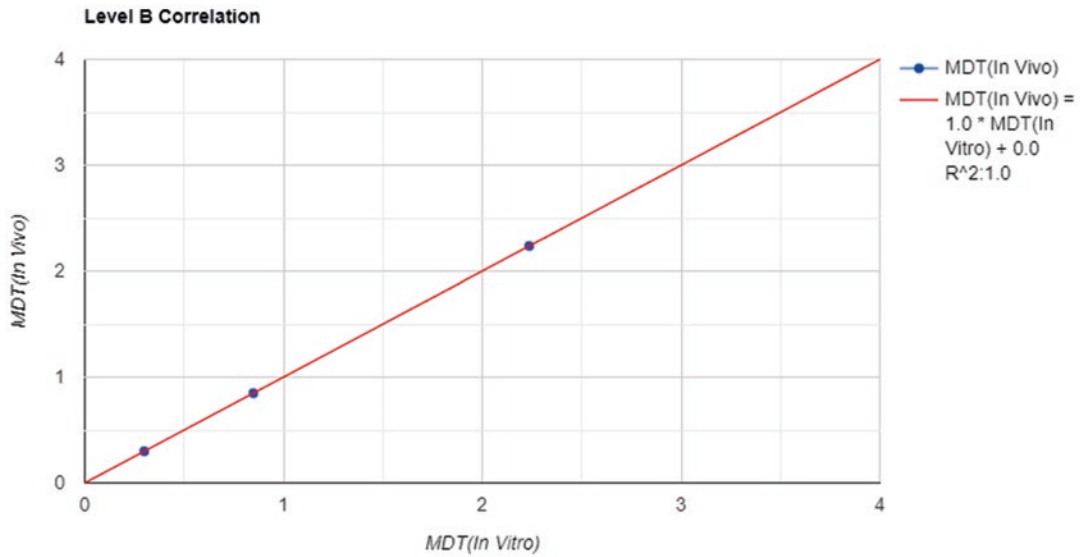


Fig. 7.16 Level B correlation for MDT (in vivo) and MDT (in vitro)

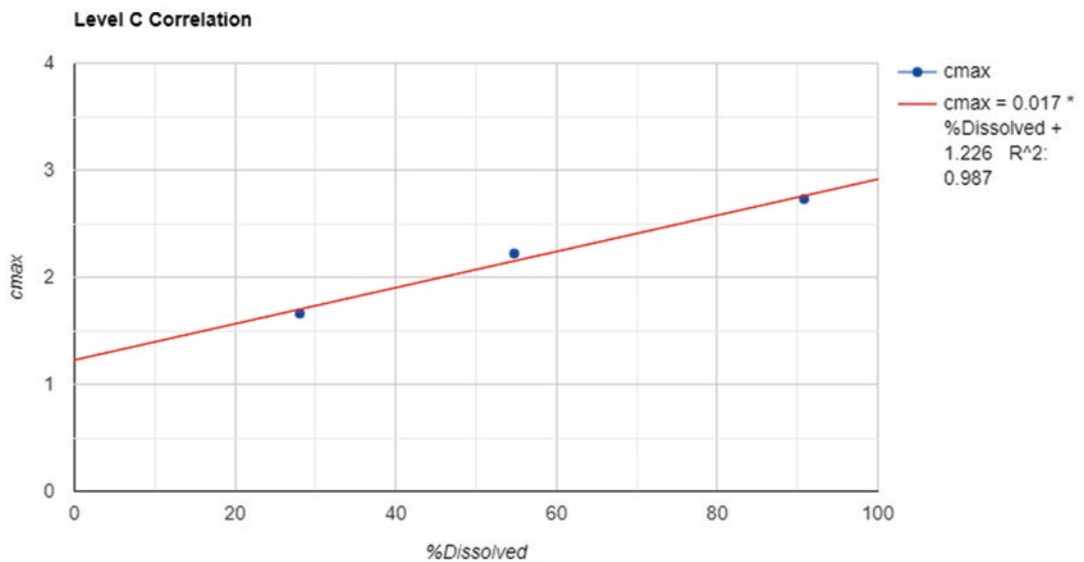


Fig. 7.17 Level C correlation for C_{max} and % dissolved at a time for three formulations

26.1 Pharmacokinetic Simulation

Pharmacokinetic simulations can be performed for single and multiple doses based on explicit equations as shown in Table 7.14 for 1-CBM, 2-CBM, and 3-CBM models for oral, IV bolus, or IV infusion. An example of a 1-CBM oral multiple dosing is shown in Fig. 7.18.

26.2 Pharmacodynamic Simulation

Pharmacodynamic simulations can be performed based on explicit equations as shown in Table 7.16, and an example of the simulation for inhibitory E_{max} model is shown in Fig. 7.19.

Fig. 7.18 Simulation of multiple oral doses for a 1-CBM using K_e , 0.1 (/hr); K_a , 1.0 (/hr); V_d , 10 (L); τ , 12 hr; dose, 100 mg; number of doses, 6; and step size, 0.25

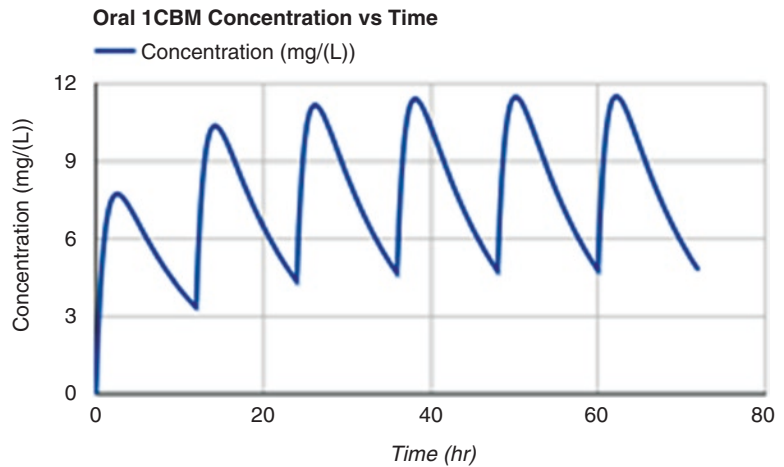
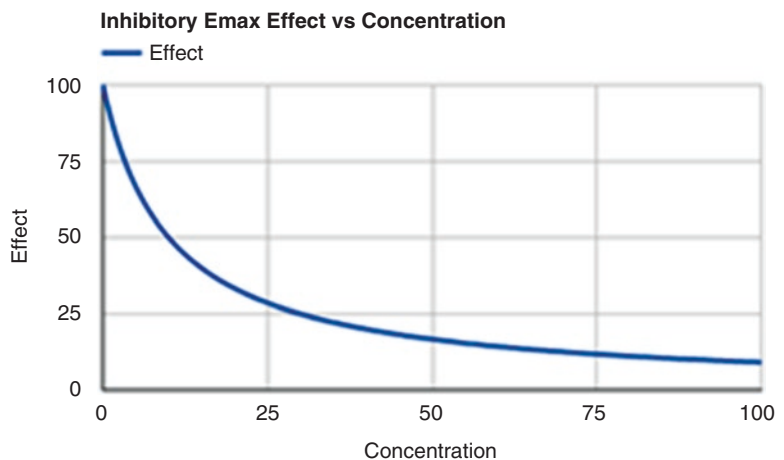


Fig. 7.19 Simulation plot of the effect vs. concentration for an inhibitory E_{max} model using E_{max} , 100%; EC_{50} , 10 (ng/mL); C_p (initial-final), 0–100 ng/mL; and step size, 0.5



27 IVIVC

Typically, in a formulation development, dissolution data becomes available as the first step. The data can be fitted to dissolution models such as E_{max} or Weibull functions. If the PK disposition parameters after intravenous administration, such as C_0 and K_{el} for a 1-CBM or A , α , B , and β for a 2-CBM, are available from a study or the literature, then using the convolution integral, as shown in Eq. (7.29), can be used to predict the concentrations as a product of input rate and disposition function. In Fig. 7.20, dissolution data is shown, fitted to an E_{max} model, and the model parameters are displayed. The disposition

parameters, C_0 and K_{el} , for a 1-CBM, following IV bolus administration, are used to simulate the predicted concentrations as shown in Fig. 7.20. The concentration-time data obtained from this simulation can be further evaluated for NCA analysis, and bioequivalency simulation can be performed with the knowledge of variability, as determined by SD or CV%.

28 Bioequivalence (BE)

The concentration-time data with a measure of variability, such as SD or CV% for two treatments (Table 7.23), can be simulated using the bootstrap method. The pharmacokinetic param-

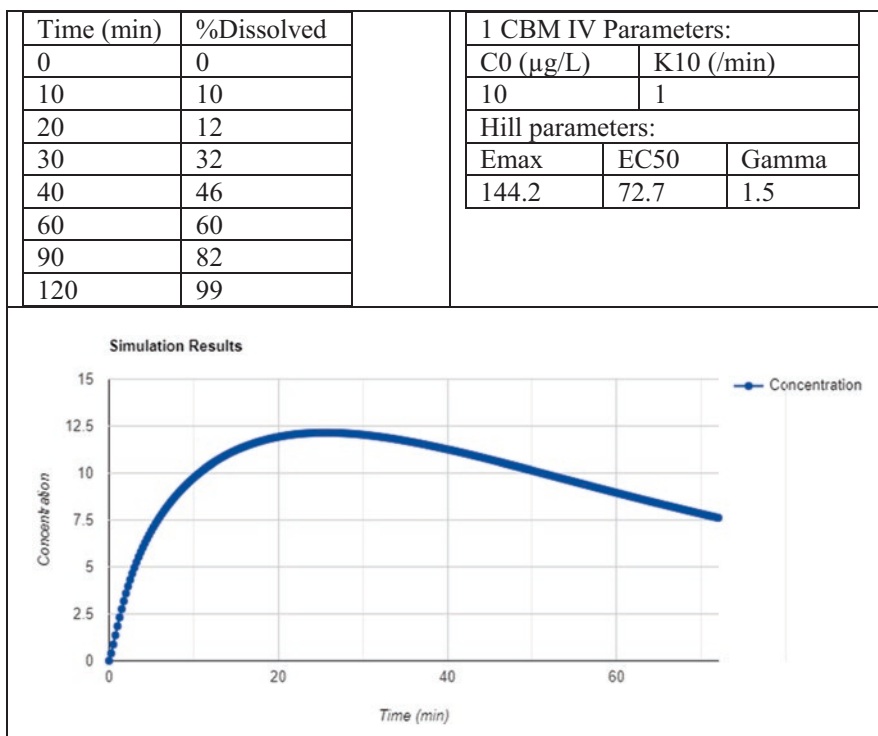


Fig. 7.20 Simulation of an IVIVC using the dissolution data and disposition parameters for a drug

Table 7.23 Observed and the bootstrap simulated concentration-time data for BE simulation

Treatment	Time (hr)	C_p observed	SD observed	C_p simulation	SD simulation	Count
Test	0	0	0	0	0	500
Test	0.5	2.685	2.333	2.821	2.18	500
Test	1	6.577	3.19	6.55	3.237	500
Test	1.5	6.825	2.136	6.632	2.247	500
Test	2	7.16	2.77	7.36	2.231	500
Test	Additional data					

ters such as AUC and C_{\max} and confidence intervals (90, 95, or 99%) are calculated. The user can compare the AUC and C_{\max} ratios for test and reference formulations to estimate bioequivalence (Table 7.24).

29 Sample Size

For bioequivalence studies using a standard two-treatment crossover design, the sample size needs to be selected with the power to

demonstrate the test and reference ratio for averages of C_{\max} , and AUC is within an 80–125% limit. The sample size is calculated using within-subject variability (SD) for the PK parameter, magnitude of subject-by-formulation interaction, the difference of the arithmetic means of the log transformed parameters (delta, usually taken as 0.05), and the 80% or 90% power [6, 31]. The sample size calculations are calculated as below and shown in Table 7.25:

$$N \geq \frac{2[t(\alpha, df = N' - 2) + t(\beta, df = N' - 2)]^2 * (2\sigma w^2 + \sigma D^2)}{(\ln(\theta) - \ln(1 - \theta))^2}$$

where

Table 7.24 Bootstrap AUC and C_{max} and 90% confidence interval estimates

Treatment	Scale	Parameter	Count	Mean	SD	CV%	90% CI lower	90% CI upper
Test	Original	AUC	500	189.6	12.9	6.8	188.4	190.7
		C_{max}	500	21.7	3.0	13.7	21.5	22
	Natural logarithm	AUC	500	5.2	0.1		5.2	5.2
		C_{max}	500	3.1	0.1		3.1	3.1
Reference	Original	AUC	500	190.9	13.1	6.9	189.7	192
		C_{max}	500	21.9	3.1	14.2	21.6	22.2
	Natural logarithm	AUC	500	5.2	0.1		5.2	5.3
		C_{max}	500	3.1	0.1		3.1	3.1

Table 7.25 Sample size calculations for a two-period, two-sequence, two-treatment crossover BE study for alpha (one-sided) = 0.05, delta = 0.05, and BE margin = 0.8

sigma_w	sigma_d	Power	
		80%	90%
01	0.15	6	8
0.1	0.15	12	14
0.15	0.15	16	22
01	0.23	12	18
0.1	0.23	18	24
0.15	0.23	22	30
01	0.3	20	28
0.1	0.3	24	34
0.15	0.3	30	42
01	0.5	54	74
0.1	0.5	58	80
0.15	0.5	64	88

$$N' \geq \frac{2[Z\alpha + Z\beta]^2 * (2\sigma w^2 + \sigma D^2)}{(\ln(\theta) - \ln(1 - \theta))^2}$$

sigma_w (σw) = within-subject variability (standard deviation) for the PK parameter

sigma_D (σD) = subject-by-formulation interaction for the PK parameter

Delta (Δ) = deviation from a perfect equivalence, 1-delta rather than 1, recommended 0.05

Power (β) = 80% or 90%

Alpha (α) = one-sided 5%, it is fixed according to regulatory convention.

BE margin (θ) = 0.8

Df = degrees of freedom

30 Differential Equation-Based Analysis (dEq)

30.1 Predefined Simulation Models

Differential equation-based analysis is a powerful tool to simulate PK/PD data. The predefined differential equations for pharmacokinetic 1-, 2-, and 3-CBM for extravascular, IV bolus, IV infusion (Table 7.14), and PD models (Table 7.16) are included, allowing simultaneous prediction of single- and multiple-dose PK/PD analysis. Additionally, an effect compartment [2] can be included in the PD analysis. The integration is performed using either by Runge-Kutta (4th order), Runge-Kutta-Cash-Karp, or Runge-Kutta-Fehlberg methods [32, 33], with appropriate step size selection. The following is an example of a model, and the simulation result is shown in Fig. 7.21.

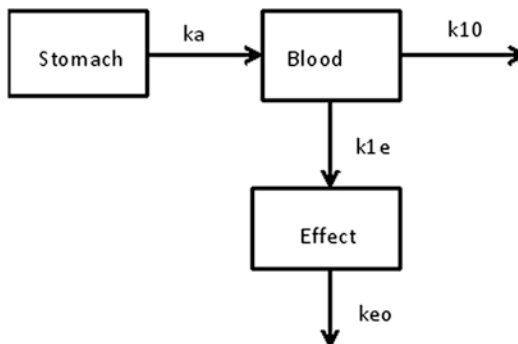
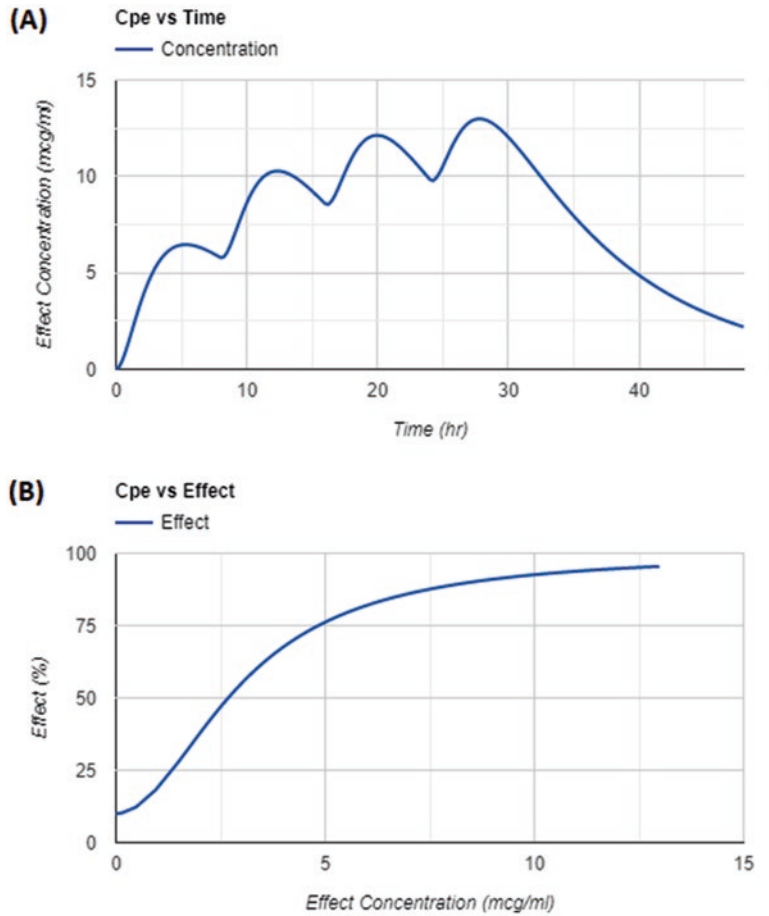


Fig. 7.21 PK/PD simulation plots using the predefined models (1-CBM oral/sigmoid E_{max}) based on the differential equations (a) concentrations in an effect compartment (C_{pe}) following multiple oral doses and (b) the effect vs. effect compartment concentrations. For simulation, parameters used were $K_{10} = 0.1$ (/hr), $K_a = 1$ (/hr), $K_{e0} = 0.5$ (/hr), $V_d/F = 10$ (L), $EC_{50} = 3$ (mcg/mL), $\gamma = 2$, step size = 0.25, dose = 100 mg q8h for 24 hours, and time frame = 0 to 48 hours



For a one-compartment model and the first-order absorption model shown above, the rate of loss of a drug from the stomach is given by

$$\frac{dX_a}{dt} = -k_a X_a \tag{7.32}$$

The rate of absorption by an apparent first-order process and the first-order elimination of a drug from the body are given by

$$\frac{dX}{dt} = k_a X_a - k_{10} X \tag{7.33}$$

X_a = amount in stomach (initial = dose),
 X = amount in blood (initial = 0), $X = VC$,
 k_a = apparent first-order absorption rate constant
 k_{10} = apparent first-order elimination rate constant

V = apparent volume of distribution of blood compartment

The rate of loss of drug concentration (C_e) from the effect compartment is given by

$$\frac{dC_e}{dt} = \frac{k_{e0} X}{V} - k_{e0} C_e \tag{7.34}$$

where

k_{e0} = rate constant for drug removal from the effect compartment

30.2 User-Defined Simulation Models

This module provides an interface for the flexibility of writing differential equations and their

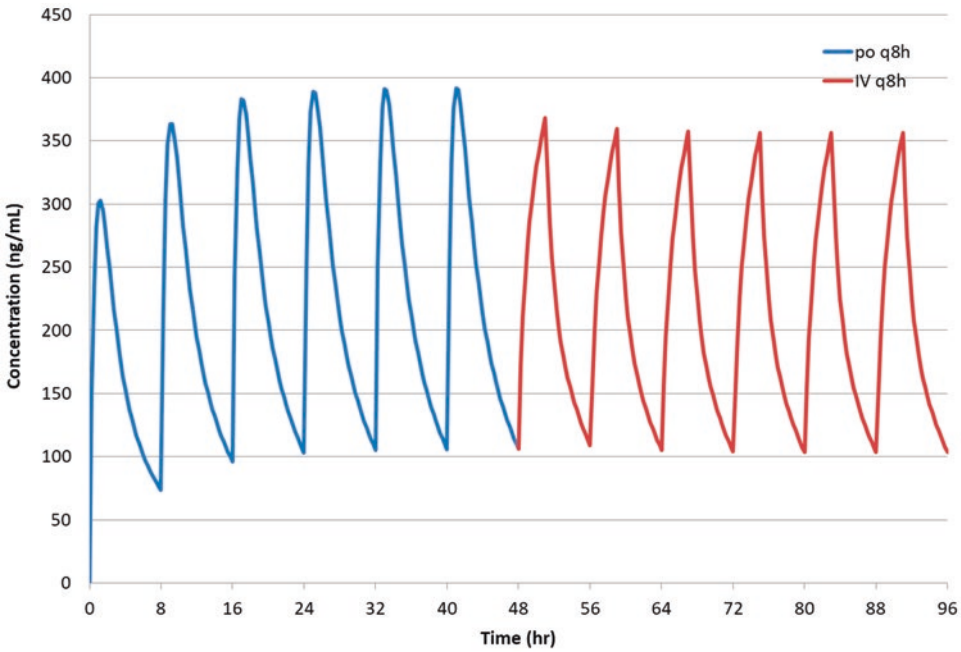


Fig. 7.22 Simulation of plasma concentrations for oral multiple doses followed by a 3-hour IV infusion q8h dosing

integration and visualizing results. The dosing routes, such as IV and extravascular, and combination of these for single and multiple doses can be easily included. The following is an example of multiple-dose oral and IV infusion for a drug with 2-CBM profile (Fig. 7.22).

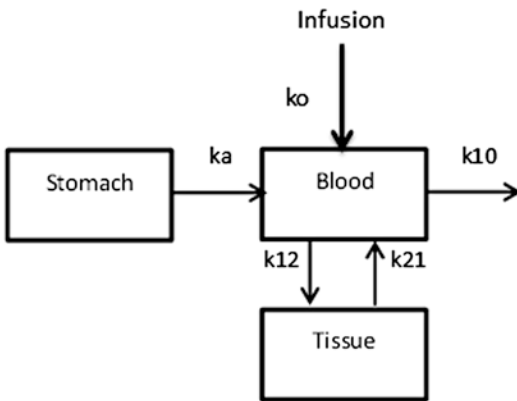
$$\frac{dX_a}{dt} = -ka \cdot X_a \tag{7.35}$$

The rate of absorption by an apparent first-order process and the rate of change of the drug from the blood (central) compartment by a first-order process are given by

$$\frac{dX}{dt} = ka \cdot X_a - k_{10} \cdot X - k_{12} \cdot X + k_{21} \cdot X_t \tag{7.36}$$

The rate of change of drug levels in the tissue (peripheral) compartment is given by

$$\frac{dX_t}{dt} = k_{12} \cdot X - k_{21} \cdot X_t \tag{7.37}$$



For a two-compartment model and the first-order absorption shown above, the rate of loss from the stomach is given by

- X_a = amount in stomach
- X = amount in blood compartment
- X_t = amount in tissue compartment
- ka = apparent first-order rate constant
- k_{10} = apparent first-order elimination rate constant
- k_{12} and k_{21} = apparent first-order inter-compartmental distribution rate constants

The screenshot shows the 'sub1.txt' data file being processed. The 'Select header' dialog has mapped the following headers to columns: Subject, Time, Concentration, and Group. The data table below shows the following values:

Subject	time(hr)	Cp(ng/mL)	Dose
1	0	0	500
1	0.5	5.359	
1	1	9.951	
1	2	17.182	
1	4	25.784	
1	6	30.774	

Below the data table, the 'User Defined Equation' section shows two equations defined:

- Enter Equation: $dG = -ka * G$ +
- Enter Equation: $dX = ka * G / V - K * X$ -

Fig. 7.23 Data input mapping and differential equations

30.3 User-Defined Differential Equation Model Optimization

The experimental data can be fitted to a mathematical model using a set of ordinary differential equations. The following is an example of a data fitted to oral 1-CBM differential equations:

$$dG = -ka.G \quad (7.38)$$

$$dX = ka.\frac{G}{V} - K.X \quad (7.39)$$

where

G = amount of drug in stomach

ka = first-order rate constant for absorption

X = amount of drug in blood

K = first-order elimination rate constant

V = apparent volume of distribution

The data input and differential equations are shown in Fig. 7.23.

The compartment, parameter, constant (for infusion input), and compartment to be optimized are selected as shown in Fig. 7.24.

Initial value of parameters, their upper and lower bound, and dosing information are provided. The optimization is achieved using either a L-BFGS-B [34], Nelder-Mead [14], or Levenberg-Marquardt [35] method using appropriate weight selection. The parameter estimates, their standard errors, and CV% are computed (Table 7.26); in addition, observed and predicted graphs (Fig. 7.25), residual plots (Fig. 7.26), and model diagnostics and iteration results are displayed.

31 Conclusions

Pharmacokinetic modeling software (PKMP) is a web-based commercial program created using the open source codes for Java coding language and R libraries. The web-based platform allows

User Defined Function

Show Equation

User Defined Mapping

Submit

Variables	Compartment	Parameter	Constant	Optimize	Units
ka	<input type="radio"/>	<input checked="" type="radio"/>	<input type="radio"/>	<input type="radio"/>	Select Unit
G	<input checked="" type="radio"/>	<input type="radio"/>	<input type="radio"/>	<input type="radio"/>	Select Unit
K	<input type="radio"/>	<input checked="" type="radio"/>	<input type="radio"/>	<input type="radio"/>	Select Unit
X	<input checked="" type="radio"/>	<input type="radio"/>	<input type="radio"/>	<input type="radio"/>	Select Unit
V	<input type="radio"/>	<input checked="" type="radio"/>	<input type="radio"/>	<input type="radio"/>	Select Unit

Fig. 7.24 Selection of compartment and parameters for differential equation optimization

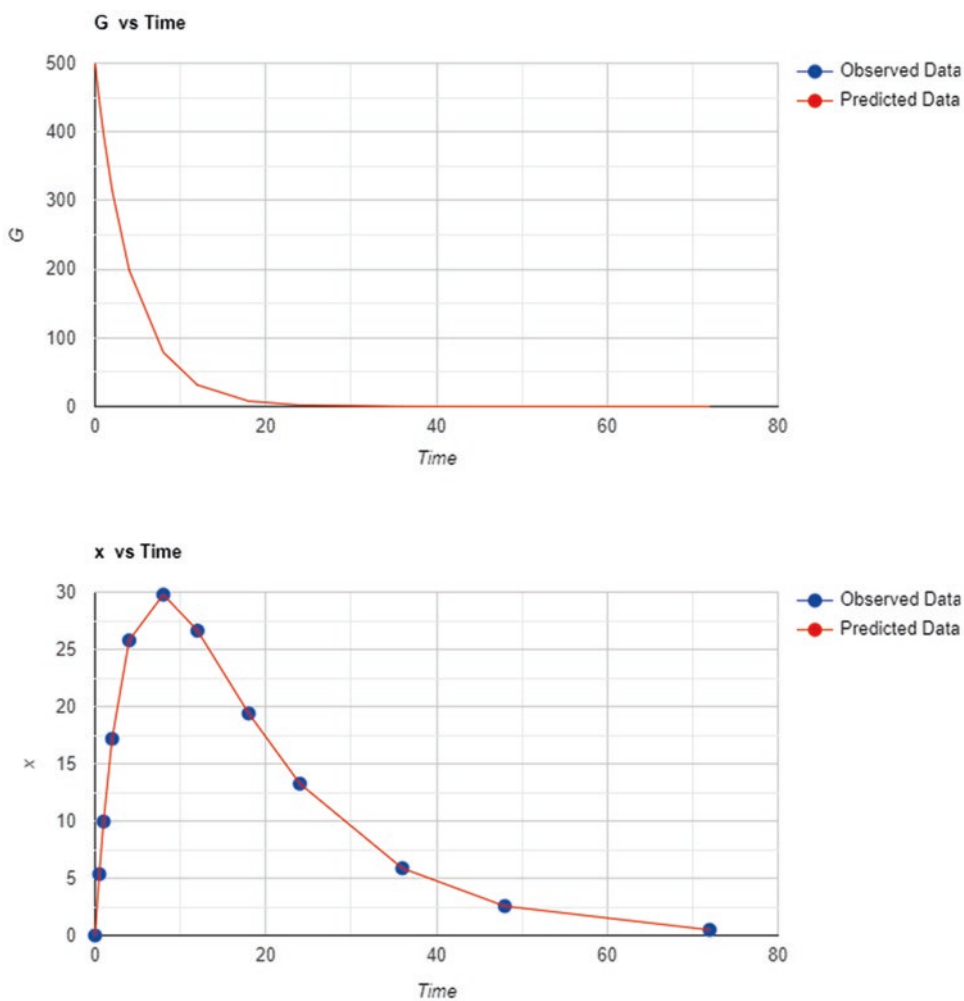


Fig. 7.25 Observed and predicted data for 1-CBM oral data fit using optimization of user-defined differential equations. For G compartment data represents amount (mg) and for X compartment data is concentration $\mu\text{g/L}$, and time is in hours

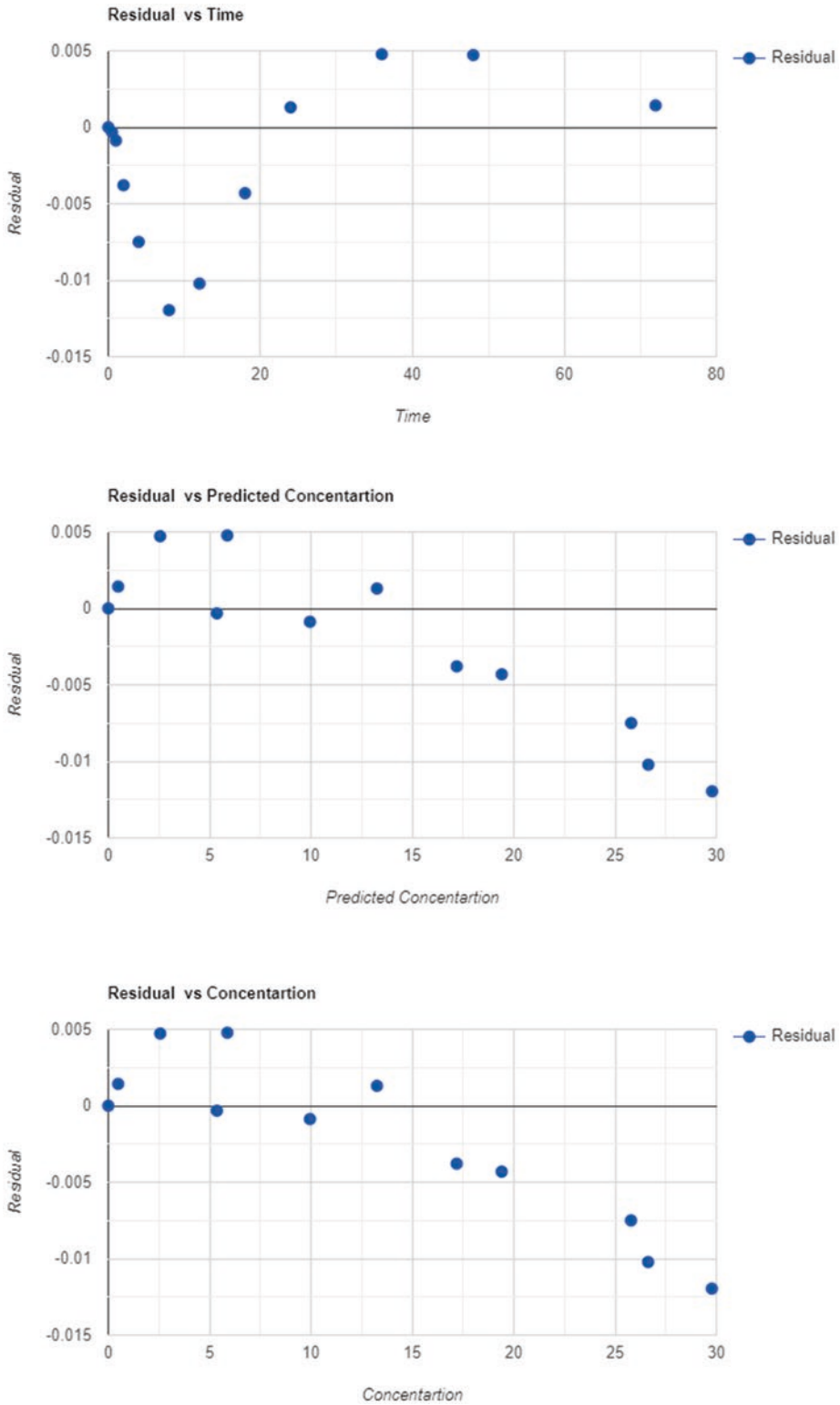


Fig. 7.26 Residual plots for 1-CBM oral data fit using optimization of user-defined differential equations

Table 7.26 1-CBM oral model parameter estimates using user-defined differential equation optimization

Parameter	Estimate	Standard error	CV%
Subject	1		
K_a (hr)	0.2308	0.0178	7.7123
K (hr)	0.0694	0.0049	7.0605
V (L)	9.9934	0.5168	5.1714

easy and secure access to the program using any Internet browser, and the program is independent of operating systems, such as MacOS or Windows. The program has been extensively tested for validation and verification of every module for its quality and functionality. Pharmacokinetic, pharmacodynamic, statistical analysis, dissolution, IVIVC, simulation, modeling, and reporting are some of its main functionalities, allowing for a wide range of data analyses to support drug product evaluation and development during different phases of drug development. The program can be accessed at <https://aplanalytics.com/>.

Acknowledgments The author would like to thank Anupama DS and programmers for their support in developing PKMP as a commercial product. The author is thankful for the critical editorial review by Soham Shah and Dr. Anant Shah.

References

1. Biopharmaceutical Research & Development: The Process Behind New Medicines. http://phrma-docs.phrma.org/sites/default/files/pdf/rd_brochure_022307.pdf.
2. Gibaldi M, Perrier D, editors. Pharmacokinetics. Revised and expanded. 2nd ed. New York: Marcel Dekker Inc; 1982.
3. Welling PG, Tse FLS, editors. Pharmacokinetics regulatory, industrial, academic, perspective. New York: Marcel Dekker, Inc; 1988.
4. Rowland M, Tozer TN. Clinical pharmacokinetics, concepts and application. Philadelphia: Lea and Febiger; 1980.
5. Bulitta JB, Holford NHG. An introductory guide to non-compartmental analysis, In: Wiley encyclopedia of clinical trials. Wiley; 2008. <https://doi.org/10.1002/9781118445112.stat06889>.
6. Guidance for industry, statistical approaches to establishing bioequivalence: U.S. Department of Health and Human Services Food and Drug Administration, Center for Drug Evaluation and Research (CDER), January 2001.
7. Bailer AJ. Testing for the equality of area under the curves when using destructive measurement techniques. J Pharmacokinet Biopharm. 1988;16:303–9.
8. Mager H, Goller G. Resampling methods in sparse sampling situations in preclinical pharmacokinetic studies. J Pharm Sci. 1988;87:372–8.
9. Boxenbaum H. Interspecies scaling, allometry, physiological time, and the ground plan of pharmacokinetics. J Pharmacokin Biopharm. 1982;10:201–27.
10. Ritschel WA, Vachharajani NN, Johnson RD, Hussain AS. The allometric approach for interspecies scaling of pharmacokinetic parameters. Comp Biochem Physiol. 1992;103C:249–53.
11. Guidance for industry: estimating the maximum safe starting dose in initial clinical trials for therapeutics in adult healthy volunteers. U.S. Department of Health and Human Services Food and Drug Administration, Center for Drug Evaluation and Research (CDER), Pharmacology and Toxicology, July 2005.
12. Penel N, Kramar A. What does a modified-Fibonacci dose-escalation actually correspond to? Med Res Methodol. 2012;12:103:1–5.
13. Gavin HP. The Levenberg-Marquardt algorithm for nonlinear least squares curve-fitting problems, September 18, 2020. <http://people.duke.edu/~hpgavin/ce281/lm.pdf>.
14. Nelder JA, Mead R. A simplex method for function minimization. Comput J. 1965;7:308–13.
15. Guidance for industry dissolution testing of immediate release solid oral dosage forms. U.S. Department of Health and Human Services Food and Drug Administration Center for Drug Evaluation and Research (CDER), August 1997.
16. Suarez-Sharp S, Abend A, Hoffelder T, Leblond D, et al. In vitro dissolution profiles similarity assessment in support of drug product quality: what, how, when—workshop summary report. AAPS J. 2020;22:74. <https://doi.org/10.1208/s12248-020-00458-9>.
17. Dash S, Murthy PN, Nath L, Chowdhury P. Kinetic modeling on drug release from controlled drug delivery systems. Acta Pol Pharm Drug Res. 2010;67:217–23.
18. Kalam MA, Humayun M, Parvez N, Yadav S, Garg A, Amin S, Sultana Y, Ali A. Release kinetics of modified pharmaceutical dosage forms: a review. Cont J Pharm Sci. 2007;1:30–5.
19. Moore JW, Flanner HH. Mathematical comparison of dissolution profiles. Pharm Technol. 1996;20:64–74.
20. Tanigawara Y, Yamaoka K, Nakagawa T, Uno T. New method for the evaluation of in vitro dissolution time and disintegration time. Chem Pharm Bull. 1982;30:1088–90.
21. Tsong Y, Hammerstrom T, Sathe P, Shah VP. Statistical assessment of mean differences between two dissolution data sets. Drug Inf J. 1996;30:1105–12.
22. FDA. Guidance for industry: extended release oral dosage forms: development, evaluation, and applica-

- tion of in vitro/in vivo correlations, September 1997. <http://www.fda.gov/cder/guidance/index.htm>.
23. Gillespie WR. Convolution based approaches for in vivo in vitro correlation modeling, in vitro in vivo correlations. *Adv Exp Med Biol.* 1997;423:53–65.
 24. Gillespie WR. Modeling strategies for in vivo in vitro correlations. In: Amidon G, Robinson JR, and Williams RL, editors. *Scientific foundation for regulating drug product quality.* Alexandria: AAPS Press; 1997. p. 275–92.
 25. Qureshi SA. In Vitro-In Vivo Correlation (IVIVC) and determining drug concentrations in blood from dissolution testing – a simple and practical approach. *Open Drug Delivery J.* 2010;4:38–47.
 26. Langenbucher F. Handling of computational in vitro/in vivo correlation problems by Microsoft Excel: III. Convolution and deconvolution. *Eur J Pharm Biopharm.* 2003;56:429–37.
 27. Langenbucher F. Numerical convolution deconvolution as a tool for correlating in vitro and in vivo drug availability. *Pharm Ind.* 1982;44:1166–71.
 28. Langenbucher F. Improved understanding of convolution algorithms correlating body response with drug input. *Pharm Ind.* 1982;44:1275–8.
 29. Loo LCK, Riegelman S. A new method for calculating intrinsic absorption rates of drugs. *J Pharm Sci.* 1968;57:918–28.
 30. Wagner JG, Metzler C. Estimation of rate constants for absorption and elimination from blood concentration data. *J Pharm Sci.* 1967;56:658–9.
 31. Diletti E, Hauschke D, Steinijans VW. Sample size determination for bioequivalence assessment by means of confidence intervals. *Int J Clin Pharmacol Therapy Toxicol.* 1991;29(1):1–8.
 32. Cash JR, Karp AH. A variable order Runge-Kutta method for initial value problems with rapidly varying right-hand sides. *ACM Trans Math Softw.* 1990;16(3):201–22.
 33. Michael Thomas Flanagan's Java Scientific Library RungeKutta Class: Numerical Solution of Differential Equations. <https://www.ee.ucl.ac.uk/~mflanaga/java/RungeKutta.html>.
 34. Byrd RH, Lut P, Nocedal J, Zhu C. A limited memory algorithm for bound constrained optimization. *SIAM J Sci Comput.* 1995;16(5):1190–208.
 35. Gavin HP. The Levenberg-Marquardt algorithm for nonlinear least squares curve-fitting problems. <https://people.duke.edu/~hpgavin/ce281/lm.pdf>.

PK/PD for Specific Nano Carriers

Incorporation of drugs into nanoparticulate drug delivery systems leads to insightful transforms in their disposition and pharmacological activity. Nanoparticulate drug delivery systems of different types, such as nanoparticles, liposomes, and drug conjugates, and of different composition are intensively explored these days in pre-clinical as well as clinical study. Exclusively, the correlations between the nanoparticulate drug delivery systems composition, effectiveness of their targeting to the projected site of action, and the degree of the preferred vs. adverse effects need to be explored. Recently, PK/PD modeling has come forward as a helpful tool with which to assess the impact of formulation and system explicit factors on the targeted disposition and therapeutic effectiveness of nanoparticulate drugs.



Pharmacokinetics and Pharmacodynamics of Liposomal Nanoparticles

Prachi Pandey, Jayvadan Patel, Samarth Kumar, and Yashwant Pathak

Contents

1	Introduction	144
2	Altered Pharmacokinetics Modify the Pharmacodynamic Efficacy and Toxicity of NPs	144
3	Factors that Influence the Pharmacokinetics, Pharmacodynamics, and Toxicology of Theranostic NPs	145
4	Theranostic Applications and Pharmacodynamics of NPs	152
5	Theranostic Nanoparticles Designed as Drug and Gene Delivery Vehicles	153
6	Challenges and Future Directions	157
	References	158

Abstract

In the past few years, some major advancements in liposome technology have induced the rapid development of new pharmaceutical

liposomal applications. For the purpose of optimizing the delivery of factors for maximum efficacy, novel methods have been proposed to increase the permeation rate of drugs temporarily and deliver the desired target compound in a time-regulated and locally restricted manner to the target site.

Lipid-based nanoparticles (LNPs) are promising delivery vectors in the treatment of cancer, inflammation, and infections and are already used in clinical practice. Numerous strategies based on LNPs are being developed to carry drugs into specific target sites. The common purpose for all of these LNP-based platforms is to improve the payload's pharmacokinetics, biodistribution, stability, and therapeutic benefits and also to reduce adverse effects to a minimum. In addition, the delivery

P. Pandey (✉)
Babaria Institute of Pharmacy, BITS Edu Campus,
Vadodara, Gujarat, India

J. Patel
Nootan Pharmacy College, Faculty of Pharmacy,
Sankalchand Patel University,
Visnagar, Gujarat, India

S. Kumar
Formulation- R & D, Sun Pharmaceutical Industries
Ltd, Vadodara, Gujarat, India

Y. Pathak
College of Pharmacy, University of South Florida
Health, Tampa, FL, USA

system must be biocompatible and nontoxic and should avoid undesirable interactions with the immune system. The rapid advancement in nanotechnology has allowed the emergence of theranostic NPs, which have shown advantages of diagnosis and drug delivery as well as targeting the biomarkers of the disease at the molecular level.

Keyword

Liposomes · Theranostic nanoparticles · Pharmacokinetics · Pharmacodynamics

1 Introduction

Liposomes were the first nanoscale drug to be approved for clinical use in 1995. Since then, the technology has grown considerably, and pioneering recent work in liposome-based delivery systems has brought about remarkable developments with significant clinical implications. This includes long-circulating liposomes; stimuli-responsive liposomes; nebulized liposomes; elastic liposomes for topical, oral, and transdermal delivery; and covalent lipid-drug complexes for improved drug plasma membrane crossing and targeting to specific organelles.

Liposomes are composite structures made of bilayered phospholipid vesicles (uni- or multilamellar) with a hydrophilic and/or aqueous inner compartment. The properties of liposomes are highly attributable to their physicochemical properties such as size, surface charge, composition, rigidity of bilayer, and preparation methods. These integrated liposome features enable the encapsulation, embedding, or association with a wide range of molecules (i.e., drugs, antigens, proteins, and nucleotides) as well as enhance the delivery of therapeutic payloads into specific tissues and cells. Liposomes also improve in vitro and in vivo stability and reduce adverse effects. The successful combination of protection of its payload molecules from one hand and its potential to be cell-specific via surface modification with various targeting agents on the other hand

made these carriers an attractive option in the field of therapeutics [5].

In the past 15 years, some major breakthroughs in liposome technology have fueled the rapid development of new pharmaceutical liposomal applications. In order to optimize the delivery of factors for maximum efficacy, novel methods have been proposed to increase the permeation rate of drugs temporarily and deliver the desired target compound in a time-regulated and locally restricted manner to the target site.

Lipid-based nanoparticles (LNPs) hold great promise as delivery vectors in the treatment of cancer, inflammation, and infections and are already used in clinical practice. Numerous strategies based on LNPs are being developed to carry drugs into specific target sites. The common denominator for all of these LNP-based platforms is to improve the payloads' pharmacokinetics, biodistribution, stability, and therapeutic benefit and to reduce adverse effects to a minimum. In addition, the delivery system must be biocompatible and nontoxic and avoid undesirable interactions with the immune system [2]. In addition, theranostic nanoparticles hold the potential to revolutionize future disease management. Since the last decade, there has been a growing interest in the engineering of various kinds of theranostic nanoparticles for simultaneous cancer imaging and therapy. Efficient targeting of theranostic nanoparticles to the tumor site is important for both diagnostic and therapeutic purposes.

2 Altered Pharmacokinetics Modify the Pharmacodynamic Efficacy and Toxicity of NPs

Nanoparticles as a drug delivery system possess numerous advantages over conventional therapies such as:

- Easy to alter the size and surface charge of nanoparticles, hence could be used for both passive and active drug targeting after parental administration.

- Altering the property of the matrix offers the chance of controlled release of medicaments.
- Nanocarriers are generally made of biodegradable substances, therefore do not remain in the body.
- Greater drug encapsulation can be obtained into the carriers without any chemical interaction; therefore, drug activity is fully retained compared to chemically modified conjugates.
- Biodistribution of therapeutics could be changed as per outer surface characteristics of the nanoparticles by late clearance of the drug in order to get the highest therapeutic potency with diminished undesired effects.
- Targeting moieties can be anchored to particle surface or guidance through magnetic-based targeting.
- Nanocarriers are designed for oral, nasal, parenteral, and ocular delivery.
- Due to their smaller size, they can penetrate through smaller capillaries, hence allowing optimal drug deposition at the target site [4].

Due to an exponential increase in surface area at nanometer levels, nanocarriers could have the capability to alter physiological interactions from the molecular level to the systemic level, creating the *in vivo* delivery of nanomaterial a fascinating research topic. The scope of nanomedicine has gone wider and wider in the last two decades. Nanocarriers are now made up of different types depends on the type of matrix used such as organic versus inorganic with an extraordinary control over the particle diameter, morphology, surface characteristics, drug encapsulation, and its release. However, their clinical transformation is comparatively slow and only a few commercial products such as liposomes or micelles. Regulatory guidelines for robust techniques of nanocarrier characterization are essential for assuring safety of nanomaterials. Novel nanocarriers are usually evaluated in terms of surface charge and ligand density, later on which decide their interactions with the cell surface. Conversely, in blood or other biological fluids, nanocarriers are easily covered with protein aura, which eventually dictates *in vivo* fates and therapeutic response [3].

3 Factors that Influence the Pharmacokinetics, Pharmacodynamics, and Toxicology of Theranostic NPs

Nanoparticles (NPs) are considered a promising tool in both diagnosis and therapeutics. Theranostic NPs possess the combined properties of targeted imaging and drug delivery within a single entity. While the categorization of theranostic NPs is based on their structure and composition, the pharmacokinetics of NPs are significantly influenced by the physicochemical properties of theranostic NPs as well as the routes of administration. Consequently, altered pharmacokinetics modify the pharmacodynamic efficacy and toxicity of NPs. Although theranostic NPs hold great promise in nanomedicine and biomedical applications, a lack of understanding persists on the mechanisms of the biodistribution and adverse effects of NPs.

Nanoparticles (NPs) possess a relatively small size in the nanorange (1–1000 nm) but have a significant advantage over atoms and molecules owing to a larger surface area per unit volume. NPs also have a greater formulating flexibility for various sizes and shapes with different chemical surface traits. Due to their versatile nature, they have been successfully used as both diagnostic and therapeutic tools. “Theranostics” refers to the development of compounds, which exhibit the characteristics of diagnostics and therapeutics in a single entity. The rapid advancement in nanotechnology has allowed the emergence of theranostic NPs, which have shown advantages of diagnosis and drug delivery as well as targeting the biomarkers of the disease at the molecular level. For the clinical use, however, the size of a NP has to be limited up to 220 nm because a standard 0.22 μm (220 nm) filter is used routinely in the clinic before injecting theranostic agents into the body. The National Nanotechnology Initiative (NNI) also defines “nanomaterials” as (1) research and technology development at the atomic, molecular, or macromolecular levels, in the length scale of approximately 1–100 nm range; (2) creating and using structures, devices,

and systems that have novel properties and functions because of their small and/or intermediate size; and (3) ability to control or manipulate at the atomic scale.

Although theranostic NPs hold great promise in nanomedicine and biomedical applications, a lack of understanding persists on the mechanisms of the biodistribution and adverse effects of NPs. An ideal theranostic NP model should possess several important properties. For delivery, NPs should act on the target tissues and demonstrate appropriate release kinetics of the drug in optimum concentrations at the site of action, illustrating their efficient therapeutic potency. Since it also possesses diagnostic abilities, it should help determine the precise location and characteristics of the disease. Along with these properties, it is very important that the NP should be nontoxic and easily excretable or eliminated from the body. There have been several reviews providing an in-depth outlook on the potential of NPs and their application in several aspects, such as their usage as theranostic agents in drug delivery and the application of theranostic NPs in cancer therapy, which is one of the most rapidly developing therapies involving nanosystems. Recognizing that the *in vivo* availability and efficacy of NPs are mainly determined by their pharmacokinetics (PK) and potential toxicity, we provide a brief review of these facets of theranostic NPs [1].

Regardless of their compositions, all theranostic NPs must be designed to have a reasonable half-life in blood, selective targetability, and effective elimination from the body after comprehensive delivery to the target site. To acquire these desired pharmacokinetic behaviors of NPs for clinical use, it is necessary to modulate the hydrodynamic diameter (HD), shape, composition, and surface characteristics of NPs. For instance, the overall HD of theranostic NPs is required to be <5.5 nm for renal clearance after complete targeting in order to achieve high signal-to-background ratio. In the following section, we discuss more details about the physicochemical properties of theranostic NPs in terms of size, shape, surface, composition, and route of administration.

The physicochemical properties of theranostic NPs are of significant importance in modulating PK because they determine the immediate pharmacological response in the body when the NPs are administered. Drugs with low bioavailability can have better drug dissolution rates by the technique of “nanosizing” a drug formulation, which would promote increased absorption of the drug. Also, NPs can prolong the half-life of drugs in blood circulation, which would otherwise be rapidly cleared or degraded. Since the PK plays a major role in determining the therapeutic efficacy and toxicity of the administered NPs, several key factors influencing the PK of NPs are discussed. In this section, we avoid reticuloendothelial system-mediated NP clearance and focus on smaller NPs and their theranostic aspects because larger NPs have slim chances of clinical translation. As previously reported, renal excretion is a preferred and desirable pathway for theranostic NPs compared with hepatic clearance because the NPs can be rapidly eliminated from the body while little cellular internalization/metabolism is involved, thus effectively minimizing body exposure to the NPs. Theranostic nanoparticles have the potential to transform cancer treatment by delivering high-quality images to the tumor. Their ability to precisely target the tumor site has been the subject of intense research.

Although theranostic nanoparticles can target tumors, their engineering still has challenges in terms of their *in vivo* capabilities. Theranostic nanoparticles are designed to be versatile and adaptable to various disease management applications. Their combined therapeutic and diagnostic capabilities can be utilized to identify and treat various diseases.

Active targeting of tumors has been shown to be very effective in the treatment of various types of cancer. Currently, theranostic nanoparticles are mainly used for target selection. However, their ability to effectively target tumors is still a major challenge. There are many ways to engineer theranostic nanoparticles. They can be used for drug delivery, photo bioimaging, and medical imaging. A similar method involves attaching contrast agents to nanoparticles. This method works by combining the therapeutic properties of

these agents with the imaging properties of the nanoparticles. Nanoshells, cages, and Cu-CuS are commonly used for achieving intrinsic and therapeutic properties. For achieving this, various surface modifications are performed. Although theranostic nanoparticles are in the early stages of their development, there are numerous efforts being made to improve their efficiency. Currently, they are being studied using various imaging and therapeutic nanoplatforms. An optimized targeting strategy for theranostic nanoparticles can prevent or minimize their accumulation in the tumor. This strategy involves the use of active molecules that can affect the vascular and lymphatic drainage of the tumor. Due to the wide variety of tumors and the unpredictable nature of their extravasation, the passive targeting strategy can be limited to its limitations in certain fast-growing tumors [7].

Theranostic nanoparticles are designed to actively target tumors. They are developed by conjugating various targeting ligands to recognize and target certain receptors that are overexpressed in tumor cells. Depending on the properties of a particular theranostic nanoparticle, its targeting ligands may be small molecules, antibodies, or protein fragments. Currently, only a few examples of these have been reported. Inspired by this, several works are being carried out to create targeted nano-beacons that can inhibit or activate the photodynamic activity of folate-controlled porphyrins after their internalization into the tumor.

Nanoparticles (NPs) are viewed as a promising tool in therapeutics. Theranostic NPs have the consolidated properties of designated imaging and medication delivery inside a solitary substance.

While the classification of theranostic NPs depends on their construction and creation, the pharmacokinetics of NPs are altogether impacted by the physicochemical properties of theranostic NPs. Thus, changed pharmacokinetics change the pharmacodynamic adequacy of NPs. In spite of the fact that theranostic NPs hold incredible guarantee in nanomedicine and biomedical applications, lesser understanding endures on the undesirable impacts of NPs.

Nanoparticles (NPs) have a moderately little size in the nanorange (1–1000 nm), NPs likewise have a more prominent defining adaptability for different sizes and shapes with various compound surface characteristics.

Because of their flexible nature, they have been effectively utilized in current drug delivery strategies. “Theranostics” display the attributes of both diagnostics and therapeutics. The quick progression in nanotechnology has permitted the development of theranostic NPs, which have shown benefits of analysis and medication conveyance just as focusing on the biomarkers of the sickness at the atomic level.

For the clinical use, nonetheless, the size of a NP must be restricted up to 220 nm on the grounds that a standard 0.22 μm (220 nm) size is utilized regularly for administration.

The National Nanotechnology Institute (NNI) likewise characterizes “nanomaterials” as examination and innovation improvement at the nuclear, sub-atomic, or macromolecular levels, in the length size of around 1–100 nm range; making and utilizing constructions, gadgets, and frameworks that have novel properties and capacities due to their little as well as halfway size; and capacity to control at the nuclear scale. In spite of the fact that theranostic NPs hold extraordinary guarantee in nanomedicine, furthermore biomedical applications, an absence of understanding perseveres on the components of the biodistribution and unfriendly impacts of NPs.

An ideal theranostic NP model ought to have a few significant properties. For drug delivery, NPs should be focused on the targeted tissues and exhibit suitable delivery of the drug at the site of activity, showing their effective strength. Since it additionally has analytic capacities, it should help decide the exact area and qualities of the illness.

Alongside these properties, it is vital that the NP ought to be non-harmful furthermore, effectively excretable or wiped out from the body. There have been a few researches giving a top to bottom point of view toward the capability of NPs and their application and their utilization as theranostic moiety in drug delivery and the use of theranostic NPs in malignant growth treatment.

Perceiving that the *in vivo* accessibility and viability of NPs are basically controlled by their pharmacokinetics (PK), it is important to mention these features of theranostic NPs [8].

The basic composition and therapeutic modality along with some pros and cons are summarized in Table 8.1.

The physicochemical properties of theranostic NPs are of critical significance in determining PK on the grounds that they decide the prompt pharmacological reaction in the body when the NPs are directed. Medications with low bioavailability can have better medication disintegration rates by the method of “nanosizing” a medication definition, which would enhance retention of the drug [12]. Also, NPs can delay the half-life of medications in blood stream. Since the PK plays a significant role in deciding the effectiveness of the regulated NPs, a few key elements impacting the PK of NPs need to be studied.

3.1 Size and Shape

The capacity of the NPs to enter the cell is dictated by both physicochemical boundaries and natural obstructions. Due to the high surface region to volume proportion (little size), they can enter the boundaries by infiltration through the cell membrane and deliver the medication inside the cell. It has been observed that an overall size range of 10–12 nm is ideal and offers high penetration and insignificant deposition in tissues. Picking an appropriate size in planning a NP is important as it coordinates which discharge pathway the medication would follow. For model, particles with a more modest size of <5.5 nm follow the course of renal excretion, though bigger estimated NPs are metabolized through the liver.

Also, selecting an appropriate carrier system is of high importance. NP frameworks, like liposomes and nanospheres, have been utilized in exact focusing of different illnesses with intravenous delivery of theranostic small particles. The drug-loaded carriers can control the effectiveness of drug delivery and furthermore ensure the safety of drug from inactivation as well as degradation, which can decrease its side effects. The

cellular take-up is likewise impacted by the state of the NPs; for instance, stretched NPs are better absorbed than circular ones [3, 4].

3.2 Surface Property

A modification in the surface of NPs has significant effect on the physical, chemical, and biological nature of the therapeutic molecules in biological systems.

NPs can impart positive or negative charges on the surface, where the interactions with cell membrane change in different ways, which affects their absorption and distribution properties. NPs with positively charged surface show higher cell uptake as compared to negatively charged NPs due to electrostatic interactions.

Alteration of the NP surface with a neutral non-ionic polymer induces stability to the NP by minimizing opsonization and increasing blood circulation time, as exemplified by NPs coated with polyethylene glycol (PEG) on their surface as reported in a study. Surface property also plays an important role when the NPs reach biological fluids (e.g., blood). The surface of NPs is coated with a layer of proteins when they come in contact with the biological fluid. This layer plays a major role in determining the attraction of the NP to the cell membrane. Different NPs form different protein layers, and, thus, every type of NPs has different affinity for a particular protein in a biological fluid, thereby affecting the physicochemical characteristics, which would subsequently affect the rate and extent of biodistribution [4, 5].

3.3 Administration Route

The PK of a drug from a NP depends upon the route by which the drug has been administered, which modifies pharmacological efficacy of the drug. For instance, when bovine insulin was given orally by means of a pH-responsive NP system of chitosan and poly(γ -glutamic acid) to rats, it showed a greater bioavailability compared with subcutaneously injected insulin in diabetic

Table 8.1 Nanoparticle composition and therapeutic modality [5]

Class	NP type	Composition	Therapeutic modality	Pros	Cons
Inorganic NPs	Magnetic NPs	Iron oxide	Chemotherapy; SiRNA; magnetic hyperthermia	Intrinsic MRI contrast; thermal therapeutic agent	Interference in imaging
	QDs	Semiconductor	Chemotherapy; SiRNA; photodynamic therapy	Broadband absorption; small size; tunable emission band	High potential toxicity
	Silica NPs	Mesoporous silica	Chemotherapy; SiRNA	Multi-functionality; facile synthesis; solubility	Stability; need contrast agents
	Carbon NPs	Graphene oxide	Photothermal therapy; photodynamic therapy; chemotherapy	Large surface area; thermal therapeutic agent	Size control; difficulty in purification
		Carbon nanotubes	Photothermal therapy; chemotherapy	Size tunability; mechanical strength	High aspect ratio; difficulty in purification; poor solubility
	Gold NPs	Gold nanoshell	Photothermal therapy; chemotherapy	Size tunability; intrinsic thermal therapeutic agent; tunable in NIR region	Potential toxicity
		Gold nanorod	Photothermal therapy		High aspect ratio; toxicity; difficulty in therapeutic payload
	Others	CuS NPs	Photothermal; chemotherapy	Thermal therapeutic agent; tunable in NIR region	Potential toxicity
		MoS2 nano sheet	Photothermal; chemotherapy; SiRNA	Large surface area; thermal therapeutic agent	Need contrast agents; difficulty in size control
Organic NPs	Biological NPs	Naturally polymers and lipoprotein	Chemotherapy; siRNA	Biocompatibility; biodegradability	Need contrast agents; difficulty in size and degradability control
	Polymer NPs	Linear and branched polymer	Photodynamic therapy; chemotherapy	Biodegradability; flexibility; size tunability	Need contrast agents
	Dendrimers	Tree-like macromolecules	Chemotherapy	Size tunability; solubility	Limited synthesis; need contrast agents
	Liposomes	Phospholipid bilayers	Chemotherapy; siRNA	Conventional drug delivery; large payload	Need contrast agents; poor stability

patients [4, 9]. These oral NPs infiltrate the mucous layer of the intestinal tract and gradually destabilize and disintegrate due to their pH sensitivity. The increased bioavailability may be attributed to the pH-sensitive insulin release from the NPs. The difference in biodistribution of insulin and prolonged reduction of glucose levels

between subcutaneous insulin and oral NPs could be because insulin, via the oral route, mimics the physiological pathway of the endogenously secreted insulin, which reaches the liver and helps to control the glucose levels in the body. In contrast, the insulin given by the subcutaneous route fails to mimic this since it enters the periph-

eral circulation, which is not the normal route of insulin production and secretion.

There are several publications concerning the effect of injection routes on the biodistribution and elimination of NPs. Very recently, the biodistribution, clearance, and tumor uptake of renally clearable carbon dots with three different injection routes, including intravenous, intramuscular, and subcutaneous administrations, were reported.

The blood clearance and urinary accumulation rate of administered NPs followed the order of intravenous > intramuscular > subcutaneous injections.

In addition, tumor uptake of carbon dots by subcutaneous and intravenous injections was higher than that by intramuscular injection. Such examples are indicative of the route-dependent therapeutic potential and clinical benefits of NP-based theranostic systems. Absorption, biodistribution, elimination, and pharmacologic and toxic effects of NPs are observed following different routes of administration [6].

The pharmacokinetics and pharmacodynamics of theranostic nanoparticles have been illustrated in Fig. 8.1.

3.4 Imaging and Therapeutic Modalities

The determination of imaging methodology is another significant segment for theranostic NPs. The utilization of negligible or noninvasive imaging methodology is valuable to portray the PK especially biodistribution as restorative adequacy of theranostic NPs. Current clinically accessible imaging modalities incorporate atomic imaging (positron emanation tomography (PET) and single photon emanation registered tomography (SPECT)), attractive reverberation imaging (MRI), processed tomography (CT), ultrasound (US), optical imaging, and photoacoustic (PA) imaging. In any case, for effective atomic imaging, the surface or center of NPs ought to be changed with different radioisotopes, paramagnetic particle chelates, or fluorophores, with the exception of utilizing inborn different NPs like iron oxide NPs, QDs, and color doped silica NPs. In view of the inborn affectability and tissue infiltration capacity of imaging modalities, the theranostic NPs could be pictured through noninvasive (more wanted) or insignificantly intrusive (less wanted) way in demonstrative techniques. The upsides and downsides of each imaging methodology are summed up in this segment; we portray remedial modalities of NPs [10, 11].

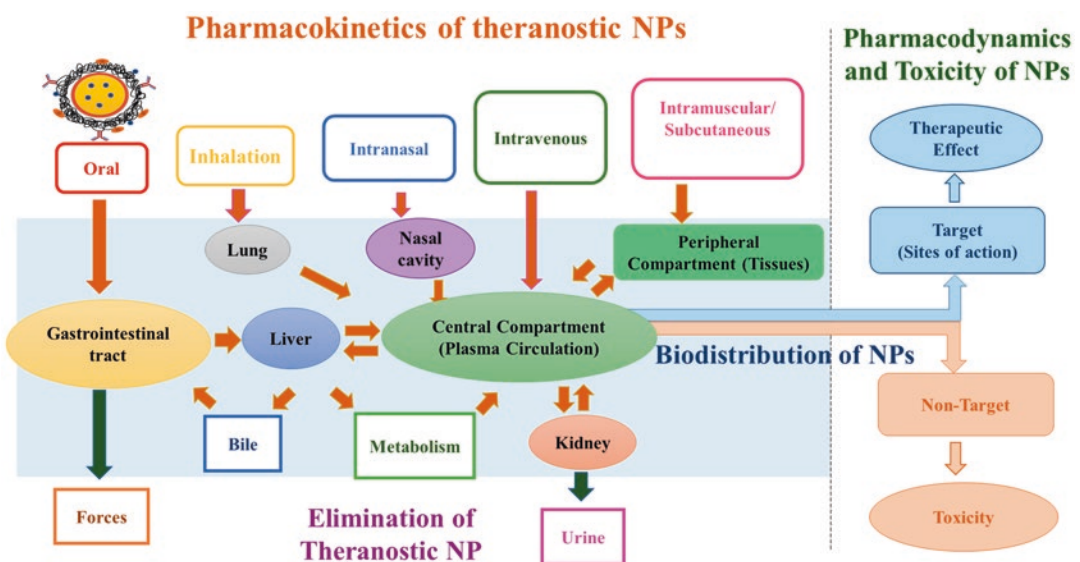


Fig. 8.1 Pharmacokinetics of theranostic NPs

3.5 Composition

Many therapeutic NPs are composed of several different elements with specific geometry/conformation such as core shell, core-satellite, linear, and hyper-branched structures. The little differences of the geometry or conformation can contribute to their *in vivo* performance such as absorption, biodistribution, elimination, as well as targeting ability [2]. In addition, the geometry/conformation changes of NPs and decomposition in *in vivo* environments can significantly affect toxicity.

The biodegradability of theranostic NPs relies on their chemical compositions. Polymeric NPs containing hydrolysable linkages, such as ester, ortho-ester, and anhydride, in their backbones are biodegradable in the body. The use of biodegradable polymers can significantly increase the elimination of NPs from the body and reduce the long-term toxicity. On the contrary, most inorganic NPs are not biodegradable. Such inorganic NPs remain for a relatively long period of time in the body due to their larger size and greater hydrophobicity compared with small molecules; therefore, concerns have been raised about the potential long-term toxicity of these NPs. Taken together, both physicochemical properties (i.e., surface charge, chemistry, and size of the NP) and exposure routes are critical factors that determine the PK of NPs, and these factors can be modified to control (enhance or decrease) the blood circulation and tissue permeation of the drug. On the other hand, poorly designed NPs can promote an enhanced delivery of the drug molecules to certain non-target tissues nonspecifically and cause undesirable side effects, which warrant the appropriate assessment of toxicity for the use of NPs [10].

3.6 Therapeutic Purpose

Chemotherapy

Since cancer is one of the leading causes of death worldwide, NP-based cancer therapy has great potential for overcoming biological barriers and selective targeting to desired sites.

Furthermore, NPs are relatively small and have greater affinity for the cell membrane, thus can easily enter the cancer cells after binding to the cell surface specifically through targeting ligands, which decreases nonspecific biodistribution and the toxicity in non-target organs. Polymeric NPs like liposomes and micelles have been used to solubilize hydrophobic drugs so that higher percentage of injected dose (%ID) can be achieved at the target site. Doxil, for example, is a PEGylated liposome coated on doxorubicin (DOX), where the PEG coating prevents the degradation of drugs by immune system and controls the release of drugs into the blood, resulting in a prolonged terminal half-life and higher drug efficacy. Another example is a QD-aptamer-DOX conjugate [QD-Apt(DOX)] for prostate cancer therapy. The QD-Apt(DOX) conjugate can perceive and render DOX at the target site by using the fluorescence resonance energy transfer (FRET) effect between DOX and QDs. The conjugate is composed of the following three parts: (1) therapeutic DOX, (2) targeted RNA aptamers, which are covalently attached onto the surface of QDs, and (3) diagnostic QDs for fluorescence imaging. This activatable system works by turning “on” the fluorescence by releasing DOX in the tumor cells, while the DOX-loaded QD-Apt is “off” in the normal cells [10].

Gene Therapy

Gene therapy implies the replacement of a faulty gene in the cell with a proficient gene or by overexpression or silencing of a gene by introducing a foreign DNA and modifying the cellular signaling. NPs have a capability to replace viral vectors as they are small in size and therefore can communicate with many biological moieties like cytokines and proteins. Although they possess some drawbacks, such as inefficient transfecting efficiency, these can be overcome by chemical modification of the functional groups. Magnetic NPs have been used in gene therapy by intercalation of the functional gene with the SPION and its effective transfection into the desired cell by high gradient magnets [13, 14].

4 Theranostic Applications and Pharmacodynamics of NPs

The application of theranostic NPs has been most successfully employed in cancer research. For theranostic and clinical applications, most NPs must have inert layer of surface coatings with polymeric or biological materials. In addition, selective targeting is also a desired property to overcome the limitations of conventional therapy and to minimize potential side effects.

There are two major strategies for efficient tumor targeting:

One is passive targeting, where, therapeutic NPs reach the tumor tissues through leaky endothelium surrounding tumor tissues through enhanced permeability and retention effect.

In contrast, active targeting is based on targeting ligands, such as antibody, aptamer, and peptide, on the NP surface which allow NPs to bind to the receptors overexpressed on cancer cells [15, 16]. In this section, several advanced examples of theranostic nanoplatfroms have been discussed.

4.1 Synthetic Polymer NPs

Photosensitizer-conjugated amine functionalized polyacrylamide NPs prepared by oil-in-water microemulsion technique have been reported in some studies.

In some studies, for tumor-specific targeting, the surface of NPs was modified with cell-permeable peptide and biologically inert PEG. Once fluorophore-embedded NPs enter the tumor, the fluorescence dye lights up the tumor cells and the drug is photosensitized by irradiation, which specifically kills the cancer cells. In addition, Liu et al. reported polyelectrolyte-based polyprodrugs which possess imaging, chemotherapeutic, and photodynamic properties. The NPs were covalently conjugated to doxorubicin through a reactive oxygen species (ROS) cleavable linker. PEGylated polyelectrolytes efficiently produce ROS under light irradiation, which then not only kill the cancerous cells by

photosensitization but also can release doxorubicin for chemotherapy. Light-triggered chemotherapy and photodynamic therapy have been combined to produce better results to cure cancers with synergistic advantages such as overcoming multiple drug resistance and improved therapeutic efficacy [13–15].

4.2 Biological NPs (Naturally Derived Polymers)

The self-assembled micellar nanocomplex (MNC) has been developed for delivery of protein drugs. Some research groups reported that simple sequential self-assembly of the epigallocatechin-3-O-gallate (EGCG) derivative, a major ingredient of green tea, with anticancer protein leads to the formation of stable micellar nanocomplex. The anticancer effect of Herceptin-loaded micellar nanocomplex (Herceptin-MNC) was investigated in vitro and in vivo and compared with those of bovine serum albumin (BSA)-MNC and free Herceptin. Herceptin-MNC exhibited a 2.3-fold greater accumulation in the tumor site, 29-fold longer blood half-life, and significantly higher anticancer effect in the tumor in comparison with free Herceptin [20–22].

4.3 Mesoporous Silica NPs

Mesoporous silica NPs have been used successfully in cancer therapy, mainly because of large surface area and pore volume and ease of surface modification. Recently, magnetic NPs or gold NPs were embedded into mesoporous silica NPs for thermally triggered drug release. An anticancer drug was loaded into porous cavities of mesoporous silica NPs, and porous structures were capped with thermally releasable molecule.

When external stimuli, such as magnetic field and NIR laser, are applied to these mesoporous silica nanoplatfroms, drug release can be controlled precisely. This controlled release behavior is a very important feature in target specific therapy as it can overcome the side effects of conventional drug delivery system [21, 22].

4.4 Magnetic NPs

Another example of theranostic NPs in cancer is the use of magnetic NPs (MNPs). MNP-based theranostics can be divided into three ways in terms of therapeutic methods:

1. Hydrophobic drug or gene delivery
2. Thermal therapy in the magnetic field
3. Magnetic/mechanical controlling in cell signaling

Theranostic MNPs normally contain a superparamagnetic iron oxide core, which is used for MRI to detect the tumor, covered by a hydrophilic surface coat on the outside. They have been reported to be linked with an anticancer drug or siRNA to treat the tumor. As one of the important examples, Moore and coworkers have reported dextran-coated SPIONs for in vivo siRNA delivery. The amine-dextran-coated SPIONs were labeled with Cy5.5 dye for simultaneous optical imaging and covalently linked to thiolated siRNA duplex and myristoylated polyarginine peptides, which are membrane translocation modules, for intracellular delivery. This study showed advancement of siRNA delivery and silencing with imaging strategies. MNPs can be also developed by conjugating chemotherapeutic drugs on the surface of NPs to target and treat cancers [18]. Lee et al. have also developed a nanocarrier containing MNP conjugated to the anticancer drug gemcitabine [13]. These NPs deliver the drug by receptor-mediated endocytosis to its target, urokinase plasminogen activator receptor, and also allows in vivo MRI of the tumor [14].

Magnetic thermal therapy utilizes heat induced from MNPs in external high-frequency alternating magnetic field, which allowed us to control heat generation after specific targeting to tumor region of interest. Although external triggering is one of the advantages in magnetic field-induced thermal therapy, the efficacy is limited even with high concentration of therapeutic MNPs. Very recently, to control cell signaling, a magnetic switch method has been developed by using zinc-doped iron oxide MNPs. The thiolated MNPs were conjugated with antibody for targeting death receptor 4 (DR4) of DLD-1 colon can-

cer cells. When a magnetic field is applied to MNP bound DR4s on DLD-1 cells, clustering of DR4s was formed and apoptosis signaling pathways were induced [22].

5 Theranostic Nanoparticles Designed as Drug and Gene Delivery Vehicles

Cellular delivery involves the transport of various drugs and biomolecules. Drugs carried by nanoparticles can be protected from enzymatic degradation and lead to better absorption and distribution. Also, drug solubility and intestinal permeability often act as obstruction to the oral bioavailability of potential drugs. As a solution to this problem, hydrophobic drugs can be incorporated into nanoscale drug delivery vehicles and transported into cells. This ability allows us to re-examine promising drugs previously dropped from development due to poor solubility.

During the past decade, liposomes, micelles, and nanoemulsions have been developed as drug and gene delivery systems. Abraxane, a nano-sized albumin-bound paclitaxel emulsion, was approved by the US Food and Drug Administration for the treatment of metastatic breast cancer in 2005. Fewer allergic reactions were observed in patients using this nanoformulation compared to free paclitaxel. A nanoemulsion of docetaxel (ANX-514) showed bioequivalence and overall safety comparable to the Taxotere formulation of docetaxel. In addition, other drug and gene delivery systems based on polymers, dendrimers, as well as biomolecules are also at different stages of preclinical and clinical development. For example, compared with a standard paclitaxel formulation, ABI-007, a nanoparticle formulation of paclitaxel which is cremophor-free, can be more efficiently and safely administered at high doses with superior response. In clinical trials of this nanoparticle formulation, prolonged survival time with no severe hypersensitivity reactions was observed when treating metastatic breast cancer [14, 17].

Development of nanodrug and gene delivery systems requires an understanding of the absorp-

tion, distribution, metabolism, and excretion profiles of the nanomaterials.

This clinical profile is required not only to optimize the clinical effects of nanomaterials but also to provide guidance for their safe use.

5.1 Nanoparticles Constructed as Drug Carriers for Efficient Delivery

Nanosized carrier systems have the potential to prolong the half-life of the encapsulated drug in the body through enhanced permeation and retention (EPR) effects. A number of nanoparticle-mediated effects, such as improved chemical stability, controlled release from the nanoparticle, and protection of the drug from the immune system, may result in prolongation of a drug's half-life and increased therapeutic window.

Incorporation of drugs into nanodelivery vehicles has resulted in a new paradigm for lowering the adverse effects of chemotherapeutic drugs. Broad application of paclitaxel and doxorubicin is limited by their physiochemical properties that result in intolerable side effects. The replacement of paclitaxel's solubilizer, Cremophor, with amphiphilic cyclodextrin nanoparticles prevents paclitaxel from undesirable recrystallization in aqueous solutions and significantly reduces the drug's side effects such as hemolysis and cytotoxicity. When doxorubicin is loaded into biodegradable poly(D,L-lactide-co-glycolide) nanoparticles for oral chemotherapy, it exhibits not only reduced cardiotoxicity compared to free doxorubicin but also improved oral bioavailability [14, 15].

One of the major challenges in drug delivery is selectively targeting diseased tissues. The efficacy of cancer chemotherapy is greatly limited by the incidence of toxicity to healthy tissues, attributed to the lack of specificity exhibited by anticancer agents for cancerous cells. Recent research has led to development of nanocarrier systems for delivery of anticancer drugs with improved therapeutic efficacy and reduced side effects. A ferrocenyl diphenol tamoxifen derivative, incorporated into lipid nanocapsules, shows antiproliferative activity specific for malignant

glioma cells, but it demonstrates low toxicity levels in normal brain cells. The biocompatible solid lipid nanoparticles has been developed for the specific delivery of docetaxel to hepatoma cells. Targeted delivery was achieved in this case by using a galactose moiety that recognized an asialoglycoprotein receptor upregulated on the hepatoma cells' surface. While increasing cellular uptake by hepatoma cells and drug accumulation in tumor, this targeted nanocarrier of docetaxel is well-tolerated in vivo, without impairing liver function, as observed histologically.

For anticancer drugs to be therapeutically effective, it is important to properly release the drug from the nanocarriers to deliver the drug into the malignant cells. Controlled release of drugs from nanoscale formulations has been observed in earlier studies. The encapsulation of temozolomide, which is a drug used to treat brain tumors, in solid lipid nanoparticles provided sustained-release of temozolomide, along with avoiding the adverse side effects such as cardiac and nephrotoxicity as usually caused by the conventional formulation.

In lung transplantation, liposomal delivery of lipophilic immunosuppressants such as tacrolimus has been observed to provide sustained release and less frequent administration of the drug, thus resulted in reduced dose-related toxicity. It has been demonstrated that an aerosolized nanoparticle formulation of the hydrophobic immunosuppressant, amorphous cyclosporine A, has an enhanced dissolution rate and, therefore, increased drug penetration and diffusion into lung tissue and the bloodstream. In addition, this nanoparticle formulation does not cause lung tissue irritation which is a frequent problem when using a solution-based pulmonary formulation [13–15].

In general, the two major challenges hampering ophthalmic drug delivery are the unique anatomical and physiochemical barriers of the eye and rapid precorneal drug loss. Liposomes and nanoparticles have been used to improve corneal penetration and achieve controlled delivery and sustained drug release. A biocompatible polymeric nanoparticle suspension loaded with sodium diclofenac has been developed. This sus-

pension does not irritate ocular tissues *in vivo* and has a favorable mean size for ophthalmic applications. Kao et al. successfully incorporated pilocarpine into chitosan/Carbopol nanoparticles for ocular applications.

These nanoparticles were observed to show little toxicity and a better prolonged release profile compared with pilocarpine in solution, gel, or liposomes. The easily modified characteristics of chitosan-based nanosystems render them suitable candidates for ophthalmic nanoformulations.

Nanoparticles can cross biological membranes in a non-destructive way without creating much toxicity. This property makes nanoparticles specially useful for improving drug bioavailability in the brain. Superoxide dismutase, a scavenger of reactive oxygen species, poorly penetrates the blood-brain barrier (BBB). When it is encapsulated in biodegradable poly(D,L-lactide-co-glycolide) nanoparticles, superoxide dismutase was demonstrated to cross the intact BBB and efficiently minimize the damage created by cerebral ischemia-reperfusion. In combination with focused ultrasound, which have the capability to locally and transiently disrupt the BBB, the magnetic nanoparticles loaded with chemotherapeutic agents can sufficiently penetrate the BBB and be deposited in the brain through both passive and active targeting, as monitored by MRI [15, 22].

5.2 Theranostic Nanoparticles for Future Customized Medication

Theranostic NPs can be employed for cancer chemotherapy, siRNA delivery, and photodynamic therapy. Small drug molecules have shortcomings including toxic side effects in normal tissues, inadequate specificity to tumor tissues, limited localization to tumor cells because of their hydrophobicity, and drug resistance. Theranostic NPs have the capabilities to overcome these problems in chemotherapy. Also, a theranostic NP delivery system can be useful for siRNA therapy. Theranostic NPs are efficient in enhancing the stability of siRNA in the blood stream after intravenous injection, thereby mini-

mizing degradation by enzymes. Accepting the fact that naked siRNA can be eliminated from the blood within 5 min after administration through intravenous injection, prolonged circulation time of siRNA in NPs can be attributed to effective therapy. Also, it is observed in some studies that negatively charged siRNA cannot easily enter the cytosol of target cells, which can be solved by theranostic NPs for siRNA therapy. During photodynamic therapy, theranostic NP-based photodynamic therapy provides benefits such as reduced systemic toxicity and improved solubility in water as compared to conventional photodynamic therapy. The selective localization of photosensitizer molecules incorporated in NPs reach the target and can significantly lower the systemic toxicity related to classical photodynamic therapy. In addition, mostly photosensitizer molecules being used in photodynamic therapy can accumulate in biological media, leading to a change in their optical characteristics [6, 16].

5.3 Diagnostic Modalities in Theranostic Approaches

In theranostic strategies and applications, diagnostic imaging becomes necessary for establishing the presence and intensity of molecular targets for certain diseases. At present, several noninvasive imaging modalities are being utilized to detect molecular targets *in vivo* such as optical imaging, ultrasound (US) imaging, MR imaging, computed tomography (CT), and nuclear imaging which are single photon emission computed tomography (SPECT) and positron emission tomography (PET). These diagnostic modalities can be broadly classified into primary molecular imaging modalities and primary morphological/anatomical imaging modalities. The primary molecular imaging modalities are characterized by high sensitivity and involve optical imaging and PET/SPECT techniques, whereas primary morphological/anatomical imaging has features of high spatial resolution such as CT, US, and MRI. Particularly, optical imaging and PET/SPECT have capacity to detect molecular targets, which are important

in a disease process, thus making it more favorable for theranostic approaches. Recently, integrated molecular/anatomical systems (e.g., SPECT/CT) have been developed to aggregate the capabilities of individual imaging modalities.

- **Diagnostic Capabilities**

The diagnostic purpose of theranostic NPs is to detect the locations of disease, the disease status, and the response of disease to treatment. The increased binding at the site of interest is achieved by either passive or active targeting. The location and extent of NP signal after intravenous administration depends on cell surface receptors and measures the tumor's size and stage of tumor. NP signal process usually utilizes radionuclides or fluorophores. Also, the NPs have an intrinsic property for contrast, for example, iron oxide for MRI. NPs are often coated with ligands that target angiogenesis markers. For example, the RGD peptide binds to $Rv\beta3$ integrin, and vascular epidermal growth factor (VEGF) binds to the VEGF receptor (VEGF-R) to identify angiogenic tumor.

Once bound, the NP can assist in monitoring resection or monitor response to therapy. Alternatively, passive targeting can be used for anatomic imaging rather than MI.

Diagnostic NPs involve superparamagnetic iron oxide (SPIO) and ultrasmall SPIO (USPIO) for MRI contrast and targeted SPIO NPs. That allows MI through MRI. Gold NPs are used for CT and radiograph contrast and MI through ligands. Silica nanoparticles have usefulness in MRI as gadolinium containers or to protect inner imaging cores. Optical diagnostic agents involve quantum dots (QDs), fluorophore-doped silica NPs, and fluorophore-doped polymeric NPs. Carbon nanotubes and gold nanorods can produce photoacoustic contrast. Surface-enhanced Raman scattering (SERS) NPs are utilized in multiplexed approaches. Some NPs are multimodal as they detect signal through more than one method such as fluorescence and MRI both [11, 14]. The diagnostic capabilities of nanoparticles are given in Table 8.2.

- **Therapeutic Capabilities**

The therapeutic capabilities of the NPs are diverse as it can assist in the drug delivery and drug release to the desired diseased areas. Conventionally, small molecule chemotherapeutics such as doxorubicin and paclitaxel were being delivered through NPs. Next-generation NP systems also can deliver siRNA for RNA interference with gene expression. It has been demonstrated that gold NPs not only assist cellular delivery of oligonucleotides but also stabilize them from nucleases. The release takes place due to the ablative effect of radionuclides loaded into NPs for degradation of the tumor cells, causing DNA damage and retarding cell growth. The release, which may also be in the form of heat or vibrational energy, can disrupt the structure of the cells and shrink the tumor size. Further, the therapeutic role also involves the surgery for tumor resection. NPs can contain an imaging agent, which can act as both diagnostic to determine tumor type, location, etc. and therapeutic that uses that image to guide tumor removal. Intraoperative imaging is visualization of diseased areas exposed during surgery and is especially useful, when the location of the tumor may change after presurgical imaging and during resection. Also, the therapeutic role can be disruption of a cellular or metabolic pathway. This approach utilizes a ligand to target the NP and disrupt cell regulation. An example of this is Herceptin-labeled NPs, which occupy the Her-2 cell surface receptors.

In drug delivery applications, the NP carrier stabilizes the payload, permitting a measured release of drug, reducing toxicity and side effects. Hydrophobic drugs are protected by the NP interior. Most therapeutic agents carrying NPs are in the form of liposomes or lipid-based complexes, as well as polymeric micelles or biodegradable polymer/drug composites. The therapeutic and diagnostic roles of nanoparticles are diverse as summarized in Table 8.3. The most common substrate is a blend of poly(lactic-co-glycolic acid) (PLGA) and polyethylene glycol (PEG) (PLGA-PEG). Metallic NPs used in tandem with infrared heating are thermoablative NPs; nanoshells and

Table 8.2 Types of NPs. The diagnostic roles of nanoparticles [4]

Technique	Limitation	NP solution	NP type
CT	Sensitivity	Contrast	Gold, silver, iodine
Optical	Signal penetration	Intense signal Fingerprint spectra	Quantum dots Raman nanoparticle
MRI	Poor multiplexing	Contrast	Iron oxide/cd ³⁺
PET/SPET	Anatomic technique	Multimodal	Radiolabeled NP
Ultrasound	Spatial resolution	Contrast	Silica, nanobubble
Resection	Anatomic technique	Border delineation	MRI and/or fluorescent
Radiation therapy	Tumor location	Radio-NPs	Sir-spheres (microparticles)

Table 8.3 Types of NPs. The therapeutic and diagnostic roles of nanoparticles [4]

NP type	Description	Therapeutic role	Diagnostic role	Example
I	NP with endogenous contrast	Targeting ligand occupies cell pathway site	Imaging with site specificity phenotyping	Iron oxide NPs
II	NP caring imaging agent	Image-guided resection	Border delineation	Radiolabeled silica, fluorescent silica
III	NP caring therapeutic agent	Therapeutic release radioablation	Typing with site specificity	pH-responsive liposomes
IV	Labeled NP caring therapeutic agent	Therapeutic release	Imaging with site specificity	Fluorescent liposomes
V	NP responsive to external stimulus	Photothermal therapy, selective drug release	Thermal imaging, CT	Magnetic nanoparticles

nanorods are the most common examples. Sir-spheres are the trademarked name of yttrium-90-loaded nanoparticles used to treat liver cancers. These particles are injected into the hepatic artery and accumulate in the tumor where they ablate the tumor in vivo [19].

6 Challenges and Future Directions

Theranostic nanoparticles have the capabilities to bring revolution in the future disease management approaches. Since the last decade, there has been an emerging interest in the development of various kinds of theranostic nanoparticles for imaging and therapy. Efficient targeting of theranostic nanoparticles to the tumor site is important for both diagnostic and therapeutic purposes. However, challenges still exist in the development of biocompatible theranostic nanoparticles with high specificity for in vivo tumor targeting potential.

There are also several studies being carried out in developing activatable theranostic nanopar-

ticles for even “smarter” cancer diagnostic imaging and chemotherapy. For example, an activatable theranostic prodrug was designed by conjugating SN-38 that is a topoisomerase inhibitor with piperazine-rhodol fluorophore using a self-immolative linker based on disulfide bonds. Such a product could assist real-time monitoring of the delivery and release of the SN-38 payload in the presence of intracellular thiols. With activatable theranostic nanoparticles, getting vital information related to the treatment response can also be possible, which can be very much useful during the decision-making process of doctors to alter treatment protocols at the right time.

Therefore, there is an inclination toward aggregating the diagnostic and therapeutic utilities of theranostic nanoparticles, resulting in more improved and customized disease management. For the purpose of clinical translation, many major challenges need to be crossed, such as the selection of the better nanoplatform, improvement in the ligand conjugation efficiency, and also in the development of an ideal synthetic technique with fewer steps, higher

reproducibility, and cost-effectiveness. Because of the high sensitivity and accurate quantification using diagnostic techniques such as positron emission tomography imaging, radiolabeling of FDA-approved therapeutic nanoparticles, such as Doxil (liposomal doxorubicin), could emerge as a highly effective strategy to enable the visualization and accurate determination of biodistribution, circulation half-life, and pharmacokinetics of theranostic nanoparticles, without compromising on drug loading capacity and safety profile. Conjugating targeting ligands to nanoparticles with intrinsic imaging and therapeutic characteristics, such as porphyrins and gold nanoshells, will be another useful way for developing future actively targeted theranostic nanoparticles for treatment of tumor.

The last decade has witnessed a wide expansion in development of several kinds of theranostic nanoparticles for cancer imaging and therapy. The studies on current status, challenges, and future prospects of actively targeted theranostic nanoparticles for cancer are the need of the hour. The development of theranostic nanoparticles which have properties of tumor specificity, safety, and simplicity will continue to be the research areas in the near future, promising a greater potential to be translated into the clinic practice.

References

- Janib SM, Moses AS, Andrew MacKay J. Imaging and drug delivery using theranostic nanoparticles. *Adv Drug Deliv Rev.* 2010;62(11):1052–63.
- Ma X, Zhao Y, Liang X-J. Theranostic nanoparticles engineered for clinic and pharmaceuticals. *Acc Chem Res.* 2011;44(10):1114–22.
- Chen F, Ehlerding EB, Cai W. Theranostic nanoparticles. *J Nucl Med.* 2014;55(12):1919–22.
- Sharma G, Sharma AR, Nam JS et al. Nanoparticle based insulin delivery system: the next generation efficient therapy for Type 1 diabetes. *J Nanobiotechnol.* 2015;13:74.
- Kang H, Mintri S, Menon AV, Lee HY, Choi HS, Kim J. Pharmacokinetics, pharmacodynamics and toxicology of theranostic nanoparticles. *Nanoscale.* 2015;7:18848–62.
- Ryu JH, Lee S, Son S, Kim SH, Leary JF, Choi K, Kwon IC. Theranostic nanoparticles for future personalized medicine. *J Control Release.* 2014;190:477–84.
- Joshi MD, Muller RH. Lipid nanoparticles for parenteral delivery of actives. *Eur J Pharm Biopharm.* 2009;71:161–72.
- Landesman-Milo D, Peer D. Altering the immune response with lipid-based nanoparticles. *J Control Release.* 2012;161(2):600–8.
- Fatemah B, Khaled G, Sebastien T. Nanotechnology in insulin delivery for management of diabetes, 2019;7:2.
- Xing H, Zheng X, Ren Q, et al. Computed tomography imaging-guided radiotherapy by targeting upconversion nanocubes with significant imaging and radiosensitization enhancements. *Sci Rep.* 2013;3:1751.
- Chen Z, Penet MF, Nimmagadda S, et al. PSMA-targeted theranostic nanoplex for prostate cancer therapy. *ACS Nano.* 2012;6:7752–62.
- Muthu MS, Leong DT, Mei L, Feng S-S. Nanotheranostics: application and further development of nanomedicine strategies for advanced theranostics. *Theranostics.* 2014;4:660–77.
- Lee GY, Qian WP, Wang L, et al. Theranostic nanoparticles with controlled release of gemcitabine for targeted therapy and MRI of pancreatic cancer. *ACS Nano.* 2013;7:2078–89.
- Bhuniya S, Maiti S, Kim EJ. An activatable theranostic for targeted cancer therapy and imaging. *Angew Chem Int Ed Engl.* 2014;53:4469–74.
- Mura S, Couvreur P. Nanotheranostics for personalized medicine. *Adv Drug Deliv Rev.* 2012;64:1394–416.
- Park J-H, Cho H-J, Yoon HY, Yoon I-S, Ko S-H, Shim J-S, Cho J-H, Park JH, Kim K, Kwon IC, Kim D-D. Hyaluronic acid derivative-coated nanohybrid liposomes for cancer imaging and drug delivery. *J Control Release.* 2014;174:98–108.
- John AE, Luckett JC, Tatler AL, Awais RO, Desai A, Habgood A, Ludbrook S, Blanchard AD, Perkins AC, Jenkins RG, Marshall JF. Preclinical SPECT/CT imaging of $\alpha\beta6$ integrins for molecular stratification of idiopathic pulmonary fibrosis. *J Nucl Med.* 2013;54:2146–52.
- Yang S, Chen Y, Ahmadi R, Ho EA. Advancements in the field of intravaginal siRNA delivery. *J Control Release.* 2013;167:29–39.
- Kim K, Kim JH, Park H, Kim Y-S, Park K, Nam H, Lee S, Park JH, Park R-W, Kim I-S, Choi K, Kim SY, Park K, Kwon IC. Tumor-homing multifunctional nanoparticles for cancer theragnosis: simultaneous diagnosis, drug delivery, and therapeutic monitoring. *J Control Release.* 2010;146:219–27.
- Lee J, Huh Y, Jun Y, Seo J, Jang J, Song H, Kim S, Cho E, Yoon H, Suh J. Artificially engineered magnetic nanoparticles for ultra-sensitive molecular imaging. *Nat Med.* 2006;13(1):95–9.
- Mintzer MA, Simanek EE. Nonviral vectors for gene delivery. *Chem Rev.* 2009;109:259–302.
- Hadjipanayis CG, Machaidze R, Kaluzova M, Wang L, Schuette AJ, Chen H, Wu X, Mao H. EGFRvIII antibody-conjugated iron oxide nanoparticles for magnetic resonance imaging-guided convection-enhanced delivery and targeted therapy of glioblastoma. *Cancer Res.* 2010;70(15):6303–12.



Pharmacokinetics of Drug-in-Polymer Matrix-Based Nanoparticulate Drug Delivery System

Sopan Nangare, Prashant Patil, Ashwini Patil, Prashant Deshmukh, Trupti Powar, Jidnyasa Pantwalawalkar, Zamir Khan, Rahul Tade, Jayvadan K. Patel, and Pravin Patil

Contents

1	Introduction	160
2	Drug-Polymer Matrix (DPM)-Based NPDDS	162
3	Applications of DPM in NPDDS and Their Pharmacokinetics	163
4	Current Challenges and Future Perspectives	170
5	Concluding Remarks	170
	References	184

Abstract

The application of nanotechnology in drug delivery is gaining much attention from researchers due to their plethora of benefits especially in the improvement of pharmacoki-

netics as compared to conventionally available dosage forms. In this line, numerous advanced approaches have been adopted that demonstrated excellent applicability in the drug delivery systems. Despite this, they are lacking the foremost limitations related to absorption, distribution, metabolism, and excretion of the drug that affect the therapeutics of the active. Noteworthy, polymeric materials

Prashant Patil contributed equally with all other contributors.

S. Nangare · P. Patil · Z. Khan · R. Tade · P. Patil (✉)
Department of Pharmaceutical Chemistry, H. R. Patel
Institute of Pharmaceutical Education and Research,
Karvand Naka,
Shirpur, Maharashtra, India

A. Patil
Department of Microbiology, R. C. Patel Arts,
Science, and Commerce College, Karvand Naka,
Shirpur, Maharashtra, India

P. Deshmukh
Department of Pharmaceutics, Dr. Rajendra Gode
College of Pharmacy, Malkapur, Maharashtra, India

T. Powar
Department of Pharmaceutics, Smt. Kashibai Navale
College of Pharmacy, Kondhwa, Maharashtra, India

J. Pantwalawalkar
Department of Pharmaceutics, Bharati Vidyapeeth
College of Pharmacy, Kolhapur, Maharashtra, India

J. K. Patel
Nootan Pharmacy College, Faculty of Pharmacy,
Sankalchand Patel University, Visnagar, Gujarat,
India

offer several advantages such as biocompatibility, biodegradability, and other tunable properties, which are playing a crucial function in advanced drug delivery systems. In recent times, a drug-in-polymer matrix (DPM)-based nanoparticulate drug delivery system (NPDDS) is majorly employed for designing different types of advanced formulations. Herein, polymeric materials are widely utilized as drug carriers that assist to accomplish the intended pharmacokinetic parameter with minimum adverse effects. Notably, published pieces of literature divulged that the DPM can effortlessly modulate the absorption, distribution, metabolism, and excretion of a drug as compared to other reported advanced approaches in drug delivery. Thus, in this chapter, we have provided the essentials for the pharmacokinetics of DPM-based NPDDS. In addition, we have discussed the different types of dosage forms based on the DPM system and their modified pharmacokinetics. Finally, we have shed light on current challenges and future prospects of DPM-based NPDDS. In conclusion, the DPM-based NPDDS can modify pharmacokinetic parameters, namely, absorption, distribution, metabolism, and excretion of the administered active. In the future, this chapter will furnish a new way of designing DPM-based advanced dosage forms with acceptable pharmacokinetics.

Keywords

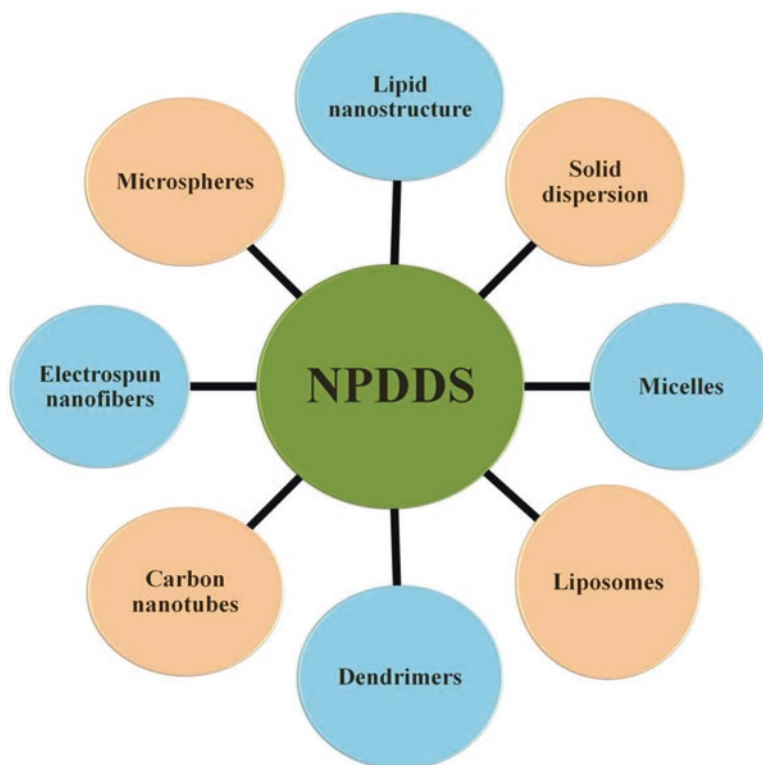
Polymer matrix · Pharmacokinetics ·
Nanoparticulate drug delivery system ·
Nanomedicine

1 Introduction

The field of advanced drug delivery systems has extensively explored in recent years because of plenteous limitations of conventionally available dosage forms [1]. This meticulous development helps to promote the modified release of drugs in

the body. In addition, it offers the targeted delivery of active that avoids several side effects and toxicities to normal cells [2]. Owing to such a plethora of merits, the advanced drug delivery systems are facilitating the improvement of the pharmacokinetics and pharmacodynamics of drugs [2, 3]. For the last two decades, nanotechnology is playing an essential role in designing advanced drug delivery systems that can conquer the disadvantages of current engaged traditional drug delivery systems [4, 5]. Therefore in this segment, we have discussed the application of nanotechnology in designing nanoparticulate drug delivery systems (NPDDS). Recently, significant progress has been achieved in the development of innovative drug delivery technologies [1] wherein nanotechnology is gaining significant consideration from researchers. Principally, it may be because of a multitude of merits in terms of improved pharmacokinetics of drugs [5]. Accordingly, the applicability of nanotechnology in research is increased extensively in an assortment of biomedical applications. It is known known that nanotechnology furnishes several noteworthy advantages as compared to the traditional dosage forms. Owing to this, numerous nanoformulations have been developed by research scholars to overcome the demerits of traditional systems as it mainly includes electrospun nanofibers [6, 7], invasomes [8], microneedles [9], transferosomes [10], nanosuspensions [11], ethosomes [12], and micelles [13]. Different types of NPDDS are depicted in Fig. 1. Recently, different advanced nanomaterials are reported on the account of NPPDS as a carrier for targeted drug delivery mainly fluorescent materials [14], graphene quantum dots (GQDs) [15], graphene derivatives such as graphene oxide (GO), and reduced GO [16]. Despite the merits of nanotechnology in biomedical, it brings new challenges in safety, efficacy, and ethical considerations [4]. Possibly, it may be because of the toxicities of carriers used for the delivery of active molecules [14, 15]. Previously, there have been gigantic developments in the field of drug delivery systems using naturally obtained materials for the delivery of active compounds to the targeted site along with

Fig. 1 Different types of nanoparticulate drug delivery systems available for delivery of a drug



modified-release patterns. Additionally, it offers a number of benefits as compared to this conventionally engaged dosage forms [17–19]. Hence, such advanced NPDDS offers negligible side effects in contrast to the conventional drug delivery systems [11, 20]. Therefore, it is an utmost requirement to develop the modified release dosage forms that assist to target the delivery of active molecules. As a result, it can facilitate improvement in pharmacokinetics, and finally, it can provide an acceptable pharmacological response [17]. Importantly, nanotechnology-based different strategies are playing a central role in effective drug delivery via advanced drug delivery systems that include NPDDS [21]. More specifically, it includes one polymer or lipid-based NPDDS. In addition, this wide variety of nanoformulation is prominently playing multiple roles like drug and gene delivery into the targeted sites of tumors [9]. It can provide the drug release depending on microenvironments [22], temperature, time, etc. Among the plenty of such advanced nanoformulations, the polymeric nano-

material/nanocarrier is an impending candidate for drug delivery application that may be due to its diverse applications. Principally, it includes the ability of modification in the release of a drug, drug delivery to the targeted site, biocompatibility, biodegradability, etc. [17]. It has been suggested that the polymer-based formulation containing nanosized dimensions of particles and their surface charge, etc., offers the active targeting as well as passive targeting of drugs [23]. In addition, the change in properties of the matrix used for the designing of dosage forms can help to regulate or modify the release patterns. The majority of the carriers used for the design of drug delivery are biodegradable and biocompatible [17–19]. It showed high drug encapsulation ability without chemical interaction that resulted in the delivery of the total quantity of drug for therapeutic action. Moreover, this NPDDS can be delivered through different routes including oral, nasal, ocular, and parental. Notably, the NPDDS offers the ability to modify the pharmacokinetic profile such as absorption, distribution,

metabolism, and excretion [24, 25]. This is because of versatile, utmost, and unique properties of carriers, mainly polymeric carrier/nanostructures. Taken as whole, the delivery of drugs through metric is an interesting area wherein the NPDDS is holding huge demand. The development of such advanced carriers reduces the dosage frequency, regulates the drug release from dosage forms, and finally maintains the blood concentration within the therapeutic range [26]. The designed NPDDS showed the different drug release profiles including zero order, first order, and Higuchi matrix [17, 27]. It has been reported that the composition of drug, polymer matrix, and excipients affects the drug release profile. In addition, physical or chemical interactions among components also influence the drug release from prepared nanocarriers [26]. Therefore, the selection of suitable carrier for designing of NPDDS is a crucial part in dosage form designing. In addition, we can design the different types of nanomaterials with special intention like imaging applications [14], pulsatile delivery [22], and different additional features like magnetic and catalytic ability [28].

2 Drug-Polymer Matrix (DPM)-Based NPDDS

The exact number of drugs along with suitable types of drug delivery systems based on different types of carriers is a key part of the treatment of different health issues [29]. Advances in the design and production of polymer-mediated nanoassemblies, nanoparticles, etc., together with advances in nanotechnology and medicine, have culminated in extraordinary polymer nanosystems applications in nanomedicine as well as pharmaceutical sciences [30]. In this regard, various types of biodegradable and non-biodegradable polymers have been suggested wherein we can maintain the drug release depending on the intention and requirement. During the development of polymer-based NPDDS, drug (active) is mixed with polymer (carrier) that plays multifarious roles that predominantly includes release modifications, solubility enhancement, and improved

dissolution rate, avoid the first-pass metabolism, targeted delivery, and increase the permeability. It helps to improve the absorption, distribution, and finally bioavailability [29]. In a nutshell, the blending of active with suitable polymers is an excellent strategy to enhance the pharmacokinetics of active which subsequently results in better pharmacological response. Therefore, DPM helps to improve the overall intended pharmacokinetics of a drug [31]. It has been revealed that the different polymeric properties such as crystallinity, hydrophilicity, hydrophobicity, molecular weight, and copolymers [32] play a crucial part in designing DPM-based NPDDS. Principally, DPM systems include polymer-based micelles, dendrimers, microsphere, nanoparticles, and microparticles. In this system, we can load the drug in the cavity as well as can form a stable drug-polymer conjugate-based matrix [31]. The example of natural polymers used in designing DPM systems includes mainly chitosan, alginate, gelatin, and dextran. In the case of semi-synthetic, ethyl cellulose, methylcellulose, hydroxypropyl methylcellulose, etc., have been reported for the development of DPM-based NPDDS [24]. In addition to this, nowadays, several synthetic polymers, for example, acrylic polymers, polyethylene glycol, and polystyrene are also majorly utilized in the development of different types of DPM-based NPDDS [31]. Recently, a hybrid polymeric microsphere using pectin/sodium carboxymethyl cellulose has been reported for targeted delivery wherein it improved the gastric resistance time, absorption rate, and finally bioavailability of the drug [33]. Drug-loaded mixed micelle can help to augment the solubility, dissolution rate, and permeability of drugs that can help to enhance the pharmacokinetics [34]. Amorphous solid dispersion of drugs with polymers showed an improved dissolution rate. Herein, the *in vivo* pharmacokinetic study revealed a significant increase in the C_{max} and relative bioavailability. Therefore, solid dispersion polymeric matrix system can be used to improve the bioavailability of poorly soluble drugs [35]. Moreover, DPM can improve the absorption efficiency of the drug. The solid dispersion of drugs and different types of polymers

such as hydroxypropyl methylcellulose and Kollicoat IR in a combination of mesoporous silica nanoparticles can help to improve the absorption efficiency of the drug [36]. Presently, drug-loaded lipid-polymer hybrid also showed improved pharmacokinetics [37]. The use of hydrophilic polymers with poor solubility and bioavailability of the drug showed enhanced solubility and dissolution rate of the drug. This means, the use of hydrophilic polymers in DPM-based NPDDS can improve the bioavailability of the drug [38]. The short duration of action is a major limitation of plenty of drug molecules. The use of a different type of polymer can help to extend the release of drug for a longer duration of action. Accordingly, it increases the absorption of the drug from the absorption site and increases the bioavailability of drug [39]. In many cases, the use of polymer for coating of DPM also resulted in improving the dissolution rate and finally pharmacokinetics of poorly bioavailable drugs [40]. Recently, the application of polymer for targeted delivery of drug has gained the huge attention in drug delivery. The eudragit S 100 coating helps to avoid the release of drug in the stomach as the well small intestine that help to targeted delivery. Accordingly, it improved the.

pharmacokinetics of the drug [22]. Interestingly, enhanced bioadhesion and reduced first-pass metabolism owing to the utilization of suitable polymers also help to modify the absorption, metabolism rate, and finally bioavailability [41]. The use of the DPM system in combination with copolymers is an open new window for the development of new dosage forms. It can be used in release modification, permeability modification, etc. As a result, it helps to improve the poor pharmacokinetics of currently engaged new active molecules [42]. The use of synthetic polymer coating (eudragit 100) to nanoparticles can enhance solubility. It can prolong the release of active and reduced enzymatic metabolism. Accordingly, the oral bioavailability of active can be modified using polymer-coated lipidic nanoparticles [43]. Polymeric nanospheres embedded into mucoadhesive films can used as alternative option to increase the permeation of drug [44]. Notably, the coating of copolymers

also showed good stability of the developed DPM system in gastric pH that resulted into significant rise in oral bioavailability [45]. Taken as whole, the application of suitable polymers in NPDDS, we can design the good dosage form that can provide the improved and acceptable pharmacokinetics.

3 Applications of DPM in NPDDS and Their Pharmacokinetics

After administering a drug (active) into the body through a different route, pharmacokinetics outlines the detailed information about absorption, distribution, metabolism, and finally excretion processes. It is noticeable that the pharmacokinetic details are important in case of confirmation of safety plus the efficacy of the drug by respective dosage forms [24]. Different evaluation of approaches has been reported by different research groups to measure the pharmacokinetics of the drug in the prepared dosage form. Specifically, in this section, we have discussed the different DPM-based NPDDS and their pharmacokinetic parameters such as absorption, distribution, metabolism, and excretion. Figure 2 demonstrates the applications of DPM in NPDDS. An abundant literature survey suggested that the pharmacokinetic study of DPM-based NPDDS can be evaluated using different evaluation strategies such as in vivo evaluation using different animals (such as rabbits, goats, and rats) and humans. Moreover, in vitro/ ex vivo evaluation approaches include different assays, namely, plasma protein binding assay and ex vivo tissue distribution [24].

In 2020, Gadalla et al. developed a hybrid polymeric microsphere using pectin/sodium carboxymethyl cellulose (NaCMC) for targeted delivery of progesterone (PG) to the colon. In brief, pharmacokinetic analysis of the polymeric microsphere revealed that the mean residence time (MRT) of PG from the microsphere formulation has been expressively improved by 2.3 folds. Herein, the prepared polymeric microspheres act as a drug reservoir that controlled the

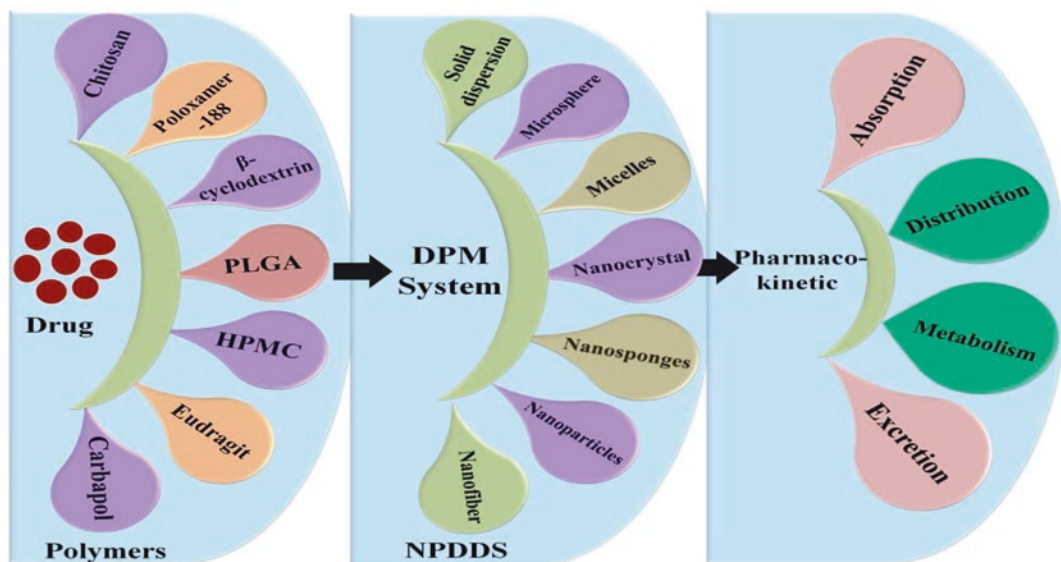


Fig. 2 DPM system-based NPDDS for improved pharmacokinetics

drug release. Accordingly, it provides a slow drug release for a prolonged time. Also, it allowed a gradual increment in drug absorption. Notably, the PG relative bioavailability was found to be 180%. Hence, it confirmed that the NaCMC-based DPM can be used to improve the pharmacokinetics of NPDDS [33]. In another work, Piazzini et al. prepared the mixed micelle of aripiprazole (ARP) using polyethylene glycol, soluplus, etc. Finally, the in vitro and in vivo evaluation of micelle was performed to check the aqueous solubility, oral bioavailability, and blood-brain barrier (BBB) permeation of ARP. In this study, the in vivo evaluation of mixed micelles showed the high ARP plasma concentration after administration of the micelles that confirmed the improved bioavailability of ARP. Therefore, polymeric mixed micelles can be used as potential candidates for increasing oral bioavailability for poorly soluble substances such as ARP [34]. Recently, Jadhav et al. developed amorphous solid dispersion of olmesartan medoxomil (OLM) using hot-melt extrusion technology for bioavailability enhancement. Herein, solid dispersion of OLM has been prepared using Kollidon VA-64 (VA-64). Briefly, the prepared solid dispersion displayed amorphous nature and it improved the dissolution

of OLM. The in vivo pharmacokinetic study revealed a significant increase in the OLM. The in vivo pharmacokinetic study revealed a significant increase in the C_{max} and relative bioavailability (201.60%) of OLM in the case of prepared solid dispersion. In conclusion, the use of Kollidon VA-64 in the development of solid dispersion can improve the pharmacokinetics of OLM and other poorly bioavailable drugs [35]. In 2020, Xi et al. reported the improved absorption efficiency of indomethacin using solid dispersion that was confirmed by in vivo assay. Herein, solid dispersion of indomethacin has been developed using hydroxypropyl methylcellulose and Kollicoat IR along with a combination of mesoporous silica nanoparticles. In vivo studies and in vitro parallel artificial membrane penetration (PAMPA) experiments signified enhanced dissolution rates of pure indomethacin in the gastrointestinal tract through oral delivery. Therefore, hydroxypropyl methylcellulose and Kollicoat IR along with mesoporous silica nanoparticles-based solid dispersion can be used to improve the oral absorption of different drug molecules [36]. In another work, Khan et al. prepared clarithromycin-loaded lipid-polymer hybrid nanoparticles and assessed them for their in vitro and in vivo evaluation. Interestingly, the

pharmacokinetic analysis of the hybrid nanoparticles revealed that a significant increase in the maximum peak plasma concentration, AUC. Accordingly, it improved the bioavailability of clarithromycin. Hence, in the future, the lipid-polymer hybrid matrix can be used to improve the pharmacokinetic parameters of clarithromycin [37]. Owing to the poor solubility and bioavailability of atorvastatin calcium, there is a huge need to develop a suitable formulation that can overcome the abovementioned limitations. In this line, Dong, Su et al. prepared atorvastatin calcium polymer-assisting solid dispersion formulation using poloxamer 188 as hydrophilic carriers through solvent evaporation system. In brief, the solubility and dissolution of atorvastatin calcium have been improved due to the hydrophilic nature of the polymer. Moreover, *in vivo* analysis confirmed that the bioavailability of atorvastatin calcium increased after taking solid dispersion orally. In that, the pharmacokinetic study indicated that the C_{max} , T_{max} , and AUC of solid dispersion have been increased. In conclusion, poloxamer 188-based atorvastatin-based solid dispersion can be used as an alternative for currently available formulations [38]. The short duration of action is a major limitation of zolpidem due to this short life. Accordingly, there is a demand for an extended-release formulation that can provide a longer duration of action. In this vein, Al-Dhubiab et al. developed the zolpidem-loaded poly (lactic-co-glycolic acid) nanospheres through the double emulsion solvent evaporation method. Finally, this nanoparticle was used for the development of buccal films. Interestingly, it provides a prolonged release and rapid onset of action as well. *In vivo* study confirmed that the administration of zolpidem nanosphere-impregnated film enhanced absorption of the drug. Additionally, it enhanced the higher peak plasma concentration and AUC. Moreover, it required 1.5 hours to reach maximum drug concentration. Taken as a whole, the prepared film shows the potential of prolonged drug release with improved pharmacokinetics of zolpidem [39]. It has been reported that the eluxadoline is a poorly water-soluble drug that affects on dissolution rate and oral bioavail-

ability of eluxadoline. In this line, Anwer et al. developed poly (lactic-co-glycolic acid) nanoparticles of eluxadoline followed by a coating of eudragit S 100 polymer. Herein, the poly (lactic-co-glycolic acid)-based nanoparticles and coating by eudragit S 100 improved the dissolution rate as well as bioavailability. Herein, poly (lactic-co-glycolic acid) nanoparticles and eudragit-coated nanoparticles improved the bioavailability by 6.8-folds and 18.5-folds, respectively. The C_{max} , T_{max} , and AUC of both eudragit-coated and non-coated formulations were significantly increased without significant changes in the elimination life ($T_{1/2}$, half-life). In short, the pharmacokinetic of eluxadoline has been increased due to targeted delivery and reduction in the first-pass metabolism. In the future, coated nanoparticles could be used for oral delivery of eluxadoline for effective treatment of irritable bowel syndrome with diarrhea [40]. It has been revealed that the oral bioavailability of curcumin is low. Therefore, there is a huge requirement for a new drug delivery system for targeted release at the colon. In this regard, Karade and co-investigators developed the curcumin-loaded chitosan microsphere for colon-specific delivery of curcumin. In brief, ascorbic acid has been used to provide an acidic microenvironment that avoids the degradation of curcumin at colonic basic pH. In addition, the eudragit S 100 coating helps to avoid the release of curcumin in the stomach as well as the small intestine. Interestingly, the stability of curcumin in alkaline pH was significantly increased. In addition, the bioavailability of curcumin in albino wistar rats has been increased. To summarize, coated curcumin-loaded chitosan nanoparticles can be used as an excellent design for the delivery of curcumin to the colon for the treatment of colonic diseases/disorders [22]. As per the literature, OLM is lacking low oral bioavailability that needs to be overcome by using different advanced strategies. In 2019, Chai et al. reported OLM microcrystal tablets and nanocrystals capsules by using milling techniques. Herein, along with the drug, different polymeric excipients have been used, namely, L-hydroxypropyl cellulose and hydroxypropyl methylcellulose. Notably, the

nanosized particles improve the solubility profile and *in vitro* dissolution. The pharmacokinetic study of OLM nanocrystal using Beagle dogs showed an increase in C_{\max} by \sim twofold and AUC by \sim 1.6 fold via the oral route. In conclusion, the low solubility and low bioavailability problems of OLM can be overcome by reducing the particle size to the nanoscale in presence of different polymers [46]. It has been mentioned that paclitaxel contained poor bioavailability. In this line, Wang et al. prepared multifunctional chitosan derivative-based polymeric micelles of paclitaxel for oral delivery. It showed sustained drug release from micelles in intestinal fluid and phosphate-buffered saline. It has been suggested that the chitosan derivative offers the enhanced bioadhesion and reduced first-pass metabolism. In addition, the micelles enhanced the solubility and permeability of paclitaxel. Finally, it improves bioavailability and its therapeutic activity. In conclusion, multifunctional chitosan-based micelle can be used as an excellent substitute for the delivery of anticancer drugs such as paclitaxel [41]. To enhance the oral bioavailability of paclitaxel, Dahmani and co-authors prepared the mixed polymeric micelles using pluronic copolymers and heparin-all-trans-retinoid acid. It provides the delayed-release, whereas *in situ* permeability study confirmed the five- to sixfold high permeability than the plain heparin-all-trans-retinoid acid-based micelle. Moreover, the mixed micelles showed higher AUC and C_{\max} that may be inhibited cytochrome P450 metabolism and P-glycoprotein efflux systems by use of pluronic copolymers. Therefore, paclitaxel mixed polymeric micelles can be an open new window for the oral delivery of anticancer drugs [42]. The short retention of acyclovir-loaded dosage form at the absorption sites (i.e. stomach) resulted in poor bioavailability. Owing to the low bioavailability of acyclovir, Dhaliwal et al. prepared thiolated chitosan-based mucoadhesive microspheres of acyclovir for the gastro retentive delivery using the emulsion-chemical crosslinking technique. In brief, it showed complete dissolution and prolonged drug release. Moreover, the mucoadhesion study demonstrated the excellent retention of the microsphere in the upper part of the

gastrointestinal tract (duodenum and jejunum). Finally, a pharmacokinetic study divulged that the mucoadhesive microsphere maintains the measurable plasma concentration for 24 hours. Herein, the thiolated chitosan-based acyclovir microsphere demonstrates the fourfold higher AUC_{0-24} . Therefore, thiolated chitosan can be used as an alternative candidate for prolonged delivery as well as improved oral bioavailability of acyclovir [47]. Recently, Kumar et al. developed eudragit 100 coated solid-lipid nanoparticles of isradipine along with rutin (bio-enhancing agent) to reduced partial dose. In this study, coated solid-lipid nanoparticles have been prepared using lipid (glycerol monostearate: soya lecithin). It showed high solubility, prolonged release, and reduction in enzymatic metabolism. The pharmacokinetic study of this study showed the enhancement of the oral bioavailability of coated formulation. Owing to enhancement in oral absorption, it shows improved biological activity. Taken as a whole, polymer-coated lipidic nanoparticles showed enhanced systemic bioavailability with consequent dose reduction of isradipine [43]. Chrysophanol is used in the management of chronic renal failure, whereas the poor oral bioavailability limited their use. In this shade, Lu et al. prepared targeted mixed polymeric micelles of chrysophanol for better oral bioavailability and anti-chronic renal failure activity. Herein, chrysophanol-loaded micelles have been achieved via the thin-film dispersion technique using polyvinylpyrrolidone K30, phospholipid, and sodium cholate. Interestingly, *in vivo* pharmacokinetic exhibited a substantial improvement in oral bioavailability of chrysophanol by using mixed micelle as compared to the free drugs. Therefore, the mixed micelles approach might be more useful for oral bioavailability improvement and concomitant enhancement of anti-chronic renal failure activity of chrysophanol [48]. Owing to the low water solubility drugs such as candesartan cilexetil, there is a prerequisite for new dosage forms that can provide adequate bioavailability. In 2019, Nekkanti et al. developed candesartan nanoparticles using polyvinyl pyrrolidone K-30, poloxamer 188, and crospovidone through wet milling technique

followed by spray drying for conversion of solid nanoparticles. As result, it improves the saturation solubility, dissolution rate, and finally oral bioavailability of candesartan. Moreover, systemic exposure in rats showed a significant rise in the rate and extent of candesartan absorption. In conclusion, these polymeric spray-dried nanoparticles can be employed for bioavailability enhancement with minimal variability [49]. In 2013, Rana and co-authors prepared the carvedilol nanosuspension-incorporated mucoadhesive buccal films. Herein, nanosuspension has been developed using 3% hydroxypropyl methylcellulose and Carbopol 934P by precipitation ultrasonication method, whereas the buccal film was designed using ethyl cellulose and hydroxypropyl methylcellulose. Interestingly, the in vivo investigation of buccal films using the rabbit model showed a 916% augmentation in the relative bioavailability as compared to a marketed oral tablet. Principally, the C_{\max} and T_{\max} of the buccal formulation have been improved owing to the high surface area of the drug plus reduced hepatic metabolism. As a result, it improves the oral bioavailability of carvedilol. In the future, a nanosuspension-based buccal film can be used as a substitute for currently engaged tablet formulation [50]. Acyclovir's oral bioavailability is restricted, owing to the gastrointestinal membrane's low permeability. Therefore, acyclovir-loaded nanospheres-based buccal films have been developed to improve the systemic bioavailability of acyclovir. In brief, acyclovir polymeric nanospheres have been developed using poly (*d,l*-lactide-co-glycolide) through a double emulsion solvent evaporation technique. After that, this polymeric nanosphere was embedded into mucoadhesive films using eudragit RL 100, hydroxypropyl methylcellulose K15, and Carbopol 974P. Ex vivo permeation studies reported the greater flux in the film, whereas in vivo study reported the significant improvement in acyclovir absorption wherein C_{\max} was increased by ~ threefold and AUC_{0- α} was by ~ eightfold as compared to oral dosing. In addition, the extended T_{\max} (6 hours) indicates the perspective of the buccal film to prolong the delivery of acyclovir. Overall, buccal film embed-

ded with acyclovir nanospheres confirmed a hopeful move toward the effectual delivery of acyclovir [44]. It has been claimed that the nanonization approaches can augment the oral bioavailability of hydrophobic drugs. In this regard, Augustine et al. established a nanoparticle-in-microparticle delivery system for darunavir and ritonavir. Herein, drug-loaded nanoparticles have been developed using sodium alginate and encapsulated into the microparticles comprised of calcium alginate and chitosan followed by a coating of polymethacrylate copolymers. Notably, the coating of copolymers ensures the stability of the developed system in gastric pH as well as offers the sustained release of the drug. Finally, the pharmacokinetic analysis using albino Sprague-Dawley rats showed a significant rise in oral bioavailability (2.3 fold). Mainly, a combination of nanonization and coating of copolymers boosted the overall performance of dosage form. Because of this, it can be a good candidate for boosting oral pharmacokinetics [45]. Presently, bioflavonoid applications for the treatment of various ailments are gaining huge importance. In this row, biochanin A is one of them, but its poor solubility leads to low bioavailability. Ultimately, there is a requirement for the development of a new alternative that can resolve the issue of poor solubility that can help to improve the bioavailability. In this vein, Han and co-authors developed the solid dispersion of biochanin A using solutol HS15 and hydroxypropyl methylcellulose that improved the solubility, dissolution rate, and extent of drug release as compared to their physical mixture. Possibly, solubility has been increased due to the reduction of crystallinity and conversion into amorphous form, whereas the hydrophilic polymeric carriers improved the dissolution rate. Pharmacokinetic investigation of the present study reported that oral administration of prepared solid dispersion increased the bioavailability of a drug. Consequently, solid dispersion of biochanin A with Solutol HS15 and hydroxypropyl methylcellulose appeared to be hopeful to get better the dissolution plus oral bioavailability of biochanin A [51]. Amphotericin B is widely used as anti-parasitic but the poor water solubility and poor membrane permeability limit

their oral bioavailability. Therefore, Javed and colleagues developed the lecithin-amphotericin-based hybrid nanocarriers, namely, nanoparticles and liposomes. In brief, initially, drug-loaded lecithin nanoparticles have been prepared using lecithin micelle concentration followed by a coating of polyethylene glycol 600 and Tween 20, whereas similar lecithin liposomes have been prepared using a critical liposomal concentration of lecithin in water. Finally, *in vivo* pharmacokinetics of both formations has been performed in rabbits that showed the improvement of oral bioavailability. The *in vitro* antileishmanial activity was found to be higher in the case of nanoparticles (6.3 fold) as compared to the liposomes (twofold) as compared to the Anfotericina FADA®. Overall, it confirmed that the application of a polymeric coating of polyethylene glycol showed more promising results due to the better interaction with membranes as well as biological systems. In the future, such nanocarriers can be used for the improvement of the bioavailability of amphotericin B [52]. It has been mentioned that heparin is lacking a short half-life and poor oral absorption. In 2002, Jiao and co-researchers developed the polymeric nanoparticles of heparin using poly-epsilon-caprolactone and poly (lactic-co-glycolic acid) along with a combination of non-biodegradable positively charged polymers, namely, eudragit RS and RL. Interestingly, oral administration of heparin-loaded polymeric nanoparticles in rabbits showed raise in anti-factor Xa activity plus activated partial thromboplastin time. Moreover, oral dosing of eudragit-based heparin-loaded polymeric nanoparticles demonstrates the improvement in bioavailability (23%). It may be because of improvement in oral absorption of heparin. Hence, encapsulation of heparin into polymeric nanoparticles can be used as a promising carrier for the oral delivery of heparin [53]. It has been reported that gemcitabine is widely used in cancer treatment. Despite this, there is a major issue of metabolism (deamination), narrow therapeutic index, and short half-life that resulted in low bioavailability. Kaur and co-authors developed the gemcitabine-loaded thiolated chitosan nanoparticles using the ionic gelation method that offers

improved oral bioavailability. It may be because of the superior mucoadhesion property of thiolated chitosan. Remarkably, it showed sustained release for 96 hours and higher mucoadhesive property and effective permeation rate. *In vivo* pharmacokinetic analysis showed a significant rise in bioavailability of gemcitabine; therefore, it can be used as an effective formulation for oral anticancer therapy [54]. In a further study, β cyclodextrin-based griseofulvin nanosponges have been reported to mask the bitter taste, improved the dissolution, and finally oral bioavailability. Herein, β cyclodextrin nanosponges were designed using cross-linker (diphenyl carbonate) by ultrasonication method and the griseofulvin loaded into that which provides the high dissolution efficiency (3.19 fold) due to the presence of the drug in nanosponges containing nanocavities plus inclusion by cyclodextrin and increases the C_{max} and T_{max} as compared to the plain griseofulvin. It can be possible due to the improved dissolution and solubility. It concludes that the designed formulation can be an excellent alternative for pediatrics. In the future, there is need to perform the clinical trials that can provide the support for presented investigation [55]. In 2020, ibandronate-loaded citrus pectin-loaded nanostructure using that improved the oral bioavailability of ibandronate. The pharmacokinetic analysis of drug has been performed in albino rats that showed the notable improvement in bioavailability than the marketed formulation [56]. Recently, Kumar et al. reported docetaxel-loaded micelles to achieve sustained drug release profile by employing oleic acid-grafted carboxymethyl chitosan as a polymer. Pharmacokinetic evaluation in Sprague-Dawley rats showed significantly enhanced C_{max} (1.97 fold), AUC (2.62 fold), T_{max} (1.33 fold), MRT (2.12 fold), and $t_{1/2}$ (1.94 fold) compared to docetaxel suspension for oral administration which assured sustained drug release. This superiority could be attributed to a polymer-induced increase in the permeability of the drug along with inhibition of enzymatic and chemical degradation. Thus, the study affirmed utility of this amphiphilic polymer to improve biopharmaceutical performance of docetaxel [57]. Shaker et al. attempted formulation of

atorvastatin-loaded ethyl cellulose nanoparticles intending to enhance oral bioavailability. Here, the emulsification-evaporation method was used for nanoparticle preparation, and further, the formulation was characterized to assess pharmacokinetic performance in New Zealand rabbits. Evaluation reports revealed the highest C_{max} for atorvastatin-loaded ethyl cellulose nanoparticles followed by Lipitor (marketed formulation), and it was least for neat atorvastatin. A similar trend was observed for AUC while $t_{1/2}$ followed the opposite order. Overall, these parameters strongly indicated improved bioavailability of atorvastatin-loaded ethyl cellulose nanoparticles compared to Lipitor and neat atorvastatin. The improved bioavailability could be attributed to the inherent ability of NPs to pass through the lymphatic circulation and consequently escaping from hepatic metabolism. Favorable reports assured the potential of nanoparticles as a carrier [58]. In 2019, Chaurasia et al. reported cationic polymer-based nanoparticles as a carrier to improve bioavailability and anticancer activity of naringenin (NRG) for oral administration. In this study, eudragit E 100 was employed as a cationic polymer to develop the NRG-EE100 nanoparticles. Briefly, NRG-EE100 nanoparticles were formulated and optimized using emulsion-diffusion-evaporation technique and design of experiment. The formulation was further subjected to check pharmacokinetic parameters (Model – Albino Wistar rats). Also, the evaluation characteristics of NRG-EE100 nanoparticles were compared with physical mixture suspension composed of NRG, EE 100, and PLX (0.027:4.7:0.85 g) and free NRG suspension. Interestingly, both physical mixture (AUC – 29.42 fold higher, C_{max} – 39.84 fold higher) and NRG-EE100 nanoparticles composite (AUC – 96.35 fold, C_{max} – 88.62 fold) showed increased AUC and C_{max} values compared to neat drug suspension thus signifying improved bioavailability. Moreover, NRG-EE100 nanoparticles showed significantly improved pharmacokinetic performance and cytotoxicity compared to the physical mixture. In addition to M cell-mediated uptake, the enhanced bioavailability can also be endorsed to the amorphous

state of active in NPs, super saturation in the intestinal lumen, and site specificity. This confirmed utility NRG-EE100 nanoparticles to improve bioavailability and anticancer potential as well [59]. Reportedly, Cheng et al. developed poly (n-butylcyanoacrylate) based nanoparticles loaded with insulin by self-polymerization. The work was specifically directed to screen the influence of insulin release rate on in vitro as well as in vivo parameters when all other variables are controlled. The insulin release rate was controlled by varying Insulin/BCA mass ratios. All batches of nanoparticles exhibited sustained hypoglycemic activity specifically 2/10 nanoparticles demonstrated higher hypoglycemic effect in 0–5 hours while 5/10 nanoparticles exhibited better hypoglycemic activity in the latter period, i.e., 5–10 hours. The supremacy in evaluation characteristics can be credited to mucoadhesion, gastrointestinal retention, and mucus penetration ability of polymer-based nanoparticles thus authenticating its potential as drug carrier composite [60]. Jin et al. designed 10-hydroxy camptothecin-loaded poly (n-butyl cyanoacrylate) nanoparticles (HCPT-PBCA-NPs) aimed to improve the bioavailability of the active compound. Then, HCPT-PBCA-NPs were further co-modified with polysorbate 80, polyethylene glycol 100, and soybean phospholipid to enhance permeation and reduce electrostatic interaction between NPs and the mucus layer. The pharmacokinetic evaluation confirmed the superiority of HCPT-PBCA-NPs with increased C_{max} (6.51 fold), AUC (7.56 fold), MRT (1.56 fold), and reduced T_{max} (two fold) compared to neat HCPT suspension. This confirmed the enhanced bioavailability of HCPT in the NPs. Here, smaller particle size could be also considered as a reason for enhanced bioavailability. The evaluation reports emphasized the potential of PBCA-NPs for controlled oral delivery of HCPT [61]. Taken as a whole, DPM offers the improved and intended pharmacokinetics wherein the types of polymers, the composition of polymers, types of DPM-based matrix, etc., play a central role. Due to plenty of meticulous merits of polymeric materials including tunability, biocompatibility, and

biodegradability, it opened new era for delivery of drugs. Table 1 demonstrates the summary of pharmacokinetic of DPM-based NPDDS.

4 Current Challenges and Future Perspectives

Research on polymer-mediated carriers for inventive drug delivery applications gained a bit more success in the last few decades in mediating safe and effective therapeutic delivery for several medical illnesses. Despite this, it has been reported that the abundant active drug molecules are lacking poor solubility and low dissolution rate. Many of the active molecules cannot reach their therapeutic concentration due to the first of metabolism. Moreover, it has been revealed that the targeted delivery of a drug is playing an important role in the effective management of the disease. The poor permeability of drugs has also limited their application in the treatment of several health issues. Taken as a whole, it affects the pharmacokinetics of drugs which is a major issue in the currently available number of drug delivery systems. Additionally, most of the new active molecules including synthetic and natural are also issue of poor pharmacokinetics that needs to be improved by using different strategies. Currently engaged NPDDS is one of them which hold a major share of drug delivery systems due to their plenty of merits. In NPDDS, there is polymer-based DPM is vastly undertaken by scientists due to the groundbreaking advantages over the other NPDDS. Mainly, the use of different types of polymers to design drug delivery systems offers the modified drug release, targeted delivery, biocompatibility, and biodegradability. In addition, it helps to enhance the pharmacokinetic parameters such as absorption, distribution, metabolism, and excretion. Herein, the use of different types of polymers offers improved solubility, dissolution rate, modified release, high entrapment and drug loading, targeted delivery, high permeability, etc. As a result, it improves the interest in pharmacokinetic parameters. In this line, different types of matrix systems have been reported by research groups that confirmed the

applicability of polymers in designing advanced drug delivery systems. Plentiful development has been already done by researchers, whereas several research groups are working on the same. Currently, several DPM-based NPDDS are available in the market that confirmed the principal role of polymer in NPDDS. Despite this, there are huge numbers of challenges that need to be overcome by using advanced strategies. As we all know, established disease treatment necessitates the accurate delivery of a prescribed dose of medicine over a specified time frame. Furthermore, to attain therapeutically relevant drug quantities in the cells, the administration of dosage form must be done in a highly regulated and site-specific way. In addition, the use of polymer combination with optimizing ratio is also a major task in designing DPM-based NPDDS. The record regarding metabolism and excretion of synthetic, semi-synthetic, and natural polymers needs to be monitored in a drug delivery system that can help to avoid adverse effects on the system. Despite improvement in the pharmacokinetics of drug-using DPM based on different evaluation strategies such as *in vivo*, *in vitro*, and *ex vivo*, there is a huge need to perform clinical trials to assure the reported results by research groups. Moreover, the development of DPM-based NPDDS systems at an industrial scale is also a major challenge for researchers. In the future, different natural phytochemicals can be used for the effective treatment of severe health ailments using DPM-based NPDDS with improved pharmacokinetics.

5 Concluding Remarks

Advances in the design and production of polymer-mediated nanoassemblies, nanoparticles, etc., together with advances in nanotechnology and medicine, have culminated in extraordinary polymer nanosystems applications in nanomedicine as well as pharmaceutical sciences. Therefore, polymers are playing an important part in the advancement of drug delivery technology. Importantly, it allow for several benefits including biocompatibility, biodegradability, modified release, targeted delivery, solubility

Table 1 Summary of the pharmacokinetics of DPM-based NPDDS

Sr. No.	Matrix type	Drug	Excipient	Final dosage form	Pharmacokinetics	Ref.
1.	Microspheres	Progesterone (PG)	Pectin/Na-CMC	Tablet	<p>Model: New Zealand male rabbits Administration: Aid of a stomach tube Data for control: Progesterone powder C_{max}: 1.61 ± 0.04 µg/mL T_{max}: 6 ± 0 hours AUC_∞: 19.4 ± 0.9 µg·h/mL Data for dosage form C_{max}: 1.37 ± 0.02 µg/mL T_{max}: 12 ± 0 hours AUC_∞: 34.9 ± 0.3 µg·h/mL Model: Rat Administration: Oral Data for control C_{max}: 437 ± 26.4 µg/mL T_{max}: 4 hours AUC_∞: 8463 ± 503 µg·h/mL</p>	[33]
2.	Mixed micelles	Aripiprazole	Polyethylene glycol, Solutplus	Solution	<p>Data for dosage form (i) For mixed micelles of aripiprazole C_{max}: 715 ± 28.5 µg/mL T_{max}: 4 hours AUC_∞: 13535 ± 539 µg·h/mL (ii) For mixed micelles of aripiprazole with borneol C_{max}: 738 ± 28.7 µg/mL T_{max}: 4 hours AUC_∞: 14181 ± 551 µg·h/mL</p>	[34]
3.	Solid dispersion	Olmesartan medoxomil (OLM)	Kollidon VA-64	Suspension	<p>Model: Sprague-Dawley rats Administration: Oral Data for control: OLM C_{max}: 1.2396 µg/mL T_{max}: 2 hours AUC_∞: 7.2344 µg·h/mL Data for dosage form C_{max}: 3.3047 µg/mL T_{max}: 0.5 hours AUC_∞: 14.5842 µg·h/mL</p>	[35]

(continued)

Table 1 (continued)

Sr. No.	Matrix type	Drug	Excipient	Final dosage form	Pharmacokinetics	Ref.
4.	Solid dispersion	Indomethacin	Hydroxypropyl methylcellulose, Kollicoat IR	Solid dispersion	<p>Model: Male Balb/c mice</p> <p>Administration: Oral</p> <p>Data for control:</p> <p>C_{max}: 124.6 ± 3.8 $\mu\text{g/mL}$</p> <p>T_{max}: 4 hours</p> <p>AUC_{∞}: 1236.5 ± 188.8 $\mu\text{g}\cdot\text{h/mL}$</p> <p>Data for dosage form</p> <p>C_{max}: 223.1 ± 44.1 $\mu\text{g/mL}$</p> <p>T_{max}: 4 hours</p> <p>AUC_{∞}: 2010.5 ± 441.9 $\mu\text{g}\cdot\text{h/mL}$</p>	[36]
5.	Nanoparticles	Clarithromycin	Eudragit, ethyl cellulose	Suspension nanoparticles formulation	<p>Model: Sprague-Dawley rats</p> <p>Administration: Oral</p> <p>Data for control: Clarithromycin</p> <p>C_{max}: 419.7 ± 85.29 $\mu\text{g/mL}$</p> <p>T_{max}: 1.21 ± 0.621 hours</p> <p>AUC_{∞}: 1734 ± 479.2 $\mu\text{g}\cdot\text{h/mL}$</p> <p>Data for dosage form</p> <p>C_{max}: 1165 ± 121.4 $\mu\text{g/mL}$</p> <p>T_{max}: 0.81 ± 0.741 hours</p> <p>AUC_{∞}: 11184 ± 1289 $\mu\text{g}\cdot\text{h/mL}$</p>	[37]
6.	Solid dispersion	Atorvastatin	loxamer-188, carboxy methylcellulose sodium	Solid dispersion	<p>Model: Wistar rats</p> <p>Administration: Oral</p> <p>Data for control: Lipitor</p> <p>C_{max}: 338.74 ± 80.38 $\mu\text{g/mL}$</p> <p>T_{max}: 0.65 ± 0.224 hours</p> <p>AUC_{∞}: $534.5-278.3$ $\mu\text{g}\cdot\text{h/mL}$</p> <p>Data for dosage form C_{max}: 972.2 ± 174.5 $\mu\text{g/mL}$</p> <p>T_{max}: 0.567 ± 0.181 hours</p> <p>AUC_{∞}: 919.0 ± 315.1 $\mu\text{g}\cdot\text{h/mL}$</p>	[38]

Sr. No.	Matrix type	Drug	Excipient	Final dosage form	Pharmacokinetics	Ref.
7.	Nanoparticles	Zolpidem	Poly(lactic-co-glycolic acid, hydroxypropyl methylcellulose, propylene glycol, polyvinyl alcohol	Films	<p><i>Model:</i> Rabbits</p> <p><i>Administration:</i> Buccal routes</p> <p><i>Data for control:</i> Oral solution</p> <p><i>C_{max}:</i> 32.34 ± 7.82 µg/mL</p> <p><i>T_{max}:</i> 1 hours</p> <p><i>AUC_∞:</i> 136.06 ± 28.72 µg·h/mL</p> <p><i>Data for dosage form</i></p> <p><i>C_{max}:</i> 52.54 ± 8.22 µg/mL</p> <p><i>T_{max}:</i> 1.5 hours</p> <p><i>AUC_∞:</i> 236.00 ± 39.51 µg·h/mL</p>	[39]
8.	Nanoparticles	Eluxadoline	Poly(lactic-co-glycolic acid, Lactel, eudragit	Nanoparticles	<p><i>Model:</i> Wistar albino rats</p> <p><i>Administration:</i> Oral</p> <p><i>Data for control:</i></p> <p><i>C_{max}:</i> 0.77 ± 0.02 µg/mL</p> <p><i>T_{max}:</i> 1.75 hours</p> <p><i>AUC_∞:</i> 5.96 ± 0.58 µg·h/mL</p> <p><i>Data for dosage form</i> <i>C_{max}:</i> 17.39 ± 3.48 µg/mL</p> <p><i>T_{max}:</i> 1.5 hours</p> <p><i>AUC_∞:</i> 110.57 ± 8.36 µg·h/mL</p>	[40]
9.	Microspheres	Curcumin	Chitosan, eudragit S 100	Suspension MS	<p><i>Model:</i> Albino rats</p> <p><i>Administration:</i> Oral gavage</p> <p><i>Data for control</i></p> <p><i>C_{max}:</i> 0.512 ± 0.020 µg/mL</p> <p><i>T_{max}:</i> 1 hours</p> <p><i>AUC_∞:</i> 2.128 µg·h/mL</p> <p><i>Data for dosage form</i></p> <p><i>C_{max}:</i> 0.655 ± 0.028 µg/mL</p> <p><i>T_{max}:</i> 6 hours</p> <p><i>AUC_∞:</i> 15.597 µg·h/mL</p>	[22]

(continued)

Table 1 (continued)

Sr. No.	Matrix type	Drug	Excipient	Final dosage form	Pharmacokinetics	Ref.
10.	Nanocrystals	Olmesartan medoxomil	Hydroxypropyl methylcellulose	Nanocrystal capsules	<p>Model: Beagle dogs Administration: Oral</p> <p>Data for control C_{max}: 327.4 ± 132 µg/mL T_{max}: 1.4 ± 0.2 hours AUC_∞: 786.0 ± 237.7 µg·h/mL</p> <p>Data for dosage form C_{max}: 678.2 ± 209.4 µg/mL T_{max}: 1.1 ± 0.5 hours AUC_∞: 1257.2 ± 402.9 µg·h/mL</p>	[46]
11.	Micelles	Paclitaxel	Chitosan	Mixed micelles	<p>Model: Rat Administration: Oral</p> <p>Data for control: Taxol C_{max}: 78 ± 34 µg/mL T_{max}: 1.5 ± 0 hours AUC_∞: 665 ± 129 µg·h/mL</p> <p>Data for dosage form C_{max}: 308 ± 103 µg/mL T_{max}: 3.0 ± 0 hours AUC_∞: 2528 ± 294 µg·h/mL</p>	[41]
12.	Micelles	Paclitaxel	Pluronic P188	Solution	<p>Model: Sprague-Dawley rats Administration: Oral</p> <p>Data for control: Taxol C_{max}: 0.119 ± 0.058 µg/mL T_{max}: 1.999 ± 0.658 hours AUC_∞: 0.916 ± 0.180 µg·h/mL</p> <p>Data for dosage form C_{max}: 1.094 ± 0.134 µg/mL T_{max}: 3.479 ± 0.694 hours AUC_∞: 20.009 ± 5.910 µg·h/mL</p>	[42]

Sr. No.	Matrix type	Drug	Excipient	Final dosage form	Pharmacokinetics	Ref.
13	Microspheres	Acyclovir	Thiolated chitosan	Microspheres	<p>Model: Sprague-Dawley Rats Administration: Oral Data for control: Drug solution C_{max}: 53.1 ± 6.8 $\mu\text{g/mL}$ T_{max} (MRT): 5.4 ± 0.5 hours AUC_{∞}: 282 ± 28 $\mu\text{g}\cdot\text{h/mL}$ Data for dosage form C_{max}: 59.7 ± 10.1 $\mu\text{g/mL}$ T_{max}(MRT): 17.9 ± 1.8 hours AUC_{∞}: 1091 ± 51 $\mu\text{g}\cdot\text{h/mL}$</p>	[47]
14	Nanoparticles	Isradipine	Eudragit 100	Solid-lipid nanoparticles	<p>Model: Goat Administration: Intestine Data for control: Drug suspension C_{max}: 18.01 ± 1.08 $\mu\text{g/mL}$ T_{max}: 2.0 hours AUC_{∞}: 245.00 ± 8.50 $\mu\text{g}\cdot\text{h/mL}$ Data for dosage form C_{max}: 49.17 ± 1.57 $\mu\text{g/mL}$ T_{max}: 8.0 hours AUC_{∞}: 1091.63 ± 22.26 $\text{g}\cdot\text{h/mL}$</p>	[43]
15	Micelles	Chrysophanol (CH)	Polyvinyl pyrrolidone K30	Micelles	<p>Model: Sprague-Dawley rats Administration: Oral Data for control C_{max}: 1.94 ± 0.18 $\mu\text{g/mL}$ T_{max}: 1.50 ± 0 hours AUC_{∞}: 8.19 ± 0.18 Data for dosage form C_{max}: 7.72 ± 0.69 $\mu\text{g/mL}$ T_{max}: 1.50 ± 0 hours AUC_{∞}: 28.10 ± 0.41 $\text{g}\cdot\text{h/mL}$</p>	[48]

(continued)

Table 1 (continued)

Sr. No.	Matrix type	Drug	Excipient	Final dosage form	Pharmacokinetics	Ref.
16	Nanocrystal	Cardesan	Hydroxyl propyl methylcellulose	Tablet	<p>Model: male Wistar rats</p> <p>Administration: oral</p> <p>Data for control - Micronized formulation</p> <p>C_{max}: 0.16 ± 0.10 $\mu\text{g/mL}$;</p> <p>T_{max}: 1.81 ± 1.13 h</p> <p>AUC_{∞}: 0.31 ± 0.07 ng-h/mL</p> <p>Data for dosage form</p> <p>C_{max}: 0.09 ± 0.03 $\mu\text{g/mL}$</p> <p>T_{max}: 1.06 ± 0.38 h</p> <p>AUC_{∞}: 0.78 ± 0.22 $\mu\text{g-h/mL}$.</p>	[49]
17	Nanocrystals	Carvedilol	Carbopol, ethylcellulose, hydroxypropyl methylcellulose	Patch	<p>Model: Rabbits</p> <p>Administration: Oral</p> <p>Data for control: Marketed Tablet</p> <p>C_{max}: 48.73 ± 14.1 ng/mL</p> <p>T_{max}: 2 hours</p> <p>AUC_{∞}: 1813.7 ± 42.53 ng-h/mL</p> <p>Data for dosage form</p> <p>C_{max}: 356.91 ± 29.5 ng/mL</p> <p>T_{max}: 4 hours</p> <p>AUC_{∞}: 4154.37 ± 80.22 g-h/mL</p>	[50]
18	Nanospheres	Acyclovir	Hydroxypropyl methylcellulose K15, Carbopol 974P, eudragit RL 100, ethyl cellulose,	Film	<p>Model: White rabbits</p> <p>Administration: Buccal mucosa</p> <p>Data for control</p> <p>C_{max}: 91.61 ng/mL</p> <p>T_{max}: 2 hours</p> <p>AUC_{∞}: 395.21 ng-h/mL Data for dosage form</p> <p>C_{max}: 306.04 ng/mL</p> <p>T_{max}: 6 hours</p> <p>AUC_{∞}: 3116.21 ng-h/mL</p>	[44]

Sr. No.	Matrix type	Drug	Excipient	Final dosage form	Pharmacokinetics	Ref.
19	Microparticle nanosuspension	Darunavir/ Ritonavir	Alginate, chitosan	Capsule	<p>Model: Sprague-Dawley rats Administration: Oral Data for control: Combination of Darunavir/ Ritonavir <i>C_{max}</i>: 0.14 µg/mL <i>T_{max}</i>: 2.63 hours <i>AUC_∞</i>: 1.17 µg•h/mL Data for nanonized drug <i>C_{max}</i>: 0.11 µg/mL <i>T_{max}</i>: 1.75 hours <i>AUC_∞</i>: 1.35 µg•h/mL Data for formulation <i>C_{max}</i>: 0.38 µg/mL <i>T_{max}</i>: 2.75 hours <i>AUC_∞</i>: 2.67 µg•h/mL</p>	[45]
20	Solid dispersion	Biochanin A	Hydroxy propyl methyl cellulose	Solid dispersion	<p>Model: Sprague-Dawley rats Administration: Oral Data for control: Biochanin A <i>C_{max}</i>: 50.4 ± 4.27 µg/mL <i>T_{max}</i>: 1.88 ± 1.55 hours <i>AUC_∞</i>: 819 ± 128 µg•h/mL Data for dosage form <i>C_{max}</i>: 662 ± 108 µg/mL <i>T_{max}</i>: 0.25 hours <i>AUC_∞</i>: 3880 ± 2490 µg•h/mL</p>	[51]

(continued)

Table 1 (continued)

Sr. No.	Matrix type	Drug	Excipient	Final dosage form	Pharmacokinetics	Ref.
21	Nanocarriers (NCs)	Soya lecithin and Amphotericin B	Poly ethylene glycol	Nanoparticles and Liposomes	<p>Model: Rabbits Administration: Oral</p> <p>Data for control: Amphotericin B C_{max}: 17.4 ± 7.8 µg/mL T_{max}: 2.5 hours AUC_∞: 81 ± 44 µg•h/mL</p> <p>Data for dosage form C_{max}: 126.4 ± 23.9 µg/mL T_{max}: 2.5 hours AUC_∞: 1824 ± 391 µg•h/mL</p> <p>Data for dosage form C_{max}: 133.5 ± 40.4 µg/mL T_{max}: 5 hours AUC_∞: 2052 ± 579 µg•h/mL</p>	[52]
22	Nanoparticles	Heparin	Poly(caprolactone), poly(DL-lactic-co-glycolic acid), eudragit RS and RL	Solution	<p>Model: New Zealand rabbits Administration: Oral</p> <p>Data for control C_{max}: 0.12 ± 0.04 µg/mL T_{max}: 5–6 hours AUC_∞: 0.32 ± 0.07 µg•h/mL</p> <p>Data for dosage form C_{max}: 0.16 ± 0.01 µg/mL T_{max}: 6–8 hours AUC_∞: 0.74 ± 0.24 µg•h/mL</p> <p>Data for dosage form C_{max}: 0.13 ± 0.06 µg/mL T_{max}: 6–8 hours AUC_∞: 0.29 ± 0.03 µg•h/mL</p>	[53]

Sr. No.	Matrix type	Drug	Excipient	Final dosage form	Pharmacokinetics	Ref.
23	Nanoparticles	Gemcitabine	Chitosan	Solution	<p>Model: Wistar rats</p> <p>Administration: Oral</p> <p>Data for control</p> <p>C_{max}: 200 ± 10 $\mu\text{g/mL}$</p> <p>T_{max}: 45 ± 2.1 Minutes</p> <p>AUC_{∞}: 6864.2 ± 125 $\mu\text{g}\cdot\text{h/mL}$</p> <p>Data for dosage form</p> <p>C_{max}: 325 ± 22 $\mu\text{g/mL}$</p> <p>T_{max}: 60 ± 3.5 Minutes</p> <p>AUC_{∞}: 14836 ± 100 $\mu\text{g}\cdot\text{h/mL}$</p>	[54]
24	Nanosponges	Griseofulvin	β -Cyclodextrin, poly vinyl pyrrolidone K.30	Nanosponges	<p>Model: Albino rats</p> <p>Administration: Oral</p> <p>Data for control: Pure drug</p> <p>C_{max}: 1809.11 $\mu\text{g/mL}$</p> <p>T_{max}: 2 hours</p> <p>AUC_{∞}: 22466.90 $\mu\text{g}\cdot\text{h/mL}$</p> <p>Data for dosage form</p> <p>C_{max}: 3855.32 $\mu\text{g/mL}$</p> <p>T_{max}: 3 hours</p> <p>AUC_{∞}: 84865.64 $\mu\text{g}\cdot\text{h/mL}$</p>	[55]
25	Nanostructured raft	Ibandronate	Citrus pectin, crosslinked carboxymethyl cellulose	Nanostructured raft	<p>Model: Rats</p> <p>Administration: Oral</p> <p>Data for control: Bonish 150 mg tablets</p> <p>C_{max}: 493 ± 0.237 $\mu\text{g/mL}$</p> <p>T_{max}: 4 ± 1.398 hours</p> <p>AUC_{∞}: 4106.81 ± 4.104 $\mu\text{g}\cdot\text{h/mL}$</p> <p>Data for dosage form</p> <p>C_{max}: 653 ± 0.097 $\mu\text{g/mL}$</p> <p>T_{max}: 2 ± 0.025 hours</p> <p>AUC_{∞}: 9058.83 ± 5.612 $\mu\text{g}\cdot\text{h/mL}$</p>	[56]

(continued)

Table 1 (continued)

Sr. No.	Matrix type	Drug	Excipient	Final dosage form	Pharmacokinetics	Ref.
27	Micelles	Docetaxel	Oleic acid modified carboxymethyl chitosan	Micelles	<p><i>Model:</i> Sprague-Dawley rats <i>Administration:</i> Oral <i>Data for control:</i> Docetaxel suspension <i>C_{max}:</i> 0.0708 ± 0.0122 µg/mL <i>T_{max}:</i> 6 hours <i>AUC₀₋₇₅:</i> 1.8168 ± 0.4272 µg.h/mL <i>t_{1/2}:</i> 31.2 ± 5.6 hours <i>Data for dosage form:</i> DTX-OACMCS micelles <i>C_{max} (h):</i> 8 hours <i>AUC:</i> 4.7627 ± 1.4082 µg.h/mL <i>t_{1/2}:</i> 60.9 ± 15.3 hours</p>	[57]
28	Nanoparticles	Atorvastatin	Ethyl cellulose	Minicapsule	<p><i>Model:</i> New Zealand rabbits <i>Administration:</i> Oral <i>Data for control:</i> Atorvastatin <i>C_{max}:</i> 515 ± 32 ng/mL <i>T_{max}:</i> 1.79 ± 0.2 hours <i>AUC₀₋₁₂:</i> 2517 ± 330 ng.h/mL <i>t_{1/2} (h):</i> 1.26 ± 0.20 <i>Data for control:</i> Lipitor <i>C_{max}:</i> 635 ± 32 ng/mL <i>T_{max}:</i> 2.07 ± 0.2 hours <i>AUC₀₋₁₂:</i> 4367 ± 494 ng.h/mL <i>t_{1/2}:</i> 2.90 ± 0.84 hours <i>Data for dosage form</i> <i>C_{max}:</i> 940 ± 35 ng/mL <i>T_{max}:</i> 3.15 ± 0.2 hours <i>AUC₀₋₁₂:</i> 8759 ± 0.407 ng.h/mL <i>t_{1/2}:</i> 3.38 ± 1.25 hours</p>	[58]

Sr. No.	Matrix type	Drug	Excipient	Final dosage form	Pharmacokinetics	Ref.
29	Nanoparticle	Naringenin	Eudragit 100	Nanoparticles	<p>Model: Albino Wistar rats Administration: Oral Data for control: Naringenin suspension <i>C_{max}</i>: 10.004 ± 0.500 ng/mL <i>T_{max}</i>: 0.5 ± 0.0 hours <i>AUC₀₋₁₂</i>: 29.862 ± 1.167 ng.h/mL <i>t_{1/2}</i>: 2.623 ± 0.022 hours</p> <p>Data for dosage form: Physical mixture suspension <i>C_{max}</i>: 398.753 ± 19.937 ng/mL <i>T_{max}</i>: 0.25 ± 0.0 hours <i>AUC₀₋₁₂</i>: 878.569 ± 27.873 ng.h/mL <i>t_{1/2}</i>: 2.913 ± 0.0257 hours</p> <p>Data for dosage form: Nanoparticle <i>C_{max}</i>: 886.635 ± 44.332 ng/mL <i>T_{max}</i>: 0.5 ± 0.0 hours <i>AUC₀₋₁₂</i>: 2877.204 ± 62.321 ng.h/mL <i>t_{1/2}</i>: 4.298 ± 0.198 hours</p>	[59]

(continued)

Table 1 (continued)

Sr. No.	Matrix type	Drug	Excipient	Final dosage form	Pharmacokinetics	Ref.
30	Nanoparticles	Insulin	Poly(n-butylcyanoacrylate)	Nanoparticles	<p>Model: Male Wistar rats</p> <p>Administration: Oral</p> <p>Data for control: Insulin solution</p> <p>C_{max} (mIU/L): ---</p> <p>T_{max} (h): ---</p> <p>AUC: 10.72 ± 5.44 mIUh/mL</p> <p>Administration: Injection</p> <p>Data for control: Insulin solution</p> <p>C_{max}: 111.79 ± 18.61 mIU/L</p> <p>T_{max}: 1 hours</p> <p>AUC: 222.76 ± 25.77 mIUh/mL</p> <p>Data for formulation: Ins/BCA (2/5)</p> <p>Administration: Oral</p> <p>C_{max}: 23.11 ± 6.08 mIU/L</p> <p>T_{max}: 4 hours</p> <p>AUC: 127.45 ± 17.47 mIUh/mL</p> <p>Data for formulation: Ins/BCA (2/10)</p> <p>Administration: Oral</p> <p>C_{max}: 28.40 ± 5.08 mIU/L</p> <p>T_{max} (h): 4</p> <p>AUC: 162.54 ± 20.84 mIUh/mL</p> <p>Data for formulation: Ins/BCA (2/15)</p> <p>Administration: Oral</p> <p>C_{max}: 34.65 ± 13.05 mIU/L</p> <p>T_{max}: 6 hours</p> <p>AUC: 172.40 ± 20.02 mIUh/mL</p>	[60]

Sr. No.	Matrix type	Drug	Excipient	Final dosage form	Pharmacokinetics	Ref.
31	Nanoparticles	10-Hydroxycaptotecin	Poly(n-butyl cyanoacrylate)	Nanoparticles	<p>Model: Sprague-Dawley rats</p> <p>Administration: Oral</p> <p>Data for control: Suspension C_{max}: 5.08 ± 1.96 ng/mL T_{max}: 1 hours</p> <p>AUC_{0-t}: 12.72 ± 2.78 ng/mL</p> <p>MRT: 2.20 ± 0.43 hours</p> <p>Data for formulation C_{max}: 33.12 ± 5.96 ng/mL</p> <p>T_{max}: 0.50 hours</p> <p>AUC_{0-t}: 96.21 ± 11.43 ng-h/mL</p> <p>MRT: 3.44 ± 0.88 hours</p>	[61]

^a C_{max} (maximal drug concentration; ng/mL), T_{max} (time for maximal drug concentration; h) and AUC_{0-t} (area under the curve; ng-h/mL)

enhancement, and improved dissolution rate. In addition, it can be used for both hydrophilic and hydrophobic actives. In this chapter, we have summarized the different pharmacokinetics of DPM-based NPDDS. Interestingly, the use of polymers in designing advanced drug delivery systems improves the performance of dosage form in terms of pharmacokinetics including absorption, distribution, metabolism, and excretion. In this line, different types of NPDDS have been designed using natural, semi-synthetic, and synthetic polymers depending on the problem that needs to be overcome. As a result, these DPM systems showed remarkable presentation, which overcomes poor pharmacokinetics. Owing to this, several DPM-based marketed formulations are introduced by different pharmaceutical companies. Despite victorious development based on polymer matrix in drug delivery, a thorough explanation of such polymer nanosystems' regarding absorption, distribution, metabolism, and elimination processes in living systems has yet to be obtained. In the future, it will pave the new pathway for delivery of poor pharmacokinetics containing synthetic and natural actives.

Acknowledgments The authors are thankful to H. R. Patel Institute of Pharmaceutical Education and Research, Shirpur, for providing the necessary facilities.

Conflict of Interest The authors declare no conflict of interest.

References

1. Yang W-W, Pierstorff E. Reservoir-based polymer drug delivery systems. *J Lab Autom.* 2012;17(1):50–8.
2. Safari J, Zarnegar Z. Advanced drug delivery systems: nanotechnology of health design a review. *J Saudi Chem Soc.* 2014;18(2):85–99.
3. Liu M, et al. Recent advances in electrospun for drug delivery purpose. *J Drug Target.* 2019;27(3):270–82.
4. Saha RN, et al. Nanoparticulate drug delivery systems for cancer chemotherapy. *Mol Membr Biol.* 2010;27(7):215–31.
5. Mishra M, et al. Nanotechnology: revolutionizing the science of drug delivery. *Curr Pharm Des.* 2018;24(43):5086–107.
6. Nangare S, et al. Pharmaceutical applications of electrospinning. In: *Annales pharmaceutiques francaises.* Elsevier; 2020.
7. Shitole MM, et al. Pharmaceutical applications of electrospun nanofibers: a state-of-the-art review. *Asian Journal of Pharmacy and Technology.* 2020;10(3):187–201.
8. Nangare S, Dugam S. Smart in vivo synthesis, characterizations, pharmaceutical applications, and pharmacokinetic perspective: a review. *Future J Pharm Sci.* 2020;6(1):1–21.
9. Dugam S, et al. Emerging era of microneedle array for pharmaceutical and biomedical applications: recent advances and toxicological perspectives. *Future J Pharm Sci.* 2021;7(1):1–26.
10. Nangare S, et al. Development of novel freeze-dried mulberry leaves extract-based transdermal gel. *Turk J Pharm Sci.* 2019;98624. <https://doi.org/10.4274/tjps>.
11. Powar TA, Hajare AA. QbD based approach to enhance the in-vivo bioavailability of ethinyl estradiol in Sprague-Dawley rats. *Acta Chim Slov.* 2020;67(1):283–303.
12. Shitole MM, et al. Review on drug delivery applications of ethosomes: Current developments and prospects:(TJPS-2021–0031. R1). *Thai J Pharm Sci.* 2021E;
13. Mahajan HS, Patil PH. Central composite design-based optimization of lopinavir vitamin E-TPGS micelle: in vitro characterization and in vivo pharmacokinetic study. *Colloids Surf B: Biointerfaces.* 2020;194:111149.
14. Dugam S, et al. Carbon dots: a novel trend in pharmaceutical applications. In: *Annales Pharmaceutiques Françaises.* Elsevier; 2020.
15. Tade RS, et al. Recent advancement in bioprecursor derived graphene quantum dots: synthesis, characterization and toxicological perspective. *Nanotechnology.* 2020;31(29):292001.
16. Tade R, Nangare SN, Patil PO. Fundamental aspects of graphene and its biosensing applications. *Funct Compos Struct.* 2021;
17. Nangare S, et al. Silk industry waste protein: isolation, purification and fabrication of electrospun silk protein nanofibers as a possible nanocarrier for floating drug delivery. *Nanotechnology.* 2020;32(3):035101.
18. Nangare S, et al. Pharmaceutical applications of citric acid. *Future J Pharm Sci.* 2021;7(1):1–23.
19. Shitole M, et al. Pharmaceutical applications of silk sericin. In: *Annales pharmaceutiques francaises.* Elsevier; 2020.
20. Miele E, et al. Nanoparticle-based delivery of small interfering RNA: challenges for cancer therapy. *Int J Nanomedicine.* 2012;7:3637.
21. Patra JK, et al. Nano based drug delivery systems: recent developments and future prospects. *J Nanobiotechnol.* 2018;16(1):1–33.
22. Karade PG, Jadhav NR. Colon targeted curcumin microspheres laden with ascorbic acid for bioavailability enhancement. *J Microencapsul.* 2018;35(4):372–80.

23. Shetab Boushehri MA, Lamprecht A. Nanoparticles as drug carriers: current issues with in vitro testing. *Nanomedicine*. 2015;10(21):3213–30.
24. Feitosa RC, et al. Pharmacokinetic aspects of nanoparticle-in-matrix drug delivery systems for oral/buccal delivery. *Front Pharmacol*. 2019;10:1057.
25. Jain AK, Thareja S. In vitro and in vivo characterization of pharmaceutical nanocarriers used for drug delivery. *Artif Cells Nanomed Biotechnol*. 2019;47(1):524–39.
26. Son G-H, Lee B-J, Cho C-W. Mechanisms of drug release from advanced drug formulations such as polymeric-based drug-delivery systems and lipid nanoparticles. *J Pharm Investig*. 2017;47(4):287–96.
27. Bacaita S, et al. Drug release kinetics from polymer matrix through fractal approximation of motion. *Smart Mater Res*. 2012;
28. Marinescu L, et al. Optimized synthesis approaches of metal nanoparticles with antimicrobial applications. *J Nanomater*. 2020;2020
29. Macha IJ, et al. Drug delivery from polymer-based nanopharmaceuticals—an experimental study complemented by simulations of selected diffusion processes. *Front Bioeng Biotechnol*. 2019;7:37.
30. Zhao Q-H, Qiu L-Y. An overview of the pharmacokinetics of polymer-based nanoassemblies and nanoparticles. *Curr Drug Metab*. 2013;14(8):832–9.
31. Bhatt P, et al. Polymers in drug delivery: an update. In: *Applications of polymers in drug delivery*. Elsevier; 2021. p. 1–42.
32. Kamaly N, et al. Degradable controlled-release polymers and polymeric nanoparticles: mechanisms of controlling drug release. *Chem Rev*. 2016;116(4):2602–63.
33. Gadalla HH, et al. Colon-targeting of progesterone using hybrid polymeric microspheres improves its bioavailability and in vivo biological efficacy. *Int J Pharm*. 2020;577:119070.
34. Piazzini V, et al. Enhanced dissolution, permeation and oral bioavailability of aripiprazole mixed micelles: in vitro and in vivo evaluation. *Int J Pharm*. 2020;583:119361.
35. Jadhav P, et al. Bioavailability enhancement of olmesartan medoxomil using hot-melt extrusion: in-silico, in-vitro, and in-vivo evaluation. *AAPS PharmSciTech*. 2020;21(7):1–17.
36. Xi Z, et al. Evaluation of the solid dispersion system engineered from mesoporous silica and polymers for the poorly water soluble drug indomethacin: in vitro and in vivo. *Pharmaceutics*. 2020;12(2):144.
37. Khan MA, et al. Clarithromycin loaded lipid polymer hybrid nanoparticles: fabrication, in vitro and in vivo evaluation. *Pak J Pharm Sci*. 2020;33(3):1303–13.
38. Dong W, et al. Preparation, characterization, and in vitro/vivo evaluation of polymer-assisting formulation of atorvastatin calcium based on solid dispersion technique. *Asian J Pharm Sci*. 2018;13(6):546–54.
39. Al-Dhubiab BE. In vitro and in vivo evaluation of nano-based films for buccal delivery of zolpidem. *Braz Oral Res*. 2016;30
40. Anwer MK, et al. Preparation, evaluation and bioavailability studies of eudragit coated PLGA nanoparticles for sustained release of eluxadoline for the treatment of irritable bowel syndrome. *Front Pharmacol*. 2017;8:844.
41. Tu L, et al. Multi-functional chitosan polymeric micelles as oral paclitaxel delivery systems for enhanced bioavailability and anti-tumor efficacy. *Int J Pharm*. 2020;578:119105.
42. Dahmani FZ, et al. Enhanced oral bioavailability of paclitaxel in pluronic/LHR mixed polymeric micelles: preparation, in vitro and in vivo evaluation. *Eur J Pharm Sci*. 2012;47(1):179–89.
43. Kumar V, Chaudhary H, Kamboj A. Development and evaluation of isradipine via rutin-loaded coated solid-lipid nanoparticles. *Interv Med Appl Sci*. 2018;10(4):236–46.
44. Al-Dhubiab BE, et al. Formulation and evaluation of nano based drug delivery system for the buccal delivery of acyclovir. *Colloids Surf B: Biointerfaces*. 2015;136:878–84.
45. Augustine R, et al. Nanoparticle-in-microparticle oral drug delivery system of a clinically relevant darunavir/ritonavir antiretroviral combination. *Acta Biomater*. 2018;74:344–59.
46. Chai R, et al. In vitro and in vivo evaluation of Olmesartan Medoxomil Microcrystals and nanocrystals: preparation, characterization, and Pharmacokinetic comparison in beagle dogs. *Curr Drug Deliv*. 2019;16(6):500–10.
47. Dhaliwal S, et al. Mucoadhesive microspheres for gastroretentive delivery of acyclovir: in vitro and in vivo evaluation. *AAPS J*. 2008;10(2):322–30.
48. Gu M, et al. Improved oral bioavailability and anti-chronic renal failure activity of chrysophanol via mixed polymeric micelles. *J Microencapsul*. 2021;38(1):47–60.
49. Vijaykumar N, et al. Development and characterization of solid oral dosage form incorporating candesartan nanoparticles. *Pharm Dev Tech*. 2009;14:290–8.
50. Rana P, Murthy R. Formulation and evaluation of mucoadhesive buccal films impregnated with carvedilol nanosuspension: a potential approach for delivery of drugs having high first-pass metabolism. *Drug Deliv*. 2013;20(5):224–35.
51. Han H-K, Lee B-J, Lee H-K. Enhanced dissolution and bioavailability of biochanin a via the preparation of solid dispersion: in vitro and in vivo evaluation. *Int J Pharm*. 2011;415(1–2):89–94.
52. Javed I, et al. Synthesis, characterization and evaluation of lecithin-based nanocarriers for the enhanced pharmacological and oral pharmacokinetic profile of amphotericin B. *J Mater Chem B*. 2015;3(42):8359–65.
53. Jiao Y, et al. In vitro and in vivo evaluation of oral heparin-loaded polymeric nanoparticles in rabbits. *Circulation*. 2002;105(2):230–5.
54. Kaur A, et al. Thiolated chitosan nanoparticles for augmented oral bioavailability of gemcitabine: prepara-

- ration, optimization, in vitro and in vivo study. *J Drug Deliv Sci Technol.* 2021;61:102169.
55. Omar SM, Ibrahim F, Ismail A. Formulation and evaluation of cyclodextrin- based nanosponges of griseofulvin as pediatric oral liquid dosage form for enhancing bioavailability and masking bitter taste. *Saudi Pharm J.* 2020;28(3):349–61.
 56. Hanif M, et al. Enhancement of oral bioavailability of ibandronate through gastroretentive raft forming drug delivery system: in vitro and in vivo evaluation. *Int J Nanomedicine.* 2020;15:4847.
 57. Kumar R, et al. Polymeric micelles based on amphiphilic oleic acid modified carboxymethyl chitosan for oral drug delivery of bcs class iv compound: intestinal permeability and pharmacokinetic evaluation. *Eur J Pharm Sci.* 2020;153:105466.
 58. Shaker MA, et al. Enhancement of atorvastatin oral bioavailability via encapsulation in polymeric nanoparticles. *Int J Pharm.* 2021;592:120077.
 59. Chaurasia S, et al. Potential of cationic-polymeric nanoparticles for oral delivery of naringenin: in vitro and in vivo investigations. *J Pharm Sci.* 2018;107(2):706–16.
 60. Cheng H, et al. Design of self-polymerized insulin loaded poly (n-butylcyanoacrylate) nanoparticles for tunable oral delivery. *J Control Release.* 2020;321:641–53.
 61. Jin X, et al. In vitro and in vivo evaluation of 10-hydroxycamptothecin-loaded poly (n-butyl cyanoacrylate) nanoparticles prepared by miniemulsion polymerization. *Colloids Surf B: Biointerfaces.* 2018;162:25–34.



Pharmacokinetics of Long Circulating Inorganic Nanoparticulate Drug Delivery Systems

Namrata Gautam, Anushka Kulkarni, Debopriya Dutta, and Sushama Talegaonkar

Contents

1	Introduction	188
2	Pharmacokinetic Considerations for Inorganic Nanoparticles	191
3	Pharmacokinetic Models for Inorganic Nanoparticles	197
4	Possible Degradation Mechanisms of Inorganic Nanoparticles	198
5	Pharmacokinetics of Long Circulating Inorganic Nanoparticles	200
6	Pharmacokinetic Fate of Inorganic Nanoparticles	202
7	Toxicity Concerns of Long Circulating Inorganic Nanoparticles [64–66] ...	203
8	Conclusion	205
	References	206

Abstract

Inorganic nanoparticles impose huge opportunities to clinicians in field of theranostics. Currently FDA has approved hundreds of inorganic nanoparticles for their clinical investigation in different fields of nanomedicine, cosmetics, nutraceuticals, diagnostics, and so on. Potential properties like tunable size, tailorability of surface, targeting at cellular level, and penetrability entail them as system of choice. Despite the tremendous applications, clinical translation of

these nanosystems is still a big challenge. The major debatable concern is their non-acceptable toxicity due to accumulation in RES organs. Interestingly in the last few decades, researchers are quite focused on nanoengineering to optimize physiochemical properties and their impact on PK of these nanosystems. The current chapter provides an overview of pharmacokinetic considerations, effect of various factors, physiologically based pharmacokinetic models, and fate and toxicity of inorganic nanoparticles. The chapter highlights over diverse factors optimized while designing these nanoparticulate systems to achieve desired pharmacokinetics.

N. Gautam · A. Kulkarni · D. Dutta
S. Talegaonkar (✉)
Department of Pharmaceutics, School of
Pharmaceutical Sciences, Delhi Pharmaceutical
Sciences & Research University, Pushp Vihar,
New Delhi, India
e-mail: stalegaonkar@dpsru.edu.in

Keywords

Pharmacokinetic · Diagnostics ·
Biodistribution · Reticuloendothelial system

Abbreviations

ADME	Absorption-distribution-metabolism-elimination
NPDDS	Nanoparticulate drug delivery systems
NPs	Nanoparticles
PBPK	Physiologically based pharmacokinetic models
PK	Pharmacokinetics
RES	Reticuloendothelial system

1 Introduction

Recent advances in formulation and development have led to the emergence of nanoparticles as a novel drug delivery system. Nanoparticles constitute the involvement of matter at the atomic levels. When we can see these particles with our naked eye, the bulk properties dominate which are the aggregate of the quantum forces. However, as we go on decreasing the size and reach a particular level like nanoscale, these bulk properties no longer dominate, and, instead, what we see is the control of individual quantum effects like melting point, fluorescence, magnetic behavior, etc. Taking an example, we see that even though large-scale gold particles appear yellow, at nanoscale, the electrons of the atoms are confined, making them interact differently with light. This is why we see a red- to purple-colored solution of gold nanoparticles rather than a yellow one. Conventionally, nanoparticles have a range of 1–100 nm.

1.1 Classification of Nanoparticles

Nanoparticles can be classified into two major broad categories based on composition as given in Fig. 10.1 [1]:

- (a) Organic
- (b) Inorganic

They can be classified into different types according to their size, morphology, and physical and chemical properties. Some of them are carbon-based nanoparticles (carbon nanotubes (CNTs) and fullerenes, graphene, nanodiamond), ceramic nanoparticles (hydroxyapatite (HA), zirconia (ZrO_2), silica (SiO_2), titanium oxide (TiO_2), and alumina (Al_2O_3)), metal nanoparticles, (silver, gold, and iron), semiconductor nanoparticles (ZnS , CdS , CdS GaN , GaP), polymeric nanoparticles (biodegradable and nonbiodegradable), and, lipid-based nanoparticles (liposomes, solid lipid nanoparticles, and nanostructured lipid carriers).

Organic nanoparticles are biodegradable and nontoxic in nature and include liposomes, dendrimers, micelles, etc. They are also called polymeric nanoparticles.

Inorganic nanoparticles can be classified into metallic nanoparticles, ceramic nanoparticles, carbon nanotubes, and quantum dots. The consideration of carbon-based nanoparticles as inorganic is justified as carbon nanotubes and graphene are entirely made of carbon atoms and not bound to any hydrogen atom to be considered as organic compounds [2].

Metallic nanoparticles have gained popularity in recent times as therapeutics and diagnostic agents in a myriad of sectors ranging from medical, biomedical, engineering, to agriculture. The adaptability of these metallic nanoparticles to be modified with various functional groups opens the pathway to utilize them for targeted drug delivery and as contrast agents for diagnostic purposes. At nanometer level, there is a vast change in the physical and chemical behavior of these metallic elements owing to their large size to volume ratio and quantum effects.

Metallic nanoparticles can be further divided into magnetic that includes iron oxide nanoparticles and nonmagnetic that includes gold, silver, and zinc nanoparticles. We'll now look into each of these in brief.

All of the metals mentioned above have a partially filled d-orbital that is responsible for their higher oxidation states and, thus, higher reactivity [3, 4]. The transition elements of the periodic

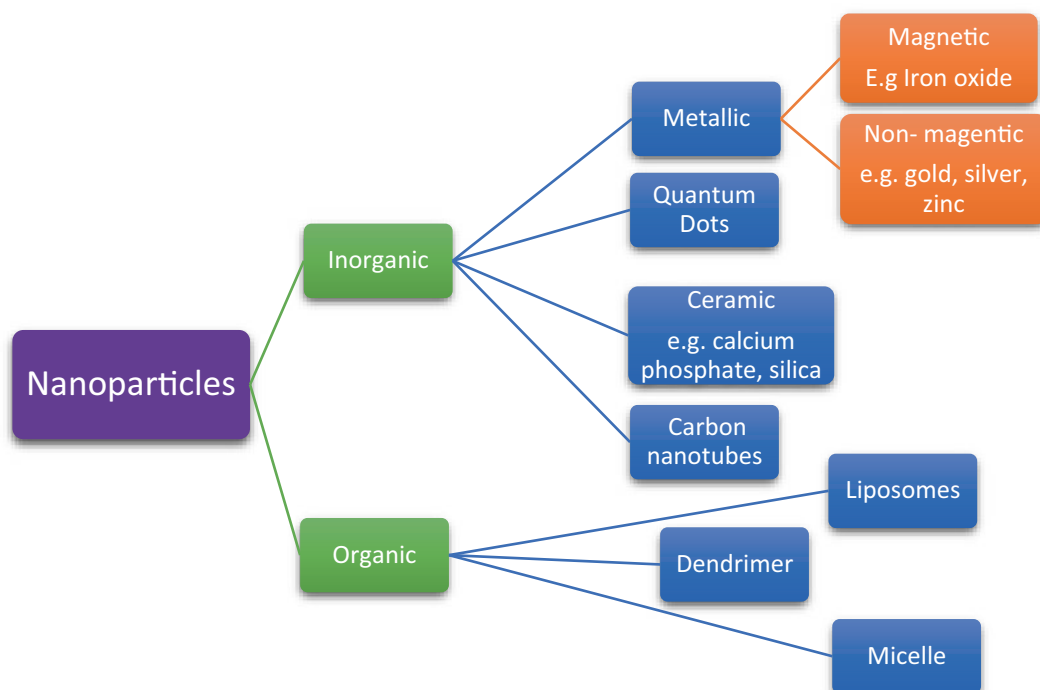


Fig. 10.1 Classification of nanoparticles

table presently used as nanoparticles include gold [gold nanoparticles (GNPs)], silver [silver nanoparticles (SNPs)], iron [iron oxide nanoparticles (IONPs)], and zinc (zinc oxide nanoparticles).

Gold Nanoparticles (GNPs)

The most widely discussed and utilized include the gold nanoparticles. They have applications in cancer therapy as well as diagnostics. Such agents are called theranostics (by combining the words therapeutic and diagnostic) [5, 6]. GNPs have a size range of 1–100 nm. Those in the range of 20–50 nm have been shown to be most promising for cellular uptake and treatment of tumors [7, 8]. The synthesis of GNPs can be done by chemical means as well as through newer sustainable method known as “green synthesis.” One of the chemical method is the citrate reduction method utilizing trisodium citrate to reduce gold chloride [9, 10]. Green synthesis, on the other hand, is a sustainable and environment-friendly technique of enzymatic reduction of gold parti-

cles using plants and microorganisms. When using plants, the plant extract is added to the auric solution resulting in formation of nanoparticles. The concentration of auric solution depends on the species and plant part used [11].

Silver Nanoparticles (SNPs)

Silver is a noble element of the transition metal series known for its healing ability. Silver as nanoparticles is useful in the destruction of cancer cells. It does so by acting as a ROS that kills the mitochondria of the tumor cells [12, 13]. Various methods are used for the synthesis of SNPs. The most widely used is the chemical reduction method.

Iron Oxide Nanoparticles (IONPs)

Iron (II) oxide is paramagnetic in nature, whereas iron (II, III) oxide/ Fe_3O_4 is super paramagnetic in nature. These properties enable them to be successfully used as contrast agents in magnetic resonance imaging (MRI) and magnetic separation technologies like DNA sequencing [8].

Quantum dots are small-sized semiconductor crystals having the ability to showcase intensive fluorescence. They are routinely used as agents in drug delivery and imaging techniques [14].

Ceramic nanoparticles have a porous structure owing to which they can be easily fabricated to suit various needs of sizes and shapes. Few examples of ceramic nanoparticles include calcium phosphate, silica, calcium carbonate, etc. Since these have strong covalent bonds between them, they are relatively stable than metal nanoparticles and, thus, show low thermal and electrical conductivity and low corrosiveness [1].

Carbon nanotubes, as the name suggests, consist of small hollow tubes made entirely of hexagonally arranged carbon atoms. The hollow interior allows it to act as a drug carrier. They are mainly produced through laser ablation method [9, 15].

1.2 Formulation and Development

The synthesis of nanoparticles can be achieved using a wide variety of methods. Traditionally, there are mainly two approaches that are utilized in the synthesis of nanoparticles (Fig. 10.2):

1. Top-down approach
2. Bottom-up approach

Top-Down Approach

It involves the breakdown of larger particles into smaller ones (miniaturization) using processes like milling and attrition. Methods that utilize these processes include laser ablation, mechanical milling, and arc discharge. It requires a lot of energy and effort which is one of the disadvantages of the technique [16, 17].

Bottom-Up Approach

This technique involves the formation of nanoparticles starting from smallest of particles like atoms or molecules and builds on further to form nuclei via process of nucleation. The

nucleation can take place in any medium. The size of the particles can be carefully controlled. Small-size particles can be obtained when almost every particle enters into the nuclei stage simultaneously. It is a simple, fast, and low-cost technique. Methods like sol-gel, microemulsion, and co-precipitation are included in this [16] [17].

One method cannot be applied to all the elements as the choice of method depends on the physical and chemical properties of the element.

Green Synthesis

Abundant research is being carried on newer methods like “green synthesis” to provide an environment-friendly and sustainable approach to nanoparticle synthesis. Traditional techniques led to the excessive use of noxious and hazardous chemicals and even produced harmful by-products at times.

Green synthesis is a comparatively safer alternative to synthesize nanoparticles that uses plants, bacteria, fungi, and algae to synthesize nanoparticles (Fig. 10.2). The phytochemicals present in plant extracts, namely, alkaloids, flavonoids, etc., obtained from plant waste act as reducing agents, thereby reducing the costs of reducing agents used in chemical synthesis methods [18]. Several studies have been carried out showcasing the success of this technique. To take an example, Latha and Gowri, in 2014, synthesized the ferric (II, III) oxide nanoparticles using *Carica papaya* leaf extract [4]. The synthesis of metallic nanoparticles inside the bacteria, fungi, algae, and yeast takes place through several mechanisms that reduce them to their elemental form. These mechanisms majorly include enzymatic reactions and other reactions like precipitations, complexation, and efflux transporters [19]. One recent study even found that biogenic silver nanoparticles were similarly effective but less toxic in eukaryotes compared to chemically synthesized silver nanoparticles [20]. The use of green technology in mass scale production of nanoparticles seems promising in coming years given the large amount of research carried on it.

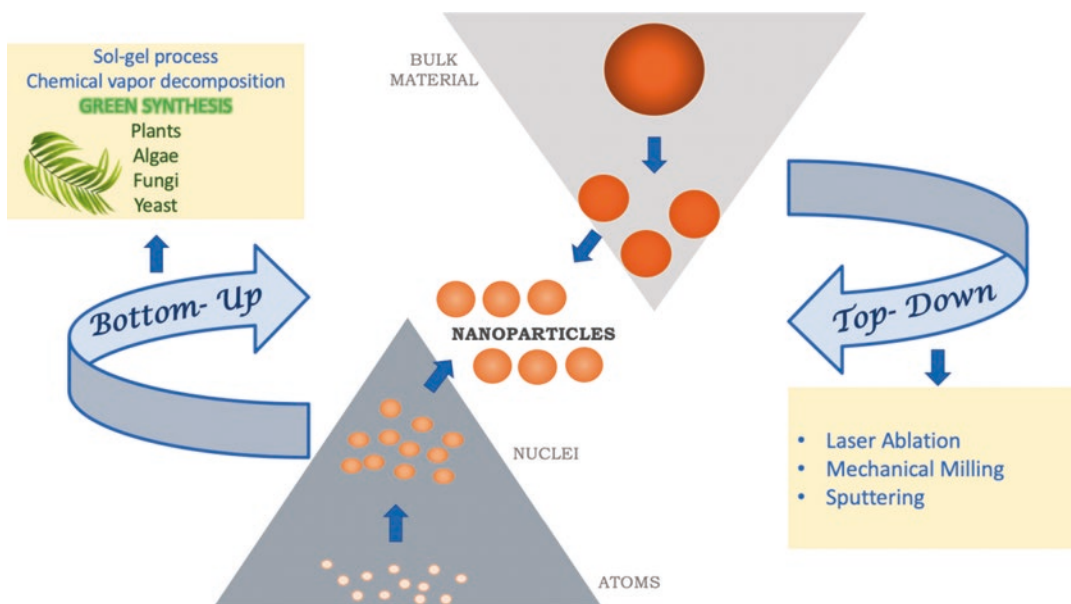


Fig. 10.2 Top-down and bottom-up approaches for preparation of nanoparticles

1.3 Evaluation of Inorganic Nanoparticles

Inorganic nanoparticles can be evaluated by several methods as mentioned in Fig. 10.3 based on the particle and drug characteristics. These parameters ultimately affect the performance of these nanoparticles inside our body, i.e., in vivo [8]. Evaluation of nanoparticles in vivo depends on the disease and the tissue or organ it is affecting.

1.4 Applications of Inorganic Nanoparticle

Owing to their low toxicity, targeted drug delivery, and, significant role in imaging, inorganic nanoparticles have found use in numerous sectors. Few applications of inorganic nanoparticles are summarized in Table 10.1. Some inorganic nanoparticle formulations which are presently marketed are given in Table 10.2.

There are numerous nanoparticulate formulations that have received approval from various regulatory agencies for its use in therapeutics and imaging. Some marketed formulations and for-

mulations of inorganic nanoparticles under clinical trials along with its use are given in Table 10.2 [39].

2 Pharmacokinetic Considerations for Inorganic Nanoparticles

In the fascinating era of nanotechnology, inorganic nanoparticles (both ceramic and metallic) offer various exciting approaches to diagnostics and therapeutics to the scientific community. Among various classes of nanosystems, inorganic nanoparticles exhibit distinctive features and biological effect over conventional organic counterparts. For targeted drug delivery, inorganic NPDDSs should reach to target tissues in optimum concentrations and show appropriate release kinetics, illustrating their efficient therapeutic potency. Also, it is very important that inorganic NPDDS should be nontoxic and easily eliminated from the body. Despite of several demerits, inorganic nanoparticles are system of choice for theranostics due to ease of their formulation-development, easier detection in biological fluids and accurate monitoring of their

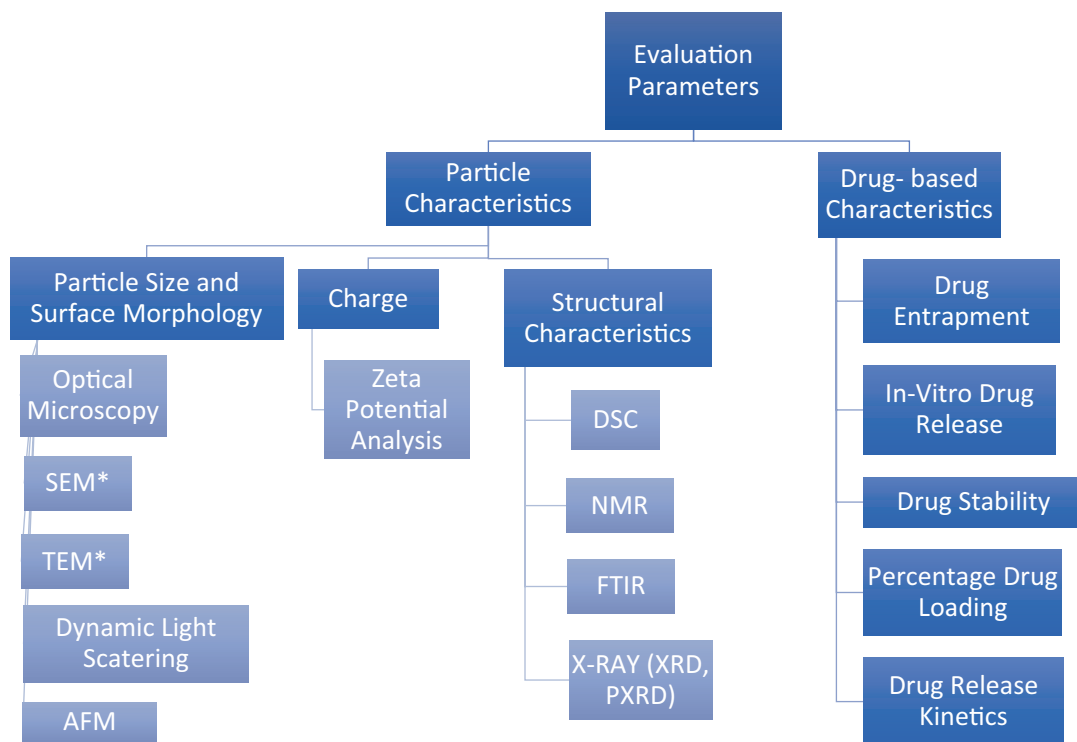


Fig. 10.3 Evaluation parameters of inorganic nanoparticles. *NMR nuclear magnetic resonance, SEM scanning electron microscopy, TEM transmission electron micros-

copy, AFM atomic force microscopy, DSC differential scanning calorimetry, FTIR Fourier transform infrared spectroscopy

kinetics. In contrast, though organic nanoparticles exhibit simple formulation and biodegradability, it is quite difficult to identify them in biological system. Also, their characterization and traceability are problematic. Some exemplary inorganic nanomaterials include quantum dots, fullerenes, carbon nanotubes, graphene, inorganic nanotubes and metallic nanoparticles (NPs). Among all inorganic nanomaterials, highly exploited ones are gold, silver iron oxide, titanium dioxide (TiO₂), and zinc oxide nanoparticles which are also approved by the FDA as theranostics [39]. Gold nanoparticles have been extensively studied in treatment of tumors or rheumatoid arthritis, also adopted as carriers for drug and gene delivery; however silver nanoparticles are employed as antibacterial agents for coating catheters, orthopedic implants, wound dressings, and scaffolds. Major utilization of iron oxide (FeO) NPs is for diagnostics as bioimaging and biosensing, whereas titanium oxide (TiO₂)

and zinc oxide (ZnO) NPs are highly consumed in cosmetics and toiletries [40].

It is the bitter truth that very few inorganic nanomaterials have been made from bench to bedside translation due to their potential toxicities to major organs. Thus, it is a major challenge to exercise more efforts investigating the toxicity mechanisms to ensure their clinical safety.

In this regard, a systematic understanding of fundamental pharmacokinetics is crucial for proper risk assessment. The pharmacokinetics of these long circulating inorganic NPDDS is strongly dependent on various physiochemical attributes including shape, size, charge, and coating material. Furthermore, biopharmaceutical factors like protein binding, route of administration, dose and dosage regimen, patient-related factors, and genetic factors also contribute in their cellular uptake and biodistribution. Literature reveals that oral, dermal, or inhalational absorption of these inorganic nanoparticles

Table 10.1 Application of inorganic nanoparticles in various sectors

Types of inorganic nanoparticles	Application in various sectors			References
	Therapeutics	Diagnostic	Food Industry	
Gold nanoparticles (AuNPs)	Anticancer drug carriers, e.g., gemcitabine Photothermal killing of cancer cells using gold nanorods	Biosensors: surface-enhanced Raman spectroscopy (SERS)	Functional yogurt having radical scavenging properties using AuNP	[21, 22]
Silver nanoparticles (AgNPs)	Anticancer effects Antimicrobial effects	Electromagnetic enhancement of spectral signals	Quercetin capped AgNP antibacterial effect against <i>S. typhi</i>	[23, 24]
Zinc nanoparticles	ZnO maintenance of insulin (antidiabetic role) Anticancer role In sunscreen as UV absorbant	ZnS:Mn for multiphoton imaging	ZnO as animal feed: Enhanced bioavailability and antimicrobial properties; UV absorbers in light-sensitive food	[25–28]
Iron (II, III) oxide nanoparticles	Colloidal carriers of drug; gene therapy Treatment of iron deficiency anemia	As imaging probes in MRI	Colorants and dietary iron source	[8, 25, 29, 30]
Quantum dots (QD)	Photodynamic therapy in cancer treatment Real-time monitoring of drug release	Cadmium-loaded QD two-photon imaging probes Fluorescence imaging Monitor ATP, Cu ²⁺ , glutathione (GSH)	–	[9, 31–33]
Silica nanoparticles	Carrier for hydrophobic drugs to protect them against acidic pH of the stomach	Ultrasound imaging contrast agents	SiO ₂ as anticaking agents in salt, sugars	[13, 30, 34]
Calcium phosphate	Anticancer drug carriers to reduce systemic toxicity Bone tissue engineering	–	–	[1, 35]
Carbon nanotubes	Thermal therapy to kill cancer cells Carrier for therapeutic molecules Tissue engineering and regeneration additives	Biosensors Imaging	Eliminate need for CO ₂ and harmful flavors	[36–38]

is comparatively low, i.e., up to 5% or less. However effective cellular uptake can be improved by tuning of their size, charge, and surface modulation. Nanosize of these inorganic nanoparticles facilitates their distribution throughout the body along with accumulation in various organs like the liver, lung, spleen, kidney, and lymph node. It has been reported that inorganic metallic nanoparticles are capable of crossing the blood-brain barrier as well as placental barrier coated with biocompatible polymers. Due to rapid clearance from the blood stream via the

mononuclear phagocyte system (MPS) and reticuloendothelial system (RES), inorganic nanoparticles bypass first pass metabolism and undergo longer circulation in the body (could remain in the body up to 6 months or more) and thus high accumulation in vital organs leading to their chronic toxicity over time. Also chances of malignancy may arise in people more exposed to nanomaterials, especially those working on nanomaterial production. Therefore, huge data on in vivo and in vitro kinetics along with computational predictive toxicity is requisite for

Table 10.2 Marketed formulations of inorganic nanoparticles

Brand name	Active ingredient	Manufacturing company	Use
Marketed formulations			
Feridex I.V. Or Endorem	Ferumoxides (iron nanoparticles)	Berlex laboratories Inc. USA Guerbet S.A (Eu)	MRI contrast media: Liver tumor imaging
QuickClot	Aluminosilicate Nanoparticle-infused cotton gauze	Z-Medica	Helps blood clot faster
Vivodots	Quantum dots	Nanoco	Diagnostic imaging and phototherapy
CosmoFer	Iron dextran colloid	Pharmacosmos	Iron deficiency anemia
Ostim	Hydroxyapatite (calcium-based nanoparticles)	Heraeus Kulzer	In periodontal disease as bone substitute
Formulations under clinical trial			
AuroLase	Gold shell with silica coating	Nanospectra Biosciences Inc.	Lung tumors, head and neck tumors, prostate cancer
SilvaSorb (NCT00659204)	Silver nanoparticles	Madigan Army Medical Center	Antibacterial gel
Nano Streams (NCT03177876)	Hydroxyapatite	Cairo University	Maxillary sinus lift
Nano Care Gold (NCT03669224)	Mix of gold and silver nanoparticles in 70% isopropyl alcohol	Cairo University	Dental caries
Magnablate I (NCT02033447)	Iron nanoparticles	University College London	Thermal ablation in prostate cancer

understanding the implications on long-term usage/exposure (Fig. 10.4).

Discussing on biotransformation of nanomaterials, it is well established that organic nanoparticles inclusive synthetic polymers or biopolymers exhibit higher biocompatibility as compared to inorganic one. The prime reason behind this is their hydrodynamic behavior in vivo and tailorability of their surface with specific targeting ligands. On the other hand, due to the poor water solubility, stability issues, immunogenicity, and potential toxicity, inorganic nanomaterials are desperately required to modify their surface with a biocompatible organic coating. Thus regardless of compositions, either metallic or ceramic, mandatory requirements for designing of all types of inorganic NPDDS are targeting efficiency, half-life of drug/formulation in blood, and complete elimination from the body without any toxicity.

Various biopharmaceutical approaches are already known to estimate the pharmacokinetics of nanomaterials. Both experimental and mathematical models are utilized to determine pharmacokinetic parameters, i.e., volume of distribution

(Vd), clearance (Cl), half-life (T_{1/2}), mean residence time (MRT), maximum or peak concentration (C_{max}), area under the time concentration curve (AUC), and bioavailability (F). Pharmacokinetic data provide insights to clinicians to optimize dose and design a dose regimen within the therapeutic window of drug. Consequently modulations are done to achieve desired pharmacokinetic profile of drug in NPDDS. However in case of inorganic NPDDS, estimation of accurate pharmacokinetic parameters and establishment of safety profile of nanomaterials are tough jobs due to unavailability of pharmacokinetic models for assessment. Due to these limitations, inorganic NPDDS are still in infancy stage in the market. Besides traditional approaches of compartment modeling and non-compartmental analysis, physiological models have emerged as newer approach for pharmacokinetic assessment of inorganic NPDDS. These physiological models are purely based on mathematical equations providing a more realistic picture of ADME process in vivo. However, such models have not been explored a lot (limited number of models available); therefore efforts

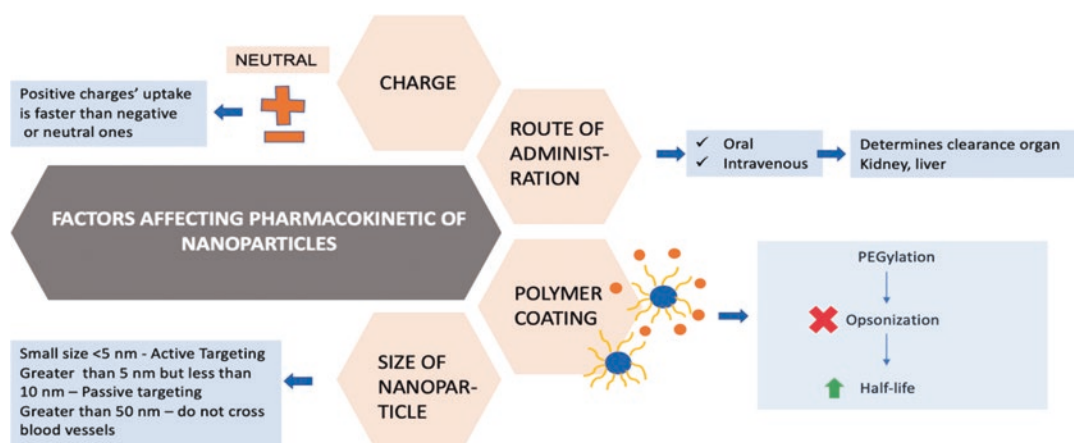


Fig. 10.4 Factors affecting pharmacokinetics of nanoparticles

are needed to fill the gap between theoretical assumptions and accurate data gap.

Thus it is quite clear that in order to attain desired pharmacokinetic parameters of inorganic NPDDS, it is necessary to modulate these systems by virtue of modifications in their physiochemical attributes, i.e., hydrodynamic diameter (HD), shape, composition, and surface characteristics [41].

2.1 Impact of Particle Size and Shape

Nanosize of inorganic material has tremendously solved the problem of their cellular uptake across biological membranes despite of their poor solubility and lipophilicity. Due to high surface area and low volume, these particles can easily penetrate various biomembranes for ease of targeting. Generally, particles in size range of 10–15 nm are easily permeated through biomembranes with limited accumulation in nontarget tissues. However, selection of appropriate particle size is crucial for its biotransformation which decides the fate of these nanosystems upon pharmacokinetic translation. It has been reported that nanoparticles having diameter around 5 nm or less prefer renal clearance, whereas particles with little larger hydrodynamic diameter undergo biliary excretion [42–44]. Nanoparticles exceeding 100 nm in size are reported to have extremely dif-

ferent pharmacokinetics and biodistribution properties, and their chances of accumulation in vital organs like the spleen, lungs, liver, and kidney arise. Therefore, optimized fabrication methods are adopted to control the mean particle diameter of these nanosystems along with adjustment in various physiochemical attributes of composition. Also, the tuning of size is done as per the requirements of target organ. For instance, in case of brain targeted drug delivery systems, to cross the tight endothelium junctions, the particles should have diameter < 20 nm. In general, the ideal size range of these inorganic NPDDS is 10–150 nm for longer circulation time and desired accumulation at target site [45]. Importantly, the smaller size of these nanosystems simulates with plasma proteins that leads to their longer circulation time and thus enhanced permeation and retention in solid tumors as well as atherosclerosis. Furthermore, it has been reported that both accumulation and penetration are required in tumors; therefore to achieve this, a wide range of nanoparticles, varying in size, are targeted to strike the tumor. Generally larger NPs show their accumulation within the tumor cells toward periphery; however the smaller ones penetrate quite deeper inside the tumor cells.

Inorganic nanoparticles could be of various shapes like spherical, cubic, rod-like, or worm-like which directly influence their cellular uptake. Different absorption patterns have been observed in terms of shape of these NPDDS. In an example

of gold nanoparticles, it was observed that among different shapes, i.e., cubic, spherical, and rod-like nanoparticles, the net quantity of nanoparticles absorbed (weight) was higher for spherical particles, whereas total count of nanoparticles was comparatively more for rod-shaped ones [46].

2.2 Impact of Surface Modulation

In the current scenario of precision medicine, huge research is going on for tailoring of inorganic nanoparticles by surface modulation to obtain intelligent nanoparticles with improved targeting efficiency and low toxicity. Functionalization of nanoparticles significantly affects the physical, chemical, and biological nature of the entire formulation and thereby impacts on its pharmacokinetics too. Surface modulation can be done in terms of attachment of ligands, ions, antibodies, coating with proteins, genetic material, polymers, etc., and currently a number of FDA-approved metallic nanoparticles are available as nanomedicines for treatment of tumors, osteoporosis, and rheumatoid arthritis [47].

The surface charge of these inorganic NPDDS interacts with surface proteins of biomembranes and thereby affects absorption and distribution across the membrane. It is well established that positively charged NPDDS show better absorption in comparison to negative ones due to electrostatic interactions. However NPs surface coated with neutral non-ionic polymer imparts stability and hence reduced immunogenicity. Furthermore, surface attributes of these inorganic NPDDS have a crucial role when come in contact with biological fluids. Generally protein-coated inorganic NPDDS show different affinities toward different proteins of biological fluid which ultimately decides their fate of biodistribution.

2.3 Impact of Route of Administration

Administration route of NPDDS impacts biodistribution imperatively due to differential interac-

tion with enzymes, hormones, proteins, ions at the site of administration, as well as site of absorption, and thus a significant change in PK parameters is obtained. Huge research has already been done to elucidate the fate of inorganic nanoparticles in vivo upon administering them through different routes. For instance, it has been reported that when PLGA NPs are administered through intravenous route, they get accumulated in the liver and spleen, but upon subcutaneous or intranodal administration, they are found to get accumulated in the lymph nodes specifically. Therefore one can easily target lymph nodes by administering drug via subcutaneous route, which could be beneficial in certain immunotherapeutic applications [48].

It is well established that altering route of administration can avoid several demerits related to both dosage form and undesirable first pass metabolism. For instance, in case of lung targeting, NPDDS are preferably administered as inhalation rather by parenteral route for maximal accumulation in the lungs before reaching to systemic circulation. In one more example, comparison between different modes of pulmonary administration was studied in mouse. For this, intratracheal instillation, intratracheal spraying, and intranasal instillation were selected to deliver PLGA nanoparticles. The report on accumulation and bioavailability of drug revealed heterogeneous biodistribution and accumulation of NPDDS in lung tissues [49].

Huang X et al. [7] studied over impact of different parenteral routes on biodistribution of carbon dots. They reported that upon administering them via intravenous, intramuscular, and subcutaneous individually, different values of PK parameters were obtained. They drew a comparison in clearance and urinary accumulation/excretion rate of NPDDS and concluded that the particles exhibit following order for above mentioned PK parameters: intravenous > intramuscular > subcutaneous injections. However accumulation and selective uptake of carbon dots in tumor cells was found to be comparatively higher by subcutaneous and intravenous route in comparison to intramuscular injection. Hence such examples potentiate route-dependent

changes in ADME of theranostics and thus their bioavailability. Although tremendous preclinical studies are continuously being done to identify the best routes for a specific target, biodistribution of these inorganic NPDDS is still a big challenge.

2.4 Impact of Composition of Nanomaterial

Most of the inorganic theranostic NPs are composed of either metallic (transition metals) or ceramic compounds having specific configuration and geometry (linear or branched). They exhibit larger size, greater hydrophobicity, and poor biodegradability as compared to organic NPDDS. Such physiochemical features of inorganic NPDDS impact their in vivo performance and affect absorption, biodistribution, elimination, as well as targeting ability. Also due to non-biodegradability, inorganic NPs remain in the body for a relatively long period of time compared to small molecules, and thus concerns have been raised for their potential toxicities. Due to their long circulation time, abrupt changes in PK parameters have been observed (increased $t_{1/2}$, reduced clearance, increased volume of distribution, lesser excretion rate, increased mean residence time).

2.5 Impact of the Dose

The relationship between dose and pharmacokinetic process depends upon the order of kinetics followed by inorganic nanoparticles. It could be linear (dose dependent), nonlinear (dose independent), or mixed order, decided by physiological and anatomical attributes of the body during ADME process [50]. In a study by Reeves, *L et al.* [51], gold nanoparticles (size range of 12–15 nm) were administered in consecutive three doses of 40, 200, and 400 $\mu\text{g}/\text{kg}$ to mice via intraperitoneal route up to 8 days. The biodistribution of nanoparticles was monitored at regular intervals. The initial results did not indicate any major difference in blood plasma concentration

of drug at 24 hrs. However after progression of time and examination of vital organs like the liver, spleen, lungs, kidneys, and brain, significant accumulation of gold nanoparticles was diagnosed. Also the reports revealed that the accumulation of nanoparticles was linearly related to dose administered. Thus the study confirmed about efficient and non-saturable cellular uptake of gold nanoparticles in a dose-dependent manner. Also Kim *Ys et al.* [52] confirmed dose-dependent kinetics of PEG-coated AuNPs (12–13 nm size) injected intravenously in mice. They compared two doses, 0.85 mg/kg and 4.26 mg/kg of nanoparticles, and reported a comparative increase in their cellular uptake in a dose-dependent manner in various organs like the liver, spleen, and kidneys. Therefore selection of dose for inorganic NPDDS is very important in terms of their accumulation toxicology.

3 Pharmacokinetic Models for Inorganic Nanoparticles

Physiologically based pharmacokinetic models (PBPK) are gaining importance day by day to provide very realistic description of ADME of various nanosystems using mathematical equations. These models are highly versatile and well adopted to include different doses, routes, and species to predict target tissue dosimetry and thus quite helpful to clinicians. However, only limited PBPK models have been developed for NPDDS yet. The major reason behind unavailability of these models is sophistication in nanoparticle synthesis process which limits the application of one PBPK to another as the NPs prepared by one technique are entirely different from another in their PK aspects. Therefore one PBPK model for a specific nanosystem cannot be a generalized model for another and requires new algorithms for modeling. Furthermore developments of PBPK models require thorough in vivo studies on mechanisms of cellular uptake, biodistribution in tissues, and elimination pathways. PBPK models are generally classified into two classes: blood flow rate-limited and permeation rate-limited models. Blood flow rate-limited models are based

on the assumption that there always exists equilibrium between blood and tissue compartments and transfer of nanoparticles from one compartment to another is a function of blood flow rate. However in permeation rate-limited models, it is assumed that rate of diffusion of nanoparticles from one compartment to another is dependent on tissue permeability of concerned compartments. While designing a particular PBPK model, all physiochemical attributes of nanosystems are well evaluated. For instance, size and shape of nanosystems decides their fate of accumulation, biodistribution, and elimination (hepatic or renal). Therefore such important factors are taken into account in PBPK models by inclusion of certain algorithms. In addition to this, physiological conditions (e.g., endothelium pore size in different tissues) are also integrated in PBPK models. Importantly, feasibility of manipulations in PBPK models is there so that additional approaches, like active targeting of nanoparticles, can be integrated by inclusion of selective transport mechanism and kinetics which is a virtue of affinity of the nanoformulation toward its target cells or tissues. Furthermore, other important factors including shape, surface modulation, charge, functional group, etc. can also be considered by clinicians in PBPK models. Despite of interaction of drugs with lymphatic systems, generally they are excluded in PBPK models due to their lower fluid movement rate as well as lesser absorption of drugs in comparison to blood. However, in some exceptional cases, they are incorporated in PBPK models where nanosystems are directly interacting with the lymphatic system. For instance, a nanosystem surface coated with antigen/antibody or some immunogenic ligands will definitely be impacted by lymphatic system for its deposition; in such cases inclusion of lymphatic system becomes mandatory to estimate accurate PK parameters.

Elimination kinetics is evaluated in all PBPK models by simulating with major excreting organs, i.e., liver, kidneys, lungs, and gut. However for nanosystems, elimination is little more complex due to involvement of other organs/tissues in clearance besides the former

ones. Among the various identified pathways of elimination for nanosystem, the most important ones are mononuclear phagocyte system (MPS) and reticuloendothelial system (RES). Generally PBPK models developed for animal studies are utilized as surrogate models for nanomedicines in humans which is a matter of concern since physiological parameters are not the same among different species. The most applicable PBPK animal models developed to simulate humans are based on species such as rodents, dogs, and monkeys. A sample PBPK model is illustrated in Fig. 10.5.

Bachler et al. [53] developed a PBPK model for comparative analysis of ionic silver and nanoparticles of silver on the basis of data generated in their toxicological studies. They evaluated various routes of administration for both formulations (i.v., dermal, oral, and inhalation) and compared their plasma/tissue concentration of drug as well as urinary excretion data. Furthermore the model was adopted to predict the absorption and distribution kinetics of both ionic silver and silver nanoparticles.

Various PBPK models have been designed to study the impact on pharmacodynamics of nanomedicines in treatment of several diseases like cancer, diabetes, autoimmune disorders, etc. [54, 55].

4 Possible Degradation Mechanisms of Inorganic Nanoparticles

Determination of degradation mechanism of NPDDS is quite complex and variable since it depends on several parameters. Once administered, inorganic NPDDS are exposed to several physiochemical changes that may lead to their agglomeration and yielding microscopic particle, or they may end up to unstable systems. Furthermore such unstable systems may undergo corrosion and get dissolved or may suffer structural damage. Such nanoparticles may act as reservoir for release of toxic ions produced by corrosive attacks. Chances of undesirable surface

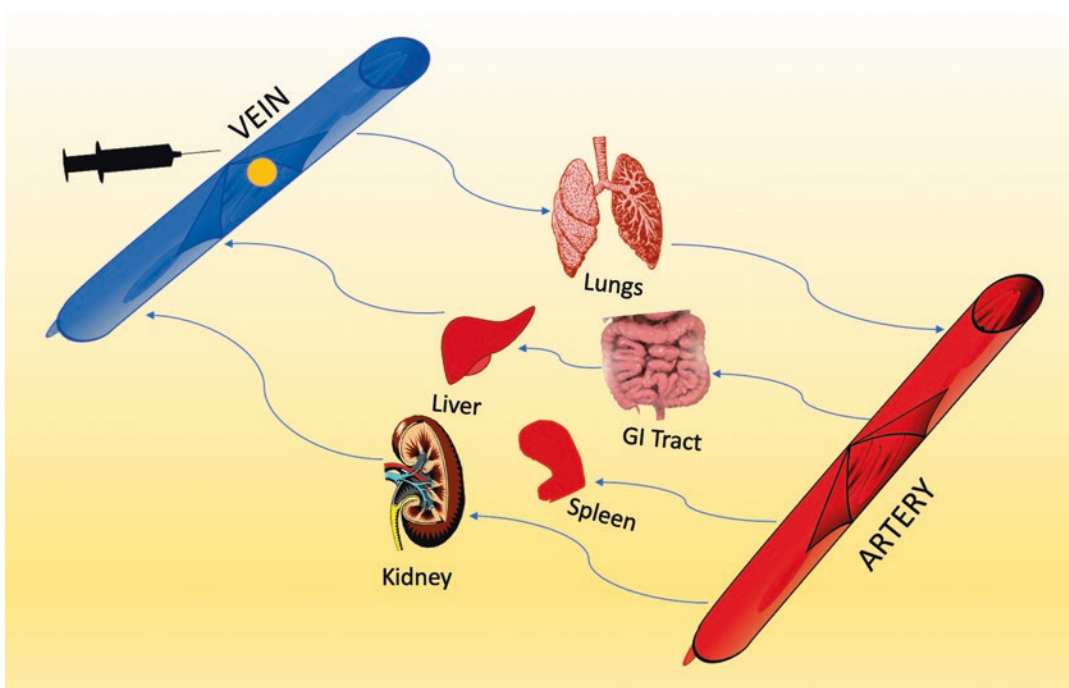


Fig. 10.5 PBPK model

modulation are also there which may impact their targeting efficiency and bioactivity. Generally, in such cases, the nanoparticle surface adsorbs the macromolecules (proteins/reactive molecules/ions) from surrounding media which may hamper its absorption and alter entire biodistribution pattern. Conclusively the pharmacokinetic fate of nanomaterials is just a virtue of physiological environment, it is exposed, and its estimation is still a challenge [56].

4.1 Agglomeration

Generally, NPDDS show some unusual behavior *in vivo*; they have strong tendency to agglomerate in biological fluid due to surface charge, coating, hyphenation, and ligands. It has been observed that the biological fluid or medium in which they are dispersed contributes in agglomeration. Various factors like ionic strength, pH as well as presence of biomolecules like proteins, enzymes and other cellular components

generally interact with these nanosystems, and a dramatic change in their state of aggregation, dispersibility, and charge may occur. This leads to destabilization of NPDDS in biological fluid, and thus their agglomeration may take place which further entails several other changes in the properties of these nanosystems, i.e., specific surface area, concentration, mobility, and so forth. Such changes occur at nanoscale leading to loss of their stability and huge changes in PK parameters leading to their undesirable uptake in nontarget tissue, accumulation, and toxicity. In case of nanopowders, it is very common phenomena.

4.2 Adsorption of Macromolecules

Concept of surface chemistry confirms that inorganic hydrophobic powders have electrostatic charges on surface and have a strong tendency to adsorb various biomolecules when come in contact of biological fluid *in vivo* or dispersed in

physiological medium. It is a serious matter of concern for inorganic NPDDS because they have also been reported to adsorb blood serum proteins to become more hydrophilic and attain stability which further leads to changes in mechanism of their attachment and interaction with biomolecules and ultimately results in PK changes of nanosystems.

4.3 Corrosive Degradation of Nanoparticles

Metallic nanoparticles are prone to release ions upon corrosion and thus induce toxicity to organ systems exposed. It has been noted that inorganic NPs upon exposure to certain pH of media, ions, or absorbing biomolecules undergo catalytic reactions and follow a disintegration pathway. A little exposure to oxygen, chlorine, free radicals, and enzymes in surrounding media is favorable for such thermodynamic processes.

Most common examples of corrosion of these metallic nanomaterials include corrosion of gold and silver nanoparticles due to presence of cysteine and chlorine in biological fluids. Several other metals like iron, zinc, and cadmium are reported to be disintegrated *in vivo*. Consequently, the corrosion leads to both morphological and chemical changes in these nanosystems and thus alters their PK parameters which ultimately results into toxicity due to metal cations.

5 Pharmacokinetics of Long Circulating Inorganic Nanoparticles

The main aim behind designing NPDDS is to achieve targeting and deliver the minimal dose in efficient manner to avoid toxicity. Also, PK parameters are programmed in designing of these nanosystems. Therefore, formulation strategies are based on thorough understanding of interaction between nanoformulations and biological systems. Additionally, the entire journey of NPDDS (ADME process) from entry to exit from the body is evaluated for both therapeutic and toxic potentials.

5.1 Absorption and Cellular Uptake [57, 58]

Inorganic NPDDS are well adapted to be delivered through different routes of administration (e.g., inhalation, oral, skin, and non-IV parenteral), but their absorption into systemic circulation and final cellular uptake is quite variable. Also absorption of these nanosystems is further dependent on several other factors like surface charge, size, shape, pH, PKa, lipophilicity, etc. It has been noted that absorption of cationic nanosystems is more efficient in comparison to anions and neutral ions from the GI tract. However in case of inhalational nanosystems, size ranging 100 nm or less, 80% of inhaled particles get trapped into respiratory tract, and their absorption takes place via olfactory nerve pathway. Furthermore, upon dermal/subcutaneous administration (50–100 nm), penetration of anionic nanosystems is found to be more efficient. Dermal penetration is also dependent upon shape and lipophilicity of NPDDS. Although injectables cause extravasations, they exhibit maximum bioavailability, reaching directly to systemic circulation.

Two basic mechanisms involved in absorption and uptake efficiency of NPDDS are opsonization and phagocytosis. Generally opsonization is responsible for phagocytic clearance in vascular system and involves attachment of opsonin proteins to foreign bodies in blood circulation, stimulation of immune systems, followed by phagocytosis. Importantly inorganic NPDDS which are nonbiodegradable bypass this opsonization rather sequestered in organs where macronuclear phagocytic system or RES systems are there, i.e., the spleen, liver, and kidney, leading to hepatotoxicity or nephrotoxicity.

5.2 Biodistribution in Tissues [55, 57]

Biodistribution of nanoformulation is an important PK parameter that decides its circulation time in the body, duration of action, and toxicity. Upon reaching to systemic circulation, NPDDS

partition between blood and adjacent tissue compartments which is basically dependent upon physicochemical properties of these nanosystems (shape, size, partition coefficient, lipophilicity, permeability) and physiological conditions of the body (organ size, body fat index, etc.). One more phenomenon, “protein-corona formation” of nanoformulations, interferes with their biodistribution [59, 60]. It involves binding of plasma proteins on the surface of nanoformulations which further influences its cellular uptake and degradation pathways of these nanosystems. The most common plasma proteins involved in protein corona formation are serum albumin, immunoglobulins, fibrinogen, and apolipoproteins, which binds to surface of nanosystems by various mechanisms like Van der Waals interactions, hydrogen bonding, and salvation. This ultimately results in drastic changes in surface characteristics and alteration in shape and size and most importantly hampers the stability of these nanosystems. Thus protein corona formation decides the PK fate of biodistribution of these NPDDS.

It has been reported that nanoformulations’ distribution mechanism is strongly dependent on their size and concentration in particular body compartment. Therefore their transport across different compartments or their accumulation in certain cells is dependent upon their diffusion rate, permeation rate, and pore size of biomembranes. Interestingly, in case of prodrugs, NPDDS and high molecular weight metallic NPs, their targeting efficiency and biodistribution are entirely dependent on their penetrating ability and retention potential. For instance, such systems are designed to accumulate in tumor cells or inflammatory sites, having high vasculature, so that large pores of tumor cells (above 100 nm) may facilitate their easier transport and thus accumulation in tumor cells. Therefore various factors are evaluated while designing PBPK models for tumor cells.

Furthermore, several physiological barriers (BBB, blood-placental barrier, blood-testis barrier etc.) play crucial roles in rate and extent of biodistribution of these nanosystems across various compartments. In literature, contribution of anatomical features of these barriers in biodistri-

bution is well established. However a thorough understanding of transport mechanism across these barriers entails bioengineering of nanosystems for better penetration and higher permeation to deliver the drug.

5.3 Elimination of Inorganic Nanoparticles [55, 57]

Despite of usual routes of elimination (hepatic and renal), nanosystems can be excreted via various other routes depending upon their route of administration. For instance, in case of inhalation, dermal, and parenteral routes of administration, elimination may take place from the lungs, skin, as well as circulatory system too. Degradation and elimination of inorganic nanoparticles is still a big challenge to clinicians. In general, the elimination of these systems involves several enzymatic and chemical degradation pathways which ultimately result in renal or biliary clearance of nanomedicines. However various PBPK models confirm that these nanoformulations do not follow usual elimination and clearance pathway; besides this, they accumulate in tissues/organs, get released slowly, and remain in blood circulation for longer durations.

Elimination kinetics of these nanosystems involves their clearance from blood, renal clearance, and biliary excretion. In blood, opsonization and phagocytosis (kind of immunogenic response produced for foreign bodies) is a major process of clearance. However bioengineered NPDDS can avoid this mechanism by surface modulation, so that they can reach to their target cells before being cleared from circulatory systems.

In the liver, macrophages produced by Kupffer cells contribute in biotransformation of nanomedicines. The concentration of these macrophages is extremely high in the liver and acts as pool for phagocytic clearance of NPs. This phagocytic clearance also involves opsonization, by virtue of binding of NPDDS with immunoglobulins. Furthermore it has been reported that extremely fine inorganic NPs engulfed by Kupffer cell produce free radicals, tumor necrosis factors,

interleukins, and other inflammatory mediators which later on lead to hepatotoxicity. Spleen also contributes in phagocytic elimination of NPDDS.

Among various routes of excretion, renal route is extremely important for clearance of nanomedicines; however due to several limitations posed in various parts of nephron (from glomerulus till distal end), their clearance becomes compromised in the kidney. The fine pore size of fenestrations in glomerular endothelium (50–100 nm) and thin basement membrane of blood capillaries restrict passage of nanoparticles and filter them out which leads to accumulation in the kidney and hence nephrotoxicity.

6 Pharmacokinetic Fate of Inorganic Nanoparticles

Inorganic nanoparticles including gold, silver, iron, cadmium, zinc, silica, phosphate, and other inorganic compounds are utilized for several biomedical applications, but their pharmacokinetic fate in vivo is quite variable in terms of their blood circulation time, retention in different organs, and mechanism of biodegradation and excretion.

It has been reported that NPs made of Ag, ZnO, CdSe, and FeO₂ undergo catalytic reaction and corrode slowly, which ultimately releases metal ions in biosystem. It is assumed that gold and silver are quite inert and thus stable against corrosion; however attachment of certain ligands like thiols, available in amino acids (glutathione) inside cells, pulls out gold ions at surface of NP, ultimately leading to its dissolution.

Balfourier et al. [61] studied over pharmacokinetic fate of gold nanoparticles in fibroblast cells up to 6 months. Their study reveals that inertness of gold is just a myth and it also undergoes degradation likewise other inorganic nanoparticles. Utilizing electron microscopy imaging and transcriptomics, they deduced that biotransformation of gold nanoparticles is a two-step mechanism. The former step involves generation of ROS in lysosomes (entrapping fine gold NPs) catalyzed by NADPH oxidase and nuclear factor erythroid. However, the latter step

is recrystallization of gold nanoparticles, which results into self-assembled nanoforms/nanoleaves of biomineralized crystals of gold. The recrystallization is favored by biological chelating agent naming metallothioneins present in cytosol. Thus they confirmed over ionic degradation of gold NPs.

Bailly et al. [62] prepared gold NPs utilizing a new laser-based technique with merits of least contaminants and better surface chemistry. They conjugated the gold NPs with dextran polymer to enhance its biocompatibility and studied the PK of NPs. In results they reported that coated gold nanoparticles prepared are highly biocompatible and nonimmunogenic (confirmed by IL-6 levels) and do not accumulate in the liver (confirmed by ALAT and ASAT activities) and kidney (creatinine clearance). Furthermore, the NPs are capable of rapid clearance from systemic circulation. However, their limited accumulation in the liver and spleen was confirmed.

Pandey .S et al. [63] prepared and evaluated calcium phosphate nanoparticles encapsulating methotrexate (MTX-CAP-NP). During pharmacokinetic evaluation, they reported selective targeting of NPDDS specifically in arthritic bones and higher concentration in blood besides entering in other organs. They disclosed that due to simulation of calcium phosphate with biominerals, they accumulate and degrade in tissues like bones and teeth like other biominerals.

Superparamagnetic iron oxide (FeOx) NPs are extremely reactive, and corrosion is their prime mechanism of disintegration, which can further be confirmed by elemental analysis using coupled plasma mass spectrometry (ICP-MS). However elemental analysis results do not portray the accurate results due to presence of higher concentration of endogenous iron inside the body. Besides this, sophisticated techniques like electron paramagnetic resonance (EPR) can be employed to differentiate between iron nanoparticles and endogenous iron, and temperature-dependent susceptibility method can be adopted. Such evaluations provide insights to biotransformation iron NPs in short and long terms. Lysosomal degradation is their prime mechanism of elimination.

Interestingly, macrophages, endothelial cells, or mesenchymal stem cells which are meant for engulfment of these nanosystems exhibit a special mechanism in biotransformation of inorganic nanoparticles. In conditions of starvation, these cells have been reported to expel FeOx NPs, Au NPs, QDs, or CNTs, in extracellular medium in form of tiny microdroplets which are further transported across the body. Thus despite of local degradation, such NPs traverse to different organ systems and may stay there for long. Hence degradation of inorganic NPS is nonlinear and unpredictable, because it is difficult to decide that up to what extent the particles injected will dissolve or will remain unmodified.

Moreover advanced technologies like TEM are quite helpful in determination of NP interaction with cell cultures within biological environment in situ. Furthermore TEM also facilitates the study over various transformations of NPs upon generation of reactive oxygen species by electron.

Conclusively we can say that inorganic NP cores can be degraded in vivo and the following strategies can be adopted to foster the degradation and elimination of inorganic theranostics:

1. Manipulation in elemental composition of inorganic NPDDS without compromising distinctive chemical, physical, and pharmaceutical properties.
2. Tuning of size can be done to harness faster elimination.
3. Hyphenation and surface modulation with biodegradable and biocompatible polymers (PEG), to reduce their uptake from RES system and faster clearance.

7 Toxicity Concerns of Long Circulating Inorganic Nanoparticles [64–66]

Huge literature is there over toxicokinetics of nanomaterials. Well, toxicity concerns associated with nanomedicines are definitely so loud that various regulations over the globe have given guidelines for preparations and utilization of

these nanosystems in different fields like agrochemicals, nutraceuticals, food, cosmetics, drugs, and so on. Irrespective of novel techniques of bioengineering applied, the core characteristics of nanosystems make them exclusive and entail toxicity concerns. The key features of these inorganic nanoparticles responsible for their toxicity are extremely fine size, penetrability at cellular level, entrapment and accumulation in RES organs, nonbiodegradability, and non-excretable through renal route. Furthermore they can cross various physiological barriers easily like BBB and placental barriers and thus may produce other toxic effects.

Due to their small size, they can penetrate both cellular and nuclear membranes and may interact with organelles and genetic material. Also due to hydrophobicity and high surface to volume ratio, they have higher adsorptive capacity, easily bind to biomolecules, and disturb the homeostasis at cellular level.

Carnovale et al. [67] synthesized and studied over uptake degradation and toxicity of gold NPs in human prostate cancer cells. They developed eight sets of NPs to study their fate in vivo, i.e., role of protein-corona formation in presence of cellular proteins and impact of shape and size in accumulation, circulation, biodistribution, and excretion. In conclusion the study disclosed that rod- and cube-shaped NPs stabilized in presence of cetyltrimethylammonium bromide (CTAB) are minimally toxic and well tolerated as compared to spherical- and prism-shaped nanoparticles. Also study confirms that serum proteins do not participate in any toxicity though they have a crucial role in cellular uptake mechanism.

In a recent review by *Sani et al.* [68], they contradicted the toxicity of gold nanoparticles. Instead they highlighted that toxicity of gold NPs is not a big concern. Furthermore they also confirmed that gold itself is inert and non-catalytic, so chances of free radical or any electron transfer reactions is minimal. A limited toxicity is reported in case of gold NPs, which can further be avoided through several means like optimization of shape and size and functionalization of surface.

Yaqoob et al. [69] reviewed over PK aspects of gold, silver, and palladium nanoparticles. In studies they also confirmed that cytotoxicity of gold NPs is size dependent and can be minimized by alterations in shape and size. However in case of silver nanoparticles, they disclosed that toxicity of silver NPs is independent of their shape and size and coating thickness. The main reason of toxicity is their catalytic behavior in aqueous medium and interaction with functional groups of amino acids like amines and thiols. Silver NPs release silver cations, which are extremely toxic to cellular components and reported to damage genetic material like DNA at nuclear level. For Pd-NPs, they revealed that like silver NPs, their cytotoxicity is due to their catalytic behavior. However sizes of NPs do have some impact on toxicity too.

Mao BH et al. [70] explored AgNPs and studied their effect at the different levels. Various doses of silver NPs were evaluated in *Drosophila melanogaster* for its lethal effect as well as cellular and molecular defects. Lethal dose delayed development cycle in embryonic stage and ultimately led to the death of developing as well as young animals; however sublethal dose impacted on tolerance to oxidative stress and shortened the life span. They also reported active participation of silver nanoparticles in surge of ROS-induced immunogenic cycle leading to apoptosis, DNA damage, and autophagy.

In a study by *Sambale F et al.* [71], toxicity of silver nanoparticles was evaluated on various human and animal cell lines, i.e., human fibroblast cell line (NIH-3 T3), human lung adenocarcinoma epithelial cell line (A-549), human hepatocellular carcinoma cell line (HEP-G2-cells), and rat adrenal pheochromocytoma cell line. In the study, they evaluated the effect of different concentrations of silver nanoparticles on the viability of the cells by MTT assay and compared it with silver ions too. Also the pharmacokinetic degradation was estimated by photometric assays. Furthermore, the data obtained was utilized in preparation of dose-response curves, determination of inhibitory concentration (IC50 value), total lethal concentration, and adverse effect concentration for individual cell lines.

They also employed electric-cell-substrate-impedance-sensing (ECIS) approach to visualize and identify cell behavior (mechanism of cell death) in real time. Conclusively, they reported that mechanism of cell death is dependent on concentration of silver nanoparticles or ions. Cell death may be either due to apoptosis mediated via Caspase 3/7 activity (nanoparticles) or necrosis (silver ions) at lethal dose.

Some of the possible mechanisms of toxicity has been discussed in the following section and depicted in Fig. 10.6.

7.1 Reactive Oxygen Species and Free Radicals

Various charges on surface of inorganic NPs are responsible for electrostatic interaction of these molecules with surrounding biomolecules in vivo. These interactions are basically electron transfer reactions which result into generation of reactive oxygen species (ROS). The formed ROS anticipate other catalytic chain reactions in biological medium and thus disturb the entire homeostasis at cellular level. Additionally, an oxidative stress is generated which further results in formation of free radicals. The oxidative stress leads to recruitment of inflammatory mediators. Moreover, free radicals generated aggravate the toxicity to next level by causing peroxidation of lipidic biomolecules, destabilization of proteins, and damage to genetic material at nuclear level. This entire cascade leads to cellular nanotoxicity in vivo.

7.2 Disruption of the Cytoskeleton Structure

As discussed earlier, inorganic nanoparticles are hydrophobic and possess surface charges; chances of their interaction with cytoskeleton are quite high. It is well known that cytoskeletal structure is very important in terms of receptor modulation and signaling pathway; therefore any changes of disruption may lead to anomalies in cellular functions. In case of diagnostics, it has been observed

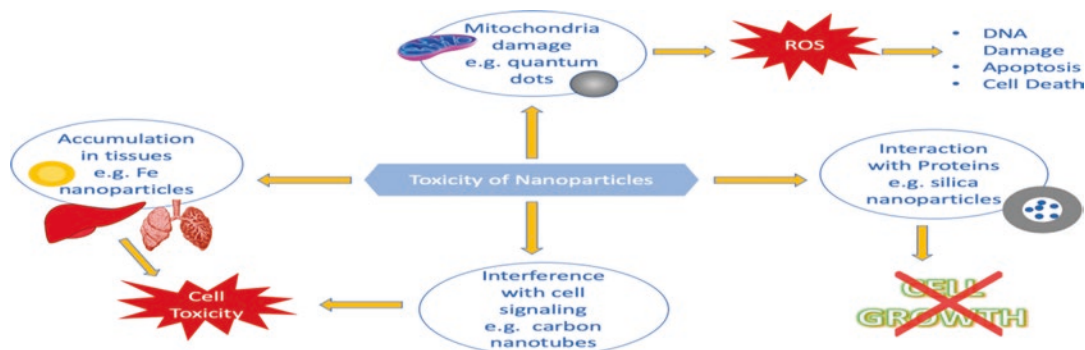


Fig. 10.6 Toxicity mechanisms of nanoparticles

that certain dyes, administered as NPs, are cytosolic in nature and diffuse inside the cells by disruption of cytoskeleton. Such cytolytic interactions have also been observed in case of blood cells, for example, hemolysis and thrombosis have been reported when these nanosystems are dispersed in blood or plasma in vitro.

7.3 Genotoxicity and Alteration of Signaling Pathway

In the previous section, penetrability of inorganic NPDDS has already been discussed. Consequently entrance of these nanosystems inside cells and nucleus cannot be denied. Additionally their capability to bind amino acids/proteins/DNA/RNA impacts the intracellular signaling pathways and thus disturbs the homeostasis of cells. This further leads to alteration in cellular mechanisms of protein synthesis, DNA transcription, RNA translation, and other biochemical processes of cell cycle. Ultimately such cellular changes lead to faulty protein/genetic material synthesis and results into genotoxicity.

7.4 Inflammation Mediated Nanotoxicity

As discussed in the previous sections, electrostatic interaction of inorganic nanoparticles induces oxidative stress inside the cells. As per pathophysiology of cellular mechanisms, it is

proven fact that oxidative stress, free radicals, and ROS inside the cells are the triggers to induce inflammatory cycle. The initial step involves recruitment of inflammatory mediators (TNF α , interleukins, β -cells, cytokines, chemokines, etc.) at the site signal induction. Later on a cascade of inflammatory cycle proceeds till cell death or phagocytosis.

For instance, most of the carbon nanoparticles including graphene and carbon nanotubes induce inflammation-mediated toxicity in various cells like keratinocytes, lung's alveoli, and epithelial cells of bronchus etc.

8 Conclusion

Upon thorough investigation it can be deduced that pharmacokinetics of long circulating inorganic nanoparticles is an outcome of their physiochemical properties and their interaction with surrounding biosystem. Although PK tracking and tracing are difficult, sophisticated technologies of imaging and development of PBPK models have solved these problems up to a great extent. However exact prediction of fate of these nanosystems prepared by different synthetic methods is not possible. The biodistribution and degradation mechanisms are unclear and unusual and require multiple labeling strategies to identify and integrate each individual component in model. However, literature proves that all inorganic (metallic and ceramic) NPDDS undergo degradation mechanism to get dissolved

or disintegrated in vivo. Thus, their circulation and retention time may vary, but ultimately they lose their identity inside biosystems.

References

1. Thomas S, Harshita BSP, Mishra P, Talegaonkar S. Ceramic nanoparticles: fabrication methods and applications in drug delivery. *Curr Pharm Des.* 2015;21(42):6165–88.
2. Inorganic compound | chemical compound | Britannica [Internet]. [cited 2021 Aug 23]. Available from: <https://www.britannica.com/science/inorganic-compound>
3. Sridharan K. The electromagnetic spectrum. In: *Spectral methods in transition metal complexes.* Elsevier; 2016.
4. Drummer S, Madzimbamuto T, Chowdhury M. Green synthesis of transition-metal nanoparticles and their oxides: a review. *Materials.* 2021;14(11):2700.
5. Warner S. Diagnostics + therapy = theranostics: strategy requires teamwork, partnering, and tricky regulatory maneuvering. *Sci.* 2004;18(16):38–9.
6. Sharma H, Mishra PK, Talegaonkar S, Vaidya B. Metal nanoparticles: a theranostic nanotool against cancer. *Drug Discov Today.* 2015;20(9):1143–51.
7. Elsayed I, Huang X, Elsayed M. Selective laser photo-thermal therapy of epithelial carcinoma using anti-EGFR antibody conjugated gold nanoparticles. *Cancer Lett.* 2006;239(1):129–35.
8. Pandey P, Dahiya M. A brief review on inorganic nanoparticles. 2016.
9. Li W, Cao Z, Liu R, Liu L, Li H, Li X, et al. AuNPs as an important inorganic nanoparticle applied in drug carrier systems. *Artif Cells Nanomed Biotechnol.* 2019;47(1):4222–33.
10. Zabielska-Koczywaś K, Wojtawicz A, Użarowska E, Klejman A, Wojtkowska A, Dolka I, et al. Distribution of glutathione-stabilized gold nanoparticles in feline fibrosarcomas and their role as a drug delivery system for doxorubicin—preclinical studies in a murine model. *Int J Mol Sci.* 2018;19(4):1021.
11. Ahmed S, Annu IS, Yudha SS. Biosynthesis of gold nanoparticles: a green approach. *J Photochem Photobiol B Biol.* 2016;161:141–53.
12. Subbaiya R, Saravanan M, Priya AR, Shankar KR, Selvam M, Ovais M, et al. Biomimetic synthesis of silver nanoparticles from *Streptomyces atrovirens* and their potential anticancer activity against human breast cancer cells. *IET Nanobiotechnol.* 2017;11(8):965–72.
13. Wei Q-Y, Xu Y-M, Lau ATY. Recent progress of nanocarrier-based therapy for solid malignancies. *Cancers.* 2020;12(10):2783.
14. Matea C, Mocan T, Tabaran F, Pop T, Mosteanu O, Puia C, et al. Quantum dots in imaging, drug delivery and sensor applications. *Int J Nanomedicine.* 2017;12:5421–31.
15. Sajid MI, Jamshaid U, Jamshaid T, Zafar N, Fessi H, Elaissari A. Carbon nanotubes from synthesis to in vivo biomedical applications. *Int J Pharm.* 2016;501(1–2):278–99.
16. Iqbal P, Preece JA, Mendes PM. Nanotechnology: the “top-down” and “bottom-up” approaches. In: *Supramolecular chemistry.* Wiley: Chichester, UK; 2012.
17. Slepíčka P, Slepíčková Kasálková N, Siegel J, Kolská Z, Švorčík V. Methods of gold and silver nanoparticles preparation. *Materials.* 2019;13(1):1.
18. Makarov VV, Love AJ, Sinitsyna OV, Makarova SS, Yaminsky IV, Taliansky ME, et al. “Green” nanotechnologies: synthesis of metal nanoparticles using plants. *Acta Nat.* 2014;6(1):35–44.
19. Ghosh S, Ahmad R, Banerjee K, AlAjmi MF, Rahman S. Mechanistic aspects of microbe-mediated nanoparticle synthesis. *Front Microbiol.* 2021:12.
20. Spagnoletti FN, Kronberg F, Spedalieri C, Munarriz E, Giacometti R. Protein corona on biogenic silver nanoparticles provides higher stability and protects cells from toxicity in comparison to chemical nanoparticles. *J Environ Manag.* 2021;297:113434.
21. Esther Lydia D, Khusro A, Immanuel P, Esmail GA, Al-Dhabi NA, Arasu MV. Photo-activated synthesis and characterization of gold nanoparticles from *Punica granatum L.* seed oil: an assessment on antioxidant and anticancer properties for functional yoghurt nutraceuticals. *J Photochem Photobiol B Biol.* 2020;206:111868.
22. Pannico M, Calarco A, Peluso G, Musto P. Functionalized gold nanoparticles as biosensors for monitoring cellular uptake and localization in normal and tumor prostatic cells. *Biosensors.* 2018;8(4):87.
23. Lotha R, Sundaramoorthy NS, Shamprasad BR, Nagarajan S, Sivasubramanian A. Plant nutraceuticals (Quercetin and afzelin) capped silver nanoparticles exert potent antibiofilm effect against food borne pathogen salmonella enterica serovar Typhi and curtail planktonic growth in zebrafish infection model. *Microb Pathog.* 2018;120:109–18.
24. Cholula-Díaz JL, Lomelí-Marroquín D, Pramanick B, Nieto-Argüello A, Cantú-Castillo LA, Hwang H. Synthesis of colloidal silver nanoparticle clusters and their application in ascorbic acid detection by SERS. *Colloids Surf B: Biointerfaces.* 2018;163:329–35.
25. Kim D, Kim J, Park Y, il, Lee N, Hyeon T. Recent development of inorganic nanoparticles for biomedical imaging. *ACS Central Sci.* 2018;4(3):324–36.
26. Yu JH, Kwon S-H, Petrášek Z, Park OK, Jun SW, Shin K, et al. High-resolution three-photon biomedical imaging using doped ZnS nanocrystals. *Nat Mater.* 2013;12(4):359–66.
27. Swain PS, Rao SBN, Rajendran D, Dominic G, Selvaraju S. Nano zinc, an alternative to conventional zinc as animal feed supplement: a review. *Animal Nutr.* 2016;2(3):134–41.

28. Jiang J, Pi J, Cai J. The advancing of zinc oxide nanoparticles for biomedical applications. *Bioinorg Chem Appl.* 2018;2018:1062562.
29. Alirezaie Alavijeh A, Barati M, Barati M, Abbasi DH. The potential of magnetic nanoparticles for diagnosis and treatment of cancer based on body magnetic field and organ-on-the-chip. *Adv Pharm Bullet.* 2019;9(3):360–73.
30. McClements DJ, Xiao H. Is nano safe in foods? Establishing the factors impacting the gastrointestinal fate and toxicity of organic and inorganic food-grade nanoparticles. *NPJ Sci Food.* 2017;1(1):6.
31. Yan Z-Y, Yao C-X, Wan D-Y, Wang L-L, Du Q-Q, Li Z-Q, Wu S-M. A sensitive and simple method for detecting Cu²⁺ in plasma using fluorescent *Bacillus amyloliquefaciens* containing intracellularly biosynthesized CdSe quantum dots. *Enzyme and microbial technology* [Internet]. 2018 [cited 2021 Aug 21];119:37–44. Available from: <https://pubmed.ncbi.nlm.nih.gov/30243385/>
32. Meng H-M, Zhao D, Li N, Chang J. A graphene quantum dot-based multifunctional two-photon nanoprobe for the detection and imaging of intracellular glutathione and enhanced photodynamic therapy. *Anal* [Internet]. 2018 [cited 2021 Aug 21];143(20):4967–73. Available from: <https://pubmed.ncbi.nlm.nih.gov/30225468/>
33. Fan H, Yu X, Wang K, Yin Y, Tang Y, Tang Y, et al. Graphene quantum dots (GQDs)-based nanomaterials for improving photodynamic therapy in cancer treatment. *Eur J Med Chem.* 2019;182:111620.
34. Chen F, Hableel G, Zhao ER, Jokerst J, v. Multifunctional nanomedicine with silica: role of silica in nanoparticles for theranostic, imaging, and drug monitoring. *J Colloid Interface Sci.* 2018;521:261–79.
35. Levingstone TJ, Herbaj S, Dunne NJ. Calcium phosphate nanoparticles for therapeutic applications in bone regeneration. *Nano.* 2019;9(11):1570.
36. Ahmed W, Elhissi A, Dhanak V, Subramani K. Carbon nanotubes. In: *Emerging nanotechnologies in dentistry.* Elsevier; 2018.
37. Simon J, Flahaut E, Golzio M. Overview of carbon nanotubes for biomedical applications. *Materials.* 2019;12(4):624.
38. Nile SH, Baskar V, Selvaraj D, Nile A, Xiao J, Kai G. Nanotechnologies in food science: applications, recent trends, and future perspectives. *Nano Micro Lett.* 2020;12(1):45.
39. Huang H, Feng W, Chen Y, Shi J. Inorganic nanoparticles in clinical trials and translations. *Nano Today.* 2020;35:100972.
40. Lin Z, Monteiro-Riviere NA, Riviere JE. Pharmacokinetics of metallic nanoparticles. *WIREs Nanomed Nanobiotechnol.* 2015;7(2):189–217.
41. Hoshyar N, Gray S, Han H, Bao G. The effect of nanoparticle size on *in vivo* pharmacokinetics and cellular interaction. *Nanomedicine.* 2016;11(6):673–92.
42. Wang Z, Malik AB. Nanoparticles squeezing across the blood–endothelial barrier via caveolae. *Ther Deliv.* 2013;4(2):131–3.
43. de Matteis V. Exposure to inorganic nanoparticles: routes of entry, immune response, biodistribution and *in vitro/in vivo* toxicity evaluation. *Toxics.* 2017;5(4)
44. Mitchell MJ, Billingsley MM, Haley RM, Wechsler ME, Peppas NA, Langer R. Engineering precision nanoparticles for drug delivery. *Nat Rev Drug Discov.* 2021;20(2):101–24.
45. Huang X, Zhang F, Zhu L, Choi KY, Guo N, Guo J, et al. Effect of injection routes on the biodistribution, clearance, and tumor uptake of carbon dots. *ACS Nano.* 2013;7(7):5684–93.
46. Niiikura K, Matsunaga T, Suzuki T, Kobayashi S, Yamaguchi H, Orba Y, et al. Gold nanoparticles as a vaccine platform: influence of size and shape on immunological responses *in vitro* and *in vivo*. *ACS Nano.* 2013;7(5):3926–38.
47. Chenthamara D, Subramaniam S, Ramakrishnan SG, Krishnaswamy S, Essa MM, Lin F-H, et al. Therapeutic efficacy of nanoparticles and routes of administration. *Biomater Res.* 2019;23(1):20.
48. Dölen Y, Valente M, Tagit O, Jäger E, van Dinther EAW, van Riessen NK, et al. Nanovaccine administration route is critical to obtain pertinent iNKT cell help for robust anti-tumor T and B cell responses. *OncImmunity.* 2020;9(1):1738813.
49. Wu L, Rodríguez-Rodríguez C, Cun D, Yang M, Saatchi K, Häfeli UO. Quantitative comparison of three widely-used pulmonary administration methods *in vivo* with radiolabeled inhalable nanoparticles. *Eur J Pharm Biopharm.* 2020;152:108–15.
50. Kang H, Mintri S, Menon AV, Lee HY, Choi HS, Kim J. Pharmacokinetics, pharmacodynamics and toxicology of theranostic nanoparticles. *Nanoscale.* 2015;7(45):18848–62.
51. Lasagna-Reeves C, Gonzalez-Romero D, Barria MA, Olmedo I, Clos A, Sadagopa Ramanujam VM, et al. Bioaccumulation and toxicity of gold nanoparticles after repeated administration in mice. *Biochem Biophys Res Commun.* 2010;393(4):649–55.
52. Kim YS, Kim JS, Cho HS, Rha DS, Kim JM, Park JD, et al. Twenty-eight-day oral toxicity, genotoxicity, and gender-related tissue distribution of silver nanoparticles in Sprague-Dawley rats. *Inhal Toxicol.* 2008;20(6):575–83.
53. von Goetz BG, Hungerbühler K. A physiologically based pharmacokinetic model for ionic silver and silver nanoparticles. *Int J Nanomed.* 2013;8:3365–82.
54. Moss DM, Siccardi M. Optimizing nanomedicine pharmacokinetics using physiologically based pharmacokinetics modelling. *Br J Pharmacol.* 2014;171(17):3963–79.
55. Yang G, Phua SZF, Bindra AK, Zhao Y. Degradability and clearance of inorganic nanoparticles for biomedical applications. *Adv Mater.* 2019;31(10):e1805730.
56. Casals E, Casals G, Puentes V, Rosenholm JM. Biodistribution, excretion, and toxicity of inorganic nanoparticles. In: *Theranostic bionanomaterials*; 2019. p. 3–26.
57. Hamidi M, Azadi A, Rafiei P, Ashrafi H. A pharmacokinetic overview of nanotechnology-based drug deliv-

- ery systems: an ADME-oriented approach. *Crit Rev Ther Drug Carrier Syst.* 2013;30(5):435–67.
58. Choi S-J, Lee JK, Jeong J, Choy J-H. Toxicity evaluation of inorganic nanoparticles: considerations and challenges. *Mol Cell Toxicol.* 2013;9(3):205–10.
 59. Saptarshi SR, Duschl A, Lopata AL. Interaction of nanoparticles with proteins: relation to bio-reactivity of the nanoparticle. *J Nanobiotechnol.* 2013;11(1):26.
 60. Tenzer S, Docter D, Kuharev J, Musyanovych A, Fetz V, Hecht R, et al. Rapid formation of plasma protein corona critically affects nanoparticle pathophysiology. *Nat Nanotechnol.* 2013;8(10):772–81.
 61. Balfourier A, Luciani N, Wang G, Lelong G, Ersen O, Khelifa A, et al. Unexpected intracellular biodegradation and recrystallization of gold nanoparticles. *Proc Natl Acad Sci.* 2020;117(1):103–13.
 62. Bailly A-L, Correard F, Popov A, Tselikov G, Chaspoul F, Appay R, et al. In vivo evaluation of safety, biodistribution and pharmacokinetics of laser-synthesized gold nanoparticles. *Sci Rep.* 2019;9(1):12890.
 63. Pandey S, Mahtab A, Kumar V, Jalees Ahmad F, Kamra Verma A, Talegaonkar S. Design and development of bioinspired calcium phosphate nanoparticles of MTX: pharmacodynamic and pharmacokinetic evaluation. *Drug Dev Ind Pharm.* 2019;45(7):1181–92.
 64. Soenen SJ, Parak WJ, Rejman J, Manshian B. (intra) cellular stability of inorganic nanoparticles: effects on cytotoxicity, particle functionality, and biomedical applications. *Chem Rev.* 2015;115(5):2109–35.
 65. de Matteis V, Rojas M, Cascione M, Mazzotta S, di Sansebastiano G, Pietro, Rinaldi R. Physico-chemical properties of inorganic NPs influence the absorption rate of aquatic mosses reducing cytotoxicity on intestinal epithelial barrier model. *Molecules.* 2021;26(10)
 66. Ahmad MZ, Abdel-Wahab BA, Alam A, Zafar S, Ahmad J, Ahmad FJ, et al. Toxicity of inorganic nanoparticles used in targeted drug delivery and other biomedical application: an updated account on concern of biomedical nanotoxicology. *J Nanosci Nanotechnol.* 2016;16(8):7873–97.
 67. Carnovale C, Bryant G, Shukla R, Bansal V. Identifying trends in gold nanoparticle toxicity and uptake: size, shape, capping ligand, and biological Corona. *ACS Omega.* 2019;4(1):242–56.
 68. Sani A, Cao C, Cui D. Toxicity of gold nanoparticles (AuNPs): a review. *Biochem Biophys Rep.* 2021;26:100991.
 69. Yaqoob SB, Adnan R, Rameez Khan RM, Rashid M. Gold, silver, and palladium nanoparticles: a chemical tool for biomedical applications. *Front Chem.* 2020;3:8.
 70. Mao B-H, Chen Z-Y, Wang Y-J, Yan S-J. Silver nanoparticles have lethal and sublethal adverse effects on development and longevity by inducing ROS-mediated stress responses. *Sci Rep.* 2018;8(1):2445.
 71. Sambale F, Wagner S, Stahl F, Khaydarov RR, Scheper T, Bahnemann D. Investigations of the toxic effect of silver nanoparticles on mammalian cell lines. *J Nanomater.* 2015;2015:1–9.



Metallic Gold Nanoparticles: In Vivo Pharmacokinetics and X-Ray Contrast Imaging Studies

Nishith Patel, Sunita Chaudhary,
and Jayvadan K. Patel

Contents

1	Introduction.....	210
2	Synthesis Strategies.....	212
3	In Vitro Analysis of Gold Nanoparticle.....	214
4	In Vivo Pharmacokinetics.....	215
5	Gold Nanoparticle in X-Ray Contrast Imaging.....	217
	References.....	222

Abstract

Among all metal nanoparticles, gold nanoparticle has emerged as a better drug delivery system, with higher efficiency and less side effects due to its unique physical, chemical, optical, and electrical properties, higher drug loading, and target transportation of drug. Due to its unique fluorescent quenching, surface-enhanced Raman spectroscopy, surface plasmon resonance properties, good binding capacity, and tunable property, gold nanoparticles have been widely used in target therapy, in vivo molecule imaging, and various sensor and molecular probe manufacturing. The most commonly used approaches for

the formulation of gold nanoparticles are categorized as physical, chemical, and biological approaches. Controlling gold nanoparticles' size, shape, and morphology plays a critical role in its in vitro analysis, pharmacokinetic study, and biomedical application. In vivo, the pharmacokinetics of gold nanoparticle depends on particle size, shape, surface charge, surface modification, and route of exposure. The generally used animal models for the pharmacokinetic studies of gold nanoparticle are rat and mice. Before checking for its pharmacokinetic study, it has to be analyzed for various in vitro studies using different analytical techniques. Gold nanoparticles act as potential X-ray contrast imaging agents with potent X-ray absorption, low toxicity with potential biocompatibility, and high absorption coefficient.

N. Patel (✉) · S. Chaudhary
Arihant School of Pharmacy and Bio-Research
Institute, Gandhinagar, Gujarat, India

J. K. Patel
Nootan Pharmacy College, Faculty of Pharmacy,
Sankalchand Patel University,
Visnagar, Gujarat, India

Keywords

Gold nanoparticle · Pharmacokinetic study ·
X-ray contrast imaging

1 Introduction

The engineered nanoparticles have attracted strong interest among researchers in the last two decades due to their excellent physicochemical, optical, and electrical properties. The hybridization with organic material makes them diverse and more valid than large-sized materials. With the use in many imaging and therapeutic meanings, nanoparticles (NPs) have proven to be a promising multi-functional platform delivery. For synthesis of NPs, different organic-inorganic or mixture of organic and inorganic resources are used, but among all these, inorganic platforms have succeeded in diagnosis and simultaneous therapy due to their flexibility in alteration, high drug loading capacity, and stability. In biological system, nanoparticle's interaction with cell and organelles varies depending on the type of the cell, targeting organelles, and routes for uptake employed, yet, surface functionalities, particle size, shape, and accumulation affect largely.

The metal nanoparticles especially gold nanoparticles (AuNPs) in recent year have drawn enormous attention and interests from diverse fields of science, due to their specific features, viz., exceptional tunable optical properties; great X-ray absorption coefficient; distinct unique electronic properties; easy and manageable synthesis; strong binding affinity to amines; disulfides, and thiols; and possible control of its physicochemical properties. The electric, magnetic, optical, and catalytic properties of metal nanostructures are influenced by their shape and size. AuNPs have abundant use in the field of biotechnology and biomedicine to deliver therapeutics because they have large surface bioconjugation with molecular probes and the variation in optical properties which are mainly concerned with localized plasmon resonance (PR).

The bulk gold is inert in nature and yellow in color, while AuNPs are having antioxidant properties and are wine red in color. The data shows that the property of AuNPs significantly depends on the particle-particle interaction and agglomeration. Depending on the shape, the size also varies from 1 nm to 5 μm . The shapes may be

spherical, octahedral, decahedral, sub-octahedral, multiple twined, icosahedral multiple twined, tetrahedral, nanotriangles, nanoprisms, nanorods, hexagonal platelets, and irregular shape. Among all these shapes, nanoprisms and triangular-shaped NPs show significant optical properties as compared to the spherical-shaped NPs. Based on morphology, AuNPs are classified into two classes: isotropic AuNPs and anisotropic AuNPs. The isotropic AuNPs due to their uniform surface characteristics exhibit just one plasmon absorption band. The anisotropic AuNPs depending on variations in morphology show multiple plasmon absorption bands, and their morphology can be tuned easily to provide better scanning deep within biological tissues. Several studies have conformed not only optical but also structural, catalytic, magnetic, and electronic properties better in of anisotropic AuNPs compared to spherical AuNPs. The limitations of Raman spectroscopy in mapping any solid liquid and gasses and even cells due to Raman scattering now become possible with the use of metal nano-materials. The phenomenon is well known as surface-enhanced Raman spectroscopy.

1.1 Characteristics and Application of Gold Nanoparticles

Surface area to volume ratio is another important characteristic where nanoparticle simply permits them to interact with other particles and possible to make diffusion faster with increasing surface area to volume ratio. The field is becoming more interesting as the treatment to affected tissue and cell targeting is possible without damaging healthy tissue and cells. The broad working range of wavelengths and high quantity factor (HQF) of AuNPs make them special for enhanced fluorescence and for therapeutic purposes. Because of small-sized particles with HQF of AuNPs, while used as targeted drug delivery respond significantly to the magnetic field that varies with time, they transfer enough toxic thermal energy to the tumor cells as hyperthermic agents. This property has enabled AuNPs in the field of radiation ther-

apy to enhance radiation. Due to HQF of AuNPs, enhanced electromagnetic field and fluorescence is generated. The AuNPs as fluorescent NPs show good biocompatibilities for molecular imaging of many metabolites and enzymes during identification of cellular functions in cancer (Fig. 11.1). The refractive index detection nanoparticles similarly have added application in the improvement of field-sensitive optical method. AuNPs have also gained advantages over traditional iodine-based X-ray CT molecular probes in CT imaging. The use of AuNPs in molecular probe has shown enhanced absorption coefficient than iodine because gold has higher atomic number as well as electron density that drastically increases CT contrast than in iodine-based molecular probes. All the above AuNPs have one more characteristic advantage that they are non-cytotoxic. Due to such characteristic properties of gold in NPs, the role of AuNPs in biological sciences has become very important. The tunable optical properties, small size with large surface, configuration, and crystallinity, nanoparticles have proven to be unique therapeutic agents with high penetration, drug loading, and cell targeting capacity. In biomedical science, the use of AuNPs in drug therapy, cell or tissue imaging for tumor,

photo-thermal therapy, and identification of pathogen in samples has become possible because of surface plasmon resonance (Fig. 11.1). The unique property of NPs in conjugation with gold to deliver has also made gene delivery possible along with its morphological characterization, protein structure elucidation, and identification of strategy for conjugation (Fig. 11.1).

AuNPs specially rod-shaped NPs have several applications in the area of in vivo imaging due to the absorption and scattering of light in the near-IR region due to its characteristics surface plasmon resonance. Due to the very small size of colloidal AuNPs, they have also expanded their potential application through chemical methods. These NPs easily penetrated to the target cells because of their characteristic small size similar to the biological molecules like proteins and DNA.

The low toxicity, good capacity to bind with a widespread choice of organic molecules, and tunable physicochemical properties make them excellent for use as therapeutic agents or drug delivery system at the target site that can provide improvised efficiency of active moiety. The use of gene gun fabricated using gold nanoparticles is very well known for providing excellent delivery

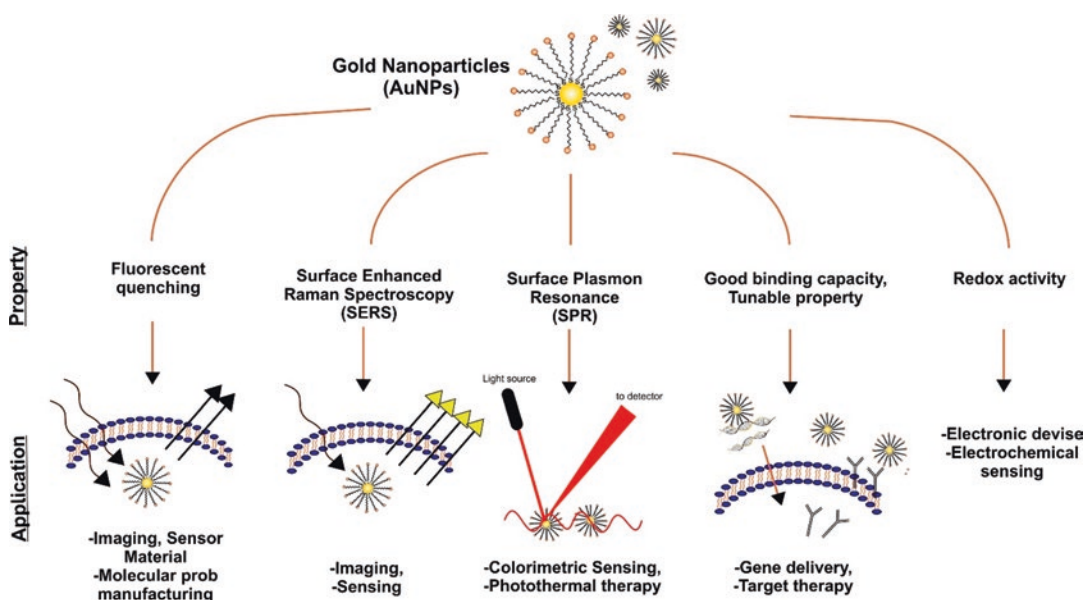


Fig. 11.1 Application of gold nanoparticles (AuNPs) according to their properties

of gene. It is being widely used for epidermal delivery of DNA vaccines, and this method is one of the finest approaches in medicine delivery.

AuNPs' strong affinity for alkynes as compared to other transition metal catalysts makes them superior to homogeneous formulations. The homogeneous systems are more costly and not environmentally friendly. Compared to that, due to quick reduction of active gold complexes into inert metallic gold all through the C-H alkyne activation, they are considered the system of choice. Due to the unique optical and electronic properties of gold nanoparticles, they have become the choice in color-detecting probes in the progress of analytical techniques.

2 Synthesis Strategies

The methods for the development of AuNPs follow the few common technique and same as the development of NPs in general. A variety of methods for the synthesis of AuNPs include chemical, physical, thermal, electrothermal, and biological methods.

2.1 Chemical Methods

In chemical methods, one of the approaches is reduction by agents, viz., hydrazine, thiols, borohydrides, amino boranes, formaldehyde, polyols, hydroxylamine, oxalic and citric acids, hydrogen peroxide, sugars, carbon monoxide, hydrogen, sulfites, acetylene, and several other reducing agents.

Another method in chemical method for the synthesis of AuNPs is the prevention of aggregation of particles using stabilizing agents, viz., sulfur ligands (thiolates), trisodium citrate dihydrate, oxygen and nitrogen-based ligands (including heterocyclic compounds), dendrimers, polymers and surfactants, and phosphorus ligands.

2.2 Turkevich Method

This method for formation of AuNPs is by reduction of hydrogen tetrachloroaurate HAuCl_4 in

boiling water using trisodium citrate (Fig. 11.2a). Citrate here is acting as stabilizing as well as reducing agent. Several modifications have been given thereafter by different researchers to provide improved and better stability, particle size, and narrow size distribution [34].

2.3 The Brust-Schiffrin Method

This method suggests the synthesis of controlled-sized AuNPs with low dispersibility. The method served an easy way to prepare AuNPs with high thermal and air stability. The method involves transfer of AuCl_4 from water to toluene phase using phase-transfer agent. Tetraoctylammonium bromide was used as the phase-transfer agent in this method along with HAuCl_4 and reduced by NaBH_4 , in the presence of dodecanethiol (Fig. 11.2b). Immediately after addition of NaBH_4 for reduction of AuCl_4 , the color changes from orange to deep brown. That clearly specifies the formation of AuNPs [7].

2.4 Reetz and Helbig Method

The method is chemical method to produce confined-sized AuNPs with the aid of cathode and anode charges and additional stabilizers. The method is also known as electrochemical method to produce AuNPs [30]. The method is based on the simple use of anode and cathode electrode cells to perform oxidation and reduction, respectively, as schematically depicted in Fig. 11.3.

The method since then has become an interest of researchers as the yield can be tuned using this simple equipment, with high precision, no requirement of high temperature, and low cost. Several modifications have been experimented and with successful results from time to time on this method to obtain AuNPs with the desired properties.

2.5 Growth Method

The method is simple and quick based on seed growth process. Narrow size distribution can be

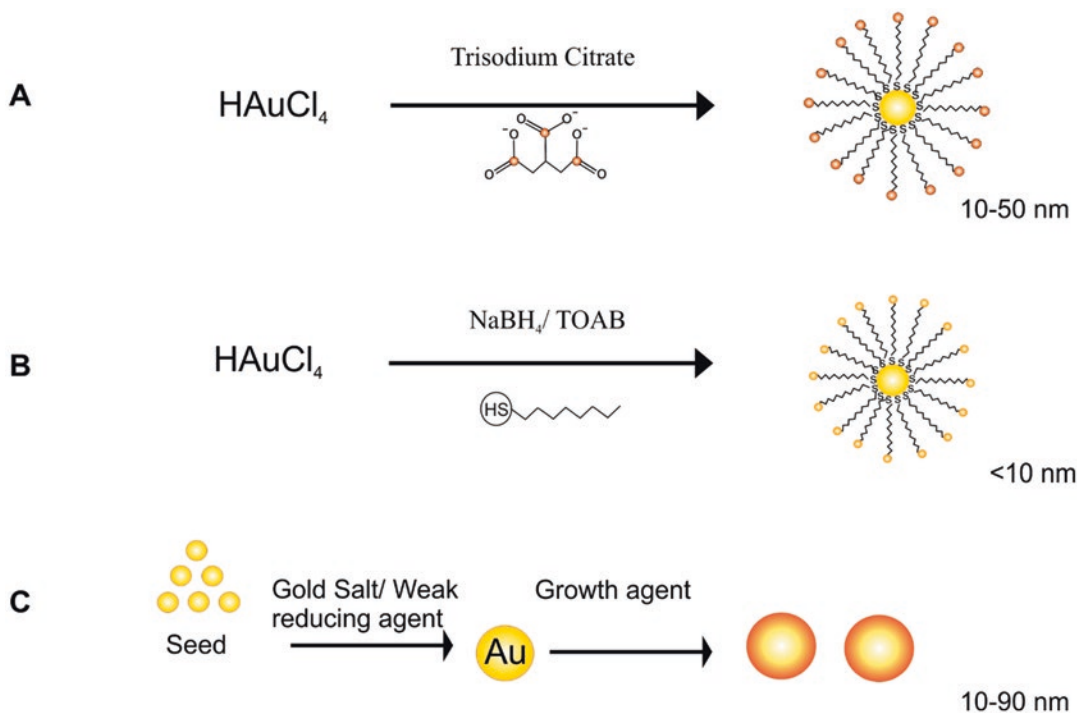


Fig. 11.2 (a) Turkevich method for the formation of AuNPs, (b) the Brust-Schiffrin method for the formation of AuNPs, (c) growth (seedling) method for the formation of AuNPs

achieved by this method. Seeds AuNPs are prepared by conventional method and then capping done by suitable metal or capping agent. The reduction method has been used for the preparation of dendrimers/Au nanoparticles. Jana et al. [19] prepared dendrimer AuNPs by the reduction of aqueous solution of HAuCl_4 and dilute solution of dendrimers by sodium borohydride (Fig. 11.2c).

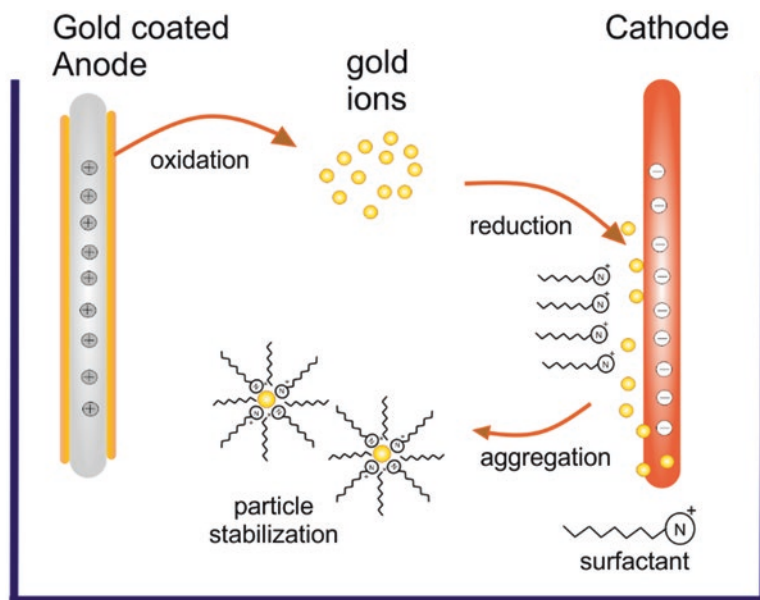
2.6 Physical Methods

The physical method uses radiation to synthesize AuNPs. The γ -irradiation, UV radiation, microwave irradiation, and even direct sunlight are also used for the synthesis of gold NPs. Among them, preparation of AuNPs using γ -irradiation is a good method that gives controlled-sized NPs with high purity. This method can provide 5–40 nm size distribution of AuNPs. Different stabilizers can be used in this method, viz., natural polysaccharide alginate and bovine serum albumin protein.

2.7 Green Method

Usually, the chemical methods are providing expensive NPs. The methods require reducing reagents for stabilization of NPs but they are toxic. The disadvantage limits the applications of NPs. The green methods for the synthesis of NPs are the methods that develop cost-effective and eco-friendly nanoparticles that do not use any toxic chemicals. The green method using plants or plant extracts is receiving importance, because of non-toxicity, source availability, low cost, and biodegradable nature. *Aloe vera*, *Medicago sativa*, *Cinnamomum camphora*, *Coriandrum sativum*, *Pelargonium graveolens*, *Terminalia catappa*, *Azadirachta indica*, *Zingiber officinale*, *Allium cepa*, and lemon-grass are the different plants that have been reported [27]. Apart from that in green method, NPs are synthesized from enzymes, animal resources, and microorganism. High-power ultrasounds and solar energy (sunlight) both can act as reducing agents for the synthesis of AuNPs.

Fig. 11.3 Reetz and Helbig method for formation of AuNPs



3 In Vitro Analysis of Gold Nanoparticle

Before going for pharmacokinetic study of AuNP, it should be necessary to evaluate for particle size and measurement of gold content. Size and morphology are very important factors for therapeutic effect and efficiency of contrast, and they also affect cellular uptake. Optical properties of AuNP are highly affected by changing shape. Dynamic light scattering (DLS) is used to measure hydrodynamic diameter, and transmission electron microscopy (TEM) is used to determine their core diameter. Zeta potential is used to measure nanoparticle surface charge. Gold concentration is measured by inductively coupled plasma optical emission spectrometry.

3.1 Dynamic Light Scattering (DLS)

Gold nanoparticles consist of two phases like gold core and coating where both phases have different refractive index. Dynamic light scattering is used to determine particle size of AuNP [20]. DLS measures the light scattering from gold core, its coating and also from adsorbed

water molecules. So DLS measurement is better for gold nanoparticle compared to TEM for complex shape determination. DLS also give determination of particle size in cell culture media to mimic particle size in biological system. Generally, it was seen that there is decrease in light scattering intensity with decrease in AuNP concentration. DLS measures fluctuation in intensity of light which are scattered from particle in suspension which undergoes Brownian motion with respect to time. Diffusion coefficient of particle is determined by measuring fluctuation intensity, and it ultimately gives particle size.

3.2 Zeta Potential

Surface charge on AuNP is determined by measuring its zeta potential. By measurement of zeta potential, properties of nanoparticle can be predicted in biological media. It was observed that highly positively charged nanoparticles tend to aggregate in serum, with less time of retention and circulation. So, it will be rapidly engulfed by reticuloendothelial system, but charge on AuNP is negative or near to neutral which makes it more stable in serum and avoid phagocytosis.

3.3 Transmission Electron Microscopy (TEM)

Size and shape of AuNP can be determined by TEM also. Generally, TEM use sample droplet on carbon-coated copper grid and then analyzed for particle size, but for complex type of structural analysis, dried droplet of sample is analyzed by TEM tomography in which sample is analyzed by many angles by rotating the grid. Then images are processed computationally which create three-dimensional image of complex AuNP which is entrapped in polymer matrix.

3.4 ICP-MS

Inductively coupled plasma is a novel technique for more precise dosing measurement of AuNP. Previously, ICP-OES technique was used for quantitative analysis of gold nanoparticle, but when more dilution of gold nanoparticle injected in animal, the sensitivity of ICS-OES is reduced. So, it requires ICP-mass spectrometry (ICP-MS). The analysis of the optimized ICP-MS method offers a quantification limit for Au (III) in colloid samples of 0.15 $\mu\text{g/L}$ that corresponds to 4.40 9109 AuNPs/L considering spherical AuNPs 15 nm sized [3].

3.5 Determination of Gold Nanoparticle Uptake

Cellular uptake of AuNP is very important in determining biomedical application. This helps to check the ability of stealth gold nanoparticle to avoid cellular uptake and also to confirm the cellular uptake by targeted cell. Study of cellular uptake is required to get information about expected therapeutic effect; less therapeutic effect is expected with minimum AuNP uptake. The effect of size and shape of gold nanoparticle on mammalian cell uptake was studied by Chithrani et al. [10]. It was observed that rod-

shaped gold nanoparticle showed less uptake than spherical shape. There is a quantitative comparison of gold nanoparticle which is surface modified by citrate and transferrin; it was found that citrate-coated gold nanoparticle showed greater cellular uptake. ICP-OES is more sensitive than CT for determining gold nanoparticle uptake.

4 In Vivo Pharmacokinetics

Before supplying any therapeutic formulation to the patient, thorough pharmacokinetic studies are required to perform. In the case of gold nanoparticles, there are several scientific literature on manufacturing rather than their pharmacokinetic study showing the reason of limited widespread application. Attention is required in pharmacokinetic studies also to explore their therapeutic purpose.

AuNPs are having large surface area so that they can be easily surface modified. Gold nanoparticle showed required sufficient physical electrical, chemical, and optical properties. So, it is widely used for various drug deliveries. The main drawback of AuNP is its safety concerning in vivo, so it requires a clear concept and understanding of gold nanoparticle pharmacokinetics and its risk assessment. Generally pharmacokinetic analysis is carried out based on physiologically based pharmacokinetic (PBPK) modeling as per literature is concerned. It involves the study of absorption, distribution, metabolism, and excretion of gold nanoparticle when given by i.v. or orally. There are various types of surface-modified gold nanoparticle studied, but the most common is PEG-coated gold nanoparticle as PEGylation is carried out to increase circulation time in *blood*. In one of the efforts to develop PEG-coated hollow gold nanoparticle, blood circulation was found to be 8 h in mice with a particle size of 43 μm [37]. It was also found that gold nanoparticle with smaller particle size up to 20 μm has longer half-life compared to larger size up to 80 nm.

4.1 Absorption

Pulmonary Absorption

It was observed that the translocation of gold nanoparticle is highly affected by particle size when passing through air-blood barrier. In one study, it was seen that by decreasing particle size of gold particle, the translocation of particles is increased in rats. To find the relationship between particle characteristics and particle size, the study of biokinetics of inhaled NPs and distribution of nanoparticle by PBPK model found that translocation was inversely related to particle size [4]. When given in vivo, higher translocation of gold nanoparticle was found with anionic surface when compared to cationic surfaces.

Gastrointestinal Absorption

The study about in vivo gastrointestinal absorption of positively and negatively charged AuNPs from gastrointestinal tract (GIT) has shown characteristic behavior of AuNPs [31]. After instillation of radiolabelled negatively (1.4–200 nm) or positively (2.8 nm) charged AuNPs intrasophageally in rats, AuNPs were able to cross the GIT, but the absorption was unfinished even after 24 h (i.e., 17.2–74.1% endured in the GIT and internal feces), and absorption competence was very low, ranging from 0.37% for small sizes (1.4–2.8 nm) to 0.01% for large size (200 nm). Few such in vivo observation shows size- and surface charge-dependent absorption of AuNPs.

Absorption and Penetration from Skin

Several factors affect any formulation to be penetrated into the skin, including physicochemical property; dose size; surface charge; lesion on the skin; age; skin disease such as irritant dermatitis, atopic eczema, and psoriasis; receptor fluid composition; ultraviolet light exposure; surfactants; and solvents. The same factor also affects penetration and absorption of AuNPs from skin. Due to metallic material during evaluation, analysis with TEM makes it easy to trace the progression of AuNPs beneath the skin.

4.2 Distribution

The factors affecting distribution of AuNPs in biological system rely on several factors including morphology with size, charges on surface, opsonization, surface characteristics, and route of administration. Looking at the effect of morphological characteristics, irrespective of size of AuNPs, distribution occurs predominant in the liver, lymph nodes, and spleen. With reduction in the size of AuNPs, more distribution, including in the liver, spleen, blood, kidney, lymph, brain, and spinal cord, occurs. Depending on the route of administration, AuNPs are distributed in the liver spleen, kidneys, and hepato-biliary system. The administration in lungs usually retains (99%) at the site only. The i.v. administration of small-sized (18 nm) AuNPs accumulated in the liver, spleen, kidneys, and hepatobiliary system, predominantly (90–95%) in the liver, while it completely gets cleared from the blood. To prolong circulation of AuNPs in blood and decrease random uptake by RES, surface coating of NPs is a very well-known phenomenon. PEG is an inert and a compatible component that have shown success in surface coating of NPs to prolong blood circulation time when the target is the tumor tissue rather than the liver, spleen, or kidneys. One more study has shown that the biodistribution of AuNPs depends on the dose of administration [23]. The biodistribution of AuNPs in several studies shows that particle size <200 nm can pass through BBB although penetration depends on size and higher in smaller NPs. The suggested mechanism of BBB penetration is to be passive translocation but limited by the pore size of tight junction or by receptor-mediated transcytosis. The pore size of a tight junction in the BBB is about 20 nm, and thus <20 nm NPs will have easy transportation capacity through this space. Tumor tissue shows good penetration due to its characteristic composition (both capillary permeability and vascular density are high) and absence of lymphatic defense system. The high penetration rate raises issue of rapid clearance and AuNPs do not remain or accumulate in tumor tissue.

4.3 Metabolism

The surface coating with PEG is biocompatible and has greatly enhanced capacity of any NPs not only to penetrate but also to retain in every desired biological site. At the time of metabolism, the polymer or similar coating component cleaved off and then degrade. This is a general metabolic pathway for bioconjugate NPs designed as drug carriers. In the case of AuNPs coated with peptides in a wide range of mammalian cells (including adherent and non-adherent cells, mouse and human cell lines), the *in vitro* studies have shown that upon internalization of biological molecules attached to AuNP surface, they are degraded within the endosomal compartments through peptide cleavage by the protease cathepsin L. Yet studies are still required further on metabolism of AuNPs.

4.4 Elimination

The AuNPs can be excreted from the body via the usual route, i.e., renal and hepatobiliary clearance. Though several factors may affect clearance of AuNPs, including size and surface chemistry, elimination of AuNPs is significantly low due to opsonization with persistent and main build-up in the body's metabolism hub liver, spleen, and mesenteric lymph node, even for smaller AuNPs.

5 Gold Nanoparticle in X-Ray Contrast Imaging

Gold nanoparticles (AuNPs) and silver nanoparticles are the regularly used in biomedical application as a nanostructure. Silver nanoparticles have minimum structural stability and maximum cellular toxicity compared to gold nanoparticle. When gold nanoparticle is compared to bulk gold, it has completely different chemical and physical properties. Due to exclusive properties of gold nanoparticle, they have various applications in biological imaging, X-ray contrast imaging and plasmonic biosensing, and contrast

enhancement of X-ray computed tomography. Iodinated molecules are having low molecular weight with high water solubility which shows low toxicity, but blood circulation time is short and easily eliminated from the kidney. So, it requires multiple injection with risk of thyroid dysfunction. In X-ray contrast imaging, AuNP has gained maximum consideration because of many advantages like high absorption coefficient, easy to handle using synthetic process, nontoxic, surface modification for stability, and targeted drug delivery.

5.1 Why Gold Particle in X-Ray Imaging

Gold solution in colloidal range has been used for various applications. One of the beneficial physical properties of Au is its high capacity of X-ray absorption when it is subjected to X-ray imaging. Compared to other contrast agent like barium sulfate and iodine, gold shows a reasonably high X-ray attenuation coefficient specially used for clinical CT at specified energy level. Contrast imaging window of AuNP is higher compared to iodinated molecules because it has longer vascular retention time and higher molecular weight. AuNPs can be easily surface modified to increase colloidal stability and targeted delivery. One of the first AuNPs developed as an X-ray contrast agent was a 1.9 nm spherical formulation and was shown to provide strong enhancement of the major vessels. However, due to the small size of the agent, the particles were rapidly washed out from renal route, so demonstration by high attenuation in the bladder is taken after 15 min of injection as an image. Increasing the size and/or modifying the surface functionality of AuNP has been shown to improve circulation time, as found in studies of AuNP whose core size was around 10 nm. After coating with PEG, the nanoparticles had an overall size of 38 nm. These nanoparticles were not renally cleared and provided vascular contrast over a period of 12–24 h [8].

Nanoparticle-based CT contrast agents and the *in vivo* studies can be divided into three main categories:

- (a) *Blood pool CT contrast agents*: Blood pool contrast agents are used to increase the retention time of nanoparticle in circulation by restricting the diffusion by the vascular membrane to allow a longer imaging time period and window.
- (b) *Passive targeting* gives broad-spectrum accumulation of AuNPs within a interested site by getting maximum advantages of enhancement of permeability and retention effect. Passive targeting allows accumulation of appropriate size nanoparticle in tumor tissue compared to normal surrounding tissues.
- (c) *Active targeting*: By active targeting, delivery of contrast agent at specific site of interest can be done, and retention of contrast agent can be increased by surface functionalization with biomolecules like peptides or antibodies which reveal a specific affinity for that site of action.

5.2 Design of AuNPs as X-Ray Contrast Agents

Gold nanoparticles are specifically designed to observe the necessary functional requirements for a contrast agent in biomedical application.

The different types of functional requirements include its mode of delivery because contrast agent should be easily delivered in vivo and also able to transport at the site of action. Secondly, the contrast agent should be non-toxic; it should not give any type of adverse effect at the time of delivery and clearance. The contrasting agent can be able to retain and accumulate at targeted site or organ like blood and cancer cell (Table 11.1). Specifically, AuNP has the capacity to increase contrast enhancement of targeted organ by increasing X-ray attenuation. In designing AuNP, it is necessary to achieve functional requirement of gold nanoparticle, and its specific properties can be controlled by its structural modification. Many properties of gold nanoparticle like its X-ray attenuation coefficient, stability of colloidal Au in body fluid and during storage, retention time in blood circulation, and its biodistribution

and cytotoxicity are major concern. Many structural properties size, shape, morphology, molecular functional group, mass concentration, and composition of AuNP are considered for governing the physical, chemical, and biological properties of nanoparticle [21]. AuNP when used as contrasting agent can accommodate higher payload compared to small molecules contrast agent. And it is widely used in specific biomedical applications due to their shape, size, and surface chemistry. AuNP showed long blood circulation time in terms of hours, while iodinated contrast agent media has less circulation time of few minutes. Higher attenuation properties of AuNP are due to its high density and higher atomic number, i.e., 79. Additionally, it is inert and biocompatible with other moieties for surface modification using different ligands. They have strong affinity to interact with molecules which contains sulfur which generally includes thiols, disulfides, and amino acids. And there is a formation of self-assembled monolayers formed by capping of AuNP with sulfur-containing molecules [5]. This binding is used to modify surface properties of particle, e.g., stability of AuNP is increased by surface modification of AuNP using tri-n-octylphosphine oxide (TOPO), oleylamine, and octadecyl. Many key properties required for designing of AuNP are presented below.

Composition

Composition plays a very important role in X-ray attenuation and hence its ability to enhance contrast effect, is directly related to the X-ray attenuation, its density in bulk, atomic number, spectrum of x ray source energy and presence of x ray absorption edges.

Size

X-ray imaging ability of AuNP is highly affected by particle size; it finally affects biocompatibility and therapeutic application. Many scientists have focused their research on the effect of size, shape, and concentration of AuNP on cellular uptake of gold nanoparticle for the cellular contrasting application. AuNP when used in size range of 3–50 nm has greater enhancement in contrast topography imaging and also radiotherapy. It was

Table 11.1 X-ray contrast study in animal using surface-functionalized gold nanoparticle

AuNP dose	AuNP size	Surface	Model	Delivery Method	Contrast enhancement	References
1.4 mg/kg	28 (7 nm and 38 (8 nm	Hetero bi-functional polyethylene glycol (h-PEG)	Mouse	i.v.	Lymph node	[12]
85 mg kg ⁻¹	20 nm	(GA-AuNP)	Swine	i.v.	Phantom	[6]
2700, 1350	1.9 nm	Citrate	Mouse	i.v.	Tumor	[15]
1.28 gkg ⁻¹	3–6 nm	Alpha-lactalbumin	Mice	i.v.	Breast tumor	[35]
36 mg/ml	0.8 μm,	Lipiodol microemulsions-Au nanoparticle colloids	Mice	i.v.	Tumor	[9]
200 mg/mL	1.9 nm	Gold nanoparticle	Mouse	i.v.	Kidney	[26]
2.5 μmol Au/g body weight)	38 nm	PEG-coated colloidal AuNPs	Mice	iv	Tumors	[8]
65 μg per one million cells	5 and 40 nm	Citrate-coated spherical AuNPs	Mice	iv	Cancer	[17]
2.7 mg/g	10–15 nm.	citrate	Mice	i.v.	Infected muscles	[1]
100 μl	20 nm	PEG	Mice	i.v.	Myocardial infarction	[33]
2.7 g Au/kg	1.9 nm	AuNP	Mice	i.v.	Tumor	[15]
3 × 10 ³ μg/ml, 200 μL)	13 nm	FA-Cys-AuNPs	Mice	i.v.	Tumor	[22]
200 mg/mL	1.9 nm	AuNPs	mouse	i.v.	Tumor	[38]
3.2 g Au/kg	38.5 nm	AuNP	mice	Intraperitoneal	Tumor	[2]
500 mg per kilogram	3.1 nm	Au-HDL	mice	i.v.	Atherosclerosis	[11]

found that among the given range of size of gold nanoparticle, specifically 13 nm particles have excellent contrast ability and significant radioactive disruption [18]. Ultimately requirement for greater attenuation is small size with higher concentration exhibit greater effect.

X-Ray Attenuation

Capacity of substance or tissue to absorb X-rays' energy is dependent on its atomic number and density. Higher atomic number and density of tissue can absorb more X-rays. So, elements like barium, iodine, and gold exhibit higher atomic number, revealing a high mass attenuation coefficient (μ/ρ). Thus, gold can be excellent candidates for X-ray contrast agents specifically in soft tissues. Among all different elements used for contrast imaging, gold has an atomic number of 79 which is higher compared to iodine, i.e., 53, and barium, i.e., 56, and also a density of 19.3 g/cm³. So it can able to absorb more X-rays at specific energy levels. Initial intensity (I_0) of X-ray photon energy autonomously influences the X-ray attenuation coefficient. As the increase of

incident photon energy from the X-ray source, it decreases the mass attenuation coefficient. Gold can be able to give improved contrast enhancement due to high X-ray attenuation coefficient compared with both iodine and barium. The photon attenuation coefficients of gold at 100 KeV is 5.16 and for iodine at same energy of radiation is 1.94. It means that gold has a tendency to give 2.7 times higher contrast X-ray imaging per unit mass than iodine. Various sizes and shapes of AuNP affect the scattering of visible light and its absorption of visible light.

Mass Concentration

The X-ray attenuation capacity of element with high atomic number is primarily directed by photoelectric absorption, which depends on variation in mass concentration. The higher is the mass concentration, the greater is its X-ray attenuation. So ultimately, it increases higher pay load at site of delivery which enhance the contrast in imaging. There is a possibility of adverse effect in vivo by giving large dose of exogenous contrast media. Therefore, there is a need to determine

exact dose of contrast agent to enhance contrast effect by avoiding cytotoxicity. Relatively higher mass concentration of contrast agent is required in computational topography (CT) compared to other techniques for imaging; it is the main limitation of CT. Thus, a body organ like bone having a high background X-ray attenuation will require a higher mass concentration of gold to produce same enhancement in contrast imaging compared to organ with low-attenuating background like tumor [24].

Contrast Enhancement

Contrast enhancement is directly related to the mass concentration at site of application. Generally, differential contrast of 30 house field unit (HU) is necessary to detect 80 keV. Based on the background signals at the site of application, dose of AuNP is differing depending upon the need of contrast enhancement. Based on mass attenuation coefficient with the change in mass fraction of the contrast agent, the minimum detectable mass fraction can be calculated.

5.3 X-Ray Imaging Technology Using Gold Nanoparticle

Magnetic Resonance Imaging (MRI)

Magnetic resonance imaging (MRI) is a non-invasive technique for imaging normally used for diagnosis of disease, molecular imaging, and cell tracing. This is due to its more ability to give high geotemporal resolution with its excellent ability to contrast soft tissue. AuNPs having a diameter of less than 2.5 nm behave like a semiconducting quasimolecules and possess magnetic properties based on their attached ligand for protection. The synthesis and characterization of new derivatives of gold nanoparticles as MRI contrast agents also have been carried out [32]. Gold nanoparticles are stabilized by dimethylaminopyridine (DMAP). Average diameter of nanoparticle was found to be 2.25 nm. The DMAP molecules were then replaced by Gd-DTPA-based chelates along with butanethiol molecules. The 38% higher relaxivity for butanethiol molecules inserted gadolinium-DTPA nanoparticle is highly attrib-

uted to the restricted tumbling of ligand molecules at the gold nanoparticle surface.

Computed Tomography (CT) and Nuclear Imaging

Computed tomography (CT) is a commonly used technique for imaging that uses X-rays, and it uses detector array which create cross-sectional images of the body with high geotemporal resolution [28]. This imaging technique gives idea about 3D details of organs for diagnosis of disease and their therapy. Main drawback of this imaging is sensitivity towards soft tissue. And CT contrast agents are used to improve the sensitivity of CT imaging. AuNP is extensively used to investigate the effect of contrast agent to improve imaging in CT. AuNP has a capacity to absorb X-ray due to higher electron density compared to tissue, so that it can produce direct contrast effect at its own position. The investigation shows that the effect of AuNP is threefold higher compared to iodine as contrasting agent in CT at 100 keV [16]. The advancement in CT machine minimizes the movement in objects and is able to get more enhanced imaging of coronary arteries with gold, even in obese patients.

Fluorescence Imaging

AuNP exhibits special optical property of surface plasmon resonance, but when size of particle is reduced to sub-nanometer range, then gold particle exists in the form of nanoclusters and possesses photoluminescence. AuNPs possess optical properties by which they are activated by light and will produce oxygen free radical. Due to these optical properties, it becomes good candidates as photosensitizers for photodynamic therapy of cancers. The synthesis and characterization of highly luminescent folate-functionalized Au₂₂ cluster Au₂₂-FA showed the brightness of 4.77 mM⁻¹ cm⁻¹ [29]. The presence of folate groups on gold particle gives rise to additional luminescence enhancement by energy transfer sensitization.

Photoacoustic Imaging

Photoacoustic imaging (PAI) is also a non-invasive imaging technique which observes the

anatomy physiology and functional and molecular signals of diseased tissue with great resolution. Due to the absence of ionizing radiation, photoacoustic imaging is safer than nuclear imaging and fluorescence imaging. AuNPs exhibit surface plasmon resonance (SPR) effect due to its strong and tunable optical absorption; it can be possible by the presence of free charges on the surface of AuNPs which oscillate with the electromagnetic field, which gives optical absorption. Photoacoustic imaging using AuNP is utilized to study brain vasculature and its functionality in small animals. The research demonstrated that the application of PEGylated AuNPs having central core of silica is used for PA imaging given by i.v. [36]. It is analyzed in NIR region to improve contrast of the brain vasculature of a rat compared to background tissue. The images present a gradual enhancement of the optical absorption in the brain vessels by up to 63% after three sequential administrations of AuNPs. The photoacoustic images confirmed the good clarity in vasculature of brain in rat with effective enhancement in absorption in blood. It showed 81% over the intrinsic contrast after 2 h from injection.

X-Ray Fluorescence Imaging (XRF)

Generally, X-ray fluorescence imaging technique involves the excitation of XRF photon with the X-rays. XRF photons and scattered photons get identified and analyzed to quantify the distribution of element in tissue. This process is known as X-ray fluorescence computed tomography (XFCT), and this is one of the promising approaches for identification, quantification, and distribution across the space of organ for that element. This technique works better over X-ray imaging and fluorescence imaging. Due to high energy of XRF (30–70 keV), it is easy to penetrate biological tissues for imaging in deeper organ compared to other techniques. In one of the study, the localization of AuNP in early detection of tumor and pharmacokinetic parameters were studied. They demonstrated specific localization to sites of disease by adapting gold nanoparticles with small targeting ligands in murine spinal cord

injury models using X-ray fluorescence imaging (XRF) X-ray imaging technology [14].

5.4 Toxicity of Gold Nanoparticles

When any nanomaterial is subjected to in vivo, then potential toxicity is a matter of concern when it is evaluated in vitro and in vivo for safety. There is a variation in interaction of AuNP with biological molecules because of difference in parameters like size, shape, surface charge, and coating material for surface modification. It is generally said that plain gold nanoparticle is toxic compared to surface-modified AuNP. By proper surface modification, toxicity can be reduced or even eliminated. AuNPs of less than 2 nm in size have the ability to bind irreversibly with biomolecules like DNA, so they induce more toxicity compared to particle with size more than ≥ 3 nm. It was found in the study that AuNPs with more than 3 nm particle size are considered to be nontoxic in the body as well as in vitro. However, depending upon the retention time of AuNP in specific organ, it will have more impact on long-term toxicity. Some laboratories have investigated the cellular toxicity of gold nanoparticles with regard to particle size, shape, and surface group. In one more study, gold nanoparticles with 2 nm diameter were analyzed which were surface modified with cationic and anionic group on surface in three types of cells [13]. It was observed that cationic is more toxic even in less concentration compared to anionic. This is due to the electrostatic interaction between cationic particle and anionic membrane. The study of different sizes and shapes of gold nanoparticle for its cellular uptake in cell line of human cervical cancer cell was done [10]. They found that average particle size around 50 nm spheres was easily taken up by cell line compared to small and larger size than 50 nm, and it was also seen that sphere-shaped particle can be easily taken up than nanorods. AuNP surface modification is required to reduce toxicity, and also its biocompatibility can be increased for biomedical application. The generally used technique for modification is

PEGylation. The most commonly used surface modification is PEGylation. It was found that PEG is more likely to enhance the solubility, which reduce nonspecific binding, thus can improve the biocompatibility and circulation half-life of AuNPs by using thiolated polyethylene glycol. Au-S covalent bonding is useful for exchange of surfactant using PEG ligand [25].

References

- Ahangari A, Salouti M, Saghatchi F. Gentamicin-gold nanoparticles conjugate: a contrast agent for X-ray imaging of infectious foci due to *Staphylococcus aureus*. *IET Nanobiotechnol.* 2016;10(4):190–4.
- Al-Neami AQ, Al-Karam LQ, Humadi MD, Alwan MH. Applications and advantages of gold nanoparticles as X-ray contrast agent. *J Biomed Eng Med Devic.* 2017;2(128):2.
- Allabashi R, Stach W, de la Escosura-Muñiz A, Liste-Calleja L, Merkoçi A. ICP-MS: a powerful technique for quantitative determination of gold nanoparticles without previous dissolving. *J Nanopart Res.* 2009;11(8):2003–11.
- Bachler G, Losert S, Umehara Y, von Goetz N, Rodriguez-Lorenzo L, Petri-Fink A, Rothen-Rutishauser B, Hungerbuehler K. Translocation of gold nanoparticles across the lung epithelial tissue barrier: combining in vitro and in silico methods to substitute in vivo experiments. *Part Fibre Toxicol.* 2015;12(1):1–18.
- Boca SC, Astilean S. Detoxification of gold nanorods by conjugation with thiolated poly(ethylene glycol) and their assessment as SERS-active carriers of Raman tags. *Nanotechnology.* 2010;21(23):235601.
- Boote E, Fent G, Kattumuri V, Casteel S, Katti K, Chanda N, Kannan R, Katti K, Churchill R. Gold nanoparticle contrast in a phantom and juvenile swine: models for molecular imaging of human organs using x-ray computed tomography. *Acad Radiol.* 2010;17(4):410–7.
- Brust M, Walker M, Bethell D, Schiffrin DJ, Whyman R. Synthesis of thiol-derivatised gold nanoparticles in a two-phase liquid–liquid system. *J Chem Soc Chem Commun.* 1994;7:801–2.
- Cai QY, Kim SH, Choi KS, Kim SY, Byun SJ, Kim KW, Park SH, Juhng SK, Yoon KH. Colloidal gold nanoparticles as a blood-pool contrast agent for X-ray computed tomography in mice. *Investig Radiol.* 2007;42(12):797–806.
- Chien CC, Wang CH, Wang CL, Li ER, Lee KH, Hwu Y, Lin CY, Chang SJ, Yang CS, Petibois C, Margaritondo G. Synchrotron microangiography studies of angiogenesis in mice with microemulsions and gold nanoparticles. *Anal Bioanal Chem.* 2010;397(6):2109–16.
- Chithrani BD, Ghazani AA, Chan WCW. Determining the size and shape dependence of gold nanoparticle uptake into mammalian cells. *Nano Lett.* 2006;6(4):662–8.
- Cormode DP, Roessler E, Thran A, Skajaa T, Gordon RE, Schlomka JP, Fuster V, Fisher EA, Mulder WJ, Proksa R, Fayad ZA. Atherosclerotic plaque composition: analysis with multicolor CT and targeted gold nanoparticles. *Radiology.* 2010;256(3):774–82.
- Eck W, Nicholson AI, Zentgraf H, Semmler W, Bartling S. Anti-CD4-targeted gold nanoparticles induce specific contrast enhancement of peripheral lymph nodes in X-ray computed tomography of live mice. *Nano Lett.* 2010;10(7):2318–22.
- Goodman CM, McCusker CD, Yilmaz T, Rotello VM. Toxicity of gold nanoparticles functionalized with cationic and anionic side chains. *Bioconjug Chem.* 2004;15(4):897–900.
- Grüner F, Blumendorf F, Schmutzler O, Stauffer T, Bradbury M, Wiesner U, Rosentreter T, Loers G, Lutz D, Richter B, Fischer M, Schulz F, Steiner S, Warmer M, Burkhardt A, Meents A, Kupinski M, Hoeschen C. Localising functionalised gold-nanoparticles in murine spinal cords by X-ray fluorescence imaging and background-reduction through spatial filtering for human-sized objects. *Sci Rep.* 2018;8(1):16561.
- Hainfeld JF, Slatkin DN, Focella TM, Smilowitz HM. Gold nanoparticles: a new X-ray contrast agent. *Br J Radiol.* 2006 Mar;79(939):248–53.
- Hainfeld JF, Slatkin DN, Smilowitz HM. The use of gold nanoparticles to enhance radiotherapy in mice. *Phys Med Biol.* 2004;49(18):N309.
- Han S, Bouchard R, Sokolov KV. Molecular photoacoustic imaging with ultra-small gold nanoparticles. *Biomed Opt Express.* 2019;10(7):3472–83.
- Iqbal M, Usanase G, Oulmi K, Aberkane F, Bendaikha T, Fessi H, Zine N, Agusti G, Errachid E-S, Elaissari A. Preparation of gold nanoparticles and determination of their particles size via different methods. *Mater Res Bull.* 2016;79:97–104.
- Jana NR, Gearheart L, Murphy CJ. Seeding growth for size control of 5–40 nm diameter gold nanoparticles. *Langmuir.* 2001;17(22):6782–6.
- Jans H, Liu X, Austin L, Maes G, Huo Q. Dynamic light scattering as a powerful tool for gold nanoparticle bioconjugation and biomolecular binding studies. *Anal Chem.* 2009;81(22):9425–32.
- Kannan RM, Nance E, Kannan S, Tomalia DA. Emerging concepts in dendrimer-based nanomedicine: from design principles to clinical applications. *J Intern Med.* 2014;276(6):579–617.
- Khademi S, Sarkar S, Shakeri-Zadeh A, Attaran N, Kharrazi S, Ay MR, Azimian H, Ghadiri H. Targeted gold nanoparticles enable molecular CT imaging of head and neck cancer: an in vivo study. *Int J Biochem Cell Biol.* 2019;1(114):105554.
- Lasagna-Reeves C, Gonzalez-Romero D, Barria MA, Olmedo I, Clos A, Ramanujam VS, Urayama A, Vergara L, Kogan MJ, Soto C. Bioaccumulation and toxicity of gold nanoparticles after repeated admin-

- istration in mice. *Biochem Biophys Res Commun.* 2010;393(4):649–55.
24. Lee N, Choi SH, Hyeon T. Nano-sized CT contrast agents. *Adv Mater.* 2013;25(19):2641–60.
 25. Liu H, Doane TL, Cheng Y, Lu F, Srinivasan S, Zhu J-J, Burda C. Control of surface ligand density on PEGylated gold nanoparticles for optimized cancer cell uptake. *Part Part Syst Charact.* 2015;32(2):197–204.
 26. Manohar N, Reynoso FJ, Diagaradjane P, Krishnan S, Cho SH. Quantitative imaging of gold nanoparticle distribution in a tumor-bearing mouse using benchtop x-ray fluorescence computed tomography. *Sci Rep.* 2016;6:22079.
 27. Parida UK, Bindhani BK, Nayak P. Green synthesis and characterization of gold nanoparticles using onion (*Allium cepa*) extract. *World J Nano Sci Eng.* 2011;1(04):93.
 28. Popovtzer R, Agrawal A, Kotov NA, Popovtzer A, Balter J, Carey TE, Kopelman R. Targeted gold nanoparticles enable molecular CT imaging of cancer. *Nano Lett.* 2008;8(12):4593–6.
 29. Pyo K, Ly NH, Yoon SY, Shen Y, Choi SY, Lee SY, Joo S-W, Lee D. Highly luminescent folate-functionalized Au₂₂ nanoclusters for bioimaging. *Adv Healthc Mater.* 2017;6(16):1700203.
 30. Reetz MT, Helbig W. Size-selective synthesis of nanostructured transition metal clusters. *J Am Chem Soc.* 1994;116(16):7401–2.
 31. Schleh C, Semmler-Behnke M, Lipka J, Wenk A, Hirn S, Schäffler M, Schmid G, Simon U, Kreyling WG. Size and surface charge of gold nanoparticles determine absorption across intestinal barriers and accumulation in secondary target organs after oral administration. *Nanotoxicology.* 2012;6(1):36–46.
 32. Shahid M. Water soluble gold nanoparticles based high relaxivity MRI contrast agents. *Mater Res Express.* 2020;6(12):1250h1251.
 33. Tian A, Yang C, Zhu B, Wang W, Liu K, Jiang Y, Qiao Y, Fu H, Li Z. Polyethylene-glycol-coated gold nanoparticles improve cardiac function after myocardial infarction in mice. *Can J Physiol Pharmacol.* 2018;96(12):1318–27.
 34. Turkevich J, Stevenson PC, Hillier J. A study of the nucleation and growth processes in the synthesis of colloidal gold. *Discuss Faraday Soc.* 1951;11:55–75.
 35. Yang J, Wang T, Zhao L, Rajasekhar VK, Joshi S, Andreou C, Pal S, Hsu H-T, Zhang H, Cohen IJ, Huang R, Hendrickson RC, Miele MM, Pei W, Brendel MB, Healey JH, Chiosis G, Kircher MF. Gold/alpha-lactalbumin nanoprobe for the imaging and treatment of breast cancer. *Nat Biomed Eng.* 2020;4(7):686–703.
 36. Yang X, Skrabalak SE, Li Z-Y, Xia Y, Wang LV. Photoacoustic tomography of a rat cerebral cortex in vivo with Au nanocages as an optical contrast agent. *Nano Lett.* 2007;7(12):3798–802.
 37. You J, Zhou J, Zhou M, Liu Y, Robertson JD, Liang D, Van Pelt C, Li C. Pharmacokinetics, clearance, and biosafety of polyethylene glycol-coated hollow gold nanospheres. *Part Fibre Toxicol.* 2014;11(1):26.
 38. Zhang S, Li L, Chen J, Chen Z, Zhang W, Lu H. Quantitative imaging of Gd nanoparticles in mice using benchtop cone-beam X-ray fluorescence computed tomography system. *Int J Mol Sci.* 2019;20(9):2315.



Mucoadhesive Nanoparticulate Drug Delivery System (NPDDS): In Vitro and Pharmacokinetic Studies

Sanjay Patil, Bhavin Choradiya,
and Jayvadan Patel

Contents

1	Introduction	226
2	Mucoadhesive Nanoparticles	227
3	Advantages of Nanoparticles	228
4	In Vitro Characterization of Nanoparticles	230
5	Ocular Pharmacokinetics of Nanoparticles	234
6	Conclusion	241
	References	241

Abstract

The nanocarriers approach is currently focused on the delivery of drugs or active agents to the site of action in an appropriate concentration. Entrapment of drug within nanocarriers may radically transform their bioavailability and tissue distribution profiles. These changes can augment the site-specific delivery with reduced side effects. Therefore, nanoparticles can improve the therapeutic efficiency and are excellent carriers. The mucoadhesive nanoparticles are used to prolong the residence time and bioavailability of the

entrapped drug in mucous membrane. In the last couple of decades, several methods have been developed to prepare mucoadhesive nanoparticles. The various in vitro characterization parameters used for evaluation of mucoadhesive nanoparticles are size, zeta potential, encapsulation efficiency, mucoadhesion studies, transmission electron microscopy, differential scanning calorimetry, Fourier-transform infrared spectroscopy, x-ray diffraction, in vitro drug release, in vitro assays like cytotoxicity studies, etc. Ocular pharmacokinetics is an evaluation of absorption of drug corresponding to time and quantity of administered medications. Quantity of drugs change in tissues or fluids of the eye when it is given in different concentrations through various dosage forms. Ocular pharmacokinetics is oftentimes performed by a multi-compartment model, expecting a homogeneous circulation of drugs in every eye tissue. In view of this, present chapter

S. Patil (✉) · B. Choradiya
Shri Neminath Jain Brahmacharyashram's, Shriman
Sureshdada Jain College of Pharmacy, Chandwad,
Maharashtra, India

J. Patel
Nootan Pharmacy College, Faculty of Pharmacy,
Sankalchand Patel University,
Visnagar, Gujarat, India

encompasses mucoadhesive nanoparticles with in vitro characterization and ocular pharmacokinetics.

Keywords

Mucoadhesive nanoparticles · In vitro characterization · Ocular pharmacokinetics · Animal models · Simulation models · Compartment models

1 Introduction

Mucoadhesives are naturally occurring polymeric materials with adhesive properties. It is often used to describe glue formed synthetically from biological intermediates which could consist of a variety of substances including proteins such as potato starch, corn starch, rice starch, gelatin, and cellulose. The term “mucoadhesives” could also mean synthetic and biological macromolecules and hydrocolloids which are designed to adhere to mucous membrane of the tissue. They are used for various purposes:

- Prevention of fluid (blood) escape.
- Protection of tissues (e.g., wound healing).
- As a replacement for surgical sutures (e.g., sutureless surgery).
- As a substitute for conventional drug delivery systems (e.g., “Orabase” paste containing carboxymethylcellulose, and gelatin used to deliver penicillin for the treatment of mouth ulcers).

Mucoadhesives gained commercial interest because they are often biocompatible, that is, useful for various biomedical applications. Some work in wet environment and under water, while others can stick to low surface energy substrates.

There are significant research and development (R & D) activities related to mucoadhesives not only by academia and entrepreneur institutions but also by leading adhesive manufacturers and raw material suppliers, as evidenced by innumerable publications and patent applications.

While the driving forces in academia approaches have always been the exploration of new and novel approaches with biopolymers having adhesive properties, the industrial emphasis has been the maintaining or improving adhesive properties at competitive cost [1].

In the early 1980s, the concept of mucosal adhesives, or mucoadhesives, was introduced into the controlled drug delivery area. Mucoadhesives are synthetic or natural polymers that interact with the mucus layer covering the mucosal epithelial surface and main molecules constituting a major part of mucus. The concept of mucoadhesives has alerted many investigators to the possibility that these polymers can be used to overcome physiological barriers in long-term drug delivery. Extensive research efforts throughout the world have resulted in significant advances in understanding the various aspects of mucoadhesion [2, 3].

Mucoadhesive dosage forms like solid (tablets, powders, microparticles, inserts, and lozenges), semisolid (gels, ointments), and liquid (solutions, suspensions, gel forming liquids) are being currently investigated. The primary objective of mucoadhesive dosage forms is to provide intimate contact of the dosage form with the absorbing surface and to increase the residence time of the dosage form to prolong the drug action.

Mucoadhesive dosage forms were also reported to improve the absorption and systemic bioavailability of the drugs that were normally poorly absorbed. Among several mucoadhesive polymers, poly (acrylic acid) (PAA) and its lightly cross-linked commercial form, Carbopol, usually have strong mucoadhesive properties and are known to be biocompatible. However, PAA has some limitations as a mucoadhesive drug carrier, for example, its high water solubility. The high water solubility critically limits its use as a mucoadhesive drug carrier because it may be dissolved long before the drug is delivered across the membrane. Moreover, when the mucoadhesive dosage form is administered in a tablet form, they may or may not adhere to the mucous surface as a result of the weight of the dosage form and the vigorous movement of the GI tract.

However, mucoadhesive microspheres have some advantages. These include a lightweight and a smaller dose variation due to the large number of microspheres administered [4].

The exact mechanisms of mucoadhesion, that is, polymer adhesion to mucosal/biological surfaces are not yet completely understood. However, several theories have been put forward to explain the mechanism behind mucoadhesion of polymers/macromolecules as shown in Table 12.1.

2 Mucoadhesive Nanoparticles

Nanoscale drug particles are more easily and rapidly absorbed by tissue than their bigger-scale counterparts, and their use tends to be associated with a reduced dosage requirement to achieve the same efficacy, which should result in fewer side effects as a side benefit. We can also modify them, make them hit the desired target by coating them with other molecules – indeed, we can engineer the surface properties of nanoparticles to target them for delivery to specific locations. For example, if you modify the surface to have a ligand that binds a certain cell type, or one that undergoes receptor-mediated endocytosis on a target cell, then you can have a highly specific targeting mechanism for drug or gene delivery. Nanomaterials are an increasingly important product of nanotechnologies. They contain nanoparticles, smaller than 100 nanometers in at least one dimension. Nanomaterials are coming into use in healthcare, electronics, cosmetics, and other areas [5].

Nanoparticles for the pharmaceutical purposes are defined as solid, colloidal, submicron-sized drug carriers (ranging in size from 1 to 1000 nm) that may or may not be biodegradable. Nanoparticles can be broadly divided into two categories: nanospheres and nanocapsules. Nanospheres are matrix-type system in which drug molecules are either encapsulated within the matrix or may be adsorbed on the particle surface. Nanocapsules are vesicular structures in which the drug is either confined to a cavity consisting of an inner liquid core or dispersed in the

Table 12.1 Various theories of mucoadhesion

Theory	Mechanism and key attributes
Wetting theory	Is primarily applied to liquid or low viscosity mucoadhesive systems Affinity of the liquid to the mucosal surface inversely dependent on the contact angle
Adsorption theory	Adhesive interaction among substrate surface depends upon the intermolecular forces such as hydrogen bond and van der Waals' forces Interaction across the interface occurs as a result of strong covalent bonding
Diffusion interlocking theory	This theory proposes the time-dependent diffusion of mucoadhesive polymer chains into the glycoprotein chain network of the mucus layer Electron transfer among surfaces resulting in attractive forces
Electronic theory	Bonding occurs due to electron transfer between polymeric system and the mucus membrane epithelium
Fracture theory	This theory relates the force required for polymer detachment from the mucus to the strength of their adhesive bond
Mechanical theory	This theory considers adhesion due to the filling of irregularities on a rough surface by a mucoadhesive liquid Such irregularity increases the interfacial area available for interactions

surrounded polymeric membrane, depending on the nature of drug [6, 7]. The nanocarriers approach is currently focused on the delivery of drugs or active agents to the site of action in an appropriate concentration. Entrapment of drug within nanocarriers may radically transform their bioavailability and tissue distribution profiles. These changes can augment the site-specific delivery with reduced side effects. Therefore, nanoparticles can improve the therapeutic efficiency and are excellent carriers for biological molecules, including enzymes, recombinant proteins, and nucleic acid. The nanocarriers also protect the drug molecules from the enzymatic or chemical degradation. The controlled release of drug from the formulation is one of the most important advantages of the nanocarrier system.

Recently, polymeric nanoparticles have been extensively explored as a particulate

nanocarrier system for the delivery of drugs and macromolecules. Various advantages of polymeric nanoparticles such as a controlled release, targeted delivery, monodisperse size, high drug payload, and excellent biocompatibility make them drug carriers of choice. A number of distinct synthetic, semi-synthetic, and natural polymers are used to prepare nanoparticles depending upon nature of drugs, site of action, and duration of action (controlled/sustain release). The various examples of polymers used for preparation of mucoadhesive nanoparticles are shown in Table 12.2.

In the last couple of decades, several methods have been developed to prepare polymeric nanoparticles, which have broadly classified according to whether the particle formation involves a polymerization of monomer units or arises from a macromolecule or preformed polymer. The monomer polymerization methods are further classified into the emulsion and interfacial polymerization [7]. The preparation methods of polymeric nanoparticles from preformed polymers include solvent displacement, emulsion-diffusion, salting out, dialysis, and supercritical fluid technology [8]. The various methods used for preparation of nanomaterials are shown in Fig. 12.1.

The choice of preparation method depends on a number of factors, such as nature of drugs, desired particle size, particle size distribution, and site of application [9].

The mucoadhesive polymers are used in the form of nanoparticles to prolong the residence time and bioavailability of the entrapped drug in mucous membrane. The nanoparticles get adhered to the mucous membrane and then swells and expand. Subsequently, chemical interaction occurs and the drug from the nanoparticles gets penetrated through the mucous membrane into the systemic circulation. The whole phenomenon of mucoadhesion of nanoparticles is shown in Fig. 12.2.

Table 12.2 Mucoadhesive polymers used for nanoparticles

Type of mucoadhesive polymer	Examples
1. Natural polymers	Chitosan and its derivatives, alginate, guar gum, xanthan gum, pectin, carrageenan, hyaluronic acid, gelatin, etc.
2. Synthetic polymers	Poly (acrylic acid) and poly (methacrylic acid) derivatives; poly (ethylene glycol) and poly (ethylene oxide) and its copolymers; poly (vinyl pyrrolidone); etc.
3. Semi-synthetic polymers	Methyl cellulose, ethyl cellulose, sodium carboxymethyl cellulose, hydroxypropyl cellulose, hydroxypropyl methyl cellulose, hydroxyethyl cellulose, etc.

3 Advantages of Nanoparticles

Nanoparticles prepared from diverse materials with unique architectures are used as drug delivery systems (DDS) as they offer several advantages over conventional DDS [10]. The advantages of nanoparticles as DDS are as follows:

1. Increase the solubility of the drugs: Poorly soluble drugs are formulated as nanocrystals or nanosuspension to improve the aqueous solubility by increasing effective surface area. This also improves the bioavailability and reduces the dose of the drug.
2. Protect the drugs/proteins from degradation: Nanoparticles prevents exposure of drug/protein molecules encapsulated inside them to harsh body environments (acidic pH of the stomach) and various enzymes (in GI tract, nasal cavity).
3. Provide controlled release of drug: The drug molecules encapsulated in nanoparticles are released in a controlled manner following degradation of nanoparticle material.

Some of the nanoparticles also offer prolonged drug release due to their slow degradation and by controlling drug diffusion through their matrix.

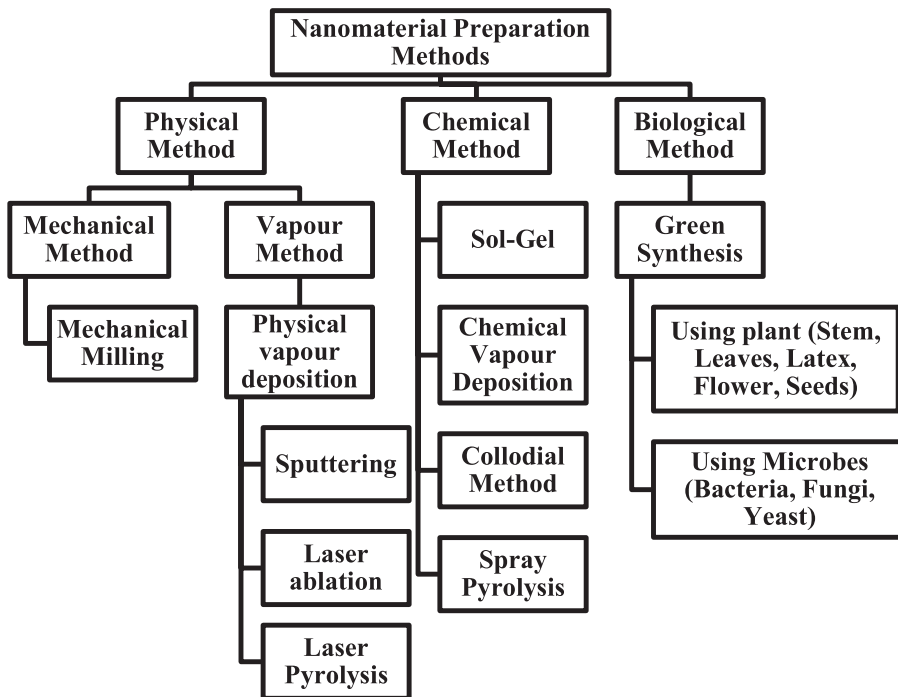


Fig. 12.1 Nanoparticle preparation methods

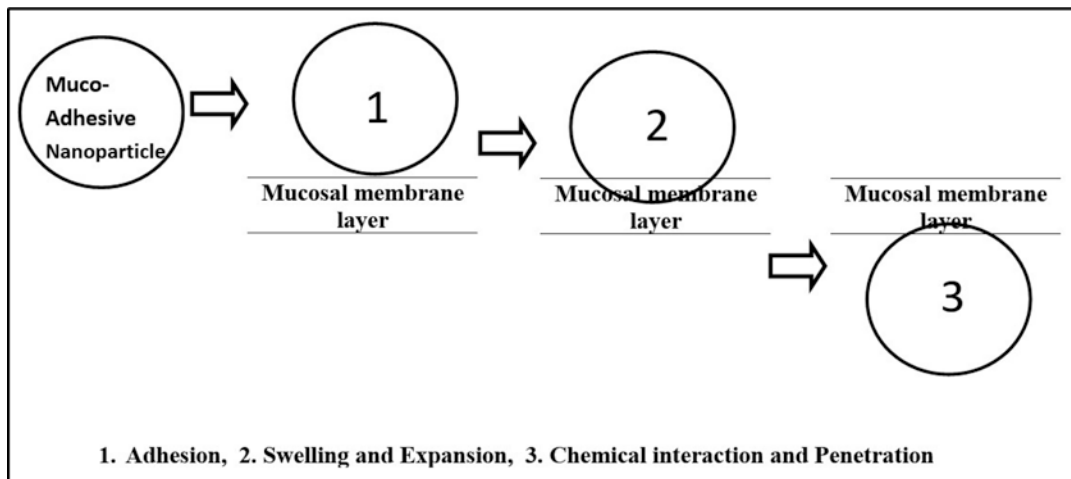


Fig. 12.2 Mucoadhesion mechanism for nanoparticles

4. Targeted drug delivery: Surface functionalization of nanoparticles with target cell specific ligands helps in target specific delivery of drugs. Folate-coated super paramagnetic iron oxide nanoparticles are used to target cancer cells and monitoring the progress of treatment.
5. Decrease the toxic side effects of drugs: Due to improvement in bioavailability, the dose of drugs is reduced and thus the side effects. Moreover, targeted delivery of cytotoxic drugs (anticancer drugs) also reduces toxic side effects on normal cells.

6. Application through various routes of administration: Nanoparticles can be formulated in various dosage forms and administered through the desired route of administration.
7. Vaccine adjuvants: In the case of vaccine delivery, nanoparticles also act as adjuvants depending upon materials used and potentiate the immune response. Higher uptake of nanoparticles by dendritic cells and macrophages improves immune response by specific vaccine antigens.

4 In Vitro Characterization of Nanoparticles

The various in vitro characterization parameters used for the evaluation of mucoadhesive nanoparticles are enlisted in Table 12.3.

4.1 Particle Size and Size Distribution

Particle size distribution is a term demonstrating what sizes (molecule size) of particles are available in what extents (relative particles sum as a rate where the aggregate sum of particles is 100%) in the sample subjected for estimated. Numerous strategies are being utilized to quantify the size distribution of nanoparticle like electron microscopy (EM), laser dispersing methods (e.g., dynamic and static light scattering, laser diffraction), and field flow fractionation (FFF) [11].

4.2 Zeta Potential

It is a technique for the estimation of the electrostatic potential at the electrical double layer encompassing a nanoparticle in formulation. Nanoparticles with a zeta potential somewhere in the range of -10 and $+10$ mV are viewed as roughly neutral, while nanoparticles with zeta potential of more than $+30$ mV or under -30 mV are viewed as explicitly cationic or definitely anionic, individually. Since most cell films are

Table 12.3 Various characterization parameters for evaluation mucoadhesive nanoparticles with suitable instrumentation

Sr. no.	Method of characterization	Instruments (model/make)
1.	Particle size and size distribution	Particle size analyzers (PSAs) like Malvern Mastersizer, Malvern Nanosizer, Anton Paar PSA 1190.
2.	Zeta potential	Malvern Nanosizer
3.	Encapsulation efficiency and drug loading	HPLC, UPLC, and other content determination equipment
4.	Mucoadhesion studies	Bespoke equipment, Anton Paar MCR 702e, and MCR 702e MultiDrive
5.	Transmission electron microscopy	Jeol CRYO ARM™ 300 II
6.	Fourier-transform infrared spectroscopy (FTIR)	Perkin Elmer Spectrum 3 FT-IR, Spectrometer, Thermo Fisher Nicolet iS50 FTIR Spectrometer
7.	Differential scanning calorimetry (DSC)	Mettler Toledo DSC 3, Perkin Elmer DSC 4000, and DSC 8000
8.	X-ray diffraction (XRD)	Malvern: Aeris, Empyrean range, X'Pert ³ MRD, X'Pert ³ MRD XL

contrarily charged, zeta potential can influence a nanoparticle's inclination to pervade layers, with cationic particles by and large showing greater harmfulness related with cell divider disturbance. This procedure is exhibited for two kinds of nanoparticles usually utilized in natural applications: colloidal gold (emphatically anionic) and amine-ended PAMAM dendrimer (firmly cationic) [12].

4.3 Encapsulation Efficiency and Drug Loading

Exemplification proficiency is the level of medication that is effectively ensnared into the micelle

or nanoparticle. Epitome proficiency or EE% is determined by deducting the complete medication added from the free non-captured drug isolated by the absolute medication added. Stacking limit is the measure of medication stacked per unit weight of the nanoparticle, demonstrating the level of mass of the nanoparticle that is because of the embodied medication.

Stacking limit (LC %) can be determined by the measure of all out ensnared drug isolated by the all out nanoparticle weight. In drug conveyance, yield, given as a percent, is an impression of the measure of medication conveyed per sum embodied [13].

4.4 Mucoadhesion Studies

The mucoadhesive capacity of a dose structure is reliant upon an assortment of elements, including the idea of the mucosal tissue and the physico-chemical properties of the polymeric detailing. Engineered bodily fluid plans are created to examine bodily fluid rheology and the dissemination of nanoparticles in vitro. Albeit these bodily fluid definitions are not gotten from people, they can summarize basic bodily fluid properties, for example, microstructure and viscoelasticity. Manufactured bodily fluid can enough mimic mass bodily fluid properties, despite the fact that it needs basic parts of a biologic framework, like natural physiological connections and cell subatomic segments [14]. The methods used to determine mucoadhesion potential includes mucin particles method, microgravimetric method, atomic force microscopy, optical techniques, diffusion/particle tracking methods, etc.

4.5 Transmission Electron Microscopy (TEM)

The transmission electron magnifying lens (TEM) is the ideal instrument for primary and synthetic portrayal at the nanoscale. Imaging, diffraction, and microanalytical data are effortlessly delivered and afterward joined to give nitty gritty bits of knowledge into the properties and

conduct of nanostructured materials. Boundaries, for example, molecule size, grain size, cross section type, morphological data, crystallographic subtleties, synthetic piece, stage type, and dispersion can be gotten by transmission electron micrographs. Electron diffraction examples of nanomaterials are likewise used to get quantitative data containing size, stage ID, direction relationship and gem absconds in the cross-section structure, and so on [15].

4.6 Fourier-Transform Infrared Spectroscopy (FTIR)

Fourier-transform infrared spectroscopy (FTIR) is a procedure which is utilized to acquire infrared range of retention, emanation, and photoconductivity of strong, fluid, and gas. It is utilized to identify diverse useful gatherings. Fourier-transform infrared spectroscopy is utilized to explore in situ the surface responses occurring at the outside of semiconductor nanoparticles and at the same time screen the varieties of the free-transporter thickness. The connection between the surface responses and the progressions in the infrared absorbance under gas adsorption/desorption cycles gives data on the synthetic wonders liable for electrical conductivity varieties and consequently for the gas location [16].

4.7 Differential Scanning Calorimetry (DSC)

DSC is a thermodynamical tool for direct assessment of the heat energy uptake, which occurs in a sample within a regulated increase or decrease in temperature. The calorimetry is particularly applied to monitor the changes of phase transitions. DSC is commonly used for the study of biochemical reactions, which is named as a single molecular transition of a molecule from one conformation to another. Thermal transition temperatures (T_t ; melting points) of the samples are also determined in solution, solid, or mixed phases such as suspensions [17].

4.8 X-Ray Diffraction (XRD)

XRD gives data about the game plan of molecules inside a glasslike material. For bigger particles (measurement >10 nm), mass polycrystalline investigation techniques are by and large fitting, since these particles are commonly little precious stones of a mass construction. For exceptionally little nanoparticles (measurement <10 nm), large numbers of the mass examination strategies fizzle and different procedures are required, which we will talk about at the appropriate time [18]. At the point when occasional constructions of a given dividing are enlightened with light of a similar frequency, diffraction emerges through useful impedance. X-rays have frequencies of the request of 1 \AA and diffract from planes of particles in a precious stone as per the Bragg condition, $2d \sin \theta = n\lambda$, where d is the partition between nuclear planes (the “d-dispersing”), θ is half of the diffraction point, n is a number, and λ is the X-beam frequency. This condition can likewise be communicated as far as the extent of the dissipating vector, $Q = 2\pi/d = (4\pi/\lambda) \sin \theta$, which is free of the X-ray frequency. Investigation of the position, width, and state of the diffraction pinnacles can yield data about the translucent stages present, the crystallite size, strain, particular direction (surface), shape anisotropy, and centralization of stacking shortcomings and other precious stone deformities [19].

4.9 In Vitro Assay: Cytotoxicity

In vitro cytotoxicity investigations of nanoparticles utilizing diverse cell lines, brooding occasions, and colorimetric measures are very important. In any case, these investigations incorporate a wide scope of nanoparticle focuses and openness times, making it hard to decide if the cytotoxicity noticed is physiologically significant. Moreover, various groups decide to utilize different cell lines just as refined conditions, which make direct comparisons cytotoxicity, perceive that phone societies are touchy to changes in their current circumstance like vacillations in temperature, pH, and supplement and waste

focuses, notwithstanding the centralization of the conceivably poisonous specialist being tried. Along these lines, controlling the test conditions is urgent to guarantee that the deliberate cell passing relates to the harmfulness of the additional nanoparticles versus the unsound refined conditions [20]. Moreover, as nanoparticles can adsorb colors and be redox dynamic, it is significant that the cytotoxicity measure is proper. Leading various tests is profitable to guarantee substantial ends are drawn. One straightforward cytotoxicity test includes visual investigation of the cells with brilliant field microscopy for changes in cell or on the other hand atomic morphology. Fiorito et al. utilized this procedure while assessing the cytotoxicity of single-walled carbon nanotubes (SWNTs). In any case, most of cytotoxicity tests utilized all through distributed nanoparticle consider measure cell demise through colorimetric strategies [21]. These colorimetric techniques can be additionally sorted into tests that measure plasma film uprightness and mitochondrial action. Openness to certain cytotoxic specialists can think twice about the cell layer, which permits cell substance to spill out. Suitability tests dependent on this incorporate the unbiased red and Trypan blue measures. Unbiased red, or toluene red, is a powerless cationic color that can cross the plasma film by dissemination. This color will in general aggregate in lysosomes inside the cell. On the off chance that the cell layer is modified, the take-up of non-partisan red is diminished and can spill out, taking into account insight among live and dead cells. Cytotoxicity can be evaluated by taking spectrophonic estimations of the impartial red take-up under fluctuating openness conditions. Two investigations by Flahaut et al. also, Monterio-Riviere et al. investigating the cytotoxicity of carbon nanotubes used the impartial red test. Trypan blue, a diazo color, is simply penetrable to cells with compromised layers; in this manner, dead cells are stained blue while live cells stay vapid. The measure of cell passing can be resolved through light microscopy. This measure was utilized by Bottini et al. what is more, Goodman et al. to decide the cytotoxicity of SWNTs and gold nanoparticles [22].

4.10 Oxidative Stress Tests

Oxidative pressure assumes a basic part in nanotoxicity. Different kinds of nanoparticles are known to instigate oxidative pressure by creating intracellular receptive oxygen species (ROS). Cell take-up of nanoparticles and intracellular metal particle discharge are significant elements for intracellular ROS age. Moreover, ROS age can result from associations of nanoparticles and cells that lead to mitochondrial brokenness. In vivo, nanoparticles actuate the discharge of cytokines, which, thusly, instigate optional oxidative pressure through age of ROS and free revolutionaries [23]. In any case, not all nanoparticles initiate oxidative pressure. Intracellular ROS age by nanoparticles relies upon their physical and synthetic properties, like the glasslike stage, adsorption capacity, and dissolvability. Regardless of whether the molecule size is nanoscale (1–100 nm), genuinely and synthetically latent particles do not instigate oxidative pressure. Accordingly, the molecule size is definitely not a direct impacting factor in nanoparticle-instigated oxidative pressure. Biomarkers of oxidative pressure are significant devices for the assessment of nanoparticle harmfulness [24].

Oxidative Pressure Markers Are Partitioned into Three Kinds:

1. Compound specialists that respond with ROS, receptive nitrogen species (RNS), and extremists, the prompt triggers of oxidative pressure. For instance, 2',7'- dichloro dihydrofluorescein diacetate (DCFH-DA) is habitually utilized for the estimation of revolutionaries. Dihydroethidium (DHE) is additionally utilized for the location of ROS. Stream cytometry is an incredible asset to recognize intracellular ROS level utilizing these tests.
2. Oxidized natural particles and their optional items; oxidized lipids, proteins, and nucleic acids are incorporated. For instance, malondialdehyde (MDA) and 8-hydroxy-2'- deoxyguanosine (8-OHdG) are utilized as oxidative pressure markers.
3. Organic particles identified with the counter oxidative pressure framework. For instance, cancer prevention agent proteins, for example, heme oxygenase-1 (HO-1), superoxide dismutase (SOD) and cell reinforcement particles, for example, glutathione (GSH), ascorbic corrosive, and tocopherol are assessed as oxidative pressure markers. These biomolecules are actuated by oxidative pressure and are likewise connected with variation to oxidative pressure [25].

4.11 In Vitro Release Studies

The in vitro discharge study is a basic test to evaluate the security, viability, and nature of nanoparticle-based medication conveyance frameworks. Drug discharge from nano-sized dose structures can be surveyed utilizing one of the accompanying three classes, specifically, test and isolated (SS), nonstop stream (CF), and dialysis layer (DM) strategies. Medication discharge is observed by truly isolating the nanoparticles from the delivery media, trailed by investigation of the previous or the last mentioned [26].

4.12 Permeation Study

Nanoparticles have drawn in much consideration as a critical material for new biomedical and drug applications. For achievement in these applications, the nanoparticles are needed to move across the cell layer and to reach to within the cell. Among a few movement pathways of nanoparticles, the immediate penetration pathway enjoys an incredible benefit because of its high conveyance adequacy. In any case, notwithstanding many exploration endeavors, key properties and elements for driving the immediate penetration of nanoparticle and its hidden instruments are a long way from being perceived [27]. In this article, trial and computational investigations in regard to the immediate penetration of nanoparticles across a cell layer will be audited. Right off the bat, exploratory investigations on the nanoparticle-cell collabo-

rations, where unconstrained direct pervasion of nanoparticles was noticed, are checked on. From the exploratory investigations, potential key physico-substance properties of nanoparticles for their immediate penetration are discussed. Furthermore, actual techniques, for example, electroporation and nonoperation for conveying nanoparticles into cells are surveyed. Current status of innovations for working with the immediate saturation of nanoparticle is introduced. At last, we audit sub-atomic elements reproduction studies and present the most recent discoveries on the basic sub-atomic instruments of the immediate penetration of nanoparticle [28].

5 Ocular Pharmacokinetics of Nanoparticles

Ocular pharmacokinetics is an evaluation of absorption of drug corresponding to time and quantity of administered medications. Quantity of drugs change in tissues or fluids of the eye when it is given in different concentrations through various dosage forms. Eye tissue obstructions cause significant difficulties in conveying drug at proper site of action. To examine pharmacokinetics, imaginary body spaces should be considered through which drug particles cross and distribute. These areas contain the extracellular and intracellular spaces.

alongside the intravascular compartment. To study the ocular pharmacokinetics, eye parts, for example, (a) anterior chamber, (b) retro or periocular space, (c) tear film and cul-de-sac, and (d) vitreous cavity should be considered as key compartments. Each eye could be considered as an individual and might be as a multi-component structure. Ocular pharmacokinetics is oftentimes performed by a multi-compartment model, expecting a homogeneous circulation of drugs in every eye tissue. A significant downside of the compartmental model is an absence of point-by-point data on local circulation in different eye structures [29].

5.1 Ocular Compartments

In regard to visual medication conveyance, eye can be clinically divided into multiple compartments. To portray ocular pharmacokinetic parameters, the fundamental spotlight should be on ocular compartments which consist of the anterior chamber, retro- or periocular space, tear film, cul-de-sac, and vitreous cavity. In later subsections, pharmacokinetics of these compartments investigating various medications and courses of organization are talked about [30]. The various compartments of the eye are shown in Fig. 12.3.

Cul-de-Sac and Tear Film Compartment

Cul-de-sac is now and again alluded to as the conjunctival sac. It is a limited pocket where palpebral and bulbar conjunctiva meets in the lower eyelid, with more profound break in the upper eyelid. It is the space between lower part of the eyelid and globe. Following effective organization, the portion comes into contact with the cornea. Assimilation of topically controlled medication is through penetration across the cornea from precorneal tear film or through foundational retention through nearby blood vessels at parkway. Tear film and circular drive may extend up to 30 μl in volume under broadened conditions. In any case, this development is not sufficient to hold 40 to 70 μl of a business effective eye plan. Subsequently, the vast majority of the portion is cleaned out quickly following instillation. Thus, under 5% of the medication comes to intraocular tissues. Skin drugs and their metabolites might be killed through different components. The most well-known ones are the

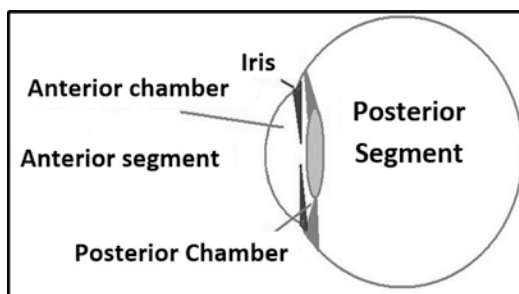


Fig. 12.3 Ocular compartments

underlying outpouring of medication by flickering system of the eyelids and through the nasolacrimal course. Directed portion in the foremost chamber might be dispensed with through watery humor outpouring [31].

Anterior Chamber

Topically controlled specialists are retained through the cornea then, at that point moved into the foremost chamber. The portion is then moved by watery stream and by dispersion into the blood dissemination through front uvea. Medication particles can saturate through the corneal epithelium by using two pathways, for example, transcellular pathway for lipophilic medications or paracellular pathways for hydrophilic medications. Lipophilic medications might be sequestered in epithelial cells from which atoms are bit by bit delivered to the corneal stroma and further foremost chamber. The lipophilic idea of corneal epithelium goes about as the rate restricting boundary for hydrophilic medications. When the medication compasses to the watery humor, it can without much of a stretch be disseminated to the iris and the ciliary body. Medication atoms can tie to melanin and make a repository, from which the medication is gradually delivered to the encompassing cells, consequently dragging out drug movement. Presence of esterase and lysosomal catalysts in the foremost chamber assumes a significant part in the bioreversion of amino corrosive prodrugs. Medication end from front compartment principally happens through fluid humor by two unique components. The first incorporates the chamber point and Sclemm's channel, and the second instrument includes blood stream in foremost uvea. A few medications are cleared through uveal blood stream. By and large, lipophilic medications are all the more quickly dispensed with comparative with hydrophilic medications [32].

Vitreous Cavity

Drugs controlled intravitreally offer direct admittance to glassy pit and retina. Once infused into the glassy pit, it might require a few hours for medication to diffuse across the whole glassy humor. Medication saturation from the glassy

cavity to the choroid is delayed because of obstruction by RPE though drug dissemination from the glassy to the retina is confined by the interior restricting film (ILM). A few components control the medication fixation in glassy cavity. Such factors incorporate starting portion, volume of appropriation, and the pace of disposal. In the glassy hole, medication can be wiped out through front as well as back routes. End of medication can be affected essentially by two variables: volume of dissemination and end half-life [33].

Retro-/Periocular Space

Periocular alludes to outskirts or the area encompassing eyeball, inside the circle. Medications controlled through a periocular course can be considered as a viable course for drug conveyance to the back eye portion. Medications regulated through this course can arrive at the back portion through a few pathways, for example, transscleral pathway, foundational dissemination, and choroidal blood stream. The foremost pathway characterizes tear film, cornea, watery humor, and glassy humor. Since periocular space is the area encompassing eye, it can create comparative pharmacokinetics inside the foremost or glassy compartments, which have effectively been examined before [34].

5.2 Pharmacokinetic Compartment Models in Ocular Drug Delivery

A few pharmacokinetic compartment models of visual medication conveyance have been produced for depicting the assimilation, appropriation, and end of visual medications in the eye. Segments of the eye, for example, tear film, cornea, watery humor, focal point, and glassy humor are straightforward. These segments have no immediate blood supply. The blood supply to the eye is intricate: it is provided by the ophthalmic vein and choroidal plexus. Choroidal veins permit simple medication conveyance from the circulatory system to the extravascular choroid. In any case, access of choroidal drug into the retina is restricted by the RPE obstruction. Foundational

drugs flow through iris, ciliary body, choroid, and retina. However, vein dividers in the iris and retina have tight intersections between the endothelial cells that slow drug permeation across the vessel dividers [35].

To examine compartment models, every part of the eye can be considered as the unmistakable compartment isolated by an obstruction from the other compartment. Consequently, stream between contiguous compartments takes additional time than dissemination. For instance, thinking about tear as one compartment with steady turnover than inflow of the lachrymal liquid is consistent and equivalent to the surge through the puncta. When hydrophilic medication imparted, it blended quickly and tear stream diverts a part for each unit time subject to the medication focus present. Essentially cornea can likewise be considered as one compartment. This is communicated by the accompanying condition from Eq. 12.1

$$\frac{dC_d}{dt} = k_0 C_d t \quad (12.1)$$

Where, C_d = the centralization of medication in tears at time t . dC_d/dt = the adjustment of concentration C_d during a time period.

k_0 = a proportionality steady of medication misfortune to the nasolacrimal channel subject to the stream rate and volume of the tear compartment.

It is normal that 99% of the medication is lost from the precorneal region. The most extreme measure of the medication is assimilated into the fundamental dissemination by means of the conjunctival layer and the nasolacrimal waste framework. When the medication is in the blood dissemination, it conveyed to different pieces of the body which is considered as the fringe compartment, trailed by digestion and discharge. End courses of the eye additionally influence the neighborhood tissue fixation. Subsequently, the focus in the fluid chamber and the glassy body is not homogeneous yet appropriate complicatedly as indicated by the end rate across the encompassing tissues. Nonetheless, if 1% of imparted sum enters the corneal epithelial obstruction and enters the stroma, then cornea is considered as

second compartment. As indicated by the two-compartment model, drug is diffused across the obstruction from low fixation to high focus in light of Fick's first law of dispersion (Eq. 12.2).

$$\frac{dC_d}{dt} = k_{dc} A (C_d - C_y) \quad (12.2)$$

Where, dC_d/dt = the net drug moving from tears to cornea per unit of time. A = the area of the tear-corneal interface.

C_d = concentration of drug in tears.

C_y = concentration of drug in cornea.

K_{dc} = the permeability constant from tears to the cornea.

The permeability constant in the reverse direction would be k_{cd} .

When the fixation in the two compartments, for example, tears and the cornea came to the balance, medication can presently do not infiltrate internal. Also, dispersion of the medication from the cornea to watery humor is similarly as of tears to cornea. To finish the model, the disposal move coefficient from the fluid to the blood plasma is given by Eq. 12.3 [32].

$$\frac{dC_4}{dt} = k_{dc} A (C_d - C_y) \quad (12.3)$$

Where, dC_d/dt = the amount of drug penetrating the barrier during a unit of time. A = the area of the tear-corneal interface.

C_c = concentration of drug in cornea.

C_d = concentration of drug in aqueous.

k_{dc} = the permeability constant from cornea to aqueous.

The more complex pharmacokinetic model depends on Fick's second law of dissemination which accepts a round adjusted barrel-shaped eye for visual conveyance. This model showed the three pathways for drug transport across the outside of the eye. These pathways are foremost fluid chamber, the back watery chamber, and the retina/choroids/scleral layer covering the glassy body. The three-compartment pharmacokinetic model has been exhibited to decide the pharmacokinetics of different peptide medications like insulin, glucagon, luteinizing chemical delivering chemical (LHRH), and leu-enkephalin through visual highways. The significant

compartments are the precorneal region, cornea, and fluid humor [36].

5.3 Pharmacokinetic Simulation Model

The porousness pattern of medications and design of blood-ocular barrier (BOB) have been known for quite a long time. In any case, no reports accessible for the dispersion of medication from blood to the eye. Any model for visual medication conveyance would be a useful device in drug revelation. The reproduction model could be a huge way to deal with gauge the conveyance of visual medications. The study proposed by Urtii et al. anticipated the visual dissemination of fundamental medications by utilizing a reenactment model. The circulation leeway among glassy and plasma was acquired from a Quantitative Structure Property Relationship (QSPR) model for freedom of intravitreal drugs [31]. The solid expectations were acquired utilizing computational worth of visual appropriation leeway, fundamental convergences of unbound medication, and a basic pharmacokinetic model. In rundown, a pharmacokinetic recreation model has been worked for expectation of medication fixations in the glassy. It depends on the unbound medication focuses in the plasma and the computational gauge for the conveyance leeway between blood dissemination and the eye. This model could precisely foresee the medication dispersion to the eye [37].

The necessity of the recreation study is that the medication convergences of plasma and glassy should be accessible. Accordingly, in light of the writing, hare reenactments were performed for 10 mixtures and human recreations with one medication. A pharmacokinetic model dependent on computational appropriation leeway and free medication fixations in plasma was equipped for anticipating the medication focuses in glassy. The vitreal centralizations of the contemplated intensifies traversed a 1000-crease scope of focuses, but the reproduced drug fixations were generally near the exploratory qualities for each situation. The reproductions with computational

and trial upsides of dissemination leeway showed comparative consistency [38].

5.4 Pharmacokinetic Animal Models

Determining the pharmacokinetic boundaries in visual tissues are a significant test due to the perplexing life structures and dynamic physiological hindrance of the eye. In drug improvement measure, human pharmacokinetics is for the most part surveyed after per os or intravenous organization by inspecting plasma at various time stretches. In any case, for drugs controlled through visual course with a neighborhood helpful impact cannot be inspected. A few exemptions are made, for example, checking of medication levels in biopsies or watery humor gathered from patients exposed to ophthalmic surgeries. In this manner, creature models are utilized to consider the medications conveyance in visual tissues. The visual attributes of creature models license to extrapolate to human pharmacokinetics [39].

A few pharmacokinetic creature models have been created to contemplate the dissemination and end of visual medications for various courses of organization. The bunny is an ordinarily utilized animal groups for preclinical visual PK contemplates. The pharmacokinetic boundaries in the hare have shown the anticipated boundaries in human. Despite the fact that the natural eye has a higher retina vascular and bigger glassy depression, more modest focal point and bigger serum compartment than bunnies, these both offer normal qualities. These variables may contribute slight distinction in pharmacokinetics of the medication in human and bunny. All things considered, bunny model is set up to examine the pharmacokinetic boundaries during visual medication advancement. Ozcimen et al. utilized hare uveitis model to consider visual pharmacokinetics of intravenously controlled tigecycline in different compartments. Huge low remedial levels were seen in glassy and fluid humor, while a higher fixation was seen in plasma. This outcome proposes that intravenous organization of

tigecycline is not a reasonable course for the treatment of bacterial endophthalmitis. In another examination, Dutch-belted hares were utilized to analyze the pharmacokinetics of intravitreal bevacizumab and ranibizumab [40].

The half-existence of bevacizumab was 4.32 days and ranibizumab was 2.88 days in hare; greatest focus in the glassy cavity was 400 $\mu\text{g}/\text{mL}$ at day 1 and ranibizumab was 162 $\mu\text{g}/\text{ml}$. Since bevacizumab (149 KD) has bigger atom size than ranibizumab (48 KD), ranibizumab could have higher retina entrance and quicker disposal. In another investigation, Xu L. et al., have revealed that the one-compartment model is the best-fit model of the pharmacokinetics of ranibizumab in 674 patients with age-related macular degeneration. It was seen that ranibizumab is wiped out from foundational course by the main request end. The disposal half-life in the glassy was 9 days and characteristic foundational end half-life is 2 hours [41].

Contrasted with hare model, pharmacokinetics of ranibizumab is marginally extraordinary in monkey creature model. Gaudreault J et al. have revealed that half-existence of 0.5 mg ranibizumab was 2.6 days contrast with 2.88 days in hare and glassy depression most extreme fixation was 169 $\mu\text{g}/\text{ml}$ at 6 hours contrast with 162 $\mu\text{g}/\text{ml}$ at day 1 in hare study. Proksch et al. additionally read the visual pharmacokinetics for mapracorat, a specific glucocorticoid receptor agonist, in bunny and monkey. Mapracorat was regulated single or rehashed with a portion range from 0.01 to 3000 $\mu\text{g}/\text{eyes}$ for bunny and 50 to 3000 $\mu\text{g}/\text{eyes}$ for monkey. In the two species, mapracorat focus was conveyed higher in cornea, conjunctiva than fluid humor, and iris/ciliary body.

Those distinctions are worthy to have some plan to anticipate about the pharmacokinetic profile of any medications. Le et al. have likewise explored the lampalizumab end following the intravitreal infusion. The lethargic visual end was noticed contrasted with fundamental end. Besides, Drolet DW et al. have shown the pharmacokinetic and security profile of pegatanib in rhesus monkeys to help the human clinical preliminary. It has likewise anticipated the human plasma freedom and glassy humor convergence of pegatanib.

Pharmacokinetic/pharmacodynamics (PK/PD) model of Factor D hindrance in monkeys by lampalizumab for the treatment of geographic decay was created by Le et al. Likewise, intravitreal organization of lampalizumab showed restorative levels at the objective site while limiting fundamental medication openness to the patient. Intravitreal infusion of lampalizumab brought about sluggish visual disposal contrasted with fundamental end. These outcomes might be useful in anticipating human PK/PD for lampalizumab [42].

Notwithstanding the way that rodent models have presented different difficulties in visual pharmacokinetic, a few examinations have demonstrated to be significant in deciding various boundaries that are significant in building up PK/PD connections. Liu et al. read subconjunctival biodegradable microfilms for supported medication conveyance to the front fragment of rodents. Microfilm was made out of prednisolone stacked poly (lactide-co- ϵ -caprolactone) drug conveyance framework which was subconjunctivally embedded into rodent eyes. These movies had the option to convey the medication for 90 days at a pace of 0.002 mg/day. Moreover, Tommaso et al. explored the impact of micelle stacked with Cyclosporin A (CsA) for effective conveyance on rodent model for anticipation of corneal unite dismissal after keratoplasty strategy. Results uncovered that CsA-micelle plan had the option to infiltrate every single corneal layer, a 73% accomplishment in cornea join relocate, 50% decrease in neovascularization, and huge lower edema in vivo.

Pharmacokinetics of topically managed ciprofloxacin (0.3%) through circular drive in equine with no ophthalmic sicknesses was concentrated by Hendrix et al. Tears were examined from parkway at various time focuses post measurements and broke down for the centralization of ciprofloxacin. Ciprofloxacin levels stayed above least inhibitory focus important to hinder the development of 90% of life forms for 6 hours post organization. These outcomes might be reproduced in human as pharmacokinetics of ciprofloxacin in ordinary ponies is practically identical to that of hare and human [43].

Ward et al. examined the visual PK properties of besifloxacin in hares, monkeys, and people, utilizing a vigorous PK study plan, and to look at the subsequent PK boundaries (C_{max} and AUC) against the common microorganisms detached from patients with bacterial conjunctivitis. For this examination, Dutch-belted and New Zealand composite bunnies and cynomolgus monkeys were utilized. The male Dutch-belted bunnies got a 50- μ L instillation of besifloxacin ophthalmic suspension (0.6%) into the conjunctival sac of each eye as a solitary bolus portion. At foreordained time spans subsequent to dosing, hares were euthanized and the eyes enucleated, frozen, and analyzed, with tissues gathered independently for each eye. Cynomolgus monkeys (guys and females) were utilized to research the visual and foundational PK following effective visual organization of besifloxacin ophthalmic suspension (0.6%) into the conjunctival sac of each eye as a solitary bolus portion. To survey fundamental PK, sequential blood tests (~0.5 mL) were gathered from a femoral vein from one partner of three monkeys at coordinated stretches from 5 min to 24 h following effective visual dosing. After a predefined assortment times, monkeys were euthanized and eyes were enucleated and snap-frozen for additional examination. For human investigation, 64 sound male or female volunteers were enlisted in the open-name study and besifloxacin was surveyed in human tear liquid [38].

Generally, the visual PK profile of besifloxacin following effective visual organization was comparative in bunnies and monkeys. The consequences of this examination showed that effective dosing of besifloxacin exhibits great visual entrance in bunnies and monkeys. Likewise, accomplishes supported levels in tears to people. Somewhat, lower maximal besifloxacin levels were seen in people contrasted and hares or monkeys. This distinction is part of the way because of the squint rate and tear turnover rate influences the elements of medication maintenance on the outside of the eye.

Creature models with harmed BRB prompted higher medication disposal rate contrasted with ordinary creatures. Likewise, a higher intravitreal

leeway was seen in sick creatures. These outcomes recommended that PK/PD result relies upon different factors, for example, drug properties just as would be expected or sickness model. Subsequently, suitable plan and determination of creature model to explore visual PK/PD is urgent. In addition, appropriate definition to beat these hindrances is the way to propel visual medication conveyance [44].

Pharmacokinetics of Nanoparticles with Suitable Examples:

1. γ -Cyclodextrin Nanoparticle Dexamethasone (DexNP) and Dorzolamide (DorzNP) Eye Drops,

Johannesson et al. created γ -cyclodextrin nanoparticle dexamethasone (DexNP) and dorzolamide (DorzNP) eye drops. These plans were relied upon to give supported high medication fixations on the eye surface. It was found that dexamethasone top fixation (ug/mL \pm standard deviation) from DexNP eye drops (636 ± 399.1) was 19-fold higher comparative with effective ophthalmic steroid suspension of dexamethasone 0.1% Maxidex® (39.3 ± 18.9) ($p < 0.001$). After 4 hr., DexNP was as yet multiple times higher than Maxidex®. Furthermore, DexNP brought about 30-fold higher convergence of dexamethasone in tear liquid throughout expanded time span permitting higher medication adds up to parcel into different visual tissues. Dorzolamide fixation from DorzNP (59.5 ± 76.9) was about half higher comparative with Trusopt® (40.0 ± 76.7) ($p < 0.05$) [45].

2. Loteprednol Etabonate 0.4% Mucus-Penetrating Nanoparticles

A 3- to 40- μ m layer of bodily fluid on cornea and conjunctiva presents a novel test for topically applied restorative specialists. A chance of decreased danger of intraocular pressure height for loteprednol etabonate (LE) ophthalmic arrangement (0.5%), has been contrasted with other corticosteroids. LE displayed comparative adequacy when contrasted with different cortico-

steroids such as prednisolone acetic acid derivation. Notwithstanding, IOP was diminished to more prominent degree, in this manner introducing its further developed profile over different corticosteroids. Schopf et al. have led an examination to further develop drug infiltration into visual tissues fundamental to the mucous boundary with a novel bodily fluid entering molecule (MPP) innovation. Studies were led in contrast with Lotemax® (loteprednol etabonate ophthalmic suspension, 0.5%) which has shown generally higher conveyance in corneal tissues, with diminished infiltration into the fluid humor and iris/ciliary body. Effective organization of the two definitions (LE-MPP 0.4% and Lotemax 0.5%) in 48 bunnies (96 eyes) brought about a T_{max} of 0.5 h. Furthermore, LE-MPP 0.4% showed 3-fold higher C_{max} and 2-fold higher $AUC_{0-12\text{ h}}$ rather than Lotemax 0.5% in fluid humor. Comparative examples were displayed by LE-MPP 0.4% in the cornea (3.6-fold C_{max} and 1.5-fold $AUC_{0-12\text{ h}}$), conjunctiva (2.6-fold C_{max}), and other visual tissues. These outcomes demonstrate that use of such conveyance frameworks is able to improve drug fixation in visual tissues just as to lessen dosing recurrence for the treatment of different confusions [46].

Pharmacokinetics of Mucoadhesive Nanoparticles Under Diseased Conditions

The corneal stroma is primarily made out of collagen and water which shape an imposing hindrance for topically applied hydrophobic medications. Moreover, an enormous number of sicknesses are known to adjust visual pharmacokinetics of different medications and their definitions. Such sick conditions may hasten different physiological conditions which may likewise modify the bioavailability of medication atoms. For example, patients with contagious keratitis show constant irritation at the cornea bringing about helpless infiltration of the medication in visual tissues. Other visual diseases incorporate uveitis, cytomegalovirus retinitis, and proliferative vitreoretinopathy. To defeat such manifestations, drugs are regulated in a few unique manners. In dry-eye patients, drugs are managed alongside a vehicle/emul-

sion to keep away from dissipation of restricted regular tears. A few ionized medications are crashed into visual tissues by coulomb-controlled iontophoresis to conquer helpless infiltration. A couple of other significant illnesses that have fundamentally added to the changed visual pharmacokinetics are retinoblastoma and glaucoma [47].

5.5 Pharmacokinetics of Mucoadhesive Drugs in Glaucoma

Glaucoma is a weakening illness which prompts visual impairment in a huge populace of Americans. It exacts a colossal cost as far as cost in medical services and personal satisfaction. Glaucoma causes breakdown of BRB just as choroidal and retinal neovascularization as the infection advances. It is important to contemplate the pharmacokinetic profile against glaucoma drugs in creature models to decide adequacy in the treatment of glaucoma in patients in the end. Pharmacokinetic boundaries of these medications are distinctive in typical and ailing visual tissues. In the investigation performed by Shen et al., it was seen that AUC and C_{max} for both the medications were fundamentally lower in the illness model contrasted with ordinary creatures. This is normal as BRB separates; there is a diminished openness of medications to sick visual tissues. This focuses to require for portion heightening which may prompt portion-related poisonousness. Visual and fundamental pharmacokinetics of brimonidine and dexamethasone in creature models with and without blood retina boundary separated was contemplated following single intravitreal infusion [48].

5.6 Pharmacokinetics of Mucoadhesive Drugs in Retinoblastoma

Retinoblastoma (Rb) addresses malignancy of the retina that happens for the most part in kids younger than five. It begins in the retina and

spreads through the optic nerve. Carboplatin is generally utilized for the treatment of Rb. Subsequently, pharmacokinetic boundaries of these medications ought to be resolved to evaluate adequacy and decide portion. Hayden et al. announced that no poisonous effect was seen in histopathology areas of hare eyes after six back-to-back subconjunctival infusions of carboplatin at a portion of 5.0 mg. Pinnacle grouping of carboplatin in retina was more noteworthy (53.3 ng/mg) in visual tissues and optic nerve comparative with intravitreal infusion (21.7 ng/mg) which is the favored course. Comparative outcomes were noticed for choroid and optic nerve. Another medication that is being examined for treatment of Rb is digoxin. As detailed by Winter et al., following a portion of 10 µg of digoxin, C_{max} in glassy is determined to be 8.5 µg/ml. Subsequently the medication is required to be inside the remedial window for 24 hours following intravitreal organization. It was additionally seen that digoxin focus in plasma was essentially underneath the lower furthest reaches of the remedial window following a solitary portion [49]. Digoxin has a fundamentally high volume of dispersion. This is because of its limiting with skeletal and heart muscles and kidney. Winter et al. have additionally detailed no quantifiable grouping of digoxin in the kidney and heart in hares. Notwithstanding, this portion was discovered to be harmful to retina in bunnies. In this way, it may not be deciphered in human in its current structure. In this way, there is a dire requirement for improvement of designated drug conveyance frameworks [50].

6 Conclusion

A wide range of studies have proved interaction of mucoadhesive materials with mucins and mucosal surfaces which demonstrated a promising background for the development of new mucoadhesive drug delivery systems. This research area is rapidly expanding and several mucoadhesive materials have shown good adhesion characteristics. Mucoadhesive nanoparticles

as a drug delivery system has various beneficial properties such as intimate contact of mucoadhesive system at the mucosal surface increased residence, and reproducible drug penetration and absorption. Before starting the preclinical and clinical studies of nanoparticles, a detailed in vitro characterization is required. Nanoparticles are evaluated for size, morphology, and surface charge, using highly advanced microscopic techniques such as scanning electron microscopy (SEM), transmission electron microscopy (TEM), and atomic force microscopy (AFM). Zeta potential is used to know the colloidal stability and the surface charge present on nanoparticles. Differential scanning calorimetry (DSC) is used to characterize particles and drug interaction. Mucoadhesivity of nanoparticles is evaluated by various in vitro mucoadhesion tests. The drug release and permeation properties from nanoparticles are also important characterization parameters for nanoparticles. The dose of drug in the ophthalmic formulation and its mechanism of action are important for its efficacy. Hence, the pharmacokinetic models are very important in assessing the efficacy. Therefore, these models should be simple and incorporate all the important pharmacokinetic parameters of the process.

References

1. Khanlari S, Dube MA. Bioadhesives: a review. *Macromol React Eng.* 2013;7(11):573–87.
2. Patil SB, Murthy RSR, Mahajan HS, Wagh RD, Gattani SG. Mucoadhesive polymers: means of improving drug delivery. *Pharma Times.* 2006;38(4):25–8.
3. Kamath KR, Park K. Mucosal adhesive preparations. In: Swarbrick J, Boylon JC, editors. *Encyclopaedia of pharmaceutical technology*, vol. 10. New York: Marcel Dekker; 1994. p. 133.
4. Patil SB, Sawant KK. Mucoadhesive microspheres: a promising tool in drug delivery. *Curr Drug Deliv.* 2008;5(4):312–8.
5. Zhang Y, Li H, Wang Q, et al. Rationally designed self-assembling nanoparticles to overcome mucus and epithelium transport barriers for oral vaccines against *helicobacter pylori*. *Adv Funct Mater.* 2018;28(33):1802675.
6. Couvreur P, Dubernet C, Puisieux F. Controlled drug delivery with nanoparticles: current possibilities and future trends. *Eur J Pharm Biopharm.* 1995;41(1):2–13.

7. Pinto Reis C, Neufeld RJ, Ribeiro AJ, Veiga F. Nanoencapsulation I. Methods for preparation of drug-loaded polymeric nanoparticles. *Nanomedicine*. 2006;2(1):8–21.
8. Devadasu VR, Bhardwaj V, Kumar MNVR. Can controversial nanotechnology promise drug delivery? *Chem Rev*. 2003;113(3):1686–735.
9. Rao JP, Geckele KE. Polymer nanoparticles: preparation techniques and size-control parameters. *Prog Polym Sci*. 2011;36(7):887–913.
10. Parveen S, Misra R, Sahoo SK. Nanoparticles: a boon to drug delivery, therapeutics. *Diagnostics Imaging Nanomed*. 2012;8(2):147–66.
11. Caputo F, Clogston J, Calzolari L, et al. Measuring particle size distribution of nanoparticle enabled medicinal products, the joint view of EUNCL and NCI-NCL. A step by step approach combining orthogonal measurements with increasing complexity. *J Control Release*. 2019;299:31–43.
12. Rasmussen MK, Pedersen JN, Marie R. Size and surface charge characterization of nanoparticles with a salt gradient. *Nat Commun*. 2020;11(1):1–8.
13. Liu Y, Yang G, Jin S, Xu L, Zao C. Development of high-drug-loading nanoparticles. *ChemPlusChem*. 2020;85(9):2143–57.
14. Silva MM, Calado R, Marto J, Bettencourt A, Almeida A, Goncalves LMD. Chitosan nanoparticles as a mucoadhesive drug delivery system for ocular administration. *Mar Drugs*. 2017;15(12):370.
15. Casciardi S, Sisto R, Diociaiuti M. The analytical transmission electron microscopy: a powerful tool for the investigation of low-dimensional carbon nanomaterials. *J Nanomater*. 2013;2013:1–15.
16. Ahimou F, Boonaert CJP, Andriaensen Y, et al. XPS analysis of chemical functions at the surface of *Bacillus subtilis*. *J Colloid Interface Sci*. 2007;309(1):49–55.
17. Coleman NJ, Craig DQM. Modulated temperature differential scanning calorimetry: a novel approach to pharmaceutical thermal analysis. *Int J Pharm*. 1996;135(1–2):13–29.
18. Abderrafi K, García Calzada R, Gongalsky MB, et al. Silicon nanocrystals produced by nanosecond laser ablation in an organic liquid. *J Phys Chem C*. 2019;115(12):5147–51.
19. Lewinski NA. Nanoparticle cytotoxicity. In: Bhushan B. (eds) *Encyclopedia of nanotechnology*; Springer, Dordrecht, 2012. p. 1644–51.
20. Bhowmick T, Yoon D, Patel M, Fisher J, Ehrman S. *In vitro* effects of cisplatin-functionalized silica nanoparticles on chondrocytes. *J Nanopart Res*. 2010;12(8):2757–70.
21. Black MJ, Brandt RB. Spectrofluorometric analysis of hydrogen peroxide. *Anal Biochem*. 1974;58(1):246–54.
22. Kongsinlark A, Rempel GL, Prasassarakich P. Hydrogenated polyisoprene-silica nanoparticles and their applications for nanocomposites with enhanced mechanical properties and thermal stability. *J Nanopart Res*. 2013;15(5):1–16.
23. Alsarra IA, Hamed AY, Alanazi FK, Neau SH. Rheological and mucoadhesive characterization of poly(Vinylpyrrolidone) hydrogels designed for nasal mucosal drug delivery. *Arch Pharm Res*. 2011;34(4):573–82.
24. Avci G, Kadioglu H, Sehirli AO, et al. Curcumin protects against ischemia/reperfusion injury in rat skeletal muscle. *J Surg Res*. 2012;172:39–46.
25. Baptista P, Pereira E, Eaton P, et al. Gold nanoparticles for the development of clinical diagnosis methods. *Anal Bioanal Chem*. 2008;391:943–50.
26. Galloway NR, Amoaku WMK, Galloway PH, Browning AC. *Common eye diseases and their management*. London: Springer; 2011.; 100(2). p. 360.
27. Achouri D, Alhanout K, et al. Recent advances in ocular drug delivery. *Drug Dev Ind Pharm*. 2013;39(11):1599–1617.
28. Ghate D, Edelhofer HF. Ocular drug delivery. *Expert Opin Drug Deliv*. 2006;3(2):275–87.
29. Kaur IP, Garg A, Singla AK, Aggarwal D. Vesicular systems in ocular drug delivery: an overview. *Int J Pharm*. 2004;269(1):1–14.
30. Almeida H, Amaral MH, Labao P, Lobo JMS. *In situ* gelling systems: a strategy to improve the bioavailability of ophthalmic pharmaceutical formulations. *Drug Discov Today*. 2014;19(4):400–12.
31. Okada AA, Wakabayashi T, Morimura Y, et al. Trans-Tenon's Retrobulbar triamcinolone infusion for the treatment of uveitis. *Br J Ophthalmol*. 2003;87(8):968–71.
32. Del Amo EM, Urtti A. Rabbit as an animal model for intravitreal pharmacokinetics: clinical predictability and quality of the published data. *Exp Eye Res*. 2015;137:111–24.
33. Chiou GC. Systemic delivery of polypeptide drugs through ocular route. *J Ocul Pharmacol*. 1994;10(1):93–9.
34. Iyer MN, He F, Wensel TG, et al. Intravitreal clearance of moxifloxacin. *Trans Am Ophthalmol Soc*. 2005;103:76–83.
35. Xu L, Lu T, Tuomi L, et al. Pharmacokinetics of ranibizumab in patients with neovascular age-related macular degeneration: a population approach. *Invest Ophthalmol Vis Sci*. 2013;54(3):1616–24.
36. Le KN, Gibiansky L, Good J, et al. A mechanistic pharmacokinetic/pharmacodynamic model of factor D inhibition in cynomolgus monkeys by lamalizumab for the treatment of geographic atrophy. *J Pharmacol Exp Ther*. 2015;355(2):288–96.
37. Ng EWM, Shima DT, Calias P, et al. Pegaptanib, a targeted anti-VEGF aptamer for ocular vascular disease. *Nat Rev Drug Discov*. 2006;5(2):123–32.
38. Proksch JW, Granvil CP, Siou-Mermet R, et al. Ocular pharmacokinetics of Besifloxacin following topical administration to rabbits, monkeys, and humans. *J Ocul Pharmacol Ther*. 2009;25(4):335–44.
39. Mathews D, Mathews J, et al. Low-dose cyclosporine treatment or sight-threatening uveitis: efficacy, toxicity, and tolerance. *Indian J Ophthalmol*. 2010;58(1):55–8.

40. Akpek EK, Vittitow J, et al. Ocular surface distribution and pharmacokinetics of a novel ophthalmic 1% azithromycin formulation. *J Ocul Pharmacol Ther.* 2009;25(5):433–9.
41. Kapanigowda UG, Nagaraja SH, Ramaiah M, Boggarapu PR. Improved intraocular bioavailability of ganciclovir by mucoadhesive polymer based ocular microspheres: development and simulation process in Wistar rats. *Daru.* 2015;23:49.
42. Bakri SJ, Snyder MR, Reid JM, et al. Pharmacokinetics of intravitreal bevacizumab (Avastin). *Ophthalmology.* 2007;114(5):855–9.
43. Edelhauser HF, Rowe-Rendleman CL, Robinson MR, et al. Ophthalmic drug delivery systems for the treatment of retinal diseases: basic research to clinical applications. *Invest Ophthalmol Vis Sci.* 2010;51(11):5403–20.
44. Mannermaa E, Vellonen KS, Urtti A. Drug transport in corneal epithelium and blood- retina barrier: emerging role of transporters in ocular pharmacokinetics. *Adv Drug Deliv Rev.* 2006;58(11):1136–63.
45. Hariharan S, Gunda S, Mishra GP, Pal D, Mitra AK. Enhanced corneal absorption of erythromycin by modulating P-glycoprotein and MRP mediated efflux with corticosteroids. *Pharm Res.* 2009;26(5):1270–82.
46. Majumdar S, Hingorani T, Srirangam R, et al. Transcorneal permeation of L- and D- aspartate Ester prodrugs of acyclovir: delineation of passive diffusion versus transporter involvement. *Pharm Res.* 2009;26(5):1261–9.
47. Gunda S, Hariharan S, Mitra AK. Corneal absorption and anterior chamber pharmacokinetics of dipeptide monoester prodrugs of ganciclovir (GCV): *in vivo* comparative evaluation of these prodrugs with Val-GCV and GCV in rabbits. *J Ocul Pharmacol Ther.* 2006;22(6):465–76.
48. Kansara V, Hao Y, Mitra AK. Dipeptide monoester ganciclovir prodrugs for Transscleral drug delivery: targeting the oligopeptide transporter on rabbit retina. *J Ocul Pharmacol Ther.* 2007;23(4):321–34.
49. Vadlapudi AD, Vadlapatla RK, Earla R, et al. Novel biotinylated lipid prodrugs of acyclovir for the treatment of Herpetic Keratitis (HK): transporter recognition, tissue stability and antiviral activity. *Pharm Res.* 2013;30(8):2063–76.
50. Boddu SHS, Gunda S, Earla R, Mitra AK. Ocular microdialysis: a continuous sampling technique to study pharmacokinetics and pharmacodynamics in the eye. *Bioanalysis.* 2010;2(3):487–507.



Pharmacokinetic and Tissue Distribution Study of Solid Lipid Nanoparticles

13

Himanshu Paliwal, Bhupendra G. Prajapati,
Dignesh Khunt, Chilakapalli Shirisha,
Jayvadan K. Patel, and Yashwant V. Pathak

Contents

1	Introduction	246
2	Composition of SLN	247
3	Pharmacokinetics and Biodistribution of SLNs Administered via Different Routes	247
4	SLNs for Oral Administration	248
5	SLNs for Injectable Administration	250
6	SLNs for Targeted Delivery	252
7	SLNs in Biologic and Diagnostic Products	253
8	SLNs for Topical Delivery	254
9	SLNs for Ocular Delivery	255
	References	257

Abstract

In recent times, the development of therapeutic products by using nanoparticle technology has given rise to progressive increment in a number of investigations based on improvement of solubility, penetrability, stability, etc. Solid lipid nanoparticles (SLN) involve absorption and localization through transcellular and paracellular mechanism which is one of the advanced nanoparticle-based formulations of the low solubility of drugs. This chapter entails the outline of the vital features of solid lipid nanoparticles and describes the pharmacokinetic and distribution outcomes of the SLN formulation designed for various

The original version of this chapter was revised. The correction to this chapter is available at https://doi.org/10.1007/978-3-030-83395-4_23

H. Paliwal · B. G. Prajapati (✉) · D. Khunt
C. Shirisha
Shree S.K. Patel College of Pharmaceutical
Education and Research, Ganpat University,
Mahesana, Gujarat, India

J. K. Patel
Nootan Pharmacy College, Faculty of Pharmacy,
Sankalchand Patel University, Visnagar, Gujarat,
India

Y. V. Pathak
University of South Florida Health, Tampa, FL, USA

routes. The key benefits of using such a nano-carrier in specific therapeutic circumstances and to resolve production and delivery issues are discussed. The major portion covers the explanation on pharmacokinetic studies undertaken in some of the recent researches categorized for oral delivery, injectable administration, topical delivery, biologic and diagnostic products, and ocular delivery. The aim was to present a fresh perspective over the pharmacokinetic and tissue distribution characteristics by means of current state-of-the-art of SLN research.

Keywords

Solid lipid nanoparticles · Pharmacokinetics · Tissue distribution · Oral delivery · Bioavailability · Targeted delivery · Nanocarrier · Topical delivery

1 Introduction

Lipid components are used from so many years in pharmaceutical fields for the development of various forms such as lotion, suppository, and ointments, among others. The lipid components receive higher approvals for parenteral and oral delivery formulation due to their high binding ability with the stratum corneum and inertness [1].

The first choice for lipid vehicles is the phospholipid which have different properties such as multifunctionality, amphiphilic nature, and biocompatibility [2]. Different lipid-based delivery systems include microemulsion, microspheres, vesicle based, and SLNs.

The origination of SLN system has been attributed to resolve the issues associated with the preparation, drug entrapment, and scalability of delivery systems such as liposomes, nano-emulsions, and polymeric nanoparticles. SLNs are expected to be more stable than vesicular systems, and their fabrication requires application high-pressure homogenization. In addition to these, SLNs allow surface modifications to produce smart delivery system for targeted delivery of active molecules [2].

In the 1990s, Muller et al. (2002) [3] formulated two novel carriers, i.e., solid lipid nanoparticles (SLNs) and nanostructured lipid nanoparticles (NLC) using lipid material. The aim of the development of SLN and NLC is to utilize the advantages of nanoparticles and also lipid components [4]. Solid lipid nanoparticles (SLNs) are colloidal carriers with a size range of 1–1000 nm where lipid cores are stability using emulsifiers [5]. It has emerged as a novel carrier for the delivery of different classes of therapeutics moiety and also in other fields such as imaging agent, cosmetics, agriculture, and also in nanoreactors. Recently, novel cationic SLNs have attracted attention due to their application for the delivery of genes and also cationic nature which helps bind DNA and also protects against enzymatic degradation [6–9]. One of the promising benefits of SLN is overcoming the reticulo-endothelial system and prolong the duration of active components in the body [5, 10]. Other numerous benefits of SLN include the following: encapsulation of hydrophilic and lipophilic drugs, provide physical stability, low cost in comparison with liposomes, and easy to manufacture [11, 12]. In addition, SLNs are a good choice for brain targeting [13, 14], epidermis targeting [1], and also as controlled-release vehicles [15].

SLNs are a safe and flexible carrier for the delivery of drug, gene, and nucleic acid and safe for particular administration routes [16]. New technologies have been developed for SLN production and are currently under investigation to obtain the optimum encapsulation of different drug categories and to deliver the bioactive compounds at the desired site. Details of different materials, methods, and characterizations are already covered by Geszke-Moritz and Moritz (2016) [17] and Mehnert (2001) [11]. But, SLNs have a strong lipophilic nature which hurdles dispersion in aqueous media, so a sufficient lower size is needed to spontaneously disperse them in water. For that reason, it required higher energy input to reduce size. One of the common steps in all SLN methods is applying the energy in different forms such as high pressure [18, 19], probe sonication [5], and microwaves [20]. High energy decreases the lipid components' size and

increases surface area. These higher surface area-containing particles need to be dispersed in aqueous media and for that needs stearic or electrostatic stabilizers [11]. Surfactants play two crucial roles in the stabilization of SLNs: (a) dispersion of the lipid melt in aqueous phase and (b) providing the stability of lipid nanoparticles after cooling [21]. Different types of surfactants are used for the stability of SLN. Broadly, surfactants are classified into amphoteric (such as phosphatidylcholines families), non-ionics (such as polysorbate 20, polysorbate 80), and ionic (such as sodium oleate, sodium taurodeoxycholate, sodium cholate). In comparison to the ionic lipid, non-ionic lipids have low toxicity and also irritation and that is why they are the first choice for oral and parenteral routes [21]. Major concern related to clinical safety is probability of toxicity due to surfactants for parenteral dosage forms while for oral and transdermal not problematic [22]. Lower size and higher surface increase the absorption of drugs which increase the bioavailability of drugs [23].

In spite of numerous merits, SLNs also have demerits such as physical instability which is characterized by the particle growth and burst release of drug. Particle aggregation and growth are major drawbacks for the parenteral route which can lead to emboli formation and also many more complications [24].

Different types of lipids, viz., cationic lipids, anionic lipids, and non-ionic lipids, are used for the formulation of SLN. Again, these lipids are different based on different fatty acids with chain lengths of hydrocarbon (stearic acid, palmitic acid, dodecanoic acid, and myristic acid), glycerides (tripalmitin, caprylate triglycerides, tribehenin), fatty ester (cetyl palmitate), fatty alcohols (oleyl alcohol, stearyl alcohol), and mixture of glyceryl esters (glyceryl behenate, glyceryl monostearate, glyceryl hydroxystearate). Different cationic lipids such as chloroquine phosphate, benzalkonium chloride, octadecylamine (stearylamine), dimethyldioctadecylammonium bromide, and cetylpyridinium chloride are used for the preparation of cationic SLN [21]. Different advantages and their challenges are shown in Fig. 13.1.

2 Composition of SLN

SLNs are generally spherical with smooth exterior which also governs in vitro and in vivo performance. They are mostly comprised of solid lipid (at room temperature), emulsifiers, therapeutic moiety, and suitable solvents. Based on the loading of therapeutics moiety, SLNs are classified with different models, such as (a) shell-loaded therapeutics moiety, (b) core-loaded therapeutics moiety, and (c) matrix-type model.

Shell-loaded therapeutics moiety is developed when the solid lipid is melted into the hot liquid droplets which are further subjected to separation during cooling phase [26]. Precipitation is one of the common mechanisms for the formulation of nanoparticles. In the case of SLNs, rapid cooling leads to solidification of melted liquid lipid droplets and completion of cooling leads to the formation of SLNs. The lipid is solidified initially before the therapeutics moiety, so that therapeutics moiety gets encapsulated in the shell. On the other hand, the core-loaded therapeutic moiety is based on the fact that therapeutic moiety is crystallized first and crystallized drug gets encapsulated by lipid undergoing crystallization. This model is the best for the sustained release of therapeutics moiety. Matrix-type models are commonly applied for the highly hydrophobic therapeutics moiety where therapeutics moieties are uniformly mixed inside the lipid matrix [2].

3 Pharmacokinetics and Biodistribution of SLNs Administered via Different Routes

SLNs have shown their potential in enhancing the therapeutic activity of active ingredients against various diseases, primarily owing to the alteration of physicochemical and biopharmaceutical characteristics. These lipid-based nanoparticles may be developed for targeted distribution and enhanced pharmacokinetic profile [27]. The disease target of SLNs has been a num-

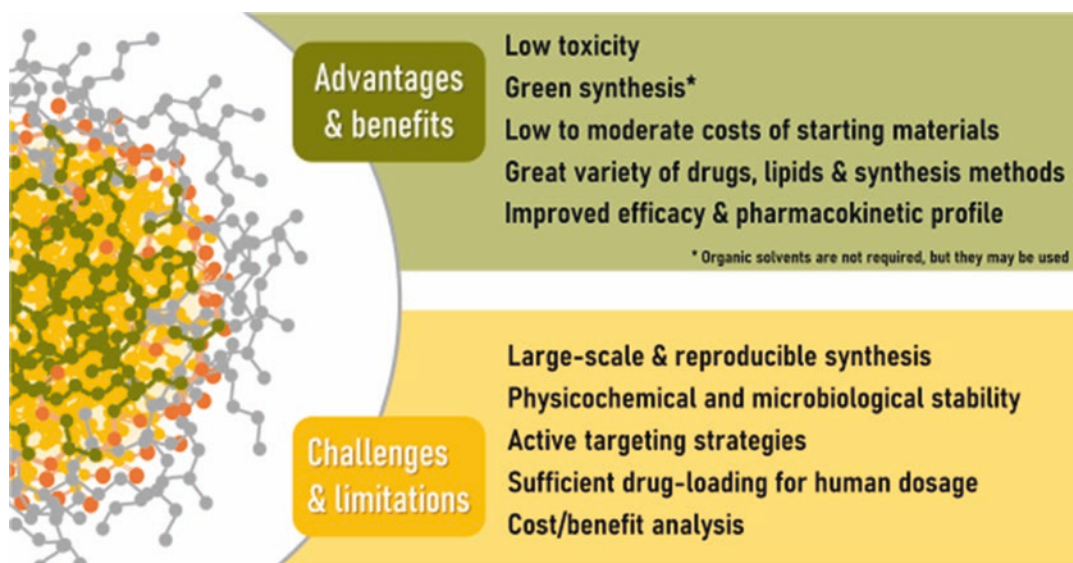


Fig. 13.1 Different benefits, challenges, and limitations of solid lipid nanoparticles (reproduced from Scioli Montoto (2020) [25], an open-access article distributed

under the Creative Commons Attribution License that permits unrestricted use, distribution, and reproduction in any medium)

ber of fatal and epidemic diseases, wherein advanced therapeutic products are desired. A great deal of efforts have been made for cancer treatment to encapsulate and deliver lipophilic as well as hydrophilic molecules in a targeted manner [28]. The following explains about the various therapeutic strategies of SLNs employed for using specific route of administration to deliver drug and/or biologicals. The main focus is on the discussion about pharmacokinetics and tissue distribution of the nanoparticles to indicate their therapeutic potential.

4 SLNs for Oral Administration

In recent times, the use of oral nanoparticles for improving solubility, permeability, and stability for various drugs has been tried out extensively. The absorption of SLNs via paracellular and transcellular routes has shown a lot of promise to deal with issues faced due to low water-soluble drugs [29]. Enteric SLNs for targeting the duodenum were formulated incorporating tilmicosin

with regard to specific region of absorption and mechanism of transport. Tilmicosin is a veterinary antibiotic which faces problems of low solubility, low penetrability, presystemic metabolism, lack of release at desired sites, etc. The outcomes of $T_{1/2}$, mean residence time (MRT), and oral absorption for enteric SLNs of tilmicosin increased several folds as compared to the commercial preparation tilmicosin. The low C_{max} (755 ng/ml) and high AUC ($11.31 \mu\text{g}\cdot\text{h}\cdot\text{mL}^{-1}$) values of enteric SLN formulation was due to rapid release in gastric region and slow release in intestine. These SLNs went on to achieve sustained release along with better oral absorption owing to reduced metabolism and duodenal-specific localization of drug [30]. The enteric SLNs containing enrofloxacin was prepared to enhance the bioavailability and reduce unwanted gastric mucosa response and stability issues. The formulation was developed by employing hot homogenization and ultrasonic emulsification method. The SLNs were injected through intragastric route which initially led to rapid increase in plasma concentration of enrofloxacin up to

0.52 $\mu\text{g}/\text{mL}$ upon completion of 3.33 h, followed by slow reduction in concentration up to 0.03 $\mu\text{g}/\text{mL}$ at 72 h. The area under curve and mean residence time was 4.26 $\mu\text{g h}/\text{mL}$ and 6.80 h, respectively, for powder drug which increased up to 11.24 $\mu\text{g h}/\text{mL}$ and 17.97 h for enteric SLNs of drug. In comparison with the powder drug, the bioavailability, $T_{1/2}$, and MRT raised to about 2.64-, 2.67-, and 2.64-fold, respectively, after being formulated as enteric SLNs. The outcomes have shown that the SLNs can prove to be a useful technique for overcoming other similar formula-related issues as well [31].

Dronedarone HCl is a potent antiarrhythmic drug which faces bioavailability issues due to low water solubility. A recent literature has explained about the development of SLNs of dronedarone HCl by using glyceryl monostearate. The pharmacokinetic studies of the prepared SLNs showed improvement in bioavailability by 2.68-fold as compared to the pure drug suspension. The outcomes were favorable for using the oral SLNs of dronedarone HCl to counter problems like low bioavailability and first pass effect. However, the bioavailability of the drug reduced from SLNs when given along with chlorpromazine which showed the uptake of SLN takes place via endocytosis [32]. Figure 13.2 shows the diagrammatic representation of different pathways of absorption of oral SLNs. To improve oral bioavailability of felodipine, SLNs were developed by using effervescent dispersion technique in order to have some edge over tradition preparation techniques. Pharmacokinetic studies performed on beagle dogs showed rise in area under curve up to 3.17-fold after oral administration. Furthermore, the C_{max} increased from 34.9 $\mu\text{g}/\text{L}$ for free felodipine to 329.42 $\mu\text{g}/\text{L}$ for the SLN formulation. The observations were impressive and suggested that bioavailability of the drug increased considerably due to increase in solubility. The higher absorption could also be possibly due to absorption of drug lymphatic route which led to diminishing the presystemic metabolism [33].

The curcumin-loaded SLNs were prepared using surfactants such as tristearin and polyethyl-

ene glycol. These emulsified SLNs with varied concentration of surfactants were tested for their pharmacokinetic profile by using male Sprague–Dawley rats. The high and comparable C_{max} , AUC, T_{max} , and bioavailability values were observed for SLNs prepared with both 17.1 mM and 46.9 mM PEG100SE concentration. The PEGylated SLNs possess no charge on the micelle which allowed rapid permeation of the SLNs through mucus layer of epithelium [34]. A study was published by Kumar et al. where they prepared SLNs by incorporating all-trans retinoic acid (ATRA) by employing novel microemulsification method. However, ATRA is known for its effectivity against several inflammatory disorders, but low solubility and instability hinder the therapeutic efficiency. SLNs of ATRA improved their solubility and stability to a great extent and thereby can be looked upon as potential carrier. Nevertheless, pharmacokinetics and biodistribution studies may be performed to further confirm the therapeutic potential of the product [35].

Camptothecin (CPT) is a potent anticancer agent whose activity is hindered due to low bioavailability and undesirable side effects. CPT was linked with palmitic acid by using disulfide linker and loaded into SLNs to generate a redox sensitive formulation (CPT-SS-PA) for successful oral delivery. The CPT-SS-PA SLN showed sustained release as compared to CPT SLN and plain CPT suspension with the peak concentration at 4 h of 2.31 $\mu\text{g}/\text{mL}$ and area of curve of 8.66 $\mu\text{g}/\text{L.h}$. Although the pharmacokinetic profiles of CPT-SS-PA SLN and CPT SLNs are comparable, CPT-SS-PA SLN showed significantly higher bioavailability. The study claimed that such modified strategies can be useful in improving oral bioavailability as well as decreasing chances of side effects [36]. The macrophage internalization of camptothecin-containing SLNs studied by using fluorescent marking is included from the research published by Martins et al. (Fig. 13.3). A group of scientists prepared SLN of lurasidone hydrochloride by using high-pressure homogenization method to improve its absorption and bioavailability when administered

through oral route. The C_{max} from SLNs was about 578.23 ng/ml, which was 2.76-fold higher than the plain drug suspension. The area under curve and T_{max} for SLN was reported to be 5871.84 ng.h/ml and 6 h, respectively, and prolonged $t_{1/2}$ and MRT showed slow elimination of drug from SLNs. The bioavailability of drug from SLN was 5.16-fold higher than drug suspension which is probably due to smaller particle and large surface area of the nanoparticles. High bioavailability may also be resulted because of lymphatic uptake of SLNs, thereby bypassing the presystemic metabolism. Furthermore, the study also established that intestinal lymphatic transport is an important mechanism for the absorption of the drug. The results of C_{max} and AUC reduced in the presence of cycloheximide because of inhibition of generation of chylomicrons from

the enterocytes and lymphatic transport of drug also decreased [37].

5 SLNs for Injectable Administration

The nanoparticles administered through intravenous route are swiftly taken up and cleared from the circulation by reticuloendothelial system which are primarily accumulated in the spleen and liver. The development of SLNs or even modifying them with the help of emulsifiers may result in prolonged retention in the circulation. Loureiro et al. developed the SLNs containing resveratrol and grape skin and seed extracts for the treatment of Alzheimer’s disease. Resveratrol is quickly metabolized into glucuronic acid and sulfate conjugates in the liver and epithelial cells

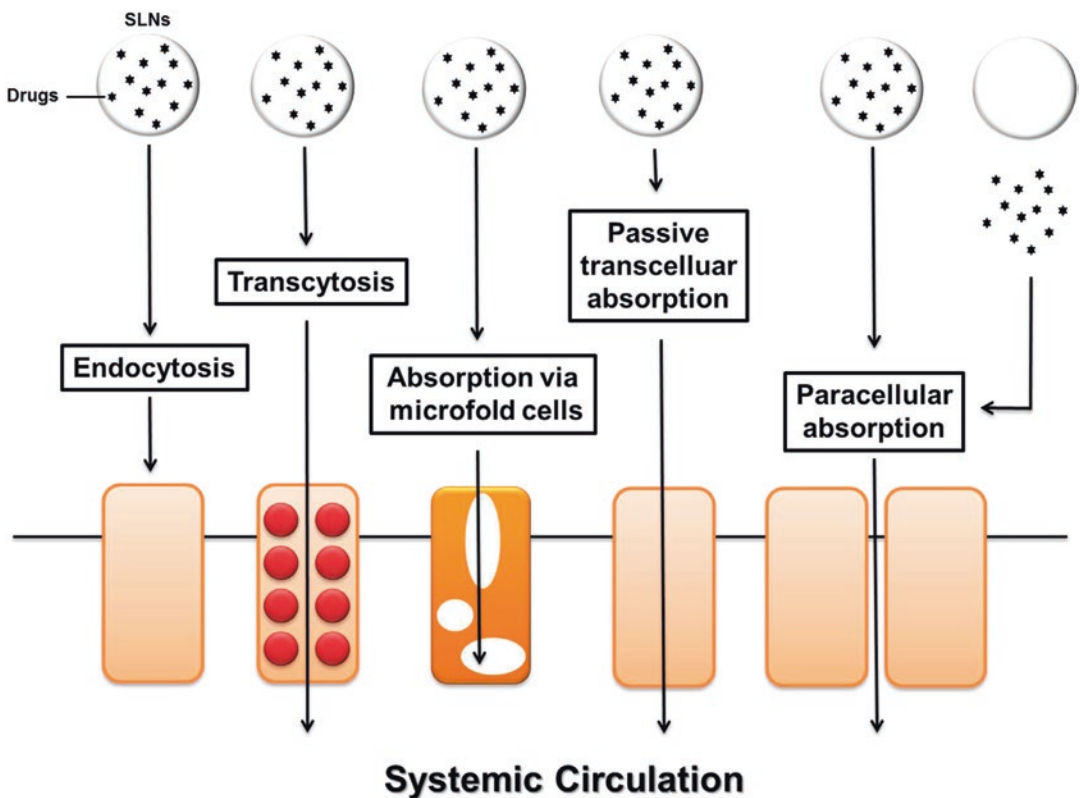


Fig. 13.2 Diagrammatic illustration of different pathways of SLN absorption via oral route (reproduced from Lin CH 2017 [38], an open-access article distributed

under the Creative Commons Attribution License that permits unrestricted use, distribution, and reproduction in any medium)

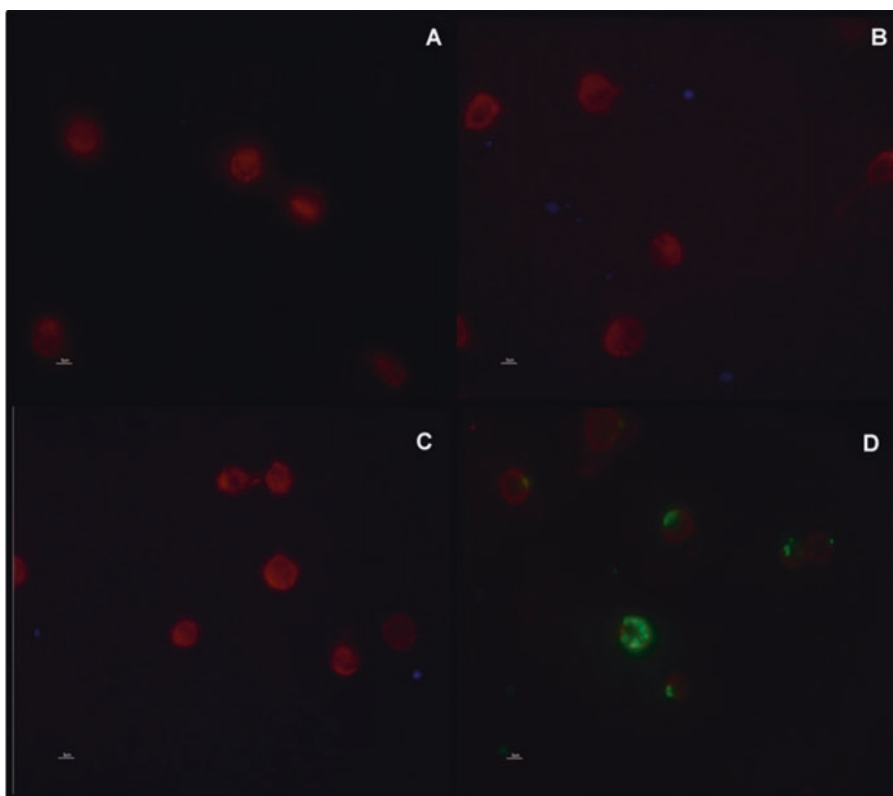


Fig. 13.3 Illustration of macrophage internalization of SLNs containing camptothecin with the help of fluorescent marking. The literature indicated that different lipids incorporated within the formulations were indicated

with blue color in the images (a–c). FluoSpheres® and Alexa Fluor® 594 internalization was represented around macrophage layer by green and red color (d), respectively [39]

of the intestine, followed by elimination from the body. To deal with these issues, SLNs were associated with anti-transferrin receptor monoclonal antibody (OX26) to facilitate the transportation of the active product to the brain. The OX26 SLNs demonstrated considerable cellular uptake as compared to the normal SLNs indicating the better transcytosis of the functionalized SLNs [40]. A group of scientists developed cationic SLNs for the delivery poorly water-soluble drugs and biotechnology products. They investigated the toxicological profile of cationic SLNs by evaluating the distribution of drug in different organs at 24 and 72 h post intravenous injection. It was reported that migration of macrophages in the liver, lungs and spleen took place after administration of cationic SLNs. The permeability across blood-brain barrier was indicated as cationic SLNs moved to brain parenchyma with no damaging effects to the barrier [41].

An attempt was made to develop SLNs of buparvaquone by using modified nanoprecipitation method to improve splenic uptake of the drug. SLNs were radiolabeled with ^{99m}Tc to provide adequate stability and targeting characteristic. The biodistribution studies indicated maximum localization of SLNs in the organs of reticuloendothelial system, with considerably high accumulation in the spleen as compared to the liver. A remarkable high spleen to liver concentration ratio (11.94 at 3 h) affirmed high uptake by spleen which is probably due to circumventing the Kupffer cells and low molecular weight of the SLNs. The study was admirable in targeting the spleen for drug delivery, especially in the cases of theileriosis and other spleen-specific infections [42]. Agomelatine, a novel antidepressant, undergoes substantial presystemic metabolism which leads to very low absolute bioavailability. An attempt was made to

develop SLN of agomelatine for improving bioavailability and penetration across blood-brain barrier, and pharmacokinetic studies were carried out for comparison of intravenous and intranasal delivery routes. The C_{max}, area under curve, and absolute bioavailability of SLNs were 759 ng/mL, 7805.69 ng.min/mL, and 44.44%, respectively, which are significantly higher as compared to oral suspension of the drug. The optimized formulation showed better targetability from intranasal route as compared to intravenous route. The formulation also displayed direct transport % of 47.37 which showed drug delivery in the brain predominantly takes place directly from the nose to brain pathway [43].

6 SLNs for Targeted Delivery

Some of the active pharmaceutical ingredients and biotechnology products require targeting a specific organ or tissue to achieve maximum therapeutic efficiency with minimum adverse effects. SLNs and their modified derivatives may be utilized for subjugating the intracellular and extracellular barriers that have significant impact over delivery. A number of literatures pondering over detailed description of the specific type of solid lipid nanoparticles to incite targeted delivery and their pharmacokinetics study are included in this portion of the chapter [44]. The targeting of alveolar macrophages was carried out by the researcher who prepared SLN assemblies modified on the surface with mannosylated surfactant (hexadecanoic acid (aminoethyl α -D-mannopyranoside) amide) containing rifampicin as model drug for tuberculosis. The biodistribution studies were carried out over the SLNs functionalized with mannosylated surfactant, and outcomes were compared with plain drug and non-functionalized SLNs post intratracheal administration in mice. The functionalized SLNs displayed the maximum retention in pulmonary region while low distribution in extra-pulmonary regions. This outcome could be possible because of significant phagocytosis by alveolar macrophages as compared to non-functionalized SLNs. Therefore, the surface modification of lipid

nanoparticles may allow better treatment focusing over the specific organ which is majorly affected by the disease [45].

A targeted oral SLN-based product for veterinary use has already been discussed previously, wherein enteric granules of tilmicosin were formulated SLNs. The product is designed for targeted delivery to the duodenum region for maximizing the oral absorption [30]. The use of glucocorticoid therapy for prolonged duration in high concentration for the treatment of rheumatoid arthritis may give rise to unwanted adverse effects. Prednisolone was incorporated in to SLNs and encapsulated with hyaluronic acid to prepare a targeted formulation against rheumatoid arthritis. The main reason behind coating the SLNs with hyaluronic acid (HA) is that it leads to prolonged circulation and localization at the inflammation site for targeted delivery. The biodistribution study showed considerable reduction in plasma drug concentration in animals administered with free drug in comparison with animals administered with HA-coated SLNs upon completion of 4 h after injection. The retention of HA-coated SLNs also translated into greater localization at the joints which is desirable in the case of rheumatoid arthritis [46].

One approach to improve bioavailability is to target the lymphatic route, especially for those drugs which are hampered by presystemic metabolism. Quetiapine fumarate was formulated into SLNs to be administered through intraduodenal injection targeting lymphatic system. SLNs were prepared using various lipids by employing microemulsion technique and subjected to *in vivo* pharmacokinetic studies. The optimized SLN was compared with plain drug suspension to assess the pharmacokinetic parameters. The results suggested that area under curve of the optimized SLN was considerably higher than the drug suspension. The bioavailability was also obtained similar to area under curve results, as SLNs showed 2.76 times higher bioavailability in comparison with plain drug suspension [47]. Pinheiro et al. developed quercetin lipid with surface functionalized with RVG29 peptide for targeting the brain better and improve neuronal uptake for the treatment

of Alzheimer's disease. The permeability studies using in vitro blood-brain barrier model showed 1.5 times improvement in penetrability when functionalized nanoparticles were compared with non-functionalized ones. Although the results were impressive, pharmacokinetic and biodistribution studies should be performed to assess the in vivo behavior and targetability of the formulation [48].

7 SLNs in Biologic and Diagnostic Products

Solid lipid nanoparticles are considered to be one of the promising carriers for the biological products, such as vaccines, serum, protein, and peptide drugs, as an efficient and safe substitute for the treatment of various diseases. The main attributes of SLNs are its ability to deal with challenges with regard to stability against degradation, better cell uptake, intracellular accumulation, targetability potential, etc. Furthermore, they offer several benefits with regard to their safety as SLNs are fabricated with tolerated excipients and ease of scalability [49–51]. The oral delivery of insulin has been mostly challenging because of degradation by gastrointestinal enzymes and inadequate absorption through intestine. An attempt was made to develop insulin-loaded cetyl palmitate-based SLNs and characterizing their potential as carrier system. SLNs were fabricated using modified solvent emulsification and evaporation method, and in vivo behavior of the product was estimated. The study displayed that after administration of SLNs into the male Wistar rats, the minimum plasma glucose concentration reached to about 73.2% of the initial concentration within 14 h of period. Apart from that, relative bioavailability of insulin-loaded in SLNs (5%) was higher than that from the oral insulin solution (1.6%). The outcomes suggested that SLNs avoid degradation of insulin and improve intestinal absorption. It was also seen that plasma glucose levels reduced significantly after oral administration of SLNs as compared to the oral insulin solution after 24 h [52]. Muntoni et al. developed the SLNs of insulin and glargine-

insulin by utilizing the fatty acid coacervation technique to protect the insulin from enzymatic degradation. The pharmacokinetic studies revealed that differential gastric emptying on the uptake of drug and absorption maxima is achieved upon completion of 30 min post administration. The bioavailability obtained after duodenal and gavage administrations was observed to be 6.10% and 4.5%, respectively. The concentration estimated in the lymph was about 2.0 $\mu\text{g/mL mg}^{-1}$ at 1.5 h post duodenal administration, which showed that intestinal uptake of drug is primarily dependent upon lymph. The outcomes of the glucose responsiveness were estimated in healthy rats which showed considerable reduction in glucose at 2.5 h and even slow reduction was observed upon completion of 6 h [53].

The modification of SLNs with the help of ligand attachment may serve to achieve better bioavailability, in the case of protein drugs and peptides. Fan et al. reported the fabrication of salmon calcitonin-containing SLNs which were attached with two different peptides to form two types of SLNs. One of the products was sCT CSK-SLNs, which was presumed to have more affinity for goblet cells and sCT IRQ-SLNs for imparting cell penetrating power. The investigation conformed about superior protection to active pharmaceutical ingredient and internalization of drug through the mucosal cells of the duodenum. The mucus layer was a significant barrier to the movement of the drug across membrane, but modified SLNs showed enhanced drug absorption. The absolute bioavailability of the sCT CSK-SLNs and sCT IRQ-SLNs was found out to be 12.41% and 10.05%, respectively. There was close to twofold rise for the modified SLNs in comparison with unmodified SLNs [54]. The strategy of modification by using peptides was taken even further by Juang et al. who prepared pH-sensitive SLNs modified using peptides for effective delivery of irinotecan. Irinotecan is a potent anticancer agent for colorectal cancer, which was incorporated into a specialized carrier to possess targeted pH-dependent release and better cell internalization. The outcomes of the in vivo studies showed that targeting by pH-responsive carriers was successful as they sup-

pressed the colorectal tumor growth and decreased associated toxicity [55].

The nanotechnology-based diagnostic agents furnish more efficient along with negligible issues with regards to safety. Correspondingly, the diagnosis through imaging techniques is considered to have potential for future prospects by using novel nano-based imaging contrasting agents. A SLN-based diagnostic product was prepared to improve contrasting characteristics while performing magnetic resonance imaging for the diagnosis of colorectal cancer. The two types of SLNs were fabricated by incorporating the gadolinium diethylenetriaminepentaacetic acid and fluorescein isothiocyanate. The prepared SLNs were intravenously administered into mice, and magnetic resonance colonography was performed for the examination of colon. The signal to noise ratio raised from 1.54- to 1.74-fold in colorectal tumors after administration of gadolinium fluorescein isothiocyanate-containing SLNs. In case of SLNs containing gadolinium diethylenetriaminepentaacetic acid, signal to noise ratio raised from 1.39- to 1.57-fold [56].

8 SLNs for Topical Delivery

SLNs have also displayed promise as an advanced drug carrier for the topical delivery of a number of active pharmaceutical ingredients. The conventional drug delivery systems of some topical agents are associated with moderate to severe side effects which hamper their therapeutic potential. Presumably, the reduction of side effects and enhancement of therapeutic activity are attainable by formulating these topical agents as SLN carriers. Despite showing a lot promise, there is still obscurity about the absorption mechanisms and cellular uptake of the topical lipid nanoparticles. This portion of the chapter entails the discussion about some of the important researches on topical SLN with their pharmacokinetic considerations [57–59]. The SLNs of penciclovir, a potent and highly selective inhibitor of herpes viruses, was formulated and proved that penciclovir-loaded SLNs are a promising carrier for topical delivery. The *in vitro* percutaneous

permeation and skin uptake behaviors in the rat skin penetration indicated twofold increase compared to commercial cream as a control at 12 h. The microscopic examination of the skin surface showed the apparent morphology of stratum corneum and broke the close conjugation of corneocyte layers. The amount of penciclovir penetrated into dermis from SLNs increased by 130% [60]. Meloxicam-loaded hydrogel of SLNs was studied by Kahlil et al. The 48 h *in vitro* study showed sustained release of drug. The formulation further studied for suppression of UV-induced erythema compare to commercial gel (0.5%) as a reference product in adult male Wistar rats. The results of the degree of erythema upon exposure to UVB radiation was monitored over 72 h and concluded that 67% of rats receiving SLN gel showed complete suppression of erythema evidenced by high mean erythema score value. Similarly, histopathological analysis of excised skin sections also proved superiority of formulation and showed normal histology with SLN-loaded hydrogel [61].

Bhalekar et al. studied piperine (a natural alkaloid) SLN dispersion for the treatment of rheumatoid arthritis. CFA-induced arthritis model was used for *in vivo* pharmacodynamic study in rat. Photomicrographs of joint section obtained during histopathology study indicated that piperine SLN gel showed minimal infiltration of inflammatory cells and connective tissue proliferation as compared to test group. TNF α assay by ELISA study showed that activated macrophages was seen to have considerably decreased as related to arthritic control group it may be attributed to the selective accumulation of piperine SLNs in inflamed site, thus reducing the secretion to TNF α from the activated macrophages [62]. SLNs were used as a carrier for topical ocular delivery of tobramycin by a group of scientists and compared with marketed formulation Tobral[®]. Dispersion of SLNs containing 0.3% w/v was administered to eye of rabbits to evaluate the ocular tolerance and potential irritation. The pre-ocular retention study by fluorescence in conjunctival sac and on corneal surface suggested four times longer retention in eye. The aqueous humor concentra-

tion of the drug was measured for 6 h indicating that the C_{max} ($36.30 \mu\text{g}/\text{mL}^{-1}$), T_{max} (4.0 h), and high AUC ($155.08 \mu\text{g}\cdot\text{h}\cdot\text{mL}^{-1}$) of SLNs dispersion were significantly higher compared to solution [63].

Nair et al. investigated clarithromycin-loaded SLNs to increase the ocular permeation and improve the therapeutic potential of the drug in topical ocular drug delivery. The permeation study of SLNs showed significantly higher permeation ($30.45 \text{ g}/\text{cm}^2/\text{h}$; $p < 0.0001$) as compared to control (solution). Pharmacokinetics data demonstrated significant improvement of clarithromycin bioavailability ($p < 0.0001$) from SLN formulation, as evidenced by a 150% increase in C_{max} ($\sim 1066 \text{ ng}/\text{mL}$) and a 2.8-fold improvement in AUC ($5736 \text{ ng h}/\text{mL}$) ($p < 0.0001$) as compared to control drug solution (C_{max} ; $655 \text{ ng}/\text{mL}$ and AUC; $2067 \text{ ng h}/\text{mL}$) [62]. Minoxidil is currently known for the treatment of androgenic alopecia, but it needs to be formulated into carrier with good penetration and non-corrosive characteristics. A 5% minoxidil was incorporated with the help of combination of polysorbates and sorbitan oleate. The skin penetration studies revealed that minoxidil is primarily distributed within the outermost layer of the skin, and only little amount was able to get to the dermis. However, the distribution of minoxidil was similar in the epidermis and dermis layer upon completion of 24 h after administration [65]. The SLNs for the topical delivery of tretinoin have also been reported as this potent anti-psoriatic agent unleashes irritating side effects, such as erythema and peeling. A biocompatible SLN of tretinoin was prepared to enhance its cutaneous delivery, stability, and pharmacodynamic features. The confocal laser screening microscopy showed that after topical application of the SLN formulation, it has penetrated into the different layers of the skin. The investigation involved preparation and examination of several nano-carriers for the delivery of tretinoin, and SLNs came out to be one of the promising systems from the study [66].

9 SLNs for Ocular Delivery

The conventional oral products face bioavailability issues because of brief contact time with ocular structures and quick washout due to tear production. Furthermore, the efficient delivery to the posterior region of the eye is difficult, and opting for alternate route may be required [67]. To resolve these issues, SLNs emerged as suitable carriers for delivery of drug as well as biotechnological agents. Lipid nanoparticles integrate the benefits of other systems like polymeric nanoparticles, nanoemulsions, and liposomes, while evading their shortcomings [68]. The ocular SLN carrier was prepared for topical administration of tobramycin. The formulation composed of ion-pair complex of tobramycin and hexadecyl phosphate was fabricated by employing warm microemulsion method. The pharmacokinetic study of SLN was performed in aqueous humor for estimating the AUC, C_{max} , T_{max} , and bioavailability. The outcomes suggested that bioavailability of tobramycin produced by SLN was much higher as compared to the reference eye-drops. The SLN produced increment in C_{max} , T_{max} , and AUC up to 1.5-, 8-, and 4-fold as compared to the reference solution. The greater bioavailability resulted from the SLN was probably due to prolonged retention which was estimated from the retention study. It was also suggested in the literature that the use of permeation enhancer like Epikuron 200 may have boosted up the corneal passage of the drug [69].

The tetrandrine-containing SLNs were developed by melt emulsification and ultra-sonication method. The observations of AUC ($6581.50 \mu\text{g}/\text{h}/\text{L}$) and C_{max} ($1103.43 \mu\text{g}/\text{L}$) were all determined to be considerably higher in comparison with tetrandrine solution. In addition to these, the prolonged $t_{1/2}$ (13.86 h) and MRT (19.37 h) were estimated for SLNs. The biodistribution study showed that the highest concentration showed up in lungs post intravenous administration. The SLN uptake was also significantly higher in reticuloendothelial system organs than normal drug solution. It was also

ascertained that SLNs were taken to the liver and spleen through the phagocytosis or endocytosis mechanism. The localization of drug from SLN was lower than drug solution in the heart and kidney [70].

Ahmad et al. developed the SLN containing etoposide for the effective ocular delivery, specifically to the posterior region. The preparation of SLN was carried out by using melt emulsification and ultra-sonication method. The etoposide-containing SLNs displayed prolonged release of etoposide for 1 week in vitreous humor with C_{max} of 46.75 µg/mL, and concentration of etoposide was maintained constant throughout the week. Contrarily, the animals administered with etoposide solution showed C_{max} of 73.18 µg/

mL, but very little amount of observed at day 2 after administration. AUC (657.9 µg.h/mL) and t_{1/2} (7.75 h) were also significantly higher in case of SLN as compared to etoposide solution. The scintigraphic study was performed by labelling the SLNs with Tc-99m to understand their distribution. It was observed that radiolabelled nanoparticle showed relatively homogeneous distribution throughout the vitreous. The nanoparticle formulation was retained at the retinal region for long period with no or little concentration observed in systemic circulation until 24-h post administration [71]. Table 13.1 summarises outcomes of pharmacokinetic studies performed on solid lipid nanoparticles administered through various routes.

Table 13.1 Summary table of outcomes of pharmacokinetic studies performed on solid lipid nanoparticles administered through various routes

Sr. No.	API/Drug	Route of administration	Pharmacokinetic parameters	References
01	Tilimicosin	Oral	Sevenfold increase in MRT and t _{1/2}	[30]
02	Enrofloxacin	Oral	The oral bioavailability, T _{1/2} , and MRT raised to about 2.64-, 2.67-, and 2.64 fold	[31]
03	Dronedarone HCl	Oral	Bioavailability increased 2.68-fold	[32]
04	Felodipine	Oral	AUC rise to 3.17-fold	[33]
05	Camptothecin (SLN of drug linked with palmitic acid)	Oral	Significantly higher bioavailability	[36]
06	Lurasidone	Oral	Bioavailability is 5.16-fold higher	[37]
07	Cannabinoid	Oral	Twofold to eightfold higher bioavailability	[72]
08	Nitrendipine	Oral	Three- to fourfold increase in bioavailability	[73]
09	Ganciclovir (borneol-modified)	Injectable	Enhances the transport of to the brain	[74]
10	Resveratrol (SLNs associated with anti-transferrin receptor monoclonal antibody)	Injectable	Considerable cellular uptake in brain	[40]
11	Buparvaquone	Injectable	Improve splenic uptake	[42]
12	Agomelatine	Intranasal	Effective delivery via nose to brain route	[45]
13	Tenofovir	Vaginal	Enhance cellular uptake of hydrophobic microbicides and outdistance the virus during the HIV/AIDS infection process	[75]
14	Quetiapine fumarate	Injectable (intraduodenal)	2.76 times higher bioavailability	[47]
15	Enrofloxacin	Injectable (IM)	Increased the bioavailability by 6.79-fold and extended the mean residence time (MRT) of the drug 10.60 h to 180.36	[76]
16	Isoniazid	Oral	Improvement in relative bioavailability in plasma (6 times) and brain (4 times)	[77]
17	Doxorubicin	Injectable (IV)	Prolonged circulation time	[78]
18	Idarubicin	Injectable (IV)	AUC and elimination half-life were 21 times and 30 times higher, respectively	[79]

(continued)

Table 13.1 (continued)

Sr. No.	API/Drug	Route of administration	Pharmacokinetic parameters	References
19	Clozapine	Injectable (IV)	AUC increased up to 2.91-fold and clearance was decreased up to 2.93-fold	[80]
20	Resveratrol	Injectable (IV)	Increase the brain intake to five-fold	[81]
21	Arteether	Oral	Relative bioavailability increased to 169.99%	[82]
22	Haloperidol	Intranasal	C _{max} in brain achieved 329.17 ± 20.89 ng/mL, T _{max} 2 h was significantly higher than intravenous and intranasal solution	[83]
23	Berberine	Oral	Enhanced absorption and anti-diabetic action	[84]
24	Puerarin	Oral	T _{max} shorter to 40 min vs. 110 min, AUC increased to 2.48 vs. 0.80 mg h/L, g h/L	[85]
25	Tetrandrine	Injectable (IV)	Higher plasma concentration and lower clearance, high uptake in reticuloendothelial system organs	[70]
26	Penciclovir	Topical	Twofold increase in rat skin penetration, dermis penetration increased by 130%	[60]
27	Meloxicam	Topical	Erythema visual scoring: 67% of rats receiving SLN gel showed complete suppression of erythema evidenced by high mean erythema score value	[61]
28	Piperine	Topical	Significantly decreased the secretion to TNF α from the activated macrophages compared to arthritic control group	[62]
29	Tobramycin	Ocular	Significantly higher bioavailability in the aqueous humor, C _{max} : 36.30 μg ml ⁻¹ and T _{max} 4.0 h compared to marketed formulation	[63]
30	Clarithromycin	Ocular	Significantly higher permeation (30.45 g/cm ² /h), bioavailability increased to 150% and 2.8-fold improvement in AUC	[64]
31	Minoxidil	Topical	Non corrosive, non-irritative	[65]
32	Tretinoin	Topical	Enhanced photostability, skin transport and anti-psoriatic activity <i>vis-à-vis</i> the vesicular carriers (liposomes, ethosomes) and the marketed product	[66]

References

- Rodrigues LBO, Lima FA, Alves CPB, et al. Ion pair strategy in solid lipid nanoparticles: a targeted approach to improve epidermal targeting with controlled adapalene release, resulting reduced skin irritation. *Pharm Res.* 2020;37:1–14.
- Tekade RK, Maheshwari R, Tekade M, Chougule MB. Solid lipid nanoparticles for targeting and delivery of drugs and genes. Elsevier Inc.; 2017.
- Muller R, Radtke M, Wissing SA. Solid lipid nanoparticles (SLN) and nanostructured lipid carriers (NLC) in cosmetic and dermatological preparations. *Adv Drug Deliv Rev.* 2002;54:S131.
- Naseri N, Valizadeh H, Zakeri-Milani P. Solid lipid nanoparticles and nanostructured lipid carriers: structure, preparation and application. *Adv Pharm Bull.* 2015;5(3):305–13.
- Shah B, Khunt D, Bhatt H, Misra M, Padh H. Application of quality by design approach for intranasal delivery of rivastigmine loaded solid lipid nanoparticles: effect on formulation and characterization parameters. *Eur J Pharm Sci.* 2015;78:54–66.
- Bondi ML, Azzolina A, Craparo EF, et al. Novel cationic solid-lipid nanoparticles as non-viral vectors for gene delivery. *J Drug Target.* 2007;15:295–301.
- Doroud D, Vatanara A, Zahedifar F, et al. Cationic solid lipid nanoparticles loaded by cysteine proteinase genes as a novel anti-leishmaniasis DNA vaccine delivery system: characterization and in vitro evaluations. *J Pharm Pharm Sci.* 2010;13:320–35.
- Tenchov R, Bird R, Curtze AE, Zhou Q. Lipid nanoparticles—from liposomes to mRNA vaccine delivery, a landscape of research diversity and advancement. *ACS Nano.* 2021;15(11):16982–7015.
- Almeida AJ, Runge S, Müller RH. Peptide-loaded solid lipid nanoparticles (SLN): influence of production parameters. *Int J Pharm.* 1997;149:255–65.

10. Brioschi AM, Calderoni S, Zara GP, Priano L, Gasco MR, Mauro A. Solid lipid nanoparticles for brain tumors therapy: state of the art and novel challenges. *Prog Brain Res.* 2009;180:193–223.
11. Mehnert W, Mäder M. Solid lipid nanoparticles: production, characterization and applications. *Adv Drug Deliv Rev.* 2001;47:165–96.
12. Ghadiri M, Fatemi S, Vatanara A, et al. Loading hydrophilic drug in solid lipid media as nanoparticles: statistical modeling of entrapment efficiency and particle size. *Int J Pharm.* 2012;424:128–37.
13. Topal GR, Mészáros M, Porkoláb G, et al. ApoE-targeting increases the transfer of solid lipid nanoparticles with donepezil cargo across a culture model of the blood–brain barrier. *Pharmaceutics.* 2021;13:38.
14. Mostafa DAE, Khalifa MKA, Gad SS. Zolmitriptan brain targeting via intranasal route using solid lipid nanoparticles for migraine therapy: formulation, characterization, in-vitro and in-vivo assessment. 2020.
15. Pole S, Williams AC, Barry BW, et al. Docosahexaenoic acid–mediated, targeted and sustained brain delivery of curcumin microemulsion. *Drug Deliv.* 2016;10:1–14.
16. H Muller R, Shegokar R, M Keck C. 20 years of lipid nanoparticles (SLN & NLC): present state of development & industrial applications. *Curr Drug Discov Technol.* 2011;8:207–27.
17. Geszke-Moritz M, Moritz M. Solid lipid nanoparticles as attractive drug vehicles: composition, properties and therapeutic strategies. *Mater Sci Eng C.* 2016;68:982–94.
18. Ramzan M, Kaur G, Trehan S, et al. Mechanistic evaluations of ketoconazole lipidic nanoparticles for improved efficacy, enhanced topical penetration, cellular uptake (L929 and J774A. 1), and safety assessment: in vitro and in vivo studies. *J Drug Delivery Sci Technol.* 2021;65:102743.
19. Vinchhi P, Patel JK, Patel MM. High-pressure homogenization techniques for nanoparticles. In: *Emerging technologies for nanoparticle manufacturing.* Cham: Springer; 2021. p. 263–85.
20. Shah RM, Rajasekaran D, Ludford-Menting M, Eldridge DS, Palombo EA, Harding IH. Transport of stearic acid-based solid lipid nanoparticles (SLNs) into human epithelial cells. *Colloids Surf., B.* 2016;140:204–12.
21. Rajabi M, A. Mousa S. Lipid nanoparticles and their application in nanomedicine. *Curr Pharm Biotechnol.* 2016;17:662–72.
22. Souto EB, Doktorovová S. Solid lipid nanoparticle formulations. Pharmacokinetic and biopharmaceutical aspects in drug delivery. *Methods Enzymol.* 2009;464:105–29.
23. Harde H, Das M, Jain S. Solid lipid nanoparticles: an oral bioavailability enhancer vehicle. *Expert Opin Drug Deliv.* 2011;8(11):1407–24.
24. Wissing SA, Kayser O, Müller RH. Solid lipid nanoparticles for parenteral drug delivery. *Adv Drug Deliv Rev.* 2004;56:1257–72.
25. Scioli Montoto S, Muraca G, Ruiz ME. Solid lipid nanoparticles for drug delivery: pharmacological and biopharmaceutical aspects. *Front Mol Biosci.* 2020;7:1–24.
26. Jennings V, Thünemann AF, Gohla SH. Characterisation of a novel solid lipid nanoparticle carrier system based on binary mixtures of liquid and solid lipids. *Int J Pharm.* 2000;199:167–77.
27. Paliwal R, Paliwal SR, Kenwat R, et al. Solid lipid nanoparticles: a review on recent perspectives and patents. *Expert Opin Ther Pat.* 2020;30(3):179–94.
28. Abdel Hady M, Sayed OM, Akl MA. Brain uptake and accumulation of new levofloxacin–doxycycline combination through the use of solid lipid nanoparticles: formulation; optimization and in-vivo evaluation. *Colloids Surf B Biointerfaces.* 2020;193:111076.
29. Salah E, Abouelfetouh MM, Pan Y, et al. Solid lipid nanoparticles for enhanced oral absorption: A review. *Colloids Surf B Biointerfaces.* 2020;196:111305.
30. Zhou K, Yan Y, Chen D, et al. Solid lipid nanoparticles for duodenum targeted oral delivery of tilimicosin. *Pharmaceutics.* 2020;12(8):731.
31. Li C, Zhou K, Chen D, et al. Solid lipid nanoparticles with enteric coating for improving stability, palatability, and oral bioavailability of enrofloxacin. *Int J Nanomedicine.* 2019;14:1619–31.
32. Gambhire VM, Gambhire MS, Ranpise NS. Solid lipid nanoparticles of dronedarone hydrochloride for oral delivery: optimization, in vivo pharmacokinetics and uptake studies. *Pharm Nanotechnol.* 2019;7(5):375–88.
33. He Y, Zhan C, Pi C, et al. Enhanced oral bioavailability of felodipine from solid lipid nanoparticles prepared through effervescent dispersion technique. *AAPS PharmSciTech.* 2020;21(5):170.
34. Ban C, Jo M, Park YH, et al. Enhancing the oral bioavailability of curcumin using solid lipid nanoparticles. *Food Chem.* 2020;302:125328.
35. Kumar M, Sharma G, Singla D, et al. Enhanced oral absorption of all-trans retinoic acid upon encapsulation in solid lipid nanoparticles. *Pharm Nanotechnol.* 2020;8(6):495–510.
36. Du Y, Ling L, Ismail M, et al. Redox sensitive lipid–camptothecin conjugate encapsulated solid lipid nanoparticles for oral delivery. *Int J Pharm.* 2018;549(1–2):352–62.
37. Patel MH, Mundada VP, Sawant KK. Fabrication of solid lipid nanoparticles of lurasidone HCl for oral delivery: optimization, in vitro characterization, cell line studies and in vivo efficacy in schizophrenia. *Drug Dev Ind Pharm.* 2019;45(8):1242–57.
38. Lin CH, Chen CH, Lin ZC, Fang JY. Recent advances in oral delivery of drugs and bioactive natural products using solid lipid nanoparticles as the carriers. *J Food Drug Anal.* 2017;25(2):219–34.
39. Martins S, Tho I, Reimold I, et al. Brain delivery of camptothecin by means of solid lipid nanoparticles: formulation design, in vitro and in vivo studies. *Int J Pharm.* 2012;439(1–2):49–62.

40. Loureiro JA, Andrade S, Duarte A, et al. Resveratrol and grape extract-loaded solid lipid nanoparticles for the treatment of Alzheimer's disease. *Molecules*. 2017;22(2):277.
41. Mendonça MCP, Radaic A, Garcia-Fossa F, da Cruz-Höfling MA, Vinolo MAR, de Jesus MB. The in vivo toxicological profile of cationic solid lipid nanoparticles. *Drug Deliv Transl Res*. 2020;10(1):34–42.
42. Maithania HV, Mohanty BS, Chaudhari PR, Samad A, Devarajan PV. Shape mediated splenotropic delivery of buparvaquone loaded solid lipid nanoparticles. *Drug Deliv Transl Res*. 2020;10(1):159–67.
43. Fatouh AM, Elshafeey AH, Abdelbary A. Intranasal agomelatine solid lipid nanoparticles to enhance brain delivery: formulation, optimization and in vivo pharmacokinetics. *Drug Des Devel Ther*. 2017;11:1815–25.
44. Jorge A, Pais A, Vitorino C. Targeted siRNA delivery using lipid nanoparticles. *Methods Mol Biol*. 2020;2059:259–83.
45. Truzzi E, Nascimento TL, Iannuccelli V, et al. In vivo biodistribution of respirable solid lipid nanoparticles surface-decorated with a mannose-based surfactant: a promising tool for pulmonary tuberculosis treatment? *Nanomaterials (Basel)*. 2020;10(3):568.
46. Zhou M, Hou J, Zhong Z, Hao N, Lin Y, Li C. Targeted delivery of hyaluronic acid-coated solid lipid nanoparticles for rheumatoid arthritis therapy. *Drug Deliv*. 2018;25(1):716–22.
47. Yasir M, Gaur PK, Puri D, Shehkar P, Kumar SS. Solid lipid nanoparticles approach for lymphatic targeting through intraduodenal delivery of quetiapine fumarate. *Curr Drug Deliv*. 2018;15(6):818–28.
48. Pinheiro RGR, Granja A, Loureiro JA, et al. RVG29-functionalized lipid nanoparticles for quercetin brain delivery and Alzheimer's disease. *Pharm Res*. 2020;37(7):139.
49. Del Pozo-Rodríguez A, Solinís MÁ, Rodríguez-Gascón A. Applications of lipid nanoparticles in gene therapy. *Eur J Pharm Biopharm*. 2016;109:184–93.
50. Rajpoot K. Solid lipid nanoparticles: a promising nanomaterial in drug delivery. *Curr Pharm Des*. 2019;25(37):3943–59.
51. Hsu CY, Wang PW, Alalaiwe A, Lin ZC, Fang JY. Use of lipid nanocarriers to improve oral delivery of vitamins. *Nutrients*. 2019;11(1):68.
52. Sarmento B, Martins S, Ferreira D, Souto EB. Oral insulin delivery by means of solid lipid nanoparticles. *Int J Nanomedicine*. 2007;2(4):743–9.
53. Muntoni E, Marini E, Ahmadi N, et al. Lipid nanoparticles as vehicles for oral delivery of insulin and insulin analogs: preliminary ex vivo and in vivo studies. *Acta Diabetol*. 2019;56(12):1283–92.
54. Fan T, Chen C, Guo H, et al. Design and evaluation of solid lipid nanoparticles modified with peptide ligand for oral delivery of protein drugs. *Eur J Pharm Biopharm*. 2014;88(2):518–28.
55. Juang V, Chang CH, Wang CS, et al. pH-responsive PEG-shedding and targeting peptide-modified nanoparticles for dual-delivery of irinotecan and microRNA to enhance tumor-specific therapy. *Small*. 2019;15(49):e1903296.
56. Wang H, Ding W, Peng L, et al. Gadolinium-loaded solid lipid nanoparticles for colorectal tumor in MR colonography. *J Biomed Nanotechnol*. 2020;16(5):594–602.
57. Trombino S, Mellace S, Cassano R. Solid lipid nanoparticles for antifungal drugs delivery for topical applications. *Ther Deliv*. 2016;7(9):639–47.
58. Mu H, Holm R. Solid lipid nanocarriers in drug delivery: characterization and design. *Expert Opin Drug Deliv*. 2018;15(8):771–85.
59. Liu M, Wen J, Sharma M. Solid lipid nanoparticles for topical drug delivery: mechanisms, dosage form perspectives, and translational status. *Curr Pharm Des*. 2020;26(27):3203–17.
60. Lv Q, Yu A, Xi Y, et al. Development and evaluation of penciclovir-loaded solid lipid nanoparticles for topical delivery. *Int J Pharm*. 2009;372(1–2):191–8.
61. Khalil RM, Abd-Elbary A, Kassem MA, et al. Nanostructured lipid carriers (NLCs) versus solid lipid nanoparticles (SLNs) for topical delivery of meloxicam. *Pharm Dev Technol*. 2014;19(3):304–14.
62. Bhalekar MR, Madgulkar AR, Desale PS, Marium G. Formulation of piperine solid lipid nanoparticles (SLN) for treatment of rheumatoid arthritis. *Drug Dev Ind Pharm*. 2017;43(6):1003–10.
63. Cavalli R, Gasco MR, Chetoni P, et al. Solid lipid nanoparticles (SLN) as ocular delivery system for tobramycin. *Int J Pharm*. 2002;238(1–2):241–5.
64. Nair AB, Shah J, Al-Dhubiab BE, et al. Clarithromycin solid lipid nanoparticles for topical ocular therapy: optimization, evaluation and in vivo studies. *Pharmaceutics*. 2021;13(4):523.
65. Padois K, Cantiéni C, Bertholle V, et al. Solid lipid nanoparticles suspension versus commercial solutions for dermal delivery of minoxidil. *Int J Pharm*. 2011;416(1):300–4.
66. Raza K, Singh B, Lohan S, et al. Nano-lipoidal carriers of retinoin with enhanced percutaneous absorption, photostability, biocompatibility and anti-psoriatic activity. *Int J Pharm*. 2013;456(1):65–72.
67. Battaglia L, Serpe L, Foglietta F, et al. Application of lipid nanoparticles to ocular drug delivery. *Expert Opin Drug Deliv*. 2016;13(12):1743–57.
68. Uner M, Yener G. Importance of solid lipid nanoparticles (SLN) in various administration routes and future perspectives. *Int J Nanomedicine*. 2007;2(3):289–300.
69. Sánchez-López E, Espina M, Doktorovova S, Souto EB, García ML. Lipid nanoparticles (SLN, NLC): overcoming the anatomical and physiological barriers of the eye - part II - ocular drug-loaded lipid nanoparticles. *Eur J Pharm Biopharm*. 2017;110:58–69.
70. Li S, Ji Z, Zou M, et al. Preparation, characterization, pharmacokinetics and tissue distribution of solid lipid nanoparticles loaded with tetrandrine. *AAPS PharmSciTech*. 2011;12(3):1011–8.
71. Ahmad I, Pandit J, Sultana Y, et al. Optimization by design of etoposide loaded solid lipid nanoparticles for ocular delivery: characterization, pharmacokinetic

- and deposition study. *Mater Sci Eng C Mater Biol Appl.* 2019;100:959–70.
72. Kaufman RC. U.S. Patent No. 10,028,919. Washington, DC: U.S. Patent and Trademark Office. 2018.
 73. Kumar VV, Chandrasekar D, Ramakrishna S, et al. Development and evaluation of nitrendipine loaded solid lipid nanoparticles: influence of wax and glyceride lipids on plasma pharmacokinetics. *Int J Pharm.* 2007;335(1–2):167–75.
 74. Ren J, Zou M, Gao P, et al. Tissue distribution of borneol-modified ganciclovir-loaded solid lipid nanoparticles in mice after intravenous administration. *Eur J Pharm Biopharm.* 2013;83(2):141–8.
 75. Alukda D, Sturgis T, Youan BC. Formulation of tenofovir-loaded functionalized solid lipid nanoparticles intended for HIV prevention. *J Pharm Sci.* 2011;100(8):3345–56.
 76. Xie S, Zhu L, Dong Z, et al. Preparation, characterization and pharmacokinetics of enrofloxacin-loaded solid lipid nanoparticles: influences of fatty acids. *Colloids Surf B Biointerfaces.* 2011;83(2):382–7.
 77. Bhandari R, Kaur IP. Pharmacokinetics, tissue distribution and relative bioavailability of isoniazid-solid lipid nanoparticles. *Int J Pharm.* 2013;441(1–2):202–12.
 78. Fundarò A, Cavalli R, Bargoni A, et al. Non-stealth and stealth solid lipid nanoparticles (SLN) carrying doxorubicin: pharmacokinetics and tissue distribution after i.v. administration to rats. *Pharmacol Res.* 2000;42(4):337–43.
 79. Zara GP, Bargoni A, Cavalli R, et al. Pharmacokinetics and tissue distribution of idarubicin-loaded solid lipid nanoparticles after duodenal administration to rats. *J Pharm Sci.* 2002;91(5):1324–33.
 80. Manjunath K, Venkateswarlu V. Pharmacokinetics, tissue distribution and bioavailability of clozapine solid lipid nanoparticles after intravenous and intraduodenal administration. *J Control Release.* 2005;107(2):215–28.
 81. Jose S, Anju SS, Cinu TA, et al. In vivo pharmacokinetics and biodistribution of resveratrol-loaded solid lipid nanoparticles for brain delivery. *Int J Pharm.* 2014;474(1–2):6–13.
 82. Dwivedi P, Khatik R, Khandelwal K, et al. Pharmacokinetics study of arteether loaded solid lipid nanoparticles: an improved oral bioavailability in rats. *Int J Pharm.* 2014;466(1–2):321–7.
 83. Yasir M, Sara UVS. Solid lipid nanoparticles for nose to brain delivery of haloperidol: in vitro drug release and pharmacokinetics evaluation. *Acta Pharm Sin B.* 2014;4:454–63.
 84. Xue M, Yang MX, Zhang W, et al. Characterization, pharmacokinetics, and hypoglycemic effect of berberine loaded solid lipid nanoparticles. *Int J Nanomedicine.* 2013;8:4677–87.
 85. Luo CF, Yuan M, Chen MS, et al. Pharmacokinetics, tissue distribution and relative bioavailability of puerarin solid lipid nanoparticles following oral administration. *Int J Pharm.* 2011;410(1–2):138–44.



Factors Affecting the Clearance and Biodistribution of Polymeric Nanoparticles

14

Komal Parmar, Jayvadan Patel,
and Yashwant Pathak

Contents

1	Introduction	261
2	Pharmacokinetic Functions	262
3	Factors Affecting Biodistribution and Clearance of Nanoparticles	264
4	Conclusion	268
	References	268

Abstract

Nanoparticles are promising drug delivery for various therapeutic applications. Pharmacokinetics is important to study the in vivo fate of nanoparticles. Biodistribution and clearance are the important parameters of pharmacokinetics to be considered. Impact of various characteristics of polymeric nanoparticles affects biodistribution and clearance of nanoparticles. The chapter focuses on four important characteristics of polymeric nanoparticles affecting their biodistribution and clearance.

K. Parmar (✉)
ROFEL, Shri G.M. Bilakhia College of Pharmacy,
Vapi, Gujarat, India

J. Patel
Nootan Pharmacy College, Faculty of Pharmacy,
Sankalchand Patel University,
Visnagar, Gujarat, India

Y. Pathak
College of Pharmacy, University of South Florida
Health, Tampa, FL, USA

Keywords

Clearance · Biodistribution · Polymeric
nanoparticles

1 Introduction

Nanodelivery systems are a comparatively new but quickly emerging field in which nanoscale materials are used as diagnostic tools or to administer therapeutic medicines to precise targets in a controlled mode [30, 57, 82, 84]. Nanoparticles can be turned into intelligent devices, encapsulating medicinal and imaging chemicals while also having stealth properties, by manipulating their size, surface features, and composition [69]. They are intended to alter the biodistribution and pharmacokinetics of the drugs, allowing for a higher dose to be delivered to a targeted disease tissue, in order to improve the therapeutic efficacy and render reduced toxicity. Many different materials and shapes of nanoparticles have been

produced for use in disease therapy, and many of them have shown to be effective [59, 61, 78]. Currently, there are a number of nanopharmaceutical products in the market [10, 19, 29, 31, 34, 42, 43]. When using nanoparticles, several factors must be considered: distribution efficiency, therapy effects, and clearance [53, 66, 90, 95]. Clinical uses for nanoparticles with great efficacy and good biosafety are on the horizon. Therapeutic effectiveness of nanoparticles is inextricably tied to pharmacological and toxicological characteristics. The most significant elements for establishing a high therapeutical index and related clinical performance are drug target residence, maximal tolerated dose, and selectivity [7, 40, 49]. Optimizing drug pharmacokinetic qualities to improve therapeutic effects and prevent adverse effects is an important feature of nanoparticle formulation design, which involves considering not just the characteristics of nanoparticles but also pharmacokinetic characteristics. The interaction between body systems and nanoparticles is responsible for all therapy outcomes.

The shape and polymer content in the core and periphery of polymeric nanoparticles characterize them. Drug is either adsorbed on the surface or encapsulated inside the core part of the polymeric nanoparticles. Delivery formulation governs the release of drug either to be controlled, sustained, or triggered release [3]. Furthermore, the surface of the polymeric nanoparticles can be attached with functional groups to obtain certain added characteristics such as prolonged systemic residence time, minimal non-specific distribution, and/or target specific cell or tissue, for example, coating the surface of the nanoparticles with polyethylene glycol to prolong the systemic circulation of the particulate system. PEGylation of nanoparticles defends the surface of the nanoparticles from protein absorption which leads to aggregation, opsonization, and phagocytosis, thereby providing extended systemic retention [52, 89]. The resultant elimination is due to phagocytosis by the monomolecular phagocyte system. Because of the large number of phagocytic cells in the liver and spleen, the majority of opsonized particles are removed by a receptor-mediated mechanism in less than a few minutes,

or they are expelled. Thus, numerous approaches are explored by the investigators to help retain the nanoparticles in the systemic circulation, so that drug delivery system can deliver the drug for prolonged period of time with specific distribution [9, 12, 83]. The effects of physiological tissue deficits and polymeric nanoparticle physicochemical characteristics on clearance and biodistribution will be discussed in this chapter to consider probable means for their advancement.

2 Pharmacokinetic Functions

Investigators have explored various factors such as physicochemical properties, administration route, dosing, and coating, affecting distribution and clearance of nanoparticles. However, all these variables are dependent on the physiological environment. Optimization of such variables after understanding of pharmacokinetics of body will help to obtain the successful drug delivery using polymeric nanoparticles.

Briefly, once the nanoparticles are introduced into systemic circulation, they are distributed to various tissues and organs where they are encountered with physical and biological challenges that may change their properties and affect their deposition and are concurrently cleared later [85] (Fig. 14.1). The interactions between nanoparticles and each organ are unique. In vivo, the major clearance process for polymeric nanoparticles is reticular endothelial system (RES) also termed as mononuclear phagocyte system (MPS) [13, 75]. Phagocytosis of polymeric nanoparticles is usually initiated by opsonization process. Opsonization occurs when opsonins, a heterogeneous group of proteins or protein fragments including C3, C4, and C5, immunoglobulins, fibronectin, and apolipoproteins, are deposited on the surface of nanoparticles and interact with a variety of surface receptors on RES cells, including complement, Fc, and fibronectin receptors [4, 71]. Proteins other than opsonins also get attached on the surface of nanoparticles forming a corona which further enables the scavenger receptors to categorize [80]. This adds an alternative way by which RES clears polymeric nanoparticles. Once

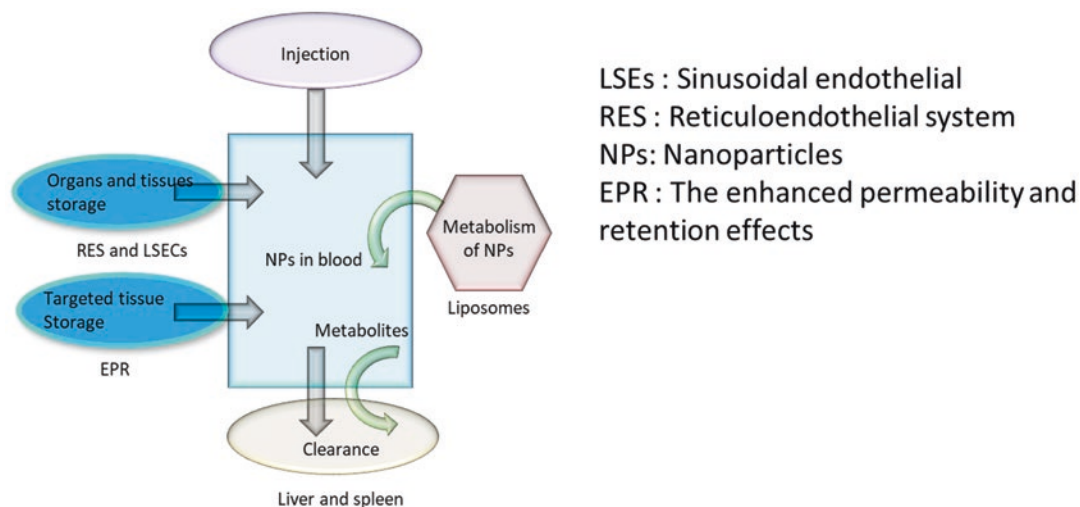


Fig. 14.1 Schematic diagram illustrating biodistribution and clearance of polymeric nanoparticles

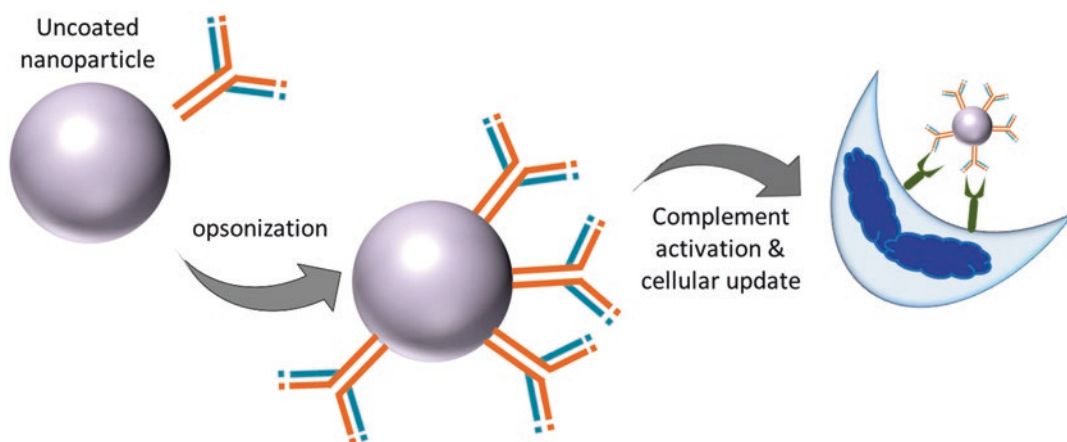


Fig. 14.2 Opsonization and uptake of uncoated polymer nanoparticles

opsonized and transported from the systemic circulation, a polymeric nanoparticle is usually localized in one of the MPS organs, mainly the liver and spleen [62] (Fig. 14.2). There are numerous such biological barriers naturally designed to safeguard the human body from foreign material. Among these barriers are the immune system's cellular and humoral arms, as well as mucosal barriers. Nanoparticles must overcome such constraints in order to reach their desired target. Nanoparticles are exceptionally well adapted to overcoming these limitations due

to their nanoscale size and ability to surface functionalize to encompass desired properties.

Important nutrients, oxygen, and other molecules are transported throughout the body via blood vessels. Circulatory system plays an important role in continuous transportation of materials in the body. The endothelium of the blood vessels has been classified as continuous, fenestrated, or discontinuous (sinusoidal), depending on the arrangement of cells. Arteries and vessels of the brain, lungs, skin, and heart have continuous endothelium. Fenestrated endo-

thelium is found in capillaries of exocrine and endocrine glands, gastric and intestinal mucosa, choroid plexus, glomeruli, and a subpopulation of renal tubules (fenestrae of approximately 70 nm in diameter). Discontinuous endothelium is found in certain sinusoidal vascular beds, most particularly the liver with fenestrations of 100–200 nm in diameter [1]. Blood vessel endothelial cells can react to the physiological conditions, culminating in angiogenic activity. The creation of new blood vessels is known as angiogenesis. Endothelial cells, which line the inside walls of blood arteries, migrate, proliferate, and differentiate during this process. Chemical impulses in the body influence the process of angiogenesis. Angiogenesis results in a weak lymphatic drainage system and a faulty hyper-vasculature during tumor growth [60]. These openings help the passive movement of nanoparticles to target tumors through the enhanced permeability and retention effect (EPR) [41], wherein the macromolecules or nanoparticles accumulate and diffuse into tumor tissue releasing the therapeutic drug locally [5, 6, 26].

3 Factors Affecting Biodistribution and Clearance of Nanoparticles

Over the last few years, research investigators have developed various types of nanoparticles with exclusive functions and characteristics for targeting purpose. Characteristics such as different therapeutic or imaging functions, special drug loading and release competences, particle sizes, type of materials, different surface charges, hydrophilic or hydrophobic properties, biodegradability, biocompatibility, and different molecular-targeting capabilities aid the nanoparticles to achieve the desired performance. However, among all the listed properties of nanoparticles, only four factors are considered to be critical for their biodistribution and clearance, namely, particle size, shape, surface charge, and surface modification. Table 14.1 demonstrates various polymeric nanoparticles and the factors associated with their pharmacokinetics. Figure 14.3 illustrates various forms of polymeric nanoparticles.

Table 14.1 Factors affecting pharmacokinetics of various polymeric nanoparticles

Polymeric nanoparticles	Pharmacokinetics	Factor	Reference
PLGA/polyvinyl acid nanospheres	Hepatic uptake	Particle size: 200 nm	Di Mascolo et al. [23]
PLAcore/PVAshell nanoparticles	Hepatic uptake	Particle size: 273.1 nm	Canup et al. [8]
Chitosan	Hepatic uptake	Particle size: 210–279 nm	Xiao et al. [88]
Polyethylenimine nanoparticles	Hepatic uptake	Particle size: 150–200 nm	Iranpur Mobarakeh et al. [39]
Polymeric nanoparticle	Lung and spleen uptake	Shape: Rod	Kolhar et al. [46]
Copolymer of poly[(ethylene glycol) methyl ether methacrylate] and poly(glycidyl methacrylate) nanoparticles	RES uptake	Shape: Cylinder Particle size: 35–1200 nm	Müllner et al. [58]
Glyceryl monostearate nanoparticles	Spleen uptake	Particle size: 350–500 nm	Patil et al. [64]
Carboxylated polystyrene nanoparticles	Lungs uptake	Surface modification: ICAM-antibody-coating	Anselmo et al. [2]
Phosphatidylcholine/cholesterol liposomes	Liver uptake	Surface charge	Levchenko et al. [50]
PLGA nanoparticles	Tumor uptake	Surface modification with chitosan or Eudragit® RS 100	Kırımlioğlu and Görgülü [44]
Polystyrene nanoparticles	M1 macrophage uptake reduced	Surface modification with PEG	Qie et al. [68]
PEG-b-PLA nanoparticles	Tumor uptake enhanced	Positive charge	Wang et al. [81]

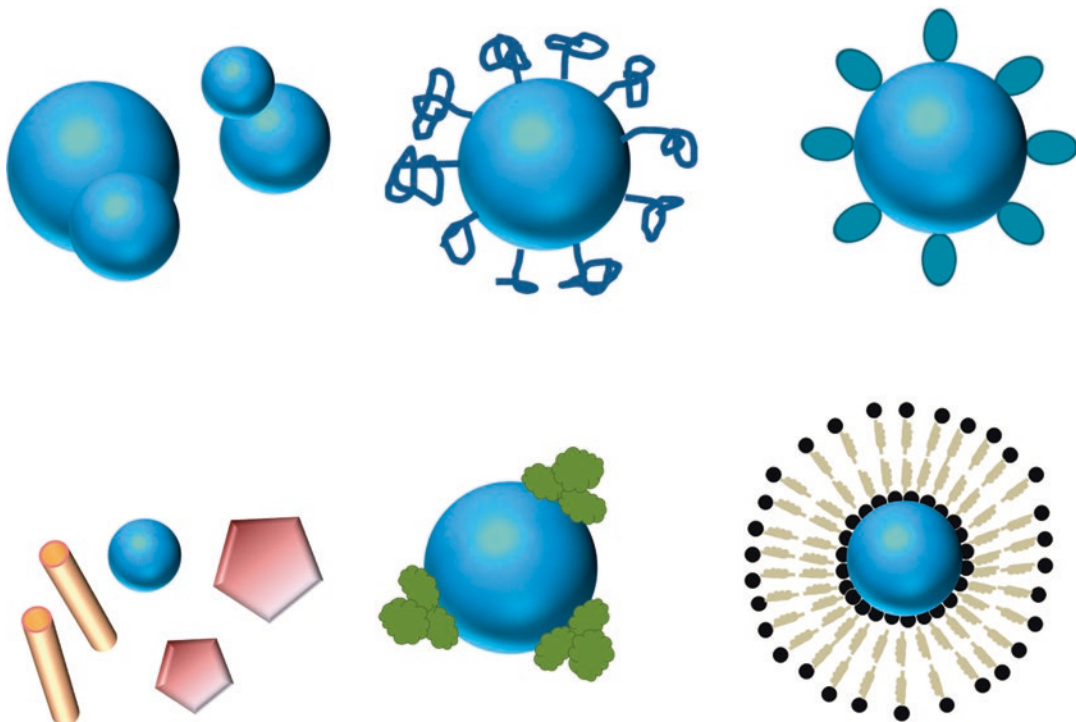


Fig. 14.3 Various shapes and surface modifications of nanoparticles

3.1 Particle Size

It is obvious, based on physiological characteristics including hepatic filtration, tissue extravasation, tissue diffusion, and kidney excretion, that the size of the nanoparticles has a significant impact on their distribution and clearance. The systemic life of employed nanoparticles in blood is determined by not only the organs' clearance efficiency, their ability to target tumors using the EPR effect, and the degradation duration in the blood, but also the particles' physicochemical features. Thus, as one of the most important attributes of a nanoparticle, size should be addressed first when tailoring drug loading and other therapeutic characteristics. Furthermore, polymeric nanoparticles' aggregation ability in tumors may be reduced if they are removed too quickly, yet too long retention in the body might contribute to greater toxicity. As a result, a nanoparticle size optimization is necessary to improve the applications of nanoparticles.

Circulation half-lives, extravasation through leaky vasculature, and macrophage uptake are all driven by size and have discrete cut-off size ranges. Various researchers have investigated optimized nanoparticle size for systemic retention resulting in desired therapeutic efficacy. From the studies, it is concluded that particle size less than 6 nm are easily filtered out through the kidney [16, 54]. In one study, *in vivo* biodistribution results of PLGA nanoparticles with consistent composition and particle size 160 nm showed intrahepatic delivery and therapeutic efficacy [48]. In another study, the *in vivo* spleen administration of the degradable poly(amine-co-ester) nanoparticles encapsulating siRNA protein with a size of 240–300 nm allowed up to 60% Nogo-B protein suppression [17]. Particles in the micrometer range have been demonstrated to efficiently aggregate within pulmonary capillaries, potentially providing a special benefit when targeting among the most major intersections of metastatic malignancy [32]. Pore sizes in leaky tumor vasculatures have been observed to range between

380 and 780 nm [35, 93]. Thus, due to the EPR effect, only nanoparticles smaller than 600 nm can be employed. In one study, PLGA nanoparticles encapsulating curcumin were investigated for cellular uptake by cervical cancer cells. Results demonstrated that polymeric curcumin nanoparticles of 132 nm in size were targeted to P-glycoprotein on the cell surface membrane of KB-V1 cells [67]. Drug carriers' size has a significant impact on their *in vivo* circulation time. It is found that as particle size increases, *in vivo* circulation time also increases [65]. This does not, however, imply that an unlimited increase in particle size leads to an infinitely long *in vivo* circulation duration. If merely considering the size difference in nanoparticle clearance, nanoparticles with diameters between 100 and 200 nm are more acceptable for utilization since they have a longer blood circulation and a lower rate of MPS absorption [47, 86, 94]. However, the size of nanoparticles is determined by the desired properties of nanoparticles and their application significance. For instance, a few smaller nanoparticles have been developed by some investigators because of their ease of clearance, which reduces the risk of chronic toxicity, or their high infiltration and retaining behavior, which improves the targeting outcome [20].

3.2 Particle Shape

The spherical shape of nanoparticles is the most frequent since it has the fewest dimensions and is the easiest to make. Diverse forms of nanoparticles have been found to have a major impact on their biodistribution and clearance, giving specific roles in medical applications. Wire [38], sphere [25], ellipsoid [21], rod [18], cylinder [37], sheet [94], cube [56], needle [45], and cluster-like [11] nanoparticle forms have been identified. The effect of shape of nanoparticles can be traced to a variety of factors. For instance, it is observed that nanoparticles with irregular shapes were more likely to settle in the spleen [22].

Various investigators have reported selective uptake of spherical nanoparticles by MPS over

rod-shaped counterparts [14, 15]. Li and co-researchers reported that cellular uptake of nanoparticles was in the sequence of sphere > cube > rod > disk in an *in vitro* cell uptake examination of various shaped PEGylated nanoparticles. This is likely owing to the ease of folding the cell membrane around the particles [51]. The oblate form of particles helps them circulate in the bloodstream because macrophages have lower uptake [72]. Intravenously injected filamentous micelles lasted ten times longer in circulation than spherical polymersomes, lasting up to 1 week [27]. Rod-like camptothecin-conjugated PEGylated dendrimers [99] showed faster cell uptake *in vitro* and longer circulation half-life along with high tumor uptake *in vivo* as compared to nanospheres. In one study, the renal system efficiently cleared single-walled carbon nanotubes with rod lengths ranging from 100 to 500 nm and diameters of 0.8–1.2 nm; driven by flow-induced orientation, the rods' long-axis went readily through the glomerular capillary fenestrations [70].

3.3 Surface Charge

Remarkably, certain nanoparticles' surface physicochemical characteristics can alter when used *in vivo*, modifying biodistribution and clearance. It has been proven that a polymeric nanoparticle's physicochemical attributes, such as surface charge and functional groups, can influence its uptake by phagocytic cells. For instance, when compared to neutral or negatively charged formulations, positively charged nanoparticles have a higher rate of cell uptake. In a study, less negatively charged rhodamine B-carboxymethyl chitosan-grafted nanoparticles and more positively charged rhodamine B-chitosan hydrochloride-grafted nanoparticles were tended to be more efficiently internalized by both L02 and SMMC-7721 cells, suggesting that surface charge played an important role in cellular uptake of polymeric nanoparticles [33]. In most situations, the nanoparticle surface contributes the driving forces for cellular internalization (electrostatic, hydrophobic, and hydrophilic (polar)

forces) and determines the uptake pathway. Nanoparticles with a positively charged surface are projected to have a high nonspecific internalization rate because of their effective binding to negatively charged groups on the cell surface and tend to have a short half-life in the bloodstream [63, 79, 94, 95]. Furthermore, an excess of positive charge on the complexes can result in nonspecific binding and absorption by cells that are not targeted. For complexes containing a targeting ligand, a weakly positively charged surface is desirable for receptor-mediated endocytosis selective binding. In a study, an amphoteric hyaluronic acid derivative with polyethylenimine chains for gene delivery overcome the disadvantages of polyethylenimine as gene carrier including the cytotoxicity caused by excess of positive charge, non-specific interaction and aggregation in the blood, and non-target gene delivery [92]. In another study, effect of surface charge on the cellular uptake and in vivo fate of PEG-oligocholeic acid-based micellar nanoparticles was reported. After opsonization in fresh mouse serum, RAW 264.7 murine macrophages took up nanoparticles with a high surface charge, whether positive or negative. In vivo biodistribution experiments

revealed that strongly positively or negatively charged nanoparticles had very high liver absorption, which is likely owing to active phagocytosis by macrophages in the liver [87].

3.4 Surface Modification

Due to the ease of detection by the RES, most uncoated nanoparticles can be swiftly removed from blood circulation when utilized in vivo, resulting in a significant loss in targeting ability [76]. Surface functionalization of nanoparticles mainly comprises PEG, the negative carboxyl ($-\text{COOH}$) group, neutral functional groups like hydroxyl ($-\text{OH}$) groups, and the positive amine ($-\text{NH}_2$) group. The increase in ($-\text{NH}_2$) resulted in a higher positive surface charge, which increased the cellular uptake of nanoparticles [55]. Rate of blood clearance of non-PEGylated nanoparticles is found to be more than PEGylated nanoparticles. PEGylation provides stealth properties to the nanoparticles surface protecting further from uptake by MPS (Fig. 14.4) [24, 91]. In one investigation, in vivo study in ICR mice showed polyethylene glycol and heparin (PEG/

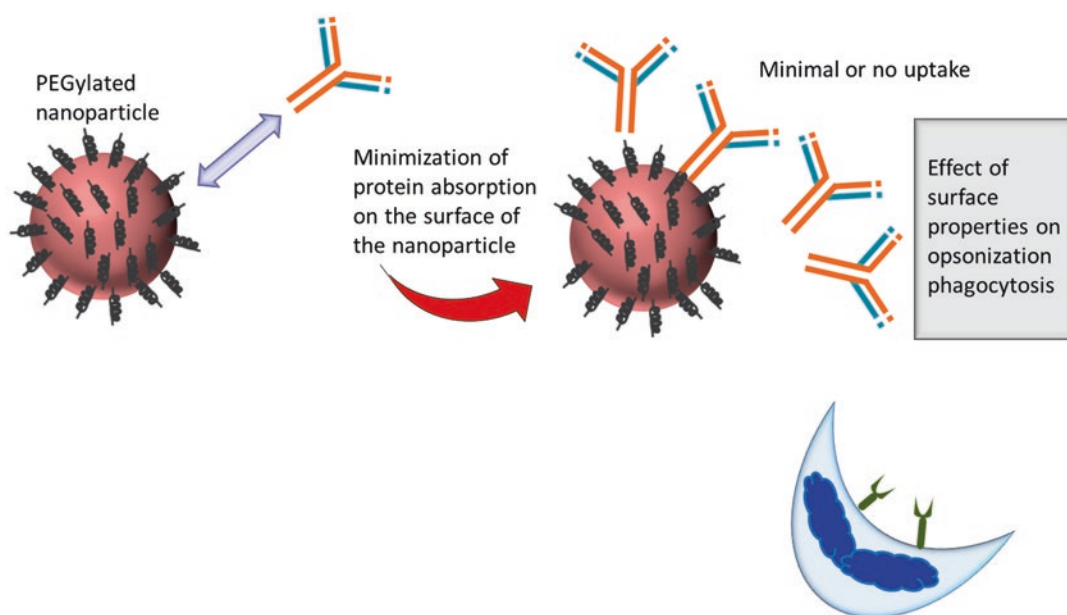


Fig. 14.4 Effect of PEGylation on nanoparticle pharmacokinetics

HEP) coating increased the blood circulation half-life of lipid polymer hybrid nanoparticles (LPHNPs) from 0.3 to 72.6 h. Moreover, PEG/HEP LPHNPs exhibited dramatically reduced liver accumulation when compared to LPHNPs [73]. In a similar study, researchers had developed polyethylene glycol and human serum albumin coating of nanoparticles carrying resveratrol for pancreatic tumor therapy. The surface-modified nanoparticles demonstrated prolonged blood circulation approximately 5.43-fold [28]. Doxorubicin-loaded nanoparticles based on polyethylene glycol-conjugated chitosan oligosaccharide-arachidic acid were explored for potential application to leukemia therapy. Results illustrated higher uptake of the conjugated nanoparticles by K562 cells with slower in vivo clearance rate, subsequently extending the blood circulation [77].

4 Conclusion

The development of a complete concept of nanoparticle pharmacokinetics in order to recognize their distribution and clearance is influenced by physiological factors and nanoparticle component such as particle size, shape, surface charge, and modification. Various investigators have been studying these characteristics since long time. Because the interactions between nanoparticles and the body are so complicated and variable, it is important to understand and follow past knowledge and principles for nanoparticle design.

References

- Aird WC. Phenotypic heterogeneity of the endothelium: I. Structure, function, and mechanisms. *Circ Res.* 2007;100(2):158–73. <https://doi.org/10.1161/01.RES.0000255691.76142.4a>.
- Anselmo AC, Kumar S, Gupta V, Pearce AM, Ragusa A, Muzykantov V, Mitragotri S. Exploiting shape, cellular-hitchhiking and antibodies to target nanoparticles to lung endothelium: synergy between physical, chemical and biological approaches. *Biomaterials.* 2015;68:1–8. <https://doi.org/10.1016/j.biomaterials.2015.07.043>.
- Begines B, Ortiz T, Pérez-Aranda M, Martínez G, Merinero M, Argüelles-Arias F, Alcudia A. Polymeric nanoparticles for drug delivery: recent developments and future prospects. *Nanomaterials (Basel).* 2020;10(7):1403. <https://doi.org/10.3390/nano10071403>.
- Behzadi S, Serpooshan V, Tao W, Hamaly MA, Alkawareek MY, Dreaden EC, Brown D, Alkhalany AM, Farokhzad OC, Mahmoudi M. Cellular uptake of nanoparticles: journey inside the cell. *Chem Soc Rev.* 2017;46(14):4218–44. <https://doi.org/10.1039/c6cs00636a>.
- Bertrand N, Wu J, Xu X, Kamaly N, Farokhzad OC. Cancer nanotechnology: the impact of passive and active targeting in the era of modern cancer biology. *Adv Drug Deliv Rev.* 2014;66:2–25. <https://doi.org/10.1016/j.addr.2013.11.009>.
- Bort G, Lux F, Dufort S, Crémillieux Y, Verry C, Tillement O. EPR-mediated tumor targeting using ultrasmall-hybrid nanoparticles: from animal to human with theranostic AGuIX nanoparticles. *Theranostics.* 2020;10(3):1319–31. <https://doi.org/10.7150/thno.37543>.
- Bottino DC, Patel M, Kadakia E, Zhou J, Patel C, Neuwirth R, Iartchouk N, Brake R, Venkatakrishnan K, Chakravarty A. Dose optimization for anticancer drug combinations: maximizing therapeutic index via clinical exposure-toxicity/preclinical exposure-efficacy modeling. *Clin Cancer Res.* 2019;25(22):6633–43. <https://doi.org/10.1158/1078-0432.CCR-18-3882>.
- Canup BS, Song H, Le Ngo V, Meng X, Denning TL, Garg P, Laroui H. CD98 siRNA-loaded nanoparticles decrease hepatic steatosis in mice. *Dig Liver Dis.* 2017;49(2):188–96. <https://doi.org/10.1016/j.dld.2016.11.008>.
- Chambers E, Mitragotri S. Prolonged circulation of large polymeric nanoparticles by non-covalent adsorption on erythrocytes. *J Control Release.* 2004;100(1):111–9. <https://doi.org/10.1016/j.jconrel.2004.08.005>.
- Chao Y, Makale M, Karmali PP, Sharikov Y, Tsigelny I, Merkulov S, Kesari S, Wrasidlo W, Ruoslahti E, Simberg D. Recognition of dextran-superparamagnetic iron oxide nanoparticle conjugates (Feridex) via macrophage scavenger receptor charged domains. *Bioconjug Chem.* 2012;23(5):1003–9. <https://doi.org/10.1021/bc200685a>.
- Chen K, Liao S, Guo S, Zheng X, Wang B, Duan Z, Zhang H, Gong Q, Luo K. Multistimuli-responsive PEGylated polymeric bioconjugate-based nano-aggregate for cancer therapy. *Chem Eng J.* 2020;391:123543. <https://doi.org/10.1016/j.cej.2019.123543>.
- Chen S, Zhong Y, Fan W, Xiang J, Wang G, Zhou Q, Wang J, Geng Y, Sun R, Zhang Z, Piao Y, Wang J, Zhuo J, Cong H, Jiang H, Ling J, Li Z, Yang D, Yao X, Xu X, Zhou Z, Tang J, Shen Y. Enhanced tumour penetration and prolonged circulation in blood of polyzwitterion-drug conjugates with cell-membrane

- affinity. *Nat Biomed Eng.* 2021;5(9):1019–37. <https://doi.org/10.1038/s41551-021-00701-4>.
13. Chenthamara D, Subramaniam S, Ramakrishnan SG, Krishnaswamy S, Essa MM, Lin FH, Qoronfleth MW. Therapeutic efficacy of nanoparticles and routes of administration. *Biomater Res.* 2019;23:20. <https://doi.org/10.1186/s40824-019-0166-x>.
 14. Chithrani BD, Chan WC. Elucidating the mechanism of cellular uptake and removal of protein-coated gold nanoparticles of different sizes and shapes. *Nano Lett.* 2007;7(6):1542–50. <https://doi.org/10.1021/nl070363y>.
 15. Chithrani BD, Ghazani AA, Chan WC. Determining the size and shape dependence of gold nanoparticle uptake into mammalian cells. *Nano Lett.* 2006;6(4):662–8. <https://doi.org/10.1021/nl052396o>.
 16. Choi HS, Liu W, Misra P, Tanaka E, Zimmer JP, Itty Ipe B, Bawendi MG, Frangioni JV. Renal clearance of quantum dots. *Nat Biotechnol.* 2007;25(10):1165–70. <https://doi.org/10.1038/nbt1340>.
 17. Cui J, Piotrowski-Daspit AS, Zhang J, Shao M, Braccaglia LG, Utsumi T, Seo YE, DiRito J, Song E, Wu C, Inada A, Tietjen GT, Pober JS, Iwakiri Y, Saltzman WM. Poly(amine-co-ester) nanoparticles for effective Nogo-B knockdown in the liver. *J Control Release.* 2019;304:259–67. <https://doi.org/10.1016/j.jconrel.2019.04.044>.
 18. Darwish WMA, Bayoumi NA. Gold nanorod-loaded (PLGA-PEG) nanocapsules as near-infrared controlled release model of anticancer therapeutics. *Lasers Med Sci.* 2020;35(8):1729–40. <https://doi.org/10.1007/s10103-020-02964-w>.
 19. de Freitas CSM, Soares AN. Efficacy of Leuproreline acetate (Eligard®) in daily practice in Brazil: a retrospective study with depot formulations in patients with prostate cancer. *Int Braz J Urol.* 2020;46(3):383–9. <https://doi.org/10.1590/S1677-5538.IBJU.2019.0212>.
 20. Dehaini D, Fang RH, Luk BT, Pang Z, Hu CM, Kroll AV, Yu CL, Gao W, Zhang L. Ultra-small lipid-polymer hybrid nanoparticles for tumor-penetrating drug delivery. *Nanoscale.* 2016;8(30):14411–9. <https://doi.org/10.1039/c6nr04091h>.
 21. Desai P, Venkataramanan A, Schneider R, Jaiswal MK, Carrow JK, Purwada A, Singh A, Gaharwar AK. Self-assembled, ellipsoidal polymeric nanoparticles for intracellular delivery of therapeutics. *J Biomed Mater Res A.* 2018;106(7):2048–58. <https://doi.org/10.1002/jbm.a.36400>.
 22. Devarajan PV, Jindal AB, Patil RR, Mulla F, Gaikwad RV, Samad A. Particle shape: a new design parameter for passive targeting in splenotropic drug delivery. *J Pharm Sci.* 2010;99(6):2576–81. <https://doi.org/10.1002/jps.22052>.
 23. Di Mascolo D, Lyon CJ, Aryal S, Ramirez MR, Wang J, Candeloro P, Guindani M, Hsueh WA, Decuzzi P. Rosiglitazone-loaded nanospheres for modulating macrophage-specific inflammation in obesity. *J Control Release.* 2013;170(3):460–8. <https://doi.org/10.1016/j.jconrel.2013.06.012>.
 24. Essa S, Rabanel JM, Hildgen P. Characterization of rhodamine loaded PEG-g-PLA nanoparticles (NPs): effect of poly(ethylene glycol) grafting density. *Int J Pharm.* 2011;411(1–2):178–87. <https://doi.org/10.1016/j.ijpharm.2011.02.039>.
 25. Evans CW, Latter MJ, Ho D, Peerzade SAMA, Clemons TD, Fitzgerald M, Dunlop SA, Iyer KS. Multimodal and multifunctional stealth polymer nanospheres for sustained drug delivery. *New J Chem.* 2012;36:1457–62. <https://doi.org/10.1039/C2NJ40016B>.
 26. Ge Z, Liu S. Functional block copolymer assemblies responsive to tumor and intracellular micro-environments for site-specific drug delivery and enhanced imaging performance. *Chem Soc Rev.* 2013;42(17):7289–325. <https://doi.org/10.1039/c3cs60048c>.
 27. Geng Y, Dalhaimer P, Cai S, Tsai R, Tewari M, Minko T, Discher DE. Shape effects of filaments versus spherical particles in flow and drug delivery. *Nat Nanotechnol.* 2007;2(4):249–55. <https://doi.org/10.1038/nnano.2007.70>.
 28. Geng T, Zhao X, Ma M, Zhu G, Yin L. Resveratrol-loaded albumin nanoparticles with prolonged blood circulation and improved biocompatibility for highly effective targeted pancreatic tumor therapy. *Nanoscale Res Lett.* 2017;12(1):437. <https://doi.org/10.1186/s11671-017-2206-6>.
 29. Goel N, Stephens S. Certolizumab pegol. *MAbs.* 2010;2(2):137–47. <https://doi.org/10.4161/mabs.2.2.11271>.
 30. Gonzalez-Valdivieso J, Girotti A, Muñoz R, Rodriguez-Cabello JC, Arias FJ. Self-assembling ELR-based nanoparticles as smart drug-delivery systems modulating cellular growth via Akt. *Biomacromolecules.* 2019;20(5):1996–2007. <https://doi.org/10.1021/acs.biomac.9b00206>.
 31. Gordon EM, Hall FL. Rexin-G, a targeted genetic medicine for cancer. *Expert Opin Biol Ther.* 2010;10(5):819–32. <https://doi.org/10.1517/14712598.2010.481666>.
 32. Harsha NS, Rani RHS. Drug targeting to lungs by way of microspheres. *Arch Pharm Res.* 2006;29:598–604. <https://doi.org/10.1007/BF02969272>.
 33. He C, Hu Y, Yin L, Tang C, Yin C. Effects of particle size and surface charge on cellular uptake and biodistribution of polymeric nanoparticles. *Biomaterials.* 2010;31(13):3657–66. <https://doi.org/10.1016/j.biomaterials.2010.01.065>.
 34. Herzog C, Hartmann K, Künzi V, Kürsteiner O, Mischler R, Lazar H, Glück R. Eleven years of Inflflex V-a virosomal adjuvanted influenza vaccine. *Vaccine.* 2009;27(33):4381–7. <https://doi.org/10.1016/j.vaccine.2009.05.029>.
 35. Hobbs SK, Monsky WL, Yuan F, Roberts WG, Griffith L, Torchilin VP, Jain RK. Regulation of transport pathways in tumor vessels: role of tumor type and microenvironment. *Proc Natl Acad Sci U S A.* 1998;95(8):4607–12. <https://doi.org/10.1073/pnas.95.8.4607>.

36. Hu J, Li HY, Williams GR, Yang HH, Tao L, Zhu LM. Electrospun poly(N-isopropylacrylamide)/ethyl cellulose nanofibers as thermoresponsive drug delivery systems. *J Pharm Sci.* 2016;105(3):1104–12. [https://doi.org/10.1016/S0022-3549\(15\)00191-4](https://doi.org/10.1016/S0022-3549(15)00191-4).
37. Hubbe H, Mendes E, Boukany PE. Polymeric nanowires for diagnostic applications. *Micromachines (Basel).* 2019;10(4):225. <https://doi.org/10.3390/mi10040225>.
38. Iranpur Mobarakeh V, Modarressi MH, Rahimi P, Bolhassani A, Arefian E, Atyabi F, Vahabpour R. Optimization of chitosan nanoparticles as an anti-HIV siRNA delivery vehicle. *Int J Biol Macromol.* 2019;129:305–15. <https://doi.org/10.1016/j.ijbiomac.2019.02.036>.
39. Juretić D, Golemac A, Strand DE, Chung K, Ilić N, Goić-Barišić I, Pellay FX. The spectrum of design solutions for improving the activity-selectivity product of peptide antibiotics against multidrug-resistant bacteria and prostate cancer PC-3 cells. *Molecules.* 2020;25(15):3526. <https://doi.org/10.3390/molecules25153526>.
40. Kalyane D, Raval N, Maheshwari R, Tambe V, Kalia K, Tekade RK. Employment of enhanced permeability and retention effect (EPR): nanoparticle-based precision tools for targeting of therapeutic and diagnostic agent in cancer. *Mater Sci Eng C Mater Biol Appl.* 2019;98:1252–76. <https://doi.org/10.1016/j.msec.2019.01.066>.
41. Kanaparthy A, Kukura S, Slenkovich N, AlGhamdi F, Shafy SZ, Hakim M, Tobias JD. Perioperative Administration of Emend® (Aprepitant) at a Tertiary Care Children's Hospital: a 12-month survey. *Clin Pharmacol.* 2019;11:155–60. <https://doi.org/10.2147/CPAA.S221736>.
42. Kim JY, Do YR, Song HS, Cho YY, Ryoo HM, Bae SH, Kim JG, Chae YS, Kang BW, Baek JH, Kim MK, Lee KH, Park K. Multicenter Phase II Clinical Trial of Genexol-PM® with gemcitabine in advanced biliary tract cancer. *Anticancer Res.* 2017;37(3):1467–73. <https://doi.org/10.21873/anticancerres.11471>.
43. Kırmılioğlu GY, Görgülü S. Surface modification of PLGA nanoparticles with chitosan or Eudragit® RS 100: characterization, prolonged release, cytotoxicity, and enhanced antimicrobial activity. *J Drug Deliv Sci Technol.* 2021;61:102145. <https://doi.org/10.1016/j.jddst.2020.102145>.
44. Kolhar P, Doshi N, Mitragotri S. Polymer nanoneedle-mediated intracellular drug delivery. *Small.* 2011;7(14):2094–100. <https://doi.org/10.1002/sml.201100497>.
45. Kolhar P, Anselmo AC, Gupta V, Pant K, Prabhakarandian B, Ruoslahti E, Mitragotri S. Using shape effects to target antibody-coated nanoparticles to lung and brain endothelium. *Proc Natl Acad Sci U S A.* 2013;110(26):10753–8. <https://doi.org/10.1073/pnas.1308345110>.
46. Kulkarni SA, Feng SS. Effects of particle size and surface modification on cellular uptake and biodistribution of polymeric nanoparticles for drug delivery. *Pharm Res.* 2013;30(10):2512–22. <https://doi.org/10.1007/s11095-012-0958-3>.
47. Kurniawan DW, Jajoriya AK, Dhawan G, Mishra D, Argemi J, Bataller R, Storm G, Mishra DP, Prakash J, Bansal R. Therapeutic inhibition of spleen tyrosine kinase in inflammatory macrophages using PLGA nanoparticles for the treatment of non-alcoholic steatohepatitis. *J Control Release.* 2018;288:227–38. <https://doi.org/10.1016/j.jconrel.2018.09.004>.
48. Lee KSS, Yang J, Niu J, Ng CJ, Wagner KM, Dong H, Kodani SD, Wan D, Morisseau C, Hammock BD. Drug-target residence time affects in vivo target occupancy through multiple pathways. *ACS Cent Sci.* 2019;5(9):1614–24. <https://doi.org/10.1021/acscentsci.9b00770>.
49. Levchenko TS, Rammohan R, Lukyanov AN, Whiteman KR, Torchilin VP. Liposome clearance in mice: the effect of a separate and combined presence of surface charge and polymer coating. *Int J Pharm.* 2002;240(1–2):95–102. [https://doi.org/10.1016/S0378-5173\(02\)00129-1](https://doi.org/10.1016/S0378-5173(02)00129-1).
50. Li Y, Kroger M, Liu WK. Shape effect in cellular uptake of PEGylated nanoparticles: comparison between sphere, rod, cube and disk. *Nanoscale.* 2015;7:16631–46. <https://doi.org/10.1039/C5NR02970H>.
51. Li M, Jiang S, Simon J, Paßlick D, Frey ML, Wagner M, Mailänder V, Crespy D, Landfester K. Brush conformation of polyethylene glycol determines the stealth effect of nanocarriers in the low protein adsorption regime. *Nano Lett.* 2021;21(4):1591–8. <https://doi.org/10.1021/acs.nanolett.0c03756>.
52. Lin YS, Hurley KR, Haynes CL. Critical considerations in the biomedical use of mesoporous silica nanoparticles. *J Phys Chem Lett.* 2012;3(3):364–74. <https://doi.org/10.1021/jz2013837>.
53. Longmire M, Choyke PL, Kobayashi H. Clearance properties of nano-sized particles and molecules as imaging agents: considerations and caveats. *Nanomedicine (Lond).* 2008;3(5):703–17. <https://doi.org/10.2217/17435889.3.5.703>.
54. Lorenz MR, Holzapfel V, Musyanovych A, Nothelfer K, Walther P, Frank H, Landfester K, Schrezenmeier H, Mailänder V. Uptake of functionalized, fluorescent-labeled polymeric particles in different cell lines and stem cells. *Biomaterials.* 2006;27(14):2820–8. <https://doi.org/10.1016/j.biomaterials.2005.12.022>.
55. Margulis K, Zhang X, Joubert LM, Bruening K, Tassone CJ, Zare RN, Waymouth RM. Formation of polymeric nanocubes by self-assembly and crystallization of dithiolane-containing triblock copolymers. *Angew Chem Int Ed Engl.* 2017;56(51):16357–62. <https://doi.org/10.1002/anie.201709564>.
56. Mitchell MJ, Billingsley MM, Haley RM, Wechsler ME, Peppas NA, Langer R. Engineering precision nanoparticles for drug delivery. *Nat Rev Drug Discov.* 2021;20(2):101–24. <https://doi.org/10.1038/s41573-020-0090-8>.
57. Müllner M, Dodds SJ, Nguyen TH, Senyschyn D, Porter CJ, Boyd BJ, Caruso F. Size and rigidity of cylindrical polymer brushes dictate long circulating

- properties in vivo. *ACS Nano*. 2015;9(2):1294–304. <https://doi.org/10.1021/nn505125f>.
58. Nima ZA, Alwbari AM, Dantuluri V, Hamzah RN, Sra N, Motwani P, Arnaoutakis K, Levy RA, Bohliqa AF, Nedosekin D, Zharov VP, Makhoul I, Biris AS. Targeting nano drug delivery to cancer cells using tunable, multi-layer, silver-decorated gold nanorods. *J Appl Toxicol*. 2017;37(12):1370–8. <https://doi.org/10.1002/jat.3495>.
59. Nishida N, Yano H, Nishida T, Kamura T, Kojiro M. Angiogenesis in cancer. *Vasc Health Risk Manag*. 2006;2(3):213–9. <https://doi.org/10.2147/vhrm.2006.2.3.213>.
60. Numata M, Grinkova YV, Mitchell JR, Chu HW, Sligar SG, Voelker DR. Nanodiscs as a therapeutic delivery agent: inhibition of respiratory syncytial virus infection in the lung. *Int J Nanomedicine*. 2013;8:1417–27. <https://doi.org/10.2147/IJN.S39888>.
61. Owens DE 3rd, Peppas NA. Opsonization, biodistribution, and pharmacokinetics of polymeric nanoparticles. *Int J Pharm*. 2006;307(1):93–102. <https://doi.org/10.1016/j.ijpharm.2005.10.010>.
62. Panariti A, Miserocchi G, Rivolta I. The effect of nanoparticle uptake on cellular behavior: disrupting or enabling functions? *Nanotechnol Sci Appl*. 2012;5:87–100. <https://doi.org/10.2147/NSA.S25515>.
63. Patil RR, Gaikwad RV, Samad A, Devarajan PV. Role of lipids in enhancing splenic uptake of polymer-lipid (LIPOMER) nanoparticles. *J Biomed Nano*. 2008;4(3):359–66. <https://doi.org/10.1166/jbn.2008.320>.
64. Perrault SD, Walkey C, Jennings T, Fischer HC, Chan WC. Mediating tumor targeting efficiency of nanoparticles through design. *Nano Lett*. 2009;9(5):1909–15. <https://doi.org/10.1021/nl900031y>.
65. Prabhakar U, Maeda H, Jain RK, Sevick-Muraca EM, Zamboni W, Farokhzad OC, Barry ST, Gabizon A, Grodzinski P, Blakey DC. Challenges and key considerations of the enhanced permeability and retention effect for nanomedicine drug delivery in oncology. *Cancer Res*. 2013;73(8):2412–7. <https://doi.org/10.1158/0008-5472.CAN-12-4561>.
66. Punfa W, Yodkeeree S, Pitchakarn P, Ampasavate C, Limtrakul P. Enhancement of cellular uptake and cytotoxicity of curcumin-loaded PLGA nanoparticles by conjugation with anti-P-glycoprotein in drug resistance cancer cells. *Acta Pharmacol Sin*. 2012;33(6):823–31. <https://doi.org/10.1038/aps.2012.34>.
67. Qie Y, Yuan H, von Roemeling CA, Chen Y, Liu X, Shih KD, Knight JA, Tun HW, Wharen RE, Jiang W, Kim BY. Corrigendum: surface modification of nanoparticles enables selective evasion of phagocytic clearance by distinct macrophage phenotypes. *Sci Rep*. 2016;6:30663. <https://doi.org/10.1038/srep30663>.
68. Rizvi SAA, Saleh AM. Applications of nanoparticle systems in drug delivery technology. *Saudi Pharm J*. 2018;26(1):64–70. <https://doi.org/10.1016/j.jsps.2017.10.012>.
69. Ruggiero A, Villa CH, Bander E, Rey DA, Bergkvist M, Batt CA, Manova-Todorova K, Deen WM, Scheinberg DA, McDevitt MR. Paradoxical glomerular filtration of carbon nanotubes. *Proc Natl Acad Sci U S A*. 2010;107(27):12369–74. <https://doi.org/10.1073/pnas.0913667107>.
70. Salmaso S, Caliceti P. Stealth properties to improve therapeutic efficacy of drug nanocarriers. *J Drug Deliv*. 2013;2013:374252. <https://doi.org/10.1155/2013/374252>.
71. Sharma G, Valenta DT, Altman Y, Harvey S, Xie H, Mitragotri S, Smith JW. Polymer particle shape independently influences binding and internalization by macrophages. *J Control Release*. 2010;147(3):408–12. <https://doi.org/10.1016/j.jconrel.2010.07.116>.
72. Sheng Y, Chang L, Kuang T, Hu J. PEG/heparin-decorated lipid-polymer hybrid nanoparticles for long-circulating drug delivery. *RSC Adv*. 2016;6:23279–87. <https://doi.org/10.1039/C5RA26215A>.
73. Song G, Petschauer JS, Madden AJ, Zamboni WC. Nanoparticles and the mononuclear phagocyte system: pharmacokinetics and applications for inflammatory diseases. *Curr Rheumatol Rev*. 2014;10(1):22–34. <https://doi.org/10.2174/1573403x10666140914160554>.
74. Suk JS, Xu Q, Kim N, Hanes J, Ensign LM. PEGylation as a strategy for improving nanoparticle-based drug and gene delivery. *Adv Drug Deliv Rev*. 2016;99(Pt A):28–51. <https://doi.org/10.1016/j.addr.2015.09.012>.
75. Termsarasab U, Yoon IS, Park JH, Moon HT, Cho HJ, Kim DD. Polyethylene glycol-modified arachidyl chitosan-based nanoparticles for prolonged blood circulation of doxorubicin. *Int J Pharm*. 2014;464(1–2):127–34. <https://doi.org/10.1016/j.ijpharm.2014.01.015>.
76. Torres-Martinez EJ, Cornejo Bravo JM, Serrano Medina A, Pérez González GL, Villarreal Gómez LJ. A summary of electrospun nanofibers as drug delivery system: drugs loaded and biopolymers used as matrices. *Curr Drug Deliv*. 2018;15(10):1360–74. <https://doi.org/10.2174/1567201815666180723114326>.
77. Verma A, Stellacci F. Effect of surface properties on nanoparticle-cell interactions. *Small*. 2010;6(1):12–21. <https://doi.org/10.1002/sml.200901158>.
78. Walkey CD, Olsen JB, Guo H, Emili A, Chan WC. Nanoparticle size and surface chemistry determine serum protein adsorption and macrophage uptake. *J Am Chem Soc*. 2012;134(4):2139–47. <https://doi.org/10.1021/ja2084338>.
79. Wang HX, Zuo ZQ, Du JZ, Wang YC, Sun R, Cao ZT, Ye XD, Wang JL, Leong KW, Wang J. Surface charge critically affects tumor penetration and therapeutic efficacy of cancer nanomedicines. *NanoToday*. 2016;11(2):133–44. <https://doi.org/10.1016/j.nantod.2016.04.008>.
80. Wang J, Hu X, Xiang D. Nanoparticle drug delivery systems: an excellent carrier for tumor peptide vaccines. *Drug Deliv*. 2018;25(1):1319–27. <https://doi.org/10.1080/10717544.2018.1477857>.

81. Wang Y, Zhou C, Ding Y, Liu M, Tai Z, Jin Q, Yang Y, Li Z, Yang M, Gong W, Gao C. Red blood cell-hitchhiking chitosan nanoparticles for prolonged blood circulation time of vitamin K1. *Int J Pharm.* 2021;592:120084. <https://doi.org/10.1016/j.ijpharm.2020.120084>.
82. Wen R, Umeano AC, Kou Y, Xu J, Farooqi AA. Nanoparticle systems for cancer vaccine. *Nanomedicine (Lond).* 2019;14(5):627–48. <https://doi.org/10.2217/nmm-2018-0147>.
83. Wilhelm S, Tavares AJ, Dai Q, Ohta S, Audet J, Dvorak HF, Chan WCW. Analysis of nanoparticle delivery to tumours. *Nat Rev Mater.* 2016;1:16014. <https://doi.org/10.1038/natrevmats.2016.14>.
84. Wisse E, Jacobs F, Topal B, Frederik P, De Geest B. The size of endothelial fenestrae in human liver sinusoids: implications for hepatocyte-directed gene transfer. *Gene Ther.* 2008;15(17):1193–9. <https://doi.org/10.1038/gt.2008.60>.
85. Xiao K, Li Y, Luo J, Lee JS, Xiao W, Gonik AM, Agarwal RG, Lam KS. The effect of surface charge on in vivo biodistribution of PEG-oligocholic acid based micellar nanoparticles. *Biomaterials.* 2011;32(13):3435–46. <https://doi.org/10.1016/j.biomaterials.2011.01.021>.
86. Xiao B, Ma P, Ma L, Chen Q, Si X, Walter L, Merlin D. Effects of tripolyphosphate on cellular uptake and RNA interference efficiency of chitosan-based nanoparticles in Raw 264.7 macrophages. *J Colloid Interface Sci.* 2017;490:520–8. <https://doi.org/10.1016/j.jcis.2016.11.088>.
87. Yadav D, Dewangan H. PEGYLATION: an important approach for novel drug delivery system. *J Biomater Sci Polym Ed.* 2021;32(2):266–80. <https://doi.org/10.1080/09205063.2020.1825304>.
88. Yamashita F, Hashida M. Pharmacokinetic considerations for targeted drug delivery. *Adv Drug Deliv Rev.* 2013;65(1):139–47. <https://doi.org/10.1016/j.addr.2012.11.006>.
89. Yang Q, Jones SW, Parker CL, Zamboni WC, Bear JE, Lai SK. Evading immune cell uptake and clearance requires PEG grafting at densities substantially exceeding the minimum for brush conformation. *Mol Pharm.* 2014;11(4):1250–8. <https://doi.org/10.1021/mp400703d>.
90. Yao J, Fan Y, Du R, Zhou J, Lu Y, Wang W, Ren J, Sun X. Amphoteric hyaluronic acid derivative for targeting gene delivery. *Biomaterials.* 2010;31(35):9357–65. <https://doi.org/10.1016/j.biomaterials.2010.08.043>.
91. Yuan F, Dellian M, Fukumura D, Leunig M, Berk DA, Torchilin VP, Jain RK. Vascular permeability in a human tumor xenograft: molecular size dependence and cutoff size. *Cancer Res.* 1995;55(17):3752–6.
92. Yue ZG, Wei W, Lv PP, Yue H, Wang LY, Su ZG, Ma GH. Surface charge affects cellular uptake and intracellular trafficking of chitosan-based nanoparticles. *Biomacromolecules.* 2011;12(7):2440–6. <https://doi.org/10.1021/bm101482r>.
93. Zhang J, Liu J, Zhao Y, Wang G, Zhou F. Plasma and cellular pharmacokinetic considerations for the development and optimization of antitumor block copolymer micelles. *Expert Opin Drug Deliv.* 2015;12(2):263–81. <https://doi.org/10.1517/17425247.2014.945417>.
94. Zhang YN, Poon W, Tavares AJ, McGilvray ID, Chan WCW. Nanoparticle-liver interactions: cellular uptake and hepatobiliary elimination. *J Control Release.* 2016;240:332–48. <https://doi.org/10.1016/j.jconrel.2016.01.020>.
95. Zhao F, Zhao Y, Liu Y, Chang X, Chen C, Zhao Y. Cellular uptake, intracellular trafficking, and cytotoxicity of nanomaterials. *Small.* 2011;7(10):1322–37. <https://doi.org/10.1002/sml.201100001>.
96. Zhao Y, Wei C, Chen X, Liu J, Yu Q, Liu Y, Liu J. Drug delivery system based on near-infrared light-responsive molybdenum disulfide nanosheets controls the high-efficiency release of dexamethasone to inhibit inflammation and treat osteoarthritis. *ACS Appl Mater Interfaces.* 2019;11(12):11587–601. <https://doi.org/10.1021/acsami.8b20372>.
97. Zhou Z, Ma X, Jin E, Tang J, Sui M, Shen Y, Van Kirk EA, Murdoch WJ, Radosz M. Linear-dendritic drug conjugates forming long-circulating nanorods for cancer-drug delivery. *Biomaterials.* 2013;34:5722–35. <https://doi.org/10.1016/j.biomaterials.2013.04.012>.



PKPD of PLGA-PEG-PLGA Copolymeric Micelles

15

Shirleen Miriam Marques and Lalit Kumar

Contents

1	Introduction	274
2	Synthesis and Purification of PLGA-PEG-PLGA Copolymer	274
3	Characterization of PLGA-PEG-PLGA Triblock Copolymer	275
4	Factors Affecting the Formation and Characteristics of the PLGA-PEG-PLGA Copolymeric Micelles	277
5	Pharmacokinetics (PK) and Pharmacodynamics (PD) of Copolymeric Micelles Based on PLGA-PEG-PLGA	279
6	Conclusion	288
	References	289

Abstract

Much research has been undertaken on stimuli-sensitive polymers and their applications in biochemistry, biomedicine, and a plethora of domains over the last decade. Stimuli-sensitive gelling polymers or in situ forming hydrogels, in particular, have drawn a lot of interest as prospective injectable implant systems with low invasiveness. Drugs or cells can be readily combined with the aqueous copolymer solution at low temperatures, and then injected into the body at a specific spot to form a semisolid

matrix. Nanoparticles composed of amphiphilic block copolymers with biodegradable core-forming blocks are extremely appealing for the development of long-acting drug delivery systems. The FDA-approved PLGA-PEG-PLGA triblock copolymer possesses the capability to provide sustained release of various biologicals. Polymer solutions having an ability to convert from sol to gel at physiological temperatures can be used for in situ gel formation and injectability. Drug delivery systems with more complicated architectures are being developed as technology advances. As a result, the processes of drug absorption and disposition following the administration of these newer delivery systems have grown extremely complicated. Thus, knowledge of the pharmacokinetics and pharmacodynamics could be

S. M. Marques · L. Kumar (✉)
Department of Pharmaceutics, Manipal College of
Pharmaceutical Sciences, Manipal Academy of
Higher Education, Manipal, Udipi, Karnataka, India
e-mail: lalit.kumar@manipal.edu

utilised to disentangle these complexities and increase our understanding of these drug delivery systems' *in vivo* behaviour, hence guiding their preclinical-to-clinical translation and clinical development.

Keywords

PLGA-PEG-PLGA · Copolymeric micelle · Amphiphilic · Pharmacokinetics · Pharmacodynamics · Hydrogel

1 Introduction

The use of polymeric nanoparticles in medicine to achieve site-specific medication delivery has recently piqued interest. Polymeric micelles, in particular, are now recognised as one of the most potential transporters [1]. The polymer poly(lactide-co-glycolic acid) (PLGA) which has received approval from the FDA has been examined for its biocompatibility and toxicity [2, 3]. To lengthen the release period of linked pharmaceuticals, the D,L-lactide (LA) to glycolide (GA) ratio, molecular weight, and hydrophilic properties of the polymer can be adjusted. The release of the drug in a controlled manner, reduced cytotoxicity, and few adverse events have all been demonstrated with PLGA nanoparticles. When chemically attached to the PLGA block, polyethylene glycol (PEG) displays a sluggish removal from the circulation, thereby resulting in a greater drug release and reduced absorption of PLGA nanoparticles by the reticuloendothelial system in comparison to the non-conjugated PLGA [2].

PEG/PLGA [4, 5], PEG/poly(caprolactone) [6], PEG/poly(propylene glycol)/polyester, PEG/peptide [7, 8] and poly(phosphazenes) [9, 10] are examples of biodegradable thermoresponsive copolymers that undergo sol-gel transitions in water when the temperature rises [11]. Self-assembled nano-micelles composed of the amphiphilic PEG and PLGA copolymers are used for the incorporation of hydrophobic as well as hydrophilic medicines and offer prolonged release of the therapeutic cargo [12]. Unlike poloxamer copoly-

mers, which have an exterior hydrophilic block, this block copolymer has hydrophilic inside blocks, which results in a distinct gelation mechanism. In this instance, gelation is likely to occur via flower-like micelle aggregation and the creation of an irregular percolated network [13]. In water, copolymers made up of hydrophobic and hydrophilic segments result in the formation of micelles, reducing free energy mostly due to hydrophobic interactions [14].

The release of drugs from these copolymers is accomplished by the following mechanisms: (i) diffusion of the drug present in the hydrogel during the early release period, and (ii) release of the drug via hydrogel matrix erosion during the latter phase [15]. Poly(lactide-co-glycolide)-poly(ethylene glycol)-poly(lactide-co-glycolide) (PLGA-PEG-PLGAs) possessing water solubility at ambient temperature allows for easy cargo loading and injection administration. In addition, the structure of the gel might be able to safeguard and release the trapped drug in a controlled manner [16]. PLGA-PEG-PLGA (Fig. 15.1) displays properties of a possible thermogel matrix, demonstrating a less invasive method of transporting cells and bioactive compounds. At low temperatures (4 °C), the PLGA-PEG-PLGA copolymer dissolves in water, but the solution gels spontaneously at 37 °C as seen in Fig. 15.2 [17]. Due to its ease of synthesis, remarkable reproducibility, and widespread acceptance of safety, the thermosensitive and biodegradable PLGA-PEG-PLGA hydrogel has attracted a lot of attention. Triblock PLGA-PEG-PLGA polymer is a suitable choice for drug carriers because of its non-cytotoxicity, outstanding temperature sensitivity, outstanding biocompatibility, and biodegradability and have been used for various clinical applications as depicted in Fig. 15.3 [18, 19].

2 Synthesis and Purification of PLGA-PEG-PLGA Copolymer

Zentner et al. outlined a traditional ring opening method to synthesize the PLGA-PEG-PLGA copolymer [20]. An appropriate amount of PEG was added into a stainless steel reactor, and the

Fig. 15.1 Structure of PLGA-PEG-PLGA copolymer

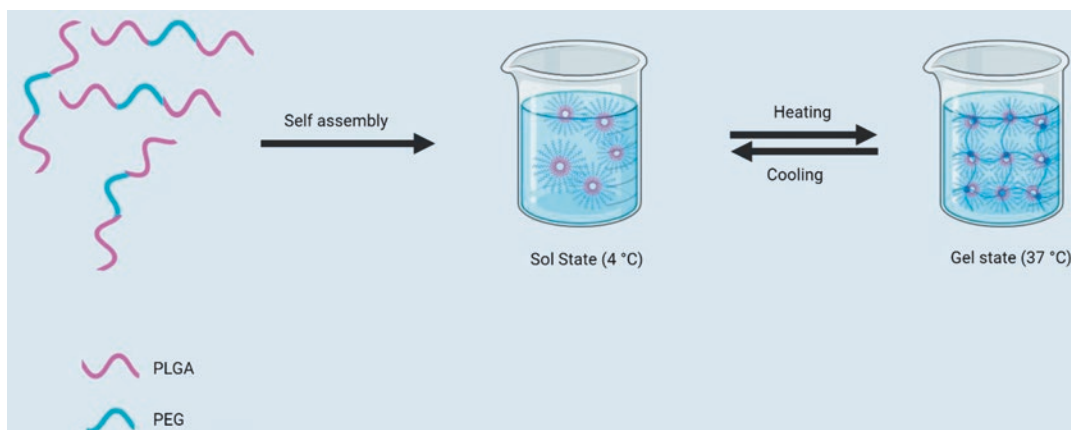
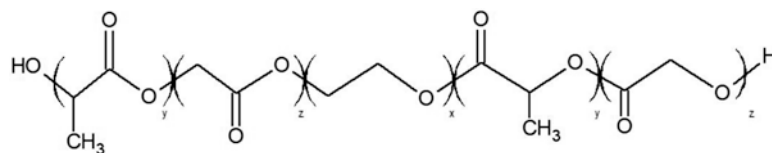


Fig. 15.2 Gelation mechanism of PLGA-PEG-PLGA copolymeric micelles

heating was carried out for 2 h at a temperature of 150 °C under 5 mmHg vacuum; after which, the desired quantities of LA and GA were loaded into the reactor. For 30 minutes, the reactor was operated at a temperature of 150 °C. A catalyst, stannous 2-ethylhexanoate, was introduced and was subsequently followed by heating the contents of the reactor at a temperature of 160 °C for duration of 6 hours below 5 mmHg vacuum [21–23].

In a study conducted by Yu and co-workers, the arrangement of the PLGA blocks in the copolymer of PLGA-PEG-PLGA was discovered to be influenced due to different polymerization conditions. Variations in the reaction affinity between LA and GA in ring opening polymerization, as well as post-polymerization transesterification, were blamed for the different arrangements in the triblock copolymer. The sol-gel conversion which was temperature induced in water was observed in an aqueous solution of the triblock copolymer. Moreover, the gelling behaviours could be adjusted by modifying the arrangement in the PLGA segment. The current research also revealed that the thermosensitive nature of the triblock copolymer was determined to be affected by the sequence structure present in the PLGA

segment. The transesterification in the polymerization process is primarily responsible for the differences in sequence structure among the copolymers. The balance in the hydrophobic and hydrophilic nature is altered by different sequence structures and polydispersities, which is essential for determining the micellization behaviour of these copolymers in water [24].

3 Characterization of PLGA-PEG-PLGA Triblock Copolymer

3.1 ¹H Nuclear Magnetic Resonance (NMR)

Copolymer structural analysis is crucial from both a theoretical and an industrial standpoint. In the study of copolymers, high-resolution NMR analysis is especially useful because it exposes structural and sequence information that cannot be deduced by other methods. NMR, especially ¹H NMR, is a simple and accurate method for determining copolymer composition, and it is generally more accurate than other conventional

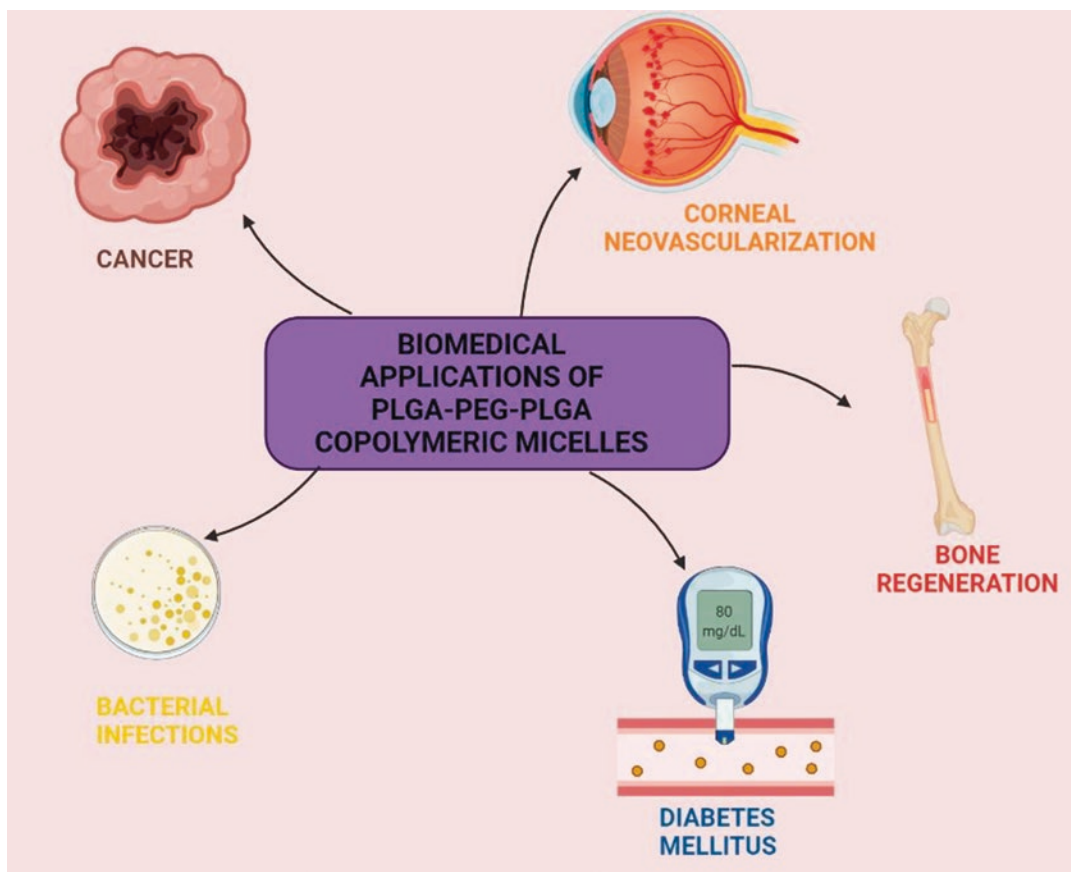


Fig. 15.3 Biomedical applications of PLGA-PEG-PLGA copolymeric micelles

analytical methods such as elemental analysis [25]. Ghahremankhani and group performed the structure analysis and estimation of molecular weight of the PLGA-PEG-PLGA copolymer using the ^1H NMR spectrum. Signals for PLGA-PEG-PLGA are found at = 5.1 ppm (a for CH of LA), 1.45 ppm (b for CH_3 of LA), 4.7 ppm (c for CH_2 of GA), 3.52 and 4.2 ppm (d and e for CH_2 of ethylene GA), and 3.52 and 4.2 ppm (d and e for CH_2 of ethylene glycolide) [26]. Similarly in order to elucidate the structure of the copolymers, determine the LA/GA ratio, and determine the number average molecular weight (M_n) of the PLGA-PEG-PLGA copolymers, ^1H NMR was performed by Khodaverdi and co-workers. The CH of LA, the CH_2 of GA, a CH_2 of PEG, another CH_2 of PEG, and the OH and CH_3 of LA, respectively, are the signals that appeared at 5.2, 4.8, 4.3, 3.5, 2.6, and 1.5 ppm. Moreover, the ratios of

the monomers that were used initially in the polymerization process matched very well with the LA-to-GA quantities which were calculated by ^1H NMR [27].

3.2 Gel Permeation Chromatography (GPC)

GPC was utilized to deduce information regarding the molecular weight and molecular weight distribution. In the study conducted by Chen and co-workers, the triblock copolymer was found to have a retention time of about 18 minutes, while the remaining two peaks in the chromatogram (retention time of about 21 minutes) were found to be of the solvent. Both copolymers were found to have a polydispersity of about 1.3, with a symmetric peak and a comparatively small

MWD. Further, the formation of the triblock polymer was confirmed by a single GPC trace along with a low polydispersity value [28].

3.3 Fourier Transform Infrared (FTIR)

FTIR spectroscopy is an important tool for determining the properties of both polymeric and biopolymeric materials. This technique has been effectively implemented for the assessment of polymerization process, characterization of the polymer structure, polymer surface, polymer degradation, and polymer modification, as well as in the identification and characterization of homopolymers, copolymers, and polymer composites [29]. The structure of PLGA-PEG-PLGA was validated by FTIR in a study done by Mohajeri and colleagues. The presence of both blocks can be seen in the FTIR spectrums of PLGA-PEG-PLGA at 1100 cm^{-1} (etheric C-O of PEG) and 1700 cm^{-1} (ester carbonyl of PLGA) [30]. The methods used for characterization of the triblock copolymer have been tabulated in Table 15.1.

4 Factors Affecting the Formation and Characteristics of the PLGA-PEG-PLGA Copolymeric Micelles

4.1 Molecular Weight Distribution (MWD) of PEG Block

MWD is among the most fundamental molecular properties of a synthetic polymer. The impact of the PEG block's MW and MWD on the micellization and phase transition of the PLGA-PEG-PLGA aqueous system was investigated by Chen and co-workers. PEG is a one-of-a-kind polymer because of its characteristics, particularly since its solubility in water and hydrophobicity rise with temperature. PEG has a chemical structure that encourages the creation of hydrogen bonds with water. The loss of water entropy can be credited to

Table 15.1 Characterization parameters for PLGA-PEG-PLGA polymer

Method	Analytical target	Reference
^1H NMR	Number-average molecular weight M_n and the molar composition	[31]
Gel permeation chromatography	Average molecular number (M_n), molecular weight (M_w), and M_w/M_n ratio (i.e. polydispersity index (PDI))	[32]
Fourier transform infrared	Functional group characterization	[33]
Differential scanning calorimetry	Glass transition temperature (T_g)	[34]

the extremely localised arrangement of the water molecules that surrounded the PEG chain. The hydrophilic PEG blocks are also found in the micellar corona of PLGA-PEG-PLGA, and in a dispersed sample, the micelle sizes may be heavily influenced by the longer PEG chains. As a result, larger micelles and looser micelle coronae emerged from a wider dispersion of PEG block. At low temperatures, a larger MWD of the PEG segment produced bigger copolymer micelles, and the resulting system which was concentrated was found to become viscous and even physically gelled [35]. A decreased solubility promoted the hydrophobic association-driven physical gelation. The samples with smaller MWDs physically gelled not just at lower concentrations but also at lower temperatures in our thermosensitive macromolecular system. This could be due to the fact that it has a higher local hydrophobicity. Because of the increased local hydrophobicity, the micelles were more stable, allowing them to maintain their gel state over a larger temperature range [36].

4.2 LA and GA Sequences in the PLGA Block

In general, the type of initiators used together with the transesterification process during ring opening polymerization, which results in a random arrangement of the monomer units in the polymer chains,

is known to influence the sequence structures of PLGA. Yu et al. created and characterised a couple of PLGA-PEG-PLGA copolymers in which the arrangement of the PLGA segment in the PLGA-PEG-PLGA triblock copolymers was modified by varied polymerization settings. Differences in reaction affinity between LA and GA in ring opening polymerization, as well as post-polymerization transesterification, were blamed for the different arrangement in the copolymers. The temperature-sensitive sol-gel conversion in water was seen in the aqueous system of the PLGA-PEG-PLGA triblock copolymers, and the gelling behaviours were shown to be controllable by modifying the arrangement in the PLGA segment. Different profiles of micellization behaviours were found as the temperature increased the copolymers, demonstrating that self-assembly of the PLGA-PEG-PLGA copolymers in water depended on the sequence structures [24].

4.3 Length of PEG Block

A study conducted by Khorshid and co-workers aimed to determine the effect of the length of the hydrophilic PEG segment on the structural changes of the PLGA-PEG-PLGA triblock copolymer during gelation. The length of the hydrophobic PLGA block was held constant in this study, whereas the length of the hydrophilic PEG block was changed ($n = 1000$ and $n = 1500$). The change was found to produce a profound effect on the phase behaviour of aqueous samples as well as the polymer structure in both dilute and semi-dilute solutions. The results of turbidity and viscosity studies on dilute copolymer solutions imply that loose intermicellar structures arise when the temperature is raised initially, after which there was species contraction and disintegration to micelles at elevated temperatures. Both copolymers exhibit a similar pattern of action; however, the properties of the copolymer with long PEG spacer appear at significantly higher temperatures [37].

4.4 LA/GA Ratio

Sulaiman and co-workers used a factorial design technique to evaluate the co-block polymer behaviour and properties of a nanopolymeric micelle which were affected by PLGA formation (constituent components ratio) and PEG concentration. With respect to the solubility behaviour, the solubility was found to be the maximum at the highest LA-to-GA ratio. In terms of the polydispersity index (PDI), a polydisperse system was favoured by the low LA-to-GA ratio, which produced two peaks in the particle size distribution. Conversely, with a high LA-to-GA ratio, a monodisperse system was seen. The variation in co-block length was the main driver of particle size distribution. Co-blocks with a longer length were found to produce larger particles than those with a shorter length [38].

In a study conducted by Qiao and group, the effect of the LA/GA molar ratio on release of the drug from the triblock copolymer hydrogel was determined, wherein 5-fluorouracil was chosen as the hydrophilic drug and indomethacin was chosen as the hydrophobic drug. The molar ratio of LA to GA was found to have a minor impact on drug release driven by diffusion, while it had a considerable impact on the release of the drug release which was governed by erosion of the hydrogel. The reason for this could be attributed to the drugs being distributed in various regions of the hydrogel. Indomethacin partitions into the hydrogel's hydrophobic PLGA region and just a little quantity into the PEG region, whereas the hydrophilic 5-fluorouracil partitions into the PEG region. The drug present in the hydrophilic region was released by diffusion via the hydrophilic channels of the hydrogel that were relatively less affected by changes in the LA/GA ratio, whereas the hydrophobic indomethacin dispersed within the PLGA region was released due to erosion of the hydrogel [23].

4.5 Effect of PEG/PLGA Ratio

In a study conducted by Cespi and group, a thorough investigation was conducted to characterise a panel of copolymers of PLGA-PEG-PLGA so as to determine their thermal characteristics in the solid state and the rheological properties of their aqueous solutions. As a result, 15 tri-block copolymers were produced as well as analysed, each with a different MW and hydrophobicity (PEG/PLGA ratio). The DSC analysis conducted for the aforementioned produced copolymers revealed that copolymers having a PEG/PLGA ratio less than 1 in which the percent of PLGA block is dominant have an amorphous solid form (PLGA-like copolymers). PEG-like copolymers, on the other hand, have lower T_g values (-35°C), with crystallization and melting events ranging from -25°C to 0°C and 10°C to 35°C . Also at greater PEG/PLGA ratios, M_n has a noticeable effect on rheological characteristics. Copolymers that possess a PEG/PLGA ratio of 0.4 to 1 are either fully or partially hydrated, resulting in complete or partial thermogelling, or sol dispersions, depending on the structural features of the copolymers (PEG/PLGA ratio and M_n), at least up to a M_n of 8 kDa. The dispersions which had a M_n of 5 kDa and 5.9 kDa, respectively, and a PEG/PLGA ratio of 0.43 and 0.51, displayed thermogelling behaviour, thus verifying the restricted window of MW and PEG/PLGA ratio where thermogelling systems in aqueous solutions can be generated, irrespective of the concentration [39]. Gelling temperature and release of a model drug were tested by Steinmann and co-workers using triblock copolymers of PLGA-PEG-PLGA with different PEG lengths. As expected, increasing the hydrophobic PLGA block resulted in a lower gelling temperature because the system required less energy to overcome the hydrogen bonding between hydrophilic PEG segments via PLGA-PLGA hydrophobic interactions. A linear association between declining PLGA block length and gelling temperature was discovered [40]. Table 15.2 represents a summary of the factors affecting the characteristics of the copolymeric micelles composed of PLGA-PEG-PLGA.

Table 15.2 Parameters affecting formation and characteristics of PLGA-PEG-PLGA copolymeric micelles

Parameter	Finding	Reference
MWD of PEG block	Larger micelles and looser micelle coronae emerged from a wider dispersion of PEG block	[35]
LA and GA sequence in the PLGA block	Gelling and micellization behaviour were shown to be controllable by modifying the sequence structure in the PLGA block	[24]
Length of PEG block	Short PEG block produce asymmetric (ellipsoid) forms in dilute solution, and a longer PEG block may be characterised using a spherical core-shell model	[37]
LA/GA ratio	A polydisperse system was favoured by the low LA-to-GA ratio, and a monodisperse system was seen with a high LA-to-GA ratio	[38]
PEG/PLGA ratio	Increasing the hydrophobic PLGA block resulted in a lower gelling temperature	[40]

5 Pharmacokinetics (PK) and Pharmacodynamics (PD) of Copolymeric Micelles Based on PLGA-PEG-PLGA

The link between pharmacokinetics and pharmacodynamics is an essential component in the pharmaceutical industry's discovery and development of novel medications. Scientists can use effective PK/PD study design, analysis, and interpretation to better comprehend the correlation between PK and PD, as well as discover PK features for further improvement and optimal drug design and development [41]. PK-PD modelling has been extensively employed to increase insight of the in vivo behaviour of these complicated delivery systems and aid their development since it allows for the separation of drug-, carrier-, and pharmacological system-specific factors [42]. It connects the concentration-time profile measured by pharmacokinetics to the magnitude of the observed reaction measured by pharmacodynamics [43].

Localized cancer therapies involving a mixture of medications have lately surfaced as novel strategies for preventing tumour progression and recurrence. Ma et al. designed a new method for treating osteosarcoma by employing thermosensitive PLGA-PEG-PLGA hydrogels to offer targeted delivery of more than a single medication, which included doxorubicin (DOX), cisplatin (CDDP), and methotrexate (MTX). In a nude mouse model containing human osteosarcoma Saos-2 xenografts, the drug-loaded hydrogels' anticancer efficacies were assessed *in vivo*. Within the neighbourhood of the tumours, the mice were administered a single injection of drug-loaded hydrogels or solutions of the free drug. Treatment with drug-loaded hydrogels exhibited improved *in vivo* tumour inhibition efficacies for up to 16 days in comparison to treatment with the free drug. The reason for this is likely due to the hydrogels' long-term drug release characteristics, which result in sustained tumour suppression *in vivo* [44].

In another study, Jiang and co-workers used multifunctional dendritic nanoparticles in a thermoresponsive injectable hydrogel matrix made of PLGA-PEG-PLGA to create a localised drug delivery vehicle so as to combine chemotherapy and immunotherapy. PLGA-PEG-PLGA allows for targeted, long-lasting drug administration as well as co-loading of medicinal substances for combination therapy. The dendritic nanoparticles were created with a fourth-generation L-arginine-rich dendritic architecture (G4-Arg) and a hydrophobic interior that could hold the anticancer medication DOX. The 4 T1 murine breast cancer model established from BALB/C mice was used to assess the anticancer impact of the various formulations *in vivo*. After a 24-day therapy, the Gel/G4-Arg/DOX group had the strongest tumour growth suppression efficacy of all the groups. The results also revealed that the tumour volume of the doxorubicin-loaded *in situ* thermosensitive hydrogel group was less as compared to the free doxorubicin group given intravenously. At the end of the treatment period, the group that received Gel/G4-Arg/DOX only once had a stronger tumour growth suppression than the free DOX group, which received free DOX four

times. *In vivo*, the level of NO in tumour tissue in the G4-Arg groups was considerably greater. The better penetrability of G4-Arg, as well as the synergism of NO created by the L-arginine in G4-Arg, can be attributed to the Gel/G4-Arg/ improved DOX's antitumor efficiency [45].

The idea of PLGA-PEG-PLGA micelles encapsulating US597 was conceived by Chen and co-workers with the goal of establishing a delivery system for prolonged oral cancer therapy. The peak plasma concentration of US597@micelles was recorded to be nearly 4 times greater as compared to free US597. US597@micelles had a 4.2-fold faster peak plasma concentration of US597 as compared to free US597. Thus, the US597@micelles were absorbed more rapidly than free US597 in Sprague-Dawley rats, and the degree of absorption as measured by peak plasma drug concentration was substantially greater. There were also alterations in the pharmacokinetic characteristics for US597@micelles, which revealed substantial modifications. US597@micelles had a two-fold shorter elimination half-time ($t_{1/2}$) than free US597 (8.716 ± 7.003 hours for US597@micelles and 16.433 ± 8.821 hours for US597), indicating that US597 was eliminated from the rat plasma more quickly for US597@micelles than for free US597. Furthermore, the change in AUC_{0-t} from $0.274 \pm 0.265 \mu\text{g}\cdot\text{h}\cdot\text{ml}^{-1}$ for US597 to $0.424 \pm 0.22 \mu\text{g}\cdot\text{h}\cdot\text{ml}^{-1}$ for US597@micelles (1.54-fold) suggested that US597@micelles would have better bioavailability as compared to the free drug. Collectively, this evidence suggests that the US597@micelles had better absorption, metabolism, and excretion than free US597, as well as a longer drug action time thereby having a higher solubility and anti-tumour efficacy [46].

In order to co-deliver DOX and β -cyclodextrin curcumin (CD CUR) to tumour regions, Yang and co-workers utilised a hydrogel composed of PLGA-PEG-PLGA. Using K 7 tumour-bearing mice, the anticancer efficacy of various techniques was assessed *in vivo*. Although the group treated with free DOX showed significant anticancer effects, the gel+DOX group had a smaller tumour volume than the free DOX group because the former relied on the sustained release of DOX

from hydrogel to keep a reasonably high DOX concentration at tumour locations for a long period. The ability of curcumin (CUR) to down-regulate Bcl 2, added to the effectiveness of the combination therapy of gel+DOX + CD CUR in killing tumour cells as compared to free DOX. As a result, although gel+CD CUR had a weak anticancer effect, the combination therapy based on gel+DOX + CD CUR had a greater antitumor activity over monotherapy. DOX and CD CUR could be delivered to the tumour region simultaneously using this localised dual medication delivery mechanism. Also, the hydrogel functioned as a drug depot, allowing for long-term medication efficacy thereby proving to be a promising method for slowing down tumour growth [47].

In another study conducted by Nagahama et al., a DOX delivery method that was both safe and effective for localised cancer chemotherapy was developed. Self-assembly of PLGA-PEG-PLGA copolymer micelles, clay nanodisks (CNDs), and DOX resulted in a novel biodegradable injectable gel. In vivo investigations employing human xenograft tumours in nude mice were used to investigate the antineoplastic effect of P3k/CND/DOX hybrid gels. When the tumour volume was 300 mm³, a hybrid gel precursor solution of 300 litres (210 g of DOX) was injected directly into the tumour. Treatment with the P3k/CND/DOX hybrid gel, the tumour volume decreased gradually. Most notably, the reduction lasted for a period of 21 days following a single hybrid gel injection, with no signs of dermatitis. Thus, the P3k/CND/DOX hybrid gel's anticancer efficacy was ascertained. The P3k/CND/DOX hybrid gel's prolonged antineoplastic action was related to the gradual release of DOX and improved cellular uptake of the DOX that was released due to the formation of nanostructures made of DOX with P3k/CND hybrid micelles. As a result, it is determined that a DOX-delivery system for focused cancer treatment requires long-term continuous gradual release of DOX devoid of "burst release" could be provided by an injectable P3k/CND/DOX gel [48].

Recently, an injection of a liposome DOX-loaded PLGA-PEG-PLGA-based thermogel was

produced by Cao and co-workers. Further, in orthotopic 4 T1 breast tumour-bearing BALB/c female mice, the anticancer efficacy of DOX-loaded formulations was investigated in vivo. Free DOX, DOX liposomes, DOX gel, and DOX-loaded liposomal gel groups had tumour inhibition rates of 56.2%, 59.7%, 75.9%, and 86.5%, respectively. Tumour volume was substantially less in the DOX gel and DOX-loaded liposomal gel sustained-release groups, implying that the peritumoural injection had higher antitumour effectiveness. DOX-loaded liposomal gel had the lowest tumour volume of all, measuring 269.9 ± 61.7 mm³, showing the greatest tumour suppression [49].

In order to demonstrate the superiority of the prodrug thermogels, in vivo antitumor effectiveness in a female H22 hepatoma-bearing mice model was studied by Zhang et al. The Gel-CAD(*cis*-aconitic anhydride-functionalized DOX) + DTX group as well as the Gel-SAD(succinic anhydride-modified DOX) + DTX group had stronger tumour inhibition efficacy than the DOX+ docetaxel (DTX) group, which was attributed to the DOX-conjugated thermogels' prolonged drug release profile. Owing to the synergism of a DNA intercalator DOX with a microtubule-interfering DTX, the Gel-CAD + DTX group had the most effective tumour inhibition of all the testing circumstances. Thus, an effective combination of a complimentary medication and a tumour microenvironment-labile polymeric prodrug thermogel presented considerable promise for in situ antineoplastic therapy [33].

By employing a fatty acid-modified Gem derivative as a drug and a thermosensitive hydrogel as the carrier, Yang and group were able to develop a long-acting Gem delivery system. The hydrogels were easily made by combining two types of PLGA-PEG-PLGA copolymers in the right proportions. BALB/c mice with 4 T1 mammary tumours were given different therapies to assess the anticancer efficiency of GemC16@Gel alone as well as the synergetic chemoradiotherapy treatment when paired with irradiation. The best tumour growth suppression was achieved with a single injection of GemC16@Gel with

three times of X-ray exposure (GemC16@Gel + X ray). This was related to GemC16's long-term release as well as its long-lasting radiosensitizing action over multiple X-ray exposures [50].

Very recently, the use of collagenase to modify the extracellular matrix with abundant collagen in solid tumours has been shown to improve interstitial transport and antibody antitumor effectiveness. Thus, Pan and co-workers created a PLGA-PEG-PLGA polymer-based thermosensitive hydrogel for peritumoural injection that included a HER2-targeted monoclonal antibody trastuzumab and collagenase (Col/Tra/Gel). HER2-positive BT474 tumour-bearing mice were chosen, in which the Col/Tra/Gel treatment showed the highest reduction of tumour growth. When compared to the other groups, the drug-loaded hydrogel preparations displayed substantial inhibitory action on tumours. Furthermore, throughout the experiments, all groups of mice preserved their usual weight. These findings showed that subcutaneous therapy with Col/Tra/Gel improved trastuzumab antitumor effectiveness [51].

Jin et al. formulated thermosensitive and formation of *in situ* hydrogels comprising of PLGA-PEG-PLGA that could deliver corilagin and low-molecular-weight chitosan (LC) directly to the tumour tissue by intratumour administration while altering the tumour microenvironment to increase drug penetration. Surprisingly, when corilagin/LC/PPP thermosensitive hydrogels (CCPH) were combined along with Abraxane®, the synergistic tumour inhibition impact could reach 61.24% with the best anticancer activity. This could be attributable to tumour stroma remodelling and increased drug accumulation. After injection, the corilagin/LC/PPP solution efficiently transformed into CCPH in the mice's subcutaneous tissues; its concentration steadily declined. Further, it was totally destroyed on the 12th day, thereby confirming its use as well as its *in vivo* biodegradability. The biodegradation properties of CCPH showed that after the therapy was completed, the CCPH which was implanted could be removed without causing any harm to the body. As a result, when used in clinical settings, the treatment was considered to be safe and

also prevents the need for surgical removal after treatment [52].

To improve anticancer activity and bioavailability *in vivo*, andrographolide was encapsulated in a micelle composed of PLGA-PEG-PLGA. The $AUC_{0-\infty}$ was calculated to be 17.167 h g/ml for andrographolide micelles, which was 2.65-fold higher than the 6.463 h g/ml for free andrographolide suspensions, showing that the micelles encapsulating andrographolide have significantly increased bioavailability. Andrographolide micelles also had a substantially greater mean retention duration with a smaller elimination rate constant (K_{el}), indicating that eliminating the drug from the blood may be much slower and that the medication may remain in the body for a prolonged period for greater efficiency. Thus, these findings proved that PLGA-PEG-PLGA-based micelles enhanced the andrographolide pharmacokinetic behaviour *in vivo*, thereby acting as a promising delivery strategy for long-term drug release [53].

Ci and co-workers reported a preparation containing irinotecan along with PLGA-PEG-PLGA. Data obtained from the study revealed an excellent sustained release profile as well as considerable augmentation of the proportion of the active form of the drug by the thermogel. The tumour volume was also found to grow somewhat after irinotecan/thermogel injection, and then reduced dramatically. On day 21, the relative tumour volumes in the irinotecan/thermogel groups were 0.2 and 0.1, respectively, for medication dosages of 45 and 90 mg/kg/w. The final tumour volume was barely 10% of the initial size, showing that the tumour had shrunk dramatically. In conclusion, the prolonged release of irinotecan from the triblock-based thermogel had a remarkable anticancer efficacy in human SW620 colon carcinoma [54].

Corneal neovascularization (CNV) is a leading cause of ocular surface diseases. Subconjunctival delivery of anti-angiogenic drugs inhibits neovascularization by administering anti-angiogenic drugs in a targeted and effective manner. Liu et al. utilized the triblock copolymer of PLGA-PEG-PLGA in order to deliver metformin and levofloxacin hydrochloride

in a sustained manner. By using a mouse model of corneal alkali burn, the *in vivo* efficiency of subconjunctival administration of the metformin (MET) + levofloxacin hydrochloride (LFH)-loaded thermosensitive hydrogel in suppressing CNV was investigated. The MET+LFH-loaded hydrogel significantly prevented the development of CNV as compared to a single injection of MET or LFH loaded thermosensitive hydrogel. The combination of a long-acting MET together with an antibiotic (LFH) produced a synergistic effect. Therefore, subconjunctival injection of MET and LFH utilising PLGA-PEG-PLGA-based thermosensitive hydrogel holds a lot of promise for ocular anti-angiogenic therapy. Thus, co-delivery of MET and LFH may have a better inhibitory effect on CNV growth [55].

In a study conducted by Chan and co-workers, a continuous evaluation for the formation of neovascularization following an alkali-burn was conducted by scoring the degree of corneal opacity, burn stimulus, neovascularization of vessel growth, and inflammatory response of biomarker IL-6 in a rat model in order to determine the efficiency of dexamethasone (DEX)-loaded PLGA-PEG-PLGA thermogel following subconjunctival administration in the treatment of CNV. The mean scores of the negative control groups were substantially greater in comparison to the groups that received the drug solution and the drug-loaded thermogel in the corneal opacity evaluation, suggesting that the DEX which was subconjunctivally injected was effective in lowering corneal opacity of the burn region following an alkali-burn. The iris features were marginally blurred in the group that received the DEX solution but instead was recognisable in the group that was treated with the DEX-loaded thermogel. Similar to the DEX solution treatment group, eyeballs that received an injection of the drug-loaded thermogel had lower scores in the burn stimulus as well as neovascularization after 7 days of treatment [56].

Zhang and co-workers aimed to create an injectable intravitreal implant made of thermogel that would administer DEX to the posterior portion of the eye for a prolonged time period. The thermogel matrix was formulated using various

block ratios of PLGA-PEG-PLGA copolymers, and the micelles created using the copolymer aided in solubilizing the hydrophobic drug in an aqueous media. The vitreous retention period of DEX suspension proved to be very short for the treatment of chronic eye diseases. Fortunately, the thermogel dramatically delayed DEX intravitreal release, with a 28-fold increase in $MRT_{(0-\infty)}$ of DEX as compared to the suspension (from 4.1 h to 115.8 h). Moreover, initially the concentration of DEX given by the thermogel in the vitreous was well-maintained at less than 10 $\mu\text{g}/\text{mL}$ that is nearly twofold lower as compared to the suspension's peak concentration. Thus, this property suggested that, once delivered, the aqueous copolymeric solution quickly converted to a semisolid gel in the physiological milieu of the eye, inhibiting the first burst release considerably [57].

Xie and colleagues developed an injectable thermo-sensitive Avastin®/PLGA-PEG-PLGA hydrogel to determine the feasibility of an intravitreal injection of the PLGA-PEG-PLGA hydrogels. Avastin® was released in the retina of a rat model for at least 6 weeks after intravitreal injection of Avastin®/hydrogel. The C_{max} in the retina of rats that received an injection of the aqueous solution of Avastin® was 38.05 ± 15.56 ng/mg. The data showed that intravitreal injections of Avastin®/PLGA-PEG-PLGA hydrogel might significantly lengthen Avastin® *in vivo* half-life in the vitreous humour and retina. The *in vivo* pharmacokinetic study indicated that the PLGA-PEG-PLGA hydrogel was able to prolong the release of Avastin® in the vitreous humour and retina in comparison to injection of an aqueous solution of Avastin® [58].

Buprenorphine is an extremely lipophilic opioid partial agonist which inhibits the signs and symptoms caused due to withdrawal syndrome. Kamali and co-workers developed a long-acting buprenorphine injectable implant comprising of PLGA-PEG-PLGA and N-methyl-2-pyrrolidone (NMP) that possessed increased therapeutic efficacy. As a result, combining PLGA-PEG-PLGA with NMP proved to be an excellent formulation in order to obtain a long-acting, controlled-release, injectable

buprenorphine solution-delivery system devoid of the initial burst release. Additionally, in comparison to the subcutaneous administration of the solution, the AUC of buprenorphine and Norbuprenorphine was increased when the in situ forming gel and in situ forming implant were used. In contrast to the in situ forming gel and in situ forming implant formulations, a considerable percentage of administered buprenorphine solution in NMP seemed to be unabsorbed and did not enter blood circulation from the site of administration. In addition, the AUC and serum concentration (C) range of buprenorphine with regard to the in situ forming gel (AUC = 2721.38 69, C = 1.87–7.12) preparation were almost the same as the in situ forming implant (RBP-6000) (AUC = 2727.36 71, C = 1.75–10), thereby suggesting that the in situ forming gel could achieve the required therapeutic concentration required to treat opioid and alcohol addiction [59].

Bacterial infection is a major stumbling block in the treatment of wounds, as it promotes the development of exudate and slows the healing cycle. In order to distribute teicoplanin, which is a glycopeptide antibiotic that is employed for cutaneous wound healing, Xu and co-workers developed a thermogelling dressing system consisting of two triblock copolymers of PLGA-PEG-PLGA featuring varying block lengths. At room temperature, the teicoplanin-loaded thermogel was observed to be a free-flowing sol that solidified into a semi-solid gel at physiological temperature. In order to test the efficiency of the teicoplanin-loaded thermogel formulation, a full-thickness excision wound model in Sprague-Dawley rats was created. The thermogel was found to reduce the inflammatory response, improve the collagen disposition, boost angiogenesis, as well as hasten the closure of the wound and healing in Sprague-Dawley rats, according to gross and histopathologic data. The increased wound healing activity was due to the union of teicoplanin's bioactivity and the acidic composition of the thermogel matrix. The application of the thermogel suppressed inflammatory response, expedited re-epithelization, enhanced collagen production and disposition, and stimulated angiogenesis in in vivo experiments, conse-

quently improving wound healing. As a result, the teicoplanin-incorporated PLGA-PEG-PLGA thermogel is a viable option for full-thickness excision wound healing as a wound dressing [60].

El-Zaafarany and co-workers investigated a duo of thermo-responsive hydrogels and emulsomes which were lipid-based in drug transportation from the nose to the brain. In comparison to simple solutions, the application of nanocarriers for direct delivery from the nose to the brain offers immense potential for increasing brain drug levels. The antiepileptic medication oxcarbazepine was encapsulated in emulsomes and further incorporated into a thermogel made of PLGA-PEG-PLGA. The intranasal emulsomal thermogel instillation at a T_{\max} of 120 minutes yielded the greatest C_{\max} of 3818.8 ng/mL ($p < 0.01$), which was followed by Trileptal® suspension and intranasally administered emulsomes, which yielded C_{\max} values of 2567.6 and 2514.4 ng/mL at T_{\max} values of 45 and 120 minutes, respectively, and ultimately the intranasally administered oxcarbazepine solution yielded the least. The greatest AUC_{0–2880min} was obtained ($p < 0.05$) in the following order: intranasal thermogel, intranasal oxcarbazepine emulsomes, Trileptal® suspension, and intranasal oxcarbazepine solution. Moreover, the MRT in plasma for emulsomes and thermogel preparations was 58.7- and 76.5-fold higher as compared to the intranasal oxcarbazepine solution, respectively. The plasma half-life of the thermogel was reported to be 1.2-fold higher than that of the oxcarbazepine emulsomes, and significantly greater than the OX solution and Trileptal® suspension, at 6.4 and 5.3 times, respectively ($p < 0.05$). The lipophilic character of the emulsomes may facilitate the partitioning of the drug present in the emulsomes into the cell membrane of the nasal epithelium and deeper into the systemic circulation, thereby explaining the lengthy plasma residency of oxcarbazepine when supplied in conjunction with emulsomes. The emulsomal thermogel's substantial absorption of oxcarbazepine, as seen by the AUC_{0–2880min} and lengthy mean residence time in comparison to intranasal oxcarbazepine-solution, could be due

in part to the gel formulation's high viscosity, which increased the time of contact with the nasal mucosa, boosting the penetrability of oxcarbazepine-emulsomes and/or free oxcarbazepine via the nasal mucosa into the systemic circulation. In comparison to the free drug, the pharmacokinetic data showed that the emulsomes encapsulating oxcarbazepine reduced the rate of its elimination, maintained a high amount of the drug in the circulation, together with a greater circulatory time in the animals [61].

Similarly, nasal oxcarbazepine-emulsome delivery led to the greatest C_{\max} of oxcarbazepine in the brain, which was about 3.3-, 22.9-, and 4.8-fold greater as compared to the emulsome-loaded thermogel, intranasal solution, and the marketed preparation of Trileptal® suspension, respectively. On the contrary, the oxcarbazepine-emulsome-loaded thermogel exhibited greater mean residence durations in the brain than the oxcarbazepine-emulsomes, intranasal oxcarbazepine solution, and Trileptal® suspension. Furthermore, oxcarbazepine was found in the brain even 48 hours after intranasal administration of the emulsomal thermogel, potentially resulting in greater seizure control in patients for an extended duration. Despite the fact that intranasal administration of emulsomal thermogel resulted in a reduced C_{\max} in the brain, the MRT data was higher. When opposed to antiepileptic drug therapies that release the medicines quickly, formulations with prolonged brain residence allow for a longer dosage interval, which not only improves compliance by the patient but also reduces the chances of a seizure occurrence following a missed dose. Likewise, prolonged oxcarbazepine formulations were found to have superior tolerability and greater maintenance dosages than rapid action formulations in treating focal epilepsy [61].

Albendazole, a commonly used anthelmintic, is thought to be effective against helminths because of its major metabolite, albendazole sulfoxide. Feng and group effectively synthesised an albendazole sulfoxide-loaded thermo-sensitive hydrogel. When compared to plain albendazole sulfoxide, *in vivo* pharmacokinetics data suggested that albendazole sulfoxide-loaded hydro-

gel was a more preferable candidate for sustained release. An intraperitoneal injection of albendazole sulfoxide solution (30 mg/kg) resulted in a maximal concentration of (131.98 ng/ml) after 2 hours and then a progressive drop over 72 hours, whereas intraperitoneal administration of albendazole sulfoxide-loaded hydrogel resulted in a maximum concentration of 178.09 ng/ml after 120 hours after which there was a steady reduction. Meanwhile, the albendazole sulfoxide-loaded hydrogel had a longer mean residence time ($MRT_{0-\infty}$) (66.892 h) than the albendazole sulfoxide solution (46.931) [62].

Tissue expanders are useful tools for creating additional skin for reconstructive surgery. The use of hydrogel tissue expanders eliminates the need for fluid injections on a regular basis. If there is not an exterior membrane, the cross-linked network of hydrophilic polymer allows for intrinsically regulated swelling. A rat skin animal model was used by Garner et al. to characterise these novel hydrogel expanders *in vivo*. The amount of hydrophobic polyester in the hydrogel was found to minimise swelling velocity to a rate and volume that eliminated the risk of the premature swelling from rupture of the sutured region. Furthermore, enhancing the cross-linking density gave the hydrogel considerable mechanical resilience to permit full post-swelling clearance without breaking or crumbling. Also, the addition of more hydrophobic PLGA is expected to impede the breakdown of the cross-linker, resulting in persistent swelling [63].

The encapsulation of propranolol-loaded liposomes in microspheres constructed with PLGA-PEG-PLGA copolymer was suggested by Guo and group, for topical application so as to achieve prolonged release of the drug in order to lessen the undesirable effects as well as the frequent administration of propranolol in the treatment of infantile hemangioma. Tumour inhibition of subcutaneous infantile hemangioma in nude mice was investigated. The therapy led to an 84% reduction in the volume of the hemangioma by day 35, but the liposomes and propranolol therapy only led in a 44% and 13% reduction in the volume of the hemangioma, respectively. In comparison to the starting hemangioma volume of

25 mm³, the volume of the hemangioma had risen 7.2 times and 4.8 times in the mice that were administered propranolol and in the mice that received the propranolol liposomes, respectively. The gradual decline in the release of propranolol from the microspheres could ultimately produce a lower cytotoxic impact. The extended and continuous release of propranolol from the microspheres, on the other hand, would dramatically slow hemangioma angiogenesis [64].

Li and co-workers synthesised a thermoresponsive PLGA-PEG-PLGA copolymer, and further the safety and efficiency of the PLGA-PEG-PLGA thermogel in preventing peridural fibrosis in an adult rat laminectomy model was assessed. Anatomical inspections and histological investigations were conducted after 30 days following the surgical procedure to assess the thermogel's efficacy in the prevention of epidural fibrosis. Clinical observation revealed that the freedom of nerve roots was unaffected by the expansion of the thermogel during the gelling process, implying that the swelling was minor and the thermogel was sufficiently soft to avoid compression [65].

Huang and co-workers used a rat model of brachial plexus avulsion to determine the therapeutic efficacy of a quercetin incorporated PLGA-PEG-PLGA based hydrogel. Results of the study indicated that the hydrogel with a higher amount of quercetin may be more effective at reducing oxidative stress and inflammation in secondary injury, as well as protecting nerve tissues in the initial phases of nerve damage. The quercetin-loaded hydrogel sustained-release technology was thought to act by suppressing the neuronal autophagy and death through activation of the PI3K/Akt pathway and inhibition of the ERK1/2 pathway, together with lowering oxidative stress and inflammation. An increased number of motor neurons present in the damaged spinal cord were preserved following treatment with hydrogels possessing varying concentrations of quercetin, thereby laying a foundation for further nerve healing. Thus, the results indicate that the quercetin-loaded copolymeric gel had the ability to increase axon intrinsic growth as well as improve peripheral nerve function recovery [66].

For reducing the first burst release, an in situ forming composite of naltrexone was developed by Kamali and co-workers, by utilising PLGA-PEG-PLGA and N-methyl-2-pyrrolidone. The developed formulation (in situ forming composite) was able to reduce the first burst release, according to the C_{\max} data. In addition, the AUC, absolute bioavailability, and range of serum naltrexone concentrations for the in situ forming composite were similar to those for Vivitrol®. The in situ forming composite system was thus found to be biocompatible and an effective formulation for naltrexone continuous release with low initial burst release [67].

Recently Rong et al. produced a delivery system for insulin by incorporating chitosan nanoparticles into a PLGA-PEG-PLGA hydrogel. Subconjunctival administration of the hydrogel decreased the decline in scotopic B-wave amplitude, relieved micro- and ultrastructural abnormalities in the retina, and decreased apoptosis of the retinal cell in diabetic retinopathy rats as compared to the other groups. However, in the ICNPH group, there was a significant decrease in vascular endothelial growth factor as well as glial fibrillary acidic protein expression, together with a substantial rise in the expression of occludin, in comparison to the sham treatment group. These findings proved that subconjunctival injection of ICNPH had a considerable neuroprotective impact on retinas in diabetic retinopathy rats and promoted regulated insulin delivery [68].

A series of PCLA-PEG-PCLA and PLGA-PEG-PLGA mixed hydrogels were produced and studied by Wang et al. A mixed hydrogel was also chosen for the preparation of the Depot-gel-in-Ms-in-Matrix-gel system for the treatment of type 2 diabetes mellitus. PLGA microspheres (Ms) were used to encapsulate exenatide-loaded hydrogels, which were then enclosed in blank hydrogel. Injecting the above prepared formulation resulted in a stable blood glucose concentration in the treated mice as well as well-maintained body weight for a period of 20 days in the pharmacodynamics investigation. The effects of Ms. and Depot-gel-in-Ms-in-Matrix-gel were compared using OGTT on the 20th day after the injection. The blood glucose fluctuations of both

the Depot-gel-in-Ms-in-Matrix-gel and the exenatide solution groups were reduced. The Ms. group, on the other hand, experienced just as much variation as the blank medium solution group. These findings revealed that in the Depot-gel-in-Ms-in-Matrix-gel group, high bioactive exenatide release was maintained, whereas in the Ms. group, it was terminated. Thus, the Depot-gel-in-Ms-in-Matrix-gel was found to be a potential exenatide-loaded long-acting preparation for treating diabetes [69].

Wang and group created a kartogenin-loaded thermoresponsive gel for intra-articular administration in order to bring forth such a carrier for prolonged release of cartilage-protective agent for the possible use of osteoarthritis (OA) treatment. As a kartogenin carrier for intra-articular injection, a PLGA-PEG-PLGA thermogel was formulated. A rabbit OA model was used to determine the *in vivo* effect of the kartogenin thermogel. A knee OA model utilising the ACLT technique was developed to confirm the possibility of employing kartogenin thermogel to treat OA. Histological staining, OARSI score, and synovial fluid measurement of inflammatory cytokines revealed that OA knees that received treatment with kartogenin thermogel had considerably higher cartilage regeneration and decreased inflammatory joints. The *in vivo* findings strongly suggested that kartogenin has anti-arthritic and chondroprotective properties for the treatment of arthritis [70].

In another study, Yan and group synthesised PLGA-PEG-PLGA loaded with simvastatin. A rat bone defect model was also used to illustrate the properties of this composite *in vivo*. In comparison to samples treated with PLGA-PEG-PLGA and control samples, bone deformities injected with simvastatin/PLGA-PEG-PLGA hydrogel demonstrated higher new bone growth. Therefore, this study's findings showed that simvastatin/PLGA-PEG-PLGA may have therapeutic prospective for bone repair [71].

In the work carried out by Liu et al., PLGA-PEG-PLGA solution was combined with a compound of salmon calcitonin (sCT) and oxidised calcium alginate (OCA) in this work. This preparation was then administered to female Sprague-

Dawley rats suffering from osteopenia to create a hydrogel that would provide long-term treatment. The polymer formulation groups received sCT therapy, which resulted in a near-complete repair of the bone structure physiologically as well as biomechanical qualities in the rat femora of Sprague-Dawley due to the sustained and consistent release of sCT. As a result of the prolonged and consistent release of sCT, the capacity for deformation of the bone was dramatically increased. Hydrogels that released sCT partially repaired the femora of MPA-induced osteopenic Sprague-Dawley rats. As a result, the formulated hydrogel containing the incorporated sCT-OCA complex showed a lot of promise for long-term osteopenia treatment [72].

Recently Xu and co-workers created a thermoresponsive PLGA-PEG-PLGA-based hydrogel supported by upconversion hollow microtubes (UCHMs) with great mechanical properties together with a strong upconversion luminescence to monitor noninvasive bone regeneration. The monitoring of the bone deformities mending procedure was realised, which included the degradation of composite hydrogel scaffold material as well as regeneration of the bone in the defect location, owing to the upconversion luminous feature of the composite hydrogel. After 4 weeks, the composite hydrogel scaffolds were entirely destroyed, and following 6 weeks of bone regeneration, the defect site was totally healed. Thus, the hydrogel provides considerable promise during the clinical therapy of bone defects based on bone healing efficiency, real-time monitoring capability, and biological safety [73].

Kartogenin (KGN), a new chondroinductive non-protein small molecule, was introduced in a thermogel composed of PLGA-PEG-PLGA in order to produce a microenvironment of bone marrow mesenchymal stem cells for the regeneration of cartilage. The group which administered the aforementioned formulation had the most cartilage regeneration, and the flaw was completely healed after a period of 3 months. Even after 8 weeks, the group which administered the thermogel was found to have the best ICRS macroscopic score values. The implantation of the thermogel revealed the best histological

repair of the cartilage, most efficient ECM deposition, and greatest mechanical strength, indicating one of the most successful in-vivo cartilage regeneration [74].

Zheng and colleagues created a thermosensitive PLGA-PEG-PLGA-based injectable hydrogel containing baricitinib (Bari-P hydrogel). In vivo results revealed that Bari-P hydrogel therapy inhibits JAK2, STAT3 phosphorylation, suppresses inflammatory cytokine production, and lowers neuronal death. Bari-P hydrogel also prevented neuronal death during the early stages of damage as well as promoted enhanced functional recovery during later stages, according to histopathological and behavioural testing. Therefore, by blocking the JAK2-STAT3 pathway and limiting the expression of inflammatory cytokines during the early phases of damage, Bari-P hydrogel decreased neuronal death and enhanced functional recovery in spinal cord damaged rats [75].

Animal contraception and control of fertility are in high demand in the livestock and pet industries. To achieve long-acting animal contraception, Chen et al. proposed a preparation comprising of an injectable and biodegradable thermogel for the sustained delivery of a hormonal contraceptive, i.e. levonorgestrel. The PLGA-PEG-PLGA micelles generated in water by amphiphilic polymer carriers could act as a repository for hydrophobic levonorgestrel molecules to be dissolved. The utilization of PLGA-PEG-PLGA thermogel increased the release of levonorgestrel following subcutaneous injection in SD rats, according to in vivo pharmacokinetic experiments. As a result, this research found that, injecting a PLGA-PEG-PLGA thermogel was a possible contender for long-term levonorgestrel release, and that it offered an appealing choice for long-term animal contraception and reproductive control due to its ease of fabrication, ease of administration, and low cost. To assess in vivo pharmacokinetics, two levonorgestrel-loaded gel formulations with the same drug dosage (2.5 mg/mL, 0.6 mL and 5 mg/mL, 0.3 mL) were subcutaneously administered into SD rats. The two gel formulations both had a minor initial burst. The C_{\max} of 7.20 ± 0.93 ng/mL was reached in the first

4 hours after injection of the 2.5 mg/mL levonorgestrel-loaded gel formulation, and the C_{\max} of 6.40 ± 1.07 ng/mL was similarly achieved in the first 4 hours following injection of the 5 mg/mL LNG-loaded thermogel system. Following that, for 2.5 and 5 mg/mL levonorgestrel-loaded thermogel systems, respectively, the drug plasma concentration remained stable above the minimal effective plasma concentration of levonorgestrel (0.2 ng/mL) for 2 and 3 weeks, demonstrating that a single administration of levonorgestrel-loaded gel formulation might exert a sustained contraceptive action for several weeks. Although the two gel formulations including levonorgestrel had identical bioavailability due to the same drug dosage, the 2.5 mg/mL levonorgestrel-loaded thermogel had a shorter mean residence time ($MRT_{0..t}$) than the 5 mg/mL gel formulation. The in vivo data was very similar to the in vitro release profiles, with the extended release period due to increased drug loading quantities. The levonorgestrel-loaded PLGA-PEG-PLGA thermogel system appears to be one of the most promising animal contraception solutions in the future, especially given the low cost of raw materials and ease of manufacture and administration [76]. Table 15.3 enlists few of the applications of the copolymeric micelles comprising of PLGA-PEG-PLGA in drug delivery.

6 Conclusion

The application of thermo-responsive copolymers has grown in popularity since the past couple of years, notably in the sector of controlled release. In drug delivery research, they are arguably one of most investigated class of environment-sensitive polymers. At a given temperature, these hydrogels can quickly transform from a low viscosity fluid into a highly viscous gel. The triblock copolymers possess thermo-responsive features wherein the solution state of these polymers undergo conversion to a highly viscous gel form at body temperature. Due to their biodegradability and since they have a high safety profile, PLGA-PEG-PLGA triblock copo-

Table 15.3 Applications PLGA-PEG-PLGA copolymeric micelles in drug delivery

Therapeutic cargo	Disease Condition	Drug delivery system	References
Combretastatin	Cancer	Nano-micelles	[77]
Doxorubicin	Osteosarcoma	Hydrogel scaffold	[78]
Bovine serum albumin		Hydrogel	[79]
Brimonidine	Glaucoma	Layered double hydroxide (LDH) nanoparticle/thermogel	[80]
Amphotericin B	Cryptococcal meningitis	Thermogel	[81]
Voriconazole	Keratomycosis	Thermogel	[82]
Berberine	Hypercholesterolemia	Nanoparticles	[83]
Bupivacaine	Peripheral nerve blockade	Hydrogels	[84]

lymers are appealing materials. Simple compounding, filtration sterilisation, and the usage of water as a solvent are just a few of the benefits. Although these triblock copolymers are excellent prospects for further investigation in the field of medication delivery, there is still a significant need for additional studies before it can be employed in the clinical setting.

Acknowledgments The authors are thankful to MAHE for providing fellowship to Miss. Shirleen Miriam Marques. The authors acknowledge the support of Manipal College of Pharmaceutical Sciences, Manipal Academy of Higher Education, Manipal, Karnataka, India, for providing infrastructural facilities.

Conflict of Interest The authors report no conflicts of interest in this work.

References

- Song Z, Feng R, Sun M, et al. Curcumin-loaded PLGA-PEG-PLGA triblock copolymeric micelles: preparation, pharmacokinetics and distribution in vivo. *J Colloid Interface Sci.* 2011;354(1):116–23.
- Hirani A, Grover A, Lee YW, et al. Triamcinolone acetate nanoparticles incorporated in thermoreversible gels for age-related macular degeneration. *Pharm Dev Technol.* 2016;21(1):61–7.
- Zheng L, Wang L, Qin J, et al. New biodegradable implant material containing hydrogel with growth factors of lyophilized PRF in combination with an nHA/PLGA scaffold. *J Hard Tissue Biol.* 2015;24(1):54–60.
- Babos G, Biró E, Meiczinger M, Feczko T. Dual drug delivery of sorafenib and doxorubicin from PLGA and PEG-PLGA polymeric nanoparticles. *Polymer.* 2018;10(8):895.
- Wilkosz N, Łazarski G, Kovacik L, et al. Molecular insight into drug-loading capacity of PEG-PLGA nanoparticles for itraconazole. *J Phys Chem B.* 2018;122(28):7080–90.
- Yen Y, Yu L, Qian H, et al. In vivo evaluation of cisplatin-loaded PEG-PCL block copolymeric nanoparticles for anticancer drug delivery. *Ann Oncol.* 2019;30:v191.
- Balci B, Top A. PEG and PEG-peptide based doxorubicin delivery systems containing hydrazone bond. *J Polym Res.* 2018;25(4):1–12.
- Crowley ST, Poliskey JA, Baumhover NJ, Rice KG. Efficient expression of stabilized mRNA PEG-peptide polyplexes in liver. *Gene Ther.* 2015;22(12):993–9.
- Zhou N, Zhi Z, Liu D, et al. Acid-responsive and biologically degradable polyphosphazene nanodrugs for efficient drug delivery. *ACS Biomater Sci Eng.* 2020;6(7):4285–93.
- Hou S, Chen S, Dong Y, Gao S, Zhu B, Lu Q. Biodegradable cyclomatrix polyphosphazene nanoparticles: a novel pH-responsive drug self-framed delivery system. *ACS Appl Mater Interfaces.* 2018;10(31):25983–93.
- Yu L, Zhang Z, Zhang H, Ding J. Mixing a sol and a precipitate of block copolymers with different block ratios leads to an injectable hydrogel. *Biomacromolecules.* 2009;10(6):1547–53.
- Khaledi S, Jafari S, Hamidi S, Molavi O, Davaran S. Preparation and characterization of PLGA-PEG-PLGA polymeric nanoparticles for co-delivery of 5-fluorouracil and Chrysin. *J Biomater Sci Polym Ed.* 2020;31(9):1107–26.
- Zahoranova A, Vojtova L, Dusicka E, Michlovska L, Krivankova N, Baudis S. Hybrid hydrogel networks by photocrosslinking of thermoresponsive α , ω -Itaconyl-PLGA-PEG-PLGA micelles in water: influence of the lithium Phenyl-2, 4, 6-Trimethylbenzoylphosphinate photoinitiator. *Macromol Chem Phys.* 2020;221(17):2000165.
- Jeong B, Bae YH, Kim SW. Biodegradable thermosensitive micelles of PEG-PLGA-PEG tri-

- block copolymers. *Colloids Surf B: Biointerfaces*. 1999;16(1-4):185–93.
15. Makadia HK, Siegel SJ. Poly lactic-co-glycolic acid (PLGA) as biodegradable controlled drug delivery carrier. *Polymers*. 2011;3(3):1377–97.
 16. Wang X, Zhang Y, Xue W, Wang H, Qiu X, Liu Z. Thermo-sensitive hydrogel PLGA-PEG-PLGA as a vaccine delivery system for intramuscular immunization. *J Biomater Appl*. 2017;31(6):923–32.
 17. Wang SJ, Zhang ZZ, Jiang D, et al. Thermogel-coated poly (ϵ -caprolactone) composite scaffold for enhanced cartilage tissue engineering. *Polymers*. 2016;8(5):200.
 18. Chen Y, Shi J, Zhang Y, et al. An injectable thermo-sensitive hydrogel loaded with an ancient natural drug colchicine for myocardial repair after infarction. *J Mater Chem B*. 2020;8(5):980–92.
 19. Wang M, Zhan J, Xu L, et al. Synthesis and characterization of PLGA-PEG-PLGA based thermosensitive polyurethane micelles for potential drug delivery. *J Biomater Sci Polym Ed*. 2020;32:613–34.
 20. Zentner GM, Rath R, Shih C, et al. Biodegradable block copolymers for delivery of proteins and water-insoluble drugs. *J Control Release*. 2001;72(1-3):203–15.
 21. Ghahremankhani AA, Dorkoosh F, Dinarvand R. PLGA-PEG-PLGA tri-block copolymers as an in-situ gel forming system for calcitonin delivery. *Polym Bull*. 2007;59(5):637–46.
 22. Michlovská L, Vojtová L, Mravcová L, Hermanová S, Kučerík J, Jančář J. Functionalization conditions of PLGA-PEG-PLGA copolymer with Itaconic anhydride. *Macromol Symp*. 2010;295(1):119–27.
 23. Qiao M, Chen D, Ma X, Liu Y. Injectable biodegradable temperature-responsive PLGA-PEG-PLGA copolymers: synthesis and effect of copolymer composition on the drug release from the copolymer-based hydrogels. *Int J Pharm*. 2005;294(1-2):103–12.
 24. Yu L, Zhang Z, Ding J. Influence of LA and GA sequence in the PLGA block on the properties of thermogelling PLGA-PEG-PLGA block copolymers. *Biomacromolecules*. 2011;12(4):1290–7.
 25. Kitayama T, Hatada K. *NMR spectroscopy of polymers*. Dordrecht, Holland: Springer Science & Business Media; 2013.
 26. Ghahremankhani AA, Dorkoosh F, Dinarvand R. PLGA-PEG-PLGA tri-block copolymers as in situ gel-forming peptide delivery system: effect of formulation properties on peptide release. *Pharm Dev Technol*. 2008;13(1):49–55.
 27. Khodaverdi E, Tekie FSM, Mohajeri SA, Ganji F, Zohuri G, Hadizadeh F. Preparation and investigation of sustained drug delivery systems using an injectable, thermosensitive, in situ forming hydrogel composed of PLGA-PEG-PLGA. *AAPS PharmSciTech*. 2012;13(2):590–600.
 28. Chen S, Pieper R, Webster DC, Singh J. Triblock copolymers: synthesis, characterization, and delivery of a model protein. *Int J Pharm*. 2005;288(2):207–18.
 29. Kowalczyk D, Pitucha M. Application of FTIR method for the assessment of immobilization of active substances in the matrix of biomedical materials. *Materials*. 2019;12(18):2972.
 30. Mohajeri SA, Yaghoubi S, Abdollahi E, et al. In-vivo study of naltrexone hydrochloride release from an in-situ forming PLGA-PEG-PLGA system in the rabbit. *J Drug Deliv Sci Technol*. 2016;36:156–60.
 31. Vojtova L, Michlovska L, Valova K, et al. The effect of the thermosensitive biodegradable PLGA-PEG-PLGA copolymer on the rheological, structural and mechanical properties of thixotropic self-hardening tricalcium phosphate cement. *Int J Mol Sci*. 2019;20(2):391.
 32. Mohammadpour F, Kamali H, Hadizadeh F, et al. The PLGA microspheres synthesized by a thermosensitive hydrogel emulsifier for sustained release of risperidone. *J Pharm Innov*. 2021:1–13.
 33. Zhang Y, Zhang J, Xu W, Xiao G, Ding J, Chen X. Tumor microenvironment-labile polymer–doxorubicin conjugate thermogel combined with docetaxel for in situ synergistic chemotherapy of hepatoma. *Acta Biomater*. 2018;77:63–73.
 34. Nasrollahi P, Khajeh K, Tamjid E, Taleb M, Soleimani M, Nie G. Sustained release of sodium deoxycholate from PLGA-PEG-PLGA thermosensitive polymer. *Artif Cells Nanomed Biotechnol*. 2018;46(sup2):1170–7.
 35. Chen L, Ci T, Yu L, Ding J. Effects of molecular weight and its distribution of PEG block on micellization and thermogellability of PLGA-PEG-PLGA copolymer aqueous solutions. *Macromolecules*. 2015;48(11):3662–71.
 36. Chen L, Ci T, Li T, Yu L, Ding J. Effects of molecular weight distribution of amphiphilic block copolymers on their solubility, micellization, and temperature-induced sol–gel transition in water. *Macromolecules*. 2014;47(17):5895–903.
 37. Khorshid NK, Zhu K, Knudsen KD, Bekhradnia S, Sande SA, Nyström B. Novel structural changes during temperature-induced self-assembling and gelation of PLGA-PEG-PLGA triblock copolymer in aqueous solutions. *Macromol Biosci*. 2016;16(12):1838–52.
 38. Sulaiman TNS, Larasati D, Nugroho AK, Choiri S. Assessment of the effect of PLGA co-polymers and PEG on the formation and characteristics of PLGA-PEG-PLGA co-block polymer using statistical approach. *Adv Pharm Bull*. 2019;9(3):382.
 39. Cespi M, Bonacucina G, Tiboni M, Casettari L, Cambriani A, Fini F, Perinelli DR, Palmieri GF. Insights in the rheological properties of PLGA-PEG-PLGA aqueous dispersions: Structural properties and temperature-dependent behaviour. *Polymer*. 2021;213:123216.
 40. Steinman NY, Haim-Zada M, Goldstein IA, et al. Effect of PLGA block molecular weight on gelling temperature of PLGA-PEG-PLGA thermoresponsive copolymers. *J Polym Sci A Polym Chem*. 2019;57(1):35–9.

41. Tuntland T, Ethell B, Kosaka T, et al. Implementation of pharmacokinetic and pharmacodynamic strategies in early research phases of drug discovery and development at Novartis Institute of Biomedical Research. *Front Pharmacol.* 2014;5:174.
42. Zou H, Banerjee P, Leung SSY, Yan X. Application of pharmacokinetic-pharmacodynamic modeling in drug delivery: development and challenges. *Front Pharmacol.* 2020;11:997.
43. Derendorf H, Lesko LJ, Chaikin P, et al. Pharmacokinetic/pharmacodynamic modeling in drug research and development. *J Clin Pharmacol.* 2000;40(12):1399–418.
44. Ma H, He C, Cheng Y, et al. Localized co-delivery of doxorubicin, cisplatin, and methotrexate by thermosensitive hydrogels for enhanced osteosarcoma treatment. *ACS Appl Mater Interfaces.* 2015;7(49):27040–8.
45. Jiang L, Ding Y, Xue X, et al. Entrapping multifunctional dendritic nanoparticles into a hydrogel for local therapeutic delivery and synergetic immunotherapy. *Nano Res.* 2018;11(11):6062–73.
46. Chen X, Chen J, Li B, et al. PLGA-PEG-PLGA triblock copolymeric micelles as oral drug delivery system: in vitro drug release and in vivo pharmacokinetics assessment. *J Colloid Interface Sci.* 2017;490:542–52.
47. Yang Z, Liu J, Lu Y. Doxorubicin and CD-CUR inclusion complex co-loaded in thermosensitive hydrogel PLGA-PEG-PLGA localized administration for osteosarcoma. *Int J Oncol.* 2020;57(2):433–44.
48. Nagahama K, Kawano D, Oyama N, Takemoto A, Kumano T, Kawakami J. Self-assembling polymer micelle/clay nanodisk/doxorubicin hybrid injectable gels for safe and efficient focal treatment of cancer. *Biomacromolecules.* 2015;16(3):880–9.
49. Cao D, Zhang X, Akabar M, et al. Liposomal doxorubicin loaded PLGA-PEG-PLGA based thermogel for sustained local drug delivery for the treatment of breast cancer. *Artif Cells Nanomed Biotechnol.* 2019;47(1):181–91.
50. Yang X, Chen X, Wang Y, Xu G, Yu L, Ding J. Sustained release of lipophilic gemcitabine from an injectable polymeric hydrogel for synergistically enhancing tumor chemoradiotherapy. *Chem Eng J.* 2020;396:125320.
51. Pan A, Wang Z, Chen B, et al. Localized co-delivery of collagenase and trastuzumab by thermosensitive hydrogels for enhanced antitumor efficacy in human breast xenograft. *Drug Deliv.* 2018;25(1):1495–503.
52. Jin X, Fu Q, Gu Z, Zhang Z, Lv H. Injectable coriagin/low molecular weight chitosan/PLGA-PEG-PLGA thermosensitive hydrogels for localized cancer therapy and promoting drug infiltration by modulation of tumor microenvironment. *Int J Pharm.* 2020;589:119772.
53. Zhang J, Li Y, Gao W, Repka MA, Wang Y, Chen M. Andrographolide-loaded PLGA-PEG-PLGA micelles to improve its bioavailability and anticancer efficacy. *Expert Opin Drug Deliv.* 2014;11(9):1367–80.
54. Ci T, Chen L, Yu L, Ding J. Tumor regression achieved by encapsulating a moderately soluble drug into a polymeric thermogel. *Sci Rep.* 2014;4(1):1–13.
55. Liu D, Wu Q, Zhu Y, et al. Co-delivery of metformin and levofloxacin hydrochloride using biodegradable thermosensitive hydrogel for the treatment of corneal neovascularization. *Drug Deliv.* 2019;26(1):522–31.
56. Chan PS, Li Q, Zhang B, To KK, Leung SS. In vivo biocompatibility and efficacy of dexamethasone-loaded PLGA-PEG-PLGA thermogel in an alkali-burn induced corneal neovascularization disease model. *Eur J Pharm Biopharm.* 2020;155:190–8.
57. Zhang L, Shen W, Luan J, et al. Sustained intravitreal delivery of dexamethasone using an injectable and biodegradable thermogel. *Acta Biomater.* 2015;23:271–81.
58. Xie B, Jin L, Luo Z, et al. An injectable thermosensitive polymeric hydrogel for sustained release of Avastin® to treat posterior segment disease. *Int J Pharm.* 2015;490(1-2):375–83.
59. Kamali H, Khodaverdi E, Hadizadeh F, Mohajeri SA. In-vitro, ex-vivo, and in-vivo evaluation of buprenorphine HCl release from an in situ forming gel of PLGA-PEG-PLGA using N-methyl-2-pyrrolidone as solvent. *Mater Sci Eng C.* 2019;96:561–75.
60. Xu WK, Tang JY, Yuan Z, et al. Accelerated cutaneous wound healing using an injectable teicoplanin-loaded PLGA-PEG-PLGA thermogel dressing. *Chin J Polym Sci.* 2019;37(6):548–59.
61. El-Zaafarany GM, Soliman ME, Mansour S, et al. A tailored thermosensitive PLGA-PEG-PLGA/emulsomes composite for enhanced oxcarbazepine brain delivery via the nasal route. *Pharmaceutics.* 2018;10(4):217.
62. Feng Y, Wang F, Zhang XW, Bhutani H, Ye B. Characterizations and bioactivities of abendazole sulfoxide-loaded thermo-sensitive hydrogel. *Parasitol Res.* 2017;116(3):921–8.
63. Garner J, Davidson D, Eckert GJ, Barco CT, Park H, Park K. Reshapable polymeric hydrogel for controlled soft-tissue expansion: in vitro and in vivo evaluation. *J Control Release.* 2017;262:201–11.
64. Guo X, Zhu X, Liu D, Gong Y, Sun J, Dong C. Continuous delivery of propranolol from liposomes-in-microspheres significantly inhibits infantile hemangioma growth. *Int J Nanomedicine.* 2017;12:6923.
65. Li X, Chen L, Lin H, et al. Efficacy of poly (D, L-lactic acid-co-glycolic acid)-poly (ethylene glycol)-poly (D, L-lactic acid-co-glycolic acid) thermogel as a barrier to prevent spinal epidural fibrosis in a postlaminectomy rat model. *Clin Spine Surg.* 2017;30(3):E283–90.
66. Huang C, Fu C, Qi ZP, et al. Localised delivery of quercetin by thermo-sensitive PLGA-PEG-PLGA hydrogels for the treatment of brachial plexus avulsion. *Artif Cells Nanomed Biotechnol.* 2020;48(1):1010–21.

67. Kamali H, Khodaverdi E, Hadizadeh F, et al. Comparison of in-situ forming composite using PLGA-PEG-PLGA with in-situ forming implant using PLGA: in-vitro, ex-vivo, and in-vivo evaluation of naltrexone release. *J Drug Deliv Sci Technol.* 2019;50:188–200.
68. Rong X, Ji Y, Zhu X, et al. Neuroprotective effect of insulin-loaded chitosan nanoparticles/PLGA-PEG-PLGA hydrogel on diabetic retinopathy in rats. *Int J Nanomedicine.* 2019;14:45.
69. Wang P, Zhuo X, Chu W, Tang X. Exenatide-loaded microsphere/thermosensitive hydrogel long-acting delivery system with high drug bioactivity. *Int J Pharm.* 2017;528(1-2):62–75.
70. Wang SJ, Qin JZ, Zhang TE, Xia C. Intra-articular injection of kartogenin-incorporated thermogel enhancing osteoarthritis treatment. *Front Chem.* 2019;7:677.
71. Yan Q, Xiao LQ, Tan L, et al. Controlled release of simvastatin-loaded thermo-sensitive PLGA-PEG-PLGA hydrogel for bone tissue regeneration: in vitro and in vivo characteristics. *J Biomed Mater Res A.* 2015;103(11):3580–9.
72. Liu Y, Chen X, Li S, et al. Calcitonin-loaded thermosensitive hydrogel for long-term antiosteopenia therapy. *ACS Appl Mater Interfaces.* 2017;9(28):23428–40.
73. Xu J, Feng Y, Wu Y, et al. Noninvasive monitoring of bone regeneration using NaYF₄: Yb³⁺, Er³⁺ upconversion hollow microtubes supporting PLGA-PEG-PLGA hydrogel. *React Funct Polym.* 2019;143:104333.
74. Li X, Ding J, Zhang Z, et al. Kartogenin-incorporated thermogel supports stem cells for significant cartilage regeneration. *ACS Appl Mater Interfaces.* 2016;8(8):5148–59.
75. Zheng XQ, Huang JF, Lin JL, et al. Controlled release of baricitinib from a thermos-responsive hydrogel system inhibits inflammation by suppressing JAK2/STAT3 pathway in acute spinal cord injury. *Colloids Surf B Biointerfaces.* 2021;199:111532.
76. Chen X, Li F, Feng L, Yu L, Ding J. An injectable Thermogel containing levonorgestrel for long-acting contraception and fertility control of animals. *J Biomed Nanotech.* 2017;13(11):1357–68.
77. Atanasov G, Kolev IN, Petrov O, Apostolova MD. Synthesis of PLGA-PEG-PLGA polymer Nanomicelles—carriers of Combretastatin-like antitumor agent 16Z. In: *Nanoscience and nanotechnology in security and protection against CBRN threats.* Dordrecht: Springer; 2020. p. 449–58.
78. Yang Z, Yu S, Li D, et al. The effect of PLGA-based hydrogel scaffold for improving the drug maximum-tolerated dose for in situ osteosarcoma treatment. *Colloids Surf B Biointerfaces.* 2018;172:387–94.
79. Patel N, Ji N, Wang Y, Li X, Langley N, Tan C. Subcutaneous delivery of albumin: impact of thermosensitive hydrogels. *AAPS PharmSciTech.* 2021;22(3):1–8.
80. Sun J, Lei Y, Dai Z, et al. Sustained release of brimonidine from a new composite drug delivery system for treatment of glaucoma. *ACS Appl Mater Interfaces.* 2017;9(9):7990–9.
81. Lin W, Xu T, Wang Z, Chen J. Sustained intrathecal delivery of amphotericin B using an injectable and biodegradable thermogel. *Drug Deliv.* 2021;28(1):499–509.
82. Mora-Pereira M, Abarca EM, Duran S, et al. Sustained-release voriconazole-thermogel for subconjunctival injection in horses: ocular toxicity and in-vivo studies. *BMC Vet Res.* 2020;16:1–14.
83. Ochin CC, Garelnabi M. Berberine encapsulated PLGA-PEG nanoparticles modulate PCSK-9 in HepG2 cells. *Cardiovasc Haematol Disord Drug Targets (Formerly Current Drug Targets-Cardiovascular & Hematological Disorders).* 2018;18(1):61–70.
84. Ning C, Guo Y, Yan L, et al. On-demand prolongation of peripheral nerve blockade through bupivacaine-loaded hydrogels with suitable residence periods. *ACS Biomater Sci Eng.* 2018;5(2):696–709.

PKPD in Diseased Conditions for NPDDS

The interface of bio-nano science and cancer medicine is an area experiencing much progress; thus, researchers explore new directions for the field of cancer nanomedicine. An essential consideration of how imaging nanoparticulate systems are cleared from normal organs/tissues but preserved in tumors is essential for their upcoming clinical applications in early diagnosis of cancer and treatment. Synergetic addition of effectual renal clearance and improved permeability and retention effect proposes a talented trail to plan low-toxicity as well as high-contrast-enhancement imaging nanoparticulate systems that can convene with the medical translational prerequisites of regulatory agencies. Moreover, pulmonary delivery of nanoparticulate systems by inhalation presents an advantageous alternative to oral and intravenous routes of administration, which avoids enzymatic degradation in the gastrointestinal tract and hepatic first pass metabolism and also limits off-target adverse side effects upon healthy tissues. Optimization of physicochemical characteristics, preferred drug, and inhalation design can significantly manipulate the pharmacokinetic performance of inhaled nanoparticulate systems and their payloads. In addition, contrast agents targeted to molecular markers of ailment are presently being urbanized with the aim of recognizing disease early and assessing effectiveness of therapy with noninvasive imaging modalities like magnetic resonance imaging.



Bridging Bio-Nanoscience and Cancer Nanomedicine

16

Alka, Raquibun Nisha, Priya Singh, Ravi Raj Pal, Neelu Singh, Nidhi Mishra, and Shubhini A. Saraf

Contents

1	Introduction	296
2	How Nanoscience Helps Cure Cancer	298
3	Nanoscale Drug Delivery Systems	300
4	Tumor Targeting	306
5	Marketed Formulations and Patents	308
6	Next Generation of Cancer Nanomedicine and Prospects	309
	References	310

Abstract

Cancer is a deadly disease that has claimed the lives of millions of people worldwide. It uses the abilities of nanoscience and nanotechnology to improve patient outcomes. Nanotechnology can improve cancer treatments by providing monitoring tools and technological platforms that may be employed in terms of detection, diagnostic moieties with the programmable release, bioanalysis, and imaging. Nanoparticles have the inherent potential to overcome a variety of obstacles in cancer treatment. The “enhanced permeability

and retention (EPR) effect,” a particular feature of tumor cells, is used to provide targeted administration of anticancer medicines. As a result, nanotechnology-based drug delivery devices have been designed to improve the penetration and selective drug retention in tumor tissues, reducing the adverse effects of standard treatment. The chapter also discusses several nanotechnology platforms for cancer treatments as well as patents. Currently, various diagnostics and therapeutic agents that are enabled by nanotechnology are being clinically studied, and several have already received FDA approval and are available on the market globally. This communication will offer an overview of the current state of nanomedicine research and industrial manufacturing, as well as prospective customized medicine potential in the coming years.

Alka · R. Nisha · P. Singh · R. R. Pal · N. Singh · N. Mishra · S. A. Saraf (✉)
Department of Pharmaceutical Sciences, Babasaheb
Bhimrao Ambedkar University, Vidya Vihar,
Raebareli Road, Lucknow, Uttar Pradesh, India

Keywords

Cancer · Nanoscience · Nanotechnology platforms · EPR effect · Drug delivery · Approved products and in clinical development · Patents

1 Introduction

Our ever-improving capacity to design nanomaterials with customized characteristics has laid a solid platform for use in various biological contexts. Inorganic (e.g., gold, silver, iron oxide, or silica) and organic (e.g., lipid-based, cell-membrane generated, and layer-by-layer constructed) nanoparticles have been developed to date. These breakthroughs have sparked a surge of curiosity in the field of nanomedicine, which aims to enhance patient outcomes by utilizing the potential of nanoscience and nanotechnology [1].

Cancer nanomedicine is the use of nanotechnology in cancer treatment, and though the subject has made significant progress lately, more can be done [2, 3]. Cancer is a disease that is extremely diverse and varied. Based on the severity of the disease and the patient's overall clinical condition, the treatment method is either curative or noncurative. Both imaging and direct viewing procedures can be used to determine the amount of disease ("staging") (e.g., endoscopy). The goal of curative ("radical") surgery, or surgery coupled with radiation and chemotherapy, is to remove the entire tumor. Several primary tumors (tumors at the site of cancer development) can be cured with these well-established treatment methods, but the ones that become malignant cause the majority of cancer-related fatalities. When a cure is not possible, the focus switches to enhancing survival and quality of life with targeted chemotherapeutics (e.g., antibodies and molecular targeted agents) [4].

Consequently, metastatic diseases remain an appealing target for the research of novel drugs aimed at improving patient survival. Several nanomedicines for cancer have been developed to date, but only a few dozen have received clinical approval [5]. The significant advantage of

these is reducing adverse effects such as nausea, anemia, hair loss, and cardiotoxicity. Although some latest clinical trials have shown promise, the longevity benefit offered by nanomedicines over standard therapy is often modest. In a particular study, no difference in survival was found in a meta-analysis comparing liposomal with non-liposomal chemotherapy (2589 patients, 14 clinical trials in total). These findings contrast sharply with preclinical mouse studies, which showed a considerable increase in survival [6]. Probably, it is the better quality of life offered via fewer side effects that need to be documented along with the advantages of targeted delivery.

1.1 Nanoparticles in Cancer Therapy

Nanoparticles (NPs) have recently been considered as potential medication carriers. Drug pharmacokinetic properties are altered by nanocarriers, which improve their efficacy while reducing adverse effects [7, 8]. Various components, like metal particles, polymers, lipids, etc., are used to construct NPs employed in drug delivery. NPs of varying sizes and shapes can be made depending on the structure of these components [9]. Nanocarrier-based drug delivery systems (DDS) have made their way into the global pharmaceutical product pipeline. Upcoming research should focus on the diverse functionalities of NPs, such as drug targeting with concomitant imaging [10]. Protein-, lipid-, and polymer-based materials are the most used biocompatible nanocarriers in clinical studies. Four reviews are featured in this category [11].

Gou et al. provided a complete overview of protein-based nano-preparations for cancer theranostics. They detailed albumin, gelatin, ferritin, and transferrin nanocarriers. Imaging modalities such as computed tomography, near-IR fluorescence, positron emission tomography, magnetic resonance imaging, and photoacoustic imaging were also discussed. The authors also looked at issues including repeatability, colloidal stability, drug-loading, and drug accumulation in the reticuloendothelial system [12].

Rezvantab et al. studied the potential of PLGA-based NPs in cancer therapy in a systematic way. The review paper outlines the characteristics of PLGA NPs as well as the techniques to produce them. A focus on passive and active tumor targeting, as well as combination therapy, is also present. They stated that investigators must evaluate the size, shape, amount of drug in formulation, biodegradability, and content uniformity whenever considering clinical feasibility. The authors also suggested that NP pharmacokinetics and pharmacodynamics be better understood, as well as the utilization of extrinsic stimuli in the case of combination therapies [13].

Raut et al. present a detailed study of drug delivery methods based on recombinant high-density lipoprotein (rHDL) in cancer therapy. rHDLNPs have the intrinsic ability to overcome various biological hurdles to cancer therapy. This platform is desirable for chemotherapeutic drugs that incur off-target effects due to its tiny size, endosomal escape, inherent targeting ability, and safety in humans and other animals [14].

In somewhat acidic environments, the size of Mu and Yan nanoparticles in cancer therapeutics altered substantially, but in neutral conditions, it remained stable. In this area, Qi et al. developed PEG-DiHyd-PLA triblock copolymers containing a hydrazone bond. These copolymers could self-assemble into micelles with confined size distribution and uniform sizes smaller than 100 nm. The prototype drug doxorubicin was efficiently loaded into the micelles in acidic conditions and demonstrated complete and prompt drug release (pH 5.0). The prepared doxorubicin NPs displayed a significant antitumor activity, destroying cancer cells while sparing normal cells [15].

1.2 Advantages

Nanotechnology is investigating several factors for cancer treatment, including the following [2]:

- (a) Increasing drug delivery efficiency while lowering side effects and, as a result, toxicity.
- (b) Active components are targeted specifically in cells and tissues.

- (c) Increasing the stability, solubility, half-life, and tumor aggregation of pharmacologically active medicines.
- (d) Creating drug release in response to stimuli.
- (e) Increasing the number of medications encapsulated or coupled to biomacromolecules like proteins and mRNA.
- (f) To overcome constraints such as drug resistance, treatment efficiency can be improved by administering numerous active agents to a specifically targeted spot.
- (g) Breaking beyond biological barriers.
- (h) Improving the sensitivity of tumorous site diagnosis and imaging.
- (i) Linking anticancer active ingredients to imaging molecules to provide a real-time assessment of the medications' in vivo efficacy.
- (j) Creating novel routes to produce synthetic vaccinations.
- (k) Using scaled-down medical gadgets to improve cancer diagnosis and imaging.

1.3 Disadvantages [16]

- (a) May trigger the immune response
- (b) Toxicity
- (c) Complex synthetic route
- (d) Occasional cytotoxicity (need of surface modifications)

1.4 Comparative Study with Standard Treatment

The main tools of traditional cancer treatment are surgery, chemotherapy, radiation, photodynamic, hormone, and biologic therapy:

- (a) Surgery is one of the therapeutic choices. That is, the malignant component must be removed. However, the disadvantage is that if the organ is lost, cancer may reappear. Furthermore, not all cancers are appropriate for surgery [17].
- (b) Radiation therapy is the second option. Radiation of a specified frequency band and strength is used to burn malignant cells. The disadvantage of this procedure is that even

healthy cells are injured, and the damage/burning is uneven, resulting in the burnt section being dead and non-functional [18].

- (c) Chemotherapy is the third option. Cancerous cells are eliminated by medications that are poisonous to cells, or by preventing cancerous cells from obtaining nutrients necessary for cell division, or by interrupting the cell division mechanism. In most cases, a combination of medications is administered to address all three components of cancer treatment. The main stumbling block is the possibility that the treatment will destroy normal blood cells [19].
- (d) Photodynamic therapy (PDT) is another method for treating localized cancer that is still in development. The attraction of “hematoporphyrin” molecules is exploited by PDT. After the sensitizer is given, the tumor area is illuminated with a specific frequency of light, either from the outside or with inserted fiber optics. Light energy initiates the chemical reaction, which generates oxygen and causes physical damage to kill cancer cells [20].
- (e) Hormonal therapy has proven to be effective in treating cancers that are “hormone-dependent.” Drugs regulate hormones that are produced inside. Drugs attach to receptors present on the surface of tumor cells, preventing their growth. In general, such treatments must be administered for a long time after surgery, on a specialist’s prescription, to prevent metastatic disease [21].
- (f) “Biologic therapy,” the newest technique in conventional cancer therapy, is defined as “cancer treatment that primarily relies on the activity of natural host defense systems or the introduction of natural mammalian chemicals to achieve antitumor effects.” Biologic cancer treatments are very recent and are referred to as “biotherapy.” They were developed in the late 1800s based on observations and testing. Biotherapy is based on the idea that cancer cells are immunologically “distinct” from normal cells and that the immune system can be manipulated to eliminate cancer cells. Hair loss, lack of appetite, nutritional concerns, peripheral

neuropathy, diarrhea, and skin damage are all common side effects of this therapy [22].

- (g) Nanotechnology has proven to be a successful cancer treatment that is far safer than traditional chemotherapy. Nanotechnology has the potential to improve cancer research and clinical approaches to cancer therapy for various reasons:
- (h) Most biological activities, including those that contribute to cancer, occur at the nanoscale. The ability of nanoscale devices to quickly explore the interior of a living cell gives substantial advantages for cancer researchers on both the primary and clinical research fronts [23].
- (i) The ability to interact with nucleic acids and proteins at the molecular level simultaneously will aid researchers to comprehend better the intricate regulatory systems that monitor the cell activity in their normal state and malignant cell transformation [24].

2 How Nanoscience Helps Cure Cancer

Nanotechnology is a relatively new discipline with the potential to revolutionize cancer detection, treatment, and prevention. It offers the possibility to enhance the accuracy of medicines with a single, highly specialized task, which is detecting and destroying cancer cells or tumors. Drug delivery systems are more likely to remain in the circulation for longer periods, accumulate at pathological areas with disrupted and leaky vasculature owing to their enhanced permeability and retention, and facilitate targeted delivery in areas with limited access to specific drugs and drug carriers [25]. It was a watershed moment in the anticancer drug industry when Maeda and his team discovered the enhanced permeability and retention effect in the 1980s [26, 27]. Because of the unique tumor vasculature and potential to achieve extended plasma or local half-lives, nanoparticles and macromolecular drugs can extravasate more selectively at tumor tissues than in normal tissues [27].

A promising approach to distributing a wide variety of molecules to specific locations in the body is to combine therapeutic drugs with nanoparticles that have unique physical, chemical, and biological characteristics and to design their routes for appropriate targeting [25]. Since this targeted approach increases the concentration of the therapeutic drugs in cells/tissues, low doses may be used, precisely when the therapeutic action and toxic effects of the agent conflict. In biological systems, increasing therapeutic drug concentration in the target site enhances the therapeutic index by increasing efficacy and tolerance.

2.1 Cancer Theranostics, Cure, and Prevention

The term “theranostics” combines the words “therapeutics” and “diagnostics” to describe a therapeutic approach that combines a nanoscale cancer diagnostic imaging examination with targeted therapy relying on the imaging results; in other words, a leap toward personalized medicine. Theranostic nanomedicine is a comprehensive nanotherapeutic system that utilizes nanotechnology and its applications to diagnose, offer targeted therapy, track the delivery system in real time, and control the release mechanism and response of the action before, during, and after the drug delivery to the target site. Nanotechnology applications for cancer diagnosis and therapy are now possible, providing a slew of new tools and alternatives, including early detection and enhanced imaging to improved, efficient, effective, and customized treatments.

2.2 EPR Mechanism in Cancer

The EPR effect is divided into two parts: increased permeation and increased retention. As solid tumor cells attain a diameter of 150–200 μm , they develop their vasculature system and begin to rely on it for nutrition, blood, and oxygen [28]. This is due to hypoxic tumor cells secreting vascular endothelial growth factors, which cause angiogenesis [29]. The basement membrane of tumor blood vessels is aberrant,

and the vascular structure is unusual, with a diverse spatial distribution, disproportionately wide interendothelial junctions, and transendothelial channels [30]. Owing to its aberrant form and high fenestrations that vary from 200 to 2000 nm, tumor vasculature turns leaky and deeply permeable in particular tumor regions, culminating in augmented permeation [29, 31]. To keep interstitial fluids balanced, extra fluid is continuously pumped into the lymphatic system of natural tissues [30].

Molecules smaller than 4 nm cannot stay in the tumor tissue long enough to accumulate. Meanwhile, high-hydrodynamic radii nanoparticles and macromolecules accumulate in the tumor interstitium [29]. Furthermore, tumor tissue can hold macromolecules and nanoparticles due to slow venous return and weak lymphatic drainage. This improved retention effect, like higher permeability, is time-dependent; for an anticancer drug to reach an optimal concentration in tumor tissue for a prolonged time, it takes almost 6 hours. Factors like protein binding and nanoparticle aggregation might also influence the EPR effect due to the larger size of the nanoscale system due to complex formation [32]. Figure 16.1 depicts the notion of the EPR effect in the tumor.

2.3 Tools for Targeting the Theranostic Agents in Cancer

The kidneys quickly excrete the drug molecules with a diameter of less than 10 nm. These molecules also accumulate in normal tissue due to their smaller size, causing toxicity and resulting in the unexpected death of a cancer patient. The EPR effect, which is a common way to deliver a therapeutic molecule, has been linked to cancer. Only by developing a suitable carrier mechanism and avoiding drug distribution to normal tissues can various therapeutic and diagnostic agents be administered to tumorous tissue [33].

Chemotherapeutic drugs and carrier complexes, ranging between 10 and 200 nm, extravasate inside the tumor tissues' leaky vasculature. Furthermore, due to an inadequate lymphatic

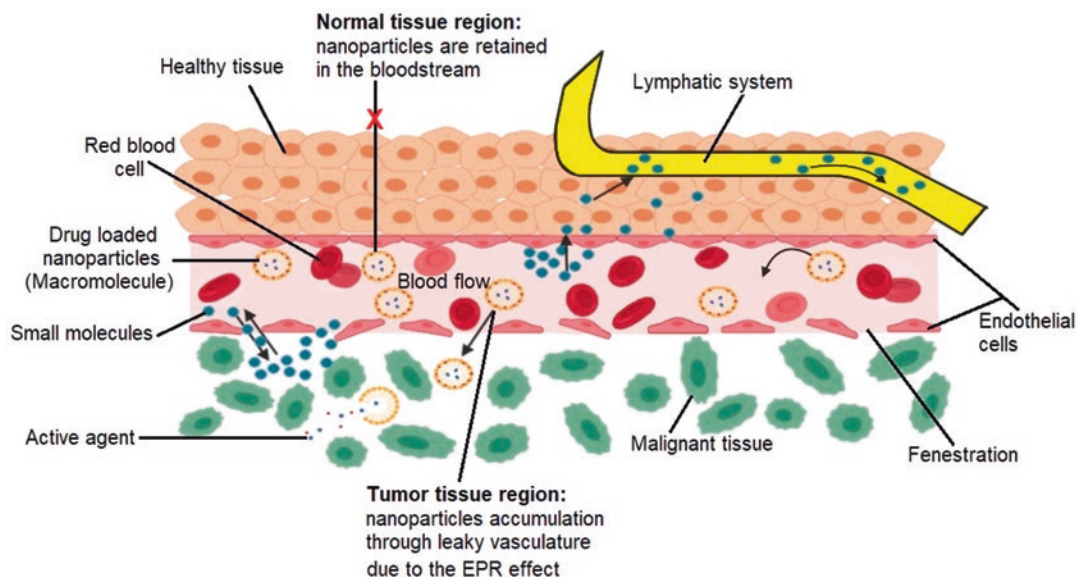


Fig. 16.1 A schematic illustration of the EPR effect (passive targeting) of drug-loaded nanoparticles as delivery of drug carriers in malignant tissue and the accumulation of

nanoparticles in the tumor vasculature with fenestrations ranging from 200 to 2000 nm, leading to increased permeation

drainage system, they are retained in tumor tissues for an extended time [25].

Cancer must be diagnosed early in its growth to be fully eradicated from the body. Nanoparticles have a wide surface area and can be coated or conjugated with numerous molecules for a variety of detection systems. They can also be employed as a delivery vehicle for anticancer drugs and other biomolecules to tumor cells. Various noninvasive imaging modalities, including single-photon emission computed tomography (SPECT) [34], computed tomography (CT) [34, 35], positron emission tomography (PET) [34, 35], magnetic resonance imaging (MRI) [34, 36, 37], and optical [34, 38] or fluorescence imaging [39] are used to diagnose cancer.

Nanotechnology provides several drug delivery methods that are especially useful. In nanomedicine, the advantage of using various materials while formulating the delivery system can help to make formulations with required release characteristics, minimal toxicity, and maximum protection of the therapeutic agent within the dosage form [40]. A priority of developing cancer nanomaterials includes the following [41]: (i) multifunctionality, (ii) increasing power and multivalence, (iii) therapeutic potential, (iv) increased target selectivity,

(v) controlled synthesis, (vi) controlled release and kinetics, (vii) loss of immunogenicity, (viii) altered pharmacokinetics, (ix) novel properties and interactions, and (x) improved physical stability. On the surface or hollow cores of such nanoparticles, diagnostic agents like superparamagnetic or paramagnetic metals or radionuclides can be inserted. Employing semiconductor quantum dots with unique electronic and optical attributes properties, a novel class of nanoparticle probes for cellular, molecular, and in vivo diagnostics, has been developed. Nanotechnology can revolutionize cancer diagnostics by developing more sensitive and precise fluorescence markers and diagnostic imaging methods [42]. As seen in Table 16.1, many therapeutic agents can be targeted via the EPR effect, and see description in various nanotechnology platforms for the cancer therapeutics in Sect. 3.1.

3 Nanoscale Drug Delivery Systems

Conventional chemotherapy of cancer is limited to surgery, radiation, chemotherapy, normal tissue damage, toxic effects, insufficiency of drug availability, and drug resistance, which failed to

Table 16.1 List of therapeutic molecules approved for cancer therapy

Nanotechnology	Delivery system	Therapeutic agents	Disease	Function	Ref.
Carbon nanotubes (CNTs)	Naringenin functionalized multi-walled CNTs	Naringenin	Lung cancer	CNTs exhibit high surface area, high aspect ratio, very less density, favorable electrical properties, and chemical stability. Functionalization of naringenin-loaded CNTs via non-covalent interactions augmented the anticancer activity in malignant lung carcinoma cells (A549)	[83]
	Glycopolymers-anchored multi-walled carbon nanotubes (GMCNTs)	Doxorubicin (DOX)	Breast carcinoma	GMCNTs have a needle-shaped structure, which gives them an advantage in cell uptake. It also improves DOX solubility and dispersibility, making it easier to target both the glucose transporter protein (GLUT5) and the folic acid receptors (FR)	[84]
	Multi-walled carbon nanotubes (MCNTs)	Doxorubicin	Breast carcinoma	Doxorubicin-loaded MCNTs were functionalized with tocopheryl succinate and hyaluronic acid, which enhanced cellular uptake and anticancer activity by targeting CD44 receptors	[85]
Dendrimers	Polyamidoamine (PAMAM) dendrimer	Curcumin and Bcl-2 siRNA	Cervical cancer	PAMAM dendrimers carrying siRNA are stable enough in the systemic circulation to survive before extravasation through cancer's vascular endothelium to enter the cancer cells. The combined effect of curcumin and Bcl-2 siRNA on cervical cancer cells results in maximum apoptotic induction	[86]
	One-step PAMAM dendrimers (OS-PAMAM)	Methotrexate (MTX)	Breast carcinoma	OS-PAMAM dendrimers have unique properties, including internal cavity structure, tunable size, and monodispersity, and presented different functional groups for chemical modification. OSPAMAM-MTX was found to be cell targeting and had better cytotoxic properties against breast carcinoma than plain MTX	[87]
	Hybrid nanoparticles	Caffeic acid- and siRNA-loaded lipid-polymer hybrid nanoparticles (CA:SIRNA:LPNPs)	Breast carcinoma	The application of a magnetic field improves (CA:SIRNA:LPNPs) cellular internalization, with siRNA and NP accumulation for apoptosis induction in breast carcinoma cells	[62]
Liposomes	Folate-decorated carboplatin and paclitaxel loaded lipid-polymer hybrid nanoparticles (FA:CBP:PTX:LPNPs)	Carboplatin and paclitaxel	Cervical cancer	FA:CBP:PTX:LPNPs integrate the benefits of liposomes and polymers into a single platform, making them the ideal system for combinatorial delivery. pH-responsive drug release, greater uptake, noticeable cytotoxicity, better tumor distribution, and enhanced antitumor activity	[54]
	Transferrin-decorated docetaxel liposomes (LIP-DTX-TF)	Docetaxel (DTX)	Prostate cancer	LIP-DTX-TF introduced prolonged release and cellular internalization in tumor cells resulting in greater anticancer potential against prostate cancer	[88]
	pH-sensitive liposomes	SIRT1 shRNA and docetaxel	Breast carcinoma	pH-sensitive liposomes induce apoptosis in breast carcinoma cells by combining liposomes with pH-sensitive cytosolic tumors	[89]

(continued)

Table 16.1 (continued)

Nanotechnology	Delivery system	Therapeutic agents	Disease	Function	Ref.
Micelles	Curcumin conjugated pH-sensitive micelles	Curcumin	Breast adenocarcinoma	pH-sensitive micelles are stable under physiological conditions, but they rapidly become activated to release bioactive agents under acidic conditions to enhanced cellular uptake to directly target breast adenocarcinoma	[90]
Nanoshells	Gold nanoshells (GNs)	Silica nanorattles	Photothermal cancer, hepatocellular carcinoma	Specialty modifications of GNs with positive silica nanorattles, which have introduced a synergistic effect of GNs with photothermal treatment and chemotherapy, which lead to a specific delivery to carcinoma cells	[91]
	Gold nanoshells (GNs)	Platinum(II)	Colorectal cancer	The photothermal effect of GNs is remarkable, allowing for synergistic chemo-photothermal therapy. Light exposure to GNs leads to a further cooling of the gold tray through the transmission of heat to the local environment between electrons that are oscillated and the lattice electron. GNs are an extraordinary mediator for photothermal treatment and lead to excellent anticancer potential in colorectal carcinoma	[92]
Polymeric micelles	Resveratrol-loaded polymeric micelles (Rsv-PMCs)	Resveratrol	Breast carcinoma	Polymeric micelles having amphiphilic block copolymers consist of hydrophobic and hydrophilic segments. Rsv-PMCs successfully internalized in breast carcinoma cells	[50]
Polymeric nanoparticles (PNPs)	PNP delivery of combination therapy	Cisplatin and paclitaxel	Ovarian cancer	PNPs facilitate the highest drug loading and sustained release, decreased tumor growth, enhanced survival time, highest accumulation at the tumor site, and reduced renal toxicity in contrast to free cisplatin and paclitaxel against ovarian cancer	[93]
	Poly(sarcosine), poly(ethylene glycol), and poly(lactic-co-glycolic acid) polymeric nanoparticles (PSar-PLGA-PEG)	Docetaxel	Glioma brain cancer, colorectal cancer, cervical cancer, gastric carcinoma	PSar-PLGA-PEG enhanced bioavailability and reduced long-circulating plasma protein adsorption to the material surface. PSar and PEG chains are responsible for steric repulsion, the reduction of conformational entropy, and the formation of hydrated loops improved DOX half-life by increasing tissue distribution, resulting in increased anticancer activity	[52]
	pH-responsive charge switchable PEGylated e-poly-L-lysine polymeric nanoparticles (PEG-EPLYS-DOX)	Doxorubicin	Breast carcinoma	To harvest PEG-EPLYS-DOX polymer-drug conjugate, an acid-cleavable imine bond was used to insert DOX into the polymer side chain, and the amino groups in the EPLYS section were amidated to protect the positively charged NPs for longer blood circulation. NPs accumulated in tumor tissue after intravenous injection, enhancing tumor cell internalization and resulting in excellent breast cancer activity	[94]

Quantum dots	Biofunctionalized graphene quantum dots (GQD)	Graphene	Detection of small cell lung cancer	GQD has emerged as an energy donor owing to its remarkable optical and electronic properties. GQD introduced a new window for zero-dimensional fluorescent materials for several biomedical applications, like gene delivery, bioimaging, biosensing, and drug delivery and diagnosis of carcinomas	[95]
	Aqueous colloidal folic acid quantum dots (FA-QD)	Folic acid	Detection of folate receptors in breast cancer	FA-QD is unique fluorescent probe, with resistance to photobleaching, high brilliance, and a versatile/active surface for bioconjugation. FA tracking analyzed in living cells with QD for the understanding of breast cancer, it also improves the site-specific detection of folate receptor during breast carcinoma	[96]
Superparamagnetic nanoparticles	Paclitaxel-loaded folate-conjugated superparamagnetic iron oxide nanoparticles (SPIONs)	Paclitaxel	Nasopharyngeal carcinoma	SPIONs accumulate in the tumor tissue through the EPR effect and using superparamagnetic properties under an external magnetic field. SPIONs coupled with FA for tissue targeting in cancerous conditions and introduces apoptosis	[63]
	Magnesium ferrite superparamagnetic nanoparticles (MgFe ₂ O ₄ -SPMNP)	Magnesium ferrite spinel	Radiosensitizer for breast carcinoma	MgFe ₂ O ₄ -SPMNP is prepared by the hydrothermal reaction method. MgFe ₂ O ₄ -SPMNP introduced as a radiosensitizer has low cytotoxicity and high cell distribution, which leads to excellent radiotherapy in breast cancer cells	[97]
	Dextran-coated superparamagnetic nanoparticles	Vinblastine	Pancreatic cancer	SPIONs have low toxicity and rapid EMF reaction leads to potential cancer detection and treatment. SPIONs were coated with dextran on the surface and conjugated with FA to enhance uptake and targeted delivery of vinblastine in pancreatic cancer cells	[98]

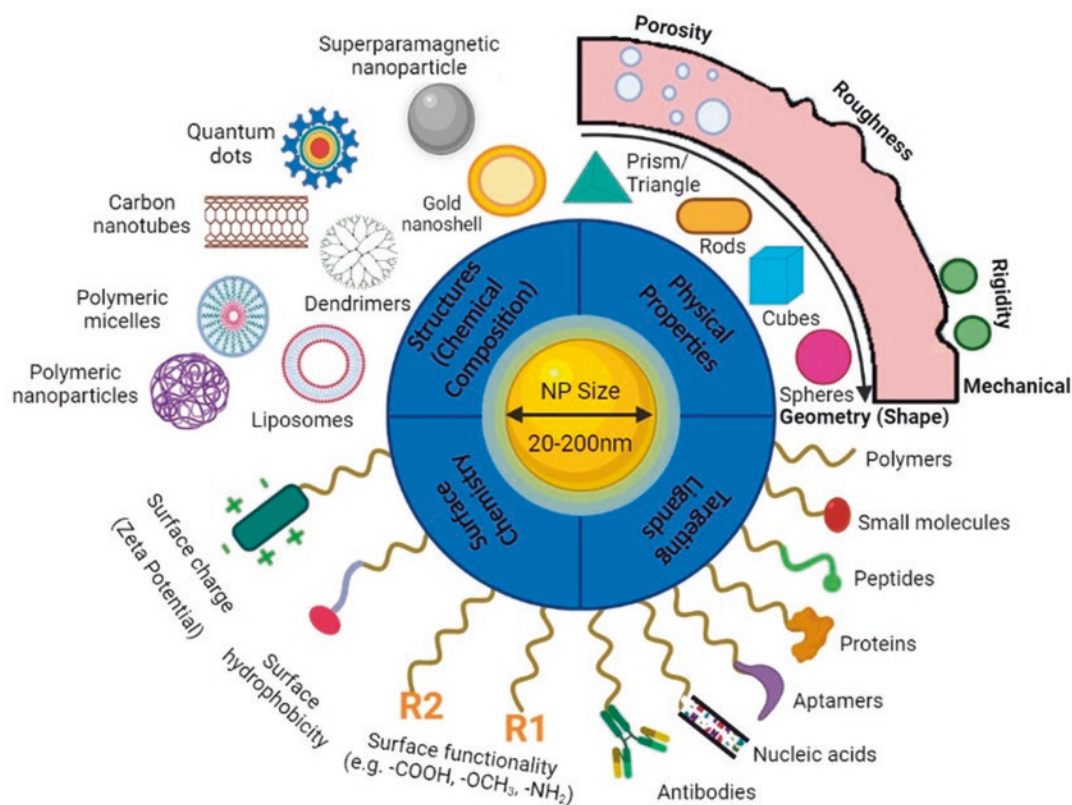


Fig. 16.2 A schematic presentation of different nanotherapeutic platforms with various structures and physicochemical properties with an array of targeting ligands for developing cancer nanomedicine

attain desired therapeutic efficacy. At present, nanotherapeutics is a rapidly advancing field of cancer research aimed at resolving several restrictions on conventional delivery [43]. Various nanotherapeutics-based drug delivery systems like polymeric nanoparticles, liposomes, polymeric micelles, hybrid nanoparticles, quantum dots, dendrimers, etc. are used to deliver anticancer drugs. A schematic illustration of various nanotherapeutic platforms to prepare the nanomedicines for applications in cancer therapy is presented in Fig. 16.2. Nanotherapeutics have extraordinary specificity of targeting (active and passive) which directly delivered drugs to the tumor cells [44]. Although there is a vast range of medicines available for cancer therapy, the problem is selective cancer cell killing and toxicity reduction for normal cells. Nanotherapeutics holds an excellent promise; a large numbers of therapeutic drugs can be enclosed into nanopar-

ticles, and can remove biological boundaries and improve their adequacy and decrease morbidity, lower immunogenicity, control release, extend half-life, minimize side effects, be used for theranostics, and enhance the pharmacokinetic profile and therapeutic effectiveness [41, 45].

3.1 Nanosystems for Cancer Therapeutics

Liposomes

Liposomes are self-assembled phospholipid bilayer structurally similar to lipid vesicles with an inner aqueous core where drugs can be encapsulated, varying between some nanometers (nm) to several micrometers (μm) [46]. The hydrophilic drugs are present in an inner aqueous compartment, while lipophilic drugs and amphiphilic drugs are attached to the lipid bilayers. This

nanosystem can be formulated via different techniques and classified according to their size, i.e., small unilamellar vesicles, multilamellar vesicles, and large unilamellar vesicles, which can be up to 20–100 nm, 5 μm , and 100–250 nm, respectively [47]. These are relatively stable and biodegradable, do not evoke any immunogenic reaction, and are mainly used for targeting the delivery of hydrophobic drugs. It is used for diverse applications like cancer, gene therapy, genetic engineering, nutrition and dietary supplements, or cosmetics [47, 48].

Polymeric Micelles

In drug delivery targeting, micelles are typically used to deliver the lipophilic drug to tumor sites. Micelles are mostly amphiphilic copolymers and comprise both hydrophobic and hydrophilic monomer units. Polymer micelles (PMs) are a promising way of self-assembling spontaneously into nano-size ranges (10–100 nm). Amphiphilic copolymers usually include a polyethylene glycol (PEG) hydrophilic shell, and hydrophobic segments can be assembled at a concentration above their critical micelle concentration (CMC) into PMs. These systems are utilized as effective delivery of lipophilic drugs to the tumor site, and it shows enhanced circulation time to accumulate a large concentration of medication at the tumor site [49, 50].

Polymeric Nanoparticles

Polymeric NPs are an attractive approach to improve the delivery of chemotherapeutic agents. It can facilitate the high loading of hydrophobic drugs with a suitable selection of the polymer and regulate drug release. The physiochemical properties can also be potentially modulated to ensure drug stability during storage [51]. Moreover, biodegradable polymers such as poly-caprolactone (PCL), polylactic acid (PLA), polylactic-co-glycolic acid (PLGA), etc. are used to evade the nanocarrier accumulation. PLGA is the most popular polymer, regulating the nanoparticles' degradation rate. For cancer treatment, there are many advantages of polymeric NPs, viz., ease of preparation, controlled and targeted release of the drug, drug uptake via internalization at the tar-

geted site with a higher concentration, and avoiding phagocytosis with enhanced drug bioavailability and reduction of its toxic effect [52].

Hybrid Nanoparticles

Lipid-polymer hybrid NPs, a promising drug delivery system mainly used to treat cancer (i.e., pancreatic, breast, and prostate), comprise an internally polymeric core and the outer lipid shell [53]. To achieve a more significant therapeutic outcome, hybrid NPs can combine the high biocompatibility of lipids with the structural integrity of polymer NPs, which allows the encapsulation of both hydrophilic and hydrophobic drugs. Moreover, hybrid NPs can be successfully internalized through cancer cells and hamper rapid clearance via the reticuloendothelial system (RES) [54].

Gold Nanoshells

For detecting tumors and metastases, gold nanoshells are helpful in various solid tumors. Gold has an advantage in its potential to detect cancer and treat cancers in the near-infrared region. When irradiated at 820 nm and for what cm^{-2} , it was able to treat mammary gland carcinoma. This system was available to selectively target the disease cell utilizing the increased temperature when it was irradiated with light [55].

Carbon Nanotubes

Carbon nanotubes (CNTs) were first reported at the end of the 1980s as a distinct molecular form of carbon atomics. The CNTs are adapted to form carbon atoms arranged by cylindrical layers in condensed aromatic rings [56]. CNTs show the lowest density, high appearance, larger surface area, good electrical characteristics, and stability. Due to the interactions between van der Waals, the CNTs exhibit high hydrophobicity and agglomeration. Additionally, the shape and patterns of CNTs are accountable for toxicity. The hydrophobicity and adverse effect are reduced with the help of surface functionalization by attaching specific molecules to their surface [56]. The larger surface area of CNTs allows for many molecules to be functionalized and facilitates the

endocytosis or passive diffusion pathway, promoting intracellular accumulation. In the cancer therapeutics area, CNTs were mainly used in cancer therapy for the transport of DNA cargo into the cell and thermal ablation therapy [57].

Dendrimers

Dendrimers are spherical shape polymers having less than 5 nm in diameter. Their chief benefit is the polymer branches, which offer a large surface area in which targeting molecules and therapeutic agents can be linked. In the presence of a hydrophobic core and hydrophilic surface, dendrimers can carry hydrophobic and hydrophilic drugs. Dendrimer shape, size, and pharmacokinetic parameters are all predisposed to the generation number, the chemical composition of the nucleus, branches, and the functional group. The biodistribution and pharmacokinetics of dendrimers may also be significantly altered by chemical modifications [58]. The dendrimer can be designed to change conformation when it enters a tumor target cell. Dendrimers are an outstanding nanocarrier for tumor targeting and therapy because of their size and capacity to load many drugs concurrently without increasing their interactions [59].

Quantum Dots

The peculiar physical characteristics of quantum dots (QDs) can be employed to diagnose malignant tumors. QDs typically comprise an inorganic transition metal core which includes indium arsenide, indium phosphide, cadmium telluride, cadmium selenide, and a shell system mainly zinc sulfide. The primary reasons for the enormously effective in vivo cancer detection agents of these composite (inorganic-organic) NPs are their small sizes which provide them with free access to blood circulation and, simultaneously, the ability to combine the targeted molecules which directly accumulated in specific tumor areas [60].

QDs also have enough surface area, like other nanoparticles, to link chemotherapeutic agents and tumor-specific moieties for concurrent drug delivery, bioimaging, and tissue engineering. QDs can emit light through the visible and infra-

red wavelength spectrum, depending on their size and core/shell system so that anyone can select an acceptable light emission color [61].

Superparamagnetic Nanoparticles

Superparamagnetic iron oxide nanoparticles (SPIONs) are targeted nanocarriers, 10 nm in diameter, highly biocompatible, fabricated through green synthesis, and, mainly, guided through an external magnetic field (EMF). However, a coating layer is needed to avoid nanoparticle exterior spin disorder, unconfined oxidation, and aggregation [62]. SPION biodistribution can be shifted by EMF to a specified organ. SPIONs allow for drug delivery, specific cellular targeting, magnetic resonance imaging (MRI), and prolonging blood circulation [63].

4 Tumor Targeting

As the pharmaceutical industries shift from modern medicine to personalized medicine, the drug delivery system is also upgrading from conventional delivery systems to a targeted delivery system. Anticancer drugs have an extremely low safety margin and require precise delivery at the target site for maximum action. The nanotechnology-based formulation delivered the drug at a specific site by taking advantage of the microenvironment. These nanoformulations are designed to modulate their properties within the target site based on the physiological microenvironment to release these drugs. Nanoformulation is a newer-generation delivery system that plays multiple roles with the body, from drug delivery to imaging application [64, 65]. The varieties of nanoformulations like lipidic, polymeric, metallic, proteinaceous, etc. were utilized for cancer targeting. These include NLCs, SLNs, micro- and nanoemulsions, cubosomes, and SLN.

Cancer is a multifactorial pathological condition that creates a microenvironment near the tumor site, including multiple, often imperfect tight junctions, leading to the classic enhanced permeability [66]. The altered retention is due to the imperfect vascular capillaries, which hamper the smooth flow out of the tumor. While design-

ing targeted nanoformulations, we have to be cautious about the physiology and environment that the dosage form encounters. It defines the penetration and retention of the targeted molecules within the tumor site. The EPR and hypoxia-like properties could be utilized for targeted drug delivery. The NPs take advantage of the EPR effect and accumulate in the cancer cells, providing maximum therapeutic efficacy with minimum off-target effect [67].

Many anticancer drugs as such do not enter treatment domains because they do not fulfill the Lipinski rules like pKa and other drugability parameters like low aqueous solubility, high toxicity, large doses, and shorter half-life. Nanotechnology-based formulations overcome the pharmacokinetic obstacles of these drugs for effective and precise treatment at the molecular level with reduced off-target effect [67]. Cancer cell targeting is achieved based on the tumor microenvironment. Broadly targeting of tumor cells through nanoparticles is achieved by multiple strategies, namely, active targeting and passive targeting.

4.1 Passive and Inverse Targeting

Passive targeting utilizes nanoparticles' small size and the tumor microenvironment like enhanced permeability and retention. Simply by virtue of size, the particles can permeate and reach the target tissue or organ [68]. In inverse targeting, the RES uptake mechanism is foiled by saturating the uptake sites by giving placebo NPs, just before administering the medicated NPs.

4.2 Active Targeting

Active targeting of nanoparticulate matter for cancer drug delivery utilized multiple approaches including receptor-dependent and stimuli-responsive. Whenever some surface modification is made, it is called active targeting. The NPs are made long circulatory through PEGylation and surface modification or modification in particle

surface charge and size. PEGylation increases circulation time resulting in increased drug penetration and deposition within cancer cells, enabling enhanced anticancer potential entrapped drug. The PEGylated liposomes were reported for the improved co-delivery of docetaxel and thymoquinone in the drug-resistant breast cancer cells [69]. A variety of surface receptors are overexpressed in various pathological conditions, including neoplasm, and can be utilized for drug delivery through surface-decorated nanoparticles (NPs). The surface of the particulate material is decorated with a specific legend which has an affinity toward overexpressed receptors on cancer cell surface utilizes for cancer cell targeting. The materials which are used for surface decoration include anisamide, glucosamine, hyaluronic acid, transferrin, folic acid, and many more for active targeting of cancer cells. The CD44 receptor has overexpressed a variety of cancers [70]. Hyaluronic acid (HA)-coated NPs target triple-negative breast cancer cells through specific binding with overexpressed CD44 receptors on cancer cells [71].

The stimuli-responsive NPs for active targeting are designed based on tumor microenvironments such as pH, catalytic enzymes or hyperthermia, or external stimuli such as pressure, magnetic field, or ultrasonication. The stimuli-sensitive NPs retain their physicochemical character, including structure, during their circulation. They are triggered upon exposure to small modulation within the tumor microenvironment or through external stimuli which lead to rapid modulation (permeability, aggregation, and disruption) to deliver the loaded drug molecule. The cross-linked guar gum-g-poly(acrylic acid-co-acrylonitrile) utilized pH-driven delivery of thymoquinone [72]. An ethylene glycol and polyvinylpyrrolidone (PVP) surface decorated NPs of Fe₃SO₄ pH-dependently delivered loaded drug in triple-negative breast cancer cell lines (MDA-MB-231) [73]. The NP surface modulation with PVP improved aqueous solubility and released drugs in the acidic environment, which enhanced drug cytotoxic potential.

5 Marketed Formulations and Patents

Nanomedicine has the potential to have a tremendous influence on society in the future. Nanotechnology has the potential to revolutionize almost every industry, but it will have a particularly significant influence on health care and medicine. Nanoparticles as drug delivery carriers, cancer biomarkers, and cancer therapeutic agents, magnetic nanoparticles for theranostics, and quantum dots for bioimaging are all examples of nanoparticles being used to diagnose and treat cancer and other disorders. These nanotechnology applications have not only piqued the interest of pharmaceutical firms and academic researchers but have also resulted in the development of novel candidates in clinical trials and even commercial applications in the worldwide market. The commercialized formulations are listed in Table 16.2 based on the stud-

ies. In a nutshell, the nanocarrier products have been widely utilized to treat disorders including autoimmune illness, HIV-related Kaposi sarcoma, cancer, and acute lymphoblastic leukemia, among others. It has also been extensively used for diagnostic reasons and is commercially accessible. The immensity of this research is demonstrated by a database search of current patents on bio-nanocarriers which highlights nanotechnology's potential in drug delivery. These innovations are useful for both targeted drug delivery and tumor cell inhibition. The nanoparticles showed several benefits, including a prolonged circulation half-life, tumor-targeting ability, and a cost-effective and simple formulation aspect, making them an excellent alternative. Patenting nanoscience technologies or procedures related to possible nanocarriers to elicit therapeutic advantages has become increasingly popular. Most recent and related patents are highlighted in Table 16.3.

Table 16.2 Therapeutic FDA-approved nanomedicines for drug delivery currently available on the market

Trade name/ marketed name	Manufacturer/company	Therapeutic active agent/ type of nanoformulation	Disease/route of administration	References
MTX-HAS	Access Pharmaceuticals, Inc. (Dallas, Texas, USA)	Methotrexate covalently linked to human serum albumin combined with cisplatin	Cancer and autoimmune diseases/ intravenous	[99]
Aldoxorubicin	CytRx, Inc. (Los Angeles, California)	Doxorubicin-loaded albumin nanoparticles	Cancer/intravenous	[100]
Abraxane	Celgene (Summit, New Jersey, USA)	Albumin-bound paclitaxel nanoparticles	Various cancers/ intravenous	[101]
Eligard	Tolmar (Fort Collins, Colorado, USA)	Leuprolide acetate polymeric nanoparticles	Prostate cancer/ intravenous	[101]
Myocet	Elan Pharmaceuticals/ Sopherion Therapeutics, Zenus Pharma (East Brunswick, New Jersey, USA)	Liposome-encapsulated doxorubicin	Breast cancer/ intravenous	[102, 103]
Oncaspar	Enzon Pharmaceuticals, Inc. (Bridgewater, New Jersey, USA)	Pegaspargase polymer conjugate	Acute lymphoblastic leukemia/intramuscular or intravenous	[102]
DaunoXome	Gilead Sciences, Ltd. (Foster City, California)	Liposome-encapsulated daunorubicin	HIV-related Kaposi sarcoma/intravenous	[103]
Genexol-PM	Samyang Biopharm (Seongnam, South Korea)	Paclitaxel-loaded polymeric micelles	Breast cancer, small cell lung cancer/ intravenous	[102]
Marqibo	Talon Therapeutics (Mississauga, Ontario, Canada)	Vincristine encapsulated in sphingomyelin liposomes	Philadelphia chromosome-negative lymphoblastic leukemia/intravenous	[104]

Table 16.3 List of patents on nanoformulations for cancer management

Patent number	Inventor	Claim product and activity	References
CN105997943B	Wang Hangxiang and Chen Jianmei	This relates to camptothecin-loaded human serum albumin nanoparticles, capable of inhibiting the reproduction of tumor cells	[105]
KR101473078B1	Ham Seung-ju, Heo Yong-min, et al.	The patent is related to organic/inorganic nanocomposite for diagnosis and treatment of cancer in which magnetic nanoparticles are formed in a cluster form inside conductive polymer particles	[106]
CN104368003A	Zhang Huijuan, Chen Qianqian, et al.	The patent is related to the preparation method of hyaluronic acid decorated Au-doped titanium dioxide nanotube that can be strong in targeting and used for achieving comprehensive therapies of cancers	[107]
US20060121119A1	Maurizio Zenoni and Simone Maschio	This is related to the process for preparing paclitaxel-loaded albumin nanoparticles. The method takes less time, incurs lower cost than that of the known art, and has potent antitumor activity	[108]
US8697181B2	Alexandru S. Biris, Yang Xu et al.	The invention is related to a magnetic oxide-quantum dot nanocomposite and methods of synthesizing it for hyperthermia cancer treatments	[109]
CN110075296B	Wu Liming Mao, Zhengwei Yang et al.	This relates to the preparation method and application of gold nanoflowers for liver cancer targeting and radiotherapy sensitivity enhancing characteristics	[110]
WO2017101653A1	Liu Feng, Lai Shuting et al.	The invention is related to hyaluronic acid-albumin conjugate for targeting tumor cells	[111]

6 Next Generation of Cancer Nanomedicine and Prospects

The translation of cancer nanotherapeutics for cancer management has been sluggish and inadequate, only with a handful of outcomes presently being applied in routine clinical practice, some of which are discussed in the sections below. The FDA approved PEGylated and non-PEGylated liposomal formulation of doxorubicin in the trade name of Doxil® (Janssen Pharmaceutical) [74], Lipodox® (Sun Pharma Global FZE) [75], and Myocet® (Sopherion Therapeutics) [76] for metastatic management. Another drug paclitaxel was also approved in the nanocarrier form of liposome (Lipusu® (Sike Pharmaceutical Co. Ltd.)) [77], albumin (Abraxane® (Celgene) [78]), and N-isopropyl acrylamide NIPAM-VP (Nanoxel® (Fresenius Kabi India Pvt. Ltd.)) [79]. Despite these, biologic drugs (trastuzumab/DM) were also approved with the name of Kadcyla® (Hoffmann-La Roche) for metastatic HER2+ management [80].

The factors such as the implementation of a complex good manufacturing process, quality by design, higher cost, and low reproducibility halt the clinical translation of nanomedicines. In contrast to the performance predictability limitations of drug molecules, anticancer nanoparticles show crucial properties like accessible pharmacokinetics, biodistribution, drug release pattern, and tumor retention and penetration at the tumor site. However, all these factors differ extensively when comparing human patients to animal models [81].

Therefore, cautiously validating characterization and implementing standard culture condition of the cell lines employed for the nanomedicines represent a crucial part of the experiment to ensure reproducibility [82]. The development of improved/identical animal models of human physiology as a translational bridge between preclinical models and the realities of the human tumor microenvironment should be a focus of existing and prospective research.

References

- Björnmalm M, et al. Bridging bio-nano science and cancer nanomedicine. *ACS Nano*. 2017;11(10):9594–613.
- Shi J, et al. Cancer nanomedicine: progress, challenges and opportunities. 2017;17(1):20.
- von Roemeling C, et al. Breaking down the barriers to precision cancer nanomedicine. 2017;35(2):159–71.
- Massagué J, Obenauf ACJN. Metastatic colonization by circulating tumour cells. 2016;529(7586):298–306.
- Schroeder A, et al. Treating metastatic cancer with nanotechnology. 2012;12(1):39–50.
- Petersen GH, et al. Meta-analysis of clinical and pre-clinical studies comparing the anti-cancer efficacy of liposomal versus conventional non-liposomal doxorubicin. 2016;232:255–64.
- Aghebbati-Maleki A, et al. Nanoparticles and cancer therapy: perspectives for application of nanoparticles in the treatment of cancers. 2020;235(3):1962–72.
- Karra N, S.J.C.d.m. Benita. The ligand nanoparticle conjugation approach for targeted cancer therapy. 2012;13(1):22–41.
- De Jong WH, P.J.J.l.j.o.n. Borm. Drug delivery and nanoparticles: applications and hazards. 2008;3(2):133.
- Jarzyna PA, et al. Multifunctional imaging nanoprobos. 2010;2(2):138–50.
- Mu Q, B.J.F.i.p. Yan. Nanoparticles in cancer therapy-novel concepts, mechanisms, and applications. 2019;9:1552.
- Gou Y, et al. Bio-inspired protein-based nanoformulations for cancer theranostics. 2018;9:421.
- Rezvantab S, et al. PLGA-based nanoparticles in cancer treatment. 2018;9:1260.
- Raut S, et al. Reconstituted HDL: drug delivery platform for overcoming biological barriers to cancer therapy. 2018;9:1154.
- Thakur N, et al. Nanoparticles as smart carriers for enhanced cancer immunotherapy. 2020;8:1217.
- Lamberti M, et al. Advantages and risks of nanotechnologies in cancer patients and occupationally exposed workers. 2014;11(7):1087–101.
- Tohme S, Simmons RL, A.J.C.r. Tsung. Surgery for Cancer: a trigger for metastases. 2017;77(7):1548–52.
- Baskar R, et al. Cancer and radiation therapy: current advances and future directions. 2012;9(3):193.
- Huang C-Y, et al. A review on the effects of current chemotherapy drugs and natural agents in treating non-small cell lung cancer. 2017;7(4)
- Agostinis P, et al. Photodynamic therapy of cancer: an update. 2011;61(4):250–81.
- Puhalla S, Bhattacharya S, N.E.J.M.o. Davidson. Hormonal therapy in breast cancer: a model disease for the personalization of cancer care. 2012;6(2):222–36.
- Schirmacher, V.J.I.j.o.o. From chemotherapy to biological therapy: a review of novel concepts to reduce the side effects of systemic cancer treatment. 2019;54(2):407–19.
- Ediriwickrema A, W.M.J.A.b.s. Saltzman, and Engineering. Nanotherapy for cancer: targeting and multifunctionality in the future of cancer therapies. 2015;1(2):64–78.
- Mahmoodi NO, et al. A comparative study on the nanoparticles for improved drug delivery systems. 2016;162:681–93.
- Golombek SK, et al. Tumor targeting via EPR: strategies to enhance patient responses. 2018;130:17–38.
- Matsumura Y, H.J.C.r. Maeda. A new concept for macromolecular therapeutics in cancer chemotherapy: mechanism of tumorotropic accumulation of proteins and the antitumor agent SMANCS. 1986;46(12 Part 1):6387–92.
- Fang J, et al. N-(2-hydroxypropyl) methacrylamide polymer conjugated pyropheophorbide-a, a promising tumor-targeted theranostic probe for photodynamic therapy and imaging. 2018;130:165–76.
- Forster JC, et al. A review of the development of tumor vasculature and its effects on the tumor micro-environment. 2017;5:21.
- Bertrand N, et al. Cancer nanotechnology: the impact of passive and active targeting in the era of modern cancer biology. *Adv Drug Deliv Rev*. 2014;66:2–25.
- Dewhirst MW, Secomb TWJNRC. Transport of drugs from blood vessels to tumour tissue. 2017;17(12):738–50.
- Pal RR, et al. Recent findings on thymoquinone and its applications as a nanocarrier for the treatment of cancer and rheumatoid arthritis. 2021;13(6):775.
- Taurin S, Nehoff H, K.J.J.o.c.r. Greish. Anticancer nanomedicine and tumor vascular permeability; where is the missing link? 2012;164(3):265–75.
- Steichen SD, Caldorera-Moore M, N.A.J.E.j.o.p.s. Peppas. A review of current nanoparticle and targeting moieties for the delivery of cancer therapeutics. 2013;48(3):416–27.
- Mendes LP, Lima EM, Torchilin VP. Targeted nanotheranostics for selective drug delivery in cancer. In: *Handbook of nanomaterials for cancer theranostics*. Elsevier; 2018. p. 245–77.
- Czernin J, et al. PET/CT in oncology: current status and perspectives. 2013;1(3):177–90.
- Guimaraes MD, et al. Functional magnetic resonance imaging in oncology: state of the art. 2014;47(2):101–11.
- Rosenkrantz AB, et al. Current status of hybrid PET/MRI in oncologic imaging. 2016;206(1):162–72.
- Herranz M, A.J.J.o.o. Ruibal. Optical imaging in breast cancer diagnosis: the next evolution. 2012;2012
- Ardehripour Y, et al. Using in-vivo fluorescence imaging in personalized cancer diagnostics and therapy, an image and treat paradigm. 2011;10(6):549–60.

40. Saraf S. Applications of novel drug delivery system for herbal formulations. *Fitoterapia*. 2010;81(7):680–9.
41. Scheinberg DA, et al. Conscripts of the infinite armada: systemic cancer therapy using nanomaterials. 2010;7(5):266–76.
42. Rotomskis RJTJ. Optical biopsy of cancer: nanotechnological aspects. 2008;94(2):200–5.
43. Zhu L, et al. Chitosan-coated magnetic nanoparticles as carriers of 5-fluorouracil: preparation, characterization and cytotoxicity studies. 2009;68(1):1–6.
44. Tran S, et al. Cancer nanomedicine: a review of recent success in drug delivery. 2017;6(1):1–21.
45. Babu P, Saranya S, Mallepogu VJAJNN. Nanoformulations as drug delivery vehicles for cancer treatment. 2015;3(1):1038.
46. Carita AC, et al. Recent advances and perspectives in liposomes for cutaneous drug delivery. 2018;25(5):606–35.
47. Eloy JO, et al. Liposomes as carriers of hydrophilic small molecule drugs: strategies to enhance encapsulation and delivery. 2014;123:345–63.
48. Biswas AK, et al. Nanotechnology based approaches in cancer therapeutics. 2014;5(4):043001.
49. Masood FJMS, E. C. Polymeric nanoparticles for targeted drug delivery system for cancer therapy. 2016;60:569–78.
50. Gregoriou Y, et al. Resveratrol loaded polymeric micelles for theranostic targeting of breast cancer cells. 2021;5(1):113.
51. Ferrari R, et al. Polymer nanoparticles for the intravenous delivery of anti-cancer drugs: the checkpoints on the road from the synthesis to clinical translation. 2018;10(48):22701–19.
52. Bhattacharya, S.J.J.o.D.D.S. and Technology. Fabrication of poly (sarcosine), poly (ethylene glycol), and poly (lactic-co-glycolic acid) polymeric nanoparticles for cancer drug delivery. 2021;61:102194.
53. Webb JL, et al. Microtubule disruption inhibits autophagosome-lysosome fusion: implications for studying the roles of aggresomes in polyglutamine diseases. 2004;36(12):2541–50.
54. Wang, J.J.D.d., Development and Therapy. Combination treatment of cervical cancer using folate-decorated, pH-sensitive, carboplatin and paclitaxel co-loaded lipid-polymer hybrid nanoparticles. 2020;14:823.
55. Mousa SA, Bharali DJJC. Nanotechnology-based detection and targeted therapy in cancer: nano-bio paradigms and applications. 2011;3(3):2888–903.
56. Hosnedlova B, et al. Carbon nanomaterials for targeted cancer therapy drugs: a critical review. 2019;19(2–3):502–22.
57. Liu Z, et al. Carbon materials for drug delivery & cancer therapy. 2011;14(7–8):316–23.
58. Kojima C, et al. Synthesis of polyamidoamine dendrimers having poly (ethylene glycol) grafts and their ability to encapsulate anti-cancer drugs. 2000;11(6):910–7.
59. Cheng Y, et al. Pharmaceutical applications of dendrimers: promising nanocarriers for drug delivery. 2008;13(4):1447–71.
60. Kim J, et al. Highly fluorescent CdTe quantum dots with reduced cytotoxicity—a robust biomarker. 2015;3:46–52.
61. Kulkarni NS, et al. Exploring potential of quantum dots as dual modality for cancer therapy and diagnosis. 2019;49:352–64.
62. Cristofolini T, et al. Multifunctional hybrid nanoparticles as magnetic delivery systems for siRNA targeting the HER2 gene in breast cancer cells. 2020;109:110555.
63. Gui G, et al. Optimization, characterization and in vivo evaluation of paclitaxel-loaded folate-conjugated superparamagnetic iron oxide nanoparticles. 2021;16:2283.
64. Pal RR, et al. Tamanu oil potentiated novel sericin emulgel of levocetirizine: repurposing for topical delivery against DNCB-induced atopic dermatitis, QbD based development and in vivo evaluation. *J Microencapsul*. 2019;36(5):432–46.
65. Pal RR, et al. A comparative study of levocetirizine loaded vesicular and matrix type system for topical application: appraisal of therapeutic potential against atopic dermatitis. *J Pharm Innov*. 2020;
66. Mahaur S, Upadhyay S, Pal RR. Indolizine: in-silico identification of inhibitors against mutated BCR-ABL protein of chronic myeloid leukemia. *Res J Pharm Pharm*. 2020;12(4):151–8.
67. Maurya P, et al. Chapter 20 – Albumin-based nanomaterials in drug delivery and biomedical applications. In: Bera H, Hossain CM, Saha S, editors. *Biopolymer-based nanomaterials in drug delivery and biomedical applications*. Academic Press; 2021. p. 465–96.
68. Pal RR, Rajpal V. Recent findings on thymoquinone and its applications as a nanocarrier for the treatment of cancer and rheumatoid arthritis. 2021;13:6.
69. Odeh F, et al. Co-encapsulation of thymoquinone with docetaxel enhances the encapsulation efficiency into PEGylated liposomes and the chemosensitivity of MCF7 breast cancer cells to docetaxel. *Heliyon*. 2019;5(11):e02919.
70. Li M, et al. Drug delivery systems based on CD44-targeted glycosaminoglycans for cancer therapy. *Carbohydr Polym*. 2021;251:117103.
71. Bhattacharya S, et al. Delivery of thymoquinone through hyaluronic acid-decorated mixed Pluronic® nanoparticles to attenuate angiogenesis and metastasis of triple-negative breast cancer. *J Control Release*. 2020;322:357–74.
72. Pal RR, et al. Synthesis of pH-sensitive crosslinked guar gum-g-poly(acrylic acid-co-acrylonitrile) for the delivery of thymoquinone against inflammation. *Int J Biol Macromol*. 2021;182:1218–28.
73. Kumar SR, et al. Synergetic effects of thymoquinone-loaded porous PVPylated Fe₃O₄ nanostructures for efficient pH-dependent drug release and anti-

- cancer potential against triple-negative cancer cells. *Nanoscale Adv.* 2020;2(8):3209–21.
74. Barenholz YC. Doxil®—the first FDA-approved nano-drug: lessons learned. *J Control Release.* 2012;160(2):117–34.
 75. Aulic S, et al. Breast cancer nanomedicine market update and other industrial perspectives of nanomedicine. In: *Nanomedicines for breast cancer theranostics.* Elsevier; 2020. p. 371–404.
 76. Lao J, et al. Liposomal doxorubicin in the treatment of breast cancer patients: a review. *J Drug Deliv.* 2013;2013
 77. Wang F, et al. Preclinical development of drug delivery systems for paclitaxel-based cancer chemotherapy. *J Control Release.* 2017;267:100–18.
 78. Li Y, et al. Pharmacologic sensitivity of paclitaxel to its delivery vehicles drives distinct clinical outcomes of paclitaxel formulations. *Mol Pharm.* 2015;12(4):1308–17.
 79. Ranade A, et al. Clinical and economic implications of the use of nanoparticle paclitaxel (Nanoxel) in India. *Ann Oncol.* 2013;24:v6–v12.
 80. Von Minckwitz G, et al. Trastuzumab emtansine for residual invasive HER2-positive breast cancer. *N Engl J Med.* 2019;380(7):617–28.
 81. Metselaar JM, Lammers T. Challenges in nanomedicine clinical translation. *Drug Deliv Transl Res.* 2020;1–5.
 82. Ioannidis JP, Kim BY, Trounson A. How to design preclinical studies in nanomedicine and cell therapy to maximize the prospects of clinical translation. *Nat Biomed Eng.* 2018;2(11):797–809.
 83. Morais RP, et al. Naringenin-functionalized multi-walled carbon nanotubes: a potential approach for site-specific remote-controlled anti-cancer delivery for the treatment of lung cancer cells. 2020;21(12):4557.
 84. Ozgen PSO, et al. Glycopolymer decorated multi-walled carbon nanotubes for dual targeted breast cancer therapy. 2020;8(15):3123–37.
 85. Singhai NJ, et al. CD44 receptor targeted 'smart' multi-walled carbon nanotubes for synergistic therapy of triple-negative breast cancer. 2020;35:100235.
 86. Ghaffari M, et al. Co-delivery of curcumin and Bcl-2 siRNA by PAMAM dendrimers for enhancement of the therapeutic efficacy in HeLa cancer cells. 2020;188:110762.
 87. Torres-Pérez SA, et al. Glycosylated one-step PAMAM dendrimers loaded with methotrexate for target therapy in breast cancer cells MDA-MB-231. 2020;58:101769.
 88. Fernandes MA, et al. Transferrin-functionalized liposomes for docetaxel delivery to prostate cancer cells. 2021;611:125806.
 89. Swami R, et al. pH sensitive liposomes assisted specific and improved breast cancer therapy using co-delivery of SIRT1 shRNA and Docetaxel. 2021;120:111664.
 90. Rashidzadeh H, et al. pH-sensitive curcumin conjugated micelles for tumor triggered drug delivery. 2021;32(3):320–36.
 91. Ma T, et al. Fabrication of gold nanoshells for improvement of cell apoptosis and its application in photothermal cancer therapy. 2020;10(8):1204–12.
 92. Lee S-Y, M.-J.J.A.a.m. Shieh, and Interfaces. Platinum (II) drug-loaded gold nanoshells for chemo-photothermal therapy in colorectal cancer. 2020;12(4):4254–64.
 93. Levit SL, Tang CJN. Polymeric nanoparticle delivery of combination therapy with synergistic effects in ovarian cancer. 2021;11(4):1048.
 94. Guo Z, et al. pH-Responsive charge switchable PEGylated ϵ -poly-L-lysine polymeric nanoparticles-assisted combination therapy for improving breast cancer treatment. 2020;326:350–64.
 95. Kalkal A, et al. Biofunctionalized graphene quantum dots based fluorescent biosensor toward efficient detection of small cell lung cancer. 2020;3(8):4922–32.
 96. Monteiro CA, et al. Evaluating internalization and recycling of folate receptors in breast cancer cells using quantum dots. 2020;209:111918.
 97. Meidanchi A, Motamed AJCI. Preparation, characterization and in vitro evaluation of magnesium ferrite superparamagnetic nanoparticles as a novel radiosensitizer of breast cancer cells. 2020;46(11):17577–83.
 98. Albukhaty S, et al. Investigation of dextran-coated superparamagnetic nanoparticles for targeted vinblastine controlled release, delivery, apoptosis induction, and gene expression in pancreatic cancer cells. 2020;25(20):4721.
 99. Bolling C, et al. Phase II study of MTX-HSA in combination with cisplatin as first line treatment in patients with advanced or metastatic transitional cell carcinoma. 2006;24(6):521–7.
 100. Kratz, F.J.J.o.c.r. A clinical update of using albumin as a drug vehicle—a commentary. 2014;190:331–6.
 101. Ventola, C.L.J.P. and Therapeutics. Progress in nanomedicine: approved and investigational nanodrugs. 2017;42(12):742.
 102. Pillai G. Nanomedicines for cancer therapy: an update of FDA approved and those under various stages of development. *SOJ Pharm Pharm Sci.* 2014;1(2):13.
 103. Salama L, et al. Emerging nanopharmaceuticals and nanonutraceuticals in cancer management. 2020;8(9):347.
 104. Wicki A, et al. Nanomedicine in cancer therapy: challenges, opportunities, and clinical applications. 2015;200:138–57.
 105. Wang Hangxiang CJ. A kind of nano particle and its preparation method and application of human serum albumins load camptothecin. Google Patents; 2019.
 106. Ham Seung-ju, Moon HY, Kim Eun-jeong, Choi Ji-hye, Kim Bong-Jun, *Organic/inorganic nanocom-*

- posite for diagnosis and treatment of cancer. 2014, Google Patents.
107. Zhang Huijuan CQ, Yandan J, Xiaojing J, Lin H, Zhenzhong Z, Hongling Z, editors. Preparation method and application of hyaluronic acid modified au-doped titanium dioxide nano-tube. Google Patents; 2017.
 108. Zenoni M, Maschio S. Process for producing nanoparticles of paclitaxel and albumin. Google Patents; 2006.
 109. Biris AS, Xu Y, Wang D. Multifunctional Fe₃O₄ cored magnetic-quantum dot fluorescent nanocomposites for RF nano-hyperthermia of cancer cells. Google Patents; 2014.
 110. Wu Liming MZ, Hongyu Y, Qingwei Z, Fu Z. Gold nanoflowers with liver cancer targeting and radiotherapy sensitization characteristics and preparation and application thereof. Google Patents; 2020.
 111. Liu Feng LS, Fuchun C, Yang Z, Yuanfa L. Targeted hydrophobic anti-tumour medicine nanometre preparation and preparation method thereof. Google Patents; 2017.



Clearance Pathways and Tumor Targeting of Imaging Nanoparticles for Diagnostics

Palak K. Parikh, Nisha H. Parikh, Jayvadan K. Patel, and Yashwant V. Pathak

Contents

1	Introduction	316
2	Clearance Pathways	317
3	Tumor Targeting with NPs	324
4	Conclusion	326
	References	327

Abstract

Nanotechnology provides numerous opportunities in the early detection of cancers and helps to reduce cancer-related mortality. Nanoparticles with diverse and tunable properties represent a promising strategy for molecular imaging. Nanoparticle-based imaging

agents have a great potential to provide enhanced sensitivity and specificity for tumor imaging. However, their prolonged tissue retention and potential toxicities have resulted in their restricted clinical translation to date. In the present compilation, clearance pathway and tumor targeting of imaging nanoparticles are summarized. The impact of size, shape, surface modification, and surface charge of NPs on their clearance is discussed. Tumor targeting strategies, i.e., active and passive targeting, are also described in the present compilation.

P. K. Parikh (✉)

L.M. College of Pharmacy, Navrangpura, Ahmedabad, Gujarat, India

N. H. Parikh (✉)

L.M. College of Pharmacy, Navrangpura, Ahmedabad, Gujarat, India

Arihant School of Pharmacy & Bio Research Institute, Adalaj, Gandhinagar, Gujarat, India

J. K. Patel

Nootan Pharmacy College, Faculty of Pharmacy, Sankalchand Patel University, Visnagar, Gujarat, India

Y. V. Pathak

College of Pharmacy, University of South Florida Health, Tampa, FL, USA

Keywords

Nanoparticles · Diagnosis · Cancer · Clearance · Tumor targeting · EPR effect

Abbreviations

AuNPs	Gold nanoparticles
CD-1 mice	Originated from Swiss mice

CDI	Color Doppler ultrasound imaging
cRGD	Monomeric cyclic Arg-Gly-Asp peptide
CT	Computed tomography
CTAB	Cetyltrimethylammonium bromide
Cys	Cystine
DHLA	Dihydrolipoic acid
DTPA	Diethylenetriaminepentaacetic dianhydride
EPR effect	Enhanced permeability and retention effect
GBM	Glomerular basement membrane
Gly	Glycine
GPI	(2-[(3-Amino-3-carboxypropyl)(hydroxy)phosphinyl]-methyl)pentane-1,5-dioic acid)
GS	Glutathione
HD	Hydrodynamic diameter
ID	Injected dose
IONPs	Iron oxide nanoparticles
KFT	Kidney filtration threshold
MPS	Mononuclear phagocyte system
MRI	Magnetic resonance imaging
MUA	Mercaptoundecanoic acid
NPs	Nanoparticles
p.i.	Post-injection
PEG	Poly(ethylene glycol)
PEI	Polyethylenimine
PET	Positron emission tomography
PVP	Poly(vinyl pyrrolidone)
QDs	Quantum dots
RES	Reticuloendothelial system
SPECT	Single-photon emission computed tomography
SWCNTs	Single-walled carbon nanotubes
TEM	Transmission electron micrographs
TPPMS	Triphenylphosphine monosulfonate
US FDA	US Food and Drug Administration
US	Ultrasonography
ZW800-CDPL	Zwitterionic 800- β -cyclodextrin-conjugated ϵ -polylysine

1 Introduction

According to GLOBOCAN statistics, cancer is one of the leading causes of mortality with around 10 million deaths all around the globe in 2020. The total number of new cancer cases is projected to rise from 19.3 million in 2020 to 30.2 million in 2040 [1]. Despite impressive progress in the therapy of cancer, early detection of cancer is of paramount importance for the treatment and has a great potential to reduce cancer mortality [2]. Different cancer diagnostic techniques mainly include noninvasive imaging techniques like computed tomography (CT), single-photon emission computed tomography (SPECT), magnetic resonance imaging (MRI), color Doppler ultrasound imaging (CDI), positron emission computed tomography (PET), ultrasonography (US), and biochemical indicators, but having their intrinsic limitations. Molecular imaging probes for imaging modalities may facilitate more accurate and earlier detection of tumors. However, their nonspecific distribution throughout the body, rapid metabolism, unwanted side effects, and low imaging contrast make their use limited [3–6]. Therefore, the development of technologies for the early detection of cancer presents a major challenge.

Cancer nanotechnology is an emerging interdisciplinary research field involving chemistry, biology, engineering, and medicine and is expected to have a great potential of early diagnosis and treatment of cancer [7, 8]. Nanoparticles (NPs) are smaller than several hundred nanometers in size in at least one dimension and are of wide class of materials that include particulate substances. Nanotechnology developments have provided a platform to design multiple components loaded nanostructures that manifest their activity through electrical, optical, magnetic, and catalytic properties by the virtue of their tunable composition, sizes (1–100 nm at least in one dimension), shapes, and structure and have been widely investigated for their applications in cancer diagnosis and treatment, bioimaging, drug delivery, and tissue repair [6, 9, 10]. During recent decades, various strategies have been undertaken for designing of NP-based contrast

agents. As per the requirements by the US FDA, all injected imaging contrasts require to be cleared from the body in a reasonable time period [11]. Therefore, renal clearable imaging contrasts are regarded as an essential prerequisite for their success in clinical practice in the future. In clinical practice, the most common contrast agents are small molecule-based contrast agents as they have smaller size than the kidney filtration threshold (KFT) of around 5.5 nm and can be quickly removed via the urinary system from the body [12]. The emergence of inorganic NP-based contrast agents has revealed a new paradigm for imaging of tumors at early stage. For instance, quantum dots (QDs) are very small semiconductor particles with tunable emission, large Stokes shift, bright fluorescence, and high photostability and have displayed a great potential for early tumor detection [13]. Due to unique electrical and optical properties, gold NPs have served as agents in MRI, fluorescence imaging, photoacoustic imaging, CT, and nuclear imaging [14, 15]. Iron oxide nanoparticles (IONPs) are magnetic NPs having their applications in magnetic fluid hyperthermia, MRI contrast agents, and thermoablation and biosensing [16, 17]. Owing to the advantages of NPs including small size, decent biocompatibility, and high atomic number, they have gained importance. However, inorganic NPs are often quickly shuttled off from the blood and captured by the reticuloendothelial system (RES), thereby prolonging the elimination time and increasing the safety risks [18]. Surface coating of inorganic NPs by poly(ethylene glycol) (PEG) is a surface chemistry strategy undertaken to reduce and slow down the severe and rapid uptake by RES. However, a majority of NPs with PEG coating still end up in the spleen and liver after circulation, resulting in low specificity in tumor targeting and potential long-term toxicity. Therefore, the development of NPs having efficient renal clearance is highly anticipated in clinically translatable nanomedicines. Properties needed to be considered for designing renal clearable NPs include particle size, particle shape, surface area, surface chemistry, and charge. Renal clearable NPs are expected to show rapid distribution to various organs and tissues,

efficient renal clearance, less RES organ accumulation, passive tumor targeting via enhanced permeability and retention (EPR) effect, and favorable two-compartment pharmacokinetics for enhancing tumor targeting efficiency [19].

2 Clearance Pathways

After intravenous administration, NPs enter the circulatory system and interact with cells, coagulation factors, platelets and plasma, as well as serum proteins from blood but will most probably be further distributed to peripheral tissues and organs. The physicochemical properties of NPs have a great influence on their distribution to various peripheral organs, degradability, and clearance [20–22]. Nevertheless, NPs that are not efficiently eliminated from the body have a higher possibility of interacting with cells, tissues, and organs and accumulating in the body due to their extended circulation time. Excretion of NPs follows two major pathways, viz., renal and hepatobiliary (processed through liver cells followed by biliary system and become excreted via the GI) excretion [23]. Clearance through the renal route is the most effective excretion. However, NPs having a hydrodynamic diameter (HD) of <6 nm can pass through the glomerular capillary wall easily and are cleared through this route, while NPs (>10 nm) are frequently sequestered from the blood and are eliminated by the mononuclear phagocyte system (MPS) [24, 25].

2.1 Clearance of Conventional Non-renal Clearable Nanoprobes

Conventional nanoprobes usually possess HDs above the KFT (~5.5 nm) in the biological environment, and hence they do not be cleared from the body by the renal route unless they can degrade into smaller fragments. They are frequently trapped in RES organs for a long duration. As summarized by Zheng J and co-worker, non-renal clearable NPs accumulate in the liver in the range of 10–100% injected dose (ID) g^{-1} at

4–48 h post-injection (p.i.) and 10–1000 times higher than liver uptake of small molecular probes. NPs having a larger core size (10–500 nm) is responsible for their higher HDs as observed for spherical AuNPs, Au nanocages, QDs, iron oxide NPs, single-walled carbon nanotubes, silica NPs, etc. [26–31]. The surface of NPs adsorbs proteins upon entering systemic circulation and alters their HDs. Sometimes, severe retention of NPs in RES organs is caused by serum protein (opsonin) adsorption induced by ligands on NP surface, which leads to a significant increase in their HDs and results in enhanced hepatic uptake [32, 33]. Surface coating and aggregation of NPs are other reasons for an increase in their HDs [34, 35]. CdSe/ZnS QDs were modified by surface coating which led to an increase in their HDs. In a PK study, coating of QDs with mercaptoundecanoic acid (MUA) with lysine cross-linking (QD-LM) led to an increase in HD from 7 nm to 25 nm, and conjugation of QDs to bovine serum albumin (QD-BSA) resulted in an increase of HD to 80 nm. Both QDs showed first-order kinetics in plasma with a half-life of 58.5 ± 17.0 min and clearance of 0.84 ± 0.30 mLmin⁻¹ kg⁻¹ for QD-LM and a half-life of 38.7 ± 3.5 min and clearance of 1.22 ± 0.20 mLmin⁻¹ kg⁻¹ for QD-BSA in rats, indicating fast clearance of QD-BSA from systemic circulation. Both QDs were sequestered in RES cells and were not detected in urine or feces for up to 10 days after intravenous administration [36]. Liu H and co-workers reported interactions between proteins and Au nanorods. The adsorption of serum albumin to nanorods resulted in an increase in HD due to aggregate formation, whereas immunoglobulins led to formation of stable protein corona on the surface of nanorods [37]. Lysine cross-linked MUA CdSe_{0.25}Te_{0.75}/CdS QDs displayed sequestration in the liver and spleen with rapid clearance from the blood. Adsorption or conjugation of PEG to the NP surface is a common approach to decrease the opsonization. PEGylation of NPs prolongs blood circulation half-life and can slow RES uptake [38]. However, PEGylation-induced enlargement of NPs may elevate RES uptake [39]. The phospholipid micelle-encapsulated CdSe/CdS/ZnS

QDs did not display any toxicity-related evidence during the pilot study in rhesus macaques. More than 90% ID of QDs retained in various organs including the spleen, liver, and kidneys after 90 days p.i. via intravenous route [40]. The cetyltrimethylammonium bromide (CTAB)-capped Au nanorods displayed quick uptake by tissues due to protein-Au nanorod complex formation and were retained in liver and spleen tissues for 28 days in rats after post-intravenous administration [41]. Different NPs displayed long retention in various organs and very slow elimination (weeks, months, to years) from the body as observed for silica NPs, CdSe-ZnS QDs with a ligand-stabilized surface, and citrate-coated AuNPs [42–44]. As NP with larger core size has prolonged residence time in bloodstream, it allows more space for functionalization and efficient targeting of diseased tissues. However, the decreasing kidney filtration making prolonged residence time in the living system may result in potential toxicities. As inorganic NPs are relatively difficult to degrade and excrete, it induces a long-term accumulation in the body. Furthermore, the degradation products of some inorganic NPs comprise heavy metal ions or their intermediates, which may cause adverse effects and damage to the organs during metabolic processes. From these respects, biodegradability enhancement for inorganic NPs may not be a desirable solution. Therefore, the development of NP-based contrast agents with efficient renal clearance is a more promising approach for their clinical translation [45].

2.2 Clearance of Renal Clearable Nanoprobes

The renal clearable NPs generally possess renal clearance efficiency of more than 50% ID within a short period of duration, i.e., of 48 h p.i. It is of great importance to minimize the retention of NPs in the body and long-term exposure of hazards for safety regulations compared to the non-renal clearable NPs [46]. To address challenges and limitations associated with non-renal clearable NPs, several renal clearable ultrasmall NPs

have been designed by various research groups during the past decades which include QDs, gold NPs, silica NPs, silver NPs, iron oxide NPs, carbon dots, copper NPs, as well as nanoclusters (NCs) [47–53]. Ravi Singh and co-workers synthesized single-walled carbon nanotubes (SWCNTs) with a mean diameter of 1 nm and length of 300–1000 nm. In the clearance study, The SWCNTs displayed efficient renal elimination, and it was the first observed investigation for renal elimination of inorganic material [54]. Since the development of renal clearable QDs by Choi HS and co-workers, various kinds of NPs have been developed for biomedical applications, and some representative NPs with their renal clearance efficiencies are listed in Table 17.1 [55].

Various parameters that greatly influence the designing of renal clearable inorganic NPs include particle size, morphology, surface chemistry, and charge.

Size

Generally, the renal clearance pathway is dependent on the glomerular filtration barrier which comprises endothelial cells, endothelial glycocalyx, podocytes, and glomerular basement membrane (GBM) in the kidney and has been commonly noticed in the clearance of globular proteins. The KFT is typically of 6–8 nm on the glomerular filtration barrier [79, 80]. Therefore, ultrasmall-sized NPs having the HD near or below the KFT can be easily cleared by the renal route. To determine renal filtration threshold, Choi HS and co-workers synthesized a series of CdSe/ZnS QDs possessing HDs of 4.36 nm to 8.65 nm, and their biodistribution and clearance were studied in rodents. The study revealed that QDs having an HD of less than 5.5 nm can be efficiently eliminated via the renal system with more than 50% ID renal clearance at 4 h p.i. (Fig. 17.1) [55]. In another study, Zhou C and co-workers reported the renal clearance of different sized glutathione (GS)-coated AuNPs with HDs of 2, 6, and 13 nm. Renal clearance kinetic studies showed 50% ID, 4% ID, and 0.5% ID in urine (24 h p.i.) for 2, 6, and 13 nm sized NPs, respectively [47]. The above mentioned studies estab-

lished a relationship between HD of NPs and renal clearance.

Shape

In addition to size, the shape of NPs also affects their renal clearance. Typically, spherical NPs with rigid structure have KFT of about 6–8 nm, whereas linear-shaped NPs with flexible structure show higher size thresholds compared to rigid structured spherical NPs and can be cleared through the kidneys [81]. SWCNTs having diameters of 0.8–1.2 nm and a rigid rod lengths of 100–1000 nm displayed renal clearance around 65% of ID (20 min p.i.). During filtration through kidney, the SWCNTs aligned to the long axis toward the glomerular capillary pores opening due to flow. Thus, SWCNTs with a molecular weight of 300–500 kDa are much larger as compared to the renal clearable proteins with a molecular weight of 30–50 kDa; they can still be efficiently eliminated through the renal route [82]. Therefore, the aspect ratio of one-dimensional nanostructures plays a crucial role in directional diffusion, which can be considered for the designing of one-dimensional nanostructures having efficient renal clearance.

Surface Chemistry

Along with size, the surface chemistry of NPs determines their interactions with biological systems. After entering systemic circulation, around 3000 serum proteins could interact with the surface of NPs and form “protein corona.” Surface properties of NPs can make an important contribution for uptake by macrophages in the spleen, liver, and lymph nodes (RES organs), leading to long-term accumulation and unpredicted localization in the body [83–85]. Hydrophobic surface possessing NPs are preferably taken up by the liver and then by the spleen and lungs. On the other hand, NPs possessing hydrophilic surfaces prepared from poly(vinyl pyrrolidone) (PVP) exhibit negligible (less than 1%) uptake by the liver and spleen, and around 5–10% of these NPs remain present in circulation (8 h after intravenous injection) [86, 87]. Choi HS and team synthesized a series on near-infrared fluorescent InAs

Table 17.1 Renal clearable inorganic NPs

Core structure of NPs	Surface modification	Surface charge	Core size/HD	Renal clearance	Imaging Technique	References
⁸⁹ Zr-DFO-PSMAi-PEG-Cy5-Cornell Prime Dots	PEG, ≈0.5 kDa	–	3.4/6.2	~26% ID in 4 h p.i.	PET	[56]
AuNPs	Gly-Cys	Negative	2.3/3.1	~42% ID in 24 h p.i.	Fluorescence	[57]
AuNPs	Cys		2.3/225	~22% ID in 24 h p.i.		
AuNPs, ⁶⁴ Cu-doped	GS	Negative	2–3/2.6	>75% ID in 24 h p.i.	PET	[58]
Nitrogen-doped carbon dots	Ethanolamine	–	3/–	–	Photoacoustic (PA) and photothermal therapy	[59]
Carbogenic small molecular complexes	–	–	>10 nm/(<1000 Da)	~80% ID in 24 h p.i.	Fluorescence	[60]
Porphyrin-PEG (2 kDa) polymer	PEG	–	Molecular mass = 16.2 kDa	~80% ID in 24 h p.i.	Fluorescence	[61]
ZW800-CDPL ⁺	–	Positive	–/4.4	45% ID in 4 h p.i.	Fluorescence	[62]
ZW800-CDPL [±]	–	Zwitterionic	–/4.6	85% ID in 4 h p.i.		
ZW800-CDPL [–]	–	Negative	–/4.9	80% ID in 4 h p.i.		
ZW800-CDPLAc	–	Neutral	–/4.8	90% ID in 4 h p.i.		
CuNPs, ⁶⁴ Cu-doped	GS	Negative	2/2.2	~80% ID in 24 h p.i.	PET	[52]
CuS, ⁶⁴ Cu-doped	PVP	Positive	4.3/5.6	~95% ID in 24 h p.i.	PET	[63]
VivoTag-680XL and ⁸⁹ Zr co-labeled dextran NPs	Succinic anhydride	Negative	13/5	75% ID g ^{–1} in 3 h p.i.	Fluorescence	[64]
¹²⁴ I-cRGDY-PEG-C dots	PEG ≈0.5 kDa	–	10/7	~50% ID in 24 h p.i. and ~72% ID in 96 h p.i.	PET	[65]
Iron oxide NPs	Dopamine sulfonate	Zwitterionic	3/4.7	65% ID in 4 h p.i.	MRA and MRI	[66]
Gadolinium-embedded iron oxide NPs	Dopamine sulfonate	Zwitterionic	2.8/4.18	<10% ID remaining in the blood 4 h p.i. for 4.8 nm NPs	T1 contrast	[50]
			3.5/5.61	–		
			4.8/6.50	–		

(continued)

Table 17.1 (continued)

Core structure of NPs	Surface modification	Surface charge	Core size/HD	Renal clearance	Imaging Technique	References
AuNPs	GS	–	2.5/3.3	<10% ID remaining in the normal tissue for >24 h p.i.	Fluorescence	[33]
Cy7-labeled graphene QDs	PEG 2000	–	3–5/5.5	>50% ID in 4 h p.i.	Fluorescence	[67]
⁶⁴ Cu-labeled carbon dots	PEG	Neutral	3/4.1	250% ID g ⁻¹ in 30 min p.i.	Fluorescence and PET	[68]
CDP-based siRNA	PEG	Weakly positive	60–100/	33% ID cm ⁻³ in 10 min p.i.	PET	[69]
¹⁹⁸ Au-doped gold NPs	GS	–	2.6/3	>50% ID in 48 h p.i.	Fluorescence and SPECT	[70]
InP/ZnS QDs	Dendron molecule and DHLA-PEG-COOH	–	~5/12	~60% ID in 24 h p.i.	Fluorescence	[71]
AuNPs	GS	–	2/2	50% ID in 24 h p.i.	X-ray CT	[47]
		Negative	1.7/2.4	52.5% ID in 24 h p.i.		
		Negative	6/–	4% ID in 24 h p.i.		
AuNPs	TPPMS	Negative	5/12.1	0.07% ID in 24 h p.i.	TEM	[72]
			18/21	0.003% ID in 24 h p.i.		
AuNPs	PEG	Negative	51.4/78.8	–	TEM	[73]
	PEG	Neutral	2.3/5.5	~50% ID in 24 h p.i.		
Short-rod mesoporous silica NPs doped with FITC	UnPEGylated	Neutral	Aspect ratio ≈1.5, length ≈185 nm	180 μg silica per gram urine 2 h p.i.	Fluorescence	[74]
	PEG	Neutral	Aspect ratio ≈1.5, length ≈185 nm	120 μg silica per gram urine 2 h p.i.		
Long rod mesoporous silica NPs doped with FITC	UnPEGylated	Weakly positive	Aspect ratio ≈5, length ≈720 nm	100 μg silica per gram urine 2 h p.i.	Fluorescence	[75]
	PEG	Neutral	Aspect ratio ≈5, length ≈720 nm	50 μg silica per gram urine 2 h p.i.		
InAs/ZnS	DHLA-PEG4	Neutral	3.2/5.6	47% ID at 4 h p.i.,	Fluorescence	[75]
	DHLA-PEG14	Neutral	3.2/8.7	~0% ID in 4 h p.i.		
CdSe/ZnCdS QDs	Cys	Zwitterionic	3.4/5.5	>65% ID in 4 h p.i.	Fluorescence	[76]

(continued)

Table 17.1 (continued)

Core structure of NPs	Surface modification	Surface charge	Core size/HD	Renal clearance	Imaging Technique	References
C-dots	PEG, ≈ 0.5 kDa	Neutral	~ 3.3	73% ID in 48 h p.i.	PET	[48]
		Neutral	~ 6	64% ID in 48 h p.i.		
SWCNT- [[^{86}Y] DOTA] (AF488) (AF680)]	–	Neutral	Diameter ≈ 1 nm, $100 \leq$ length ≤ 500 nm	$\sim 20\%$ ID g^{-1} in 60 min p.i.	Fluorescence	[77]
^{111}In -labeled MWNTs	DTPA	–	Diameter = 20–30 nm, length = 0.5–2 μm	12% ID g^{-1} in 24 h p.i.	SPECT	[78]
$^{99\text{m}}\text{Tc}$ -CdSe/ ZnS	Cys	Zwitterionic	2.85/4.36	75.13% ID in 4 h p.i.	Fluorescence	[55]
			3.02/4.99	62.18% ID in 4 h p.i.		
			3.3/5.52	43.65% ID in 4 h p.i.		
			3.8/6.7	23.35% ID in 4 h p.i.		
			4.31/8.65	18.02% ID in 4 h p.i.		
$\text{Au}_{10-11}\text{SG}_{10-11}$	GS	Negative	$< 1/-$	19.07% ID in 24 h p.i.	Fluorescence	[24]
$\text{Au}_{15}\text{SG}_{13}$	GS	Negative	$< 1/-$	22.90% ID in 24 h p.i.		
$\text{Au}_{18}\text{SG}_{14}$	GS	Negative	$< 1/-$	26.82% ID in 24 h p.i.		
$\text{Au}_{25}\text{SG}_{18}$	GS	Negative	$\sim 1/-$	51.57% ID in 24 h p.i.		

(ZnS) core (shell) QDs by varying surface chemistry using PEGs of different chain lengths. Dihydropolipoic acid (DHLA)-PEG2-coated QDs having an HD of 5.1 nm were retained in the liver despite their small size. On the other hand, DHLA-PEG4-coated QDs having a HD of 5.6 nm passed through glomerular filter slits and displayed rapid renal clearance. Even though PEG is an inert molecule, variation in chain length and chemical structure exhibited different surface chemistry and led to the altered biodistribution and renal clearance. Rapid clearance of DHLA-PEG4-coated QDs was attributed to hydrophilicity, and QDs with ultrashort-chain PEG2 were remained in the liver either due to hydrophobic character or specific recognition of the short chain [75]. Another surface chemistry approach used to minimize the surface protein binding is the use of zwitterionic ligands. The cysteine-coated

QDs having a small HD of 5.5 nm can effectively be cleared from the body. As cysteine ligand can enhance renal clearance, cysteine-coated AuNPs with a size of 3.5 ± 0.9 nm were prepared, and these NPs were found unstable and formed aggregates of 220 ± 60 nm quickly in phosphate-buffered saline before in vivo administration. Similar results were also found for citrate-coated AuNPs. Furthermore, tripeptide GS was used and luminescent GS-AuNPs of the size 2 nm were synthesized. Biodistribution and renal clearance revealed more than 50% of ID was eliminated from urine after intravenous administration and only $3.7 \pm 1.9\%$ of ID was found in the liver [22, 47, 88]. Comparison of zwitterionization and PEGylation of luminescent AuNP surface modifications revealed different effects on biodistribution and tumor targeting. Both surface modification modalities led to efficient renal

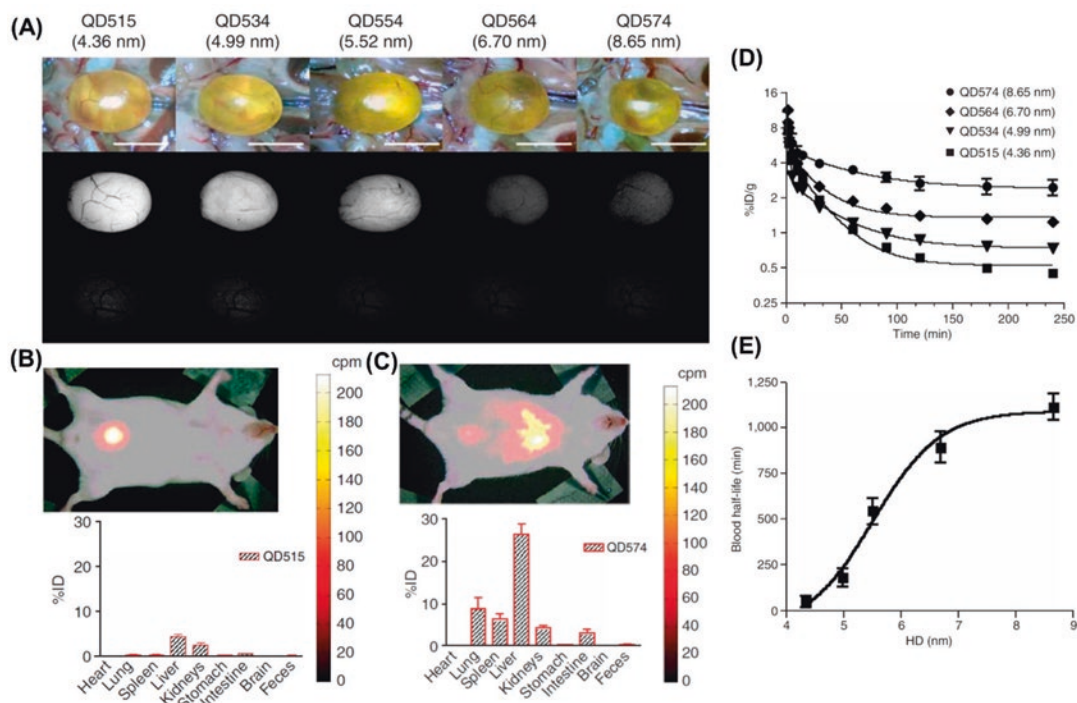


Fig. 17.1 (a) Surgically exposed CD-1 mouse bladders after intravenous injection of QD515, QD534, QD554, QD564, or QD574 of defined hydrodynamic diameter. Shown are color video (top) and fluorescence images (bottom) for un.injected control bladder and 4 h after injection (middle) for each QD. (b) Radioscintigraphic images of ^{99m}Tc -QD515 (4.36 nm) at 4 h p.i. (c) In vivo body clearance analysis of ^{99m}Tc -QD574 (8.65 nm) as

described for 1(B). (d) Blood concentration ($\% \text{ID g}^{-1}$) of ^{99m}Tc -labeled QDs after intravenous injection into CD-1 mice. Each data point is the mean \pm s.d. from $N = 5$ animals. (e) Blood half-life (mean \pm 95% confidence intervals) as a function of hydrodynamic diameter calculated from the data in 1(D). (Reproduced with permission [55]. Copyright 2007, Springer Nature)

clearance and comparable low uptake in the RES. PEG-AuNPs exhibited high tumor targeting efficiency and specificity, whereas GS-AuNPs displayed rapid tumor detection [33].

Surface Charge

The charges on the surface of NPs also play a critical role in renal filtration as the glomerular capillary wall possesses a negative charge due to the presence of heparan sulfate proteoglycan in the endothelial glycocalyx and can act as a barrier with selective charge [89, 90]. Hence, cationic NPs can easily cross the kidney filtration barrier due to favorable electrostatic interactions, whereas anionic NPs or neutral NPs can accumulate in the kidney due to disfavored interactions. For instance, posi-

tively charged gold composite nanodevices with 5 nm size displayed rapid renal clearance than negatively charged gold composite nanodevice of the same size [91]. In another study for effect of charge on renal clearance, ultrasmall cationic and anionic QDs with HDs of 5.67 nm and 3.7 nm were synthesized, and their clearance was determined. The anionic mercaptosuccinic acid (MSA)-capped QDs were retained in the kidney due to charge-dependent repulsion with negatively charged GBM, whereas cationic polyethylenimine (PEA)-conjugated QDs were detected in renal tubules and quickly eliminated via the kidney. The failure of MSA QDs to be excreted by the renal route was unlikely due to an increase in the size caused by protein binding after injection [92].

3 Tumor Targeting with NPs

The vascular system in tumorous tissues has unique characteristics of leaky vessels and pores through endothelial gaps (100 nm to 2 μ m) and defective lymphatic system. This defective vascularate disables drainage of the intratumoral components and leads to their accumulation into tumoral tissues [93, 94]. The relatively effective and selective tumor-accumulating properties of NPs are due to the EPR effect [93]. In 1986, the concept of the EPR mechanism was demonstrated by Matsumura and Maeda in solid murine tumors [95]. Various studies confirmed the accumulation of macromolecules like plasma proteins, protein-polymer conjugates, DNA complexes, liposomes, micelles, and even inorganic NPs in tumor tissues than in normal tissues due to the EPR effect. However, biocompatible macromolecules with a molecular weight greater than 40KDa tend to target tumor tissues via the EPR effect [96–98]. In the study reported by Sykes EA and co-workers, it was detected that perfusion of AuNPs was dependent on their size as well as the size of the tumor. From the study, it was concluded that AuNPs with a size less than 45 nm can permeate easily into the tumor without bothering its size, and these NPs can be used for the diagnosis or treatment of cancer [99]. NPs can accumulate at tumor sites through active or passive targeting, and tumor targeting by NPs is due to the fact that they can escape rapid renal filtration and circulate in blood plasma at higher concentration for a longer duration of period [100, 101]. Nonetheless, once the NPs are renal clearable, the EPR effect may become negligible due to rapid renal clearance and low tumor targeting. Some studies were undertaken to resolve the dilemma between the effective accumulation of NPs into tumor tissues and renal clearance [102].

3.1 Passive Tumor Targeting

The passive targeting comprises the site-specific accumulation of NPs through the leaky vasculature of the tumor and thus making the EPR effect a basis for passive tumor targeting by NPs [103].

To understand effective tumor accumulation and renal clearance of NPs, Liu J and co-workers reported passive tumor targeting and renal clearance of IRdye 800CW and GS-AuNPs (HD of 3.3 nm). During *in vivo* fluorescence imaging of MCF-7 tumor-bearing nude mice, both probes displayed rapid distribution in mice after intravenous injection, and maximum accumulation at the sites of tumors was observed within 40 min. However, retention kinetics of both probes in normal tissues as well as in tumors were found significantly distinct. Both probes showed two-compartment pharmacokinetics with a distribution half-life around 5 min, whereas the elimination half-lives were found 8.5 ± 2.1 h for GS-AuNPs and 0.98 ± 0.08 h for IRdye 800CW. A significant decrease in fluorescence from tumor in mouse was observed at 12 h p.i. and less than 5% of the maximum fluorescence was detected at the tumor site after 24 h p.i., which indicated rapid clearance of the dye. GS-AuNPs displayed different retention kinetics in normal tissue and tumor. More than 90% of GS-AuNPs were cleared out from the normal tissue (half-life of 43.4 min) which was more than three times faster than the IRdye 800CW. Tumor uptakes for GS-AuNPs and IRdye 800CW were found $2.3 \pm 0.2\%$ ID/g and $0.2 \pm 0.02\%$ ID/g, respectively, at 12 h p.i. which indicated long tumor retention of NPs. The contrast index (the parameter used to quantify the quality of imaging) of the GS-AuNPs increased quickly and reached the tumor detection threshold (CI = 2.5) which was almost three times faster than IRdye 800CW (Fig. 17.2). This prolonged retention of renal clearable NPs (HD = 3.3 nm) in the tumor is due to passive targeting through the EPR effect. The origin of the EPR effect in renal clearable GS-AuNPs is expected since these luminescent AuNPs evaded the uptake of the RES organs and remained present in blood plasma with slow renal elimination (half-life of 8.5 h) [104]. Factors responsible for the EPR effect include vascular permeability; MPS activity; intratumor pressure; tumor type, size, and location; as well as circulation time of NPs [105, 106]. Several physicochemical properties of NPs that influence EPR-based tumor targeting include particle size,

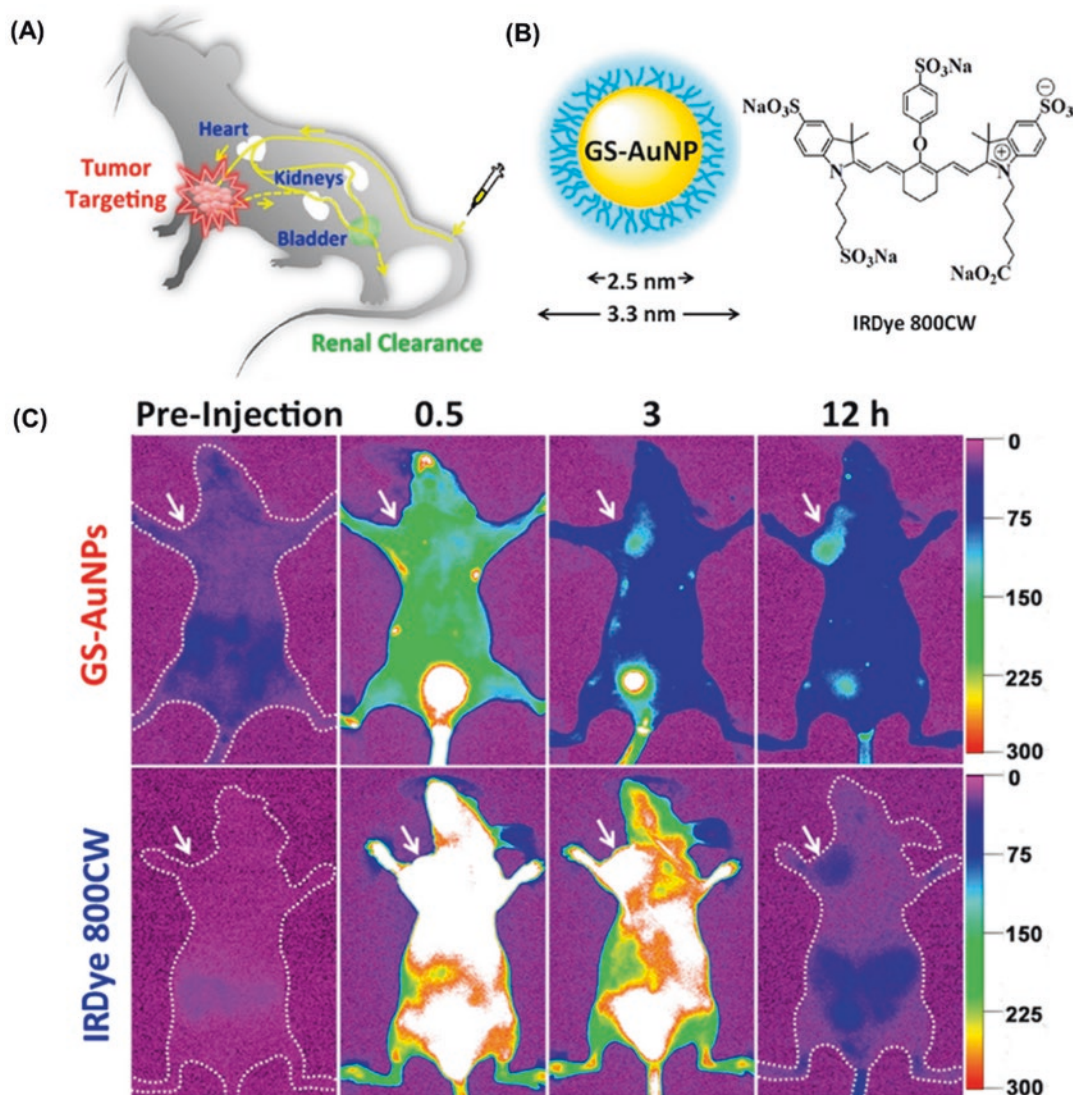


Fig. 17.2 (a) Scheme of passive tumor targeting of renal clearable probes. In vivo tumor targeting and clearance kinetics can be measured by fluorescence imaging in real time after intravenous injection of the probes into nude mice. (b) Schematic representation of a glutathione-coated luminescent gold nanoparticle (GS-AuNP) and the

structure of IRDye 800CW. (c) Representative in vivo NIR fluorescence images of MCF-7 tumor-bearing mice IV-injected with GS-AuNPs and IRDye 800CW. The tumor areas are indicated with arrows. (Reprinted with permission [104]. Copyright 2013, American Chemical Society)

shape, surface charge, etc. [94, 105]. Liu J et al. observed the effect of PEGylation on AuNPs for passive tumor targeting and renal clearance. In the kinetic study through in vivo fluorescence imaging, the PEG-AuNPs acquired around 12 h to reach the contrast index threshold ($\text{CI} = 2.5$) and were retained until 48 h p.i. in nude mice bearing MCF-7 tumor. Compared to zwitterionic

GS-AuNPs, PEG-AuNPs exhibited three times higher tumor targeting efficiency, although both displayed comparable low RES uptake. The PEG-AuNPs displayed tumor targeting efficiency with a tumor/blood ratio of 9.0 ± 1.3 at 48 h p.i., and from that, they came to the conclusion that the strong EPR effect was enhanced due to their extended retention time and higher concentration

of in the blood. The distribution half-life for PEG-AuNPs was found 56.1 ± 9.7 min, which was one order longer than that of GS-AuNPs (5.4 ± 1.2 min), whereas the elimination half-lives of PEG-AuNPs (9.2 ± 3.9 h) and GS-AuNPs (8.5 ± 2.1 h) were found comparable. The area under the curve for PEG-AuNPs was 142.8% ID h g^{-1} , which was three times higher than that for the GS-AuNPs (47.2% ID h g^{-1}) at 24 h p.i. The study revealed that larger AUC of PEG-AuNPs in blood is responsible for high tumor targeting efficiency and is basically a result of the fact that PEGylation can increase the EPR effect of renal clearable AuNPs relative to zwitterionization. However, the limitation of PEGylation in tumor imaging is that it acquired much longer time for the PEG-AuNPs to reach the desired CI than the GS-AuNPs because of the slow tumor accumulation and normal tissue clearance of the PEG-AuNPs [33].

3.2 Active Tumor Targeting

In addition to passive targeting based on the EPR effect, active targeting was employed as a complementary approach for improving tumor localization of NPs by increasing their accumulation and retention at the target site. In this approach, different ligands on the surface of NPs are utilized to recognize receptors overexpressed on the cell surface of tumor tissues [105, 107, 108]. The first indication of this phenomenon was proposed for the fluorescent liposomes covalently coupled with antibodies [109]. In the study on renal clearable QDs, the CI value was found 1.8, i.e., lower than that of GS-AuNPs (CI = 3.0). Furthermore, conjugating QDs with targeting ligands like cRGD (monomeric cyclic Arg-Gly-Asp peptide) and GPI (2-[(3-amino-3-carboxypropyl)(hydroxy)phosphinyl]-methyl]pentane-1,5-dioic acid) led to an increase in CI values to 6.9 and 5.0, respectively [76, 110]. Gao X and co-workers reported three different surface modification strategies for semiconductor QDs, viz., amphiphilic tri-*n*-octylphosphine oxide (TOPO) coating (-COOH groups), PEG coating and conjugation of PEG plus prostate-specific mem-

brane antigen (PSMA) monoclonal antibody. During *in vivo* imaging in mice, -COOH group bearing probes did not show any tumor signals and PEG-coated probes exhibited only weak tumor signals (passive targeting). However, PEG-PSMA antibody conjugated probes displayed intense tumor signals due to active targeting. The imaging results were found consistent with the histological examinations. The study revealed that active tumor targeting with a tumor-specific ligand/antibody was found much faster and more efficient as compared to passive targeting [111]. Sykes EA and co-workers investigated the effect of NP size on active and passive targeting using spherical AuNPs with different core sizes (15, 30, 60, and 100 nm). Surface modification strategies were employed using PEG or PEG-conjugated OPSS-modified transferrin for active and passive targeting of MDA-MB-435 orthotopic tumor xenografts. The study revealed that the active targeting only increased the tumor uptake of NPs having 60 nm size when compared to their passive counterparts, whereas 15, 30, and 100 nm NPs did not display any significant differences [112]. This investigation proposes the complexity involved with manipulating the active targeting of tumors by NPs.

4 Conclusion

During the past years, advanced nanotechnology has shown great promise in the diagnosis and treatment of cancer, and significant progress has been made in the development of NP-based cancer diagnostics. Compared to the conventional cancer diagnostics available in the clinic, a variety of NP-based imaging probes presented improvement in terms of selectivity and sensitivity that could not be achieved with traditional approaches. However, clinical translation of diagnostic NPs has been hindered due to their prolonged tissue retention and potential toxicities. The ultrasmall inorganic NPs with efficient renal clearance provide fast kidney filtration and thereby minimize their tissue retention and promote their clinical application. Owing to the anatomy of kidneys, various physicochemical

properties of NPs, such as particle size, particle shape, surface chemistry, and charge determine their interactions with different compartments of the kidney and thus affect their in vivo transport along with their clearance. The tumor accumulation of NPs depends on the EPR effect. Furthermore, the integration of tumor targeting by EPR effect and efficient renal clearance results in the synergistic effect on tumor imaging. A variety of renal clearable NPs including QDs, gold NPs, silica NPs, iron oxide NPs, carbon dots, copper NPs, as well as nanoclusters (NCs) have displayed their potential in cancer diagnosis. These NPs generally possess a small core size, i.e., below the KFT which facilitates their rapid excretion from the body through the renal route. Moreover, the renal clearable NPs have reduced accumulation rate in RES organs and toxicities caused by their retention in the body, making them a good application prospect in the treatment of cancer such as drug loading and photothermal therapy. NPs possessing both diagnostic and therapeutic functionalities in a single formulation open an opportunity for the delivery of nanomedicine into clinical cancer therapy. In spite of the enhanced and prolonged tumor retention of various NPs that is extensively detected in the preclinical investigation, most NP-based drug delivery systems exhibit limited improvements in the overall progression-free survival of patients compared with free drugs, which stress continuing the efforts with close collaboration among researchers from various disciplines to deeply understand the clearance and tumor targeting of NPs, so that they can be translated into clinical practices.

References

1. Global cancer observatory. <https://gco.iarc.fr/>. Accessed 13 Jul 2021.
2. Chen X, Gole J, Gore A, et al. Non-invasive early detection of cancer four years before conventional diagnosis using a blood test. *Nat Commun.* 2020;11:1–10. <https://doi.org/10.1038/s41467-020-17316-z>.
3. Fass L. Imaging and cancer: a review. *Mol Oncol.* 2008;2:115–52.
4. Frangioni JV. New technologies for human cancer imaging. *J Clin Oncol.* 2008;26:4012–21.
5. Leng F, Liu F, Yang Y, et al. Strategies on nanodiagnostics and nanotherapies of the three common cancers. *Nano.* 2018;8:1–15. <https://doi.org/10.3390/nano8040202>.
6. Ma YY, Jin KT, Wang SB, et al. Molecular imaging of cancer with nanoparticle-based theranostic probes. *Contrast Media Mol Imaging.* 2017;2017:1026270.
7. Ferrari M. Cancer nanotechnology: opportunities and challenges. *Nat Rev Cancer.* 2005;5:161–71. <https://doi.org/10.1038/nrc1566>.
8. Laroui H, Rakhya P, Xiao B, et al. Nanotechnology in diagnostics and therapeutics for gastrointestinal disorders. *Dig Liver Dis.* 2013;45:995–1002. <https://doi.org/10.1016/j.dld.2013.03.019>.
9. Jeevanandam J, Barhoum A, Chan YS, et al. Review on nanoparticles and nanostructured materials: history, sources, toxicity and regulations. *Beilstein J Nanotechnol.* 2018;9:1050–74. <https://doi.org/10.3762/bjnano.9.98>.
10. Liang R, Wei M, Evans DG, Duan X. Inorganic nanomaterials for bioimaging, targeted drug delivery and therapeutics. *Chem Commun.* 2014;50:14071–81. <https://doi.org/10.1039/C4CC03118K>.
11. Prasad R, Jain NK, Conde J, Srivastava R. Localized nanotheranostics: recent developments in cancer nanomedicine. *Mater Today Adv.* 2020;8:100087. <https://doi.org/10.1016/j.mtadv.2020.100087>.
12. Hussain T, Nguyen QT. Molecular imaging for cancer diagnosis and surgery. *Adv Drug Deliv Rev.* 2014;66:90–100.
13. Valizadeh A, Mikaeili H, Samiei M, et al. Quantum dots: synthesis, bioapplications, and toxicity. *Nanoscale Res Lett.* 2012;7:480.
14. Luo D, Wang X, Burda C, Basilion JP. Recent development of gold nanoparticles as contrast agents for cancer diagnosis. *Cancers (Basel).* 2021;13:1825. <https://doi.org/10.3390/cancers13081825>.
15. Kumar A, Mazinder Boruah B, Liang XJ. Gold nanoparticles: promising nanomaterials for the diagnosis of cancer and HIV/AIDS. *J Nanomater.* 2011;2011:202187.
16. Martinkova P, Brtnicky M, Kynicky J, Pohanka M. Iron oxide nanoparticles: innovative tool in cancer diagnosis and therapy. *Adv Healthc Mater.* 2018;7(5):1700932. <https://doi.org/10.1002/adhm.201700932>.
17. Hernández-Hernández AA, Aguirre-Álvarez G, Cariño-Cortés R, et al. Iron oxide nanoparticles: synthesis, functionalization, and applications in diagnosis and treatment of cancer. *Chem Pap.* 2020;74:3809–24.
18. Nie J, Li Y, Han G, Qiu J. In vivo clearable inorganic nanophotonic materials: designs, materials and applications. *Nanoscale.* 2019;11:12742–54.
19. Yu M, Zheng J. Clearance pathways and tumor targeting of imaging nanoparticles. *ACS Nano.* 2015;9:6655–74. <https://doi.org/10.1021/acsnano.5b01320>.

20. Gattoo MA, Naseem S, Arfat MY, et al. Physicochemical properties of nanomaterials: implication in associated toxic manifestations. *Biomed Res Int*. 2014;2014:498420. <https://doi.org/10.1155/2014/498420>.
21. Feliu N, Docter D, Heine M, et al. In vivo degeneration and the fate of inorganic nanoparticles. *Chem Soc Rev*. 2016;45:2440–57. <https://doi.org/10.1039/c5cs00699f>.
22. Longmire M, Choyke PL, Kobayashi H. Clearance properties of nano-sized particles and molecules as imaging agents: considerations and caveats. *Nanomedicine*. 2008;3:703–17. <https://doi.org/10.2217/17435889.3.5.703>.
23. Poon W, Zhang YN, Ouyang B, et al. Elimination pathways of nanoparticles. *ACS Nano*. 2019;13:5785–98. <https://doi.org/10.1021/acsnano.9b01383>.
24. Du B, Jiang X, Das A, et al. Glomerular barrier behaves as an atomically precise bandpass filter in a sub-nanometre regime. *Nat Nanotechnol*. 2017;12:1096–102. <https://doi.org/10.1038/nnano.2017.170>.
25. Li X, Wang B, Zhou S, et al. Surface chemistry governs the sub-organ transfer, clearance and toxicity of functional gold nanoparticles in the liver and kidney. *J Nanobiotechnol*. 2020;18:45. <https://doi.org/10.1186/S12951-020-00599-1>.
26. Zhang G, Yang Z, Lu W, et al. Influence of anchoring ligands and particle size on the colloidal stability and in vivo biodistribution of polyethylene glycol-coated gold nanoparticles in tumor-xenografted mice. *Biomaterials*. 2009;30:1928–36. <https://doi.org/10.1016/j.biomaterials.2008.12.038>.
27. Wang Y, Black KCL, Luehmann H, et al. Comparison study of gold nanohexapods, nanorods, and nanocages for photothermal cancer treatment. *ACS Nano*. 2013;7:2068–77. <https://doi.org/10.1021/nl304332s>.
28. Hong G, Robinson JT, Zhang Y, et al. In vivo fluorescence imaging with Ag₂S quantum dots in the second near-infrared region. *Angew Chem Int Ed Engl*. 2012;51:9818–21. <https://doi.org/10.1002/anie.201206059>.
29. Song X, Gong H, Yin S, et al. Ultra-small iron oxide doped polypyrrole nanoparticles for in vivo multimodal imaging guided Photothermal therapy. *Adv Funct Mater*. 2014;24:1194–201. <https://doi.org/10.1002/adfm.201302463>.
30. Liu Z, Cai W, He L, et al. In vivo biodistribution and highly efficient tumour targeting of carbon nanotubes in mice. *Nat Nanotechnol*. 2007;2:47–52. <https://doi.org/10.1038/nnano.2006.170>.
31. Chen F, Hong H, Zhang Y, et al. In vivo tumor targeting and image-guided drug delivery with antibody-conjugated, radiolabeled mesoporous silica nanoparticles. *ACS Nano*. 2013;7:9027–39. <https://doi.org/10.1021/nl3043617j>.
32. Alexis F, Pridgen E, Molnar LK, Farokhzad OC. Factors affecting the clearance and bio-distribution of polymeric nanoparticles. *Mol Pharm*. 2008;5:505–15. <https://doi.org/10.1021/mp800051m>.
33. Liu J, Yu M, Ning X, et al. PEGylation and zwitterionization: pros and cons in the renal clearance and tumor targeting of near-IR-emitting gold nanoparticles. *Angew Chem Int Ed Engl*. 2013;52:12572–6. <https://doi.org/10.1002/anie.201304465>.
34. Guerrini L, Alvarez-Puebla RA, Pazos-Perez N. Surface modifications of nanoparticles for stability in biological fluids. *Materials (Basel)*. 2018;11:1154.
35. Maguire CM, Rösslein M, Wick P, Prina-Mello A. Characterisation of particles in solution—a perspective on light scattering and comparative technologies. *Sci Technol Adv Mater*. 2018;19:732–45.
36. Fischer HC, Liu L, Pang KS, Chan WCW. Pharmacokinetics of nanoscale quantum dots: in vivo distribution, sequestration, and clearance in the rat. *Adv Funct Mater*. 2006;16:1299–305. <https://doi.org/10.1002/adfm.200500529>.
37. Liu H, Pierre-Pierre N, Huo Q. Dynamic light scattering for gold nanorod size characterization and study of nanorod-protein interactions. *Gold Bull*. 2012;45:187–95. <https://doi.org/10.1007/s13404-012-0067-4>.
38. Owens DE, Peppas NA. Opsonization, biodistribution, and pharmacokinetics of polymeric nanoparticles. *Int J Pharm*. 2006;307:93–102. <https://doi.org/10.1016/j.ijpharm.2005.10.010>.
39. Thi TTH, Pilkington EH, Nguyen DH, et al. The importance of Poly(ethylene glycol) alternatives for overcoming PEG immunogenicity in drug delivery and bioconjugation. *Polymers (Basel)*. 2020;12:298. <https://doi.org/10.3390/polym12020298>.
40. Ye L, Yong K-T, Liu L, et al. A pilot study in non-human primates shows no adverse response to intravenous injection of quantum dots. *Nat Nanotechnol*. 2012;7:453–8. <https://doi.org/10.1038/nnano.2012.74>.
41. Wang L, Li YF, Zhou L, et al. Characterization of gold nanorods in vivo by integrated analytical techniques: their uptake, retention, and chemical forms. *Anal Bioanal Chem*. 2010;396:1105–14. <https://doi.org/10.1007/s00216-009-3302-y>.
42. Kumar R, Roy I, Ohulchanskyy TY, et al. In vivo bio-distribution and clearance studies using multimodal organically modified silica nanoparticles. *ACS Nano*. 2010;4:699–708. <https://doi.org/10.1021/nl901146y>.
43. Ballou B, Ernst LA, Andreko S, et al. Sentinel lymph node imaging using quantum dots in mouse tumor models. *Bioconjug Chem*. 2007;18:389–96. <https://doi.org/10.1021/bc060261j>.
44. Sadauskas E, Danscher G, Stoltenberg M, et al. Protracted elimination of gold nanoparticles from mouse liver. *Nanomedicine*. 2009;5:162–9. <https://doi.org/10.1016/j.nano.2008.11.002>.
45. Yin R, Zhang X, Ge J, et al. Recent advances in renal clearable inorganic nanoparticles for cancer diagnosis. *Part Part Syst Charact*. 2021;38:1–17.

46. Peng C, Huang Y, Zheng J. Renal clearable nano-carriers: overcoming the physiological barriers for precise drug delivery and clearance. *J Control Release*. 2020;322:64–80. <https://doi.org/10.1016/j.jconrel.2020.03.020>.
47. Zhou C, Long M, Qin Y, et al. Luminescent gold nanoparticles with efficient renal clearance. *Angew Chem Int Ed Engl*. 2011;50:3168–72. <https://doi.org/10.1002/anie.201007321>.
48. Burns AA, Vider J, Ow H, et al. Fluorescent silica nanoparticles with efficient urinary excretion for nanomedicine. *Nano Lett*. 2009;9:442–8. <https://doi.org/10.1021/nl803405h>.
49. Tang S, Peng C, Xu J, et al. Tailoring renal clearance and tumor targeting of ultrasmall metal nanoparticles with particle density. *Angew Chem Int Ed Engl*. 2016;55:16039–43. <https://doi.org/10.1002/anie.201609043>.
50. Zhou Z, Wang L, Chi X, et al. Engineered iron-oxide-based nanoparticles as enhanced T1 contrast agents for efficient tumor imaging. *ACS Nano*. 2013;7:3287–96. <https://doi.org/10.1021/nl305991e>.
51. Skrabalak SE, Chen J, Sun Y, et al. Gold nanocages: synthesis, properties, and applications. *Acc Chem Res*. 2008;41:1587–95. <https://doi.org/10.1021/ar800018v>.
52. Yang S, Sun S, Zhou C, et al. Renal clearance and degradation of glutathione-coated copper nanoparticles. *Bioconjug Chem*. 2015;26:511–9. <https://doi.org/10.1021/acs.bioconjugchem.5b00003>.
53. Zhao Y, Sultan D, Detering L, et al. Facile synthesis, pharmacokinetic and systemic clearance evaluation, and positron emission tomography cancer imaging of 64Cu-Au alloy nanoclusters. *Nanoscale*. 2014;6:13501–9. <https://doi.org/10.1039/c4nr04569f>.
54. Singh R, Pantarotto D, Lacerda L, et al. Tissue biodistribution and blood clearance rates of intravenously administered carbon nanotube radiotracers. *Proc Natl Acad Sci U S A*. 2006;103:3357–62. <https://doi.org/10.1073/pnas.0509009103>.
55. Soo Choi H, Liu W, Misra P, et al. Renal clearance of quantum dots. *Nat Biotechnol*. 2007;25:1165–70. <https://doi.org/10.1038/nbt1340>.
56. Chen F, Ma K, Zhang L, et al. Ultrasmall renally clearable silica nanoparticles target prostate cancer. *ACS Appl Mater Interfaces*. 2019;11:43879–87. <https://doi.org/10.1021/acsami.9b15195>.
57. Ning X, Peng C, Li ES, et al. Physiological stability and renal clearance of ultrasmall zwitterionic gold nanoparticles: ligand length matters. *APL Mater*. 2017;5:053406. <https://doi.org/10.1063/1.4978381>.
58. Chen F, Goel S, Hernandez R, et al. Dynamic positron emission tomography imaging of renal clearable gold nanoparticles. *Small*. 2016;12:2775–82. <https://doi.org/10.1002/sml.201600194>.
59. Lee C, Kwon W, Beack S, et al. Biodegradable nitrogen-doped carbon nanodots for non-invasive photoacoustic imaging and photothermal therapy. *Theranostics*. 2016;6:2196–208. <https://doi.org/10.7150/thno.16923>.
60. He H, Wang Z, Cheng T, et al. Visible and near-infrared dual-emission carbogenic small molecular complex with high RNA selectivity and renal clearance for nucleolus and tumor imaging. *ACS Appl Mater Interfaces*. 2016;8:28529–37. <https://doi.org/10.1021/acsami.6b10737>.
61. Huang H, Hernandez R, Geng J, et al. A porphyrin-PEG polymer with rapid renal clearance. *Biomaterials*. 2016;76:25–32. <https://doi.org/10.1016/j.biomaterials.2015.10.049>.
62. Kang H, Gravier J, Bao K, et al. Renal-clearable organic nanocarriers for bioimaging and drug delivery. *Adv Mater*. 2016;28:8162–8. <https://doi.org/10.1002/adma.201601101>.
63. Zhou M, Li J, Liang S, et al. CuS nanodots with ultrahigh efficient renal clearance for positron emission tomography imaging and image-guided photothermal therapy. *ACS Nano*. 2015;9:7085–96. <https://doi.org/10.1021/acsnano.5b02635>.
64. Nair AV, Keliher EJ, Core AB, et al. Characterizing the interactions of organic nanoparticles with renal epithelial cells in vivo. *ACS Nano*. 2015;9:3641–53. <https://doi.org/10.1021/acsnano.5b00428>.
65. Phillips E, Penate-Medina O, Zanzonico PB, et al. Clinical translation of an ultrasmall inorganic optical-PET imaging nanoparticle probe. *Sci Transl Med*. 2014;6:1–10. <https://doi.org/10.1126/scitranslmed.3009524>.
66. Wei H, Bruns OT, Kaul MG, et al. Exceedingly small iron oxide nanoparticles as positive MRI contrast agents. *Proc Natl Acad Sci U S A*. 2017;114:2325–30. <https://doi.org/10.1073/pnas.1620145114>.
67. Chong Y, Ma Y, Shen H, et al. The in vitro and in vivo toxicity of graphene quantum dots. *Biomaterials*. 2014;35:5041–8. <https://doi.org/10.1016/j.biomaterials.2014.03.021>.
68. Huang X, Zhang F, Zhu L, et al. Effect of injection routes on the biodistribution, clearance, and tumor uptake of carbon dots. *ACS Nano*. 2013;7:5684–93. <https://doi.org/10.1021/nn401911k>.
69. Zuckerman JE, Choi CHJ, Han H, Davis ME. Polycation-siRNA nanoparticles can disassemble at the kidney glomerular basement membrane. *Proc Natl Acad Sci U S A*. 2012;109:3137–42. <https://doi.org/10.1073/pnas.1200718109>.
70. Zhou C, Hao G, Thomas P, et al. Near-infrared emitting radioactive gold nanoparticles with molecular pharmacokinetics. *Angew Chem Int Ed Engl*. 2012;51:10118–22. <https://doi.org/10.1002/anie.201203031>.
71. Gao J, Chen K, Luong R, et al. A novel clinically translatable fluorescent nanoparticle for targeted molecular imaging of tumors in living subjects. *Nano Lett*. 2012;12:281–6. <https://doi.org/10.1021/nl203526f>.
72. Hirn S, Semmler-Behnke M, Schleh C, et al. Particle size-dependent and surface charge-dependent biodistribution of gold nanoparticles after

- intravenous administration. *Eur J Pharm Biopharm.* 2011;77:407–16. <https://doi.org/10.1016/j.ejpb.2010.12.029>.
73. Choi CHJ, Zuckerman JE, Webster P, Davis ME. Targeting kidney mesangium by nanoparticles of defined size. *Proc Natl Acad Sci U S A.* 2011;108:6656–61. <https://doi.org/10.1073/pnas.1103573108>.
 74. Huang X, Li L, Liu T, et al. The shape effect of mesoporous silica nanoparticles on biodistribution, clearance, and biocompatibility in vivo. *ACS Nano.* 2011;5:5390–9. <https://doi.org/10.1021/nn200365a>.
 75. Choi HS, Ipe BI, Misra P, et al. Tissue- and organ-selective biodistribution of NIR fluorescent quantum dots. *Nano Lett.* 2009;9:2354–9. <https://doi.org/10.1021/nl900872r>.
 76. Choi HS, Liu W, Liu F, et al. Design considerations for tumour-targeted nanoparticles. *Nat Nanotechnol.* 2010;5:42–7. <https://doi.org/10.1038/nnano.2009.314>.
 77. Ruggiero A, Villa CH, Bander E, et al. Paradoxical glomerular filtration of carbon nanotubes. *Proc Natl Acad Sci U S A.* 2010;107:12369–74. <https://doi.org/10.1073/pnas.0913667107>.
 78. Lacerda L, Soundararajan A, Singh R, et al. Dynamic imaging of functionalized multi-walled carbon nanotube systemic circulation and urinary excretion. *Adv Mater.* 2008;20:225–30. <https://doi.org/10.1002/adma.200702334>.
 79. Haraldsson B, Nyström J, Deen WM. Properties of the glomerular barrier and mechanisms of proteinuria. *Physiol Rev.* 2008;88:451–87. <https://doi.org/10.1152/physrev.00055.2006>.
 80. Du B, Yu M, Zheng J. Transport and interactions of nanoparticles in the kidneys. *Nat Rev Mater.* 2018;3:358–74. <https://doi.org/10.1038/s41578-018-0038-3>.
 81. Choi HS, Frangioni JV. Nanoparticles for biomedical imaging: fundamentals of clinical translation. *Mol Imaging.* 2010;9:291–310. <https://doi.org/10.2310/7290.2010.00031>.
 82. Ruggiero A, Villa CH, Bander E, et al. Paradoxical glomerular filtration of carbon nanotubes. *Proc Natl Acad Sci.* 2010;107:12369–74. <https://doi.org/10.1073/PNAS.0913667107>.
 83. Khor SY, Vu MN, Pilkington EH, et al. Elucidating the influences of size, surface chemistry, and dynamic flow on cellular association of nanoparticles made by polymerization-induced self-assembly. *Small.* 2018;14:1801702. <https://doi.org/10.1002/smll.201801702>.
 84. Lynch I, Dawson KA. Protein-nanoparticle interactions. *Nano Today.* 2008;3:40–7.
 85. Walkey CD, Olsen JB, Guo H, et al. Nanoparticle size and surface chemistry determine serum protein adsorption and macrophage uptake. *J Am Chem Soc.* 2012;134:2139–47. <https://doi.org/10.1021/ja2084338>.
 86. Brannon-Peppas L, Blanchette JO. Nanoparticle and targeted systems for cancer therapy. *Adv Drug Deliv Rev.* 2004;56:1649–59. <https://doi.org/10.1016/j.addr.2004.02.014>.
 87. Gaur U, Sahoo SK, De TK, et al. Biodistribution of fluoresceinated dextran using novel nanoparticles evading reticuloendothelial system. *Int J Pharm.* 2000;202:1–10. [https://doi.org/10.1016/S0378-5173\(99\)00447-0](https://doi.org/10.1016/S0378-5173(99)00447-0).
 88. Dekany I, Majzik A, Patakfalvi R, Hornok V. Growing and stability of gold nanoparticles and their functionalization by cysteine. *Gold Bull.* 2009;42:113–23.
 89. Miner JH. The glomerular basement membrane. *Exp Cell Res.* 2012;318:973–8. <https://doi.org/10.1016/J.YEXCR.2012.02.031>.
 90. Menon MC, Chuang PY, He CJ. The glomerular filtration barrier: components and crosstalk. *Int J Nephrol.* 2012;2012:749010. <https://doi.org/10.1155/2012/749010>.
 91. Balogh L, Nigavekar SS, Nair BM, et al. Significant effect of size on the in vivo biodistribution of gold composite nanodevices in mouse tumor models. *Nanomedicine.* 2007;3:281–96. <https://doi.org/10.1016/j.nano.2007.09.001>.
 92. Liang X, Wang H, Zhu Y, et al. Short-and long-term tracking of anionic ultrasmall nanoparticles in kidney. *ACS Nano.* 2016;10:387–95. <https://doi.org/10.1021/acsnano.5b05066>.
 93. Siemann DW. The unique characteristics of tumor vasculature and preclinical evidence for its selective disruption by Tumor-Vascular Disrupting Agents. *Cancer Treat Rev.* 2011;37:63–74. <https://doi.org/10.1016/j.ctrv.2010.05.001>.
 94. Kalyane D, Raval N, Maheshwari R, et al. Employment of enhanced permeability and retention effect (EPR): nanoparticle-based precision tools for targeting of therapeutic and diagnostic agent in cancer. *Mater Sci Eng C.* 2019;98:1252–76. <https://doi.org/10.1016/j.msec.2019.01.066>.
 95. Matsumura Y, Maeda H. A new concept for macromolecular therapeutics in cancer chemotherapy: mechanism of tumoritropic accumulation of proteins and the antitumor agent smancs. *Cancer Res.* 1986;46:6387–92.
 96. Golombek SK, May JN, Theek B, et al. Tumor targeting via EPR: strategies to enhance patient responses. *Adv Drug Deliv Rev.* 2018;130:17–38. <https://doi.org/10.1016/j.addr.2018.07.007>.
 97. Toy R, Bauer L, Hoimes C, et al. Targeted nanotechnology for cancer imaging. *Adv Drug Deliv Rev.* 2014;76:79–97. <https://doi.org/10.1016/j.addr.2014.08.002>.
 98. Maeda H. Vascular permeability in cancer and infection as related to macromolecular drug delivery, with emphasis on the EPR effect for tumor-selective drug targeting. *Proc Jpn Acad Ser B Phys Biol Sci.* 2012;88:53–71. <https://doi.org/10.2183/pjab.88.53>.
 99. Sykes EA, Dai Q, Sarsons CD, et al. Tailoring nanoparticle designs to target cancer based on tumor pathophysiology. *Proc Natl Acad Sci U S A.*

- A. 2016;113:E1142–51. <https://doi.org/10.1073/pnas.1521265113>.
100. Bertrand N, Wu J, Xu X, et al. Cancer nanotechnology: the impact of passive and active targeting in the era of modern cancer biology. *Adv Drug Deliv Rev.* 2014;66:2–25. <https://doi.org/10.1016/j.addr.2013.11.009>.
101. Iyer AK, Khaled G, Fang J, Maeda H. Exploiting the enhanced permeability and retention effect for tumor targeting. *Drug Discov Today.* 2006;11:812–8. <https://doi.org/10.1016/j.drudis.2006.07.005>.
102. Wang Y, Wang Z, Xu C, et al. A disassembling strategy overcomes the EPR effect and renal clearance dilemma of the multifunctional theranostic nanoparticles for cancer therapy. *Biomaterials.* 2019;197:284–93. <https://doi.org/10.1016/j.biomaterials.2019.01.025>.
103. Navya PN, Kaphle A, Srinivas SP, et al. Current trends and challenges in cancer management and therapy using designer nanomaterials. *Nano Converg.* 2019;6:23. <https://doi.org/10.1186/s40580-019-0193-2>.
104. Liu J, Yu M, Zhou C, et al. Passive tumor targeting of renal-clearable luminescent gold nanoparticles: Long tumor retention and fast normal tissue clearance. *J Am Chem Soc.* 2013;135:4978–81. <https://doi.org/10.1021/ja401612x>.
105. Attia MF, Anton N, Wallyn J, et al. An overview of active and passive targeting strategies to improve the nanocarriers efficiency to tumour sites. *J Pharm Pharmacol.* 2019;71:1185–98. <https://doi.org/10.1111/jphp.13098>.
106. Prabhakar U, Maeda H, et al. Challenges and key considerations of the enhanced permeability and retention effect for nanomedicine drug delivery in oncology. *Cancer Res.* 2013;73:2412–7. <https://doi.org/10.1158/0008-5472.CAN-12-4561>.
107. Danhier F, Feron O, Préat V. To exploit the tumor microenvironment: passive and active tumor targeting of nanocarriers for anti-cancer drug delivery. *J Control Release.* 2010;148:135–46. <https://doi.org/10.1016/j.jconrel.2010.08.027>.
108. Rosenblum D, Joshi N, Tao W, et al. Progress and challenges towards targeted delivery of cancer therapeutics. *Nat Commun.* 2018;9:1410. <https://doi.org/10.1038/s41467-018-03705-y>.
109. Leserman LD, Barbet J, Kourilsky F, Weinstein JN. Targeting to cells of fluorescent liposomes covalently coupled with monoclonal antibody or protein A. *Nature.* 1980;288:602–4. <https://doi.org/10.1038/288602a0>.
110. Liu J, Yu M, Zhou C, Zheng J. Renal clearable inorganic nanoparticles: a new frontier of bionanotechnology. *Mater Today.* 2013;16:477–86. <https://doi.org/10.1016/j.mattod.2013.11.003>.
111. Gao X, Cui Y, Levenson RM, et al. In vivo cancer targeting and imaging with semiconductor quantum dots. *Nat Biotechnol.* 2004;22:969–76. <https://doi.org/10.1038/nbt994>.
112. Sykes EA, Chen J, Zheng G, Chan WCW. Investigating the impact of nanoparticle size on active and passive tumor targeting efficiency. *ACS Nano.* 2014;8:5696–706. <https://doi.org/10.1021/NN500299P>.



PLGA Nanoparticles for Oral Delivery: Nephrotoxicity and Pharmacokinetic Studies

18

Neelu Singh, Nidhi Mishra, Kaiser Raza,
and Poonam Parashar

Contents

1	Introduction	334
2	Properties of PLGA	335
3	Nephrotoxicity	336
4	Pharmacokinetic Studies	337
5	Alteration of Pharmacokinetics and Biodistribution Profiles	337
6	Peroral PLGA NPs for Delivery of Anticancer Drugs	338
7	Peroral PLGA NPs for Delivery of Drugs Employed Brain Disorders	339
8	Peroral PLGA NPs for Delivery of Cardiovascular Drugs	340
9	Peroral PLGA NPs for Delivery of Drugs for Skin Disorders	340
10	Peroral PLGA NPs for Delivery of Antidiabetic Drugs	341
11	Peroral PLGA NPs for Delivery of Anti-infectious Drugs	342
12	Peroral PLGA NPs for Delivery of Antiviral Drugs	343
13	Conclusion	343
	References	344

N. Singh · N. Mishra
Department of Pharmaceutical Sciences, Babasaheb
Bhimrao Ambedkar University (A Central
University), Lucknow, Uttar Pradesh, India

K. Raza
Department of Pharmacy, School of Chemical
Sciences and Pharmacy, Central University of
Rajasthan, Ajmer, Rajasthan, India

P. Parashar (✉)
Amity Institute of Pharmacy, Amity University Uttar
Pradesh, Lucknow Campus,
Lucknow, Uttar Pradesh, India

Abstract

Peroral administration of drug-loaded PLGA nanoparticles (NPs) is gaining utmost attention in recent years. PLGA NPs have been successfully employed for peroral delivery of varied drugs including antineoplastic agents, antibacterial agents, and small molecules (genes and proteins). PLGA NPs showed enhanced bio-efficacy of encapsulated drug ascribing to enhanced bioavailability, pro-

longed circulation, controlled release, protection against degradation/release during transit, and passive/active targeting potential. Further literatures have evidenced their swift uptake facilitated through Peyer's patches (M-cells), GALT (isolated follicles of the gut associated lymphoid tissue), and the normal intestinal enterocytes. This chapter comprehensively describes the delivery of various drugs through PLGA NPs in addition to especial discussion of the pharmacokinetic and nephrotoxicity of the same.

Keywords

Drug delivery · Peroral administration · Pharmacokinetic · Poly lactic glycolic acid

1 Introduction

Owing of its noninvasive aspect and the fact that it bypasses the pain and distress experienced with injections, as well as the risk of infection, oral drug administration route is one of the most consistently utilized routes for medication delivery. It is not practicable, however, when the active agents (drugs) have undesirable physicochemical features for gastrointestinal absorption, solubility or stabil-

ity limitations, or a noticeable decrease in bioavailability due to first-pass hepatic metabolism [1].

Biodegradable and biocompatible polymers have served an indispensable role in the targeted and controlled delivery of drugs. Due to its excellent attributes, polylactic-co-glycolic acid (PLGA) is among the most intensively explored synthetic biodegradable polymers. Based on its stimuli-sensitive nature, it is also referred as a "smart polymer." A myriad of PLGA-based drug delivery systems for the diagnosis and treatment of multiple ailments are developed [2].

Nanoparticles are solid, spherical entities with a diameter of less than 100 nm that are made from natural or synthetic polymers. Hydrophilic and hydrophobic drugs, vaccines, and bio-macromolecules could all be administered employing nanoparticles. Nanoparticles can potentially be leveraged to enable controlled drug delivery to targeted cells, tissues, or organs. As PLGA hydrolysis yields metabolite monomers, lactic acid, and glycolic acid, it is considered among the most extensively utilized biodegradable polymer. The application of PLGA for drug delivery or as biomaterial is attributed with negligible systemic toxicity because these two monomers are endogenous and efficiently metabolized by the body through the Krebs cycle [3]. Various fabricated forms of PLGA nanoparticles is shown in Fig. 18.1.

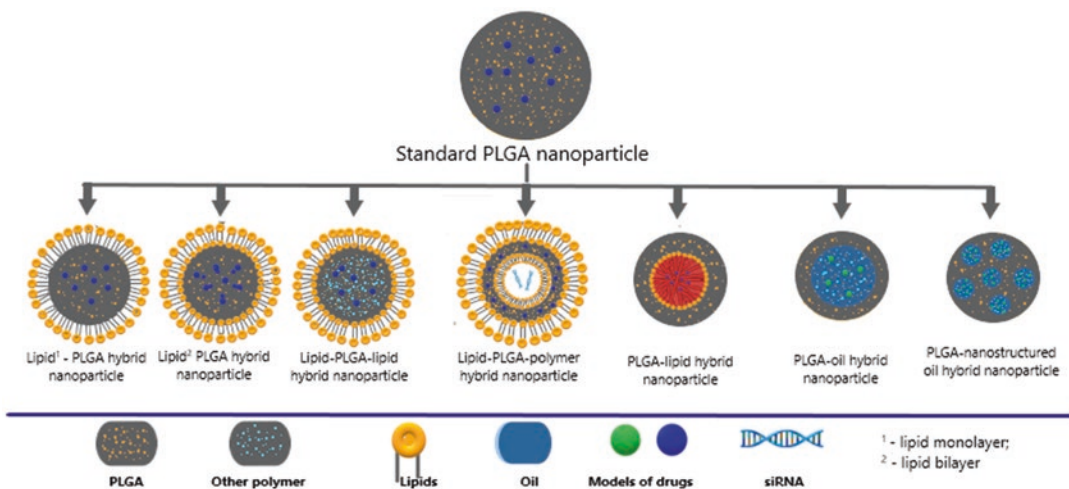


Fig. 18.1 Various types of PLGA-lipids hybrid formulations

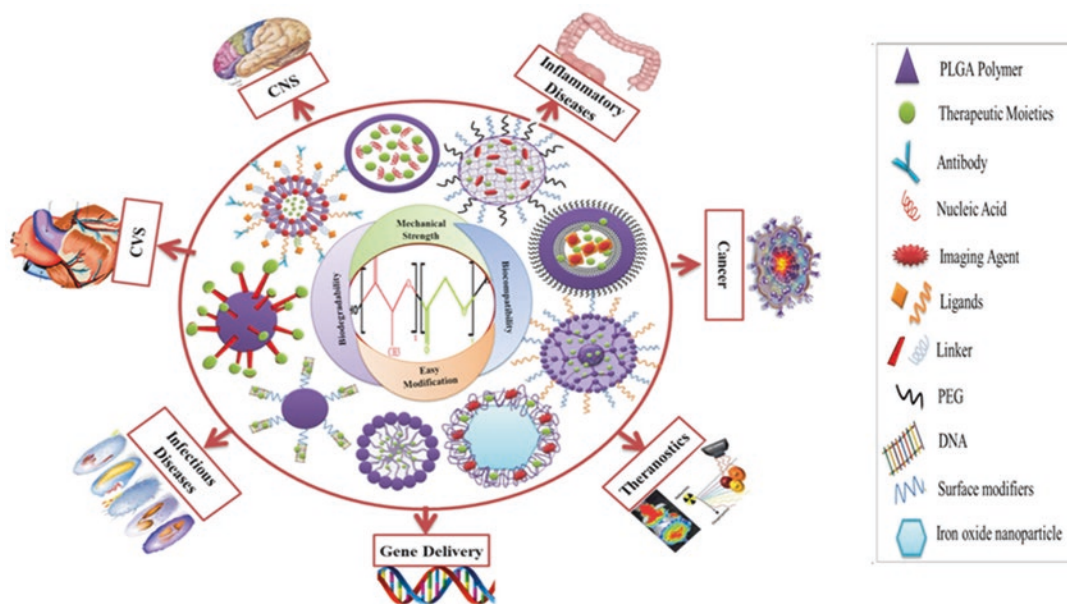


Fig. 18.2 PLGA-based nanostructures for drug delivery. Figure illustrates the salient features of PLGA (i.e., biocompatibility, biodegradability, mechanical strength, and easier to modify) owing to which this polymer is being

used for effectual designing of a wide variety of nanostructures including polymeric micelles, dendrimers, nanocapsules, nanoghosts, nanogels, and theranostic agents Reproduced with permission [5]

2 Properties of PLGA

PLGA is a copolymer synthesized by random ring opening copolymerization of two monomers, glycolic acid and lactic acid cyclic dimers (1,4-dioxane-2,5-diones).

Tin(II) 2-ethylhexanoate, tin(II) alkoxides, and aluminum isopropoxide are common catalysts utilized in the synthesis of this copolymer. During polymerization, successive monomeric units (glycolic or lactic acid) in PLGA are connected by ester bonds, resulting in a linear, amorphous aliphatic polyester product. The monomer ratio is frequently used to distinguish the different types of PLGA. PLGA 50:50, for example, refers to a copolymer composed of 50% lactic acid and 50% glycolic acid. PLGA is a popularly utilized polymer because of its biocompatibility, protracted track history in biomedical applications, and well-documented significance for extended drug release opposed to traditional systems, lasting days, weeks, or months, as well as the conve-

nience of parenteral administration using injection [4]. The applications of PLGA in delivery of various drugs have been shown in Fig. 18.2.

Polymer biodegradation: The polymer backbone with ester bonds is arbitrarily hydrolyzed if PLGA is exposed to aqueous hydrolysis. Each ester bond hydrolyzes to produce one OH group and one COOH group. The hydrophilic property of a polymer increases as its molecular weight is reduced due to scission of extended polymer chains; as the molecular weight is reduced further, water-soluble polymer fragments are generated. These fragments are then degraded subsequently to yield glycolic and lactic acids, which are physiologically inert to proliferating body cells and are excreted from the body via typical metabolic pathways [5]. The drug induced nephrotoxicity reduced significantly when formulated as nanoparticle, the nephrotoxicity of various drugs has been briefly recorded in Table 18.1.

Table 18.1 Example of nanoparticle implications on drug-induced nephrotoxic side effects

Drug name	Category	Treatment indications	Effect of NP formulation on nephrotoxicity	Ref.
Amphotericin B	Antibiotic	Fungal infections	Reduced nephrotoxic parameters in human clinical trials, decreased tubular cell damage, reduce creatinine clearance	[6, 7]
Vancomycin	Antibiotic	Bacterial infections	Reduced renal damage and kidney drug distribution	[8]
Cyclosporine	Chemotherapeutic agent	Cancer, autoimmune disorders, organ transplantation rejection	Reduced kidney drug accumulation, reduced total BUN and plasma creatinine, prevention of glomerular damage, improved drug bioavailability	[9]
Tacrolimus	Immunosuppressive	Inflamed bowel disease, organ transplantation rejection	Reduced creatinine and BUN levels, maintenance of normal kidney function compared to non-treated controls	[10]
Cisplatin	Chemotherapeutic agent	Various cancers	Prolonged anti-tumor effects, reduced nephrotoxic side effects in human clinical trials, reduce drug accumulation within kidneys, reduction in kidney cell death	[11–14]
Doxorubicin	Chemotherapeutic agent	Various cancers, tumor therapy	Enhanced drug bioavailability, increased antioxidant parameters in kidney tissue, reduced renal tissue-based lipid peroxidation	[15]

3 Nephrotoxicity

The term “nephrotoxicity” refers to a significant loss in renal function triggered by the toxic effects of drugs and chemicals. They are of several types, and some drugs may have multiple effects on renal function [16].

Nephrotoxins are chemicals that cause kidney damage (nephrotoxicity). Both glomerular and tubular repercussions due to NPs have been observed in the renal system suggesting that tubules are the preferred site detrimental activity of NPs. NPs can disturb the renal system by causing cytotoxicity in glomerular and tubular cell lines, and *in vivo* investigations have revealed that NPs can change the normal shape of the nephron, altering the kidney’s physiological activities. In general, NP renal toxicity appears to be linked to the size and chemical composition of the NP, although other parameters such as surface charge and functionalization may also have a key influence in the commencement of deleterious effects. *In vitro* studies displayed that the amount of the toxic effects is dependent on the cell types to which the NPs engage, as well as cellular functions [17].

Yuh-Feng Lin et al. developed resveratrol-loaded nanoparticles (Res NPs) conjugated with

kidney injury molecule-1 for chronic kidney disease (CKD). The toxicity of Res NPs was negligible, and they triggered autophagy. The NLRP3 inflammasome and IL-1 secretion were both suppressed by Res NPs. NLRP3 expression was shown to be higher in CKD patients’ peripheral blood monocytic cells than in healthy individuals. In a murine model of CKD, treatment with kidney injury molecule-1-Res NPs decreased creatinine and shielded against tubulointerstitial damage. Res NPs may be used to prevent CKD by inhibiting the NLRP3 inflammasome and inducing autophagy [18].

K. Sonaje et al. developed biodegradable nanoparticles for oral delivery of ellagic acid (EA) and assessed their antioxidant efficacy against cyclosporine A-induced nephrotoxicity in rats. To increase oral bioavailability of EA, a dietary antioxidant with weak biopharmaceutical characteristics was encapsulated into PLGA and polycaprolactone (PCL) nanoparticles. Intestinal absorption of EA as DMAB-stabilized nanoparticles was much higher than that of sodium carboxymethyl cellulose suspension and PVA-stabilized particles, according to *in situ* permeation studies in rats. Biochemical indicators and renal histology showed that EA and EA nanoparticles were capable of preventing CyA-induced nephrotoxicity in rats [19].

Alshamsan et al. studied the use of PLGA NPs to prevent tacrolimus (TAC)-related nephrotoxicity in mice after several doses while maintaining immunosuppressive effect. In an *ex vivo* study, TAC-loaded NPs showed a significant reduction in CD4+ and CD8+ cell proliferation, which was comparable to the control treatment (Prograf). TAC was given subcutaneously to the mice at a dose of 1 mg/kg per day for 30 days, either as a control or as TAC-loaded NPs. The *in vivo* immunosuppressive actions as well as renal function of mice were investigated after drug treatment. For TAC-loaded PLGA NPs, the results evidenced much decreased drug-associated toxicity and activity comparable to Prograf [20].

4 Pharmacokinetic Studies

Pharmacokinetics is a term derived from the Greek words *pharmakon* (drug) and *kinetikos* (movement) that describe how a substance is absorbed, distributed, metabolized, and excreted [21].

The study of the dynamic motions of foreign substances (xenobiotics) throughout their passage through the body is known as pharmacokinetics [22]. Nanoparticles are utilized to improve cellular uptake and therapeutic concentrations at specific required sites as well as to improve the pharmacokinetic and pharmacodynamic aspects of drugs. In rabbits, Akhtar et al. investigated the pharmacokinetics (PK) of chitosan-modified PLGA NPs for oral gentamicin delivery. In animal models, PK investigations suggest that therapeutically optimal gentamicin concentrations can be established with a single oral dosage of gentamicin in the form of chitosan-modified PLGA NPs for extended periods [23].

Drug delivery assessment of perorally administered PLGA NPs has been extensively explored in various studies. It has been reported in various pieces of literature that the uptake of PLGA NPs has been facilitated through M-cells in Peyer's patches, isolated follicles of GALT (gut associated lymphoid tissue), and the normal intestinal enterocytes [24]. The facilitated uptake is credited to PLGA NP physicochemical properties

comprising nanosize, favorable zeta potential, hydrophobicity, etc. [25]. A study was performed by Jani et al. reporting investigation of PLGA NPs uptake subsequent to oral administration through fluorescence microscopy (qualitative; tissue distribution) and scanning confocal microscopy (histological localization) [26]. The findings of fluorescence microscopy suggested size-dependent uptake of PLGA NPs via Peyer's patches and the order was found to be 300 nm and 1 μm > 3 μm . Further, the results of confocal microscopy indicated the particles in a size range of 300 nm and 1 μm resided into the deep region of Peyer's patches, whereas particles of >1 μm remain localized in the dome region. Additionally, the uptake was also found to be charge dependent, and Jain et al. reported that the particles possessing negative and neutral charges displayed a swift uptake by Peyer's patches when compared with positively charged particles.

5 Alteration of Pharmacokinetics and Biodistribution Profiles

Peroral delivery is the most preferred route of administration ascribing to high patient compliance, low costs, and easy handling, and thus constant efforts are been done to improve pharmacokinetic performance of drug candidates [27]. In the same context, Zhao et al. formulated vitamin E TPGS conjugated PLGA NPs of paclitaxel for oral administration [28]. The *in vitro* viability investigations revealed approximately 1.28, 1.38, and 1.12-fold enhanced cytotoxicity in MCF-7 cell lines when compared with Taxol[®] at an incubation period of 24, 48, and 72 h, respectively. Further, *in vivo* evaluation displayed significantly enhanced oral bioavailability (tenfold) of vitamin E TPGS conjugated PLGA NPs when compared with Taxol[®] along with 9.74-fold higher therapeutic efficacy and 12.56-fold extended sustainable therapeutic time.

Thus, the bestowed properties of PLGA and its pharmacokinetic profile have made it a choice of delivery of various drugs. The various encased drugs in PLGA have been recorded in Table 18.2.

Table 18.2 Various drugs incorporated in PLGA NPs for oral administration [29]

Drugs	Purpose	Disorder	References
Doxorubicin	Improvement of bioavailability and reduction toxicity	Cancer chemotherapy	[30]
Ethionamide	Sustained release	MDR tuberculosis	[31]
Insulin	Protection of insulin against self-aggregation, enzymatic degradation, and prolonged the duration of hypoglycemic effects	Diabetes	[32]
Rolipram	To target drug delivery to the inflamed gut tissues	Inflammatory bowel disease	[33]
Heparin	Improvement of absorption	Venous thrombosis and pulmonary embolism	[34]
Cyclosporin A	Improvement of bioavailability and pharmacokinetic	Immunosuppression in organ transplantation	[22, 35]
Amifostine	Improvement of absorption	Treatment of cancer as radioprotective agent	[36]
Ellagic acid	Improvement of bioavailability	Oxidative stress-induced diseases	[37]
Rifampin, isoniazid, pyrazinamide, and ethambutol	Sustained release	Cerebral tuberculosis	[38]
Coenzyme Q10	Improvement of bioavailability	Hypertension	[39]
Mifepristone	Improvement of bioavailability	Ovarian and breast cancer	[40]
Streptomycin	Improvement of bioavailability and reduction of nephrotoxicity	Tuberculosis	[41]
Voriconazole	Improvement of antifungal efficacy	Fungal infections	[42]
Atorvastatin	Sustained release	Hyperlipidemia	[43]
Paclitaxel	Improvement of bioavailability and develop cremophor EL-free polymeric drug delivery system	Breast cancer	[44]
Estradiol	Improvement of bioavailability	Postmenopausal dyslipidemia	[45]
Tamoxifen	Improvement of bioavailability and reduce hepatotoxicity	Breast cancer	[46]
Curcumin	Improvement of bioavailability	Pancreatic cancer, colon cancer, and cancer-associated multiple myeloma	[47]

6 Peroral PLGA NPs for Delivery of Anticancer Drugs

Cancer is a disease that begins from a cell. Healthy cells grow, divide, multiply, and replace old ones, sustaining the body in a state of balance and homeostasis; unfortunately, if the genetic information within the cell is mutated, cells will proliferate uncontrollably and create tumors. Cancer cells spread to other parts of the body via blood and lymphatic channels, generating tumorigenic masses of cells [48].

Surgical procedures, chemotherapy, radiation therapy, and immunotherapy are indeed

treatment options for several types of cancer. The primary flaw of chemotherapies is that the strategy involved is usually nonspecific. The size distribution, surface morphology, surface charge, surface erosion, surface chemistry, surface adhesion, drug diffusivity, inner porosity, encapsulation efficiency, stability, and release kinetics of the targeted NPs all have a significant impact on the efficacy and side effects of anticancer drug therapy. PLGA nanoparticles are routinely utilized to encapsulate a variety of cancer-related drugs and deliver them in vivo [4]. The mechanism of few commonly employed PLGA encapsulated anticancer drugs is as follows:

- Paclitaxel targets to microtubules.
- Etoposide leads to inhibition of topoisomerase-II and activation of oxidation-reduction reactions to create derivatives that bind directly to DNA and cause DNA damage.
- 9-Nitrocamptothecin targeting the enzyme topoisomerase-I.
- Cisplatin is known to crosslink DNA molecule in several ways to interfere cell division via mitosis. Damaged DNA triggers the DNA repair process.
- Dexamethasone targets to cytoplasmic receptors.
- Curcumin targets to cytoplasmic proteins [4].

DMAB-modified PLGA NPs, unmodified PLGA-TPGS NPs, and DMAB-modified PLGA-TPGS NPs were developed by Chen et al. from biodegradable PLGA-TPGS random copolymer for effective oral delivery of anticancer drugs. DMAB was utilized to extend the NP retention time on the cell surface, facilitating their uptake and oral bioavailability. The NPs were observed to be spherical, with a mean particles size of 250 nm. After DMAB modification, the surface charge of PLGA-TPGS NPs became positive. The study also revealed that DMAB-modified PLGA-TPGS NPs exhibited considerably higher cell uptake unlike DMAB-modified PLGA NPs and unmodified PLGA-TPGS NPs [49].

Italia et al. developed PLGA NPs loaded with cyclosporine for oral delivery and compared them to Sandimmune Neoral® in terms of nephrotoxicity and pharmacokinetics. The pharmacokinetic characteristics of cyclosporine-loaded nanoparticles and Sandimmune Neoral® formulations differed significantly, with the nanoparticulate formulation exhibited controlled cyclosporine release spanning 5 days whereas the marketed formulation displayed a sharp C_{max} with a 3-day drug release. In contrast to Sandimmune Neoral®, the nanoparticulate formulation elicited reduced nephrotoxicity in rats, as proved by diminished plasma creatinine (PC), blood urea nitrogen (BUN), and malondialdehyde (MDA) levels in plasma as well as the kidneys [22].

Joshi et al. developed Gemcitabine HCl loaded PLGA NPs for improving oral bioavailability

through absorption via M cells of Peyer's patches. In vivo pharmacokinetic investigations in rats revealed that NPs increased bioavailability by 21.47 times. As a result, orally administered gemcitabine HCl loaded PLGA NPs hold the possibility to improve bioavailability while preventing the negative effects of gemcitabine i.v. infusions and promoting patient compliance [50].

7 Peroral PLGA NPs for Delivery of Drugs Employed Brain Disorders

It's been difficult to target and deliver macromolecular therapies to the central nervous system (CNS). The principal barrier that must be traversed enable pharmaceuticals reach target in the brain is the blood-brain barrier (BBB). As a consequence, substantial emphasis has been invested into augmenting therapeutic drug transport across the BBB and into the CNS, through the deployment of NPs [51].

Neurological maladies are a serious global health issues, but pharmaceutical therapies are inadequate mainly because of the BBB's limitations on drug entry to the CNS. For crossing the BBB, PLGA NPs are among the most intriguing drug and gene delivery platforms. The employment of PLGA NPs to transport therapeutics across the BBB has spawned a slew of new techniques, for instance, (1) to promote passage from the injection site (pre-transcytosis approaches); (2) to improve transport over the brain endothelial cells (BBB transcytosis approaches); and (3) to enable targeting of the compromised nervous system cells (post-transcytosis approaches) [52].

Lopez et al. developed memantine loaded PLGA PEGylated nanoparticles for peroral administration for treatment of Alzheimer's disease. The in vitro and in vivo outcomes for brain drug levels demonstrated compelling proof that the formulated NPs delivered the drug to the target tissue providing sustained release premise. Owing to the bioadhesive polymer characteristics, the prepared colloidal systems boost drug concentration in the target organs and validate the efficacy of the NPs for oral route. Furthermore,

reduced dosing frequency (on alternate days) was determined to be sufficient for achieving satisfactory drug therapeutic levels in the brain [53].

Zhang et al. investigated the influence of borneol on the brain targeting ability of aprotinin-conjugated PEG-PLGA NPs (Apr-NP) and the activity of huperzine A (Hup A)-loaded NPs in AD rats. The emulsion and solvent evaporation technique was used to develop Apr-NP. Using coumarin-6 as a tracer, the uptake of Apr-NP alone or in combination with borneol in brain capillary endothelial cells (BCECs) was determined. To evaluate the brain delivery of Apr-NP in rats, *in vivo* imaging and the distribution of Hup A in the brain were examined, with or without the oral administration of borneol. The results revealed that co-incubation with borneol enhanced nanoparticle uptake in BCECs. The co-administration of borneol along with the NPs improved their delivery to the rat brain substantially. When coupled with borneol, the memory impairment in AD rats was considerably improved by Hup A-loaded NPs [54].

8 Peroral PLGA NPs for Delivery of Cardiovascular Drugs

Despite significant clinical progress, cardiovascular diseases (CVDs), which include a multitude of heart, blood vessel, and stroke conditions, remain a primary reason of death in the United States. According to the World Health Organization (WHO), CVDs will account for about 25 million deaths worldwide by 2030. A myriad of nanostructure-based drug delivery systems, particularly those composed of biodegradable PLGA with numerous functionalities, are being investigated for application in CVDs. These differ in size and shape and allow functionalization with a vast array of electrostatic charges and biomolecules [5].

For the treating CVDs, Wang et al. developed a superparamagnetic nano-silica@ quercetin encapsulated PLGA nanocomposite (SiN@ QC-PLGA). The characteristics of the SiN@ QC-PLGA nanocomposite were nearly identical

to those of the local myocardium, facilitating cell recruitment, attachment, expansion, and deposition of cardiac proteins. Thus in a nutshell, these types of antioxidant (QC) delivery systems may potentially be exploited to prevent atherosclerosis and other associated heart diseases [55].

Zhang et al. used a modified nanoprecipitation method to develop simvastatin-loaded TPGS-stabilized liposome-PLGA hybrid NPs (ST-TLPN). This method was identified to be more efficient and easier than the regular method. The influence of TPGS content inside the polymeric core and lipid shell on the physical and chemical attributes of NPs was investigated to select the best formulation. The RAW264.7 cell line showed incredible cellular uptake. When compared to ST-loaded PLGA NPs, ST-TLPN showed improved pharmacokinetics and antiatherogenic activity in *in vivo* animal model [56].

9 Peroral PLGA NPs for Delivery of Drugs for Skin Disorders

The human body's most large and diverse organ is the skin. Skin health is vital not only for aesthetic reasons, but also for health reasons. Its unpleasant appearance caused by dermatitis has an impact on the patient's psychological state, and both considerations have a role in the development and management of chronic skin disorders. Inflammation is a complex process in which the body repairs tissue damage and guards itself against detrimental stimuli, and it is triggered by pathogens, unpleasant mechanical or chemical agents, and autoimmune responses [57].

Gourishetti et al. developed a sesamol (SM)-loaded PLGA nanosuspension (SM-PLGA NPs) to promote wound healing in rats with diabetic foot ulcer. The pharmacokinetic profile of the standard drug (plain SM) and preparation showed that the C_{max} of the PLGA NPs is lower than the plain SM, but the time to achieve maximum concentration (T_{max}) was much longer. Both plain SM and PLGA NPs had pretty much identical area under the curve values; however, the mean residence time of PLGA NPs was significantly

greater than the plain SM. The elimination half-life of PLGA NPs was much greater than that of the plain SM, which could account for drug's sluggish removal from the body. The plasma concentration and time graph revealed that the plain SM got excreted from the body in 24 h of administration, while the SM-PLGA NPs remained in plasma besides 96 h. The SM-PLGA NPs exhibited controlled release of SM that considerably sped up the process of healing in foot ulcers by enhancing granulation tissue formation, augmenting re-epithelization, downregulating inflammatory mediators, collagen deposition at the site of wound, and accelerating neovascularization. All of these are essential attributes of the wound healing process that ultimately culminated in wound closure in less than 10 days [58].

Anwer et al. developed sustained release apremilast (APM)-loaded PLGA NPs, which were subsequently characterized *in vitro* and *in vivo* in rats for pharmacokinetics. The *in vitro* drug release of optimized APM NPs revealed a sustained release profile. Comparing the bioavailability of optimized APM NPs to that of normal APM suspension, the pharmacokinetic studies indicate a 2.25-fold improvement in bioavailability. Furthermore, a considerable increase in half-life and mean residence time validates optimized APM NPs' long-term retention. In once-daily regimen therapy, the increased bioavailability and long-term retention of APM-laden PLGA NPs will be favorable [59].

10 Peroral PLGA NPs for Delivery of Antidiabetic Drugs

Type 2 diabetes mellitus (T2DM) is a non-communicable metabolic condition marked by high blood glucose, insulin resistance, and a relative insulin insufficiency in the body. T2DM is a leading cause of death and suffering worldwide, attracting a lot of attention from the wider populace, policymakers, and public healthcare professionals. As per the International Diabetes Federation (IDF), global statistical data suggests that 592 million individuals will have diabetes by

2035, with T2DM increasing proportionately across every nation. Obesity, aging, dietary choices, lack of physical activity, urbanization, and an inactive lifestyle are all key risk aspects and factors of T2DM. By employing a PLGA-based polymeric nanocrystal composite system as a modified delayed drug delivery carrier for a BCS class II oral hypoglycemic drug, new potential of SGNCs (second-generation nanocrystals) application were investigated and improved. PLGA is a biocompatible and biodegradable polymer that is very widely and extensively employed as a polymeric nanoparticulate drug delivery method for a variety of therapeutic drugs.

Depending on the molecular weight and ratio of lactic-glycolide copolymer composition, the biodegradation time of PLGA polymer ranges from days to months. The protective polymer PLGA, which forms a surface-grafted polymeric molecule, assists in the inclusion of therapeutic agents for their delivery. Furthermore, the addition of an ionic or nonionic stabilizer in conjunction with the PLGA is required to maintain physical stability of the SGNC formulation, which is attained through electrostatic repulsion and steric stabilization [60].

Folate-decorated PLGA NPs (FA-PEG-PLGA NPs) were developed by Jain et al. as a strategically tailored carrier for the oral administration of insulin. The double-emulsion solvent evaporation technique was used to prepare insulin-loaded FA-PEG-PLGA NPs. In diabetic rats, the bioavailability and hypoglycemic efficacy of orally delivered FA-PEG-PLGA NPs was investigated. When compared to subcutaneously delivered standard insulin solution, FA-PEG-PLGA NPs displayed a two-fold spike in oral bioavailability with no hypoglycemia shock. These NPs sustained a constant blood glucose level for 24 h, but subcutaneous insulin only lasted 8 h and was linked with severe hyperglycemia [61].

Ren et al. employed PLGA NPs in yeast cell wall particle systems (YCWPs) to enhance the hypoglycemic activity of exenatide (EXE) through oral targeted delivery. For long-term diabetic treatment oral delivery of EXE, a high-efficiency therapeutic peptide, is vital. The

EXE-PLGA NPs @YCWPs were efficiently loaded into the YCWPs using a solvent hydration lyophilization cycle technique, as confirmed by scanning electron microscopy and confocal laser scanning microscopy. This nano-in-micro carrier provided a noticeable sustained drug release as well as a diminished burst release. Furthermore, the gastrointestinal stability of EXE in PLGA NPs @YCWPs was much greater than PLGA NPs in the simulated gastrointestinal setting, which was effective in improving EXE absorption. In biodistribution analysis, the EXE-PLGA NPs @YCWPs promptly reached the villi's root and even partially accessed the interior of villi, particularly in the ileum and Peyer's patches. In vitro studies in the macrophage RAW 264.7 cells showed efficient α -glucan receptor-mediated endocytosis and transport of EXE-PLGA NPs @YCWPs, indicating a possible intestinal macrophage guided absorptive pathway. Upon oral administration of the EXE-PLGA NPs @YCWPs, the in vivo pharmacokinetic analysis revealed a preferential hypoglycemic effect and elevated pharmacological availability ($13.7 \pm 4.1\%$). The integration of PLGA nanoparticles in the YCWP system is thought to be a promising technique for orally delivering therapeutic peptides [62].

11 Peroral PLGA NPs for Delivery of Anti-infectious Drugs

Infections have been successfully treated with drugs for centuries. However, due to the emergence of antibiotic resistance in the twenty-first century, these could turn lethal yet again. Pathogens can develop resistance through a variety of ways, including increasing the amount of time they remain within the cell, where drugs often fail to attain therapeutic concentrations. Furthermore, drugs are susceptible to a variety of issues that reduce their efficacy. This necessitates the utilization of higher doses and repeated administrations, which can result in adverse effects or toxicity. The employment of nanopar-

ticle systems can contribute in resolving such obstacles and improve therapeutic efficacy. As a consequence, their application as targeting vectors for particular tissues as vaccines, and as theranostic systems by targeting several antimicrobial agents against various pathogens such as bacteria, virus, fungi, or parasites, multidrug-resistant strains, and biofilms, is gaining momentum [63].

In vivo study to determine the efficacy, toxicity, and biodistribution of itraconazole (ITZ)-loaded PLGA-DMSA NPs for the treatment of paracoccidioidomycosis (PCM) was carried out by Azevedo et al. The biodistribution of ITZ delivered as NPs and an oral solution were studied, and it was concluded that the type of formulations and routes of administration had a significant influence on organ quantification. When compared to free drug, ITZ biodistribution from NPs exhibited higher accumulation in the lung, liver, and spleen. ITZ-NPs were found to be as effective as the free drug in the treatment of chronic PCM, with the added benefit of preventing the drug's known side effects. Considering that the administration would be repeated after 3 days, the ITZ-NP drug concentration was less than that provided by free ITZ; therefore this would help to cut the overall expense of therapy as well as the time and stress caused to the patients [64].

Nayak et al. employed solvent evaporation method to formulate, characterize, and analyze rotavirus (strain SA11) encapsulated polylactide (PLA) and PLGA NPs for oral vaccine. Serum albumin was utilized as a stabilizer to prevent denaturation of viral antigen during the emulsification process. Sodium bicarbonate (NaHCO_3) and sucrose were used in the primary emulsification stage to yield uniformly stabilized particles that entrapped rotavirus. The polymer particle surfaces were observed to have consistent porosity and roughness via scanning electron and atomic force microscopy. In contrast to soluble antigen, single-dose oral immunization with 20 mg of antigen encapsulated in PLA-PLGA particles evoked enhanced and long-lasting IgA and IgG antibody titers [65].

12 Peroral PLGA NPs for Delivery of Antiviral Drugs

Communicable diseases are the largest cause of death around the world, with viruses having a significant consequence on healthcare and economic prosperity. Furthermore, the swift emergence of drug resistance to presently known treatments, as well as adverse side effects associated with long-term usage, is a severe public health issue. As a response, novel therapeutic options must be explored and developed. The interplay of nanostructures with microorganisms is rapidly transforming the biomedical area, with improvements in diagnostic and therapeutic aspects. NPs exhibit exceptional physical characteristics that make them ideal for drug delivery. These are primarily attributable to particle size (influences bioavailability and circulation time), a large surface area-to-volume ratio (improves solubility, particularly in comparison to larger particles), a configurable surface charge of the particle with the potential of encapsulation, and the ability to accommodate large drug payloads [66].

Joshi et al. investigated the effects of orally administered lopinavir-loaded PLGA NPs on bioavailability enhancement, Caco-2 cell uptake, and intestinal transit via nanoprecipitation method. The NPs were then characterized utilizing TEM, DSC, and FTIR, and their safety was established using the MTT assay. Rats were used in the *in vivo* pharmacokinetic experiments. The NPs exhibited uniform spherical shapes with a particle size of 142.1 ± 2.13 nm and a $93.03 \pm 1.27\%$ entrapment efficiency. There was no interaction between the drug and the polymer. After oral delivery, confocal microscopy indicated the penetration and absorption of developed NPs in Caco-2 cells and the colon. NPs increased permeability by 3.04 times and bioavailability by 13.9 times. By delivering antiretroviral drugs to lymph (a significant HIV reservoir site) via direct absorption via the colon prior reaching systemic circulation, NPs could be a successful delivery system for antiretroviral drugs [67].

Sarti et al. investigated the *in vivo* potential of an oral vaccine comprising PLGA NPs with the immunostimulant monophosphoryl lipid A. The developed PLGA NPs possessed a size and zeta potential that enabled them to be taken up by M-cells of Peyer's patches, as well as a high drug loading, encapsulation efficiency for the model antigen OVA and adjuvant MPLA, and optimal release profiles for oral vaccines. When compared to the control formulation, OVA/MPLA-loaded NPs elicited greater antigen-specific IgG and IgA antibodies in mice [68].

13 Conclusion

All the above studies witnessed the potential of PLGA NPs as nanocarriers and the possibility of exploring delivery of other drugs for improved bio-efficacy. The formulation methods of drug-loaded PLGA NPs is facile that also offers easy surface engineering that leads to site-specific targeted drug delivery. Future research aimed at combatting challenges that include co-delivery of variable drugs into PLGA NPs and the scale-up from bench to bedside. Comparable to any therapy, drug-loaded PLGA NPs will be considered successful in terms of improved pharmacokinetic/pharmacodynamic activity, specific drug delivery and targeting potential, minimized toxicity, as well as superior therapeutic efficacy of loaded drug. The future demands for novel and advanced surface engineering approaches that have specificity and selectivity toward the targeted site that can further escalate therapeutic efficacy of formulation/delivery system. The approaches encompass ligand-established targeting, genetic engineering, and surface engineering with specific targeting moiety. Through the progress in technology, PLGA NPs may be investigated for broader applications but still, a long way off. Besides all new methodologies/technologies and potential of PLGA NPs, only limited commercial products are available, namely, Zoladex[®] (PLGA/PLA microparticles, AstraZeneca), ReGel[®] (PLGA-PEG-PLGA hydrogel, Macro-Med), and a few have moved to clinical trials, however founding commercial

viability. As we unveil the potential of PLGA NPs with enhanced therapeutic efficacy, we may expect newer and improved PLGA NPs that could hold success and acceptance for clinical application.

References

- Martin-Banderas L, Duran-Lobato M, Munoz-Rubio I, Alvarez-Fuentes J, Fernandez-Arevalo M, Holgado MA. Functional PLGA NPs for oral drug delivery: recent strategies and developments. *Mini Rev Med Chem.* 2013;13(1):58–69.
- Kapoor DN, Bhatia A, Kaur R, Sharma R, Kaur G, Dhawan S. PLGA: a unique polymer for drug delivery. *Ther Deliv.* 2015;6(1):41–58.
- Danhier F, Ansorena E, Silva JM, Coco R, Le Breton A, Préat V. PLGA-based nanoparticles: an overview of biomedical applications. *J Control Release.* 2012;161(2):505–22.
- Tabatabaei Mirakabad FS, Nejati-Koshki K, Akbarzadeh A, Yamchi MR, Milani M, Zarghami N, et al. PLGA-based nanoparticles as cancer drug delivery systems. *Asian Pac J Cancer Prev.* 2014;15(2):517–35.
- Mir M, Ahmed N, Rehman A. Recent applications of PLGA based nanostructures in drug delivery. *Colloids Surf B Biointerfaces.* 2017;159:217–31.
- Wingard JR, Kubilis P, Lee L, Yee G, White M, Louise W, et al. Clinical significance of nephrotoxicity in patients treated with amphotericin B for suspected or proven aspergillosis. *Clin Infect Dis.* 1999;29(6):1402–7.
- Italia J, Yahya M, Singh D, Kumar MR. Biodegradable nanoparticles improve oral bioavailability of amphotericin B and show reduced nephrotoxicity compared to intravenous Fungizone®. *Pharm Res.* 2009;26(6):1324–31.
- Hodoshima N, Masuda S, Inui K-I. Decreased renal accumulation and toxicity of a new VCM formulation in rats with chronic renal failure. *Drug Metab Pharmacokinet.* 2007;22(6):419–27.
- Italia J, Bhatt D, Bhardwaj V, Tikoo K, Kumar MR. PLGA nanoparticles for oral delivery of cyclosporine: nephrotoxicity and pharmacokinetic studies in comparison to Sandimmune Neoral®. *J Control Release.* 2007;119(2):197–206.
- Meissner Y, Pellequer Y, Lamprecht A. Nanoparticles in inflammatory bowel disease: particle targeting versus pH-sensitive delivery. *Int J Pharm.* 2006;316(1–2):138–43.
- Aryal S, Hu C-MJ, Zhang L. Polymer–cisplatin conjugate nanoparticles for acid-responsive drug delivery. *ACS Nano.* 2010;4(1):251–8.
- Liu G, Franssen E, Fitch MI, Warner E. Patient preferences for oral versus intravenous palliative chemotherapy. *J Clin Oncol.* 1997;15(1):110–5.
- Mizumura Y, Matsumura Y, Hamaguchi T, Nishiyama N, Kataoka K, Kawaguchi T, et al. Cisplatin-incorporated polymeric micelles eliminate nephrotoxicity, while maintaining antitumor activity. *Jpn J Cancer Res.* 2001;92(3):328–36.
- Uchino H, Matsumura Y, Negishi T, Koizumi F, Hayashi T, Honda T, et al. Cisplatin-incorporating polymeric micelles (NC-6004) can reduce nephrotoxicity and neurotoxicity of cisplatin in rats. *Br J Cancer.* 2005;93(6):678–87.
- Anders CK, Adamo B, Karginova O, Deal AM, Rawal S, Darr D, et al. Pharmacokinetics and efficacy of PEGylated liposomal doxorubicin in an intracranial model of breast cancer. *PLoS One.* 2013;8(5):e61359.
- Al-Naimi MS, Rasheed HA, Hussien NR, Al-Kuraishy HM, Al-Gareeb AI. Nephrotoxicity: role and significance of renal biomarkers in the early detection of acute renal injury. *J Adv Pharm Technol Res.* 2019;10(3):95.
- Iavicoli I, Fontana L, Nordberg G. The effects of nanoparticles on the renal system. *Crit Rev Toxicol.* 2016;46(6):490–560.
- Lin Y-F, Lee Y-H, Hsu Y-H, Chen Y-J, Lin Y-F, Cheng F-Y, et al. Resveratrol-loaded nanoparticles conjugated with kidney injury molecule-1 as a drug delivery system for potential use in chronic kidney disease. *Nanomedicine.* 2017;12(22):2741–56.
- Sonaje K, Italia J, Sharma G, Bhardwaj V, Tikoo K, Kumar MR. Development of biodegradable nanoparticles for oral delivery of ellagic acid and evaluation of their antioxidant efficacy against cyclosporine A-induced nephrotoxicity in rats. *Pharm Res.* 2007;24(5):899–908.
- Alshamsan A, Binkhathlan Z, Kalam MA, Qamar W, Kfoury H, Alghonaim M, et al. Mitigation of tacrolimus-associated nephrotoxicity by PLGA nanoparticulate delivery following multiple dosing to mice while maintaining its immunosuppressive activity. *Sci Rep.* 2020;10(1):1–11.
- Turfus S, Delgoda R, Picking D, Gurley B. *Pharmacokinetics pharmacognosy.* Boston: Academic; 2017.
- Mehrotra N, Gupta M, Kovar A, Meibohm B. The role of pharmacokinetics and pharmacodynamics in phosphodiesterase-5 inhibitor therapy. *Int J Impot Res.* 2007;19(3):253–64.
- Akhtar B, Muhammad F, Aslam B, Saleemi MK, Sharif A. Pharmacokinetic profile of chitosan modified poly lactic co-glycolic acid biodegradable nanoparticles following oral delivery of gentamicin in rabbits. *Int J Biol Macromol.* 2020;164:1493–500.
- Song X, Zhao X, Zhou Y, Li S, Ma Q. Pharmacokinetics and disposition of various drug loaded biodegradable poly(lactide-co-glycolide) (PLGA) nanoparticles. *Curr Drug Metab.* 2010;11(10):859–69.
- Shakweh M, Besnard M, Nicolas V, Fattal E. Poly (lactide-co-glycolide) particles of different physicochemical properties and their uptake by Peyer's patches in mice. *Eur J Pharm Biopharm.* 2005;61(1–2):1–13.

26. Jani P, Halbert GW, Langridge J, Florence AT. Nanoparticle uptake by the rat gastrointestinal mucosa: quantitation and particle size dependency. *J Pharm Pharmacol.* 1990;42(12):821–6.
27. Yin Y, Chen D, Qiao M, Lu Z, Hu H. Preparation and evaluation of lectin-conjugated PLGA nanoparticles for oral delivery of thymopentin. *J Control Release.* 2006;116(3):337–45.
28. Zhao L, Feng S-S. Enhanced oral bioavailability of paclitaxel formulated in vitamin E-TPGS emulsified nanoparticles of biodegradable polymers: in vitro and in vivo studies. *J Pharm Sci.* 2010;99(8):3552–60.
29. Kumar G, Shafiq N, Malhotra S. Drug-loaded PLGA nanoparticles for oral administration: fundamental issues and challenges ahead. *Crit Rev Ther Drug Carrier Syst.* 2012;29(2):149–82.
30. Kalaria D, Sharma G, Beniwal V, Kumar MR. Design of biodegradable nanoparticles for oral delivery of doxorubicin: in vivo pharmacokinetics and toxicity studies in rats. *Pharm Res.* 2009;26(3):492–501.
31. Kumar G, Sharma S, Shafiq N, Pandhi P, Khuller GK, Malhotra S. Pharmacokinetics and tissue distribution studies of orally administered nanoparticles encapsulated ethionamide used as potential drug delivery system in management of multi-drug resistant tuberculosis. *Drug Deliv.* 2011;18(1):65–73.
32. Carino GP, Jacob JS, Mathiowitz E. Nanosphere based oral insulin delivery. *J Control Release.* 2000;65(1–2):261–9.
33. Lamprecht A, Ubrich N, Yamamoto H, Schäfer U, Takeuchi H, Maincent P, et al. Biodegradable nanoparticles for targeted drug delivery in treatment of inflammatory bowel disease. *J Pharmacol Exp Ther.* 2001;299(2):775–81.
34. Jiao Y, Ubrich N, Marchand-Arvier M, Vigneron C, Hoffman M, Lecompte T, et al. In vitro and in vivo evaluation of oral heparin-loaded polymeric nanoparticles in rabbits. *Circulation.* 2002;105(2):230–5.
35. Jaiswal J, Gupta SK, Kreuter J. Preparation of biodegradable cyclosporine nanoparticles by high-pressure emulsification-solvent evaporation process. *J Control Release.* 2004;96(1):169–78.
36. Pamujula S, Graves RA, Freeman T, Srinivasan V, Bostanian LA, Kishore V, et al. Oral delivery of spray dried PLGA/amifostine nanoparticles. *J Pharm Pharmacol.* 2004;56(9):1119–25.
37. Bala I, Bhardwaj V, Hariharan S, Kharade SV, Roy N, Ravi Kumar M. Sustained release nanoparticulate formulation containing antioxidant-ellagic acid as potential prophylaxis system for oral administration. *J Drug Target.* 2006;14(1):27–34.
38. Pandey R, Khuller G. Oral nanoparticle-based antituberculosis drug delivery to the brain in an experimental model. *J Antimicrob Chemother.* 2006;57(6):1146–52.
39. Ankola D, Viswanad B, Bhardwaj V, Ramarao P, Kumar MR. Development of potent oral nanoparticulate formulation of coenzyme Q10 for treatment of hypertension: can the simple nutritional supplements be used as first line therapeutic agents for prophylaxis/therapy? *Eur J Pharm Biopharm.* 2007;67(2):361–9.
40. He W, Horn SW, Hussain MD. Improved bioavailability of orally administered mifepristone from PLGA nanoparticles. *Int J Pharm.* 2007;334(1–2):173–8.
41. Pandey R, Khuller GK. Nanoparticle-based oral drug delivery system for an injectable antibiotic–streptomycin. *Chemotherapy.* 2007;53(6):437–41.
42. Peng H-S, Liu X-J, Lv G-X, Sun B, Kong Q-F, Zhai D-X, et al. Voriconazole into PLGA nanoparticles: improving agglomeration and antifungal efficacy. *Int J Pharm.* 2008;352(1–2):29–35.
43. Meena A, Ratnam DV, Chandraiah G, Ankola D, Rao PR, Kumar MR. Oral nanoparticulate atorvastatin calcium is more efficient and safe in comparison to Lipicure® in treating hyperlipidemia. *Lipids.* 2008;43(3):231–41.
44. Bhardwaj V, Ankola D, Gupta S, Schneider M, Lehr C-M, Kumar MR. PLGA nanoparticles stabilized with cationic surfactant: safety studies and application in oral delivery of paclitaxel to treat chemical-induced breast cancer in rat. *Pharm Res.* 2009;26(11):2495–503.
45. Mittal G, Chandraiah G, Ramarao P, Kumar MR. Pharmacodynamic evaluation of oral estradiol nanoparticles in estrogen deficient (ovariectomized) high-fat diet induced hyperlipidemic rat model. *Pharm Res.* 2009;26(1):218–23.
46. Jain AK, Swarnakar NK, Godugu C, Singh RP, Jain S. The effect of the oral administration of polymeric nanoparticles on the efficacy and toxicity of tamoxifen. *Biomaterials.* 2011;32(2):503–15.
47. Xie X, Tao Q, Zou Y, Zhang F, Guo M, Wang Y, et al. PLGA nanoparticles improve the oral bioavailability of curcumin in rats: characterizations and mechanisms. *J Agric Food Chem.* 2011;59(17):9280–9.
48. Raj S, Khurana S, Choudhari R, Kesari KK, Kamal MA, Garg N, et al., editors. Specific targeting cancer cells with nanoparticles and drug delivery in cancer therapy. *Seminars in cancer biology.* Elsevier; 2021.
49. Chen H, Zheng Y, Tian G, Tian Y, Zeng X, Liu G, et al. Oral delivery of DMAB-modified docetaxel-loaded PLGA-TPGS nanoparticles for cancer chemotherapy. *Nanoscale Res Lett.* 2011;6(1):4.
50. Joshi G, Kumar A, Sawant K. Enhanced bioavailability and intestinal uptake of Gemcitabine HCl loaded PLGA nanoparticles after oral delivery. *Eur J Pharm Sci.* 2014;60:80–9.
51. Reynolds JL, Mahato RI. Nanomedicines for the treatment of CNS diseases. *J Neuroimmune Pharmacol.* 2017;12(1):1–5.
52. Cai Q, Wang L, Deng G, Liu J, Chen Q, Chen Z. Systemic delivery to central nervous system by engineered PLGA nanoparticles. *Am J Transl Res.* 2016;8(2):749.
53. Sánchez-López E, Ettcheto M, Egea MA, Espina M, Cano A, Calpena AC, et al. Memantine loaded PLGA PEGylated nanoparticles for Alzheimer's disease: in vitro and in vivo characterization. *J Nanobiotechnol.* 2018;16(1):1–16.

54. Zhang L, Han L, Qin J, Lu W, Wang J. The use of borneol as an enhancer for targeting aprotinin-conjugated PEG-PLGA nanoparticles to the brain. *Pharm Res.* 2013;30(10):2560–72.
55. Wang L, Feng M, Li Y, Du Y, Wang H, Chen Y, et al. Fabrication of superparamagnetic nano-silica@quercetin-encapsulated PLGA nanocomposite: potential application for cardiovascular diseases. *J Photochem Photobiol B Biol.* 2019;196:111508.
56. Zhang M, He J, Zhang W, Liu J. Fabrication of TPGS-stabilized liposome-PLGA hybrid nanoparticle via a new modified nanoprecipitation approach: in vitro and in vivo evaluation. *Pharm Res.* 2018;35(11):1–13.
57. Dawid-Pač R. Medicinal plants used in treatment of inflammatory skin diseases. *Adv Dermatol Allergol/Postępy Dermatol Alergol.* 2013;30(3):170.
58. Gourishetti K, Keni R, Nayak PG, Jitta SR, Bhaskaran NA, Kumar L, et al. Sesamol-loaded PLGA nanosuspension for accelerating wound healing in diabetic foot ulcer in rats. *Int J Nanomedicine.* 2020;15:9265–82.
59. Anwer MK, Mohammad M, Ezzeldin E, Fatima F, Alalaiwe A, Iqbal M. Preparation of sustained release apremilast-loaded PLGA nanoparticles: in vitro characterization and in vivo pharmacokinetic study in rats. *Int J Nanomedicine.* 2019;14:1587.
60. Panda BP, Krishnamoorthy R, Bhattamisra SK, Shivashekaregowda NKH, Seng LB, Patnaik S. Fabrication of second generation smarter PLGA based nanocrystal carriers for improvement of drug delivery and therapeutic efficacy of gliclazide in Type-2 diabetes rat model. *Sci Rep.* 2019;9(1):1–15.
61. Jain S, Rathi VV, Jain AK, Das M, Godugu C. Folate-decorated PLGA nanoparticles as a rationally designed vehicle for the oral delivery of insulin. *Nanomedicine.* 2012;7(9):1311–37.
62. Ren T, Zheng X, Bai R, Yang Y, Jian L. Utilization of PLGA nanoparticles in yeast cell wall particle system for oral targeted delivery of exenatide to improve its hypoglycemic efficacy. *Int J Pharm.* 2021;601:120583.
63. Zazo H, Colino CI, Lanao JM. Current applications of nanoparticles in infectious diseases. *J Control Release.* 2016;224:86–102.
64. Cunha-Azevedo EP, Py-Daniel KR, Siqueira-Moura MP, Bocca AL, Felipe MS, Tedesco AC, et al. In vivo evaluation of the efficacy, toxicity and biodistribution of PLGA-DMSA nanoparticles loaded with itraconazole for treatment of paracoccidioidomycosis. *J Drug Deliv Sci Technol.* 2018;45:135–41.
65. Nayak B, Panda AK, Ray P, Ray AR. Formulation, characterization and evaluation of rotavirus encapsulated PLA and PLGA particles for oral vaccination. *J Microencapsul.* 2009;26(2):154–65.
66. Singh L, Kruger HG, Maguire GE, Govender T, Parboosing R. The role of nanotechnology in the treatment of viral infections. *Ther Adv Infect Dis.* 2017;4(4):105–31.
67. Joshi G, Kumar A, Sawant K. Bioavailability enhancement, Caco-2 cells uptake and intestinal transport of orally administered lopinavir-loaded PLGA nanoparticles. *Drug Deliv.* 2016;23(9):3492–504.
68. Sarti F, Perera G, Hintzen F, Kotti K, Karageorgiou V, Kammona O, et al. In vivo evidence of oral vaccination with PLGA nanoparticles containing the immunostimulant monophosphoryl lipid A. *Biomaterials.* 2011;32(16):4052–7.



Pharmacokinetics of Nanoparticle Systems for Pulmonary Delivery

19

Bhupendra Prajapati, Himanshu Paliwal,
and Jayvadan Patel

Contents

1	Introduction	348
2	Pharmacokinetics and Distribution of Nanoparticle-Based Formulations for Pulmonary Delivery	354
	References	362

Abstract

The introduction of nanotechnology in the pharmaceutical field has incited the attention of researchers to develop nanoparticle-based formulations to treat pulmonary diseases. The main reason behind this popularity is because of the vast surface area of the lungs and limited barriers obstructing the penetration. The nanoparticle drug delivery systems targeting the lungs by inhalational route provides potential alternative to oral and intravenous systems of drug delivery as it not only prevents the inactivity by enzymatic degradation and first-pass metabolism, but it also restricts the undesirable adverse effects. In case of pulmonary diseases, inhalational systems furnish targeted delivery to

improve therapeutic efficiency at the specific site. The pulmonary systems have been fabricated using a variety of methods, ranging from traditional approaches like spray-drying and pulverization to the advanced techniques, such as supercritical fluid extraction, micellar solubilization, etc. In order to assess the efficacy and targetability, the pharmacokinetic and biodistribution studies of nanoparticle formulations for pulmonary delivery are very essential. The chapter aims at discussing about various nanoparticle formulations which have been developed specifically for targeting the lungs. A number of recent and relevant literatures with the outcomes of their pharmacokinetic and biodistribution studies have been talked about and compared to justify the potential of nanoparticle formulations for the management of pulmonary diseases.

B. Prajapati (✉) · H. Paliwal
Shree S.K. Patel College of Pharmaceutical
Education and Research, Ganpat University,
Mahesana, Gujarat, India

J. Patel
Nootan Pharmacy College, Faculty of Pharmacy,
Sankalchand Patel University,
Visnagar, Gujarat, India

Keywords

Pulmonary delivery · Nanoparticle formulation · Inhalational route · Pulmonary diseases · Pharmacokinetic studies · Biodistribution

1 Introduction

In recent years, there has been an increase in interest in pulmonary delivery of nanoparticles via various dry powder formulations [1]. For a long time, various systems for the treatment of a variety of lung diseases such as solid lipid nanoparticles, polymeric nanoparticles, and liposomes have been studied [2]. Hydrophobic small molecular compounds can be embedded in nanoparticles for drug delivery to improve stability and therapeutic effects [3]. The storage of DNAs or RNAs in polymer carriers with variable surface loads to improve cellular absorption and exogenous gene expression has resulted in efficient gene delivery. Drug supply systems from nanoparticles can be used to supply drugs, improve bioavailability, and support systemic drug release [4]. An improved permitted permeability and retention can achieve increased concentrations of nanoparticles in specific areas (EPR) [5].

1.1 Lung Diseases and Their Choice of Treatment

Lung Cancer

The disease of lung cancer is an abnormal development of tumors by the cells in your lungs [6]. In the Western areas, lung cancer is a major contributor toward the death count and accounts for >30% of all cancer deaths. In a phase III study, paclitaxel and albumin were formulated into nanoformulation and was shown to be more effective and having very less side effects as compared to the standard paclitaxel formulation [7]. Because EGFR is highly expressed in non-small cell lung cancer, it has been used as a tool for targeting the cancerous cells in the lungs [8].

Drug of choice: Cisplatin (dried nanoparticle), paclitaxel (polymeric nanoparticle), etc.

Asthma

Chronic obstructive airway disease, like as asthma, is characterized by mucus hypersecretion and

severe inflammation [9]. Polymeric steroid nanoformulations can accumulate and provide greater benefits at the site of airway inflammation [10]. Recent nanomedicine advances provide an opportunity for substantial improvements in current asthma therapies, and the strategy enables enhanced ICS levels to be delivered which helps to reduce systemic adverse effects [11].

Drug of choice: Beclomethasone (lipid nano-carrier), curcumin (polymeric nanoparticle), etc.

Chronic Obstructive Pulmonary Disease (COPD)

COPD is a chronic pulmonary disease that inflammates your lungs and makes breathing harder. The inflammation causes excessive mucosal production and the thickening of your lungs. When using nanoparticles as drug delivery for chronic inflammatory pulmonary diseases, there are several benefits. They offer sustainable release of medicinal products and help to overcome airway defenses and target diseased cells at the same time [12].

Drug of choice: Fluticasone (dried nanoparticle).

Pulmonary Hypertension

Pulmonary hypertension refers to high blood pressure in the lungs. Unlike high blood pressure, which affects all blood vessels, pulmonary hypertension affects only the blood vessels between heart and lungs. Hypertension nanoparticles of nifedipine are coprecipitated to form a colloid that exhibits a negative surface charge with stearic acid [13].

Drug of choice: Iloprost (liposomes), Carvedilol (polymeric nanoparticle), etc.

Interstitial Lung Disease

The interstitial lung diseases are a group of chronic disorders that involve the entire lung parenchyma as well as the alveolar interstitium [14]. Some examples are bronchiolitis obliterans and idiopathic pulmonary fibrosis (IPF).

Drug of choice: Amikacin (liposomes), tacrolimus (lipid nanoparticle), etc.

Cystic Fibrosis

Cystic fibrosis is a mostly genetic disorder; when there is mutation of CFTR, cystic fibrosis occurs [15]. Thick mucus can result from cystic fibrosis. This thick mucus can grow and make it harder to breathe in your lungs. Bacteria are much easier to grow with and the risk of lung infections is increased. Cysteamine, an FDA-approved pro-teostasis regulator for CF 30 years ago, showed promising results for CF treating cysteamine [16].

Drug of choice: Ivacaftor (nanostructured lip carriers), gene therapy by AeroEclipse nebulizer (pDNA) complexed with cationic liposome GL67A and gene transfer agents.

Respiratory Distress Syndrome

RDS is most common in premature babies, affecting nearly all newborns born before 28 weeks of pregnancy [17]. For nanotechnology treatment of RDS, a novel long-acting biocompatible phospholipid micelle was developed. It can modulate key signaling molecules which can be critical to response that are inflammatory in RDS [4].

Pneumonia

Pneumonia is an infection of the lungs which is caused by various microorganisms like bacteria, viruses, or fungi. Microorganisms multiply and thrive in the lungs, causing unpleasant symptoms. The air sacs become inflamed and may fill with fluid, causing the flow of oxygen to be disrupted [18].

Drug of choice: Amoxicillin (polymeric nanoparticle), azithromycin (PLGA-based nanoparticle), etc.

Internal Bleeding in the Lungs

Hemorrhaging of the lung is uncommon. It occurs when blood leaks into the main lung from

blood vessels in the windpipe or airways. Children of all ages can suffer from pulmonary hemorrhage. It can begin gradually and last a long time, or it can be a sudden and life-threatening event [19].

Drug of choice: Magnetically driven nanoparticle containing thrombin, hemostatic dexamethasone nanoparticles (hDNP) loaded with corticosteroid, etc.

1.2 Anatomy and Physiology of the Lungs

Two regions comprise the respiratory system: lower and upper respiratory tract. The nasal cavity, nose, and pharynx comprise the upper respiratory tract, whereas the trachea, bronchi, and bronchial tubes comprise the lower respiratory tract (Fig. 19.1). The trachea starts at the laryngeal border and separates into two bronchi before continuing into the lungs. Smaller bronchioles get divided from the bronchi in the lungs so that air channels can be generated. Terminal sections of the bronchi are called as alveoli (Fig. 19.1). The functional unit of the lungs is the alveoli which help in exchange of gases. Diffusion of oxygen into the bloodstream takes place through the walls of alveoli and the interstitial space. Diffusion of carbon dioxide takes place in the opposite way during the process of expiration [20]. Alveolus is coated with a layer of alveolar mucus and fluid, the core material of which are surface proteins and phospholipids. The surface tension in the alveoli is reduced by this phospholipid surfactant layer, which is necessary for efficient gas exchange. For the oxygen supply and elimination of carbon dioxide, collaboration of the respiratory and circulatory systems takes place [21].

Inhalation requires the employment of rib cage muscles, particularly the diaphragm, which is the largest. Contraction and flattening of the diaphragm allow the lungs to suck the air. Exhalation relaxes the diaphragm and rib cage muscles. As a result, the air is naturally expelled

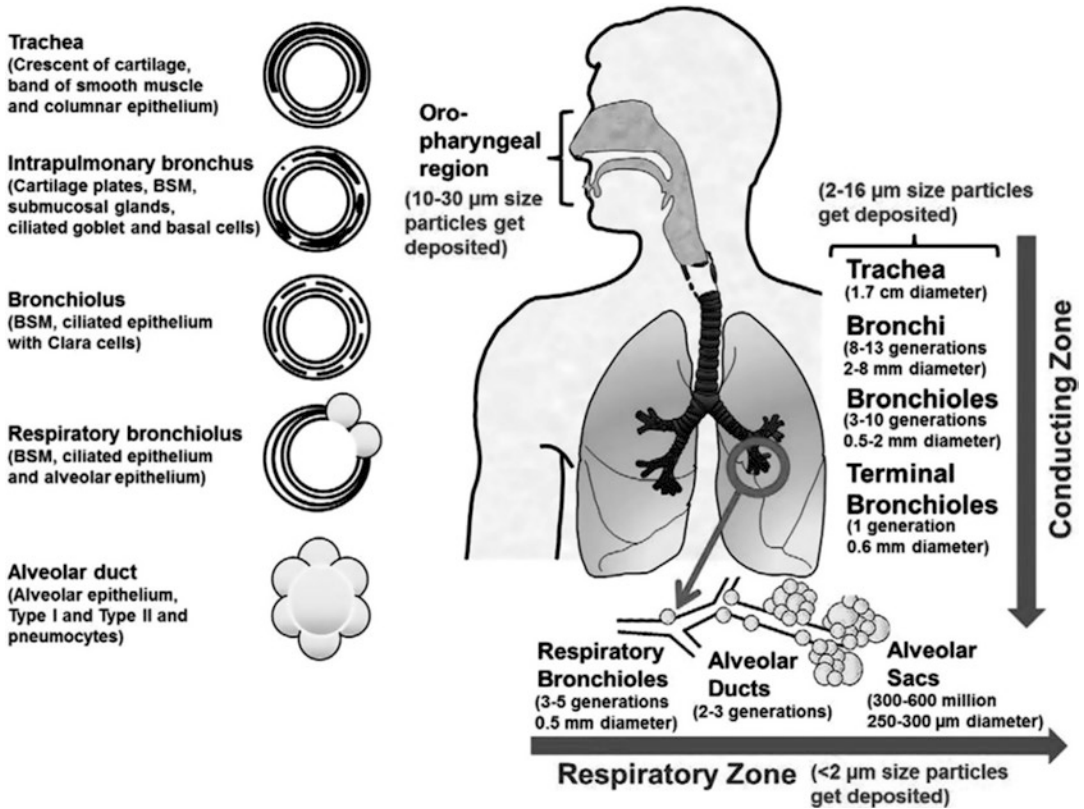


Fig. 19.1 Representation of particle deposition in the lungs according to different mechanisms related to particle size. BSM, bronchial smooth muscle [22]

from the lungs. Air is inhaled through the nose and mouth to meet oxygen demands. The mucous membrane in the nose warms and moistens the air while also trapping foreign particles. The alveoli, which are grouped in clusters like bunches of balloons, are where airways come to an end. Inhalation causes balloons to expand, allowing air to rush in to fill the vacuum. The balloons deflate, and air escapes the lungs. The blood picks up oxygen as it passes through the walls of the air sacs and transports it to the rest of the body [23]. Some of the critical factors affecting pulmonary drug delivery is illustrated in Table 19.1.

1.3 Deposition

The initial stage following inhalation is particle deposition, which is required for additional pro-

cesses to occur. There are several ways for determining particle deposition as follows:

Inertial impaction

Large particles having size of $>5 \mu\text{m}$ moves with velocity that forces the molecule out of the air stream so that it can impact into the wall. Inertial impaction is proportional to the velocity, density, and square of the particle diameter. Impaction (P1) is calculated by

$$P1 = 1 - \frac{2}{\pi} \cos^{-1}(\theta \cdot St) + \frac{1}{\pi} \sin(2 \cos^{-1}(\theta \cdot St))$$

$$St = \text{Stoke number} = \frac{\rho d^2 v}{18 \mu D}$$

θ = Angle of branching; ρ = particle density; v = velocity of particle; D = airways diameter.

Applicability of the preceding P1 equation is when $(.St)$ is less than one, however if (St) is one, the P1 is 1 [30].

Table 19.1 Factors affecting pulmonary drug delivery

Factors	Impact
Flow and quantity of air	Airflow rate, volume inhaled, and breathing life all have an effect on deposition in the lung. If the patient inhales at higher airflow rates, the impaction of the throat increases and the lung dose decreases [24]
Size of formulation	Fine aerosols on peripheral airways are distributed, but they do deposit less drugs in the surface area per unit than large particulate aerosols, which deposit more drugs per unit area, but on larger, central airways [25]
Aerodynamic impaction	The larger the particles, the more likely they are to “crash out” of the airstream and deposit on an airway. Similarly, particles traveling faster will collide more readily [26]
Bronchi	The distribution of drug deposition into the lung is also affected by an increase in bronchial impact which reduces the number of particles available on the alveoli to sediment [27]
Throat size	Smaller throats trap more particles, resulting in a lower lung dose [28]
Electrostatics	Mirror charges and field charge effects in the lung have the potential to attract particles to the airways and significantly affect deposition [29]

Sedimentation

The driving force for the particle deposition through sedimentation. Most of the particle size sedimentation is seen for the particles having size in the range of 0.5–5 μm which exceeded the impaction to arrive 5–6 generation of lungs [31]. Deposition of particle by sedimentation is calculated by

$$p_s = 1 - e^{-[4gC\rho d^2L \cos\theta / 9\pi\mu Rv]}$$

g = Force of gravitation; C = correction factor of Cunningham slip angle; R = airway radius; L = length of the tube, v = velocity of particle.

Diffusion

The deposition of particles below 0.5 μm governs the Brownian motion in the alveolar and lower airways.

Table 19.2 Mechanism of deposition in different areas of the lungs based on particle size [33]

Location	Size (μm)	Mechanism
Primary bronchi	5–10	Impaction
Secondary bronchi	1–5	Sedimentation
Bronchioles	1–3	Sedimentation
Alveoli	0.5	Brownian motion

$$p_d = \sqrt{\frac{2kTC}{3\pi\eta_d R}}$$

k = Boltzmann constant; T = temperature; η = gas viscosity.

Direct interception

Due to interception, the extended form of fibers is deposited in the upper airways. In this phenomenon, one side of the particle impacts the surface, while the other side of the particle is free and the center of gravity of the particle lies in the gas's streamline.

Electrostatic disposition

When high pressure is involved in the production of particles, they normally become charged due to which a charge is stimulated on the walls which are then neutralized by adhering to the wall. Charged particles are deposited with the help of this method [32]. Various locations of pulmonary region wherein the particles get deposited are included in Table 19.2.

1.4 Factors Affecting the Particle Deposition

The respiratory tract's dynamics and inhaled particle properties assist as the foundation for particle deposition. The nature of the dynamics involved in pulmonary delivery is flow patterns, turbulence, non-dimensional analysis association with mucus, temperature, and aerodynamic diameter. The particle properties include size, charge, density, shape, solubility, and lipophilicity [34–36]. Figure 19.2 depict critical problems

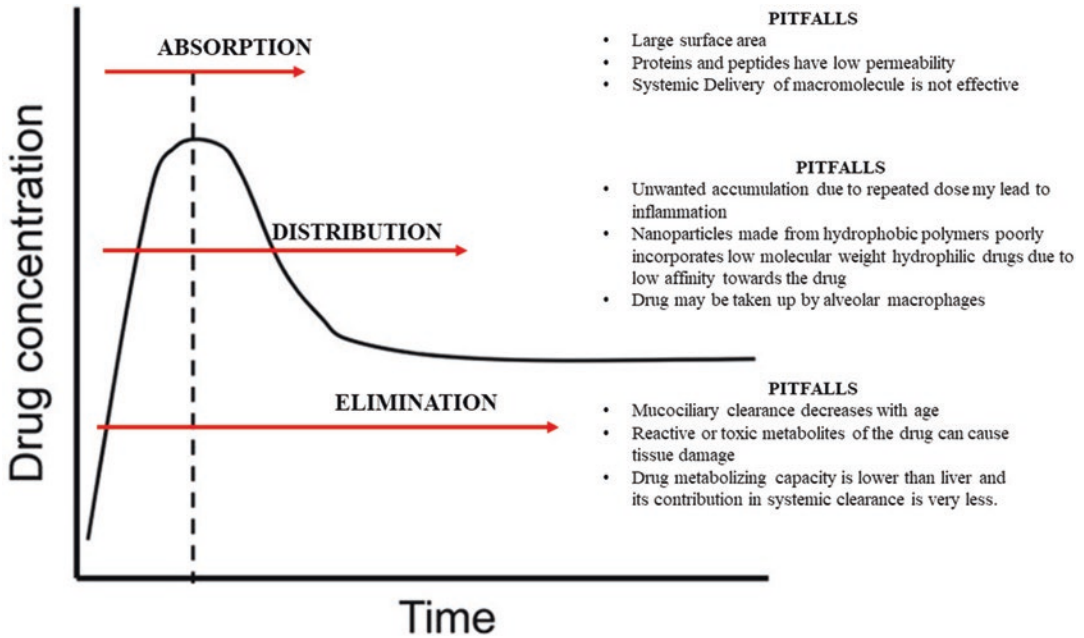


Fig. 19.2 Critical problems associated with absorption, distribution, and elimination after pulmonary drug delivery

associate with absorption, distribution and elimination after pulmonary drug delivery.

Properties of Particle

Aerodynamics

The term aerodynamic diameter (d_{ac}) refers to the diameter of a particle as the sphere having density equal to one and which can settle at equal velocity and can be determined by equation

$$d_{ac} = d_g \sqrt{\frac{\rho}{X}}$$

d_g = Geometric diameter, ρ = particle density, χ = dynamic shape correction factor.

Aerosol particle size is measured in terms of mass median aerodynamic diameter (MMAD) and geometric standard deviation (GSD) [37].

Shape

Spherical particles are desirable because they are easier to process; however, the concept of nons-

pherical particle deposition in the lungs stems from asbestosis produced by fiber deposition. As these particles are deposited in the outer areas due to interception, the particle can be made to crystallize in an extended form to target deposition [38].

Density

The particle density is inversely related to the particle's chances of reaching the deeper regions. Hollow particles, which have benefit over tiny non-porous denser particles, can be used to yield less dense, large-sized particles [39].

Charge

Particles which have positive charge are attached to the membrane having their half-life of absorption in the range of hours to days [40].

Molecular weight

Molecules whose lipid solubility is enough to pass across the membrane are not affected by the molecular weight. The absorption of lipid insoluble compounds exceeding 1000D is influenced by the molecular weight [41].

Properties of the Respiratory Tract

Airway geometry

As the branching of the respiratory area increases, the turbulence also increases, which leads to an increase in the chance of impaction deposition [41].

Inhalation pattern

The mean residence time and the tidal volume help in controlling the deposition of particles [41].

$$\text{Total deposition} = (DT_m)^{0.5} V_t^{0.49}$$

D = Diffusion coefficient, T_m = mean residence time, V_t = tidal volume.

Airflow velocity

Due to an increase in the airflow velocity by the mechanism of impaction, the oropharyngeal area deposition occurs. The residence time of particle is reduced due to high amount of airflow due to which sedimentation and diffusion deposition are also reduced. Simple and appropriate turbulent flow causes deposition in the top areas (impaction), while the sluggish pace produces deposition in the lower parts (deposition). Lower airways are affected by deposition (sedimentation and diffusion) [41, 42].

Inhalation

Nasal inhalation results in less deposition than oral inhalation.

Absorption

The particles of the drug which slowly disperse are able to retain in the lungs for hours or even days. The dissolving medium in the lungs is made up of 96% water with salts, proteins, phospholipids, and mucins having a total volume of 10–30 mL resulting in a pH of 6.6. For the absorption to take place, the drug particles are required to be present in the dissolved form, or they may be eliminated by any of the previously listed mechanism of clearance. For the drug to be absorbed or metabolized, the particles of drug

must contact the layer of surfactant. With the help of this mechanism, the solubility of the small molecules is enhanced, and the macromolecules are aggregated. The epithelium, which is thick in the trachea (50–60 m) and thin in the alveoli (0.2 m), functions as a barrier to medicament absorption [42, 43].

Clearance

The clearance of particles from the respiratory system comprises the clearing of particles from the nasopharyngeal, trachea-bronchial, and pulmonary compartments. Mucociliary and mechanical clearance from the nasopharyngeal compartment, and also absorption into the circulation, are all components of nasopharyngeal clearance. The alveolar macrophage-mediated clearance, circulatory absorption, and endocytosis into the interstitium with the help of endothelial cells are responsible for the clearance from the lungs. The rate of clearance declines with age, but workout raises the rate of clearance. In the occurrence of influenza and pneumonia, clearance might be delayed up to 3 months to a year [44].

Mucociliary clearance

The main clearance occurs by this mechanism; it is the synchronous sweeping movement by cilia and mucus. Synchronous impulses by cilia induce mucus to travel propulsively toward the larynx, where it is cleared by swallowing or coughing. This process normally removes insoluble particles larger than 6 m in size, and the majority of particles are eliminated within 24 hours following inhalation [45].

Alveolar clearance

Particles with limited solubility or those containing material for continuous release have enough time to be phagocytized by macrophages before being cleared via the lymphatic system, MCC, or enzymatic destruction. Phagocytosis is more susceptible to particles with diameters of 1.5–3 m. With increasing molecular weight, the alveolar permeability decreases [46].

Mechanical clearance

When large particles (10 μ m) are ingested, they elicit spontaneous coughing, sneezing, and swallowing. It is present in the upper airways which causes elimination of the drug [47].

2 Pharmacokinetics and Distribution of Nanoparticle-Based Formulations for Pulmonary Delivery

2.1 Liposomes

Liposome is considered as an appealing technology for drug delivery, particularly for applications in pulmonary, because they are made mostly of phospholipids, which are found naturally in the lungs. They are spherical vesicles of lipid type which can hold water within a bilayer phospholipid layer of oval structure. Liposomes are the most common vesicles having the capability of transporting both lipophilic and hydrophilic molecules. Liposomes can be manufactured by using various types of phospholipids, which has an impact on their characteristics and stability, but the widely employed agent for liposome manufacturing is PC lipids-phosphatidylcholine. The advantages of using liposomal formulations are as follows: (a) biocompatible, biodegradable, non-toxic, and non-immunogenic, (b) greater stability, (c) encapsulated drug is protected from external environment, and (d) reduces exposure of harmful medications to vulnerable tissues. Despite showing promise, the liposomes are associated with limitations such as high cost of production, possible leakage and fusion which may occur with the encapsulated drugs, short half-life, etc. [48].

Liposomal systems have also displayed a lot of potential for pulmonary delivery of therapeutic agents. The inhalational nanoliposomal carriers may improve prolong the retention of drugs in the pulmonary structures to enhance the bioavailability. A group of researchers used film removal and liposomal dispersion techniques to develop liposomes for delivery of tacrolimus. The pulmo-

nary pharmacokinetic study was performed using albino rats to determine mean pharmacokinetic parameters. The spray-dried inhalational products prepared during the investigation showed increased AUC and $t_{1/2}$ values as compared to the plain drug DPIs. The outcomes of the pharmacokinetic studies showed the retention of tacrolimus in the lungs up to 24 hours and significantly low clearance rate. The longer residence time of drug in the pulmonary region may be helpful in lowering the chances of sudden discharge and long-term rejection when tacrolimus-like drug molecules are administered for salvage therapy [49].

The pulmonary route poses problems for the delivery of peptides and protein-based therapeutic agents because of the intricate structures of respiratory system. The attempts of delivering insulin via the pulmonary route have been made wherein film shaking and membrane destabilizing methods were employed to develop liposomal carriers containing insulin. The distribution of liposomes was efficient and consistent throughout the study. The insulin-containing liposomes produced significant lowering of blood glucose level in diabetic mice. The administration of insulin through the pulmonary route provides noninvasive way of delivery with sustained release behavior [50]. The pulmonary administration of antibiotics by using nebulizer may show potential for the treatment of pulmonary infections because it increases the amount of drug reaching to the site of action and reducing the possibilities of side effects. The report of preparation of freeze-dried liposomes containing rifampicin displays such characteristics. The pharmacokinetic investigation of liposomes indicated that drug is released in a controlled fashion for prolonged duration of time. The plasma concentration of rifampicin from liposomes begins to show up after 4 hours and could be detected until 48 hours. Pharmacokinetic and disposition behavior of such formulations proffer a reasonable justification for using liposomes for treatment of tuberculosis and other diseases [51]. Liposomes of remdesivir as a nebulizable delivery system against COVID-19 was developed by using the modified hydration method, which

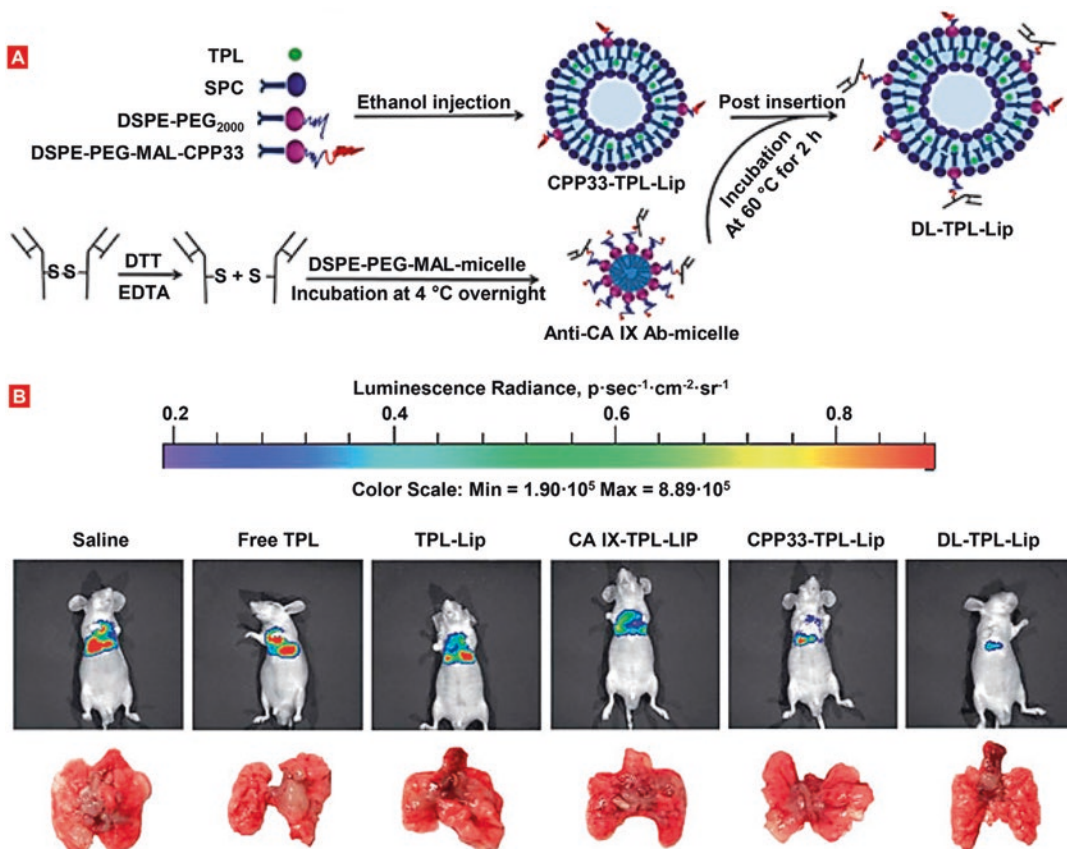


Fig. 19.3 Pictorial illustration of research investigation which involved preparation of dual-ligand triptolide-containing liposomes for the treatment of lung cancer. The

biodistribution of anticancer agent was indicated in the lung tissues of the mice, even after completion of 31 days [54]

allows scaling of dosage form for large-scale preparation. The nanoliposomes of remdesivir showed excellent characteristics during evaluation, along with low toxicity and prolonged release behavior. Although the outcomes of the investigation showed potential of reducing the dosing frequency and better therapeutic activity, the pharmacokinetic and distribution study is not performed [52]. A group of scientists studied the distribution behavior of the PEGylated liposomes delivered in the form of aerosols in the lungs of mice. The micro sprayer was utilized for delivering the aerosolized liposomes in the mice lungs with pulmonary fibrosis. The PEGylated liposomes showed prolonged retention, and their concentration was found out to be higher in bronchoalveolar lavage fluid but comparable to non-

modified liposomes in alveolar macrophages and fibrotic tissues in the lungs [53].

Figure 19.3 demonstrates that the biodistribution of anticancer agent was indicated in the lung tissues of mice, even after completion of 31 days during the study focused on dual-ligand triptolide-containing liposome formulation [54].

2.2 Solid Lipid Nanoparticles (SLNs) and Nanostructured Lipid Carriers (NLCs)

SLNs are nanoscale aqueous suspensions made up mostly of triglycerides and phospholipids. For pulmonary requests, phospholipids and triglycerides are used in the ratio of 30:70. SLNs are alike

to emulsion of lipids, except instead of oil, solid lipid is used. In order to get a stable nanoparticle dispersion having suitable stability, SLNs contain 0.1–30% w/w solid lipid and 0.5–5.0% w/w stabilizer. Because of the ordered organization of solid lipids in SLNs, drug encapsulation is low, and some of the lipids crystallize, triggering drug ejection. NLCs were created in order to solve the drawbacks of SLNs. Lipids of solid and liquid are combined in NLCs so that a matrix with more disorder allows for greater drug encapsulation. The advantages of using SLNs and NLCs are low toxicity, biocompatibility, long-term stability, easy scaling-up, sterilized, controlled drug release, targeted drug release, protection of incorporated compounds, etc. On the other hand, some of the disadvantages that hamper the use of SLNs and NLCs are unpredictable gelation tendency and unexpected polymeric transitions [55, 56].

SLNs can offer potential for pulmonary delivery as they provide opportunity of depositing the drug into the internal lung structures, predominantly due to nanoscale size, extended release, and lesser toxicity [57]. SLNs were tried out for enhancing the localization and treatment potential of amikacin. The prepared lipid nanoparticles were further labeled with ^{99m}Tc to track amikacin during the biodistribution studies. The amikacin-loaded SLNs given through the pulmonary route showed better accumulation in the lungs as compared to the free amikacin given through *IV* route. The percent injected dose/gram for lung after half-hour was 37.9 for pulmonary administration and 2.1 for *IV* route. However, the drug administered via both the route started dropping after 6 hours, but the outcomes were sufficient to prove clear benefits of using SLNs for pulmonary delivery [58].

The SLNs were also utilized for delivery of insulin by Liu et al., where they have used reverse micelle-double emulsion method to produce SLNs for delivery of insulin through the pulmonary route. Diabetic male Sprague Dawley rats were injected with 20 IU/kg insulin-containing SLNs along with blank SLNs to investigate pharmacokinetic and pharmacodynamic characteristics. Pharmacokinetic studies revealed that plasma concentration of insulin increased signifi-

cantly after administration of SLNs and achieved peak concentration of 170 $\mu\text{IU/mL}$ in 4 hours. The plasma concentration profile of insulin displayed the slow absorption of drug after pulmonary administration of insulin-containing SLNs, and mean absorption time was about 8 hours which suggests the steady clearance of insulin from the lungs, possibly because of tissue binding. The insulin released from the SLNs distributed evenly over the alveolar structures. SLNs proved to avoid generation of blocking protein aggregates which lead to increase in stability as well as improving their transmembrane movement [59].

Yang et al. demonstrated a novel technique of using poly(lactic-co-glycolic acid) microspheres to develop SLN-based carriers for simultaneous delivery of afatinib and paclitaxel. The research involved loading of afatinib into SLNs, followed by incorporating paclitaxel into micro-poly-lactidum co-glycolide. In addition to various characterization studies, the SLNs were also subjected to *in vivo* pharmacokinetic and tissue distribution studies using Sprague Dawley rats. The T_{max} of both afatinib and paclitaxel were observed to be 8 hours, while C_{max} values of afatinib and paclitaxel were found out to be 18.69 $\mu\text{g/mL}$ and 28.31 $\mu\text{g/mL}$, respectively, indicating the faster release of paclitaxel as compared to afatinib. The $T_{1/2}$ of the pulmonary SLN formulation was significantly higher than oral and intravenously administered afatinib and paclitaxel. The tissue distribution of both afatinib and paclitaxel was higher in pulmonary region, even after completion of 18 hours. The prolonged retention of drugs in the lung regions further validates the potential of pulmonary SLNs developed by the researchers [60].

Peng Ji et al. prepared solid lipid nanoparticles of a water poor soluble flavonoid compound, Naringenin was formulated and studied for pharmacokinetic in Sprague Dawley rats. The study proved that relative bioavailability of formulated SLNs was increased to 2.53-fold compared to its suspension administered by the pulmonary route [61]. Sustained release SLNs of Yuxingcao essential oil prepared and evaluated for its prolonged pulmonary retention and improve bioavailability.

The results indicated high AUC value by almost 4.5–7.7-folds compared to similar dose by intratracheal and by 257–438-folds to the intravenously dosed [62]. Pharmacokinetic and biodistribution investigation of sterically stabilized SLNs of paclitaxel was performed by Li et al. and compared with marketed product Taxol®. The study concluded that there are no statistically significant differences in pharmacokinetic parameters [63].

2.3 Dendrimers

Dendrimers are polymer molecules with extraordinary symmetry, a fast-branching rate, and a large number of modifiable terminal functional groups. The nucleus, which is located in the middle of the dendrimer molecule, branches that centrifugally extend from the nucleus, and numerous functional groups which are terminal, which are localized on the surface of dendrimer, are the three basic domains that form the dendrimer structure, and it resembles a tree. Dendrimers are globular macromolecules that are monodispersed and have a size range of 1–100 nm. They are prepared by divergent and convergent methods [64]. The benefits of employing dendrimers are as follows: (a) targeted drug delivery, (b) solubility improvement of poorly soluble drugs, (c) passes through cell membrane due to small size, and (d) high structural homogeneity. However, high production cost and probable toxicity of unmodified dendrimers may pose issues during formulation [65].

A literature discussed about preparing inhalational dendrimer system to deliver chemotherapeutic agents and comparing their activity with intravenous alternatives. PEGylated dendrimers were prepared and incorporated with doxorubicin to achieve the controlled release and retention of anticancer agent in lungs for longer duration. The modified dendrimer showed quick adsorption in the blood, as well as rapid removal from lungs in 24 hours through mucociliary clearance and about 15% of the drug concentration from the formulation retained in the lungs. The outcomes were highly in favor of using pulmonary product, as dendrimer given through the intratracheal

route showed 95% decrease in lung tumor in 2 weeks, while only 30–50% reduction achieved by intravenous administration. Therefore, it was lucid that PEGylated dendrimers can be employed as inhalational product to enhance the longer retention of anticancer agents in the lung tumor cells [66]. The targeted delivery into the lungs is vital for enhancing the drug concentration at the specific sites for the management of pulmonary disorders. Ryan et al., prepared the PEGylated dendrimers for pulmonary delivery and examined the effect of size of dendrimer and their absorption over retaining their concentration for longer duration in the lungs. The absorption of dendrimer was significantly higher in case of large-sized dendrimers (20–30% of administered does) as compared to smaller ones showing only 2% absorption. However, the higher molecular weight dendrimer results in slow absorption and better retention in lung tissues. The results explicated that PEGylated dendrimer are suitable for inhalational route to provide systemic delivery of therapeutic molecules, thereby serving as reliable substitution to injectable systems and exhibiting controlled release of drug in to the systemic circulation or lung tissues [67].

2.4 Nanoemulsions

The colloidal dispersions which are made up from surfactant, oil, or co-surfactant having the mean particle size less than 500 nm are called nanoemulsions. Nanoemulsions are capable of holding both hydrophilic (w/o) as well as hydrophobic (o/w) medicines. Nanoemulsions are appealing alternatives because of their small particle size and large surface area. Small globule size having large surface aids in improving solubility and thereby bioavailability of drugs. Furthermore, the problems such as creaming, flocculation, coalescence, sedimentation, etc. can be avoided without producing any toxicity or irritancy. Nevertheless, the fabrication of such systems is a costly affair, and employing high concentration of surfactants may produce to the lungs [68]. Self-aggregated amphiphilic graft/block copolymers having hydrophobic part on

the inside (core) and outside (shell) part having hydrophilic component are involved in generation of polymeric micelles. A polymeric micelle has a diameter of around 20–50 nm and is made up of several hundred block copolymers. Drugs with low aqueous solubility are stored in the core [69].

2.5 Polymeric Nanoparticles

Polymeric nanoparticles (NPs) have sparked a lot of interest in recent years because of their unique properties. The term “nanoparticle” refers to both nanocapsules and nanospheres, which are different in terms of size and shape. According to their morphology, nanocapsules comprise an oily core having medication dissolved and a polymeric shell which is involved in regulation of release profile of drug from the core. Continuous network of polymer nanospheres helps in having the medicine inside or outside of the sphere. Polymeric nanoparticles may be beneficial by controlling the drug release, offering protection of drug from external environment, enhancing bioavailability and therapeutic index [70].

The polymeric nanoparticles have been considered as potent carriers for the drugs as well as the diagnostic agents for dealing with pulmonary conditions. They possess the ability to subjugate drug resistance and enhancing the pharmacokinetic and distribution characteristics of the active molecules, in order to prolong the retention of drug at the site of treatment and reducing the possible systemic exposure. These nanoparticles can also be fabricated to acquire smart attributes to deliver the drug molecules in particular diseased tissues, microenvironments, or other target areas. Numerous attempts have been made in developing polymeric nanoparticles for pulmonary diseases, to provide curative effects during circulation or to get accumulated in the microstructures in the lungs [71]. A recent literature has discussed about their research work of preparing the YSA-functionalized and PLGA-based nanoparticles to improve delivery of drug in the lungs. Nanoparticles were incorporated with fluorescent dye and tissues harvested for biodistri-

bution studies were subjected to *in vivo* imaging for fluorescence determination. The cellular uptake of YSA-functionalized nanoparticles was much greater than PLGA nanoparticles. The lung-injured animals showed 1.3 times higher accumulation of YSA-functionalized nanoparticles in the lungs as compared to the PLGA nanoparticles [72].

A study depicted designing nanoparticles containing miRNA (miR-146a) for targeting and controlling the expression of the gene IRAK1. Nanoparticles with high stability and sustained release were developed using single emulsion-solvent evaporation technique. The cellular uptake of nanoparticles in A549 cell lines was observed to be dose dependent, along with 40% reduction in expression of IRAK1 [73]. Apart from these, biocompatibility and multidrug loading may be another goal for fabricating nanoparticles with specific types of adjuvants. A self-assembled nanoparticle system, also called Janus particles, was developed to contain anticancer moieties for the delivery through the pulmonary route. These nanoparticles were designed by employing combinations of biocompatible and biodegradable adjuvants. The biodistribution was evaluated by labeling the nanoparticles with red fluorescence (DiR) and estimating the concentration of drug in different organs after inhalation administration into mice. The localization of nanoparticles is predominantly dependent upon the size of particles (155 and 450 nm sized nanoparticles), as relatively smaller particles get accumulated rapidly in the lungs. Furthermore, larger nanoparticles maintained higher concentration as compared to smaller ones post 1 hour after administration. On completion of 24 hours after administration, the 150 nm particles were cleared off completely from lungs, while 450 nm particles retained their concentration. It was evident from the outcomes that 450 nm sized Janus particles were optimum for inhalation treatment of lung cancer [74]. Docetaxel-loaded cholesterol-PEG co-modified poly (n-butyl) cyanoacrylate nanoparticles was prepared by spray-drying and freeze-drying. PK study of sustained release polymeric nanoparticles indicated that plasma concentration of docetaxel was more than

24 hours. It was absorbed much faster and complete into the rat lung. There was increase in $t_{1/2}$ and AUC by 2.3- and 6.5-fold with freeze-dried product and 3.4- and 8.8-fold with spray-dried product compared to free drug after IT administration [75].

2.6 Nanocrystals

The utilization of nanocrystals may help in improving the solubility, increasing the penetration, better release control, and significant mucoadhesion, further leading to bioavailability enhancement of the drugs which makes it a suitable candidate for pulmonary delivery. A number of attempts have been made to develop nanocrystal formulations of pulmonary agents [76, 77]. In one of the studies, the nanocrystal-based dry powder inhalers (DPI) of curcumin were designed using spray-drying method. The researcher investigated the influence of different milling times over the size of particle and aerodynamic characteristics. It was observed that nanocrystals retained the constant size throughout the study and curcumin DPIs showed greater distribution in the lung as compared to other tissues. For the pharmacokinetic studies, anesthetized rabbits were administered with endotracheal insufflation and oral curcumin DPIs and blood samples were collected at different time points. There was considerable variation in between the pulmonary and oral route, as the plasma concentration of curcumin through inhalational route was much greater than the oral route. The peak plasma concentration (C_{max}) of animals administered through the pulmonary route and oral route were 27.52 mg/L and 3.64 mg/L, respectively, and time to reach the maximum plasma concentration (T_{max}) of the pulmonary and oral group of animals were found to be 0.5 hour and 3 hours, respectively. It was clear from the study that curcumin DPIs displayed better and faster absorption of curcumin, which further lead to increase the bioavailability of curcumin [78].

Another study demonstrated the preparation of nanocrystals for inhalational delivery of curcumin acetate for sustained delivery in lungs. The

curcumin acetate was milled and spray-dried to produce inhalable microparticles and nanocrystals. The pharmacokinetic and biodistribution study was conducted using rats after intrapulmonary administration of the formulation. The prolonged retention of nanocrystals of curcumin acetate was observed in pulmonary region with AUC values being 7.62-fold higher as compared to their microparticles. Additionally, there was considerable improvement in in vivo release rate (3.3-fold) and local availability of curcumin by 25.1-fold by using nanocrystal [79]. The nanocrystal technology may also assist in tackling the issues such as gastric irritability and metabolism, especially for celecoxib-like therapeutic agents. The spray-dried nanocrystals of celecoxib were prepared for the management of lung cancer. The outcomes of the study validated the efficiency of the formulation due to their aerosolization potential [80]. The budesonide containing nanocrystals were developed by anti-solvent precipitation and spray-drying method. The enhanced dissolution of drug and greater fine particular fraction of the preparation confirmed the suitability of nanocrystal formulation [81]. However, both the previous researches lack the pharmacokinetic and biodistribution studies to emphasize the in vivo performance and localization.

2.7 Niosomes

Niosomes were one of the advanced and promising vesicular carrier, prepared using non-ionic surfactants and cholesterol. Niosomes prepared for pulmonary delivery may allow slow and targeted release, better therapeutic efficiency, and enhanced mucus infusion [82]. A group of scientists prepared and characterized the niosome formulation containing clarithromycin for pulmonary delivery. The main idea was to use thin film hydration method for formulating several batches with different concentrations of surfactants. The evaluation was performed using Sprague Dawley rats for estimating various pharmacokinetic parameters. The value of C_{max} increased from 2.488 $\mu\text{g/mL}$ for plain clarithromycin to 4.321 $\mu\text{g/mL}$ for clarithromycin con-

taining niosomes. The concentration of drug after 24 hours in the plasma was also considerably higher in case of niosomal formulation. Furthermore, the outcomes of MRT, AUC, and AUMC were several folds higher for niosomes, which displayed the sustained release characteristics of the niosomes [83].

A study was conducted to augment pulmonary delivery by loading the cilomilast in the phosphatidylcholine-rich niosomes to enhance the anti-inflammatory potential. The biodistribution study of the prepared niosomes showed the extensive localization in the pulmonary region which is also a primary target organ. It was clear from the investigation that the concentration of phosphatidylcholine played important role in attaining pulmonary targetability [84]. The studies have also reported the preparation of rifampicin-loaded niosomes and comparing its biodistribution behavior with plain rifampicin solution. The organ biodistribution study was performed using albino rats to estimate the effectiveness of vesicular carriers to localize the drug at specific site. The comparative AUC study revealed better organ localization of drug from the niosome formulation in contrast to plain drug solution. The drug localization capacity in the pulmonary region after intratracheal administration rose up to 145 times from the niosomes in comparison with drug solution. The research showed enhanced bioavailability of rifampicin in the pulmonary region after intratracheal administration of the niosomes. The significant rise in value of mean residence time from the formulation was evident that niosomes prolonged the retention of the drug for improving the therapeutic potential of rifampicin in dealing with lung infections [85].

2.8 Exosomes

However, the utilization of exosomes as drug carrier is under exploration, but some of the studies have demonstrated their potential for pulmonary targeting. The researchers have focused upon employing the exosomes for delivery of agents such as anticancer, antifibrotic, immunomodulators, etc. Exosomes may prove beneficial due to their exceptional stability and low toxicity, pro-

longed retention, lack of immunogenicity, and targeted delivery [86]. A study was reported to develop the fibroblast-based exosomes for improving drug delivery for the treatment of pulmonary fibrosis. Nintedanib (angiokinase inhibitor) was incorporated in the exosomes as an anti-fibrotic agent. The prepared exosomes displayed the notable enhancement in the therapeutic action, which was probably due to increased localization of nintedanib in fibrotic tissues in the lungs as well as reduction in inflammation caused by macrophages [87].

Kim et al. explored around the possibility of development of exosomes to deliver paclitaxel for the management of multiple drug resistance cancer. The exosomes prepared in the investigation were fabricated using sonication to exhibit better loading capacity and sustained release characteristics. The biodistribution studies were carried out with female C57BL/6 mice to examine localization of drug at metastatic tumor sites in the lung within 10–12 days. Although the exosomal formulation possessed potent cytotoxic effect over tumor cells, they showed accumulation around the cancer cells in the lungs in mouse models with carcinoma pulmonary metastasis [88]. This group of researchers has further proposed to develop the engineered macrophage-derived exosomes for even better targeting at the pulmonary region. The aminoethylanisamide polyethylene glycol was employed to prepare exosomes for delivering paclitaxel as such systems can target the sigma receptor in the lungs. The exceptional outcomes were observed as the specially designed exosomes showed intense localization at the lung cancer metastases [89].

2.9 Polyplexes

The delivery of genetic material using bacterial or viral vector may be challenging due to their ability to incite immune response in the host. RNAs and DNAs may be formulated using cationic polymers to form the complexes known as polyplexes or lipoplexes. These carrier systems also protect the incorporated genetic material from the degradation and promote distribution of

drug in deeper cellular structures [90, 91]. A group of scientist researchers developed polyplexes for the delivery of CXCR4 inhibitors PEI-C poly(ethylenimine) derivative to the lungs for the management of pulmonary fibrosis. The safety and efficacy was evaluated in the mice and fluorescent labeling was done for the biodistribution studies. The outcomes of study revealed that polyplexes were mostly observed in the lungs post-intratracheal administration. The concentration of the formulation after 24 hours was maintained to about 42% of what was observed at 1 hour administration. Notably, the localization mainly took place in the lungs as signal intensity was insignificant from the other organs [92]. Dinari et al. prepared a nano-polyplex carrier comprising gold nanorods, pDNA, and poly dimethylaminoethyl acrylate with the goal to

attain peak therapeutic activity and the least adverse effect for gene delivery. This research involved the utilization of “grafting to” technique for improving activity of nanostructures with poly dimethylaminoethyl acrylate because of the attraction of gold atoms for the sulfur compounds. The developed polyplex showed high transfection capacity and limited toxicity. The results of the investigation may pave way to even more research studies focusing over development of new-generation nanoparticle polyplex carriers for efficient delivery of genetic materials. The pharmacokinetic and biodistribution studies may also be done to assess the in vivo behavior of such carrier systems [93]. Table 19.3 summarises the investigations encompassing the pulmonary delivery of nanoparticle formulations.

Table 19.3 List of research investigations encompassing the pulmonary delivery of nanoparticle formulations

Drug	Formulations	Outcomes of pharmacokinetic study	Applications	References
Levofloxacin	PLGA nanoparticles	$C_{\max} = 2.71 \mu\text{g/mL}$ $AUC_{0-\infty} = 380.2 \mu\text{g/g}\cdot\text{h}$ $AUC/MIC = 375.15$	Reaching deeper lung structures for enhancing therapeutic efficacy	[94]
Tranilast	Inhalable nanocrystalline powders	$C_{\max} = 910 \text{ ng/mL}$ $T_{1/2} = 0.250 \text{ h}$ $AUC_{0-24 \text{ h}} = 458 \text{ ng}\cdot\text{h/mL}$	Enhanced anti-inflammatory effects in lung	[95]
Glucagon	PLGA nanoparticles	$C_{\max} = 1.1 \text{ ng/mL}$ $AUC_{0-12 \text{ h}} = 1632 \text{ pg}\cdot\text{h/mL}$ $T_{\max} = 15 \text{ min}$	Extended half-life and enhanced bioavailability	[96]
VIP derivative	PLGA nanoparticles	–	Enhanced anti-inflammatory effects	[52]
Remdesivir	Aerosolized nanoliposome	–	Effective alternative for coronavirus disease	[53]
Bleomycin	Aerosolized PEGylated liposomes	Higher accumulation in bronchoalveolar lavage fluid as compared to alveolar macrophages	Improving intrapulmonary pharmacokinetics	[97]
Paclitaxel	Exosomes	–	Increased cytotoxicity	[88]
Paclitaxel	Exosomes	–	Improved targeting and therapeutic effect in pulmonary metastases	[89]
Itraconazole	Nebulized aerosols of 2-hydroxypropyl-cyclodextrin (HP β CD) solubilized solution (HP β CD-ITZ) and colloidal dispersion (URF-ITZ)	(A) HP β CD $C_{\max} = 3.38 \mu\text{g/g}$ $t_{1/2}$ distribution = 4.87 h, $t_{1/2}$ elimination = 30.9 h $AUC_{0-24 \text{ h}} = 32.0 \mu\text{g h/mL}$ (B) URF-ITZ $C_{\max} = 4.87 \mu\text{g/g}$ $t_{1/2}$ distribution = 2.91 h, $t_{1/2}$ elimination = 28.0 h $AUC_{0-24 \text{ h}} = 27.2 \mu\text{g h/mL}$	Solubilization of poorly soluble drug and enhanced drug absorption	[98]

References

- Deng Z, Kalin GT, Shi D, Kalinichenko VV. Nanoparticle delivery systems with cell-specific targeting for pulmonary diseases. *Am J Respir Cell Mol Biol*. 2021;64(3):292–307.
- Paranjpe M, Müller-Goymann CC. Nanoparticle-mediated pulmonary drug delivery: a review. *Int J Mol Sci*. 2014;15(4):5852–73.
- Bhushan B, Luo D, Schrickler SR, et al. *Handbook of nanomaterials properties*. Springer Science & Business Media; 2014.
- Sadikot RT, Kolanjiyil AV, Kleinstreuer C, Rubinstein I. Nanomedicine for treatment of acute lung injury and acute respiratory distress syndrome. *Biomed Hub*. 2017;2(2):1–12.
- Fang J, Nakamura H, Maeda H. The EPR effect: unique features of tumor blood vessels for drug delivery, factors involved, and limitations and augmentation of the effect. *Adv Drug Deliv Rev*. 2011;63(3):136–51.
- Neal RD, Sun F, Emery JD, Callister ME. Lung cancer. *BMJ*. 2019;365:11725.
- Gradishar WJ, Tjulandin S, Davidson N, et al. Phase III trial of nanoparticle albumin-bound paclitaxel compared with polyethylated castor oil-based paclitaxel in women with breast cancer. *J Clin Oncol*. 2005;23(31):7794–803.
- Mehra NK, Mishra V, Jain NK. Receptor-based targeting of therapeutics. *Ther Deliv*. 2013;4(3):369–94.
- van Rijt SH, Bein T, Meiners S. Medical nanoparticles for next generation drug delivery to the lungs. *Eur Respir J*. 2014;44(3):765–74.
- Matsuo Y, Ishihara T, Ishizaki J, et al. Effect of beta-methasone phosphate loaded polymeric nanoparticles on a murine asthma model. *Cell Immunol*. 2009;260(1):33–8.
- Cheng WC, Chen CH. Nanotechnology bring a new hope for asthmatics. *Ann Transl Med*. 2019;7(20):516.
- Passi M, Shahid S, Chockalingam S, Sundar IK, Packirisamy G. Conventional and nanotechnology based approaches to combat chronic obstructive pulmonary disease: implications for chronic airway diseases. *Int J Nanomedicine*. 2020;15:3803–26.
- Mosgoeller W, Prassl R, Zimmer A. Nanoparticle-mediated treatment of pulmonary arterial hypertension. *Methods Enzymol*. 2012;508:325–54.
- Crystal RG, Gadek JE, Ferrans VJ, et al. Interstitial lung disease: current concepts of pathogenesis, staging and therapy. *Am J Med*. 1981;70(3):542–68.
- Davies LA, Nunez-Alonso GA, McLachlan G, et al. Aerosol delivery of DNA/liposomes to the lung for cystic fibrosis gene therapy. *Hum Gene Ther Clin Dev*. 2014;25(2):97–107.
- Velino C, Carella F, Adamiano A, et al. Nanomedicine approaches for the pulmonary treatment of cystic fibrosis. *Front Bioeng Biotechnol*. 2019;7:406.
- Eworuke E, Major JM, McClain LIG. National incidence rates for Acute Respiratory Distress Syndrome (ARDS) and ARDS cause-specific factors in the United States. *J Crit Care*. 2018;47:192–7.
- Dueck NP, Epstein S, Franquet T, et al. Atypical pneumonia: definition, causes, and imaging features. *Radiographics*. 2021;41(3):720–41.
- Godfrey S. Pulmonary hemorrhage/hemoptysis in children. *Pediatr Pulmonol*. 2004;37(6):476–84.
- Rang HP, Dale MM, Ritter JM, Flower RJ. *Pharmacology*. 6th ed. New York: Churchill Livingstone; 2007.
- Adjei A, Gupta P. Pulmonary delivery of therapeutic peptides and proteins. *J Control Release*. 1994;29(3):361–73.
- Moreno-Sastre M, Pastor M, Salomon CJ, et al. Pulmonary drug delivery: a review on nanocarriers for antibacterial chemotherapy. *J Antimicrob Chemother*. 2015;70(11):2945–55.
- British Lung Foundation. How your lungs work. <https://www.blf.org.uk/sites/default/files/how%20your%20lungs%20work%20v4.pdf>.
- Usmani OS, Biddiscombe MF, Barnes PJ. Regional lung deposition and bronchodilator response as a function of β_2 -agonist particle size. *Am J Respir Crit Care Med*. 2005;172(12):1497–504.
- Ruffin RE, Dolovich MB, Wolff RK, Newhouse MT. The effects of preferential deposition of histamine in the human airway. *Am Rev Respir Dis*. 1978;117(3):485–92.
- Stevens N, Prime D. How particle size changes lung deposition: a physical modeller's perspective. *Drug Deliv Lung*. 2015;26:226–9.
- Katz IM, Schroeter JD, Martonen TB. Factors affecting the deposition of aerosolized insulin. *Diabetes Technol Ther*. 2001;3(3):387–97.
- Heyder J. Deposition of inhaled particles in the human respiratory tract and consequences for regional targeting in respiratory drug delivery. *Proc Am Thorac Soc*. 2004;1(4):315–20.
- Majid H, Winker-Heil R, Madl P, et al. Effect of oral pathway on charged particles deposition in human bronchial airways. *J Aerosol Med Pulm Drug Deliv*. 2016;9(1):24–9.
- Yeh HC, Schum GM. Models of human lung airways and their application to inhaled particle deposition. *Bull Math Biol*. 1980;42(3):61–80.
- Kim CS, Hu SC. Regional deposition of inhaled particles in human lungs: comparison between men and women. *J Appl Physiol*. 1998;84(6):1834–44.
- Yang MY, Chan JGY, Chan HK. Pulmonary drug delivery by powder aerosols. *J Control Release*. 2014;193:228–40.
- Yang W, Peters JI, Williams RO. Inhaled nanoparticles--a current review. *Int J Pharm*. 2008;356(1–2):239–47.
- Fernández Tena A, Casan Clarà P. Deposition of inhaled particles in the lungs. *Arch Bronconeumol*. 2012;48(7):240–6.
- Kaur G, Narang RK, Rath G, Goyal AK. Advances in pulmonary delivery of nanoparticles. *Artif Cells Blood Substit Immobil Biotechnol*. 2012;40(1–2):75–96.
- Musante CJ, Schroeter JD, Rosati JA, et al. Factors affecting the deposition of inhaled porous drug particles. *J Pharm Sci*. 2002;91(7):1590–600.

37. Rubin BK. Air and soul: the science and application of aerosol therapy. *Respir Care*. 2010;55(7):911–21.
38. Javadzadeh Y, Yaqoubi S. Therapeutic nanostructures for pulmonary drug delivery. In: *Nanostructures for drug delivery*. Philadelphia: Elsevier; 2017. p. 619–38.
39. Gharse S, Fiegel J. Large porous hollow particles: lightweight champions of pulmonary drug delivery. *Curr Pharm Des*. 2016;22(17):2463–9.
40. Byron PR. Physicochemical effects on lung disposition of pharmaceutical aerosols. *Aerosol Sci Technol*. 1993;18(3):223–9.
41. Patton JS, Fishburn CS, Weers JG. The lungs as a portal of entry for systemic drug delivery. *Proc Am Thorac Soc*. 2004;1(4):338–44.
42. Fischer H, Widdicombe JH. Mechanisms of acid and base secretion by the airway epithelium. *J Membr Biol*. 2006;211(3):139–50.
43. Boat TF, Cheng PW. Biochemistry of airway mucus secretions. *Fed Proc*. 1980;39(13):3067–74.
44. Liao X, Wiedmann TS. Solubilization of cationic drugs in lung surfactant. *Pharm Res*. 2003;20(11):1858–63.
45. Wanner A. Alteration of tracheal mucociliary transport in airway disease. Effect of pharmacologic agents. *Chest*. 1981;80(6 Suppl):867–70.
46. Oberdörster G. Lung clearance of inhaled insoluble and soluble particles. *J Aerosol Med*. 1988;1(4):289–330.
47. Lippmann M, Yeates DB, Albert RE. Deposition, retention, and clearance of inhaled particles. *Br J Ind Med*. 1980;37(4):337–62.
48. Liu C, Shi J, Dai Q, et al. In-vitro and in-vivo evaluation of ciprofloxacin liposomes for pulmonary administration. *Drug Dev Ind Pharm*. 2015;41(2):272–8.
49. Chougule M, Padhi B, Misra A. Nano-liposomal dry powder inhaler of tacrolimus: preparation, characterization, and pulmonary pharmacokinetics. *Int J Nanomedicine*. 2007;2(4):675–88.
50. Huang YY, Wang CH. Pulmonary delivery of insulin by liposomal carriers. *J Control Release*. 2006;113(1):9–14.
51. Patil J, Devi VK, Devi K, Sarasija S. A novel approach for lung delivery of rifampicin-loaded liposomes in dry powder form for the treatment of tuberculosis. *Lung India*. 2015;32(4):331.
52. Onoue S, Matsui T, Kuriyama K, et al. Inhalable sustained-release formulation of long-acting vasoactive intestinal peptide derivative alleviates acute airway inflammation. *Peptides*. 2012;35(2):182–9.
53. Vartak R, Patil SM, Saraswat A, et al. Aerosolized nanoliposomal carrier of remdesivir: an effective alternative for COVID-19 treatment in vitro. *Nanomedicine*. 2021;16(14):1187–202.
54. Shen AM, Minko T. Pharmacokinetics of inhaled nanotherapeutics for pulmonary delivery. *J Control Release*. 2020;326:222–44.
55. Fang CL, Al-Suwayeh SA, Fang JY. Nanostructured lipid carriers (NLCs) for drug delivery and targeting. *Recent Pat Nanotechnol*. 2013;7(1):41–55.
56. Cipolla D, Shekunov B, Blanchard J, Hickey A. Lipid-based carriers for pulmonary products: preclinical development and case studies in humans. *Adv Drug Deliv Rev*. 2014;75:53–80.
57. Weber S, Zimmer A, Pardeike J. Solid Lipid Nanoparticles (SLN) and Nanostructured Lipid Carriers (NLC) for pulmonary application: a review of the state of the art. *Eur J Pharm Biopharm*. 2014;86(1):7–22.
58. Varshosaz J, Ghaffari S, Mirshojaei SF, et al. Biodistribution of amikacin solid lipid nanoparticles after pulmonary delivery. *Biomed Res Int*. 2013;2013:1–8.
59. Liu J, Gong T, Fu H, et al. Solid lipid nanoparticles for pulmonary delivery of insulin. *Int J Pharm*. 2008;356(1–2):333–44.
60. Yang Y, Huang Z, Li J, et al. PLGA porous microspheres dry powders for codelivery of afatinib-loaded solid lipid nanoparticles and paclitaxel: novel therapy for EGFR tyrosine kinase inhibitors resistant nonsmall cell lung cancer. *Adv Healthc Mater*. 2019;8(23):1900965.
61. Wu C, Ji P, Yu T, et al. Naringenin-loaded solid lipid nanoparticles: preparation, characterization, controlled delivery, cellular uptake, and pulmonary pharmacokinetics. *Drug Des Devel Ther*. 2016;10:911–25.
62. Zhao Y, Chang YX, Hu X, et al. Solid lipid nanoparticles for sustained pulmonary delivery of Yuxingcao essential oil: preparation, characterization and in vivo evaluation. *Int J Pharm*. 2017;516(1–2):364–71.
63. Li R, Eun JS, Lee MK. Pharmacokinetics and biodistribution of paclitaxel loaded in pegylated solid lipid nanoparticles after intravenous administration. *Arch Pharm Res*. 2011;34(2):331–7.
64. Tomalia DA, Baker H, Dewald J, et al. A new class of polymers: starburst-dendritic macromolecules. *Polym J*. 1985;17(1):117–32.
65. Yousefi M, Narmani A, Jafari SM. Dendrimers as efficient nanocarriers for the protection and delivery of bioactive phytochemicals. *Adv Colloid Interface Sci*. 2020;278:102125.
66. Kaminskas LM, McLeod VM, Ryan GM, et al. Pulmonary administration of a doxorubicin-conjugated dendrimer enhances drug exposure to lung metastases and improves cancer therapy. *J Control Release*. 2014;183:18–26.
67. Ryan GM, Kaminskas LM, Kelly BD, et al. Pulmonary administration of PEGylated polylysine dendrimers: absorption from the lung versus retention within the lung is highly size-dependent. *Mol Pharm*. 2013;10(8):2986–95.
68. Nasr M, Nawaz S, Elhissi A. Amphotericin B lipid nanoemulsion aerosols for targeting peripheral respiratory airways via nebulization. *Int J Pharm*. 2012;436(1–2):611–6.
69. Mourya VK, Inamdar N, Nawale RB, Kulthe SS. Polymeric micelles: general considerations and their applications. *Indian J Pharm Educ Res*. 2011;45(2):128–38.
70. Schaffazick SR, Pohlmann AR, Dalla-Costa T, Guterres SS. Freeze-drying polymeric colloidal suspensions: nanocapsules, nanospheres and nanodisper-

- sion A comparative study. *Eur J Pharm Biopharm.* 2003;56(3):501–5.
71. Lim YH, Tiemann KM, Hunstad DA, et al. Polymeric nanoparticles in development for treatment of pulmonary infectious diseases. *Wiley Interdiscip Rev Nanomed Nanobiotechnol.* 2016;8(6):842–71.
 72. Patil MA, Upadhyay AK, Hernandez-Lagunas L, et al. Targeted delivery of YSA-functionalized and non-functionalized polymeric nanoparticles to injured pulmonary vasculature. *Artif Cells Nanomed Biotechnol.* 2018;46(sup3):S1059–66.
 73. Mohamed A, Kunda NK, Ross K, et al. Polymeric nanoparticles for the delivery of miRNA to treat Chronic Obstructive Pulmonary Disease (COPD). *Eur J Pharm Biopharm.* 2019;136:1–8.
 74. Garbuzenko OB, Winkler J, Tomassone MS, Minko T. Biodegradable Janus nanoparticles for local pulmonary delivery of hydrophilic and hydrophobic molecules to the lungs. *Langmuir.* 2014;30(43):12941–9.
 75. Hu X, Yang F, Liao Y, et al. Docetaxel-loaded cholesterol-PEG co-modified poly (n-butyl) cyanoacrylate nanoparticles for antitumor drug pulmonary delivery: preparation, characterization, and in vivo evaluation. *Int J Nanomedicine.* 2020;15:5361–76.
 76. Manish K, Nithya S, Rajnikanth PS, et al. Authors review on drug nanocrystals: a progress to targeted delivery. *Curr Nanomed.* 2020;10:1–23.
 77. Kumar M, Shanthi N, Mahato AK, et al. Preparation of luliconazole nanocrystals loaded hydrogel for improvement of dissolution and antifungal activity. *Heliyon.* 2019;5(5):e01688.
 78. Hu L, Kong D, Hu Q, et al. Evaluation of high-performance curcumin nanocrystals for pulmonary drug delivery both in vitro and in vivo. *Nanoscale Res Lett.* 2015;10(1):381.
 79. Hu X, Yang FF, Wei XL, et al. Curcumin acetate nanocrystals for sustained pulmonary delivery: preparation, characterization and in vivo evaluation. *J Biomed Nanotechnol.* 2017;13(1):99–109.
 80. Mardani S, Maghsoodi M, Ghanbarzadeh S, et al. Preparation and characterization of celecoxib agglomerated nanocrystals and dry powder inhalation formulations to improve its aerosolization performance. *Pharm Sci.* 2017;23(4):278–84.
 81. Hu J, Dong Y, Ng WK, Pastorin G. Preparation of drug nanocrystals embedded in mannitol microcrystals via liquid antisolvent precipitation followed by immediate (on-line) spray drying. *Adv Powder Technol.* 2018;29(4):957–63.
 82. Gharbavi M, Amani J, Kheiri-Manjili H, et al. Niosome: a promising nanocarrier for natural drug delivery through blood-brain barrier. *Adv Pharmacol Sci.* 2018;2018:1–15.
 83. Shilakari Asthana G, Sharma PK, Asthana A. *In vitro* and *in vivo* evaluation of niosomal formulation for controlled delivery of clarithromycin. *Scientifica.* 2016;2016:1–10.
 84. Liu FC, Yu HP, Lin CY, et al. Use of cilomilast-loaded phosphatosomes to suppress neutrophilic inflammation for attenuating acute lung injury: the effect of nanovesicular surface charge. *J Nanobiotechnol.* 2018;16(1):35.
 85. Mullaicharam AR, Murthy RSR. Lung accumulation of niosome-entrapped rifampicin following intravenous and intratracheal administration in the rat. *J Drug Deliv Sci Technol.* 2004;14(2):99–104.
 86. Ortega A, Martinez-Arroyo O, Forner MJ, Cortes R. Exosomes as drug delivery systems: endogenous nanovehicles for treatment of systemic lupus erythematosus. *Pharmaceutics.* 2020;13(1):3.
 87. Sun L, Fan M, Huang D, et al. Clodronate-loaded liposomal and fibroblast-derived exosomal hybrid system for enhanced drug delivery to pulmonary fibrosis. *Biomaterials.* 2021;271:120761.
 88. Kim MS, Haney MJ, Zhao Y, et al. Development of exosome-encapsulated paclitaxel to overcome MDR in cancer cells. *Nanomedicine.* 2016;12(3):655–64.
 89. Kim MS, Haney MJ, Zhao Y, et al. Engineering macrophage-derived exosomes for targeted paclitaxel delivery to pulmonary metastases: in vitro and in vivo evaluations. *Nanomedicine.* 2018;14(1):195–204.
 90. Tros de Ilarduya C, Sun Y, Düzgüneş N. Gene delivery by lipoplexes and polyplexes. *Eur J Pharm Sci.* 2010;40(3):159–70.
 91. Nascimento TL, Hillaireau H, Fattal E. Nanoscale particles for lung delivery of siRNA. *J Drug Deliv Sci Technol.* 2012;22(1):99–108.
 92. Ding L, Zhu C, Yu F, et al. Pulmonary delivery of polyplexes for combined PAI-1 gene silencing and CXCR4 inhibition to treat lung fibrosis. *Nanomedicine.* 2018;14(6):1765–76.
 93. Dinari A, Moghadam TT, Abdollahi M, Sadeghizadeh M. Synthesis and characterization of a Nano-Polyplex system of GNRs-PDMAEA-pDNA: an inert self-catalyzed degradable carrier for facile gene delivery. *Sci Rep.* 2018;8(1):8112.
 94. Shah SR, Prajapati HR, Sheth DB, et al. Pharmacokinetics and in vivo distribution of optimized PLGA nanoparticles for pulmonary delivery of levofloxacin. *J Pharm Pharmacol.* 2020;72(8):1026–37.
 95. Onoue S, Aoki Y, Kawabata Y, et al. Development of inhalable nanocrystalline solid dispersion of tranilast for airway inflammatory diseases. *J Pharm Sci.* 2011;100(2):622–33.
 96. Onoue S, Kuriyama K, Uchida A, et al. Inhalable sustained-release formulation of glucagon: in vitro amyloidogenic and inhalation properties, and in vivo absorption and bioactivity. *Pharm Res.* 2011;28(5):1157–66.
 97. Togami K, Maruta Y, Nanbu M, et al. Prolonged distribution of aerosolized PEGylated liposomes in the lungs of mice with bleomycin-induced pulmonary fibrosis. *Drug Dev Ind Pharm.* 2020;46(11):1873–80.
 98. Yang W, Chow KT, Lang B, et al. *In vitro* characterization and pharmacokinetics in mice following pulmonary delivery of itraconazole as cyclodextrin solubilized solution. *Eur J Pharm Sci.* 2010;39(5):336–47.



In Vivo Biodistribution and Pharmacokinetic Studies of NPDDS for Brain Targeting

20

Aishwarya Deshmukh, Jayvadan Patel,
Govind Vyas, and Mukesh Patel

Contents

1	Introduction	366
2	The Blood-Brain Barrier and Drugs	367
3	Nanotechnology for Brain Drug Delivery	368
4	Delivery and Pharmacokinetics of Nanomedicines	369
5	Quantification of the In Vivo Trafficking of Novel Drug Delivery Systems (NDDSs)	371
6	Physiological-Based Pharmacokinetic Modelling (PBPK) in Nanoparticulate Drug Delivery Systems (NPDDS) Targeting the Brain	378
7	Summary	382
	References	382

Abstract

Central nervous system (CNS) diseases have become distressing to humankind due to multiple reasons, lifestyle changes, and unrelenting decline in the environment being the major contributing factors. Since the blood-brain

barrier (BBB) and blood-cerebrospinal fluid barrier (BCSFB) are the chief physiological barriers that hold a large logjam for the efficacious treatment of CNS disorders as well as brain tumours, complex anatomical architecture, exclusive microenvironment, and discrimination for any and every foreign material including drug as well can be considered as the leading challenges for delivery of drug to the CNS. Lately, it has become a necessity to develop upright cargo, which carts drug to the CNS in concentrations not only effective but also without triggering systemic side effects. Nanoparticulate drug delivery systems (NPDDSs) have been associated to discourse the difficulties associated with treatment of neurological disorders and have proven cutting edge over the conservative CNS-related

A. Deshmukh (✉)

Smt. Kashibai Navale College of Pharmacy,
Pune, Maharashtra, India

J. Patel

Nootan Pharmacy College, Faculty of Pharmacy,
Sankalchand Patel University,
Visnagar, Gujarat, India

G. Vyas

Invahealth Inc., East Windsor, NJ, USA

M. Patel

Former Experis Engineering, Edina, MN, USA

pharmacotherapy. The mandate for efficacious nano-based methodologies emphasizes on the restoration and neuroprotection which might help significantly from sustained nanoparticulate-based approach together with the expansion in neuronal cell biology, the related pathologies, and physiologies. In addition, the ideal NPDDSs ought to deliver APIs with intended properties like sustained release with lengthy circulation time, better stability, solubility, as well as targeting. Many studies have provided pharmacokinetic information of drug-loaded NPDDSs, though a limited number of nanotechnology-based products are approved. The reason behind these limited numbers of approved products may partly be attributed to the insufficient indulgence of their pharmacokinetic properties. The present chapter deliberates current methods and developments in the bioanalysis and pharmacokinetic studies of NPDDSs.

Keywords

NPDDS · Brain targeting · Biodistribution · Pharmacokinetic

1 Introduction

Neurological disorders, due to high prevalence and/or morbidity and mortality, have a high social impact. The neurological disorders are divided into two categories, namely, neurological disorders within the neuropsychiatric category and neurological disorders from other categories, which are further used for calculating the estimates of the global burden of the disease. Neurological disorders within the neuropsychiatric category comprise diseases like epilepsy, Alzheimer and other dementias, Parkinson's disease, multiple sclerosis, and migraine, while neurological disorders from other categories consist of diseases as well as injuries having neurological consequence like cerebrovascular disease, neuro-infections, and neurological injuries. Approximately 12% of deaths occur worldwide because of various neurological disorders, 2.84%

due to Alzheimer and dementia and 8% due to cerebrovascular disease [1]. Currently, many neurological diseases have no effective therapies; however, molecular to behavioural level scientific and technological researches have been conceded but failed to develop in an interdisciplinary way, with a definitive response still to be out-looked. Thus, a number of CNS disorders remain not curable, for instance, neurodegeneration (e.g. amyotrophic lateral sclerosis, Alzheimer's, Parkinson's, Huntington disease, and Prion Disease), genetic deficiencies (e.g. lysosomal storage diseases, leukodystrophy), and quite a few types of brain cancer. Moreover, albeit drug therapy of such diseases perhaps already exists in line of principle, it cannot be currently exploited due to the presence of the BBB averting the passage, which in turn leads to insignificant access to the CNS [2].

Nanotechnology has been developing rapidly and extensively used in diagnosis and treatment of disease in the past two decades, viz. a range of nanoparticle (NP)-based drug delivery systems, such as liposomes, dendrimers, micelles, polymer nanoparticles, and inorganic nanoparticles, have been constructed employing many promising novel nanomaterials [3], carrying therapeutic drugs or imaging probes and delivering them to site of target. NPs exhibit numerous benefits, which include solubility improvement, protection of cargoes from enzymatic digestion, elevation of targeting efficiency, and increasing cellular internalization, and thus they have gained growing consideration in the field of medicine and biology. The diagnosis and treatment of CNS disorders has not been very striking, due to the constraint by BBB for drug transportation into the brain [4], with nearly 100% of the macromolecular drugs and more than 98% of the small-molecule drug candidates being incapable of entering the brain. Furthermore, only nutrients and few small lipophilic molecules (<500 Da) can efficiently cross the BBB and attain an efficient brain concentration. Thus, to surmount the BBB and deliver diagnostic and therapeutic drugs to the brain, different types of strategies have been developed, one of the most important being is using NPs as carriers [5].

2 The Blood-Brain Barrier and Drugs

The BBB, an arrangement of complex system of endothelial cells, astroglia, pericytes, and perivascular mast cells, checks the passage of most circulating cells and molecules [6]. The vascular layer of brain capillary endothelial cells are interconnected alongside tight and adherens junctions, which attributes to the BBB tightness. Additionally, tight junctions carry out two major purposes:

- (i) Preventing the entry of small molecules and ions through the space between cells, allowing passage by entering the cells either by diffusion or active transport, thus controlling the type and amount of substances allowed to pass through BBB.
- (ii) Averting the transport of integral membrane proteins between the apical and basolateral membranes of the cell, thus, each cell membrane surfaces conserve its atypical functions, for instance, exocytosis that occurs at the basolateral surface and receptor-mediated endocytosis occurring at the apical surface.

Tight junctions are made up of three integral proteins, namely, occluding and claudins (make up the backbone of junction strands), as well as junctional adhesion molecules (traffics the T-lymphocytes, neutrophils, and dendritic cells from the vascular compartment to the brain during immune inspection and inflammatory responses). Moreover, strong mechanical attachments are offered by adherens junctions, which are formed from cadherins and catenins, between adjacent cells. This condensed network of interconnections grants a transelectrical resistance $>1500 \Omega\text{cm}^2$ being highest among all other endothelial districts, to the endothelial layer of BBB. The endothelial BBB layer density prevents the entry across intercellular junctions (paracellular passage), thus restraining the likelihood of exchanges between the two compartments practically through passages transiting across the cellular body, i.e. transcellular passage.

The BBB is a dynamic biological entity which acts as a mechanical fence and controls active metabolism as well as carrier-mediated transports. Nutrients, like glucose, amino acids, and ketone bodies, penetrate the brain by specific transporters, while the uptake of large molecules, like that of neurotrophins and cytokines are mediated by receptor-mediated endocytosis [7, 8]. Moreover, brain uptake of most pharmaceuticals is prohibited by the BBB, except for small hydrophilic compounds having mass lower than 150 Da in addition to extremely hydrophobic compounds with mass lower than 400–600 Da, which can cross the BBB by passive diffusion [9]. A few drugs crossing the BBB include opiates (e.g. morphine, methadone, and meperidine), anxiolytics (diazepam, temazepam), selective serotonin reuptake inhibitors (paroxetine), and antipsychotics (chlorpromazine, promethazine) although the majority of antibiotics and antitumour are not permitted. The BBB stiffness plays a major role in averting the pharmacological therapy of a number of neurological diseases, in addition to the presence of the *P*-glycoprotein pump in the BBB, which further represents barrier for drugs in crossing the cerebral capillary endothelium and entering the brain parenchyma, though it allows the identification of molecules indispensable for the brain to enter the brain and the exclusion of other molecules including pharmaceuticals.

Thus, it is quite plausible that diverse approaches and explorative strategies must have been employed to permit pharmaceuticals to prevail over the BBB, which ranges from invasive techniques, for instance, through osmotic opening of the BBB, to chemical modifications in drugs to sought physiological carrier-mediated transports, or utilize the “Trojan horse” technology which blends BBB-impermeant pharmaceutical to molecules capable of crossing the barrier, thus taking benefit of receptor-mediated transport systems. In addition, substitute routes of administration, with the capacity to reach the brain by sidestepping the BBB (e.g. intranasal), have been vigorously investigated, although constraints are faced in this context, for instance, the limited surface of adsorption of the olfactory bulb, which is

minimal compared to that of the BBB, consequently, quantitatively dropping the prospect to attain the brain with appropriate amounts of drugs.

3 Nanotechnology for Brain Drug Delivery

Lately, advancement in nanomedicine has made it possible to explore engineered tunable devices, having size in the order of billionth of metres, as a fascinating mechanism to resolve the unmet predicament of augmenting the drug transport across the BBB [10]. Nanoparticle (NP) technology is one of the fast advancing devices. NPs are substances having size of 1–100 nm and exhibit its function as a whole unit in context to transport and properties. The motive for the expectation is being the prospect of NP multifunctionalization, together with their capacity in carrying the drug payloads including BBB-impermeant drugs. Utilization of NPs justifies because of the fact that appropriate surface multifunctionalization is promoted at the same time either by enhancing its crossing or their targeting of the BBB. Moreover, since the crossing of the BBB-impermeant drugs through the barrier will depend completely on the physicochemical and biomimetic features of the NP vehicle and will be independent of the chemical structure of the drug, which is stalled inside the NPs, the likelihood for BBB-impermeant drugs to reach the brain when vehicled by NPs will be increased. The prospect of bestowing features such as high chemical and biological stability, viability of incorporating both hydrophilic and hydrophobic pharmaceuticals, as well as the ability to be administered by a range of routes (including oral, inhalational, and parenteral) confers NP as an attractive tool for medical applications [11].

Furthermore, NPs by covalent conjugation with various ligands (such as antibodies, proteins, or aptamers) can be functionalized to target specific tissues. A huge surface area-to-volume ratio of NPs also allows attachment of numerous copies of a ligand and radially augments their binding affinity through the

multivalent functionalization [12]. However, designing NPs for clinical applications should consider the actuality that their systemic administration would produce imperative alterations, particularly the nonspecific interaction between proteins circulating in the bloodstream and the shell of NPs that might lead to the adsorption of opsonins on their surface, forming the alleged “corona”, since these proteins considerably change the bare material properties, which determine the elimination of NPs from circulation by the reticuloendothelial system (RES) (largely located in the spleen and liver). The methodologies engaged for sidestepping reticuloendothelial system are to articulate particles with neutral surface charge; to shield their surface with various types of hydrophilic surfactants, like polysorbates and polyethylene glycol (PEG); and to use small size nanoparticles (e.g. <80 nm). NPs having these features, known as “stealth”, have the capacity to shun the reticuloendothelial system and exhibit long circulation time as well as stability in blood, with opportunity to functionalize for crossing the BBB and successful target attainment [13]. The potential of NP functionalization for brain drug delivery are shown in Fig. 20.1.

Moreover, it is imperative to mention that the couture of NPs for enhancing drug delivery to the brain does not essentially entail their capacity to cross the BBB themselves, and it is expected that NPs could participate into two ways:

- (i) By escalating the concentration of drug whether inside or at the luminal surface of BBB cells, thus instituting a local high concentration gradient between the blood and brain which is higher than that obtainable post-systemic administration of the free drug, which in turn supports the improved passive diffusion of the drug. For instance, synthesizing NPs designed for targeting brain capillary endothelial cell and the feature either or not followed by their consequent uptake from targeted cells
- (ii) Movement together with their drug cargo into the CNS. For instance, facilitating NPs to target brain capillary endothelial cells and

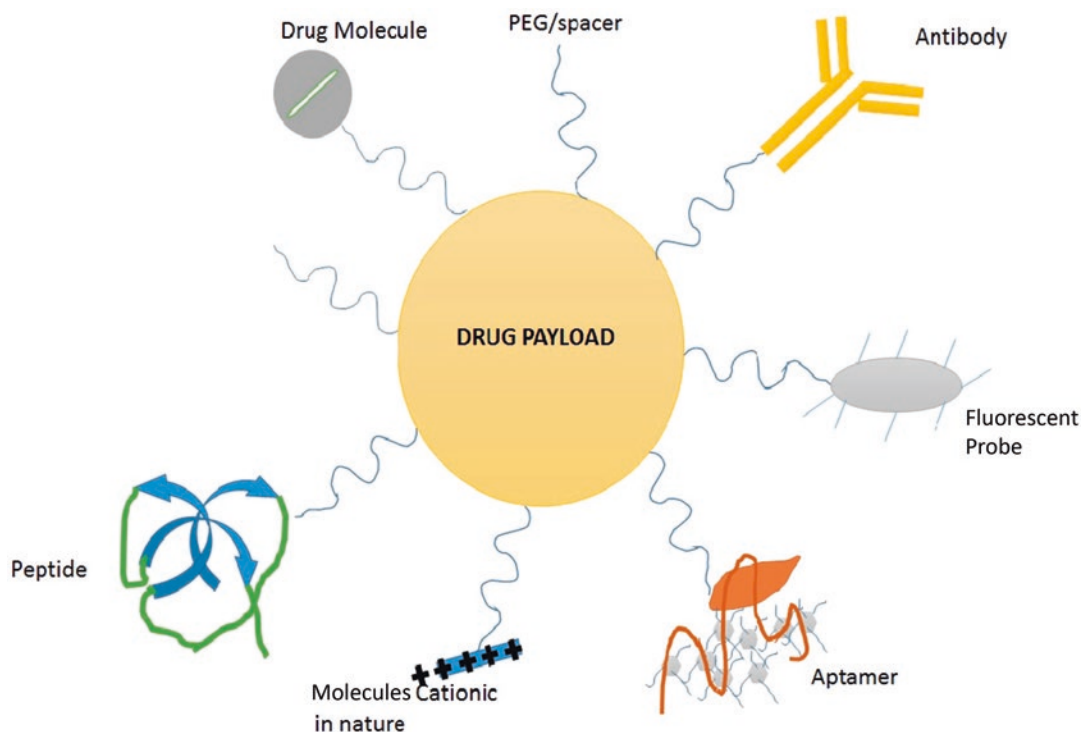


Fig. 20.1 Surface-modified NPs for brain drug delivery with various targets, viz. drugs; targeting molecules like peptides, antibody, aptamers, and cations; as well as PEG/spacers and/or fluorescent probe as a tracer

later their transcellular passage across the BBB [14]

4 Delivery and Pharmacokinetics of Nanomedicines

Alterations in pharmacokinetic properties of the active pharmaceutical ingredients (API) like extended stay in the body and better distribution to target tissues, probably snowballing their efficacy and alleviating adverse reaction, are responsible for variations in pharmacokinetic characteristics of nanomedicines. Modification in pharmacokinetics such as in vivo absorption, distribution, metabolism, and excretion in the body affects the efficacy and/or adverse reaction regulation in nanomedicines. In addition, composition and formulation of nanomedicine delineate the physiochemical properties, which eventually exert effect on their efficacy and toxicity.

Regulation of physiochemical properties of nanomedicines and alterations in the degree of binding between biomolecules and nanomedicines ultimately control the in vivo distribution of nanomedicines. For instance, it has been described in few studies that nanomedicines prepared using PEGylated particles considerably reduce the type and amount of binding proteins. Additionally, an escalation in the migration to the brain was found when polysorbate-coated particles were bound to apolipoprotein E [15, 16].

Different targeted delivery methods like cell internalization, transporter-mediated endocytosis, intracellular transport, and conjugation with antibody, protein, peptide, polysaccharide, etc. can change the pharmacokinetics of nanomedicines in the body. The delivery mechanisms for nanomedicines can be categorized into intracellular transport, epileptic transport, and other types. Intracellularization, transporter-mediated endocytosis, and permeation enhancement through interactions involving particle size and/

or cell surface regulate and assist the intercellular transport [17]. Broadly, small particle size of nanomedicines augments the intercellular transport, leading to facilitation in cell permeation, and eventually affects absorption, distribution, and excretion of nanomedicines; especially, particle size of nanomedicines plays a decisive role in cell internalization by transporter-mediated endocytosis. Large particle size of nanomedicine leads to speedy opsonization, and thus their elimination from the blood by endothelial macrophages also gets hastened. A few studies have reported that the cell surface transporter affinity for the nanomedicine differs conditional to the particle size of nanomedicines, and this might likewise influence the debauched elimination of bulky particles from the blood by macrophage cells. Furthermore, nanomedicines prepared with non-charged polymers, surfactants, or polymer coatings degrading *in vivo* owing to their hydrophilicity can interact with cell surface receptors or ligands and thus rise permeability or stimulate nanomedicine internalization [17, 18].

Furthermore, intracellular transport of active pharmaceutical ingredients has also been shown to be improved by nanomedicines through binding which includes bioadhesive polymers or chelates [18, 19]. Opening of tight junctions and/or increased membrane permeability may increase intracellular trafficking of API which is coupled to specific proteins, antibodies, and others in polymers *in vivo*. Specifically, institution of such a characteristic in anti-neoplastic agents can expand the efficacy of chemotherapy, the most relevant example can be targeting brain tumours which are highly unreachable to drugs bound by tight junctions, thus growing tumour cell targeting and dropping normal cell targeting. By using this nanomedicine strategy, cytotoxicity to normal cells can be curtailed, and anticancer efficiency can be attained. Decreased nanomedicine eradication from the lungs during inhalation leads to amplification owing to condensed degradation and elimination by lung mucosa or macrophages, subsequently augmenting the drug

retention time besides movement of drug toward the target. The enhanced permeability and retention (EPR) effect can rise the anticancer efficiency by augmenting tumour permeation and retention time. The EPR effect also aids in selectively delivering nanomedicines to target tissue by conjugation to an antibody, protein, peptide, or polysaccharide, which, in turn, are employed for modification in the delivery of nanomedicines to target tissues with receptor/ligand interactions or further physiologically precise target cell interactions, ultimately modifying the effectiveness or adverse reactions of a drug. Nanomedicines prepared by coating with hydrophilic material have been found to exhibit enhanced stability, as well as their opsonization or build-up in mucus is prevented. Nanomedicines can be retained *in vivo* by coercing the macrophage-induced or mucosal instability, for example, in lung tissue for extended periods of time through particle size, control, and evading elimination by mucus ciliates, which possibly can degrade or exert macroscopic effects in lung mucosa [19]. Consequently, multiple formulations have been developed for exploiting delivery mechanisms that regulate pharmacokinetics and pharmacodynamics of nanomedicines.

4.1 Pharmacokinetic Properties of Nanomedicines

The pharmacokinetic features of diverse nanomedicines in various formulations are assessed by chemical structure (shape), particle size, as well as surface chemical characteristics [20]. Regulation of particle size in nanomedicines enhances their target tissue retention and eliminates them swiftly when they exhibit non-target tissue distribution. For instance, nanomedicines with particle size <10 nm are excreted by the kidneys, while those with particle size >10 nm are occasionally extended and removed by the hepatic and/or the mononuclear phagocyte system (MPS). In addition, nonspecific protein

adsorption in the body forms a protein corona around nanomedicines, except if materials like polyethylene glycol (PEG) are applied on the nanoparticle through surface coating. This protein adsorption mechanism persuades protein denaturation, leading to protein aggregation or phagocytosis as a result of activated macrophages. Chemical properties and surface coatings based on nanoparticle targeting encompass active and passive targeting. Passive targeting, which comprises a nonspecific accumulation in disease tissue (generally cancer tissue), is particularly pertinent to solid cancers, wherein targeting leads to augmented blood vessel and transporter permeation and retention (i.e. enhanced permeability and retention; EPR effect) of nanomedicine and thus, their improved tumour tissue accumulation. Specific or active targeting which is a selective transport mechanism for nanomedicines containing small molecule, protein, or antibody, solitary to specific cells and/or tissues, might occur through homing to overexpressed cell surface receptors.

4.2 Future Outlooks on Nanomedicines in View of Pharmacokinetic Properties

Evaluation of nature of formulations, pharmacokinetic properties, and the approval process for nanomedicines are few of the obligatory steps to achieve clinical implications. Consequently, on the basis of current inclinations in nanomedicine development besides FDA and EMA guidelines, a guileless process system can be described to monitor the acclaimed ADME assessments of nanomedicines (Fig. 20.2). Stability during the manufacturing process and replicated human conditions govern the ADME properties of drug of interest and provision of ability to assess or not the particular drug in line. Evaluation also differs on the basis of route of administration as well as distribution. Accordingly, the projected process system offers precarious and hands-on frontiers in the development and assessment of nanomedicine [21].

5 Quantification of the In Vivo Trafficking of Novel Drug Delivery Systems (NDDSs)

The encapsulated/embedded APIs must be release from NPs to reach the target site in order to exert the anticipated biological effect. Even though NDDSs are employed as drug carriers since a long time, the pharmacokinetic studies are really focused on the total drug concentrations, with polymers being unnoticed, and thus, the representation of the systematic release profile for the drug-loaded particles tends to be inadequate. The important feature of the pharmacokinetic studies on NDDSs additionally includes encapsulated drug and carrier polymer release and disposition, apart from the conventional pharmacokinetic studies of APIs which emphasis on the released drug concentration. Quantitation and differentiation of polymer between released and encapsulated drug can be considered as the chief technical difficulties concerning the bioanalysis of NDDS. However, technology advancement has made it possible to develop and explore methods for differentiating the released and encapsulated drugs in vivo.

5.1 Quantitation Methods for the Released and Encapsulated Drug In Vivo

The NDDS encapsulation conserves the payload drugs and provide with sustained circulation time and solubilization, also referred to as a circulating “reservoir” of drug. Different methods are exploited to divulge the release profiling of NDDSs.

Liquid Chromatography with Tandem Mass Spectrometry (LC-MS/MS)

LC-MS/MS is currently not only a standardized bioanalysis method for small molecule drugs, but also the desired choice for drug release process profiling of NDDSs in vivo. LC-MS/MS utilization in differentiating encapsulated as well as released drug is a critical challenge. Study by

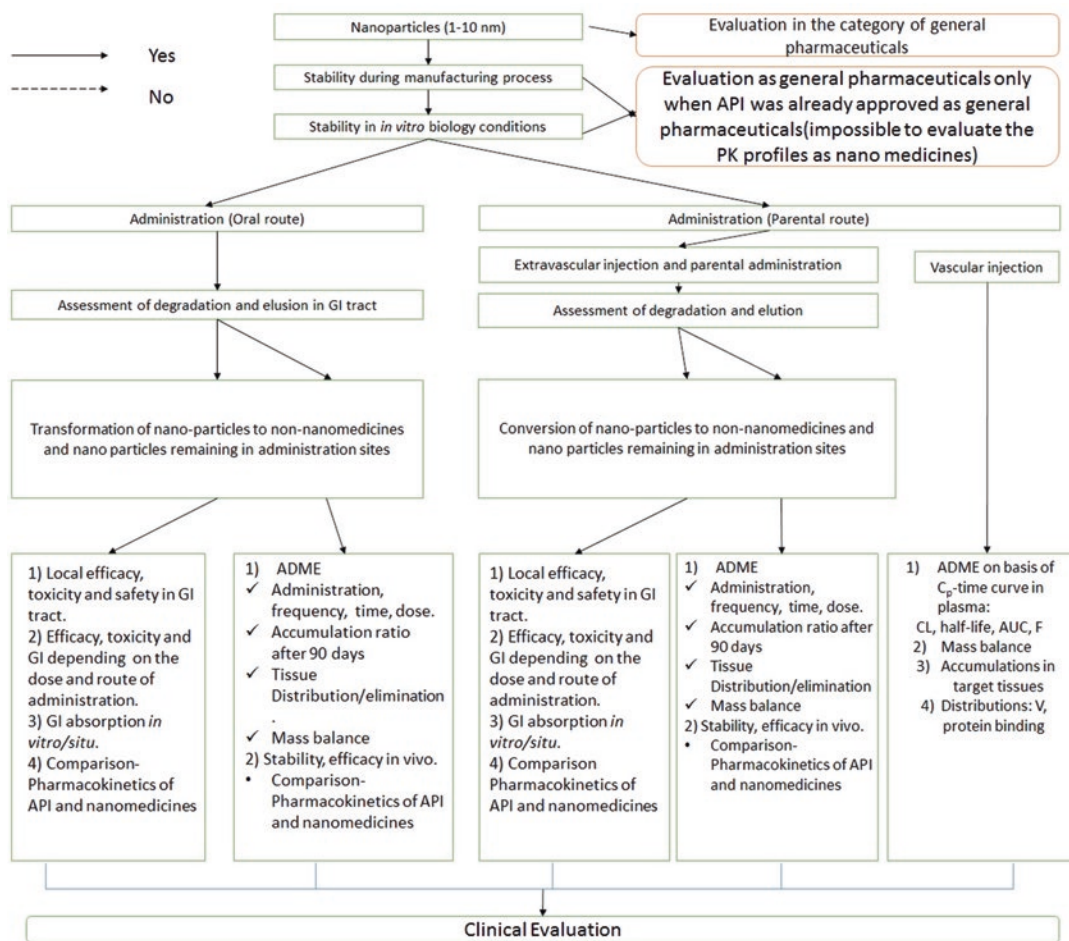


Fig. 20.2 Anticipated algorithm to evaluate ADME of nanomedicines

Smits et al. [22] testified for the very first time LC-MS/MS system for the differential quantification of encapsulated and released prednisolone phosphate-loaded liposomes in hepatic tissue as well as whole blood. The prednisolone was employed as substitute analyte for study of released drug, because prednisolone phosphate post release *in vivo* got instantaneously dephosphorylated by phosphatases. A similar study in line with this was conducted by Braal et al., which determined drug release from polymeric micelles [23]. In addition, CriPec[®], a docetaxel temporarily covalently conjugated micelle (approximately 65 nm) is stable at pH 5.0 and room temperature. The quantification of the released docetaxel, without interference of the

conjugated drug, was consequently measured. Moreover, for conjugated docetaxel quantitation, the drug ought to be isolated from micelles at 37 °C and pH 7.4 for a period of 3 days. In addition, the drug-loaded micelles should be separated first, as the LC-MS/MS method by itself cannot distinguish separated drug from the formerly released drug.

Solid-phase extraction (SPE) is a technique extensively employed for separating the released and encapsulated drug. The general SPE procedure is conducted in the following steps: (1) loading of sample; (2) water washing, hydrophilic surface containing liposomes does not get retained on SPE column; and (3) hydrophobic solvent washing, adsorbed released drug is eluted) (Fig. 20.3).

Studies by Deshpande et al. [24], Su et al. [25], and Xie et al. [26] have exploited SPE separation method for describing the pharmacokinetic profile of amphotericin B and doxorubicin (DOX) liposomes in vivo. Further, a study by Wang et al., profiled the release and uptake progressions of DOX liposome in healthy tissue and tumour [27]. The SPE separation method has been provisionally exploited for separating polymeric NPs; for instance, a study by Song et al. [28] utilized the separation method for the quantitation of gedatolisib released from poly(lactide)-poly(ethylene glycol) PLA-PEG NPs. The encapsulated gedatolisib concentration was computed by deducting the released gedatolisib values from the total values. Moreover, in deliberation of the payload drug properties, an MCX SPE column was utilized as an alternative to a HLB SPE column.

Ultrafiltration has also been deliberated as a separation method for liposomal released and encapsulated drug; study by Xie et al. [26] probed the precision of this separation method by utilizing DOX liposomes as a test sample. The study exhibited recovery rate of DOX separated by ultrafiltrate below 10%, which may be connected to the adsorption of DOX to device and plasma proteins. Furthermore, a novel separation technique was also established by Chen et al. [29], where, in consideration to the specific binding of biotin and streptavidin, streptavidin-Fe₃O₄@PDA was employed as the separation nanoprobe for separating biotin-docetaxel liposomes from plasma in the presence of a magnetic field and showed 75% recovery efficiency.

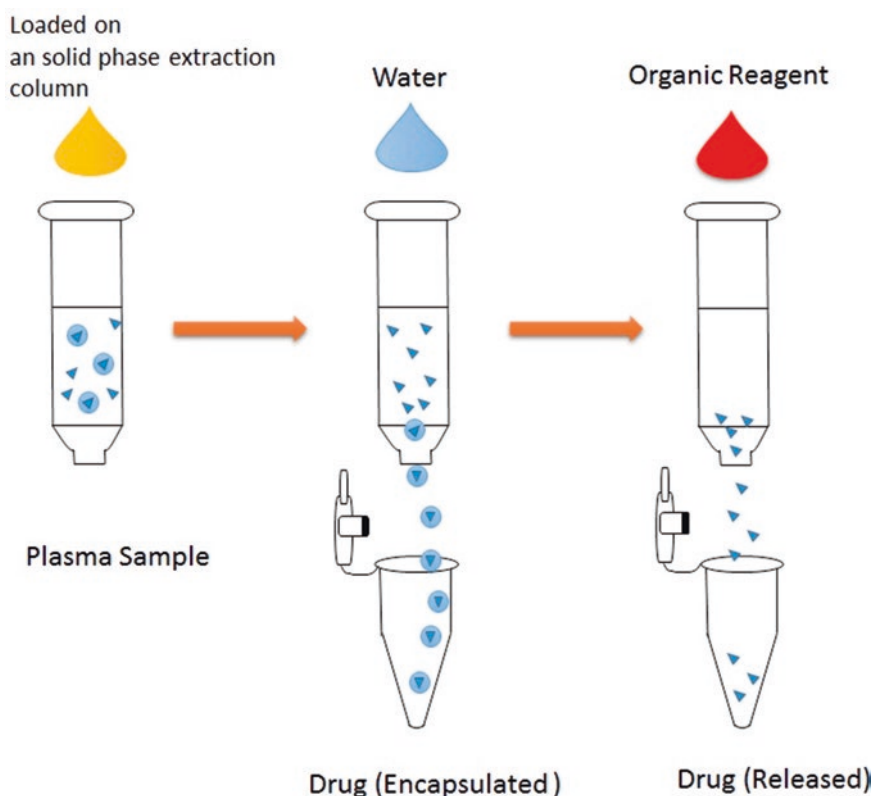


Fig. 20.3 Separation of encapsulated as well as released drug in liposomes by solid-phase extraction in plasma sample

Förster or Fluorescence Resonance Energy Transfer (FRET)

FRET is a new technique to divulge the biological fate of NDDSs *in vivo*, the principle of which encompasses transfer of energy between a donor fluorophore (in electronic excited state) and an adjacent acceptor fluorophore (1–10 nm) (Fig. 20.4). For a competent energy transfer, spectrum overlap between the donor and acceptor must be greater than 30%. Moreover, a FRET pair (donor and acceptor) must be co-encapsulated in the core of micelles, for exploring the stability and drug release of NDDSs in the FRET-based strategies. FRET signal deteriorates quickly *vis-à-vis* surpassing the energy transfer distance, which relates to the payload release, though the payload release can be made either by micelle dissociation or FRET pair diffusion. Sun et al. investigated the *in vivo* stability of the micelles by immobilization of FRET pair on the hydrophobic end of the carrier polymers, and the FRET pair loaded polymers were further altered into micelle, which further confirmed that the signal declining *in vivo* was simply associated to micelle dissociation [30]. For minimizing the influence of FRET fluorophore on micelle properties, merely a minor percentage of the hydrophobic ends were loaded with the FRET pair (1% for both), and the loading of drug was found not to be influenced. The FRET method does have some limitations:

1. Reillumination which is initiated by repartitioning into hydrophobic constructs. The FRET pairs are usually highly hydrophobic compounds and favour to repartition into hydrophobic constructs like membranes, biomacromolecule hydrophobic cavities, or physiological micelle hydrophobic cores.
2. Low sensitivity. The fluorescence intensity of the FRET system is comparatively fragile, due to the fact that the acceptor can be only get excited by the donor indirectly.

Aggregation-Caused Quenching (ACQ) Fluorophores

ACQ fluorophores are conjugated aromatic system with robust hydrophobicity, have provision

to aggregate in water or alike hydrophilic solvent, and hold exceptional fluorescent properties when dispersed in solution. The fluorescence can also be turned off if the fluorophores aggregate and form stable p–p stack with the help of process such as fluorescent quenching. On the basis of this distinctive feature, ACQ probes are encapsulated in the hydrophobic core of nanocarriers; the emission of fluorescence directs a dispersed state of ACQ that is a representation of intact nanocarriers (Fig. 20.5a). The fluorescence quenches instantaneously supplementary with the ACQ probes aggregating in the aqueous medium when the nanocarriers are dissociated. The aggregating process is reversible in which the small aggregates appear as homogenous solutions without precipitation when dispersed in the solvent. In addition, the aggregates get dissolved or dispersed into monomers again in the hydrophobic domains on introduction of new micelles and regain their fluorescence. While the ACQ probes were initially considered for imaging, a study by He et al. showed application of this approach for quantitation of mPEG-poly-DL-lactic acid (mPEG-PDLLA) polymeric micelles *in vivo*. In a study, where the near-infrared aza-BODIPY fluorescent probe P2 was encapsulated in the hydrophobic core of the polymeric micelles showed exceptional linearity of fluorescent response versus polymeric micelle concentration over the range of 9.77–625 mg/mL [31]. The pharmacokinetic study in rat specified that ACQ can be a substitute for the bioanalysis of NDDSs. However, the main shortcoming of ACQ method is reillumination and restricted application of ACQ in hydrophobic NDDSs.

Aggregation-Induced Emission (AIE) Fluorophores

AIE fluorophores display scarce emission in dilute solvent as compared to ACQ. In the state of aggregate, a restriction in the free rotation of dye molecules is observed, which vividly improves emission (Fig. 20.5b). The fluorescence of leaked AIE probes is extremely weak in the environment as far as the nanocarrier dissociation is concerned. Thus, AIE probes can be utilized to designate the nanoparticle

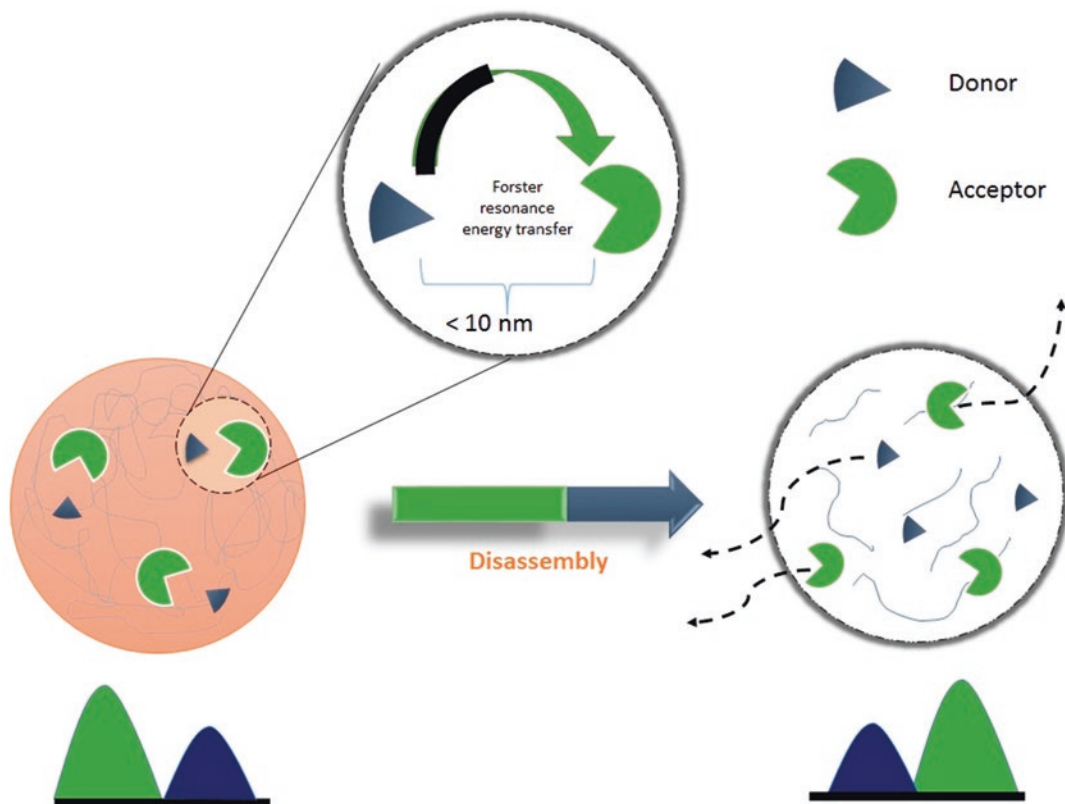


Fig. 20.4 Förster resonance energy transfer (FRET) for tracing biodistribution of NPDDS

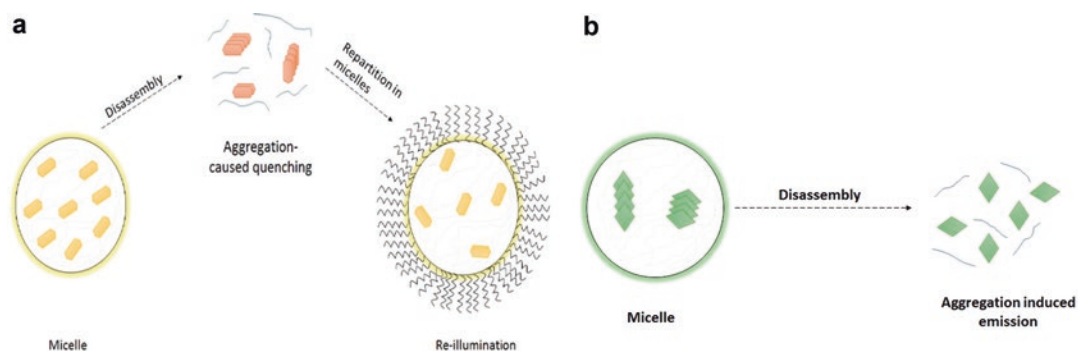


Fig. 20.5 (a) Aggregation-caused quenching and (b) aggregation-induced emission for tracing the drug encapsulated in NDDSs

state in vivo; however, few reports about monitoring in vivo fate of NDDSs with AIE strategy exists. Conservative short wavelength one-photon excited AIE material does have few disadvantages in application, like toxicity, diminutive penetration depth ($<100\text{ mm}$), intrusion of tissue autofluorescence, and pho-

toleaching phenomenon. Additionally, AIE is also delayed by scattering, a phenomenon relating to the long wavelengths of the exciting light in addition to high signal-noise ratio at a deep focal plane. As compared to one-photon excited AIE, two-photon excited AIE has the benefit of less biological damage, low-energy

irradiation, high-energy fluorescence, decrease of autofluorescence, and exceptional penetration depth. Recently in a study by Zhuang et al., a two-photon excitable AIE fluorescence probe was used for comparison of pharmacokinetic behaviour of DOX and DOX-loaded micelles in vivo [32]. The doped TBIS fluorophore accomplished mPEG-SS-poly (AEMA-co-TBIS) (mPEATss) micelles with great AIE feature devoid of any influences on the drug loading.

Enzyme-Linked Immunosorbent Assay (ELISA)

ELISA, which is an immunological assay employed for detection of biomolecules like proteins, antibodies, hormones, and cytokines, has also been explored in investigating the release profile of the biomacromolecule-loaded nanoparticles. The most predominant ELISA method is called “sandwich” ELISA, in which the analyst antigen is wedged between two kinds of antibodies; where a primary antibody is first immobilized to the surface of the plate to capture the analyst antigen in the serum, thus it is called capture antibody. The detecting antibody, an enzyme-linked antigen-specific antibody, follows and recognizes the captured antigens. The coupled enzyme assists for an optical detection, amplification of signal, and quantitation of the captured analyst antigen. Wang et al. employed the sandwich ELISA method for measuring the released payloads stromal cell-derived factor 1 (SDF-1) as well as bone morphogenetic protein 2 (BMP-2) for assessing the encapsulation efficiency and release kinetics of the chitosan oligosaccharide/heparin (CSO/H) NPs in vitro [33]. In addition, Azie et al. in the study conjugated latent transforming growth factor beta (TGF- β) to superparamagnetic iron oxide nanoparticles (SPIONs), and the release profile of the active TGF- β from the SPIONs were then monitored by ELISA [34]. Though, ELISA is sensitive, it also has some restraint, like narrow varieties of commercial ELISA kits, linear ranges, and cross-reactivity issue.

5.2 Quantitation Methods for Polymer

The polymeric material of NDDS may disassemble, distribute, metabolize, and excrete post administration. The information about the in vivo fate of the polymeric materials is insufficient as compared to the payload drug. The pharmaceutical polymer excipients and the key component of NDDS are normally deliberated to be inert ingredients; nevertheless, adverse drug reaction (ADR) reports on iatrogenic illnesses related to polymer are snowballing, for example, hypersensitivity reactions, cell vacuolation, or splenomegaly. Thus, polymer accumulation may have impending toxicity and has provoked consideration of regulatory authorities. Numerous analytical techniques have been established for bioanalysing the polymeric material in NPs. Some conventional techniques like nuclear magnetic resonance (NMR), colorimetric methods, SEC, and high-performance liquid chromatography (HPLC) are insufficient in context to sensitivity; thus, LC-MS/MS and ELISA are presently explored for in vivo polymer quantitation [35].

Liquid Chromatography Tandem Mass Spectrometry (LC-MS/MS)

LC-MS/MS is an analysis technique for small molecular drug and has lately made immense expansion in polymer bioanalysis. Polydispersity, which comprises series of homologues with different degrees of polymerization and MWs, is the main challenge for the quantitative analysis of polymers by LC-MS/MS, and to conquer this challenge, numerous mass spectroscopy data acquisition strategies, for instance, selected ion monitoring (SIM), multiple reaction monitoring (MRM), in-source collision-induced dissociation (CID), and MSALL, are employed to the polymer analysis in biological matrices.

ELISA

The application of ELISA method can be facilitated with the development of antibodies that specifically bind to PEG conjugates in PEGylated drug detection. The binding affinity of the anti-PEG antibodies to PEG conjugates is stronger to

free PEGs. Study by Richter and Akerblom for the very first time projected generation of antibodies against PEG by immunizing rabbits, and these prepared polyclonal antibodies provided lower limits of quantitation (LLOQ) of PEGylated drugs down to about 1 mg/mL [36]. For improving the sensitivity, the mouse monoclonal antibodies capable of binding PEG conjugates specifically without differentiating their conjugates were also prepared later. Therefore, sandwich ELISA could determine the concentrations of PEG conjugates in complex biological samples, and thus, detection of PEG at a concentration as low as 1.2 ng/mL could be attained with anti-PEG sandwich ELISA. A subtle LC-MS/MS method (LLOQ 0.125 mg/mL) was established by Danika et al. for PCK3145 quantification in mouse plasma. In spite of the fact that the LC-MS/MS has been utilized for quantitative bioanalysis of peptides, this method still visages substantial challenges for analysis of PEGylated peptides, like that of high polydispersity of PEG, high MW, and poor ionization efficacy. An indirect ELISA method was developed for the detection of PEGPCK3145 by means of PEGylated protein ELISA kit (Enzo Life Sciences). PCK3145 concentration was acquired from the quantification of PEG-PCK3145. A greater sensitivity (LLOQ 0.132 ng/mL) as well as wide applications for PEG conjugates was attained by anti-PEG sandwich ELISA method; nonetheless, the specificity of this expertise is yet to be established. Besides, ELISA method is considered inappropriate for the free PEG analysis, which is a restraint for its presentation in observing the biological fate of PEG-based NDDSs.

5.3 Quantitation Methods for the NPs

The delivery-related activity and uptake mechanism of NDDS are still elusive; nonetheless, an augmented cellular uptake of nanostructures has been substantiated by numerous *in vitro* and *in vivo* studies. Since the improved cellular uptake affects the biodistribution of payload drugs, it has gained abundant consideration in the

field of NDDSs; for instance, technologies like magnetic resonance imaging (MRI), radiolabeling, fluorescence spectroscopy, and laser ablation inductively coupled plasma MS (LAICP-MS) are presently employed for *in vivo* NP quantitation.

Magnetic Resonance Imaging (MRI)

MRI holds exclusive features like noninvasiveness, absence of exposure to ionizing radiation, high contrast in soft tissues, as well as high spatial resolution [37]. MRI scanner uses radio wave pulse for exciting hydrogen nuclear and measures the emitted radio frequency during the relaxation course from the excited hydrogen atoms. Furthermore, as human tissues have copious amount of hydrogen atoms in the form of water in diverse location, the amount, and bonding status, spatially localized spectra of the tissues in terms of the hydrogen nuclear density can be created. Different contrasts will be generated as per the different relaxation properties between the hydrogen atoms in different body fluids and tissues. MRI frequently necessitates the use of contrast agents for improved image quality; the FDA has approved only gadolinium (Gd)-based contrast agents for MRI to be used on patients with all types of cancers. However, Gd MRI is not suitable for quantitative clinical measures of NPs as intrinsic/background signals interferes drug distribution signals. ¹⁹F-MRI which offers a quantifiable signal, but the limitation being less sensitivity, does not makes it an ideal method either. Magnetic particle imaging (MPI), yet another modality, is a type of noninvasive imaging technique. In addition, MPI has been applied to observe the biodistribution pattern of NDDSs by using superparamagnetic nanoparticles (SPNs) as contrast agents. Consequently, MPI has shown prospects to offer an extensive range of imaging depths, linearly quantifiable signals, high sensitivity, as well as real-time imaging. A study by Zhu et al. [38] designed a superparamagnetic Fe₃O₄ nanocluster@poly(lactide-co-glycolide acid) core-shell nanocomposite loaded with DOX, which assisted as a drug delivery system as well as an MPI quantification tracer. The study further showed that nanocomposite was

degraded in a mild acidic microenvironment (pH $\frac{1}{4}$ 6.5), which further led to a constant release of DOX in addition to steady decomposition of the Fe₃O₄ nanocluster. Moreover, the decomposition-induced MPI signal decay was found to be proportionate to the release rate of DOX over time (R² $\frac{1}{4}$ 0.99). Thus, a quantitative monitoring procedure for drug release course was established effectively in the cell culture.

Radiolabeling

Tracing of nanoparticles *in vivo* and examining their biodistribution, drug targeting, and clearance quantitatively become possible when nanoparticles are labeled with radionuclides. Conventional methods for radiolabeling NPs usually comprise functionalizing the particle surface, core, or coating with radio-tag. Conversely, the chief apprehension of the orthodox radiolabeling methods is the institution of a bulky lipophilic prosthetic tag or else charged metal ion chelate-tag into the system, which in turn could impact the toxicity profiles in addition to pharmacokinetic of the original NPs. Alternative radiolabeling methods for NPs such as radiochemical doping, direct chemisorption, isotope exchange, physisorption, cation exchange, particle beam or reactor activation, and cavity encapsulation have been explored to dodge alerting their surface properties. Furthermore, modern imaging techniques like positron emission tomography (PET) can provide insights into the *in vivo* biodistribution of radiolabeled NDDSs. In a study by Engudar et al., liposomes were remote loaded ¹²⁴I and evaluated by PET/CT imaging by *in vivo* method and exhibited sustained systemic circulation half-life of 19.5 h for the radiolabeled liposomes. Moreover, radiolabeled liposomes were found to be accumulated less than usually long-circulating liposomes in the organ, viz. spleen, liver, and kidney besides tumours [39].

Fluorescence Spectroscopy

Lately, semiconductor NPs, also recognized as quantum dots (QDs), have been comprehensively applied in fluorescence technology, a proficient methodology for examination of nanostructure biodistribution in cells as well as tissues. QDs do

have optical transitions in the near-infrared region as compared conventional organic dyes and thus are accountable for minimal tissue absorption. A study conducted by Kenesei et al. [40] employed spectral imaging fluorescence microscopy for monitoring the distribution of fluorescent polystyrene nanoparticles which were modified with PEG or carboxylic acid groups in male and pregnant female mice. Visualization of nanoparticles in several tissues and overcoming the limitations caused by the high autofluorescence of native tissues was made possible by spectral imaging combined with post hoc spectrum analysis.

Laser Ablation Inductively Coupled Plasma Mass Spectroscopy (LA-ICP-MS)

ICP-MS is a sensitive analytical method for the determination of ultra-trace levels of metals and metalloids; LA-ICP-MS being a derived technology of ICP-MS is armed with a laser ablation system for vaporizing the sample. LA-ICP-MS imaging is executed by rastering a laser beam across the surface of a cryosectioning tissue sample, which in turn offers a high spatial resolution of the absorbed metallic NPs in diverse tissues. LA-ICP-MS method for quantitative imaging of biodistributions of PEGylated AuNPs was developed by Elci et al. [41]. The imaging method delivers significant tissue/organ distribution data to facilitate in the design and study of nanomaterials for biomedical applications.

6 Physiological-Based Pharmacokinetic Modelling (PBPK) in Nanoparticulate Drug Delivery Systems (NPDDS) Targeting the Brain

Although PBPK models are used for assessing pharmacokinetics (PK) of NPDDS including those which target the brain, several limitations of model design decrease the exactitude and accuracy of nanoparticle PK estimates. A complete account of the nanoparticle ADME is vital to develop the quality of the simulations, and therefore an exhaustive consideration of the

molecular and physiological progressions regulating nanoparticle disposition should be highlighted. While only a narrow range of applications have been developed until now, the prospective of this technique is tremendously promising. PBPK model was described in 2008 which predicted PK of quantum dots by whole-body PBPK in mice for a nanoformulation. Distribution coefficient was used to mimic the diffusion of nanoparticle in various tissues based on *in vitro* data and was able to envisage PK with decent correctness in animals. Consequently, different PBPK models for quantum dot PK were explored, in experiments by [42, 43]. Tissue-to-plasma coefficient values were deduced from the investigational data obtained from rat and a blood flow-limited model was established to mimic the PK of quantum dots. However, the model did not precisely envisage the tissue distribution of quantum dots, predominantly in the first hour post-dose, due to an inadequate number of compartments (blood, skin, muscle, kidney, liver, and “other tissues”) incorporated in the simulation as well as lymphatic system being absent. PBPK approach was exploited for modelling silver nanoparticle PK, for shamming the association between particle sizes, tissue penetration, and the resultant influence on toxicity and health risks. Regrettably, experimental data couldn't be harmonized entirely in the model, perhaps due to the consequence of other nanoparticle characteristics being excluded in the PBPK model, for example, surface charge and coating.

PLGA nanoparticle formulations prepared with diverse types of monomethoxypoly ethylene glycol (mPEG), viz. PLGA, PLGA-mPEG256, PLGA-mPEG153, PLGA-mPEG51, and PLGA-mPEG34, were studied by utilizing PBPK modelling to investigate the association between nanoparticle properties (e.g. size, zeta potential, and the number of PEG molecules per unit surface area) and distribution considerations. Substantial linear relationships among nanoparticle properties and distribution parameters were obtained by multivariate regression, and consequently, the same semi-mechanistic model was effectively employed to envisage the distribution yet another nanoparticle PLGA-mPEG 495 in

animal study [44]. In a study, temporal exposure and elimination of gold dendrimer composite nanodevices were studied in melanoma-induced mice, and results showed that size and charge of composite nanodevices directed their *in vivo* interactions due to lack of specific binding ligands. In yet another study, a PBPK model was established for ionic silver and nanoencapsulated silver based on toxicokinetic data obtained from *in vivo* studies. The study authenticated the model structure for both silver forms by replicating exposure conditions of *in vivo* experiments and associating simulated with real pharmacokinetic data obtained from plasma and tissues. PBPK models for NPDDS has been assimilated with the mathematical simulation of therapeutic activity and/or host toxicity, since the pharmacodynamics of nanoparticles depends on the nanoparticle penetration in tissues and the interaction with the therapeutic targets. Moreover, several factors defining complex interplay influence these phenomena which can be positively characterized through mathematics. Few studies have predicted augmented efficiency of nanoparticles by mathematical modelling frameworks based on relating drug's cellular uptake and tumour cell death rates [45].

6.1 Pharmacokinetic Analysis Laser-Synthesized Au Nanoparticles (AuNPd)

In a study by Bailly AL et al., the pharmacokinetic profile of laser-synthesized Au nanoparticles (AuNPd) in blood was investigated in athymic nude female mice which were treated with AuNPd at an exclusive dose of 1 mg/kg by IV injection, and the concentration of gold was quantified by inductively coupled plasma mass spectrometry (ICP-MS) at specific timeline of 5, 15, 30, 45, 60, 4, and 24 h post-AuNPd injection. Solutions were dosed with calibration curves performed with ionic gold standard solutions as well as gold nanoparticle standard solutions to avoid underestimation of gold concentration which might perhaps happen due to an inadequate mineralization of nanoparticulate gold. Result

showed insignificant difference with whatsoever the standard solutions were employed, endorsing validity of the measurement. In addition, AuNPD blood concentration-time curve in a semilogarithmic scale showed a quick fall in initial concentration, subsequently with additional gradual deterioration fitting into a conventional bi-compartmental pharmacokinetic model described by a quick initial distribution phase and then a terminal elimination phase at lower rate. The mean pharmacokinetic parameters considered in this bi-compartmental analysis were $T_{1/2\alpha}$ (bio-distribution half-life), $T_{1/2\beta}$ (elimination half-life), AUC, C_{max} , Cl (clearance), and Vd (volume of distribution). Results further showed that above 95% of the injected dose was eliminated from the blood circulation 1 h post injection, which was dependable with the low value of $T_{1/2\alpha}$, i.e. half-life for the distribution phase. Blood levels of gold was untraceable in 24 h post-administration, therefore clarifying the short $T_{1/2\beta}$, i.e. half-life for elimination besides high clearance value. The Vd was also found below the volume of the mice body fluid (2 mL) that suggested AuNPD accumulation in the organs. These data, thus, recommended that the amount of AuNPD in the blood (central compartment) decays quickly because of the transfer of NP to tissues (peripheral compartment) and/or to AuNPD elimination that occurs concurrently [46].

It is valuable to counterpart the biodistribution investigational data with pharmacokinetic modelling for an improved understanding of exposure, offer comprehensions on the key mechanisms accountable for biodistribution, and perhaps extrapolate the bio-behaviour from animal models to humans. PBPK models have been exploited for studying and thus predicting the biodistribution of chemicals inside the body since many years. Additionally, many PBPK models have been precisely established for nanoparticles; however, they have not been successful to explicitly address the role of phagocytosis, a key process involved in nanoparticle biodistribution.

Whole-body PBPK model built by Li et al. [47] assimilated phagocytosis; nevertheless, the model was inadequate to intravenous injection of nanoparticles.

Serum half-life and biodistribution is impacted by nanoparticle core, linker, and coating materials together with synthesis and purification techniques that are employed during the course of development; for instance, linker molecules like chitosan may sterically lead to stabilization of the corona and preclude accumulation. Synthetic polymers like PEG, polyvinyl alcohol (PVA), or polysaccharide induced surface modification of nanoparticles can increase the solubility of hydrophobic materials, diminish nonspecific binding, extend the circulation time, as well as improve tumour-specific targeting. Meanwhile in vivo fate of nanoparticles is determined by the chemical and physical properties; it is necessary to quantify pharmacokinetic profile right in the early phase of development so that this evidence can be utilized for influencing nanoparticle design as well as candidate prototype selection. Conventionally, pharmacokinetic studies were performed on the basis of either quantification of the therapeutic agent (for instance, employing HPLC and mass spectroscopy) or radiolabeling the agent and determining radioactivity in the homogenized tissue. However, these methods are comparatively affluent, time-consuming, and not in the realm of capability of several nanoparticle synthesis laboratories. Albeit pharmacokinetic data is highly essential in making choices concerning particle size, synthesis procedures, coating, and purification methods, these researches are frequently directed in the late stages of nanoparticulate development because of these barricades. A novel and cost-effective method for PK assessment of nanoparticles is using near-infrared (NIR)-based technology, which also permits the critical steps performance in early development stages of nanoparticulate research [48].

6.2 Pharmacokinetic Evaluation of Liposomes Containing Drugs

In a study by Shinde U A et al., liposomes containing atomoxetine (ATX-Lipo), ATX mucoadhesive liposomes without a vasoconstrictor phenylephrine (PHE) (ATX-Muco Lipo), and ATX mucoadhesive liposomes with a vasoconstrictor phenylephrine (PHE) (ATX + PHE-Muco Lipo) were efficiently tagged with ^{99m}Tc , and optimization was conducted for maximum radiolabeling efficiency and stability. Results showed radiochemical purity of 96.22% for ATX-Lipo post 180 min (this time period was selected for stability study of the radiolabeled formulations, as it was terminal time point before animal sacrifice); optimum SnCl_2 concentration was detected as 100 μL (1 mg/mL) for ATX liposomal formulations with 20 min of incubation time. These results showed that the radiolabeled formulations were appropriate for the pharmacokinetic study of ATX in rats. Moreover, biodistribution studies of ^{99m}Tc formulations following intranasal (i.n.) administration (ATX-Lipo, ATX-Muco Lipo and ATX + PHE-Muco Lipo) as well as intravenous (i.v.) administration (ATX-Lipo) on rats were executed, in addition to estimation of the radioactivity at different time intervals up to 180 min. Drug brain/blood ratios at all sampling time points for diverse formulations as well as pharmacokinetic parameters were calculated. The pharmacokinetic studies showed maximum concentrations (C_{max}) of the drug in the blood and brain post i.n. and i.v. administration in rats were achieved at altered t_{max} values. Bearing in mind the drug concentration attained in the brain at a specific time interval, intranasal ATX-Lipo achieved a lower C_{max} value (0.0248) at a t_{max} of 30 min, while the C_{max} (0.109) for intranasal ATX-Muco Lipo was attained at 60 min of t_{max} . Less C_{max} in the brain for intranasal ATX-Lipo would have been due to condensed residence time of the formulation owing to nasolacrimal drainage, with which upper C_{max} value for intranasal ATX-Muco Lipo (0.109) at 60 min was ascribed to mucoadhesive polymer's properties like viscous nature and cross-linking that was

incorporated in the liposomal formulation. Ugwoke, M. et al. observed an alike observation for nasal mucoadhesive delivery of apomorphine [49] in powder dosage form. The maximum C_{max} value in the brain (0.151) was attained at 30 min after ATX + PHE-Muco Lipo was administered intranasally. A vasoconstrictor, PHE, is clinically given in combination with local anaesthetics for prevention of wash away of local anaesthetic from the site of action, therefore extending its effect at that location. Comparable effect would be ascribed when ATX + PHE-Muco Lipo was administered. A study by Dhuria et al. has also confirmed greater brain uptake of intranasal therapeutic neuropeptides with phenylephrine incorporated as a vasoconstrictor in the formulation. Charlton et al. co-administered ephedrine as a vasoconstrictor along with the drug in a nasal formulation and observed higher drug blood concentrations [50]. Nonetheless, in other comparable studies, it has been described that vasoconstrictors were administered previous to commencing drug administration rather than going for co-administering with the nasal formulation. This showed that in the present study by Shinde U A et al., the use of PHE preceding intranasal administration of ATX liposomal formulation in place of co-administration may have augmented the prospect of superior transport to the brain. This study showed a significant high brain AUC for intranasal ATX-Muco Lipo (8.88 min %/g) as well as intranasal ATX + PHE-Muco Lipo (2.26 min %/g) in comparison to intravenous ATX-Lipo (1.28 min %/g), demonstrating the efficacy of the liposomes for brain targeting. ATX-Lipo (i.n.), ATX-Muco Lipo (i.n.), ATX + PHE-Muco Lipo (i.n.), and ATX-Lipo (i.v.) exhibited brain/blood uptake ratios (BBR) of 0.161, 1.255, 0.331, and 0.003, respectively, at 30 min designated larger transportation of drug to the brain post-intranasal administration of liposomal formulations in comparison to intravenous administration of liposomes. The result may be suggestive of liposomal direct transport bypassing the blood-brain barrier owing to an unswerving connection between the nose and brain due to presence of olfactory region in the nasal cavity. Pharmacokinetic data was further exploited to

calculate the drug (ATX) targeting efficiency (DTE, %) and brain drug (ATX) direct transport percentage (DTP, %) for nasally administered formulations. Comparable studies in the same line have described similar results for nose-to-brain targeted intranasal mucoadhesive micro-emulsion drug delivery systems as well [51].

7 Summary

Forthcoming standpoint for the use of nanotechnology in drug delivery to CNS is highly encouraging and has unlocked new opportunities in the treatment of neurological disorders owing to their revolutionizing prospective in CNS-targeted therapies by nanoengineering drug/carriers to cross the BBB, diffusion within brain tissues, specifically targeting of cells, and/or signalling cascades. Moreover, a complete consideration of the in vivo fate of NPDDSs is essential to guarantee their safe clinical applications due to a vast breach in pharmacokinetics between the released (in-)active ingredients and NPs. Numerous NPDDS approaches have been developed as an unconventional tactics to augment drug delivery and progress the treatment of CNS disorders. Many processes intercede the pharmacokinetics of NPDDS, with absorption, distribution, metabolism, and elimination being below par comprehended and regularly conflicting significantly from conventional formulations. Indulgence on how nanoformulation composition in addition to physicochemical properties might influence drug biodistribution and disposition in the body is of fundamental importance when developing prospect treatment strategies. The approaches for profiling biodistribution as well as pharmacokinetic behaviour of NPDDSs for brain targeting have been discussed.

References

1. Honjo K, Black SE, Verhoeff NP. Alzheimer's disease, cerebrovascular disease, and the β -amyloid cascade. *Can J Neurol Sci.* 2012;39(6):712–28.
2. Kanwar JR, Sriramaju B, Kanwar RK. Neurological disorders and therapeutics targeted to surmount

- the blood brain barrier. *Int J Nanomedicine.* 2012;7:3259–78.
3. Srikanth M, Kessler JA. Nanotechnology-novel therapeutics for CNS disorders. *Nat Rev Neurol.* 2012;8:307–18.
4. Wohlfart S, Gelperina S, Kreuter J. Transport of drugs across the blood-brain barrier by nanoparticles. *J Control Release.* 2012;161:264–73.
5. Gao H. Progress and perspectives on targeting nanoparticles for brain drug delivery. *Acta Pharm Sin B.* 2016;6(4):268–86.
6. Petty MA, Lo EH. Junctional complexes of the blood brain barrier: permeability changes in neuroinflammation. *Prog Neurobiol.* 2002;68(5):311–23.
7. Santaguida S, Janigro D, Hossain M, Oby E, Rapp E, Cucullo L. Side by side comparison between dynamic versus static models of blood-brain barrier in vitro: a permeability study. *Brain Res.* 2006;1109(1):1–13.
8. Rabanel JM, Aoun V, Elkin I, Mokhtar M, Hildgen P. Drug-loaded nanocarriers: passive targeting and crossing of biological barriers. *Curr Med Chem.* 2012;19(19):3070–102.
9. Pardridge WM. Drug transport across the blood-brain barrier. *J Cereb Blood Flow Metab.* 2012;32(11):1959–72.
10. Holmes D. The next big things are tiny. *Lancet Neurol.* 2013;12(1):31–2.
11. Petkar KC, Chavhan SS, Agatonovik-Kustrin S, Sawant KK. Nanostructured materials in drug and gene delivery: a review of the state of the art. *Crit Rev Ther Drug Carrier Syst.* 2011;28(2):101–64.
12. Montet X, Funovics M, Montet-Abou K, Weissleder R, Josephson L. Multivalent effects of RGD peptides obtained by nanoparticle display. *J Med Chem.* 2006;49(20):6087–93.
13. Gabathuler R. Approaches to transport therapeutic drugs across the blood-brain barrier to treat brain diseases. *Neurobiol Dis.* 2010;37(1):48–57.
14. Masserini M. Nanoparticles for brain drug delivery. *ISRN Biochem.* 2013;2013:18.
15. TGA. Regulation of nanomedicines by the Therapeutic Goods Administration. TGA; 2016.
16. European Medicines Agency. Nanomedicines: EMA experience and perspective. 2015. http://www.euronanoforum2015.eu/wpcontent/uploads/2015/06/2_NanomedicinesEMA-experienceperspective_DoloresHernan_10042015.pdf.
17. Petros RA, DeSimone JM. Strategies in the design of nanoparticles for therapeutic applications. *Nat Rev Drug Discov.* 2010;9:615–27.
18. Roger E, Lagarce F, Garcion E, Benoit JP. Biopharmaceutical parameters to consider in order to alter the fate of nanocarriers after oral delivery. *Nanomedicine.* 2010;5:287–306.
19. Bur M, Henning A, Hein S, Schneider M, Lehr CM. Inhalative nanomedicine—opportunities and challenges. *Inhal Toxicol.* 2009;1:S137–43.
20. FDA. Liposome drug products guidance for industry. 2015. <http://www.fda.gov/Drugs/>

- [GuidanceComplianceRegulatoryInformation/Guidances/default.htm](#).
- Choi YH, Han HK. Nanomedicines: current status and future perspectives in aspect of drug delivery and pharmacokinetics. *J Pharm Investig*. 2018;48:43–60.
 - Smits EA, Soetekouw JA, Doormalen IV, et al. Quantitative LC-MS determination of liposomal encapsulated prednisolone phosphate and non-encapsulated prednisolone concentrations in murine whole blood and liver tissue. *J Pharm Biomed Anal*. 2015;115:552–61.
 - Braal CL, Bruijn PD, Atrafi F, et al. A new method for the determination of total and released docetaxel from docetaxel-entrapped core-cross-linked polymeric micelles (CriPec(R)) by LC-MS/MS and its clinical application in plasma and tissues in patients with various tumours. *J Pharm Biomed Anal*. 2018;161:168–74.
 - Deshpande NM, Gangrade MG, Kekare MB, et al. Determination of free and liposomal amphotericin B in human plasma by liquid chromatography mass spectrometry with solid phase extraction and protein precipitation techniques. *J Chromatogr B Analyt Technol Biomed Life Sci*. 2010;878:315–26.
 - Su C, Yang H, Sun H, Fawcett JP, Sun D, Gu J. Bioanalysis of free and liposomal amphotericin B in rat plasma using solid phase extraction and protein precipitation followed by LC-MS/MS. *J Pharm Biomed Anal*. 2018;158:288–93.
 - Xie Y, Shao N, Jin Y, Zhang L, Jiang H, Xiong N, Su F, Xu H. Determination of non-liposomal and liposomal doxorubicin in plasma by LC-MS/MS coupled with an effective solid phase extraction: in comparison with ultrafiltration technique and application to a pharmacokinetic study. *J Chromatogr B Analyt Technol Biomed Life Sci*. 2018;1072:149–60.
 - Wang H, Zheng M, Gao J, Wang J, Zhang Q, Fawcett JP, et al. Uptake and release profiles of PEGylated liposomal doxorubicin nanoparticles: a comprehensive picture based on separate determination of encapsulated and total drug concentrations in tissues of tumor-bearing mice. *Talanta*. 2020;208:120358.
 - Song W, Tweed JA, Visswanathan R, Saunders JP, Gu Z, Holliman CL. Bioanalysis of targeted nanoparticles in monkey plasma via LC-MS/MS. *Anal Chem*. 2019;91(21):13874–82.
 - Chen Y, Wang L, Guo D, et al. A rapid and efficient technique for liposomal and nonliposomal drug pharmacokinetics studies using magnetic nanoprobe and its application to leakage kinetics of liposomes. *J Chromatogr A*. 2018;1580:2–11.
 - Sun X, Wang G, Zhang H, et al. The blood clearance kinetics and pathway of polymeric micelles in cancer drug delivery. *ACS Nano*. 2018;12(6):6179–92.
 - He H, Zhang J, Xie Y, et al. Bioimaging of intravenous polymeric micelles based on discrimination of integral particles using an environment responsive probe. *Mol Pharm*. 2016;13(11):4013–9.
 - Zhuang W, Ma B, Hu J, et al. Two-photon AIE luminogen labeled multifunctional polymeric micelles for theranostics. *Theranostics*. 2019;9(22):6618–30.
 - Wang B, Guo Y, Chen X, et al. Nanoparticle-modified chitosan-agarose gelatin scaffold for sustained release of SDF-1 and BMP-2. *Int J Nanomedicine*. 2018;13:7395–408.
 - Azie O, Greenberg ZF, Batich CD, Dobson JP. Carbodiimide conjugation of latent transforming growth factor b1 to superparamagnetic iron oxide nanoparticles for remote activation. *Int J Mol Sci*. 2019;20(13):3190.
 - Wang T, Zhang WD, Sun D, Gu J. Current status of in vivo bioanalysis of nano drug delivery systems. *J Pharm Anal*. 2020;10:221–32.
 - Richter AW, Akerblom E. Antibodies against polyethylene glycol produced in animals by immunization with monomethoxy polyethylene glycol modified proteins. *Int Arch Allergy Appl Immunol*. 1983;70:124–31.
 - Cai H, Dai X, Wang X, et al. A nanostrategy for efficient imaging-guided antitumor therapy through a stimuli-responsive branched polymeric prodrug. *Adv Sci*. 2020;7:1903243.
 - Zhu X, Li J, Peng P, Nassab NH, Smith BR. Quantitative drug release monitoring in tumors of living subjects by magnetic particle imaging nanocomposite. *Nano Lett*. 2019;19(10):6725–33.
 - Engudar G, Schaarup-Jensen H, Flidner FP, et al. Remote loading of liposomes with a 124I-radioiodinated compound and their in vivo evaluation by PET/CT in a murine tumor model. *Theranostics*. 2018;8(21):5828–41.
 - Kenesei K, Murali K, Czéh A, Piella J, Puentes V, Madarász E. Enhanced detection with spectral imaging fluorescence microscopy reveals tissue- and cell-type-specific compartmentalization of surface-modified polystyrene nanoparticles. *J Nanobiotechnol*. 2016;14:55.
 - Elci SG, Yan B, Kim ST, et al. Quantitative imaging of 2 nm monolayer protected gold nanoparticle distributions in tissues using laser ablation inductively-coupled plasma mass spectrometry (LA-ICP-MS). *Analyst*. 2016;141(8):2418–25.
 - Lin P, Chen JW, Chang LW, Wu JP, Redding L, Chang H, et al. Computational and ultrastructural toxicology of a nanoparticle, Quantum Dot 705, in mice. *Environ Sci Technol*. 2008;42(16):6264–70.
 - Lee HA, Leavens TL, Mason SE, Monteiro-Riviere NA, Riviere JE. Comparison of quantum dot biodistribution with a blood-flow-limited physiologically based pharmacokinetic model. *Nano Lett*. 2009;9:794–9.
 - Li M, Panagi Z, Avgoustakis K, Reineke J. Physiologically based pharmacokinetic modeling of PLGA nanoparticles with varied mPEG content. *Int J Nanomedicine*. 2012;7:1345–56.
 - Moss DM, Siccardi M. Optimizing nanomedicine pharmacokinetics using physiologically based

- pharmacokinetics modelling. *Br J Pharmacol*. 2014;171:3963–79.
46. Bail AL, Correard F, Popov A, Tselikov G, Chaspou F, Appay R, et al. In vivo evaluation of safety, biodistribution and pharmacokinetics of laser synthesized gold nanoparticles. *Sci Rep*. 2019;9(1):12890.
 47. Li D, Johanson G, Emond C, Carlander U, Philbert M, Jolliet O. Physiologically based pharmacokinetic modeling of polyethylene glycol-coated polyacrylamide nanoparticles in rats. *Nanotoxicology*. 2014;8:128–37.
 48. Lee MJ, Veiseh O, Bhattarai N, et al. Rapid pharmacokinetic and biodistribution studies using chlorotoxin-conjugated iron oxide nanoparticles: a novel non-radioactive method. *PLoS One*. 2010;5(3):e9536.
 49. Ugwoke MI, Sam E, Van Den Mooter G, Verbeke N, Kinget R. Nasal mucoadhesive delivery systems of the antiparkinsonian drug, apomorphine: influence of drug-loading on in vitro and in vivo release in rabbits. *Int J Pharm*. 1999;181:125–38.
 50. Charlton ST, Davis SS, Illum L. Evaluation of the effect of ephedrine on the transport of drugs from the nasal cavity to the systemic circulation and the central nervous system. *J Drug Target*. 2007;15:370–7.
 51. Vaidya AV, Shinde UA, Shimoi HH. Preliminary studies on brain targeting of intranasal atomoxetine liposomes. *Int J Pharm Pharm Sci*. 2016;8(3):286–92.



Enhanced Bioavailability and Intestinal Uptake of Nanoparticles After Oral Delivery

Mitali Patel and Krutika Sawant

Contents

1	Introduction	386
2	Nanoparticles for Oral Delivery	387
3	Intestinal Lymphatic System (ILS)	389
4	Bioavailability and Intestinal Lymphatic System	389
5	Approaches Used for Evaluation of Intestinal Lymphatic Uptake	391
6	Applications of Nanoparticles in Enhancing BA of Drugs Through ILS	392
7	Conclusions	394
	References	394

Abstract

Poor bioavailability (BA) has become a major issue in the drug discovery in pharmaceutical industry as majority of the new molecules have poor water solubility. Hydrophilic milieu of the gastrointestinal tract (GIT) restricts the absorption of such lipophilic entities. Most of the drugs are directly absorbed through the portal vein after oral administration but there are several lipophilic molecules which enter into the systemic circulation by lymphatic

transport. Additionally, this characteristic also hinders the development of successful delivery system. Pharmacokinetic property of drugs is also affected by presence of food as it causes delay in gastric emptying, promote gastric motility, promote bile salt secretion, etc. Nanoparticles are considered as an effective approach to overcome hurdles and the pharmacokinetic and pharmacodynamic limitations linked with such lipophilic molecules. Lipid-based nanoparticles like solid lipid nanoparticles, nanostructured lipid carriers, self-microemulsifying drug delivery system, liposomes, etc. have gained more attention for delivery of lipophilic molecules. The pharmaceutical industries are looking for another path for delivery of drugs to evade issues related with poor bioavailability. Currently for orally administered lipophilic drugs, the intestinal

M. Patel
Maliba Pharmacy College, Uka Tarsadia University,
Bardoli, India

K. Sawant (✉)
Pharmacy Department, Faculty of Pharmacy,
The Maharaja Sayajirao University of Baroda,
Vadodara, India

lymphatic system (ILS) has become an absorptive pathway to conquer such limitations, which can avoid liver-assisted first-pass metabolism and aid bioavailability. The ILS is a path which transports fat-soluble vitamins, food-derived lipids, and lipophilic peptides to systemic circulation. This chapter emphasizes on the ILS, the role of the lymphatic system in bioavailability enhancement, and application of nanoparticles for improving BA via this route.

Keywords

Bioavailability · Intestinal lymphatic system · Nanoparticles · Oral delivery

1 Introduction

The choice of oral route for drug delivery is primarily associated with its ease of administration and noninvasiveness which increases patient's compliance. Presently, around 40% drugs in the development phase and almost 60% drugs in synthesis are lipophilic in nature [1]. These newly discovered active pharmaceutical ingredients (APIs) by pharmaceutical industry have failed to be developed because of poor solubility in water, which makes their formulation difficult or even impossible. Drugs belonging to Biopharmaceutics Classification System (BCS) Class II and IV suffer from less water solubility and/or permeability which is the main reason that they suffer from poor bioavailability (BA) [2–4]. Hence, alternative drug delivery system is needed to deliver such lipophilic drug molecules by peroral route [5].

The physicochemical properties and metabolic instability of drugs in the stomach and liver negatively affect their absorption process. Upon oral administration, many drugs and macromolecules get degraded or deactivated because of gastric acid secretion, presence of enzymes in the GIT, etc. Some drugs are stable and undergo absorption from GIT, but they undergo hepatic first-pass metabolism and have low BA [6].

Upon oral administration of a formulation, the absorption starts from the stomach, but the mag-

nitude of drug absorption is limited due to short (0.5–2 h) gastric emptying time. For orally given drugs, small intestine is the chief absorption site. The intestinal absorptive surface area due to villi and microvilli is nearly 300–400 m² and hence there are more chances of absorption of majority of the molecules from this site [7, 8].

By considering all the aspects of API and oral route, there is a need to choose an alternative pathway for oral drug delivery systems. ILS is taken into consideration as a promising pathway for oral drug delivery as it sends drugs initially to the lymphatic system which subsequently reach the systemic circulation. The lymphatic transport pathway has many merits such as the following: it bypasses hepatic assisted first-pass metabolism and directly delivers drug to systemic circulation, permits transfer of macromolecules and larger size particles due to leaky capillaries of lymphatics, has ability to treat the diseases which affect lymphatic systems for example lymphomas, human immunodeficiency virus (HIV) infection, etc. Till date, two key targets (i) chylomicrons (CMs) in enterocytes and (ii) M (microfold) cells present in Peyer's patches (PP) are recognized for effective lymphatic delivery [9].

The presence of food may impact drug absorption process on account of physiological changes in the GI tract or physical or chemical interactions between API and particular food components [10]. The absorption with food may be delayed, increased, reduced, or not affected based on type and degree of interaction [11]. The high-fat meal generally increases the gastric residence time which can be a vital feature in degree of drug absorption. As the presence of food in GIT delays gastric emptying time, more time is available for drug absorption [12]. The BA enhancement with food is attributed to enhanced residence time in GIT, solubility, biliary and pancreatic secretions, permeability, decreased metabolism, reduced activity of efflux pump, changes in mesenteric and liver blood flow, and promotion of transport through lymphatic system [13]. For absorption process of lipophilic drugs, the lipidic constituent of food plays an essential role which leads to augment oral BA [14]. The meal with high fat increases the level of triglyceride (TG)-rich lipoproteins which

undergo reaction with the drugs [15] and further promote the intestinal lymphatic transport and modify pharmacokinetic profile of API. Also, GIT residence time is increased by food containing long-chain fatty acids and triglycerides [16]. The intraluminal process of formulation is influenced such as buffer capacity, pH, amount of bile salt, osmolality, surface tension, and food components [17, 18]. A guideline on “Food-Effect BA and Fed Bioequivalence Studies” was given by the Food and Drug Administration (FDA) [3]. To assess influence of foods on drug absorption process, the FDA recommends high-fat meal conditions as it markedly affect GI physiology. This fat condition includes 800–1000 cal; 50–65% from fat, 25–30% from carbohydrates, and 15–20% protein [2, 19].

2 Nanoparticles for Oral Delivery

Lipophilic drug suffers from pitfalls like slow onset of action, low oral BA, inability to attain steady-state level plasma concentration, and unwanted adverse effects. Nanotechnology is an encouraging approach for fabrication of successful drug delivery systems specifically for drugs with less water solubility, poor permeability, and BA [20, 21]. In the field of delivery of drugs, nanotechnology offers numerous merits like (i) delivery of lipophilic drugs, (ii) drug targeting to particular site in GIT, (iii) transcytosis of drug molecules across the GIT, and (iv) transcellular delivery of macromolecules. Moreover, nanoparticle-based oral drug delivery can effectively improve pharmacokinetics and pharmacodynamics of drugs [22–25].

Nowadays, oral delivery based on lipidic component has acquired interest for the fruitful delivery of lipophilic compounds [26]. Among various BA-enhancing techniques, lipid-based nanoparticles are well-known for resolving solubility and/or permeability problems [27, 28]. The exclusive properties of lipid vehicles such as biocompatibility, physiochemical diversity, and capacity to boost oral BA of lipophilic moieties through lymphatic uptake have made them as a carrier of choice for fabrication of orally given dosage forms [29].

Most of the researchers assume that lipid-based formulations are usually established for

extremely lipophilic drugs. The drugs which are less water soluble are categorized as (i) lipophilic hydrophobic (grease balls) and (ii) non-lipophilic hydrophobic (brick dust) [30]. “Grease balls” in lipid-based excipients show good solubility, whereas “brick dust” are insoluble in glyceride excipients and have tight crystal lattices, and formulations of such compounds can be developed with surfactants or cosolvents [27, 31].

In BA enhancement, lipid-based excipients provide improved solubility, assisting lymphatic transport, and/or promotion of enterocytes regulated transport and disposition of drugs [6, 32]. Lipid-based system is useful in increasing the BA of lipophilic drugs as they can hold the drug in the solubilized state in the lipid phase until it is absorbed and hence, can overcome barrier of poor dissolution and thereby can achieve improved and steady BA [33–35]. The absorption of lipid-based formulation is affected by numerous factors like size of particles, extent of emulsification, rate of dispersion, and precipitation of drug after dispersion in GIT. Furthermore, the administration of drug along with lipids augment the lymphatic transport [36, 37].

Numerous lipid-based formulations like solid lipid nanoparticles (SLNs), nanostructured lipid carriers (NLCs), lipid-polymer hybrid nanoparticles (LPHNPs) and self-microemulsifying drug delivery systems (SMEDDS) can be fabricated for successful delivery to ILS [38, 39]. The probable intestinal absorption mechanisms include increased fluidity of membrane, tight junction (TJ) opening, impeding efflux by P-gp and/or CYP450, and increasing production of chylomicron [40–42] which is depicted in Fig. 21.1.

Digestible lipids such as phospholipids, fatty acids (FA), cholesterol, triglycerides (TG), diglycerides (DG), and synthetic derivatives are considered as appropriate oils for the delivery of lipophilic molecules. The lipids affect the absorption process based on carbon chain length, extent of saturation, and their capacity to interact with water molecules [43].

Co-administration of drugs with long-chain triglyceride (LCT), instead of shorter lipids, stimulates production of lipids in the enterocytes, increasing chylomicron synthesis and thus pro-

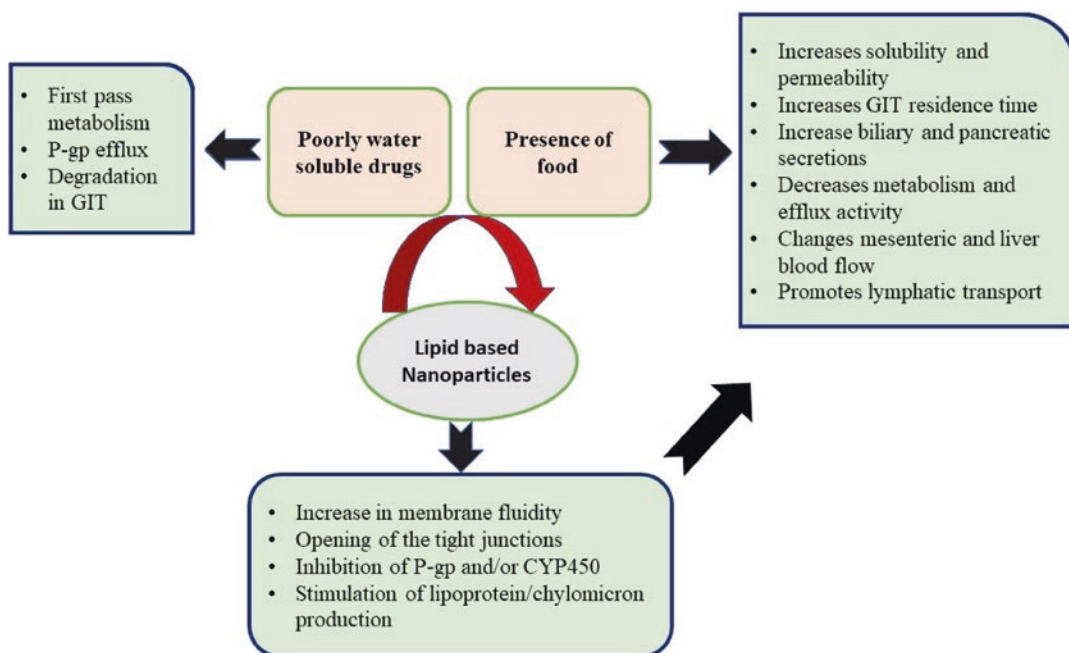


Fig. 21.1 Role of lipid-based nanoparticles in enhancement of BA

moting the lymphatic transport [44]. It has been reported by Caliph et al. that administration of halofantrine with LCT rather than medium-chain triglyceride (MCT) or short-chain triglyceride (SCT) exhibited improved BA of halofantrine (70%) by lymphatic pathway [45].

Intestinal permeability is primarily affected by components of LBDDS by inhibiting efflux transport and/or by altering the passive permeability [46]. The passive permeability is increased by using excipients like lysophospholipids, surfactants, fatty acids containing medium chain, and cosurfactants either by tight junction opening or by improving membrane solubility and fluidity [47, 48].

Upon administration, triglyceride is converted into mono-/diglycerides and fatty acids. If the drug has less solubility in triglycerides alone, then the solvent capacity of the lipid formulation can be enhanced by adding mixed glycerides during development of formulation. Moreover, mixed glycerides are alike to products of lipid digestion. In aqueous environment of GIT, the undigested triglycerides have poor miscibility which alters gastric emptying and absorption [49–51].

In GIT, absorption process of dietary lipid comprises many steps. Initially, neutral lipids undergo hydrolysis in the gut which produces fatty acids and monoglycerides. They are then transferred via the apical membrane of enterocytes where re-esterification occurs by enzymes of endoplasmic reticulum and generates TGs. Further, generated TGs along with cholesterol, cholesteryl esters, phospholipids, and Apo B are collected into CMs, and lastly, they are released from the basolateral membrane of enterocyte and reach the intestinal lymphatic lacteals [52].

The enterocytes produce CMs and lipoproteins having diameter of 200–800 nm at the end of lipid digestion which are extremely large for blood capillaries and hence uptaken through lymphatic capillaries [40].

For intestinal lymphatic absorption of nanoparticles, the mechanism responsible is that the drug undergoes intracellular association with lipophilic core of the chylomicron [53]. After that, the CMs are packed in the Golgi and then secreted to the intracellular space from the basolateral side of the enterocyte. Then it is absorbed by mesenteric lymph vessels along with lipo-

philic molecule into lymphatics until it reaches systemic blood circulation [29, 54].

For intestinal lymphatic transport, drugs having logP and solubility value more than 5 and 50 mg/mL in LCT, respectively, are considered as suitable candidates [55], though this is not true at all times. An opposite relationship has been reported among solubility of retinoids in oil and lymphatic absorption [56]. The reported combined requirements, i.e., high log P value and high solubility in LCT, are not adequate for actual estimation of transport by ILS [15]. The association of lipophilic drug with CMs present in enterocytes is a requirement to enter the lymph, which is a determinant of lymphatic transportation. The lymphatic uptake is strongly correlated with extent of association with CMs, not with only high LogP or high LCT solubility or both. The impact of physicochemical properties of API on lymphatic transport can be predicted based on connection among CM association and molecular descriptors [57].

2.1 Pharmacokinetics of Lipid-Based Nanoparticles

Nanoparticles possess pharmacokinetic merits like targeted delivery, improved stability, enhanced permeability across membrane and BA, and improved duration of action. The various properties of nanoparticles, for example, particle size, surface charge, and lipophilicity, influence process of absorption [58, 59]. Small particles undergo high transcellular uptake by follicle-associated epithelia in contrast to large particles. Generally, nanoparticles enter cells by endocytosis, whereas large size particles undergo opsonization and hence can be removed by macrophages of the reticuloendothelial system (RES). Opsonization is prevented by modifying the surface property using excipients like PEG [60, 61].

3 Intestinal Lymphatic System (ILS)

The lymphatic system in the small intestine not only solitarily controls tissue fluid homeostasis and promotes immune surveillance nevertheless

also helps in transportation of luminal substances such as fat-soluble vitamins as well as dietary fats. Possibly due to this additional role, the small intestine is a widely studied tissue lymphatic system in many species [48]. The intestine from luminal to serosal surface comprises three layers of lymphatics, viz., the lacteals present in the villi, a submucosal lymphatic network, and a lymphatic network present in the smooth muscle layer [62].

The ILS primarily comprises lymphatics' network of lymph nodes, lymphatic vessels, and lymphoid organs and mainly drains interstitial fluids. Each gut villi is drained by central lacteal out of where fluid is drained to the mesenteric lymph duct. The lymph flows by this lymph duct to the cisterni chyli and reaches the thoracic duct. The lymph is ultimately recombined at the junction of left jugular and left subclavian veins with the blood. Hence, drugs that are effectively reached in the lymph circumvent hepatic assisted first-pass metabolism [40, 49].

Various factors affect the lymphatic transport of drug molecules. Among them, chain length of free fatty acid (FFA) chain, composition, and size of the lymph lipid precursor in the enterocyte render a main part in lymphatic transport of drug. FFA with 6–12 carbon chain length undergo portal blood absorption, while FFA containing carbon chain length more than 12 undergo re-esterification and are transported by ILS [5, 62]. Moreover, higher the unsaturation, the larger the size of lymph lipoproteins, boosting the lymphatic uptake [63].

4 Bioavailability and Intestinal Lymphatic System

Intestinal absorption is prerequisite for raising BA of drugs given by the oral route. Various mechanisms such as carrier-mediated transport, passive diffusion, enzymatic and chemical modification of the molecule in the enterocyte, dissolution behavior of the drug, and interaction with food ingredients mainly affect permeation across intestinal mucosa [64]. The BA enhancement of any API by ILS can be done either by chylomicron pathway or M cell pathway which are discussed below.

4.1 Chylomicron Pathway

CMs, triglyceride-rich large particles, are produced through the intestine and play a role in transportation of compounds such as cholesterol and dietary triglycerides to peripheral tissues and liver. As the stimulation of lipid digestion, CMs (lipid spheroids) are formed in the enterocytes to aid lipid transport, particularly high lipophilic entities, for example, triglycerides (TG). The hydrophobic core of CMs consists of TG, mono-glycerides, and cholesterol esters and polar surface consists of phospholipids (6–12%), free cholesterol, and apolipoproteins [42, 65, 66].

These particles comprise apolipoproteins A-I, A-II, A-IV, A-V, B-48, C-II, C-III, and E. The core structural protein is Apo B-48 which is present in each chylomicron particle. The chylomicron size depends upon quantity of ingested fat. A meal with high fat aids generation of large size chylomicron particles because a greater number of triglycerides are transported while in fasted condition; CMs with small size are produced due to less quantity of triglycerides [67].

Normally, the fatty acid composition of post-prandial CM triglycerides fairly closely imitates that of ingested fat, though numerous studies account that the composition of fatty acid of a fatty meal is not at all times exhibited in the fatty acid composition of CM triglycerides. For example, fatty acids with low and medium chain are often poor substrates for re-esterification into triglycerides in the enterocytes and hence are not markedly transported into CMs but are rather taken up by the portal vein to the liver [66].

The intestinal lymphatic absorption process can be briefly summarized as follows: It consists of successive events such as absorption of lipophilic dietary constituents. The drug molecules are uptaken by the enterocyte, get associated with core of CMs, and are transported into lymphatic capillaries. The critical and rate-determining step in this process is the association of lipophilic molecules with CMs to establish a magnitude of intestinal lymphatic absorption. The degree of association between drug and CMs mainly depends on affinity of lipidic com-

ponent toward the core of the CMs. The amount and nature of the lipids present in formulation influence the quantity and type of lipids in the CMs [68].

4.2 M Cell Pathway

Peyer's patches (PPs) comprise aggregated lymphoid follicles and are encircled by a specific epithelium, the follicle-associated epithelium (FAE). The FAE leads to formation of interface between the gut-associated lymphoid tissue (GALT) and the luminal [69]. Microfold (M) cells are present in the intestinal epithelium which cover mucosa-associated lymphoid tissues, for example, PPs of the small intestine. M cells are widely distributed in the small intestine, specifically the ileum. Generally, they are involved in transport of antigens to lymphoid follicles [70]. They also provide openings for various particles such as CMs and lipidic particles [71].

Morphologically, the M cells contain irregular brush border, reduced glycocalyx, and reduced microvilli. They are extremely specific for phagocytosis and transcytosis uptake of macromolecules, antigens, and pathogenic microorganisms [72]. After transcytosis, antigens exit into the intraepithelial pocket beneath the M cell basolateral membrane, which contains lymphocytes and mononuclear phagocytes (MNP). This specific microenvironment underneath the M cell permits effective transmission of luminal antigens to MNP [73].

The numerous properties like particle size, hydrophobicity, surface charge, and particle shape notably impact M cell uptake [74]. Nanoparticles lower than 1 μm undergo M cell uptake and are transported to basal medium, whereas particles greater than 5 μm remain entrapped in PPs. Different ranges of particle size are reported for uptake by transcytosis by M cells but the optimal size should be smaller than 1 μm and more exactly less than 200 nm [75]. Nanoparticles prepared with hydrophobic polymers (PLGA, PLA) are transported to greater extent by M cells as compared to hydrophilic polymers.

5 Approaches Used for Evaluation of Intestinal Lymphatic Uptake

Numerous models are established for investigation of lymphatic transport. *In vitro* models mimic the function of either CMs or M cells, whereas the *in vivo* models primarily target the assessment of drug transport by lymphatic system via lymphatic cannulation.

5.1 In Vitro Caco-2 Cell Model

Intestinal absorption is a complex process and basically still not understood properly. So, drug absorption is verified experimentally during drug development practice. In view of *in vitro* analysis, *in vivo* absorption process can be predicted which further may reduce the time and cost needed for clinical studies [76]. The Caco-2 cells are mainly extracted from human epithelial colorectal adenocarcinoma cells. It is chiefly incorporated for study of intestinal absorption of compounds. Caco-2 cell line comprises monolayer of differentiated villus cells resembling the small intestine which signifies a potential tool to study drug transport [77].

When Caco-2 cells are cultured on well plate as a monolayer, they undergo differentiation and lead to formation of tight junction among cells which is used as a model to determine transport. Additionally, Caco-2 cells also exhibit efflux and transporter proteins and phase II conjugation enzymes which can be used to assess transcellular pathways and metabolic transformation of compounds [78]. But Caco-2 cells lack cytochrome P450 isozymes (specifically CYP3A4) which are present in high proportion at the intestine. However, treatment of Caco-2 cells with vitamin D3 can be used to manifest high level of CYP3A4 [79].

For determination of transcellular pathway by lipid nanoparticles, transport experiments with specific endocytosis inhibitors are carried out. In this experiment, cells are first treated with the culture medium comprising specific inhibitor, and then transport experiment is carried out with

the test compounds. Cells treated with HBSS are taken as control. The inhibitors used are methyl- β -cyclodextrin for cholesterol depletion, filipin or nystatin for inhibition of caveola-mediated endocytosis, and chlorpromazine for inhibition of clathrin-mediated endocytosis [80].

5.2 Mesenteric Lymph Duct Cannulation

The mesenteric lymph instead of the thoracic duct is an ideal site of cannulation where lymph from the intestine and other parts of body is drained. It assembles lymph from the intestine, and collecting mesenteric lymph from animals thus allows the estimation of the transport of lipoproteins from the intestine. The lipoproteins can be quantified and characterized with the benefit that mesenteric lymph lipoproteins are in a nascent state since they have not been substantially altered by enzymes such as lipoprotein lipase [81–83].

5.3 Chylomicron Blocking Pathway

The *in vivo* lipid absorption is influenced by cycloheximide. Cycloheximide is an inhibitor of protein synthesis which hampers the synthesis of apolipoproteins, thus controlling the formation of CMs [84, 85]. This model is extensively used to analyze the lymphatic transport because of invasiveness and good relationship with mesenteric lymph cannulation method. Rats are intraperitoneally administered with cycloheximide, and after 1 h, the formulation is administered. Generally, reduction in AUC of amount of drug in blood is observed and compared with non-cycloheximide-treated animal group [86].

Pluronic L-81 is a lipophilic, non-ionic polymer comprising polyoxyethylene and polyoxypropylene. It reduces the formation of triglyceride in lymph either by the inhibiting formation of chylomicron, intracellular transport of chylomicron, or inhibiting transport of the triglyceride

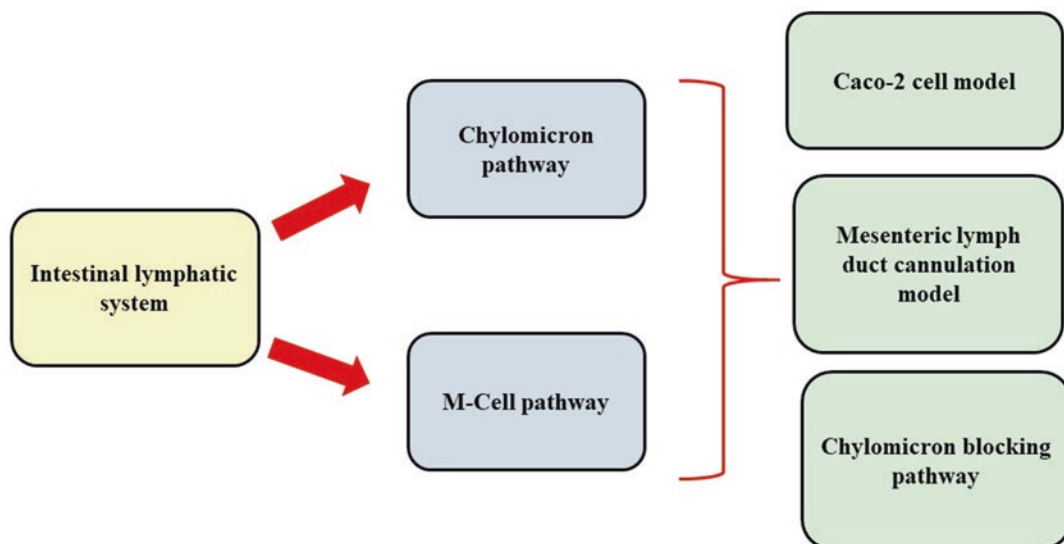


Fig. 21.2 BA enhancement by intestinal lymphatic system

into CMs. Hence, it can be utilized to analyze intestinal lymphatic transport of drugs [85].

Colchicine is an inhibitor of microtubular polymerization that decreases the capacity of enterocytes to transfer CMs by influencing movement of CMs from the Golgi body to basolateral membrane. Nevertheless, it is not chosen over pluronic and cycloheximide owing to its ability to cause lethargy and death in animals at 5 mg/kg dose. The low dose (2.5 mg/kg) is not enough to inhibit transportation of chylomicron [87].

The schematic representation of BA enhancement by intestinal lymphatic system, its mechanism, and models are depicted in Fig. 21.2.

6 Applications of Nanoparticles in Enhancing BA of Drugs Through ILS

Various lipid-based nanoparticles such as SMEDDS, SLNs, NLCs, and LPHNPs can raise the BA of poorly water-soluble drugs by ILS, and some are discussed below:

Liao et al. prepared SMEDDS of baicalein (BA) (BA-SMEDDS) and compared with conventional baicalein SMEDDS (C-SMEDDS).

The BA-SMEDDS and C-SMEDDS had droplet size 9.6 nm and 11.3 nm, respectively. The AUC was 1.31 times and Cmax was 1.87 times more with BA-SMEDDS as compared to C-SMEDDS. C-SMEDDS and BA-SMEDDS exhibited relative BA 342.5% and 448.7% in SD rats as compared to plain baicalein (BA). The lymphatic transport analysis using cycloheximide showed that 81.2% of BA was obtained in portal blood circulation, while about 18.8% was taken up by lymphatic transport. The lymphatic transport of C-SMEDDS and BA-SMEDDS was improved from 18.8% to 56.2% and 70.2%, respectively [88].

Patel et al. fabricated NLCs of nintedanib esylate (NE) to improve oral BA by lymphatic uptake. The NE-NLCs showed particle size 125.7 ± 5.5 nm, entrapment efficiency $88.5 \pm 2.5\%$, and zeta potential -17.3 ± 3.5 mV. The NE was in amorphous state after incorporation into NLCs. Tissue distribution study using intestinal tissue and uptake study by caco-2 cells displayed deep penetration of FITC-loaded NLCs. Cytotoxicity study across A549 exhibited NE-NLCs was effective in reducing viability of cells in contrast to NE suspension. The improved BA of NE (26.31 times) was observed by NE-NLCs. Intestinal lymphatic

uptake study in cycloheximide model showed involvement of ILS for boosting oral BA of NE [89].

Low solubility in water and substantial first-pass metabolism of genistein (GEN) limits its oral BA. Hence, SLNs were prepared and characterized, and *in vitro* chylomicron formation was evaluated by Obinu et al. The particle size of GEN-loaded SLNs (GEN-SLNs) was about 280 nm with more drug loading. Moreover, uptake of GEN-SLNs was mediated by Caco-2 cells. The particle size was increased indicating association between SLNs and the lipidic part of CMs. So, the results showed the ability of SLNs to augment oral BA of GEN by intestinal lymphatic transport [90].

Patel et al. prepared SLNs of asenapine maleate (AS) for improving oral BA. The AS-SLNs had particle size 114.3 nm, zeta potential -12.9 mV, and entrapment efficiency of 84.10%. The higher drug release of AS from AS-SLNs showed higher potential for lymphatic uptake. The uptake of AS-SLNs was found to be clathrin-caveola-mediated endocytosis across Caco-2 cells. Uptake of coumarin-6-loaded SLNs was high as that of plain dye. The pharmacokinetic profile in rats exhibited improved BA by AS-SLNs. The AUC was decreased in cycloheximide-treated rats showing contribution of ILS [86].

The oral BA of darunavir is 37% because of it being a substrate for cyp3A and P-gp. So Bhalekar et al. evaluated potential of darunavir-SLNs in increasing the drug BA by lymphatic transport. Endocytosis was involved in uptake of SLNs which was proved by endocytic inhibitors like chlorpromazine and nystatin. The AUC of SLN was high compared to that of marketed tablet. The AUC was decreased to 17.19 in the presence of cycloheximide, indicating involvement of lymphatic uptake in BA improvement [91].

As huperzine A (Hup-A) has low water solubility and oral BA, SMEDDS was developed by Li et al. The AUC value of Hup-A-loaded SMEDDS was markedly high than Hup-A suspension. More amount of Hup-A was observed in mesenteric lymph as compared to Hup-A suspension. The C_{max} and AUC were lowered with

Hup-A-loaded SMEDDS in chylomicron flow blocking model as that of control model. Around 40% and 5% lymphatic transport was observed with Hup-A-loaded SMEDDS and Hup-A suspension, respectively, indicating SMEDDS is able to boost the lymphatic uptake of Hup-A [92].

Jo et al. prepared a supersaturated SMEDDS (S-SMEDDS) and SMEDDS of saquinavir to boost its lymphatic transport and BA. The SMEDDS showed good emulsification ability and stability. The S-SMEDDS was prepared using hydroxypropyl methyl cellulose 2910 and SMEDDS. The concentration of drug in intestinal fluid (simulated) was high with S-SMEDDS as compared to SMEDDS. Moreover, the lymphatic transport in rats was considerably enhanced with S-SMEDDS as compared to SMEDDS [93].

Rifampicin (RF)-loaded LPHNPs (RF-LPHNPs) were prepared by Bachhav et al. to target Peyer's patches. RF-LPHNPs had mean particle size between 300 and 400 nm and drug loading higher than 12%. Complete amorphization was proved with DSC and XRD studies. High hydrophobicity and low mucoadhesion was observed with RF-LPHNPs in contrast to RF-Gantrez nanoparticles (RF-GNP). After intraduodenal administration of coumarin-loaded LPHNPs and GNP in rats showed more accumulation of RF-GzNP at the border of villi and more uptake of RF-LPHNPs by PPs. Moreover, in the liver, less accumulation of RF-LPHNPs as that of RF-GNP indicated circumvent of the portal circulation. RF-LPHNPs showed high lung: plasma concentration ratio as compared to RF-GNP which has proved the potential of LPHNPs in the therapy of disease like tuberculosis [94].

Zeng et al. prepared and evaluated LPHNPs of tilianin (TIL) (TIL-LPHNPs). The particle size, entrapment efficiency, and zeta potential of TIL-LPHNPs was 54.6 ± 5.3 nm, $86.6 \pm 3.6\%$, and -33.4 ± 4.7 mV respectively. The AUC of TIL-LPHNPs was significantly enhanced as compared to TIL solution [95].

The NLCs of olmesartan medoxomil (OLM) for oral BA enhancement was prepared by Kaithwas et al. The OLM-NLCs exhibited

decreased crystallinity of the drug. The uptake of OLM-NLCs across Caco-2 cells displayed higher uptake (5.2-folds) as that of free drug. The AUC_{total} and C_{max} of OLM-NLCs were effectively high in contrast to free drug [96].

7 Conclusions

Nanotechnology has a considerable capacity to ameliorate the oral BA and efficacy of drugs. Among different nanocarriers, lipid-based formulations are enormously used in the drug delivery attributed to their intrinsic property to boost the BA of lipophilic drugs: (i) Though diverse routes of drug administration exist which can effectively avoid the liver, the oral route is of utmost suitable and safe for patients. (ii) ILS augments the oral BA of molecules suffering from extensive first-pass metabolism in the liver. Hence, BA augmentation with ILS approach is extremely preferred for oral route of administration of lipophilic drugs. Lipid-based drug delivery can be effectively used to ameliorate absorption of lipophilic molecules by ILS. Hence, lipid-based nanoparticles can be helpful in successful development of product for oral administration.

References

- Kuentz M, Imanidis G. In silico prediction of the solubility advantage for amorphous drugs—are there property-based rules for drug discovery and early pharmaceutical development? *Eur J Pharm Sci.* 2013;48(3):554–62.
- O'Driscoll CM, Griffin BT. Biopharmaceutical challenges associated with drugs with low aqueous solubility—the potential impact of lipid-based formulations. *Adv Drug Deliv Rev.* 2008;60(6):617–24.
- Pouton CW. Formulation of poorly water-soluble drugs for oral administration: physicochemical and physiological issues and the lipid formulation classification system. *Eur J Pharm Sci.* 2006;29(3–4):278–87.
- Patel M, Joshi G, Sawant KK. Nanotechnology in oral drug delivery: salient aspects, state of art, and applications. In: Thangadurai D, Sangeetha J, Prasad R, editors. *Functional bionanomaterials. Nanotechnology in the life sciences.* Cham: Springer; 2020. p. 165–84.
- Chakraborty S, Shukla D, Mishra B, Singh S. Lipid—an emerging platform for oral delivery of drugs with poor bioavailability. *Eur J Pharm Biopharm.* 2009;73(1):1–15.
- Porter CJ, Trevaskis NL, Charman WN. Lipids and lipid-based formulations: optimizing the oral delivery of lipophilic drugs. *Nat Rev Drug Discov.* 2007;6(3):231–48.
- Trevaskis NL, Charman WN, Porter CJ. Lipid-based delivery systems and intestinal lymphatic drug transport: a mechanistic update. *Adv Drug Deliv Rev.* 2008;60(6):702–16.
- Kalepu S, Manthina M, Padavala V. Oral lipid-based drug delivery systems—an overview. *Acta Pharm Sin B.* 2013;3(6):361–72.
- Ahn H, Park JH. Liposomal delivery systems for intestinal lymphatic drug transport. *Biomater Res.* 2016;20:36.
- Mundada V, Patel M, Sawant K. Submicron emulsions and their applications in oral delivery. *Crit Rev Ther Drug Carrier Syst.* 2016;33(3):265–308.
- Welshman IR, Sisson TA, Jungbluth GL, Stalker DJ, Hopkins NK. Linezolid absolute bioavailability and the effect of food on oral bioavailability. *Biopharm Drug Dispos.* 2001;22(3):91–7.
- Shrestha H, Bala R, Arora S. Lipid-based drug delivery systems. *J Pharm (Cairo).* 2014;2014:801820.
- Rein MJ, Renouf M, Cruz-Hernandez C, Actis-Goretta L, Thakkar SK, da Silva Pinto M. Bioavailability of bioactive food compounds: a challenging journey to bioefficacy. *Br J Clin Pharmacol.* 2013;75(3):588–602.
- Rahman MA, Harwansh R, Mirza MA, Hussain S, Hussain A. Oral lipid based drug delivery system (LBDDS): formulation, characterization and application: a review. *Curr Drug Deliv.* 2011;8(4):330–45.
- Gershkovich P, Hoffman A. Effect of a high-fat meal on absorption and disposition of lipophilic compounds: the importance of degree of association with triglyceride-rich lipoproteins. *Eur J Pharm Sci.* 2007;32(1):24–32.
- Gursoy RN, Benita S. Self-emulsifying drug delivery systems (SEDDS) for improved oral delivery of lipophilic drugs. *Biomed Pharmacother.* 2004;58(3):173–82.
- Rashid M, Malik MY, Singh SK, Chaturvedi S, Gayen JR, Wahajuddin M. Bioavailability enhancement of poorly soluble drugs: the holy grail in pharma industry. *Curr Pharm Des.* 2019;25(9):987–1020.
- Horter D, Dressman JB. Influence of physicochemical properties on dissolution of drugs in the gastrointestinal tract. *Adv Drug Deliv Rev.* 2001;46(1–3):75–87.
- Sunesen VH, Vedelsdal R, Kristensen HG, Christrup L, Müllertz A. Effect of liquid volume and food intake on the absolute bioavailability of danazol, a poorly soluble drug. *Eur J Pharm Sci.* 2005;24(4):297–303.
- Sharma M, Sharma R, Jain DK. Nanotechnology based approaches for enhancing oral bioavailability of poorly water soluble antihypertensive drugs. *Scientifica (Cairo).* 2016;2016:8525679.
- Patel P, Patel M. Nanostructured lipid carriers: a versatile carrier for oral delivery of lipophilic drugs. *Recent Pat Nanotechnol.* 2021;15:154–64.

22. Koo OM, Rubinstein I, Onyukel H. Role of nanotechnology in targeted drug delivery and imaging: a concise review. *Nanomedicine*. 2005;1:193–212.
23. Mishra B, Patel BB, Tiwari S. Colloidal nanocarriers: a review on formulation technology, types and applications toward targeted drug delivery. *Nanomed Nanotech Biol Med*. 2010;6:9–24.
24. Caruthers SD, Wickline SA, Lanza GM. Nanotechnological applications in medicine. *Curr Opin Biotechnol*. 2007;18:26–30.
25. Agrawal U, Sharma R, Gupta M, Vyas SP. Is nanotechnology a boon for oral drug delivery? *Drug Discov Today*. 2014;19(10):1530–46.
26. Williams HD, Ford L, Igonin A, et al. Unlocking the full potential of lipid-based formulations using lipophilic salt/ionic liquid forms. *Adv Drug Deliv Rev*. 2019;142:75–90.
27. Savla R, Browne J, Plassat V, Wasan KM, Wasan EK. Review and analysis of FDA approved drugs using lipid-based formulations. *Drug Dev Ind Pharm*. 2017;43(11):1743–58.
28. Feeney OM, Crum MF, McEvoy CL, et al. 50 years of oral lipid-based formulations: provenance, progress and future perspectives. *Adv Drug Deliv Rev*. 2016;101:167–94.
29. Dahan A, Hoffman A. Rationalizing the selection of oral lipid based drug delivery systems by an in vitro dynamic lipolysis model for improved oral bioavailability of poorly water soluble drugs. *J Control Release*. 2008;129(1):1–10.
30. Mullertz A, Ogbonna A, Ren S, Rades T. New perspectives on lipid and surfactant based drug delivery systems for oral delivery of poorly soluble drugs. *J Pharm Pharmacol*. 2010;62(11):1622–36.
31. Veber DF, Johnson SR, Cheng HY, Smith BR, Ward KW, Kopple KD. Molecular properties that influence the oral bioavailability of drug candidates. *J Med Chem*. 2002;45:2615–23.
32. Mu H, Holm R, Mullertz A. Lipid-based formulations for oral administration of poorly water-soluble drugs. *Int J Pharm*. 2013;453:215–24.
33. Porter CJ, Pouton CW, Cuine JF, Charman WN. Enhancing intestinal drug solubilisation using lipid-based delivery systems. *Adv Drug Deliv Rev*. 2008;60(6):673–91.
34. Rane SS, Anderson BD. What determines drug solubility in lipid vehicles: is it predictable? *Adv Drug Deliv Rev*. 2008;60:638–56.
35. Hauss DJ. Oral lipid-based formulations. *Adv Drug Deliv Rev*. 2007;59:667–76.
36. Jannin V, Musakhanian J, Marchaud D. Approaches for the development of solid and semi-solid lipid-based formulations. *Adv Drug Deliv Rev*. 2008;60:734–46.
37. Souto EB, Muller RH. Lipid nanoparticles: effect on bioavailability and pharmacokinetic changes. *Handb Exp Pharmacol*. 2010;197:115–41.
38. Kim H, Seong I, Ro J, Hwang SH, Yun G, Lee J. Enhanced association of probucol with chylomicron by pharmaceutical excipients: an in vitro study. *Drug Dev Ind Pharm*. 2015;41(7):1073–9.
39. Patel MH, Sawant KK. Self microemulsifying drug delivery system of lurasidone hydrochloride for enhanced oral bioavailability by lymphatic targeting: in vitro, Caco-2 cell line and in vivo evaluation. *Eur J Pharm Sci*. 2019;138:105027.
40. O'Driscoll CM. Lipid-based formulations for intestinal lymphatic delivery. *Eur J Pharm Sci*. 2002;15(5):405–15.
41. Reddy LHV, Murthy RSR. Lymphatic transport of orally administered drugs. *Indian J Exp Biol*. 2002;40:1097–109.
42. Khan AA, Mudassir J, Mohtar N, Darwis Y. Advanced drug delivery to the lymphatic system: lipid-based nanoformulations. *Int J Nanomedicine*. 2013;8:2733–44.
43. Wasan KM. Formulation and physiological and biopharmaceutical issues in the development of oral lipid-based drug delivery systems. *Drug Dev Ind Pharm*. 2001;27(4):267–76.
44. Sek L, Porter CJ, Kaukonen AM, Charman WN. Evaluation of the in-vitro digestion profiles of long and medium chain glycerides and the phase behaviour of their lipolytic products. *J Pharm Pharmacol*. 2002;54(1):29–41.
45. Caliph SM, Charman WN, Porter CJ. Effect of short-, medium-, and long-chain fatty acid-based vehicles on the absolute oral bioavailability and intestinal lymphatic transport of halofantrine and assessment of mass balance in lymph-cannulated and non-cannulated rats. *J Pharm Sci*. 2000;89(8):1073–84.
46. Constantinides PP, Wasan KM. Lipid formulation strategies for enhancing intestinal transport and absorption of P-glycoprotein (P-gp) substrate drugs: in vitro/in vivo case studies. *J Pharm Sci*. 2007;96(2):235–48.
47. Aungst BJ. Absorption enhancers: applications and advances. *AAPS J*. 2012;14:10–8.
48. Akhtar N, Ahad A, Khar RK, et al. The emerging role of P-glycoprotein inhibitors in drug delivery: a patent review. *Expert Opin Ther Pat*. 2011;21:561–76.
49. Yanez JA, Wang SW, Knemeyer IW, Wirth MA, Alton KB. Intestinal lymphatic transport for drug delivery. *Adv Drug Deliv Rev*. 2011;63(10–11):923–42.
50. Brocks DR, Davies NM. Lymphatic drug absorption via the enterocytes: pharmacokinetic simulation, modeling, and considerations for optimal drug development. *J Pharm Pharm Sci*. 2018;21(1s):254s–70s.
51. Chaudhary S, Garg T, Murthy RS, Rath G, Goyal AK. Recent approaches of lipid-based delivery system for lymphatic targeting via oral route. *J Drug Target*. 2014;22(10):871–82.
52. Cifarelli V, Eichmann A. The intestinal lymphatic system: functions and metabolic implications. *Cell Mol Gastroenterol Hepatol*. 2019;7(3):503–13.
53. Gershkovich P, Hoffman A. Uptake of lipophilic drugs by plasma derived isolated chylomicrons: linear correlation with intestinal lymphatic bioavailability. *Eur J Pharm Sci*. 2005;26(5):394–404.
54. Nordskog BK, Phan CT, Nutting DF, Tso P. An examination of the factors affecting intestinal lymphatic

- transport of dietary lipids. *Adv Drug Deliv Rev.* 2001;50(1–2):21–44.
55. Ali Khan A, Mudassir J, Mohtar N, Darwis Y. Advanced drug delivery to the lymphatic system: lipid-based nanoformulations. *Int J Nanomedicine.* 2013;8:2733–44.
 56. Nankervis R, Davis SS, Day NH, Shaw PN. Intestinal lymphatic transport of three retinoids in the rat after oral administration: effect of lipophilicity and lipid vehicle. *Int J Pharm.* 1996;130:57–64.
 57. Lu Y, Qiu Y, Qi J, Feng M, Ju D, Wu W. Biomimetic reassembled chylomicrons as novel association model for the prediction of lymphatic transportation of highly lipophilic drugs via the oral route. *Int J Pharm.* 2015;483(1–2):69–76.
 58. Feitosa RC, Geraldes DC, Beraldo-de-Araújo VL, Costa JSR, Oliveira-Nascimento L. Pharmacokinetic aspects of nanoparticle-in-matrix drug delivery systems for oral/buccal delivery. *Front Pharmacol.* 2019;10:1057.
 59. Das S, Chaudhury A. Recent advances in lipid nanoparticle formulations with solid matrix for oral drug delivery. *AAPS PharmSciTech.* 2011;12(1):62–76.
 60. Onoue S, Yamada S, Chan HK. Nanodrugs: pharmacokinetics and safety. *Int J Nanomedicine.* 2014;9:1025–37.
 61. Lin CH, Chen CH, Lin ZC, Fang JY. Recent advances in oral delivery of drugs and bioactive natural products using solid lipid nanoparticles as the carriers. *J Food Drug Anal.* 2017;25(2):219–34.
 62. Trevaskis NL, Lee G, Escott A, et al. Intestinal lymph flow, and lipid and drug transport scale allometrically from pre-clinical species to humans. *Front Physiol.* 2020;11:458.
 63. Trevaskis NL, Porter CJ, Charman WN. The lymph lipid precursor pool is a key determinant of intestinal lymphatic drug transport. *J Pharmacol Exp Ther.* 2006;316(2):881–91.
 64. Patel MH. Formulation, optimization and evaluation of lipid based nanoformulations for improving oral bioavailability of some drugs. ProQuest Publishing; 2018. p. 10–20.
 65. Julve J, Martín-Campos JM, Escola-Gil JC, Blanco-Vaca F. Chylomicrons: advances in biology, pathology, laboratory testing, and therapeutics. *Clin Chim Acta.* 2016;455:134–48.
 66. Hussain MM. Intestinal lipid absorption and lipoprotein formation. *Curr Opin Lipidol.* 2014;25(3):200–6.
 67. Feingold KR, Anawalt B, Boyce A, et al. Introduction to lipids and lipoproteins. South Dartmouth: MDText.com, Inc.; 2000; 2021.
 68. Lawless E, Griffin BT, O'Mahony A, O'Driscoll CM. Exploring the impact of drug properties on the extent of intestinal lymphatic transport – in vitro and in vivo studies. *Pharm Res.* 2015;32(5):1817–29.
 69. Jung C, Hugot JP, Barreau F. Peyer's patches: the immune sensors of the intestine. *Int J Inflam.* 2010;2010:823710.
 70. Kobayashi N, Takahashi D, Takano S, Kimura S, Hase K. The roles of Peyer's patches and microfold cells in the gut immune system: relevance to autoimmune diseases. *Front Immunol.* 2019;10:2345.
 71. Li X, Yu M, Fan W, Gan Y, Hovgaard L, Yang M. Orally active-targeted drug delivery systems for proteins and peptides. *Expert Opin Drug Deliv.* 2014;11(9):1435–47.
 72. Mabbott NA, Donaldson DS, Ohno H, Williams IR, Mahajan A. Microfold (M) cells: important immunosurveillance posts in the intestinal epithelium. *Mucosal Immunol.* 2013;6(4):666–77.
 73. Shakweh M, Besnard M, Nicolas V, Fattal E. Poly (lactide-co-glycolide) particles of different physicochemical properties and their uptake by Peyer's patches in mice. *Eur J Pharm Biopharm.* 2005;61(1–2):1–13.
 74. Gullberg E, Leonard M, Karlsson J, et al. Expression of specific markers and particle transport in a new human intestinal M-cell model. *Biochem Biophys Res Commun.* 2000;279:808–13.
 75. Managuli RS, Raut SY, Reddy MS, Mutalik S. Targeting the intestinal lymphatic system: a versatile path for enhanced oral bioavailability of drugs. *Expert Opin Drug Deliv.* 2018;15(8):787–804.
 76. van Breemen RB, Li Y. Caco-2 cell permeability assays to measure drug absorption. *Expert Opin Drug Metab Toxicol.* 2005;1(2):175–85.
 77. Gamboa JM, Leong KW. In vitro and in vivo models for the study of oral delivery of nanoparticles. *Adv Drug Deliv Rev.* 2013;65(6):800–10.
 78. Hubatsch I, Ragnarsson EGE, Artursson P. Determination of drug permeability and prediction of drug absorption in Caco-2 monolayers. *Nat Protoc.* 2007;2(9):2111–9.
 79. Angelis ID, Turco L. Caco-2 cells as a model for intestinal absorption. *Curr Protoc Toxicol.* 2011:1–15. <https://doi.org/10.1002/0471140856.tx2006s47>.
 80. Roger E, Lagarce F, Garcion E, Benoit JP. Lipid nanocarriers improve paclitaxel transport throughout human intestinal epithelial cells by using vesicle-mediated transcytosis. *J Control Release.* 2009;140(2):174–81.
 81. Boyd M, Risovic V, Jull P, Choo E, Wasan KM. A stepwise surgical procedure to investigate the lymphatic transport of lipid-based oral drug formulations: cannulation of the mesenteric and thoracic lymph ducts within the rat. *J Pharmacol Toxicol Methods.* 2004;49(2):115–20.
 82. Trevaskis NL, Hu L, Caliph SM, Han S, Porter CJ. The mesenteric lymph duct cannulated rat model: application to the assessment of intestinal lymphatic drug transport. *J Vis Exp.* 2015;97:52389.
 83. Banan B, Wei Y, Simo O, et al. Intestinal lymph collection via cannulation of the mesenteric lymphatic duct in mice. *J Surg Res.* 2021;260:399–408.
 84. Edwards GA, Porter CJ, Caliph SM, Khoo SM, Charman WN. Animal models for the study of intestinal lymphatic drug transport. *Adv Drug Deliv Rev.* 2001;50(1–2):45–60.
 85. Ghoshal S, Witta J, Zhong J, de Villiers W, Eckhardt E. Chylomicrons promote intestinal absorption of lipopolysaccharides. *J Lipid Res.* 2009;50:90–7.

86. Patel M, Mundada V, Sawant K. Enhanced intestinal absorption of asenapine maleate by fabricating solid lipid nanoparticles using TPGS: elucidation of transport mechanism, permeability across Caco-2 cell line and in vivo pharmacokinetic studies. *Artif Cells Nanomed Biotechnol.* 2019;47(1):144–53.
87. Dahan A, Hoffman A. Evaluation of a chylomicron flow blocking approach to investigate the intestinal lymphatic transport of lipophilic drugs. *Eur J Pharm Sci.* 2005;24:381–8.
88. Liao H, Gao Y, Lian C, et al. Oral absorption and lymphatic transport of baicalein following drug-phospholipid complex incorporation in self-microemulsifying drug delivery systems. *Int J Nanomedicine.* 2019;14:7291–306.
89. Patel P, Patel M. Enhanced oral bioavailability of nintedanib esylate with nanostructured lipid carriers by lymphatic targeting: in vitro, cell line and in vivo evaluation. *Eur J Pharm Sci.* 2021;159:105715.
90. Obinu A, Burrai GP, Cavalli R, et al. Transmucosal solid lipid nanoparticles to improve genistein absorption via intestinal lymphatic transport. *Pharmaceutics.* 2021;13(2):267.
91. Bhalekar MR, Upadhaya PG, Madgulkar AR, Kshirsagar SJ, Dube A, Bartakke US. In-vivo bioavailability and lymphatic uptake evaluation of lipid nanoparticulates of darunavir. *Drug Deliv.* 2016;23(7):2581–6.
92. Li F, Hu R, Wang B, et al. Self-microemulsifying drug delivery system for improving the bioavailability of huperzine A by lymphatic uptake. *Acta Pharm Sin B.* 2017;7(3):353–60.
93. Jo K, Kim H, Khadka P, et al. Enhanced intestinal lymphatic absorption of saquinavir through supersaturated self-microemulsifying drug delivery systems. *Asian J Pharm Sci.* 2020;15(3):336–46.
94. Bachhav SS, Dighe VD, Kotak D, Devarajan PV. Rifampicin lipid-polymer hybrid nanoparticles (LIPOMER) for enhanced Peyer's patch uptake. *Int J Pharm.* 2017;532(1):612–22.
95. Zeng C, Zheng R, Yang X, Du Y, Xing J, Lan W. Improved oral delivery of tilianin through lipid-polymer hybrid nanoparticles to enhance bioavailability. *Biochem Biophys Res Commun.* 2019;519(2):316–22.
96. Kaithwas V, Dora CP, Kushwah V, Jain S. Nanostructured lipid carriers of olmesartan medoxomil with enhanced oral bioavailability. *Colloids Surf B Biointerfaces.* 2017;154:10–20.



Nanoparticle Pharmacokinetic Profiling In Vivo Using Magnetic Resonance Imaging

Bhupendra G. Prajapati, Himanshu Paliwal,
and Jayvadan K. Patel

Contents

1	Introduction	400
2	Theory and Principles of MRI	401
3	Drug Release Monitoring Using MRI	401
4	Contrasting Agents for Monitoring the Drug Release	402
5	Pharmacokinetic Profiling Using MRI	406
6	Biodistribution Studies Using MRI	409
	References	413

Abstract

The rapid progression in the field of nanotechnology has given rise to production of nanoparticles for in vivo imaging and targeted delivery. A number of novel nanoparticles may suffer from inadequate activity due to unwanted tissue localization or inappropriate

low half-lives. Pharmacokinetic profiling can assist in deriving ideas about the size of the particle, surface coating, associated moieties, etc. which can aid in resolving the undesirable outcomes. The utilization of imaging techniques such as magnetic resonance imaging (MRI) may play vital role in studying the pharmacokinetics and biodistribution of drugs or drug carriers for the treatment of several diseases. Along with the generation of anatomical images, MRI can also serve to target and quantify the radioactive or optical probe labelled nanocarriers for delivery of theranostics. The in vivo studies using MR-active nanoparticles will help in deciphering the behaviour of the synthesized nanoparticles inside the body to understand their distribution and elimination. This chapter will comprehensively focus on recent and relevant literatures and their useful outcomes with

The original version of this chapter was revised.
The correction to this chapter is available at
https://doi.org/10.1007/978-3-030-83395-4_23

B. G. Prajapati (✉) · H. Paliwal
Shree S.K. Patel College of Pharmaceutical
Education and Research, Ganpat University,
Mahesana, Gujarat, India

J. K. Patel
Nootan Pharmacy College, Faculty of Pharmacy,
Sankalchand Patel University, Visnagar, Gujarat,
India

regard to drug release studies, pharmacokinetics studies, or biodistribution studies by using MRI contrast agents.

Keywords

Magnetic resonance imaging ·
Pharmacokinetics · Nanoparticles ·
Biodistribution · Contrast agents ·
Theranostics · Nanocarriers · Elimination · In
vivo studies · Targeted delivery

1 Introduction

The discovery of novel agents with therapeutic potential requires efficient strategies for tracing delivery and disposition of drug. The pharmacokinetic studies are also vital for obtaining approval from regulatory agencies and to establish dose/effect relationship [1]. The localization of the agents at the specific site is speculated to be primarily induced by concentration gradients in the blood, interstitial fluid, or target tissue. With the advent of some novel delivery strategies, offering high loading capacity and targeting of nanoparticle-based drug/gene carrier system may provide solution to the challenges pertaining to the conventional approaches [2].

In case of such targeted carriers, the analysis of blood and tissue concentrations may not furnish the precise representation of *in vivo* pharmacokinetics and pharmacodynamics because drug release may be altered due to binding properties. Therefore, there is the need of novel approaches for characterizing the pharmacokinetics and pharmacodynamics of these carriers that can also justify the binding and delivery pattern. It is obvious that such approaches will involve more intricacies as compared to the modelling techniques used for conventional formulations [3].

The pharmacokinetic monitoring of nanoparticles is also important as various nanoparticle systems are considered to offer potential for treatment and diagnosis [4–6]. Nanoparticles may be incorporating drug into a core or dispersed into polymer matrix, which allows

designing of such systems to possess desired particle size, particle shape, surface charge, and surface chemistry. They alter delivery characteristics and pharmacological presentation of drugs incorporated in the nanoparticle [7]. Generally, the nanoparticles exhibit very slow and restricted renal clearance, and their circulation may further be extended, for, e.g. PEGylated nanoparticle of doxorubicin for tumour targeting. Owing to ambiguity in their modified disposition, new toxicity problems may be triggered. Therefore, it is prudent to track the drug disposition from nanoparticles to delineate the drug exposure-response relationship for estimating efficacy and safety [8, 9].

Magnetic resonance imaging (MRI) is a dynamic imaging tool that can obtain the images of the inner depth images of the living body or any solid material. It generates images with high temporal and spatial resolution; therefore, it is a potential alternative for characterizing the distribution and localization of delivery systems at specific site [10–12]. However, the use of MRI for studying drug delivery systems has been minimal as compared to its utilization in clinical settings. It can provide a medium to investigate the pattern of *in vitro* drug release from the dosage forms to get better idea around the pharmaceutical processes used in preparation of pharmaceutical systems. They also allow examination of *in vivo* behaviour of these delivery systems in the body. The penetration of biological solvents in the solid dosage forms is critical to their *in vivo* performance which can be studied with the help of MRI for contemplation of internal events related to these systems [13]. Even though the number of reports that focussed on *in vivo* behaviour of the dosage form has been less, there is no denying of its potential to serve as primary tool for studying pharmacokinetic behaviour of conventional as well as novel nanocarrier systems. Some of the literature which involved evaluation of dosage forms in animals and humans have demonstrated that MRI can be used to predict the release, distribution, and physiological response to the drug delivery systems ranging from conventional oral formulations to nano-based targeting carrier devices [14, 15].

The application of magnetic resonance imaging of guiding drug delivery systems has appeared as a suitable method for improving targeting of delivery vehicles at particular site. With regard to drug delivery potential, imaging may serve to locate the target region or to plan, monitor, and examine the outcomes of the therapy. Furthermore, MRI is suitable for targeted delivery of nanoparticles as it allows obtaining the images and quantitative estimation during therapy. However, it can be considered as an alternative to other image-guided drug delivery strategies, but it can also be used in conjunction to enhance invasiveness of other techniques. The use of X-ray, fluorescence imaging, etc. can be used along with MRI which enables concurrent interventional procedures to take in place controlled clinical surrounding [16, 17].

2 Theory and Principles of MRI

Nuclear magnetic resonance was reported for the first time by Bloch and Purcell (1946) [18]. Since its discovery, this technique has been advancing significantly to find its place in clinical studies [19]. Magnetic resonance imaging is a non-invasive technique which uses the nuclear magnetic resonance (NMR) signal to develop magnetic resonance (MR) images. The NMR signals are produced when certain nuclei such as hydrogen nucleus (^1H), fluorine nucleus (^{19}F), phosphorus nuclei (^{31}P), etc. are exposed to strong magnetic field and radio waves. These nuclei, owing to their magnetic moment, align themselves according to the applied field to attain equilibrium. When this equilibrium is deranged, the weak magnetization develops due to changes in orientation of the aligned nuclei. A small voltage is generated by the electromagnetic induction, and this voltage is responsible for producing NMR signals [20, 21].

The magnetization is dependent upon the applied magnetic field and magnetic moment of nuclei. However, the NMR signals are inherently weaker in nature, but its strength can be intensified by altering magnetic field or by using different nuclei. In order to generate the strong magnetic field, a cylindrical bore superconduct-

ing magnetic is usually employed [22]. MRI involves translation of difference in magnetic field into NMR signal to divulge spatial information. The frequency of NMR signals for magnetic field fluctuations according to the space is primarily governed by its position [23].

Advantages of Employing MRI for Pharmacokinetic Studies

1. MRI is a non-invasive imaging technique which allows quantitative estimation of pharmacokinetic and biodistribution of drug carriers to support production of novel therapeutic and diagnostic agents [24].
2. The potential of target delineation may aid in better dose optimization for novel nanoparticle-based drug delivery carriers [25].
3. This imaging technique not only allows patient monitoring for advancing diseases but even more critical to identify disease-modifying elements with regard to the existing therapeutic treatment [26, 27].
4. Apart from its non-invasiveness, MRI is a relatively cost-efficient and time-saving technique as compared to other imaging techniques [28].
5. Further, MRI can be modified or improved to serve optimally for specific disease condition for delivery of specific therapeutic product. For example, an early-stage intervention and targeted delivery is at the utmost priority for the treatment of cancer patients [29].

3 Drug Release Monitoring Using MRI

Owing to its potential in clinical field, it has emerged as impressive tool for studying the release characteristics, distribution, and localization of drug at particular site from delivery systems. MRI allows production of tissue level depth images with high temporal as well as spatial resolutions [10, 12]. The magnetic capabilities can be explored by using MRI contrast agents, such as gadolinium (Gd^{3+}), manganese (Mn^{2+}), iron (Fe^{3+}), etc. in order to enhance the

sensitivity and resolution of images [30, 31]. The contrasting agents may show paramagnetic behaviour due to the presence of unpaired pair of electrons, for example, gadolinium(III), dysprosium(III), etc. or may exhibit superparamagnetic characteristics comprising transitioning metal ions, for example, iron(III) oxides, etc. [30, 32, 33]. They may be inherent to the nanoparticles, chelated on the nanoparticle surface, or fused as a doping agent with matrix [34]. Figure 22.1 illustrates different classes of MRI contrasting agents.

The functioning of contrasting agent requires availability of free diffusible water molecules, hence producing distinct signals when drug molecule is attached to the surface as compared to when drug molecule is incorporated within nanocarrier [35]. In the recent past, a number of contrasting agents linked to a nanoparticulate system were formulated for monitoring pharmacokinetic parameters using MRI. Further, there are specially designed stimuli-responsive nanosystems wherein MR signals were concealed by complexation or coating. In the presence of stimulating factors, like pH, temperature, light, etc., paramagnetic ions are discharged to produce deviations in MR signals. Such techniques and others may be efficient in studying the pharmacokinetic parameters [36].

4 Contrasting Agents for Monitoring the Drug Release

4.1 Gd-Based Contrasting Agent

Gadolinium is one of the lanthanide elements consisting of seven unpaired electrons which are responsible for intense relaxation and paramagnetic behaviour. It is designed as a contrasting agent to be used for magnetic resonance imaging, positron imaging tomography, microwave applications, etc. [38, 39]. The MR images are enhanced as they reduce the T1 relaxation time of targeted tissues where Gd nanoparticles are localized. Gd containing complexes impedes the longitudinal relaxation time of protons present in water environment to generate a vivid contrast [40, 41]. The underlying mechanism is when Gd is exposed momentarily, the rate of relaxation pertaining to the solvent will be elevated. This rise is contributed as a result of proton dipole-dipole interactions and applied varying magnetic field. Several factors can affect the relaxation rate of the Gd nanoparticle such as direct interaction of the Gd ion with solvent molecules, diffusion of solvent molecules, hydration number of solvent (water), reorientation time, etc. [42]. Despite great potential of Gd-based product, their

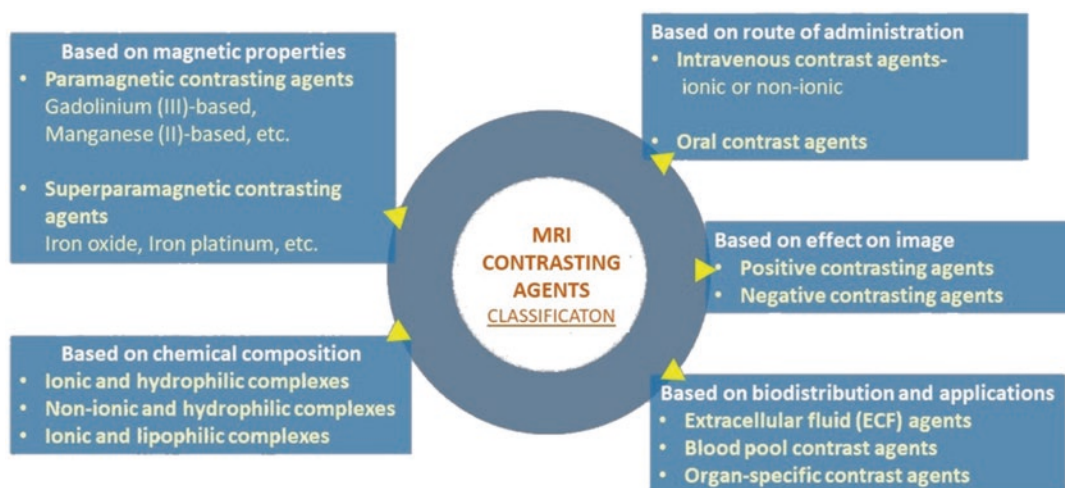


Fig. 22.1 MRI contrasting agents classified on the basis of magnetic properties, chemical composition, route of administration, effect on image, and biodistribution and applications [37]

conventional formulations show poor tissue labelling and targeting. The efforts have been made to improve localization and sensitivity of the contrasting agents by incorporating them into nanocarriers.

One such effort included the preparation of gadolinium-containing nanoparticles where drug and contrasting agents were delivered together by using nanocarriers. Gallic acid was used as a therapeutic agent and developed into formulation of gold nanoparticles to allow MR imaging. $\text{Gd}(\text{NO}_3)_3$ was utilized as a diagnostic agent and evaluated using high-resolution transmission electron microscopy, X-ray diffraction, and inductively coupled plasma atomic emission spectrometry. The outcomes of release studies showed that around 70% of gallic acid is released up to 72 h from the nanoparticles. In vitro release of gallic acid was more at pH of cancerous cells (pH = 4.8) which indicates better release control of such systems to deliver the drug into cancer cells and avoiding unintended release in systemic circulation. Furthermore, it was confirmed that nanoparticle displayed effective cytotoxic action over HepG2 cells (cancer cells) and insignificant cytotoxicity to the 3T3 cells (normal cells). The MR imaging of the prepared nanocomposite showed enhanced MRI contrast in comparison with plain $\text{Gd}(\text{NO}_3)_3$ [43].

The researchers have attempted for developing the activatable imaging nanosystems to augment MR signal for diagnosis of tumour as well as examining the treatment. It was claimed that highly effective activatable nanocarriers have been prepared with enhanced MR imaging and safer than conventional counterparts. The pH-responsive nanocarrier was prepared containing doxorubicin as a drug and gadolinium metallofullerene as contrast agent. This preparation showed better contrasting characteristics due to high relaxation effect and averting premature release of Gd ion. To analyse their drug release characteristics, the nanocarrier preparations were dialysed in HEPES (4-(2-hydroxyethyl)-1-piperazineethanesulfonic acid) buffer and MES (2-(N-morpholino) ethanesulfonic acid) buffer. The MRI indicated that nanoparticles showed that at physiological pH, decreased relaxation

rate and therefore rate of drug release was also low. Contrarily, the drug release rate was significantly higher in acidic environment. There is exceptional synchronization between the relaxation rate and drug release rate which indicates the suitability of such nanocarrier for monitoring the drug release. The pH-dependent cellular uptake was observed in HeLa cells which was analysed using confocal laser scanning microscopy and flow cytometry analysis. It was indicated that high fluorescence intensity of doxorubicin was estimated at pH 6.6 in the nucleus in comparison with that at pH 7.4. It was evident that the doxorubicin molecules are released and penetrated readily at pH 6.6 [44].

Xu et al. developed layered nanocomposites of three drugs, viz. diclofenac, ibuprofen, and naproxen. Their intercalation was performed using three different techniques: co-precipitation, ion exchange, and exfoliation-self-assembly for each drug. The characterization performed using X-ray diffraction study, elemental microanalysis, and IR spectroscopy revealed that the active molecules were efficiently integrated into the inter-layer spaces. However, the drug loading capacity was significantly better for products made out of co-precipitation method as compared to the other methods. The comparatively faster release of drug was shown by naproxen-loaded composites at pH 7.4 as about 80% release was observed after completion of 1 h, while in the case of nanocomposites loaded with diclofenac and ibuprofen, sustained drug release was noticed for about 4 h and 24 h, respectively. The composites also showed biocompatibility and effective relaxation characteristics during the investigation [45].

Theranostic delivery was recently reported by Usman et al. where chlorogenic acid and gadolinium were loaded in the Zn/Al layered double hydroxide-based nanohybrid carrier. Gold nanoparticles were coated on the surface of nanocarriers to enhance the contrast characteristics. The release studies were carried out using UV-visible spectrophotometer showing higher release in acidic pH as compared to alkaline pH. The drug release ceased upon completion of 50 h, and release was up to 90% in pH 4.8 (acidic) and about 65% in pH 7.4 (alkaline). MR imaging

was also tested to check whether signal strength was improved for nanohybrid carriers. Gold nanoparticles consist of large surface area which allows better penetration of water molecules in the layer spaces. The coating of gold nanoparticles on the surface leads to reduction of T_1 relaxation (longitudinal relaxation) time which further inflates the signal strength [46].

The formulation of responsive nanocarriers for targeted drug release can also be achieved using MR imaging technique. He et al. developed pH-sensitive nanocarriers containing doxorubicin. Gadolinium- and doxorubicin-containing nanoparticles were covered with hyaluronic acid shell for improving targeting potential. The pH-responsive nature prepared nanoparticles showed that as the pH was decreased to 5.5, the supernatant colour altered from purple to orange indicating the release of drug molecules from the nanoparticles. The retrieval of fluorescence of doxorubicin released in the solution suggests that simultaneous estimation of released drug is possible. The deviations produced in the fluorescence showed that the drug release was faster in acidic pH 5.5 and about 44.5% doxorubicin loaded in the nanoparticle released into the supernatant. However, the release for both pH of 6.8 and 7.4 was found to be below 15%. The targeting capacity of these nanosystems was examined on CD44⁺ HeLa cells and CD44⁻ NIH 3T3 cells. The observed fluorescence intensity was much higher in CD44⁺ HeLa cells than CD44⁻ NIH 3T3 cells, and further hyaluronic acid is vital for targetability as nanocarriers devoid of hyaluronic acid showed weak fluorescence [47].

4.2 Mn-Based Contrasting Agent

The manganese-based contrast agent has been used from time to time to develop MR imaging due to its effective positive contrasting behaviour. Yang et al. prepared Mn-based nanosystems containing fluorouracil, self-assembled by ligand bridging. The product formed displayed 47.7% and 82.6% of drug loading capacity and encapsulation efficiency, respectively. The tumour cells containing the acidic environment were suitable

for release of therapeutic agent (fluorouracil) as well as contrast agent (Mn^{2+}), possible due to hydration of nitrogen present. The in vitro release of the preparation was tested using standard absorption curves and inductively coupled plasma-mass spectrometry. Acid-responsive release was indicated as the percentage release of 80% for fluorouracil and 84% for Mn^{2+} was observed at pH 5.5 after completion of 4 h. On the other hand, less than 10% release was shown at pH 7.4 within 4 h. Therefore, such controlled release of constituents attains both the purposes for therapeutic delivery and diagnosis using MRI [48].

Yu et al. used manganese phosphate-based nanoparticle for diagnosis along with delivery of doxorubicin which was designed by salinization. Doxorubicin was incorporated into the hollow cavities of nanosystems, and polyethylene glycol is attached onto the surface for better targeting. The drug release studies were performed at different pH conditions, and at pH 5.4, about 90% of drug release was resulted within 72 h, and at pH 7.4, it was 15%. The pH-responsive delivery of the prepared nanosystems was exceptional when compared to performance of conventional pH-sensitive carriers. The conventional systems undergo the protonation of doxorubicin-like drugs to loosen up the interactions between drug and surfactant to release the drug. While, hollow manganese phosphate-based nanoparticles achieve quick response to acid medium because of formation of cracks in the hollow structure to affect the drug release in a controlled manner. The magnetic resonance relaxation properties also enhanced at pH 5.4 than at pH 7.4 due to better dissolution of contrasting agent at low pH. The targetability was further improved by conjugating the nanoparticles with folic acid which allows folate receptor-mediated endocytosis [49].

The development of pH-responsive nanocarriers for theranostic application were tried out by Huang et al., reporting the preparation of manganese and iron layered double hydroxide for the treatment and diagnosis of cancer. Methotrexate was incorporated as chemotherapeutic agent, and nanoparticles were evaluated to check their targeting potential towards acid environment

build-up in the tumour area. The release characteristics were examined at different pH conditions by using high-performance liquid chromatography. At pH 7.4, the rate of release of drug was only 21% which was significantly low on completion of 20 h. The acidic environment favoured the drug release because drug release after 20 h at pH 4.0, 5.0, and 6.0 were found to be 90%, 85%, and 80%, respectively. Therefore, the prepared product showed a lot of promise to function as pH-dependent drug delivery system [50].

Another approach to monitor the release of active drug is to develop monodisperse mesoporous manganese silicate coated silica nanoparticle (MMSSN) which can act as efficient vehicle for both contrast and therapeutic agent. Such a product was prepared in a simplified manner by using modified silicone dioxide sacrifice and in situ silicate growth method. Mesoporous magnesium silicate shell offers a large surface area and lavish paramagnetic sites on Mn which bestows the nanoparticles with high longitudinal relaxation effect. Moreover, the negatively charged shell imparts it with pH-dependent release of doxorubicin. In vitro drug release studies revealed that the nanocarriers exhibited the pH-dependent release behaviour. The release experiment showed that around 69.4% of drug are released at pH 5.4, while the release amount was about 9.5% at pH 7.4. Such a pH response may develop due to alterations in the electrostatic attraction between the drug molecules and pore of the carrier in the acidic medium to allow rapid dissociation and dissolution of drug. The results suggest that release of doxorubicin will be negligible in neutral pH of systemic circulation but when the nanoparticle will reach the tumour site and internalized into the tumour cell via endocytosis, the rapid drug release will take place. The sustained and intercellular release characteristics of the product were also attested from the images developed using confocal laser scanning microscopy (CLSM) [51].

Cai et al. developed hollow structured Prussian blue (HMPB) nanoparticle and coated the outer and inner surface with Mn to impart magnetic properties onto it. HMPB was produced by using

hydrothermal method based upon the mesoporous Prussian blue nanoparticle, which was further treated with chemical etching process. HMBP was then subjected to coating with combination of Mn and Fe at a fixed ratio to generate product labelled with contrasting agent, i.e. HMBP-Mn. The hollow mesoporous assembly provides high surface area for loading of chemotherapeutic agents, such as doxorubicin. It was also suggested that both Mn^{2+} and doxorubicin can be released in a controlled pH-responsive manner from the preparation, which also allows monitoring the release rate simultaneously. The drug release studies have displayed that about 20% of doxorubicin was released from HMPB-Mn at pH 7.4 and approximately 95% release at pH 5.0 within 20 h. This outcome may be due to the reason that proton contributed by acidic medium has broken down the attachment between Mn^{2+} and cyano group. This effect is highly advantageous to curtail the side effects associated with therapeutic agent before it reaches the site and improves the antitumour activity [52].

Dong et al. prepared a monodispersed calcium carbonate nanoparticle which was further modified with polyethylene glycol to achieve high loading of contrasting agent (Mn^{2+}) and drug (doxorubicin). The nanoparticles prepared were again pH sensitive like our previous discussions to provide controlled release characteristics. They studied the pH-responsive release of drug from the product by determining the longitudinal relaxation rate (T_1) using MRI. The observations indicated that longitudinal relaxivity rise intensely from 1.156 m/Ms to 11.48 m/Ms, while pH was reduced from 7.4 to 5.5. These nanoparticulate systems will allow non-invasive differentiation of tumour from the normal tissues. The research also explored around the potential of using such nanoparticles for in vivo drug release monitoring using MRI. The drug-loaded nanoparticles were injected into the tumour and muscle cells of Balb/c mice. The in vitro studies demonstrated that intense MR signals were displayed in the tumour cells post-injection which progressively increased in 2 h, while the intensity of MR signal was significantly lower in muscle cells

even after injecting the same concentration. The *in vivo* results evidently showed that nanoparticles retain their stability in the normal tissues but undergoes dissociation in the low pH of tumour [53].

4.3 Fe-Based Contrasting Agent

The iron-based nanoparticles have scarcely been investigated for monitoring the drug release, although some of the recent researches will be included in the discussion. One of the attempts included generation of temperature-sensitive products for delivery of anticancer drug. Kneepkens et al. prepared thermosensitive liposomes loaded with doxorubicin and iron-succinyl deferoxamine (Fe-SDFO). For this discussion, we will focus on MRI active preparation, i.e. Fe-SDFO. Nanovesicular systems (liposomes) were prepared using thin film hydration and extrusion method, wherein preformed Fe-SDFO is incorporated during the process of vesicle formation. The release studies were carried out for concentrations varying from 3.2 to 4 mM of Fe-SDFO. The rapid release of encapsulated Fe-SDFO was determined at 42 °C which was about 80% in 2 min, and approximately 93.5% of percentage release was observed upon completion of 10 min. Contrarily, the release of Fe-SDFO at normal body temperature (37 °C) was about 15% within 1.5 h, indicating that small amount of Fe-SDFO leaked from the liposomes. The temperature-dependent effect was also observed on the relaxation rate, because the temperature increased from 0.80 to 1.35 m/Ms. when temperature was raised from 37 °C to 42 °C. The *in vitro* studies portrayed the efficiency of such systems for image-guided stimulated release of drug. The changes due to temperature will allow clarifications with regard to release of drug within tumour [54].

Bakewell et al. developed a triblock copolymer consisting of polyethylene glycol, glutamic acid hydroxamate, and polypeptides. The portion consisting of hydroxamic acid forms association with iron by coordination bonding between polymers to provide stability to the micelles. The

above coordination product possesses low stability at low pH, furnishing it with stability dependent upon the surrounding medium to trigger the drug release in a controlled manner. The nanoparticles were characterized by time course-positive MR imaging contrast using tumour and orthotopic models. The results showed that localization of iron-based nanoparticles was observed in the subcutaneous tumour as MR signals were maximum between 24 and 48 h, diminishing after completion of 168 h. The investigation demonstrated that iron-based micelles were localized at the tumour site because of intense contrast developed in MRI; therefore, it is suitable for further exploration for theranostic potential [55].

Kaittanis et al. utilized ferumoxytol (iron oxide nanoparticles) which is also called nanophores for delivery of one or more drugs. Iron oxide nanoparticles also have magnetic properties to be used as contrasting agents for MRI. In this research, three different nanoparticles were prepared by loading fluorescent Taxol analogue Flutax1, fluorophore DiR, and doxorubicin. The characterization of the prepared nanoparticles revealed that dextran capsule allowed high loading capacity due to electrostatic interactions. Upon reaching to the acidic microenvironment similar to tumour, fast release of the loaded compound was observed which can be utilized for management of solid tumours. Additionally, the drug (or diagnostic agent) was monitored from both spatial and temporal point of view by using MRI because the release of cargo leads to restoration of longitudinal (T_1) and transverse relaxation (T_2) signals of ferumoxytol. The drug delivery system showed versatility by avoiding any possible alterations in the chemical structure of the drug and other components of the nanoparticle [56].

5 Pharmacokinetic Profiling Using MRI

During drug development process, MRI study may offer non-invasive estimation of the pharmacokinetics and biodistribution of drug from the drug carrier in animal models. This permits us to

choose superior drug delivery system among various possible alternatives. It provides answers to some of imperative queries answered like ‘Where did the drug carriers went inside the body?’, ‘How long does drug carriers retain in the body?’, ‘How are they eliminated from the body?’, ‘Will they reach to the target site?’, and ‘What amount of drug is released and how much has reached to the actual site?’. MR imaging techniques may allow us to attain the deeper knowledge on movement of the drug delivery systems inside the body. Further, a number of recent literature and their outcomes will be included in the discussion to understand how useful is this technique in pre-clinical development of drug delivery systems [57, 58]. Huang et al. prepared MnO-containing nanoparticles which were attached with PEG with the help of chelation and further conjugation with cyclic arginine-glycine-aspartic acid (cRGD). These nanosystems allow both passive and active targetability towards tumour cells. The potential of the developed product in tumour diagnosis was carried out using in vivo MRI study. The in vivo MRI study involved imaging of tumour tissues pre- and post-administration of nanoparticle. The tumour tissue in the developed images started to get lucent after 5 min of injection; subsequently the contrasting effect of the Mn^{2+} showed maximum MR signal between 30 and 120 min after injection. However, the intensity of signals got weaker after 120 min but the contrasting capacity retained up to 300 min. This precise contrast behaviour in tumour sites may be attributed to the passive targetability of cRGD employed in the fabrication of nanoparticle [59].

Pharmacokinetic study using MRI was also reported by Tian et al. where they have synthesized a novel biodegradable magnetic contrasting agent, poly(L-glutamic acid)-benzyl-diethylenetriamine pentaacetate-gadolinium chelate (PG-Gd) by utilizing difunctional and monofunctional diethylenetriamine pentaacetate precursors. For performing pharmacokinetic and biodistribution studies, firstly PG-Gd was intravenously injected (0.08 mmol Gd/kg) in normal Swiss mice. The drug was quickly distributed in first 24 h, accompanied with long elimination half-life of 50.1 h. The steady-state volume of

distribution (85.5 mL/kg) was found to be as high as total blood volume of mouse indicating that PG-Gd was highly efficiently distributed throughout the systemic circulation. Later on, pharmacokinetic study was also performed on the rhesus monkeys where the PG-Gd was compared with Magnevist (gadopentetate dimeglumine). The outcomes showed that PG-Gd released significantly higher in the first 2 h of injection in comparison to Magnevist. However, the volume of distribution of Magnevist was much higher than PG-Gd, indicating its better distribution throughout the body [60]. Fig. 22.2 represents the preparation and theranostic application of nanoparticles containing Gd-based contrast agents.

Bakewell et al. performed pharmacokinetic study in the cannulated rat model to estimate the pharmacokinetic properties of the micellar preparation in comparison with free drug. The value of plasma exposure increased from 0.96 $\mu\text{g}\cdot\text{h}/\text{mL}$ for free drug to 913.7 $\mu\text{g}\cdot\text{h}/\text{mL}$ for iron-based micelle formulation. It was clear from the results that micelles stabilized using iron showed extensive stability in systemic circulation after their administration [55]. Gobbo et al. synthesized the superparamagnetic iron oxide nanoparticles (SPIONs) by using two methods based on organic and aqueous protocols. For pharmacokinetic studies, the SPIONs were injected in the rats, and blood samples were withdrawn at different time points for concentration measurements. SPIONs followed one compartment model pharmacokinetics as they were readily removed from the systemic circulation. They were mainly distributed in the organs such as the liver, kidney, lungs and spleen which are the main sites for metabolism and excretion of xenobiotics [62].

Neubauer et al. developed a nanoparticle system containing perfluorooctyl bromide, combination of surfactants (lecithin and phosphatidylethanolamine), and glycerin which were marked with gadolinium-based contrast agent. Pharmacokinetic analysis of distribution of nanoparticle was studied using male New Zealand white rabbits. MR signals depicted that gadolinium concentration in systemic fluid dropped in a biexponential manner which is usually seen in case of perfluorocarbon type of

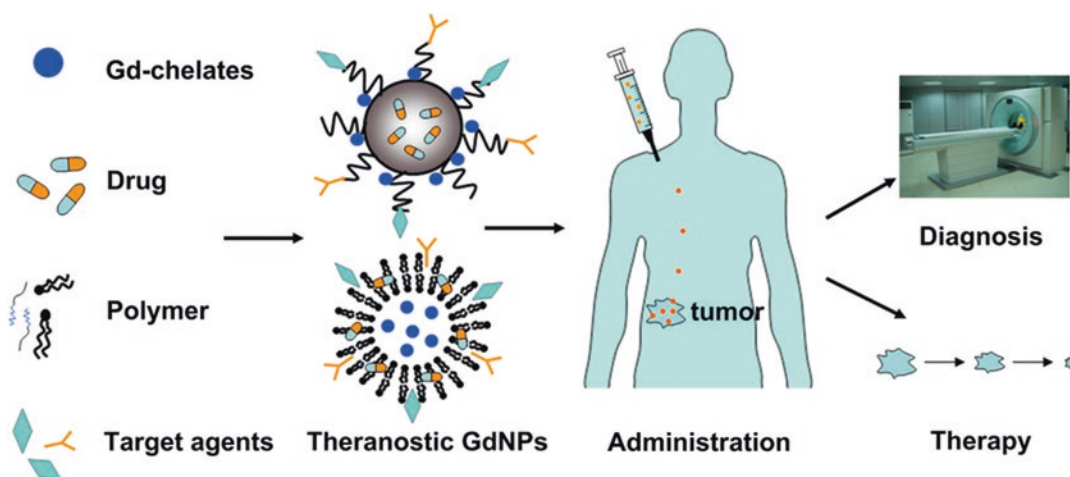


Fig. 22.2 Pictorial illustration of preparation and theranostic application of nanoparticles containing Gd-based contrast agents [61]

nanoparticles. The injected formulations showed two compartment model pharmacokinetic behaviour, and the estimated parameters did not vary among rabbits injected with targeted and non-targeted nanoparticles. The larger elimination rate constant was determined with elimination half-life of 11.9 h and distribution half-life of around 20.2 min. The main benefit of using such systems is that high intravenous doses are not mandatory for generating detectable response from the target tissue [63]. Pouliquen et al. prepared iron oxide nanoparticles by using modified Molday's method to study their pharmacokinetic characteristics in animal models. The results of pharmacokinetic studies done in Swiss female mice displayed that in the starting 30 min after injection, around 47% of the product is retained in the blood. Surprisingly, the tissue uptake of nanoparticles was faster in the first 10 min but drops down in the subsequent 20 min. The tissue distribution resumes back to faster rate after 30 min [64].

Paramagnetic chemical exchange saturation transfer (PARACEST) as a contrast agent was utilized by Ali et al. to investigate pharmacokinetics of two nanoparticles, viz. tetraglycineamide derivative of 1,4,7,10-tetraazacyclododecane-1,4,7,10-tetraacetic acid (DOTA-Gly) and polyamidoamine (PAMAM) dendrimer. The fraction of

concentration was utilized for comparing the pharmacokinetic feature of both the nanoparticles when they get distributed in the tumour tissue. Nanosystems showed suboptimal tissue penetrability as well as slow elimination of these large nanoparticles. In order to improve the application of this technology, it is required to put more emphasis on impact of magnetic field exposures during MRI studies and pH variability on relative concentration determinations [65]. Badachhape et al. formulated a gadolinium-based liposome (ADx-001) by incorporating PEG conjugated styryl pyrimidine as targeting molecule for MR imaging of amyloid plaques. Plasma concentration of Gd was estimated using ICP-MS at different time intervals post-administration of ADx-001 in cynomolgus monkeys. Due to scarcity of previous literature on circulation half-life in monkeys, the comparative data was never generated. However, pharmacokinetic studies were compared with any previously encountered prolonged circulation half-life of around 41 h [66].

The gadolinium-containing contrast agents are frequently used for MR imaging studies due to their efficiency and safety for prolonged usage in patients; in spite of that, some gadolinium-based contrasting agents are associated with detrimental effects in nephrogenic systemic fibrosis (NSF) as the deposition of Gd causes toxicity on

long-term usage. Wei et al. synthesized zwitterion containing exceedingly small superparamagnetic iron oxide nanoparticles (ZES-SPIONs) and evaluate them to check whether their pharmacokinetic and imaging characteristics are equivalent to those of Gd-based products. The renal clearance was estimated by administering the ZES-SPIONs into mice, and their urine was collected at various time intervals. The longer blood half-life (around 19 min) was deducted out of the study, which is higher than Gd-based contrast agents [67]. Ferumoxytol is used as iron source in treatment of iron deficiency anaemia, along with that it also has potential of being employed as contrast agent for MRI study, as reported in numerous studies. Wells et al. investigated pharmacokinetic behaviour of ferumoxytol in the abdominal and pelvic area by the help of MRI relaxometry. There were huge differences between its pharmacokinetic behaviour in mononuclear phagocyte system (MPS) as compared to the non-MPS organs. The MR signals were elevated throughout the MPS organs for 30 days of investigation, apart from organs such as the liver and spleen, while the signal intensity dropped for the non-MPS organs to indicate poor distribution of contrast agent in these organs in comparison to MPS organs. It was clear from the observations that distribution of ferumoxytol was dose dependent and organ specific [68]. Edge et al. developed dimercaptosuccinic acid (DMSA)-coated superparamagnetic iron oxide nanoparticles (SPIONs) of two lead-based nanoparticles (MF66 and OD15) and carried out experimentations to estimate pharmacokinetics and biodistribution of nanoparticles in the pig under anaesthesia. On the basis of particle electron paramagnetic resonance, it was ascertained that OD15 administered in 2 mg/kg dose was eliminated from blood in 30 min. The recommendations were to administer such magnetic nanoparticles as single intravenous dose for peak bioavailability. Noticeably, the circulation time is too short for it to provide substantial anticancer activity [69]. The compilation of pharmacokinetic outcomes of various research studies employing MRI is shown in Table 22.1.

6 Biodistribution Studies Using MRI

Magnetic resonance imaging allows generation for high-resolution 3-D images useful for carrying out in vivo biodistribution studies of nanoparticles. The imaging quality of this technique is much higher in comparison with optical imaging or radionuclide imaging. There is no restriction as far as penetrability is concerned with remarkable contrasting abilities [70]. This discussion will be followed up with some relevant literature to put up insights of biodistribution studies. The biodistribution studies performed by Tian et al. involved intravenously injecting six mice with 0.08 mmol Gd/kg of PG-Gd. The drug uptake at 2 h post-injection was estimated to be 8.07%ID/kg and 5.65%ID/kg in the kidney and liver, respectively. However, the drug uptake in the kidney decreased significantly after 2 days (1.07%ID/kg), which remained in negligible amounts after 7 days (0.68%ID/kg). The outcomes suggest that PG-Gd is steadily cleared from blood 2 days post-injection. Although there was increment in uptake by the liver, the heart and muscles showed fall in drug uptake after 2 days [60].

Lee et al. described about the synthesis of biodegradable nano-formulation containing superparamagnetic iron oxide (CSNP-SPIO) with hydrophobic core of poly(lactic-co-glycolic acid) covered with glycol chitosan shell. The distribution study of the formulation showed intense radioactive signals in the liver after their intravenous injection. The liver gets darker due to accumulation of nanoparticles initially; however, as the CSNP-SPIO starts to break down slowly, the liver darkness tends to lower down with time. The results suggest that CSNP-SPIO proved its effectiveness as biodegradable MR contrast agent. Additionally, the core of these nanoparticles provides substantial area for drug loading, and amine groups on the glycol chitosan shell are useful for targeting purpose. Figure 22.3 depicts how CSNP-SPIO were designed using superparamagnetic iron oxide and evaluation for biodistribution and internalization characteristics [71].

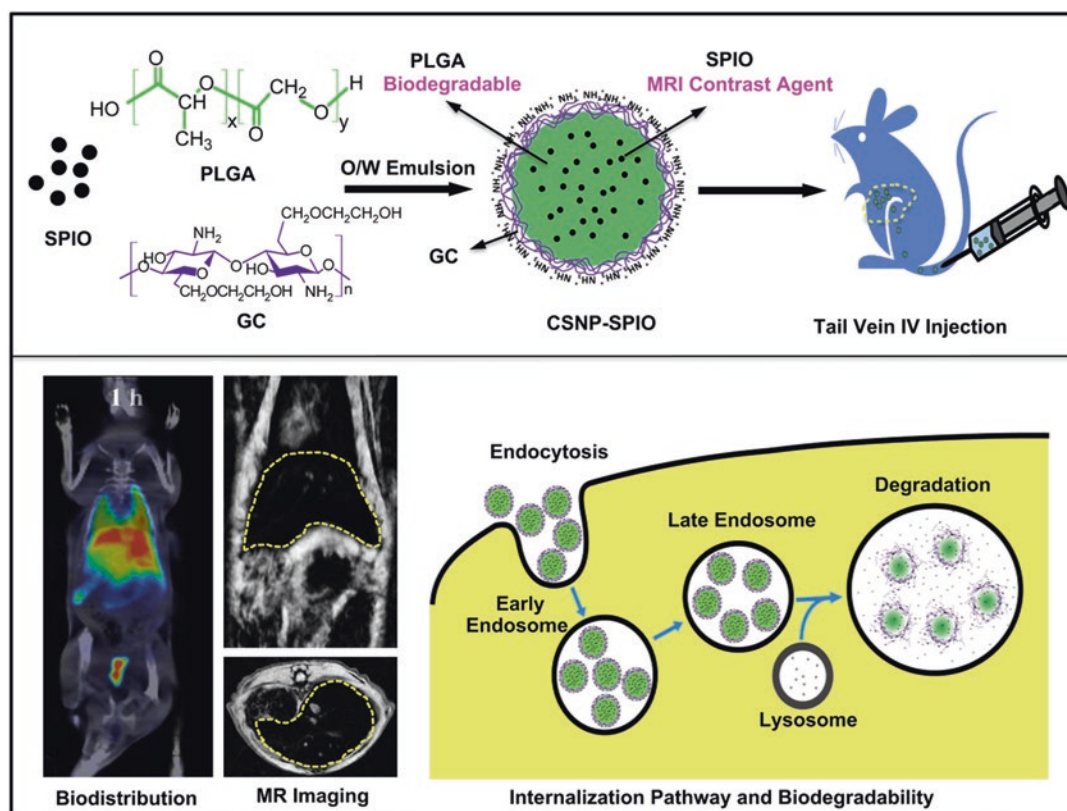
Table 22.1 Summary and significant outcomes of pharmacokinetic studies performed using MRI contrast agents

Contrast agent	Drug	Elimination half-life	Relaxivity	Applications	References
PEGylation of MnO nanoparticles and conjugation with cRGD	–	–	10.2 m/Ms (spin-lattice relaxivity)	(a) Passive and active targeting to tumour (b) High stability in storage and physiological fluids	Huang et al. [59]
Poly(L-glutamic acid)-benzyl-diethylenetriamine pentaacetate-gadolinium chelate (PG-Gd)	–	50.1 h	–	(a) Blood pool MR imaging agent	Tian et al. [60]
Triblock copolymer (PEG-glutamic acid hydroxamate-polypeptide) chelated with Fe	Daunorubicin	–	7–16 m/Ms (spin-lattice relaxivity) 36–53 m/Ms (spin-spin relaxivity)	(a) Improves stability and plasma retention (b) Enhanced antitumour activity and reduced toxicity	Bakewell et al. [55]
Superparamagnetic iron oxide nanoparticles (SPIONs)	–	32 min	–	(a) Theranostic application in cancer	Gobbo et al. [62]
Gd-based paramagnetic liquid perfluorocarbon nanoparticles	–	11.9 h	12.7 m/Ms (spin-lattice relaxivity) 10.4 m/Ms (spin-spin relaxivity)	(a) Site-targeting nanocarrier (b) Surrogate marker for drugs, especially anticancer drugs (c) Drug release monitoring at specific site	Neubauer et al. [63]
Superparamagnetic iron oxide nanoparticles (MD)	–	–	43.6 m/Ms (spin-lattice relaxivity) 368.4 m/Ms (spin-spin relaxivity)	(a) High efficiency due to increases in tissue uptake (b) Better cellular localization	Pouliquen et al. [64]
Paramagnetic chemical exchange saturation transfer (PARACEST)	–	–	Eu-DOTA-Gly: 0.0018 m/Ms Eu-G5: 0.107 m/Ms Yb-DOTA-Gly: 0.0115 m/Ms Yb-G2: 0.091 m/Ms (spin-lattice relaxivity)	(a) Selection of suitable nanoparticles based on their pharmacokinetic behaviour in tumours	Ali et al. [65]
Gadolinium-based liposome (ADx-001)	Lipid-PEG conjugated styryl-pyrimidine	41 h	31 m/Ms (spin-lattice relaxivity)	(a) High sensitivity, specificity, and prolonged retention for imaging of β amyloid plaques	Badachhape et al. [66]

(continued)

Table 22.1 (continued)

Contrast agent	Drug	Elimination half-life	Relativity	Applications	References
Zwitterion containing exceedingly small superparamagnetic iron oxide nanoparticles (ZES-SPIOs)	–	19 min	5.2 m/Ms (spin-lattice relaxivity) 10.5 m/Ms (spin-spin relaxivity)	(a) Preclinical prospect for MR-angiography	Wei et al. [67]
Dimercaptosuccinic acid (DMSA)-coated SPIOs (labelled with MF66 and OD15)	–	10 min	–	(a) Therapeutic and diagnostic carrier	Edge et al. [69]

**Fig. 22.3** Schematic representation of preparation of superparamagnetic iron oxide containing nanoparticles (CSNP-SPIO), followed by their evaluation of biodistribution, internalization, and biodegradability of the nanoparticles [71]

To understand the contrasting behaviour of Mn-based agents in tumour tissues, in vivo bio-distribution studies were done by Huang et al. The concentration of Mn in tumour tissues in comparison with other organs such as the liver, lung, spleen, intestine, kidney, etc. was determined at different time points post-injection.

There was significant localization of Mn in tumour areas, i.e. 62 g/g of the weight of tissue upon completion of 30 min after injection. The Mn concentration after 2 h of injection was still 55.7 g/g of the weight of tissue, indicating its retention in tumour for longer duration. The fine contrast during in vivo MRI study revealed the

persistent maintenance of Mn content during the time period of 30–120 min. The concentration of Mn dropped expectedly at 4 h after injection, reaching back to its pre-injection level. The distribution of Mn in the non-tumour tissues remained under 30 g/g of the weight of tissue throughout the duration of investigation. The outcomes confirmed that the prepared nanoparticles target the tumour cells efficiently and also retain into tumour for sufficient duration [59].

The biodistribution of SPIONs was examined by Gobbo et al., where the alterations in MR signals were checked in rats injected with the magnetically active products. There was no difference in signal intensity at all time intervals in rats injected with saline (control). For the rats injected with SPIONs, alterations in signal intensity were observed at different time points for individual organ. In the case of the spleen and liver, the best MR signal was observed at 3 h after injection, while the signal intensity never changed in the lungs through the study period, mainly because lung tissues are filled with air which annuls the low-density water and thereby feeble MRI signals. The drop in signal intensity was gradual as it reduced throughout the 96-h period. For the kidney, the alterations in signal reached to a constant value in both the medulla and cortex with the concentrations of 8.61% and 18.68% upon completion of 96 h [62]. Wei et al. also reported the results of biodistribution studies carried out on ZES-SPIONs formulation to estimate in vivo stability of the product. The activity of iron-based contrast agent was estimated by withdrawing the organs and blood at 24 h after injection. ZES-SPIONs show bright contrast, therefore showing considerable accumulation in the bladder at 10 min after injection. Further, the similar contrast was also observed in the heart and kidney at 6 min after injection. ZES-SPIONs get cleared off from the heart and kidney and a second dose was injected. For the subsequent study after second dose, the nanoparticles show almost similar level of accumulation in the heart and kidney in comparison with the outcomes of the first injection [67].

Gadolinium-based formulation (ADx-001) reported by Badachhape et al. was endured by rats up to the dose of 0.30 mmol/Gd/kg. The rats injected with the product did not die until necropsy underwent after 28 days, and no signs of dysfunction or impairment were seen during the period. The distribution of Gd content in different organs increased in a dose-dependent manner. From the distribution, it was deduced that the Gd content was higher in the liver and spleen and lowest in the skin and brain. The Gd content in tissues remained only up to 10% at 28 days after injection. Furthermore, intravenous injection of ADx-001 was tolerated in cynomolgus monkeys, and no adverse effects were observed [66].

Lv et al. synthesized Gd-doped iron oxide nanoparticles (GdIONPs) and monitored the in vivo distribution of the nanoparticles. For the determination of organ level distribution, GdIONPs were injected in the nonobese diabetic/severe combined immunodeficiency (NOD/SCID) mice with xenograft tumour, equivalent to 7–8 mg/kg of iron. In order to obtain direct estimation, the amount of GdIONPs in different organs was calculated in $\mu\text{g/mL}$ for blood and $\mu\text{g/g}$ for various organs. It was observed that the amount of GdIONPs increased rapidly in the blood up to 39.9 $\mu\text{g/mL}$ at 20 min post-injection and slowly decreased up to 0.8 $\mu\text{g/mL}$ after 6 h. The prolonged retention in circulation was observed may be as a result of nanoscale size of GdIONPs and coating of polyvinyl pyrrolidone-33 (PVP33) as a plasma expander on the surface. PVP33 may also provide additional stability to the nanoparticles in the biological fluids which are essential for their theranostic applications for tumours. This trend of distribution was also observed in the spleen, liver, and tumour cells as the GdIONPs content was found to be low at 1 h post-injection which increased to its peak value after 3 h, followed by slow reduction up to 48 h. GdIONPs showed minimal penetration through the blood-brain barrier, and the concentration of Gd in the brain after injection was only 1% of its concentration in tumour [72].

Table 22.2 List of experimental parameters determined during in vivo biodistribution studies using MRI

Contrast agent	Administered dose	Recipient animal	Organs of interest	References
Poly(L-glutamic acid)-benzyl-diethylenetriamine pentaacetate-gadolinium chelate (PG-Gd)	0.08 mmol Gd/kg of PG-Gd	Healthy male Swiss mice	Heart, liver, spleen, kidney, and muscle	Tian et al. [60]
PLGA-linked SPIONs (CSNP-SPIO)	227.3 ± 23.2 MBq/0.2 cc of ^{99m} Tc-labelled CSNP-SPIO	Sprague Dawley (SD) rats	Whole body, bilateral lungs, liver, spleen, bilateral kidneys, and bladder	Lee et al. [71]
PEGylation of MnO nanoparticles and conjugation with cRGD	0.5 mg Mn per kg for the weight of mouse	Tumour-bearing nude mouse	Tumour, lung, spleen, intestine, kidney, heart, brain, and liver	Huang et al. [59]
Superparamagnetic iron oxide nanoparticles (SPIONs)	100 µl of SPIONs at 10 mg Fe/mL	Female BALBc mice	Heart, liver, spleen, lungs, and kidneys	Gobbo et al. [62]
Zwitterion containing exceedingly small superparamagnetic iron oxide nanoparticles (ZES-SPIONs)	0.2 mmol [Fe]/kg	Anaesthetized mice	Liver, blood, spleen, kidney, lung, gastrointestinal tract, and heart	Wei et al. [67]
Gadolinium-based liposome (ADx-001)	0.20 and 0.15 mmol Gd/kg	Transgenic APP ^{swe} /PSEN1 ^{dE9} mice	Bone, brain, kidney, liver, and skin	Badachhape et al. [66]
Gd-doped iron oxide nanoparticles (GdIONPs)	0.74 mg/mL of Fe	NOD/SCID mice	Liver, spleen, kidney, brain, and tumour cells	Lv et al. [72]
PEG-coated IONPs	200 µg/mL of Fe	Eight-weeks old BALB/cJRj female mice	Liver, spleen, kidneys, and blood	Romero et al. [73]

IONPs developed by Romero et al. were subjected to biodistribution studies in mice, wherein two different solutions of IONPs (fresh and aged) were injected. This research was focussed on evaluating the effect of the prolonged stability of polyethylene glycol coating over biodistribution pattern of IONPs by using MRI. It was observed that both the solutions displayed distinct biodistribution behaviour during investigation. In the case of aged IONP solution, the liver and spleen got darker indicating the localization of IONPs in the reticuloendothelial organs. On the other hand, the fresh solution of IONPs showed very limited accumulation in the liver and spleen, whereas accumulation in the kidneys was much higher. These outcomes illustrated that such minor modifications on the surface of nanoparticles also contributes to significant impact over in vivo characteristics of nanoparticles [73]. Summarization of experiments with regard to biodistribution studies using MRI is listed in Table 22.2.

References

- Vrbanac J, Slaughter R. ADME in drug discovery. In: A comprehensive guide to toxicology in nonclinical drug development. 2nd ed. Elsevier Inc; 2017. p. 39–67.
- Mikhail AS, Partanen A, Yarmolenko P, et al. Magnetic resonance-guided drug delivery. *Magn Reson Imaging Clin N Am*. 2015;23(4):643–55.
- Mahmoudi M, Tachibana A, Goldstone AB, et al. Novel MRI contrast agent from magnetotactic bacteria enables in vivo tracking of iPSC-derived cardiomyocytes. *Sci Rep*. 2016;6(1):26960.
- D’Mello SR, Cruz CN, Chen ML, et al. The evolving landscape of drug products containing nanomaterials in the United States. *Nat Nanotechnol*. 2017;12(6):523–9.
- Li M, Al-Jamal KT, Kostarelos K, Reineke J. Physiologically based pharmacokinetic modeling of nanoparticles. *ACS Nano*. 2010;4(11):6303–17.
- Bawa R, Barenholz Y, Owen A. Chapter 12 the challenge of regulating nanomedicine: key issues. In: *Nanomedicines: design, delivery and detection*. Cambridge: The Royal Society of Chemistry; 2016. p. 290–314.

7. Gabizon A, Shmeeda H, Barenholz Y. Pharmacokinetics of pegylated liposomal doxorubicin. *Clin Pharmacokinet*. 2003;42(5):419–36.
8. Suk JS, Xu Q, Kim N, et al. PEGylation as a strategy for improving nanoparticle-based drug and gene delivery. *Adv Drug Deliv Rev*. 2016;99(Pt A):28–51.
9. Barenholz Y. Doxil(R)—the first FDA-approved nano-drug: lessons learned. *J Control Release*. 2012;160(2):117–34.
10. Mulder WJ, McMahon MT, Nicolay K. The evolution of MRI probes: from the initial development to state-of-the-art applications. *NMR Biomed*. 2013;26(7):725–7.
11. Langereis S, Geelen T, Grull H, et al. Paramagnetic liposomes for molecular MRI and MRI-guided drug delivery. *NMR Biomed*. 2013;26:728–44.
12. Kluza E, Strijkers GJ, Nicolay K. Multifunctional magnetic resonance imaging probes. *Recent Results Cancer Res*. 2013;187:151–90.
13. Melia CD, Rajabi-Siahboomi AR, Bowtell RW. Magnetic resonance imaging of controlled release pharmaceutical dosage forms. *Pharm Sci Technol Today*. 1998;1(1):32–9.
14. Ashraf M, Iuorno VL, Coffin-Beach D, et al. A novel nuclear magnetic resonance (NMR) imaging method for measuring the water front penetration rate in hydrophilic polymer matrix capsule plugs and its role in drug release. *Pharm Res*. 1994;11(5):733–7.
15. Rajabi-Siahboomi AR, Bowtell RW, Mansfield P, et al. Structure and behavior in hydrophilic matrix sustained release dosage forms: 2. NMR imaging studies of dimensional changes in the gel layer and core of HPMC tablets undergoing hydration. *J Control Release*. 1994;13(3):121–8.
16. Lardo AC. Real-time magnetic resonance imaging: diagnostic and interventional applications. *Pediatr Cardiol*. 2000;21(1):80–98.
17. Lederman RJ. Cardiovascular interventional magnetic resonance imaging. *Circulation*. 2005;112(19):3009–17.
18. Bloch F. Nuclear induction. *Phys Rev*. 1946;70(7–8):460–74.
19. Smith FW, Hutchison JM, Mallard JR, et al. Oesophageal carcinoma demonstrated by whole-body nuclear magnetic resonance imaging. *BMJ*. 1981;282(6263):510–2.
20. Hawkes RC, Holland GN, Moore WS, Worthington BS. Nuclear magnetic resonance (NMR) tomography of the brain: a preliminary clinical assessment with demonstration of pathology. *J Comput Assist Tomogr*. 1980;4(5):577–86.
21. Smith FW, Runge V, Permezel M, Smith CC. Nuclear magnetic resonance (NMR) imaging in the diagnosis of spinal osteomyelitis. *Magn Reson Imaging*. 1984;2(1):53–6.
22. Webb A. Chapter 1. The principles of magnetic resonance, and associated hardware. In: *New developments in NMR*. Royal Society of Chemistry; 2016. p. 1–47.
23. Cleary JOSH, Guimarães AR. Magnetic resonance imaging. In: *Pathobiology of human disease*. Elsevier Inc; 2014. p. 3987–4004.
24. Pien HH, Fischman AJ, Thrall JH, Sorensen AG. Using imaging biomarkers to accelerate drug development and clinical trials. *Drug Discov Today*. 2005;10(4):259–66.
25. Owringi AM, Greer PB, Glide-Hurst CK. MRI-only treatment planning: benefits and challenges. *Phys Med Biol*. 2018;63(5):05TR01.
26. MAGNIMS study group. MAGNIMS consensus guidelines on the use of MRI in multiple sclerosis—establishing disease prognosis and monitoring patients. *Nat Rev Neurol*. 2015;11(10):597–606.
27. Fazekas F, Soelberg-Sorensen P, Comi G, Filippi M. MRI to monitor treatment efficacy in multiple sclerosis. *J Neuroimaging*. 2007;17:50S–5S.
28. Hong H, Goel S, Zhang Y, Cai W. Molecular imaging with nucleic acid aptamers. *Curr Med Chem*. 2011;18(27):4195–205.
29. Pickhardt PJ, Park SH, Hahn L, et al. Specificity of unenhanced CT for non-invasive diagnosis of hepatic steatosis: implications for the investigation of the natural history of incidental steatosis. *Eur Radiol*. 2012;22(5):1075–82.
30. Klasson A, Ahren M, Hellqvist E, et al. Positive MRI contrast enhancement in THP-1 cells with Gd₂O₃ nanoparticles. *Contrast Media Mol Imaging*. 2008;3(3):106–11.
31. Zhang Y, Lin JD, Vijayaragavan V, et al. Tuning sub-10 nm single-phase NaMnF₃ nanocrystals as ultrasensitive hosts for pure intense fluorescence and excellent T1 magnetic resonance imaging. *Chem Commun*. 2012;48(83):10322–4.
32. Mitchell DG. Liver I: currently available gadolinium chelates. *Magn Reson Imaging Clin N Am*. 1996;4(1):37–51.
33. Shokrollahi H. Contrast agents for MRI. *Mater Sci Eng C*. 2013;33(9):4485–97.
34. Frey NA, Peng S, Cheng K, et al. Magnetic nanoparticles: synthesis, functionalization, and applications in bioimaging and magnetic energy storage. *Chem Soc Rev*. 2009;38(9):2532–42.
35. Terreno E, Castelli DD, Viale A, et al. Challenges for molecular magnetic resonance imaging. *Chem Rev*. 2010;110(5):3019–42.
36. Pham SH, Choi Y, Choi J. Stimuli-responsive nanomaterials for application in antitumor therapy and drug delivery. *Pharmaceutics*. 2020;12(7):630.
37. Xiao YD, Paudel R, Liu J, et al. MRI contrast agents: classification and application. *Int J Mol Med*. 2016;38(5):1319–26.
38. Cipreste MF, Peres AM, Cotta AA, et al. Synthesis and characterization of ¹⁵⁹Gd-doped hydroxyapatite nanorods for bioapplications as theranostic systems. *Mater Chem Phys*. 2016;181:301–11.
39. Cho HK, Cho HJ, Lone S, et al. Preparation and characterization of mri-active gadolinium nanocomposite particles for neutron capture therapy. *J Mater Chem*. 2011;21(39):15486–93.

40. Ahmadi R, Malek M, Hosseini HRM, et al. Ultrasonic-assisted synthesis of magnetite based MRI contrast agent using cysteine as the biocapping coating. *Mater Chem Phys*. 2011;131(1–2):170–7.
41. Tweedle M. The ProHance story: the making of a novel MRI contrast agent. *Eur Radiol*. 1997;7:S225.
42. Zheng XY, Li LD, Sun LD, Yan CH. Lanthanide nanoparticles: promising candidates for magnetic resonance imaging contrast enhancement. *Handb Phys Chem Rare Earths*. 2016;50:301–35.
43. Sani Usman M, Hussein MZ, Fakurazi S, et al. Gadolinium-doped gallic acid-zinc/aluminium-layered double hydroxide/gold theranostic nanoparticles for a bimodal magnetic resonance imaging and drug delivery system. *Nano*. 2017;7(9):244.
44. Wang S, Zhou Z, Wang Z, et al. Gadolinium metallofullerene-based activatable contrast agent for tumor signal amplification and monitoring of drug release. *Small*. 2019;15(16):1900691.
45. Xu Y, Goyanes A, Wang Y, et al. Layered gadolinium hydroxides for simultaneous drug delivery and imaging. *Dalton Trans*. 2018;47(9):3166–77.
46. Usman MS, Hussein MZ, Kura AU, et al. Chlorogenic acid intercalated Gadolinium–Zinc/Aluminium layered double hydroxide and gold nanohybrid for MR imaging and drug delivery. *Mater Chem Phys*. 2020;240:122232.
47. He Z, Zhang P, Xiao Y, et al. Acid-degradable gadolinium-based nanoscale coordination polymer: a potential platform for targeted drug delivery and potential magnetic resonance imaging. *Nano Res*. 2018;11:929–39.
48. Yang C, Song G, Yuan H, et al. Manganese–fluorouracil metallodrug nanotheranostic for MRI-correlated drug release and enhanced chemoradiotherapy. *CCS Chem*. 2021;3(4):1116–28.
49. Yu J, Hao R, Sheng F, et al. Hollow manganese phosphate nanoparticles as smart multifunctional probes for cancer cell targeted magnetic resonance imaging and drug delivery. *Nano Res*. 2012;5(10):679–94.
50. Huang G, Zhang KL, Chen S, et al. Manganese-iron layered double hydroxide: a theranostic nanoplatform with pH-responsive MRI contrast enhancement and drug release. *J Mater Chem B*. 2017;5(20):3629–33.
51. Li X, Zhao W, Liu X, et al. Mesoporous manganese silicate coated silica nanoparticles as multi-stimuli-responsive T1-MRI contrast agents and drug delivery carriers. *Acta Biomater*. 2016;30:378–87.
52. Cai X, Gao W, Ma M, et al. A prussian blue-based core-shell hollow-structured mesoporous nanoparticle as a smart theranostic agent with ultrahigh pH-responsive longitudinal relaxivity. *Adv Mater*. 2015;27(41):6382–9.
53. Dong Z, Feng L, Zhu W, et al. CaCO₃ nanoparticles as an ultra-sensitive tumor-pH-responsive nanoplatform enabling real-time drug release monitoring and cancer combination therapy. *Biomaterials*. 2016;110:60–70.
54. Kneepkens E, Fernandes A, Nicolay K, Grüll H, et al. Iron(III)-based magnetic resonance-imageable liposomal T1 contrast agent for monitoring temperature-induced image-guided drug delivery. *Investig Radiol*. 2016;51(11):735–45.
55. Bakewell SJ, Carie A, Costich TL, et al. Imaging the delivery of drug-loaded, iron-stabilized micelles. *Nanomedicine*. 2017;13(4):1353–62.
56. Kaittanis C, Shaffer T, Ogirala A, et al. Environment-responsive nanophores for therapy and treatment monitoring via molecular MRI quenching. *Nat Commun*. 2014;5:3384.
57. Kunjachan S, Ehling J, Storm G, et al. Noninvasive imaging of nanomedicines and nanotheranostics: principles, progress, and prospects. *Chem Rev*. 2015;115(19):10907–37.
58. Lammers T, Kiessling F, Hennink WE, Storm G. Nanotheranostics and image-guided drug delivery: current concepts and future directions. *Mol Pharm*. 2010;7(6):1899–912.
59. Huang H, Yue T, Xu K, et al. Fabrication and evaluation of tumor-targeted positive MRI contrast agent based on ultrasmall MnO nanoparticles. *Colloids Surf B Biointerfaces*. 2015;131:148–54.
60. Tian M, Wen X, Jackson EF, et al. Pharmacokinetics and magnetic resonance imaging of biodegradable macromolecular blood-pool contrast agent PG-Gd in non-human primates: a pilot study. *Contrast Media Mol Imaging*. 2011;6(4):289–97.
61. Liu Y, Zhang N. Gadolinium loaded nanoparticles in theranostic magnetic resonance imaging. *Biomaterials*. 2012;33(21):5363–75.
62. Gobbo OL, Wetterling F, Vaes P, et al. Biodistribution and pharmacokinetic studies of SPION using particle electron paramagnetic resonance, MRI and ICP-MS. *Nanomedicine*. 2015;10(11):1751–60.
63. Neubauer AM, Sim H, Winter PM, et al. Nanoparticle pharmacokinetic profiling in vivo using magnetic resonance imaging. *Magn Reson Med*. 2008;60(6):1353–61.
64. Pouliquen D, Le Jeune JJ, Perdrisot R, et al. Iron oxide nanoparticles for use as an MRI contrast agent: pharmacokinetics and metabolism. *Magn Reson Imaging*. 1991;9(3):275–83.
65. Ali MM, Yoo B, Pagel MD. Tracking the relative in vivo pharmacokinetics of nanoparticles with PARACEST MRI. *Mol Pharm*. 2009;6(5):1409–16.
66. Badachhape AA, Working PK, Srivastava M, et al. Pre-clinical dose-ranging efficacy, pharmacokinetics, tissue biodistribution, and toxicity of a targeted contrast agent for MRI of amyloid deposition in Alzheimer’s disease. *Sci Rep*. 2020;10:16185.
67. Wei H, Bruns OT, Kaul MG, et al. Exceedingly small iron oxide nanoparticles as positive MRI contrast agents. *Proc Natl Acad Sci*. 2017;114(9):2325–30.
68. Wells SA, Schubert T, Motosugi U, et al. Pharmacokinetics of ferumoxytol in the abdomen and pelvis: a dosing study with 1.5- and 3.0-T MRI relaxometry. *Radiology*. 2020;294(1):108–16.
69. Edge D, Shortt CM, Gobbo OL, et al. Pharmacokinetics and bio-distribution of novel super paramagnetic iron oxide nanoparticles (SPIONs) in the anaesthetized pig. *Clin Exp Pharmacol Physiol*. 2016;43(3):319–26.

70. Kim J, Kim HS, Lee N, et al. Multifunctional uniform nanoparticles composed of a magnetite nanocrystal core and a mesoporous silica shell for magnetic resonance and fluorescence imaging and for drug delivery. *Angew Chem*. 2008;47(44):8438–41.
71. Lee PW, Hsu SH, Wang JJ, et al. The characteristics, biodistribution, magnetic resonance imaging and biodegradability of superparamagnetic core–shell nanoparticles. *Biomaterials*. 2010;31(6):1316–24.
72. Lv YB, Chandrasekharan P, Li Y, et al. Magnetic resonance imaging quantification and biodistribution of magnetic nanoparticles using T1-enhanced contrast. *J Mater Chem B*. 2018;6(10):1470–8.
73. Carregal-Romero S, Plaza-García S, Piñol R, et al. MRI study of the influence of surface coating aging on the in vivo biodistribution of iron oxide nanoparticles. *Biosensors*. 2018;8(4):127.



Correction to: Pharmacokinetics and Pharmacodynamics of Nanoparticulate Drug Delivery Systems

Jayvadan K. Patel and Yashwant V. Pathak

Correction to:

**J. K. Patel, Y. V. Pathak (eds.), *Pharmacokinetics and Pharmacodynamics of Nanoparticulate Drug Delivery Systems*,
<https://doi.org/10.1007/978-3-030-83395-4>**

The below chapters were mistakenly published with an incorrect author name. The book has now been updated with the change mentioned below:

In Chapter 13: The 1st author's name has now been updated to Himanshu Paliwal (By mistake it was Himanshu P. Paliwal).

In Chapter 22: The 2nd author's name has now been updated to Himanshu Paliwal (By mistake it was Himanshu P. Patel).

The updated version of these chapters can be found at
https://doi.org/10.1007/978-3-030-83395-4_13
https://doi.org/10.1007/978-3-030-83395-4_22

Index

- A**
Absorption, 84
Absorption, distribution, metabolism and excretion (ADME), 371, 372
 drug-associated nanostructure, 81
 mathematical depiction, 83
Accelerated blood clearance (ABC), 86
Active drug transporters, 88
Active pharmaceutical ingredients (APIs), 42, 88, 369, 386
Active targeting, 152, 218, 307
Active tumor targeting, 326
Acyclovir-loaded nanospheres-based buccal films, 167
Acyclovir polymeric nanospheres, 167
Acyclovir's oral bioavailability, 167
ADMEWORKS DDI Simulator, 57
Administration routes, 85, 148, 150
Advanced drug delivery systems, 160
Advanced microscopic techniques, 241
Advanced nanoformulations, 161
Advanced nanomaterials, 160
Advanced technologies, 203
Advanced therapy medical products (ATMPs), 42
Adverse drug reaction (ADR), 376
Aerodynamics, 352
Agglomeration, 199
Aggregation-caused quenching (ACQ) fluorophores
 release profiling of NDDSs, 374
Aggregation-induced emission (AIE) fluorophores
 release profiling of NDDSs, 374–376
Agomelatine, 251
Airflow velocity, 353
Airway geometry, 353
Albendazole, 285
Albino Sprague-Dawley rats, 167
All-trans retinoic acid (ATRA), 249
Alveolar clearance, 353
Alveolar macrophage-mediated clearance, 353
Alveolar macrophages, 252
Alveoli, 349, 350
Alveolus, 349
Alzheimer's disease, 250, 253
Amikacin (liposomes), 349
Amikacin-loaded SLNs, 356
Amine-dextran-coated SPIONs, 153
Amine-ended PAMAM dendrimer, 230
Amitriptyline (AMI), 92
Amorphization, 393
Amoxicillin (polymeric nanoparticle), 349
Amphiphilic block copolymer NPs, 44
Amphiphilic drugs, 304
Amphiphilic tri-*n*-octylphosphine oxide (TOPO) coating
 (-COOH groups), 326
Amphotericin B, 167, 168, 373
Analysis of variance (ANOVA), 106
 parallel groups, 108, 110
 parallel/repeated groups, 108
Anisotropic AuNPs, 210
Anterior chamber, 235
Antibiotics, 7
Anticancer drugs, 152, 154, 306, 307
 gemcitabine, 153
 industry, 298
Anticancer effects, 80
Anti-neoplastic agents, 370
Anti-psoriatic agent, 255
Antiretrovirals, 92
Anti-transferrin receptor monoclonal antibody (OX26), 251
Antitumor efficacy, 95
Apolipoproteins, 390
Area between the baseline and effect curve (ABEC), 76
Area under the curve (AUC), 54
Area under the moment curve (AUMC), 54, 105
Aripiprazole (ARP), 164
Asenapine maleate (AS), 393
Asthma, 348
Atomic force microscopy (AFM), 32, 33
Atom manipulation, 11
Atorvastatin-loaded ethyl cellulose nanoparticles, 169
ATX mucoadhesive liposomes, 381
AuNPs synthesis methods
 Brust-Schiffirin method, 212
 chemical method, 212
 green method, 213
 growth method, 212, 213

- AuNPs synthesis methods (*Cont.*)
 physical method, 213
 Reetz and Helbig method, 212
 Turkevich method, 212
Azithromycin (PLGA-based nanoparticle), 349
- B**
- BA augmentation with ILS approach, 394
BA enhancement, 389
BA-enhancing techniques, 387
Basolateral membrane, 388
BBB-impermeant drugs, 368
Beclomethasone (lipid nanocarrier), 348
Besifloxacin, 239
Bestowing features, 368
 β cyclodextrin-based griseofulvin nanosponges, 168
Bevacizumab, 238
Bias exchange metadynamics (BEMD), 49
Bilayered phospholipid vesicles, 144
Bioadhesion, 166
Bioavailability (BA), 386
Biochemical fluxes, 55
Biodegradable polymers, 305
Biodistribution, 145, 205, 375, 377, 378, 380–382, 406
 anticancer agent, 355
 MRI
 CSNP-SPIO, 409, 411
 drug uptake, 409
 gadolinium-based formulation, 412
 GdIONPs, 412
 high-resolution 3-D images, 409
 in vivo studies, 413
 IONPs, 413
 Mn-based agents, 411
 PVP33, 412
 SPIONs, 412
 ZES-SPIONs, 412
 nanoparticles with red fluorescence (DiR), 358
 pattern, 87
 and pharmacokinetic, 357, 359, 361
 and PK, 83–84
 rifampicin solution, 360
 studies, 251, 252, 255
- Bioequivalence (BE)
 ANOVA, 106
 assessment, 106
 AUC, 108, 110
 average calculations, 106
 blood samples, 106
 bootstrap AUC and C_{max}, 131, 132
 concentration-time data, 130, 131
 drug ingredient/moiety, 106
 four-period crossover repeated study, 108, 110
 pharmacokinetic parameters, 130–131
 repeated BE, 106, 108–110
 sample size, 131, 132
 two-way crossover study, 106, 108
- Bioimaging technologies, 32
Biological membrane, 70
Biological method, NP synthesis, 28, 29
Biological molecules, 7
Biological NPs (naturally derived polymers), 152
Biologic therapy, 298
Biomembranes, 195
Biopharmaceuticals
 disorders treatment, 50
 Humulin, 42
 sophisticated medicines, 42
 types, 42
Biophase, 80
Biorelevant release tests, 93
Biosimilars, 42
Biosystems, 205
Biotherapy, 298
Blood–brain barrier (BBB), 31, 86, 155, 164, 251, 339
 averting, 366, 367
 cadherins, 367
 carrier-mediated transports, 367
 catenins, 367
 drugs, 367
 endothelial cells, 367
 endothelial layer, 367
 invasive techniques, 367
 occluding and claudins, 367
 pharmacological therapy, 367
 preventing, 367
 tight junctions, 367
 transcellular passage, 367
 Trojan horse technology, 367
Blood circulation half-life, 37
Blood-flow-limited PBPK model, 54
Blood flow rate-limited models, 197
Blood-ocular barrier (BOB), 237
Blood pool CT contrast agents, 218
Blood urea nitrogen (BUN), 339
Body surface area (BSA), 114
Body weight, 114
Bone morphogenetic protein 2 (BMP-2), 376
Bootstrap method, 130
Bootstrap simulation, 121, 127
Born–Oppenheimer approximation, 47
Bovine serum albumin (BSA)-MNC, 152
Brain cancer, 366
Brain drug delivery, 368, 369
Brain targeting
 laser-synthesized AuNPd, 379, 380
 limitations, 378
 liposomes containing drugs, 381, 382
 melanoma-induced mice, 379
 PLGA nanoparticle formulations, 379
 tissue-to-plasma coefficient values, 379
Breast cancer resistance protein (BCRP) inhibitors, 93
Brij 78-stabilized and F68-stabilized SLNs, 63
Bronchial smooth muscle (BSM), 350
Bronchiolitis obliterans, 348
Brownian motion, 351
Brust-Schiffirin method, 212
Bulk materials, 6
Buparvaquone, 251
Bupivacaine (BUP), 92
Buprenorphine, 283

- C**
Caco-2 monolayers, 93
Cadherins, 367
Cages, 147
Calcium phosphate nanoparticles encapsulating methotrexate (MTX-CAP-NP), 202
Camptothecin (CPT), 249
Cancer, 338
 cell targeting, 307
 chemotherapy, 80
 description, 296
 fatalities, 296
 multifactorial pathological condition, 306
 non-liposomal chemotherapy, 296
 nanomaterials development priority, 300
 types, 80
Cancer nanomedicine
 advantages, 296
 clinical approval, 296
 definition, 296
 delivery system formulations, 300
 marketed formulations and patents, 308
 nanotherapeutic platforms, 304
 next generation, 309
Cancer nanotechnology
 clinical practice, 317
 components loaded nanostructures, 316
 interdisciplinary research, 316
Cancerous cells, 298
Cancer therapy, NPs
 acidic environments, 297
 advantages, 297
 combination therapy, 297
 comparative study, 297, 298
 DDS, 296
 disadvantages, 297
 drug delivery methods, 297
 drug pharmacokinetic properties, 296
 imaging modalities, 296
 pharmacokinetics and pharmacodynamics, 297
 protein-based nano-preparations, 296
Capsules, 118
Capture antibody, 376
Captured antigens, 376
Carbon-based nanoparticles, 26, 188
Carbon-based nanoparticulate materials, 9
Carbon nanotubes (CNTs), 26, 190, 305, 306
Carboplatin, 241
Cardiotoxicity, 296
Cardiovascular diseases (CVDs), 340
Carica papaya leaf extract, 190
Carrier-mediated transports, 367
Carvedilol (polymeric nanoparticle), 348
Carvedilol nanosuspension-incorporated mucoadhesive buccal films, 167
Catenary compartmental model, 56
Catenins, 367
Cationic lipids, 247
Cationic nanosystems, 200
Cationic SLNs, 251
Caveola-mediated endocytosis, 391
Celecoxib, 359
Cell internalization, 253
Cellular nanotoxicity, 204
Cellular uptake, 35, 203
Central nervous system (CNS), 339
 diagnosis and treatment, 366
 disorders, 366
Centrifugal ultrafiltration, 34
Ceramic nanoparticles, 188, 190
Ceramic NPs, 27
Cerebrovascular disease, 366
Cetyltrimethylammonium bromide (CTAB), 203, 318
CFA-induced arthritis model, 254
CG molecular dynamics, 47
C-H alkyne activation, 212
Chemical agents, 28
Chemical method, 212
 NP synthesis, 28
Chemotherapeutic drugs, 154, 299
Chemotherapy, 151, 298
Chitosan-based mucoadhesive microspheres, 166
Chitosan-based nanosystems, 155
Chitosan oligosaccharide/heparin (CSO/H) NPs, 376
Chronic inflammatory pulmonary diseases, 348
Chronic kidney disease (CKD), 336
Chronic obstructive airway disease, 348
Chronic obstructive pulmonary disease (COPD), 348
Chrysophanol, 166
Chrysophanol-loaded micelles, 166
Chylomicron pathway, 389, 390
Chylomicrons (CMs), 386
Ciprofloxacin, 238
Cisplatin (CDDP), 280, 348
Clarithromycin bioavailability, 255
Clarithromycin-loaded SLNs, 255
Classification of nanoparticulates
 chemical composition, 9
 dimensions
 electron association, 9
 1-D, 10
 surface engineering, 10
 three-dimensional (3-D), 10–11
 two-dimensional (2-D), 10
 zero-dimensional (0-D), 10
 economic growth, 8
 material-based classification
 carbon-based, 9
 composite-based, 9
 inorganic-based, 9
 organic-based, 9
 nanometer-sized, 8
 nanostructured, 8
 origin
 natural nanoparticulate materials, 8
 synthetic (engineered) nanoparticulate materials, 8
 ultrafine-grained, 8
Claudins, 367
Clay nanodisks (CNDs), 281

- Clearance pathway
 - conventional nanoprobcs, 317–318
 - HD, 317
 - renal (*see* Renal clearable nanoprobcs)
- Clinical cancer therapy, 327
- CLOEPK, 57
- C_{max}, 252, 255
- Co-administration of drugs, 387
- Coarse-grained (CG) models, 47, 49, 50
- Coated curcumin-loaded chitosan nanoparticles, 165
- Coated solid–lipid nanoparticles, 166
- Co-deliver DOX and β -cyclodextrin curcumin (CD CUR), 280
- Colchicine, 392
- Collective variables (CVs), 48
- Collision-induced dissociation (CID), 376
- Colloidal AuNPs, 211
- Colloidal stability, 34
- Color Doppler ultrasound imaging (CDI), 316
- Colorimetric methods, 376
- Compartmental body models (CBM), 117, 119–120
- Compartmental model, 54
- Compartmental pharmacokinetics (CA-PK), 117, 119–120
 - catenary, 56
 - compartments, 55
 - demonstration, 55
 - Fick's law of diffusion, 55
 - first-order kinetics, 55
 - IV Bolus administration
 - multicompartment, 60, 61
 - one-compartment, 60
 - IV infusion administration, 61
 - mammillary, 56
 - materials/drugs, 54
 - mathematical model, 55
 - oral absorption, 61, 62
 - PBPK (*see* Physiologically based pharmacokinetic (PBPK) modelling)
 - three-compartment model, 55
- Compartmental systems, 55
- Composite-based nanoparticulate materials, 9
- Computational topography (CT), 220
- Computed tomography (CT), 155, 220, 300, 316
- Concentration-effect relationship, 118
- Concentration *vs.* pharmacological response, 70
- Confinement effect, 11, 12
- Confocal laser scanning microscopy (CLSM), 405
- Conjugating QDs, 326
- Conservative force, 49
- Contrast enhancement, 220
- Contrasting agents
 - classified, 402
 - Fe-based, 406
 - functioning, 402
 - Gd-based, 402–404
 - Mn-based, 404–406
 - paramagnetic behaviour, 402
- Conventional chemotherapy, 300
- Conventional drug delivery systems, 254
- Conventionally engaged dosage forms, 161
- Conventional non-renal clearable nanoprobcs
 - CTAB-capped Au nanorods, 318
 - HDs, 317
 - ID, 317
 - inorganic NPs, 318
 - QD-BSA, 318
 - QDs, 318
 - surface coating and aggregation, 318
 - toxicity-related evidence, 318
- Conventional therapies, 144
- Conveyance frameworks, 240
- Convolution
 - individual dissolution times, 123
 - superposition principle, 123, 125
 - 2-CBM equation, 125
- Copolymeric micelle
 - andrographolide, 282
 - antiepileptic medication oxcarbazepine, 284
 - applications, drug delivery, 289
 - bacterial infection, 284
 - brachial plexus avulsion, 286
 - CNV, 282, 283
 - corilagin/LC/PPP, 282
 - drugs, 274
 - hydrogel, 286, 288
 - hydrophobic polyester, 285
 - LFH, 283
 - microspheres, 285, 286
 - naltrexone, 286
 - NMP, 283
 - oxcarbazepine-emulsome delivery, 285
 - PK/PD, 280
 - CD CUR, 281
 - dendritic nanoparticles, 280
 - DOX, 280
 - features, 279
 - hydrogels, 280
 - long-acting Gem delivery system, 281
 - solid tumours, 282
 - thermogels, 281
 - PLGA, 274
 - PLGA-PEG-PLGA, 275
 - biomedical applications, 276
 - synthesis/purification, 274, 275
 - thermogel, 288
 - sCT therapy, 287
 - sol-gel transitions, 274
- Corneal neovascularization (CNV), 282
- Corneal stroma, 240
- Corona, 368
- Correlations
 - level A, 122
 - Hill equation, 125, 126
 - interpolation method, 125
 - Weibull equation, 126, 127
 - level B, 127, 129
 - level C, 127, 129
- Corrosive degradation, NPs, 200
- Coulomb-controlled iontophoresis, 240

- CPT-SS-PA SLN, 249
- Critical micelle concentration (CMC), 305
- Crystallographic subtleties, 231
- CSNP-SPIO, 409, 411
- Cu-CuS, 147
- Cul-de-sac, 234
- Curative (“radical”) surgery, 296
- Curcumin (polymeric nanoparticle), 348
- Curcumin-loaded chitosan microsphere, 165
- Curcumin-loaded SLNs, 249
- Customized medication, 155
- Cyclic arginine-glycine-aspartic acid (cRGD), 407
- Cycloheximide, 391
- Cyclosporin A (CsA), 238
- Cynomolgus monkeys, 239
- Cysteine-coated QDs, 322
- Cystic fibrosis, 349
- Cytotoxic effects, 80
- Cytotoxicity, 370

- D**
- Darunavir, 393
- Data analysis modules
 - extravascular/IV Bolus/IV Infusion, 103, 104
 - NCA-PK, 103
 - oral administration of drug, 103, 104
 - plasma concentration *vs.* time profile, 103, 105
- Debye–Hückel interaction energy, 48
- Deconvolution, 122
 - Loo-Riegelman method, 123, 125
 - numeric, 125
 - Wagner-Nelson method, 122, 123
- Delivery vehicles, 401
- δ -cyclodextrin nanoparticle dexamethasone (DexNP), 239
- Dendrimer-N-acetylcysteine (D-NAC), 64
- Dendrimers, 17, 64, 153, 306, 357
- Dermal penetration, 200
- Destructive sampling, 110
- Diagnostic capabilities, 156
- Diagnostic modalities in theranostic approaches
 - CT, 155
 - diagnostic capabilities, 156
 - MR imaging, 155
 - noninvasive imaging, 155
 - optical imaging, 155
 - PET/SPECT techniques, 155
 - therapeutic capabilities, 156, 157
 - US imaging, 155
- Dialysis layer (DM) strategies, 233
- 2',7'- Dichloro dihydrofluorescein diacetate (DCFH-DA), 233
- Difference factor, 121, 126, 127
- Differential equation-based analysis (dEq), 132, 133
- Differential scanning calorimetry (DSC), 231, 241
- Digestible lipids, 387
- Dihydroethidium (DHE), 233
- Dihydrolipoic acid (DHLA)-PEG2-coated QDs, 322
- Dimercaptosuccinic acid (DMSA)-coated SPIONs, 409
- Dimethylaminopyridine (DMAP), 220
- Direct covalent/non-covalent conjugation of drugs, 83
- Direct interception, 351
- Dispersion releaser technology, 93
- Dissipative particle dynamics (DPD), 47
- Dissolution
 - comparison, 121, 127
 - data analysis, 118, 120, 124–126
 - drug absorption, 118
 - mathematical models, 120, 124
 - profile comparison, 120
 - Weibull_4 model, 120, 125, 126
- Distinctive properties, 6, 7
- Distracted off-target toxicity, 7
- Distribution
 - steady-state volume, 407
- DNA complexes, 324
- DNA vaccines, 212
- Docetaxel-loaded cholesterol-PEG co-modified poly (n-butyl) cyanoacrylate nanoparticles, 358
- Dodecanethiol, 212
- Dorzolamide (DorzNP), 239
- Dosage forms, 160
- Dose–effect relationship, 92
- Dose escalation, 115, 117, 118
- Dose normalization, 109, 112
- Dose proportionality
 - dose normalization, 109, 112
 - linear model, 109, 111
 - pharmacokinetic exposure parameters, 108
 - power model, 109, 111
- Dose-response relationship, 102
- DOX liposomes, 373
- Doxil® upsurges, 88
- Doxorubicin (DOX), 151, 154, 280, 373, 400, 404, 405
- Doxorubicin (DOX) NPs, 297
- DPM-based marketed formulations, 184
- Dronedarone HCl, 249
- Drug action, 85
- Drug and gene delivery vehicles, theranostic NPs
 - customized medication, 155
 - dendrimers, 153
 - development, 153
 - diagnostic modalities, 155, 156
 - drug carriers, 150, 154, 155
 - enzymatic degradation, 153
 - liposomes, 153
 - micelles, 153
 - nanoemulsions, 153
 - oral bioavailability, 153
- Drug-associated nanostructure, 81
- Drug candidates, 70
- Drug carriers, 83, 150, 154, 155, 407
- Drug clearance, 88
- Drug concentration, 80
 - vs.* time profile, 87
- Drug conveyance frameworks, 241

- Drug delivery, 354
 - nanotechnology, 82–83
 - NPDDS (*see* Nanoparticulate drug delivery systems (NPDDS))
 - strategies, 147
 - Drug delivery systems (DDS), 228, 400
 - Drug development, 102
 - Drug disposition, 89
 - Drug distribution, 60, 84
 - Drug efficacy, 84
 - Drug encapsulation, 145, 161
 - Drug-loaded carriers, 148
 - Drug-loaded lipid-polymer hybrid, 163
 - Drug-loaded mixed micelle, 162
 - Drug-loaded nanoparticles, 64, 405
 - Drug molecule, 402
 - Drug penetration, 83
 - Drug PK modifiers, 81
 - Drug-polymer conjugate-based matrix, 162
 - Drug release, 96
 - monitoring, 401, 402
 - stimulating factors, 402
 - Drug's metabolic instability, 386
 - Drug's physicochemical property, 386
 - Drug-polymer matrix (DPM)-based NPDDS
 - acyclovir, 166, 167
 - amorphous solid dispersion, 162
 - amphotericin B, 167
 - anticancer drugs, 166
 - ARP, 164
 - atorvastatin calcium polymer-assisting solid dispersion, 165
 - AUC, 165
 - β cyclodextrin, 168
 - bioavailability, 163, 166
 - chrysophanol, 166
 - copolymer coating, 163
 - drug delivery systems, 162
 - drug plus reduced hepatic metabolism, 167
 - eluxadoline, 165
 - eudragit-coated nanoparticles, 165
 - evaluation strategies, 163
 - HCPT-PBCA-NPs, 169
 - HS15 and hydroxypropyl methylcellulose, 167
 - hybrid polymeric microsphere, 162, 163
 - ibandronate, 168
 - information, 163
 - in vitro* antileishmanial activity, 168
 - mucoadhesive microsphere, 166
 - nanonization approaches, 167
 - nanosuspension, 167
 - natural polymers, 162
 - NRG, 169
 - OLM, 164, 166
 - oral administration, 168
 - oral bioavailability of curcumin, 165
 - oral dosing, 168
 - overview, 164
 - paclitaxel, 166
 - PAMPA, 164
 - parameters, 163
 - PDM-based matrix, 169
 - pharmacokinetics, 162, 170–183
 - polyethylene glycol, 168
 - polymeric excipients, 165
 - polymeric properties, 162
 - polymer nanosystems, 162
 - roles, 162
 - synthetic polymer coating, 163
 - water solubility drugs, 166
 - zolidem-loaded poly nanospheres, 165
 - Drug-release kinetics, 87
 - Drugs of Biopharmaceutics Classification System (BCS), 386
 - Drug supply systems, 348
 - Drug suspension, 252
 - Dry powder inhalers (DPI), 359
 - Dual-ligand triptolide-containing liposomes, 355
 - Dynamic light scattering (DLS), 33, 214
- E**
- 8-Hydroxy-2'- deoxyguanosine (8-OHdG), 233
 - Elastic liposomes, 144
 - Electrical conductivity, 11
 - Electron association, 9
 - Electron paramagnetic resonance (EPR), 202
 - Electrostatic disposition, 351
 - Electrostatic interaction, 221
 - Elimination, 407, 408
 - E_{max} model, 73
 - E_{max} or Weibull functions, 130
 - Employed electric-cell-substrate-impedance-sensing (ECIS), 204
 - Emulsification-reverse salting-out method, 44
 - Encapsulated drug, 154
 - Endocytosis, 7
 - Endothelial cells, 367
 - Energy states, 8
 - Engineered nanoparticles, 210
 - Enhanced permeability and retention (EPR) effect, 38, 86, 154, 264, 300, 307, 317, 370
 - Enhanced sampling methods, 48, 49
 - Enterocytes, 388, 389
 - Enzyme-linked immunosorbent assay (ELISA)
 - polymer, 376, 377
 - release profiling of NDDSs, 376
 - Epigallocatechin-3-O-gallate (EGCG), 152
 - Epikuron 200, 255
 - Epileptic transport, 369
 - EPR-based tumor targeting, 324
 - EPR concept, 94
 - Eudragit-based heparin-loaded polymeric nanoparticles, 168
 - Exemplification proficiency, 230
 - Exenatide (EXE), 341
 - Exhalation relaxes, 349
 - Exosomes, 360
 - Expel FeOx NPs, 203
 - Extensive research efforts, 226

External magnetic field (EMF), 306
Extravascular/IV Bolus/IV infusion, 103, 104
Ex vivo permeation studies, 167
Ex vivo tissue distribution, 163

F

Factors affecting pharmacokinetics, inorganic NPs
 administration route, 196, 197
 dose impacts, 197
 nanomaterial composition, 197
 particle size and shape, 195, 196
 surface modification, 196
Fatty acids, 247
f1 comparison analysis, 121, 127
FDA and EMA guidelines, 371
FDA-approved metallic nanoparticles, 196
FDA approved PEGylated and non-PEGylated liposomal
 formulation of doxorubicin, 309
Ferromagnetic nanoparticulate materials, 15
Ferromagnetism, 15
Ferumoxytol, 409
Fick's first law of dispersion, 236
Filtration through kidney, 319
First-order absorption model, 62
First-pass metabolism, 165, 166
Fluorescence imaging, 220
Fluorescence spectroscopy, 378
Folate-controlled porphyrins, 147
Folate-decorated PLGA NPs (FA-PEG-PLGA NPs), 341
Follicle-associated epithelium (FAE), 390
Follow-on biologics, 42
Food and Drug Administration (FDA), 387
Food-Effect BA and Fed Bioequivalence Studies, 387
Force field (FF), 47, 48
Förster/fluorescence resonance energy transfer (FRET),
 374, 375
Fourier-transform infrared (FTIR), 231, 277
Four-period crossover repeated study, 108, 110
Freeze-dried liposomes, 354
Full atomistic models, 47, 48
Functionalized/tailored nanoparticles, 65

G

Gadolinium (Gd)-based contrasting agent, 402–404, 408
Gadolinium (Gd)-based formulation, 412
Galactose moiety, 154
Gallic acid, 403
Gastric irritability, 359
Gastrointestinal (GI) absorption, 216
Gastrointestinal (GI) degradation, 30, 82
Gastrointestinal tract (GIT), 216
GastroPlus™, 57, 93
Gd-doped iron oxide nanoparticles (GdIONPs), 412
Gel filtration, 34
Gel permeation chromatography (GPC), 276
Gemcitabine-loaded thiolated chitosan nanoparticles, 168
Generic drug substitutability, 42
Generic medicine, 42

Gene therapy, 151
Gene therapy products (GTPs), 42
Genetic polymorphism, 70
Genistein (GEN), 393
GEN-loaded SLNs (GEN-SLNs), 393
Geometric standard deviation (GSD), 352
Geometric variable, 6
Geometry/conformation, 151
GI absorption mechanism, 64
GIT delays gastric emptying time, 386
GI tract, 93, 94, 386
Glaucoma, 240
Glomerular basement membrane (GBM), 319
Glomerular capillary, 323
Glucocorticoid therapy, 252
Glutathione (GS)-coated AuNPs, 319
Glycocalyx, 390
Glycolide (GA), 274
Gold colloidal NPs, 29
Gold nanoparticles (GNPs), 6, 32, 63, 152, 189, 403
 anisotropic AuNPs, 210
 antioxidant properties, 210
 applications, 211
 biotechnology and biomedicine applications, 210
 cellular uptake, 215
 characteristics, 210
 features, 210
 homogeneous systems, 212
 physicochemical properties, 210
 synthesis methods (*see* AuNPs synthesis methods)
 toxicity, 221, 222
 X-ray contrast imaging (*see* X-ray contrast imaging,
 AuNPs)
Gold nanoshells, 305
Gold- or silica-coated iron oxide NPs, 32
Graphene oxide (GO), 160
Graphene quantum dots (GQDs), 160
Grease balls, 387
Green chemistry, 82
Green method, 213
Green synthesis, 189, 190
Growth method, 212, 213
GS-AuNPs, 323
Gut-associated lymphoid tissue (GALT), 390

H

HA-coated NPs, 307
HA-coated SLNs, 252
Half-maximal inhibitory concentration (IC₅₀), 75
Hemostatic dexamethasone nanoparticles (hDNP), 349
Hepatobiliary, 317
Herceptin-labeled NPs, 156
Herceptin-loaded micellar nanocomplex (Herceptin–
 MNC), 152
Higher surface area-containing particles, 246
High-performance liquid chromatography (HPLC), 34,
 376, 405
High quantity factor (HQF), 210
High-resolution 3-D images, 409

- Higuchi matrix, 162
Hill equation, 125, 126
Histopathological analysis, 254
HIV-related Kaposi sarcoma, 308
Hollow particles, 352
Hollow structured Prussian blue (HMPB), 405
Hormonal therapy, 298
Human equivalent dose (HED), 115, 117
Human immunodeficiency virus (HIV), 386
Hup-A-loaded SMEDDS, 393
Huperzine A (Hup-A), 393
Hyaluronic acid (HA), 252
Hydrodynamic diameter (HD), 146, 195, 317
Hydrophilic drugs, 304
Hydrophilic molecules, 354
Hydrophilic surfactants, 368
Hydrophobic polymers, 390
Hydrophobic therapeutics moiety, 247
Hydroxamic acid, 406
- I**
- Ibandronate-loaded citrus pectin-loaded nanostructure, 168
ICP-mass spectrometry (ICP-MS), 215
Idiopathic pulmonary fibrosis (IPF), 348
Iloprost (liposomes), 348
Imaging modalities, 150, 296
 I_{\max} , 75
Imperfect vascular capillaries, 306
Indirect pharmacodynamic response (IDR) models
 ABEC, 76
 drug molecule, 74
 estimation, 76
 I_{\max} , 75
 loss and production, 74
 model I, 75
 model II, 75
 model III, 75
 model IV, 76
 parameters and factor controlling, 74
 representation, 75
Individual quantum effects, 188
Inductively coupled plasma mass spectrometry (ICP-MS), 379
Inflammation mediated nanotoxicity, 205
Inhalational nanosystems, 200
Inhalational route, 357, 359
Inhalation pattern, 353
Inhibition responses, 74
Inhibitory Emax model, 129
Inorganic-based nanoparticulate materials, 9
Inorganic nanoparticles
 applications, 191, 193
 classification, 188–190
 degradation mechanism, 198–200
 evaluation, 191
 formulation and development
 bottom-up approach, 190
 green synthesis, 190
 top-down approach, 190
 PBPK model, 197–198
 pharmacokinetic considerations (*see* Pharmacokinetic considerations, inorganic nanoparticles)
 pharmacokinetic fate, 202–203
Inorganic NP-based contrast agents, 317
Inorganic NPDDDS, 198
Inorganic theranostics, 203
In situ polymerization, 44
Insulin-containing liposomes, 354
Insulin-containing SLNs, 356
Insulin oral delivery, 253
Internal bleeding in lungs, 349
International Organization for Standardization (ISO), 5
Inter-patient variability, 84
Interpolation method, 125
Interspecies scaling
 allometric approach, 112
 HED, 115, 117
 NCA, 114, 117
 in pharmacokinetics, 112
 PK parameters, 114
Interstitial fluid pressure (IFP), 94
Interstitial lung disease, 348
Intestinal absorption, 391
Intestinal absorptive surface area, 386
Intestinal lymphatic absorption, 388
Intestinal lymphatic system (ILS), 386
 advantages, 389
 BA, 389
 chylomicron pathway, 390
 factors affecting transport, 389
 lymphatics' network, 389
 M cell pathway, 390
 serosal surface, 389
Intestinal lymphatic transport, 387, 389
Intestinal lymphatic uptake evaluation approaches
 chylomicron blocking pathway, 391, 392
 in vitro caco-2 cell model, 391
 mesenteric lymph, 391
Intestinal permeability, 388
Intracellularization, 369
Intracellular transport, 369
Intramuscular injection, 92
Intranasal instillation, 196
Intratracheal instillation, 196
Intratracheal spraying, 196
Intravenous (IV), 61
Intravenous administration, 317
Intravenous injection, 323
Inverse of variance-covariance matrix, 121
In vitro analysis, AuNPs
 DLS, 214
 ICP-MS, 215
 TEM, 215
 zeta potential, 214
In vitro caco-2 cell model, 391
In vitro characterization, mucoadhesive nanoparticles
 DSC, 231
 evaluation, 230

- exemplification proficiency, 230
 - FTIR, 231
 - in vitro cytotoxicity, 232
 - mucoadhesion studies, 231
 - oxidative stress tests, 233
 - particle size distribution, 230
 - TEM, 231
 - XRD, 232
 - zeta potential, 230
 - In vitro cytotoxicity, 232
 - In vitro dissolution data, 121
 - In vitro–in vivo correlation (IVIVC), 93, 95–97, 121, 128, 130, 131
 - defined, 95
 - In vitro/in vivo extrapolation (IVIVE), 89
 - In vitro study, 95–96
 - In vivo
 - MRI (*see* Magnetic resonance imaging (MRI))
 - pharmacokinetic analysis, 168
 - siRNA, 153
 - systems, 94
 - In vivo pharmacokinetics, AuNPs
 - absorption and penetration from skin, 216
 - distribution, 216
 - drug deliveries, 215
 - elimination, 217
 - gastrointestinal absorption, 216
 - metabolism, 217
 - PBPK modeling, 215
 - PEGylation, 215
 - pulmonary absorption, 216
 - therapeutic purpose, 215
 - In vivo studies
 - biodistribution, 409
 - characteristics, 413
 - distribution, 412
 - MRI, 407, 411
 - pharmacokinetics, 400
 - Ionic silver, 379
 - Iron (Fe)-based contrasting agent, 406
 - Iron oxide nanoparticles (IONPs), 189, 317, 408, 413
 - Iron-succinyl deferoxamine (Fe-SDFO), 406
 - Itraconazole (ITZ), 342
 - Ivacaftor (nanostructured lip carriers), 349
 - IV infusion administration, 61
- K**
- Kartogenin (KGN), 287
 - Kel calculation, 104, 106
 - KGN-loaded thermoresponsive gel, 287
 - Kidney filtration threshold (KFT), 317
 - Kollocoat IR, 164
 - Kollidon VA-64, 164
 - Kupffer cells, 201
- L**
- Lampalizumab, 238
 - Large-scale gold particles, 188
 - Laser ablation inductively coupled plasma mass spectroscopy (LA-ICP-MS), 378
 - Laser-based technique, 202
 - Laser-synthesized Au nanoparticles (AuNPd), 379, 380
 - L-BFGS-B method, 135
 - Lecithin-amphotericin-based hybrid nanocarriers, 168
 - Level A correlation
 - deconvolution, 122
 - Hill equation, 125, 126
 - interpolation method, 125
 - IVIVC, 122
 - linear correlation, 122
 - Level B correlation, 127, 129
 - Level C correlation, 127, 129
 - Levenberg-Marquardt method, 117, 118, 135
 - Levofloxacin hydrochloride (LFH), 283
 - Linear correlation, 122
 - Linear model, 71
 - Linear time-invariant pharmacokinetics, 62
 - Linear trapezoidal rule
 - log-linear trapezoidal rule, 103–105
 - plasma concentrations, 103
 - user-defined value, 103
 - Lipid-based drug delivery, 394
 - Lipid-based excipients, 387
 - Lipid-based formulations, 387
 - Lipid-based nanoparticles (LNPs), 27, 144, 188, 387, 388
 - Lipid-based system, 387
 - Lipid components, 246
 - Lipidic component-based oral delivery, 387
 - Lipid matrices, 45
 - Lipid nanoparticles, 255
 - Lipid-polymer hybrid matrix, 165
 - Lipid-polymer hybrid nanoparticles (LPHNPs), 268, 305, 387
 - Lipid types, 247
 - Lipid vehicles, 246
 - Lipinski rules, 307
 - Lipophilic drugs, 304, 386, 387
 - Lipophilic immunosuppressants, 154
 - Lipophilic medications, 235
 - Lipophilic molecules, 354
 - Liposomal drug delivery
 - PBPK (*see* Physiologically based pharmacokinetic (PBPK) modelling)
 - tumour tissue compartment model, 91
 - Liposomes, 15, 16, 145, 153, 304, 305, 348, 354, 355
 - applications, 144
 - bilayered phospholipid vesicles, 144
 - biodistribution, 94
 - clinical implications, 144
 - containing drugs, 381, 382
 - elastic, 144
 - in vitro and in vivo stability, 144
 - long-circulating, 144
 - nebulized, 144
 - properties, 144
 - stimuli-responsive, 144
 - theranostic NPs (*see* Theranostic NPs)

- Liquid-based drug nanocarriers, 83
 - Liquid chromatography with tandem mass spectrometry (LC-MS/MS)
 - polymer, 376
 - release profiling of NDDSs, 371–373
 - LNPs application, enhancing BA
 - AS-SLNs, 393
 - darunavir-SLNs, 393
 - GEN, 393
 - Hup-A, 393
 - lymphatic transport, 392
 - NE, 392
 - NE-NLCs, 392
 - OLM-NLCs, 393
 - RF-LPHNPs, 393
 - SMEDDS, 392
 - S-SMEDDS, 393
 - TIL-LPHNPs, 393
 - water-soluble drugs, 392
 - LNPs, pharmacokinetics, 389
 - Localized surface plasma resonance (LSPR), 29
 - excitation, 29
 - spectrum, 29
 - Log-linear model, 72, 73
 - Log-linear trapezoidal rule, 103–105
 - Long-chain triglyceride (LCT), 387
 - Long circulating inorganic nanoparticles pharmacokinetics
 - absorption and cellular uptake, 200
 - elimination routes, 201, 202
 - formulation strategies, 200
 - NPDDS, 200
 - tissue biodistribution, 200, 201
 - toxicokinetics
 - AgNPs, 204
 - amino acids, 204
 - bioengineering, 203
 - cellular and nuclear membranes, 203
 - cytoskeleton structure disruption, 204, 205
 - ECIS approach, 204
 - electron transfer reactions, 203
 - gold NPs, 204
 - human prostate cancer cells, 203
 - inflammation mediated nanotoxicity, 205
 - nanomedicines, 203
 - ROS and free radicals, 204
 - signaling pathways, 205
 - toxicity mechanisms, 204, 205
 - Long-circulating liposomes, 144
 - Loo-Riegelman method, 123, 125
 - Lotemax®, 240
 - Loteprednol etabonate (LE), 239, 240
 - Lower airways, 353
 - Lower limits of quantitation (LLOQ), 377
 - Lower respiratory tract, 349, 350
 - LPHNPs of tilianin (TIL) (TIL-LPHNPs), 393
 - Lung cancer, 348
 - Lung diseases, 348
 - asthma, 348
 - COPD, 348
 - cystic fibrosis, 349
 - internal bleeding, 349
 - interstitial lung disease, 348
 - lung cancer, 348
 - mechanism of deposition, 351
 - pneumonia, 349
 - pulmonary hypertension, 348
 - RDS, 349
 - Lung transplantation, 154
 - Luteinizing chemical delivering chemical (LHRH), 236
 - Lymphatic capillaries, 388
 - Lymphatic flows, 84
 - Lymphatic system, 94
 - Lymphatic transportation, 389
 - Lymphatic transport pathway, 386
 - Lymphatic uptake, 389
 - Lyophilization, 45
 - Lysine cross-linked MUA, 318
 - Lysophospholipids, 388
 - Lysosomal degradation, 202
- ## M
- Macromolecules, 82, 199, 200
 - Macro-oriented brains, 5
 - Macrophage internalization, SLNs, 251
 - Macrophages, 86, 203
 - Magic bullets, 5
 - Magnetically driven nanoparticle containing thrombin, 349
 - Magnetic capabilities, 401
 - Magnetic contrasting agent, 407
 - Magnetic field-induced thermal therapy, 153
 - Magnetic NPs (MNPs), 152, 153
 - Magnetic particle imaging (MPI), 377
 - Magnetic properties, 15
 - Magnetic resonance colonography, 254
 - Magnetic resonance imaging (MRI), 220, 300, 316, 377, 378, 400
 - advantages, 401
 - application, 400
 - biodistribution (*see* Biodistribution)
 - in clinical settings, 400
 - contrasting agents (*see* Contrasting agents)
 - drug release (*see* Drug release)
 - internal events, 400
 - pharmacokinetic profiling, 406–411
 - theory and principles, 401
 - Magnetic thermal therapy, 153
 - Magnetization, 401
 - Mahalanobis distance, 121
 - Malondialdehyde (MDA), 233, 339
 - Mammillary compartmental model, 56
 - Manganese (Mn)-based contrasting agent, 404–406
 - Manufactured bodily fluid, 231
 - Mapracorat, 238

- MARTINI FF, 49
Mass median aerodynamic diameter (MMAD), 352
Maximum safe recommended dose (MSRD), 117, 118
M cell pathway, 390
MDA-MB-435 orthotopic tumor xenografts, 326
MD simulations, 48
MDT, 129
Mean absorption time, 356
Mean residence time (MRT), 54, 105, 163, 248
Mechanism-based model, 90
Mechanical clearance, 353, 354
Mechanical properties, 12, 13
Medication, 148
 carriers, 296
 discharge, 233
Medium-chain triglyceride (MCT), 388
Melanoma-induced mice, 379
Meloxicam-loaded hydrogel, 254
Membrane-limited organ model, 59
Mercaptosuccinic acid (MSA)-capped QDs, 323
Mercaptoundecanoic acid (MUA), 318
Mesenteric lymph duct cannulation, 391
Mesenteric lymph vessels, 388
Mesoporous manganese silicate coated silica nanoparticle (MMSSN), 405
Mesoporous silica NPs, 152
Metabolism, 217
Metal-based materials, 9
Metal ions, 202
Metallic nanomaterials, 200
Metallic nanoparticles (NPs), 16, 26, 63, 64, 188, 192
Methotrexate (MTX), 280, 404
Micelles, 145, 153
Microbe-mediated synthesis, 29
Microdroplets, 203
Microfilm, 238
Microorganism-based NP synthesis, 29
Mixed glycerides, 388
Mixed log-linear, 104
Mn-based agents, 411
MNP-based theranostics, 153
Model-independent methods, 120
Modified solvent emulsification and evaporation method, 253
Molday's method, 408
Molecular imaging probes, 316
Molecular modeling, 47
Molecular weight, 352
Monoglycerides, 388
Monomer polymerization methods, 228
Monomolecular phagocyte system, 262
Mononuclear phagocytes (MNP), 390
Mononuclear phagocyte system (MPS), 193, 198, 370, 409
Moxifloxacin, 71
MR imaging, 155
MSALL, 376
Mucins, 85
Mucoadhesion, 169
 mechanism, 227
 potential, 231
 studies, 231
Mucoadhesive
 biocompatibility, 226
 dosage forms, 226
 materials, 241
 microspheres, 227
 naturally occurring polymeric materials, 226
 purposes, 226
 R&D activities, 226
 synthetic and biological macromolecules, 226
 synthetic/natural polymers, 226
Mucoadhesive nanoparticles
 advantages, 228, 230
 drug delivery system, 241
 enzymatic/chemical degradation, 227
 in vitro discharge study, 233–234
 ocular pharmacokinetics (*see* Ocular pharmacokinetics, mucoadhesive nanoparticles)
 oxidative pressure markers, 233
 pharmaceutical purposes, 227
 phenomenon, 228
 therapeutic efficiency, 227
Mucoadhesive polymers, 228
Mucoadhesivity, 241
Mucociliary clearance, 353
Mucous membrane, 350
Mucus barrier, 85
Multicompartment IV Bolus, 60, 61
Multifunctional chitosan-based micelle, 166
Multifunctional chitosan derivative-based polymeric micelles, 166
Multilamellar vesicles, 95
Multiple reaction monitoring (MRM), 376
Multivalent functionalization, 368
Multivariate statistical difference (MSD) determination, 121, 128
- N**
NADPH oxidase, 202
Nano-based drug delivery systems, 82
Nanocages, 17
Nanocapsules, 16, 17, 43, 44, 358
Nanocarrier, 83, 87, 145, 227, 255, 394, 400, 402–404
Nanocarrier-based biopharmaceuticals, 50
Nanocarrier-based drug delivery systems (DDS), 296
Nanoclusters (NCs), 319, 327
Nanocrystals, 11, 17, 359
Nanodelivery systems, 261
Nanodrugs
 delivery systems, 65
 development, 92, 93
Nanoemulsions, 45, 153, 357, 358
Nanoencapsulated silver, 379

- Nanofluids, 13, 14, 30
- Nanoformulation, 71, 83, 160, 306
 - characteristics, 85
 - clearance, 86
 - distribution mechanism, 201
 - patents, 309
- Nanoformulation PK
 - ADME properties, 84
 - administration, distribution and elimination, 84
 - administration routes, 85
 - drug efficacy, 84
 - and human body, 84
 - oral administration, 85
 - toxicity, 84
- Nanohybrid carriers, 404
- Nanomaterials, 82, 145, 227
 - characterizes, 147
 - components, 5
 - definitions, 5, 145
 - dendrimers, 17
 - dimensions, 4
 - ISO, 5
 - liposomes, 15, 16
 - metallic nanoparticles, 16
 - nanocages, 17
 - nanocapsules, 16, 17
 - nanocrystals, 17
 - nanoparticles, 5
 - nanotubes, 17
 - polymeric micelles, 16
 - polymeric nanoparticles, 16
 - preparation methods, 228, 229
 - quantum dots, 18
 - surface-to-volume ratio, 15
- Nanomedicines, 47, 65, 82–84, 145, 309
 - ADME, 371, 372
 - anti-neoplastic agents, 370
 - API, 369
 - cell internalization, 369
 - composition and formulation, 369
 - delivery mechanisms, 369
 - EPR effect, 370
 - intracellular transport, 369
 - in vivo distribution, 369
 - macrophage-induced/mucosal instability, 370
 - non-charged polymers, 370
 - particle size, 370
 - PEGylated particles, 369
 - pharmaceutical ingredients, 370
 - pharmacokinetic characteristics, 369
 - pharmacokinetic properties, 370–371
 - physicochemical properties, 369
 - transporter-mediated endocytosis, 369
- Nano-mesenchymal stem cells, 73
- Nanonization, 167
- Nanoparticle-based CT contrast agents, 217
- Nanoparticle-mediated effects, 154
- Nanoparticles (NPs), 26, 368, 400
 - advantage, 82
 - classification, 188
 - diagnostic roles, 157
 - drug supply systems, 348
 - formulations, 256, 361
 - liposomes, 354, 355
 - NLCs, 355–357
 - SLNs, 355–357
 - PLGA, 379
 - lipid-based (*see* Lipid-based nanoparticles (LNPs))
 - liposomes (*see* Liposomes)
 - magnetic characteristics, 15
 - pharmacodynamic efficacy and toxicity, 144, 145
 - pharmacodynamics, 379
 - pharmacokinetic monitoring, 400
 - pharmacokinetics (*see* Pharmacokinetics)
 - pulmonary delivery (*see* Pulmonary delivery)
 - theranostic (*see* Theranostic NPs)
 - therapeutic and diagnostic roles, 157
- Nanoparticulate drug delivery systems (NPDDSs)
 - advancements, 42
 - chemotherapy and medications, 43
 - dendrimers, 366
 - DPM (*see* Drug-polymer matrix (DPM)-based NPDDS)
 - goal, 43
 - inorganic nanoparticles, 366
 - liposomes, 366
 - micelles, 366
 - new-generation medications, 43
 - PK perspective, 81
 - polymer nanoparticles, 366
 - types, 161
- Nanoparticulates
 - antibodies/peptides, 7
 - benefits, 6
 - vs. bulk materials, 6
 - characteristics, 7
 - chemical and physical properties, 11
 - classification (*see* Classification of nanoparticulates)
 - distinctive properties, 7
 - endocytosis, 7
 - gold nanoparticles, 6
 - healthcare products and restoration, 7
 - inimitable behavior and properties, 7
 - macro-oriented brains, 5
 - and nanoscale (*see* Nanoscale)
 - particle size, 7
 - production, 5
 - properties, 6
 - quantum effects, 6
 - shape, 5
 - size, 5
 - size-dependent properties, 11, 12
 - size reduction, 5
 - small molecule-type drugs, 7
 - solubility, 7
 - stand-alone solids/subcomponents, 5
 - structure of elements, 5
 - surface area, 5
- Nanoparticulate systems (NS), 43
- Nanophores, 406

- Nanoprecipitation, 43, 45
- Nanoscale
 - confinement effect, 11, 12
 - drug particles, 227
 - magnetic properties, 15
 - mechanical properties, 12, 13
 - nanometer size, 11
 - optical properties, 14
 - particles, 54
 - science, 7
 - size effects, 11
 - structural properties, 13
 - substances, 6
 - surface effects, 12
 - thermal properties, 13, 14
- Nanoscience
 - drug delivery systems, 298
 - EPR effect mechanism, 299
 - theranostic agents targeting tools, 299, 300
 - theranostics, 299
 - therapeutic drugs, 299
- Nanoshells, 147
- Nanosized carrier systems, 150, 154, 155
- Nanosizing, 148
- Nanospheres, 43, 227, 358
- Nanostructured lipid carriers (NLCs), 246, 355–357, 387
- Nanosystems, 199
- Nanotechnology, 4, 5, 26, 298
 - advanced drug delivery systems, 161
 - advantages, 160, 387
 - applicability, 160
 - applications, 4, 15
 - brain drug delivery, 368, 369
 - customer products, 4
 - definition, 4
 - in drug delivery, 4, 82–83, 387
 - in healthcare research, 4
 - oral BA, 394
 - therapeutics and diagnosis, 53
- Nanotechnology-based diagnostic agents, 254
- Nanotechnology-based drug delivery systems, 83
 - advantages, 26
 - polymeric matrix, 26
- Nanotechnology-based formulations, 306, 307
- Nanotherapeutics, 7, 304
 - development, 4
 - platforms, 304
- Nanotherapeutics-based drug delivery systems, 304
 - CNTs, 305, 306
 - dendrimers, 306
 - gold nanoshells, 305
 - hybrid NPs, 305
 - liposomes, 304, 305
 - PMs, 305
 - polymeric NPs, 305
 - QDs, 306
 - SPIONs, 306
- Nanotubes, 17
- Naringenin (NRG), 169
- Nasal administration, 85
- Nasal inhalation, 353
- Nasopharyngeal clearance, 353
- National Nanotechnology Initiative (NNI), 145
- Natural nanoparticulate materials, 8
- Naturally obtained materials, 160
- NCA, 114, 117
- Nebulized liposomes, 144
- Nelder-Mead method, 118, 135
- Nephrogenic systemic fibrosis (NSF), 408
- Nephrotoxicity, 336
- Neuro-infections, 366
- Neurological disorders, 366
- Neurological injuries, 366
- Neuropsychiatric category, 366
- Newton's equation of motion, 49
- Next-generation NP systems, 156
- Nifedipine, 348
- Nintedanib, 360
- Nintedanib esylate (NE), 85, 392
- Niosomes, 359, 360
- Nitrendipine, 71
- N-methyl-2-pyrrolidone (NMP), 283
- Non-anticipated biological effects, 88
- Nonbiodegradability, 197
- Noncompartmental analysis pharmacokinetic (NCA PK) parameters, 103, 105, 107
- Non-compartmental model, 54
- Non-compartmental pharmacokinetics, 62–63
- Non-corrosive characteristics, 255
- Non-functionalized SLNs post intratracheal administration, 252
- Noninvasive imaging modalities, 300
- Noninvasive imaging techniques, 316
- Nonobese diabetic/severe combined immunodeficiency (NOD/SCID) mice, 412
- Non-phagocytic pathways, 85
- Nonspherical particles, 352
- No observed adverse effect level (NOAEL), 115, 118
- Novel carriers, 246
- Novel cationic SLNs, 246
- Novel drug delivery systems (NDDSs), 80
 - bioanalysis, 371
 - in clinical applications, 81
 - DPM (*see* Drug-polymer matrix (DPM)-based NPDDS)
 - quantitation methods (*see* Quantitation methods)
- NP-based cancer diagnostics, 326
- NP-based contrast agents, 316–318
- NP-based imaging probes, 326
- NPDDS biopharmaceutical modeling
 - CG models, 49, 50
 - design and development, 46
 - enhanced sampling methods, 48, 49
 - full atomistic models, 47, 48
 - molecular modeling, 47
 - software programs, 47
- NPDDS degradation mechanism, 205
- NP-drug delivery systems, 38, 327

- NP frameworks, 148
 - NP properties affecting pharmacokinetics, drug delivery
 - biodistribution, 37
 - in vivo NP biodistribution, 37
 - overview, 36, 38–39
 - size, shape, and core composition
 - active targeting, 35, 37
 - cellular uptake, 35
 - specific location and type, 34
 - substantial correlation, 35
 - tumor permeability, 37, 38
 - NPs applications
 - brain, 31
 - diagnosis and bioimaging, 32
 - drug delivery systems, 30
 - gene delivery, 32
 - GI tract, 30
 - respiratory tract, 31
 - tissue repair, 32
 - tumor cell targeting, 31
 - NPs biodistribution, 37
 - NPs characterization
 - drug loading, 34
 - drug release, 34
 - microscopic techniques, 32
 - particle size
 - AFM, 33
 - DLS, 33
 - electron microscopy, 32
 - polymer degradation, 33
 - SEM, 33
 - surface charge, 34
 - surface hydrophobicity, 34
 - NPs classification
 - carbon-based, 26
 - ceramic, 27
 - lipid-based, 27
 - metal, 26
 - polymeric, 27
 - semiconductor, 27
 - NPs concentration methods
 - centrifugation, 45
 - dialysis method, 46
 - lyophilization, 45
 - rotary evaporation, 45
 - ultracentrifugation, 45
 - volume of administration, 45
 - NPs physicochemical properties, 317
 - NPs preparation methods
 - bottom-up method
 - biological methods, 28
 - chemical methods, 28
 - emulsification and diffusion/displacement, 44
 - emulsification and solvent evaporation techniques, 43
 - emulsification-reverse salting-out method, 44
 - in situ polymerization, 44
 - nanoemulsion, 45
 - nanoprecipitation, 45
 - techniques, 27, 28
 - top-down method
 - mechanical size reduction technologies, 27
 - physical methods, 28
 - small-drug NPs, 27
 - surface structure, 27
 - NPs properties
 - electronic and optical, 29
 - magnetic, 29
 - mechanical, 30
 - physicochemical, 29
 - thermal, 30
 - NPs types, drug delivery, 43, 44
 - NRG-EE100 nanoparticles composite, 169
 - Nuclear magnetic resonance (NMR), 275, 376, 401
 - Numeric deconvolution, 125
- O**
- Occluding, 367
 - Ocular pharmacokinetics, mucoadhesive nanoparticles
 - animal models (*see* Pharmacokinetic animal models)
 - dosage forms, 234
 - glaucoma, 240
 - intravascular compartment, 234
 - multi-compartment model, 234
 - ocular compartments
 - anterior chamber, 235
 - cul-de-sac, 234
 - eye, 234
 - retro-/periocular space, 235
 - tear film, 234
 - vitreous cavity, 235
 - pharmacokinetic compartment models (*see* Pharmacokinetic compartment models)
 - pharmacokinetic simulation model, 237
 - Rb, 240, 241
 - under diseased conditions, 240
 - Oleic acid-grafted carboxymethyl chitosan, 168
 - Olmesartan medoxomil (OLM), 164, 393
 - 1-CBM oral absorption model, 118, 120
 - 1-CBM oral model parameter estimates, 138
 - One-compartment open model IV Bolus, 60
 - One-dimensional (1-D) nanoparticulate materials, 10
 - Oposonization, 200
 - Optical imaging, 150, 155
 - Optical properties, 14
 - Optimized formulation, 252
 - Oral absorption, 61, 62
 - Oral administration, 85, 93, 105
 - of drug, 103, 104
 - of formulation, 386
 - SLNs
 - ATRA, 249
 - bioavailability, 249, 250
 - Cmax, 250
 - CPT, 249
 - dronedarone HCl, 249
 - drug lymphatic route, 249
 - enrofloxacin, 248
 - enterocytes and lymphatic transport, 250
 - modified strategies, 249

- MRT, 248
- paracellular and transcellular routes, 248
- pathways, 250
- PEG100SE concentration, 249
- pharmacokinetic studies, 249
- Oral drug bioavailability, 93, 94
- Oral route drug delivery, 386
- Organic and inorganic resources, 210
- Organic-based nanoparticulate materials, 9
- Organic nanoparticles, 188
- Organisation for Economic Co-operation and Development, 88
- Organization of PKMP data analysis modules, 103, 104
- Organ-specific accumulation, 38
- OX26 SLNs, 251
- Oxidative pressure markers, 233
- Oxidative stress tests, 233
- Oxides, 30
- Oxidised calcium alginate (OCA), 287
- Oxidized natural particles, 233
- P**
- Paclitaxel (polymeric nanoparticle), 348
- Paclitaxel mixed polymeric micelles, 166
- Paracoccidiodomycosis (PCM), 342
- Parallel artificial membrane penetration (PAMPA), 164
- Parallel tempering metadynamics (PTMD), 49
- Paramagnetic chemical exchange saturation transfer (PARACEST), 408
- Particle deposition, 351
- Particle engineering, 95
- Particle properties
 - aerodynamics, 352
 - charge, 352
 - density, 352
 - molecular weight, 352
 - shape, 352
- Particle size, 7
- Particle size distribution, 230
- Particulate drug delivery systems (PDDS), 43
- Passive targeting, 152, 218, 371
 - EPR effect, 324
 - GS-AuNPs, 324
 - in vivo fluorescence imaging, 324
 - PEG-AuNPs, 325, 326
 - PEGylation, 326
 - renal clearable probes, 325
 - site-specific accumulation, 324
- Pectin/sodium carboxymethyl cellulose (NaCMC), 163
- PEG-coated AuNPs, 197
- PEG-conjugated OPSS-modified transferrin, 326
- PEG-DiHyd-PLA triblock copolymers, 297
- PEG-PSMA antibody, 326
- PEGylated dendrimers, 357
- PEGylated drug detection, 376
- PEGylated liposomes, 307, 355
- PEGylated SLNs, 249
- PEGylation, 222, 267
- PEGylation-induced enlargement, 318
- Penciclovir, 254
- Penciclovir-loaded SLNs, 254
- Penetration pathway, 233
- Peptide-based therapies, 43
- Peptides, 354
- Perfusion-limited models, 88
- Periodic table, 188–189
- Permeability-limited models, 88
- Permeability studies, 253
- Permeation rate-limited models, 198
- Peroral delivery, 337
- PET/SPECT techniques, 155
- Peyer's patches (PPs), 386, 390
- P-glycoprotein (P-gp), 93
- Phagocytosis, 256, 353
- Pharmaceutical sciences, 170
- Pharmaceutical systems, 400
- Pharmacodynamic efficacy and toxicity, 144, 145
- Pharmacodynamic models
 - drug development process, 70
 - Emax model, 73
 - essential indirect response models (*see* Indirect pharmacodynamic response (IDR) models)
 - fixed effect model, 71
 - linear model, 71, 72
 - log-linear model, 72, 73
 - mathematical equations, 70
 - NPDDS design formulation, 71
 - prediction of effects, 70
 - quantitative relationship, 71
 - requirements, 71
 - sigmoidal Emax model, 74
 - simple direct effect model, 71
 - types, 72
- Pharmacodynamics (PD), 400
 - Levenberg-Marquardt method, 118
 - models and equations, 118, 122
 - Nelder-Mead method, 118
 - phase, 80
 - plasma concentration, 117
 - sigmoidal Emax model, 118, 122, 123
 - simulation, 129, 130
 - and theranostic applications, 152–153
- Pharmacokinetic (PK) animal models
 - besifloxacin, 239
 - best-fit model, 238
 - bevacizumab, 238
 - ciprofloxacin, 238
 - CsA, 238
 - drug improvement measure, 237
 - Dutch-belted hares, 238
 - effective visual dosing, 239
 - glucocorticoid receptor agonist, 238
 - lampalizumab, 238
 - medication disposal rate, 239
 - ophthalmic surgeries, 237
 - preclinical visual PK contemplates, 237
 - ranibizumab, 238
 - rodent models, 238
 - visual medication advancement, 237

- Pharmacokinetic (PK) compartment models
 - choroidal veins, 235
 - dissemination, 236
 - epithelial obstruction, 236
 - fixation, 236
 - hydrophilic medication, 236
 - medication conveyance, 235
 - nasolacrimal waste framework, 236
 - visual conveyance, 236
- Pharmacokinetic (PK) considerations, inorganic nanoparticles
 - biocompatible organic coating, 194
 - biological system, 192
 - biopharmaceutical approaches, 194
 - biopharmaceutical factors, 192
 - chronic toxicity, 193
 - factors affecting (*see* Factors affecting pharmacokinetics, inorganic NPs)
 - metallic nanoparticles, 193
 - nanomaterials biotransformation, 194
 - nanosystems, 191
 - NPDDS, 194
 - parameters, 194, 195
 - risk assessment, 192
 - targeted drug delivery, 191
 - toxicities, 192
- Pharmacokinetic (PK) evaluation, NPDDS
 - dendrimers, 64
 - functionalized/tailored NPs, 65
 - metallic nanoparticles, 63, 64
 - SLNs
 - drug-loaded, 63
 - oral administration, 63
 - transdermal delivery, 63
 - theranostic NPs, 64
- Pharmacokinetic modeling program (PKMP)
 - in animals and humans, 102
 - ANOVA (*see* Analysis of variance (ANOVA))
 - BE (*see* Bioequivalence (BE))
 - CA-PK, 117, 119–120
 - correlation (*see* Correlation)
 - data analysis modules (*see* Data analysis modules)
 - dEq, 132, 133
 - difference factor, 121, 126, 127
 - dissolution (*see* Dissolution)
 - dose escalation, 115, 117, 118
 - dose proportionality (*see* Dose proportionality)
 - interspecies scaling (*see* Interspecies scaling)
 - IVIVC, 121, 128
 - Kel calculation, 104, 106
 - linear trapezoidal rule, 103–105
 - MSD determination, 121, 128
 - NCA PK parameters, 105, 107
 - organization, 103, 104
 - PD, 117, 122, 123
 - similarity factor, 121, 127
 - simulation (*see* Simulation)
 - superposition analysis, 110, 114, 115
 - toxicokinetics (*see* Toxicokinetics)
 - urine data analysis, 109, 113, 114
 - user-defined differential equation model optimization, 135–137
 - user-defined simulation models, 133, 134
- Pharmacokinetic (PK) models
 - aim, 54
 - compartmental (*see* Compartmental pharmacokinetics model)
 - drug concentrations, 70
 - mathematical approach, 54
 - non-compartmental, 62, 63
 - nonlinear process, 54
 - NPDDS, 65
 - standard terms, 54, 55
- Pharmacokinetic (PK) profiling, 86–87, 161
- MRI
 - biodistribution, 406
 - cRGD, 407
 - DMSA-coated SPIONs, 409
 - drug carriers, 407
 - ferumoxytol, 409
 - gadolinium-containing contrast agents, 408
 - injected formulations, 408
 - in vivo MRI study, 407
 - iron oxide nanoparticles, 408
 - magnetic contrasting agent, 407
 - MPS, 409
 - NSF, 408
 - PARACEST, 408
 - PG-Gd, 407
 - in preclinical development, 407
 - SPIONs, 407
 - ZES-SPIONs, 409
- Pharmacokinetics (PK), 70, 144, 145, 150, 158, 261, 337
 - APIs, 88
 - creature models, 237
 - behaviour, 400
 - data analysis, 102
 - Doxil® upsurges, 88
 - drug molecule within host body, 81
 - exposure–efficacy interactions, 88
 - fate, 199, 202
 - in vivo (*see* In vivo studies)
 - methodical and quantitative analysis, 81
 - nanomedicines, 369–371
 - nanoparticle systems (*see* Nanoparticles)
 - non-anticipated biological effects, 88
 - parameters, 54, 62, 63, 65, 114, 170
 - PBPK modelling, 88–90
 - phase, 80
 - PK–PD (*see* PK–PD modelling)
 - recreation model, 237
 - simulation, 129, 130, 237
 - studies, NDDs, 54, 253, 354, 356, 359, 371, 400
- Pharmacological effects, 74
- Pharmacologically active agents, 80
- Pharmacotherapeutics, 82
- Phospholipids, 354
- Photoacoustic imaging (PAI), 150, 220, 221
- Photodynamic activity, 147
- Photodynamic therapy (PDT), 155, 298

- Photoluminescence, 220
- Photon correlation spectroscopy (PCS), 33
- pH-responsive delivery, 404
- pH-responsive nanocarrier, 403
- pH-sensitive SLNs, 253
- Physical method, 28, 213
- Physical vapor deposition (PVD), 27
- Physicochemical features of drugs, 82
- Physico-substance properties, 234
- Physiological barriers, 201
- Physiologically based pharmacokinetic (PBPK)
 - modelling, 54, 70, 83
 - active drug transporters, 88
 - amalgamation, 57
 - biological parameters, 57
 - blood drug concentration, 59
 - coalescing system data, 83
 - comparative analysis, 198
 - compartments, 56
 - concept, 88
 - development, 84, 90
 - drug clearance, 88
 - drug-dependent parameters, 57
 - drug-dependent tissues/organs, 58
 - drug-specific parameters, 89
 - elimination kinetics, 198
 - feasibility of manipulations, 198
 - humans, 198
 - humans specify ethnic population, 57
 - implementation, 89
 - integral models, 70
 - IVIVE, 89
 - lymphatic systems, 198
 - mathematical model, 57
 - modelling software, 57
 - nanomedicines, 198
 - nanoparticles
 - and biological system interaction, 91
 - dose–effect relationship, 92
 - interspecies and population translation, 92
 - in vivo systems, 94
 - IVIVC, 93
 - nanodrugs, 92, 93
 - oral drug bioavailability, 93, 94
 - nanosystem, 197, 198
 - in NPDDS, 197
 - brain targeting (*see* Brain targeting)
 - PD, 88
 - perfusion-limited models, 88
 - perfusion rate-limiting tissue/organ, 59
 - permeability-limited models, 88
 - permeability surface area product, 58, 59
 - physiological parameters, 89, 90
 - physiology- and drug-dependent information, 88
 - rate-limited kinetics, 56
 - schematic structure, 58
 - and simulation
 - mechanism-based model, 90
 - physiological factors, 90
 - simplified PBPK model, 90, 91
 - whole-body PBPK model, 90, 91
 - software, 70
 - tissue model structure, 88, 89
- Physiological models, 194
- Piperine SLNs, 254
- PK aspects
 - biodistribution, 83–84
 - distribution in tissues and organs, 85, 86
 - elimination and clearance, 86
 - nanoformulation, 84–85
- PK–PD modelling
 - in vitro study, 95–96
 - liposomal drug delivery (*see* Liposomal drug delivery)
 - and simulation, 70
 - with spatiotemporal characterisation, 94–95
- PKSIM, 57
- Plain heparin-all-trans-retinoid acid-based micelle, 166
- Plant-mediated synthesis, 29
- Plasma concentrations, 134
 - vs. time profile, 103, 105
- Plasma creatinine (PC), 339
- Plasma exposure, 407
- Plasma protein binding assay, 163
- Plasma-time curve, 60
- Plasmonic biosensing, 217
- PLGA-based nanoparticles, 358
- PLGA-based NPs, 297
- PLGA-mPEG 495, 379
- PLGA nanoparticles (NPs), 297
 - anticancer drugs, 338, 339
 - antidiabetic drugs, 341
 - anti-infectious drugs, 342
 - antiviral drugs, 343
 - brain disorders, 339
 - CVDs, 340
 - drug administration route, 334
 - drug delivery, 343
 - drug-induced nephrotoxic side effects, 336
 - drugs, 335, 338
 - formulations, 379
 - hydrolysis, 334
 - lipid hybrid formulations, 334
 - myriad, 334
 - nephrotoxicity, 336
 - peroral administration, 337
 - pharmacokinetics, 337
 - polymer biodegradation, 335
 - properties, 335
 - skin disorders, 340, 341
- PLGA-PEG-PLGA triblock copolymers, 288–289
 - effect, 279
 - factors effecting formulation/characteristics, 279
- FTIR, 277
- GPC, 276
- LA/GA ratio, 278
- LA/GA sequences, 277, 278
- MWD, PEG block, 277
- NMR, 275, 276
- PEG block length, 278

- Pluronic L-81, 391
Pneumonia, 349
Poloxamer 188-based atorvastatin-based solid dispersion, 165
Poly (acrylic acid) (PAA), 226
Poly-caprolactone (PCL), 43, 305, 336
Polydispersity, 376
Polydispersity index (PDI), 278
Polyethylene glycol (PEG), 148, 274, 305, 317, 368, 371, 404
Polyethylene glycol and heparin (PEG/HEP), 267–268
Polyethylenimine (PEA)-conjugated QDs, 323
Polylactic acid (PLA), 305, 342
Polylactic-co-glycolic acid (PLGA), 156, 274, 305, 334
 microspheres, 356
 nanoparticles, 165
Polymer, 83
 ADR, 376
 colorimetric methods, 376
 ELISA, 376, 377
 HPLC, 376
 LC-MS/MS, 376
 NDDS, 376
 NMR, 376
 pharmaceutical polymer, 376
 quantitation and differentiation, 371
 SEC, 376
Polymer-based DPM, 170
Polymer-based formulation, 161
Polymer-coated lipidic nanoparticles, 166
Polymeric micelles (PMs), 16, 305, 372
Polymeric nanomaterials, 82
Polymeric nanoparticles, 16, 27, 151, 188, 228, 305, 348, 358, 359
 biodistribution/clearance, 263
 characteristics, 264
 particle shape, 266
 particle size, 265, 266
 surface charge, 266, 267
 surface modification, 267
 components, 268
 definition, 261
 drug pharmacokinetic qualities, 262
 materials/shapes, 261
 opsonization, 263
 PEGylation, 262
 pharmacokinetics, 262, 264, 268
 shape/polymer, 262
Polymeric nanospheres, 163
Polymerization, 228
Polymer/lipid-based NPDDS, 161
Polymer-mediated carriers, 170
Polymer-mediated nanoassemblies, 170
Polymersome, 43
Polymethacrylate copolymers, 167
Polyplexes, 360, 361
Polysorbates, 368
Polyvinylpyrrolidone (PVP), 307, 319
Polyvinyl pyrrolidone-33 (PVP33), 412
Poor pharmacokinetics, 170
Positron emission tomography (PET), 150, 155, 300, 316, 378
Post duodenal administration, 253
Preclinical animal models
 drug concentration, 80
 PD and PK, 80
 PK profile (*see* Pharmacokinetic (PK) profiling)
 sustained drug delivery system, 80
Predefined simulation models, 132, 133
Prednisolone, 252
Pre-ocular retention study, 254
Primary antibody, 376
Progesterone (PG), 163
Prolonged retention, 255
Prostate-specific membrane antigen (PSMA), 326
Protein-based therapeutic agents, 354
Protein-based vaccines, 32
Protein corona, 319
Protein-corona formation, 201
Prototype drug doxorubicin, 297
Pulmonary administration, 196
Pulmonary delivery
 absorption, 352
 anatomy and physiology, 349–351
 dendrimers, 357
 deposition, 350–351
 diffusion, 351
 direct interception, 351
 distribution, 352
 electrostatic disposition, 351
 elimination, 352
 exosomes, 360
 factors, 350, 351
 inertial impaction, 350
 lung diseases (*see* Lung diseases)
 nanocrystals, 359
 nanoemulsions, 357, 358
 nanoparticle formulations, 361
 niosomes, 359, 360
 particle properties, 352
 polymeric NPs, 358, 359
 polyplexes, 360, 361
 respiratory tract, 353–354
 sedimentation, 351
Pulmonary diseases, 358
Pulmonary hypertension, 348
- Q**
QD-aptamer-DOX conjugate [QD-Apt(DOX)], 151
QDs to bovine serum albumin (QD-BSA), 318
Quantal effect model, 71
Quantitation methods
 encapsulated/embedded APIs, 371
 NDDSs, 371
 NPs
 fluorescence spectroscopy, 378
 LA-ICP-MS, 378
 MRI, 377, 378
 radiolabeling, 378

- polymer, 376–377
 - released and encapsulated (*see* Release profiling of NDDSs)
 - Quantitative biodistribution, 37
 - Quantitative Structure Property Relationship (QSPR), 237
 - Quantum confinement, 11
 - Quantum dots (QDs), 11, 18, 190, 306, 327, 378, 379
 - Quantum effects, 6
 - Quantum mechanics, 11
 - Quantum size effect, 14
 - Quetiapine fumarate, 252
- R**
- Radiation therapy, 297
 - Radiolabeling, 378
 - Raman scattering, 210
 - Raman spectroscopy, 210
 - Ranibizumab, 238
 - Rat adrenal pheochromocytoma cell line, 204
 - Reactive oxygen species (ROS), 152, 203, 204
 - Receptive nitrogen species (RNS), 233
 - Receptive oxygen species (ROS), 233
 - Receptor-mediated endocytosis, 227
 - Receptor-mediated mechanism, 31, 262
 - Receptor-mediated transcytosis, 216
 - Recombinant high-density lipoprotein (rHDL), 297
 - Recombinant human insulin (Humulin), 42
 - Reetz and Helbig method, 212
 - Refractive index detection nanoparticles, 211
 - Regulatory agencies, 65
 - Regulatory authorities, 376
 - Reillumination, 374
 - Release profiling of NDDSs
 - ACQ fluorophores, 374
 - AIE fluorophores, 374–376
 - ELISA, 376
 - FRET, 374, 375
 - LC-MS/MS, 371–373
 - Remdesivir, 354
 - Renal clearable nanoprobes, 317
 - efficiencies, 319–322
 - glomerular filtration barrier, 319
 - HDs, 319
 - ID, 318
 - NCs, 319
 - NPs shape, 319
 - parameters, 319
 - QDs, 319
 - surface charge, 323
 - surface chemistry, 319, 322
 - Renal excretion, 146
 - Repeated BE, 106, 108–110
 - Respiratory distress syndrome (RDS), 349
 - Respiratory system, 349
 - Respiratory tract, 351
 - absorption, 353
 - airflow velocity, 353
 - airway geometry, 353
 - alveolar clearance, 353
 - clearance, 353
 - inhalation pattern, 353
 - mechanical clearance, 354
 - mucociliary clearance, 353
 - nasal inhalation, 353
 - Restricted/residual maximum likelihood (REML), 106
 - Reticuloendothelial system (RES), 30, 63, 193, 198, 250, 262, 305, 317, 368
 - Retinoblastoma (Rb), 240, 241
 - Retro-/periocular space, 235
 - RF-Gantrez nanoparticles (RF-GNP), 393
 - Rifampicin (RF), 354
 - Rifampicin (RF)-loaded LPHNPs (RF-LPHNPs), 393
 - Rivaroxaban, 72
- S**
- Salmon calcitonin (sCT), 287
 - Sandwich ELISA, 376
 - Scaling factors, 84
 - Scanning electron microscopy (SEM), 32, 33
 - Scintigraphic study, 256
 - sCT CSK-SLNs, 253
 - sCT IRQ-SLNs, 253
 - SEC, 376
 - Sedimentation, 351
 - Selected ion monitoring (SIM), 376
 - Self-assembled nanoforms/nanoleaves, 202
 - Self-microemulsifying drug delivery systems (SMEDDS), 387
 - Self-polymerization, 169
 - Semiconductor nanocrystals, 18
 - Semiconductor nanoparticles, 27, 188, 378
 - Shell-loaded therapeutics moiety, 247
 - Short-chain triglyceride (SCT), 388
 - Sigmoidal Emax model, 74, 118, 122, 123
 - Silver nanoparticles (SNPs), 63, 189
 - Simcyp, 57
 - Similarity factor, 121, 127
 - Simple allometric equation, 114
 - Simplified PBPK model, 90, 91
 - Simulation
 - dose-concentration, 127
 - formulation development, 127
 - IVIVC, 130, 131
 - pharmacodynamic, 129, 130
 - pharmacokinetic simulation, 129, 130
 - Single-photon emission computed tomography (SPECT), 150, 155, 300, 316
 - Single-walled carbon nanotubes (SWNTs), 232
 - siRNA, 155
 - Size-dependent cell binding, 35
 - Size-dependent characteristics, 8
 - Skin, 85
 - Skin penetration studies, 255
 - Small molecule-based contrast agents, 317
 - Small molecule-type drugs, 7

- Solid lipid nanoparticles (SLNs), 43, 71, 85, 348, 355–357, 387
administration, 253
advantages, 246–248
anatomy and composition, 247
attributes, 246, 253
biologic and diagnostic products, 253–254
carrier, 255
colloidal carriers, 246
containing etoposide, 256
containing gadolinium diethylenetriaminepentaacetic acid, 254
diagnostic product, 254
disadvantages, 247, 248
dispersion, 254
injectable administration, 250–252
lipophilic nature, 246
modification, 253
ocular delivery, 255–257
oral administration (*see* Oral administration, SLNs)
pharmacokinetics and biodistribution, 247, 248
pharmacokinetics studies, 256–257
product, 252
safe and flexible carrier, 246
surfactants, 247
targeted delivery, 252–253
technologies, 246
topical delivery, 254–255
- Solid-phase extraction (SPE), 372
- Solid-state magnetism, 15
- Solid tumour growth, 94
- Spatial resolutions, 401
- Spatiotemporal characterisation, 94–95
- Spherical particles, 352
- Spherical-shaped NPs, 210
- Sprague–Dawley rats, 249, 356
- Spray-dried nanocrystals, 359
- Spray-drying method, 359
- Stabilizing agents, 28
- Stealth, 368
- Stimuli-responsive liposomes, 144
- Stimuli-responsive NPs, 307
- Stromal cell-derived factor 1 (SDF-1), 376
- Structural properties, 13
- Sub-atomic elements reproduction studies, 234
- Subconjunctival biodegradable microfilms, 238
- Subcutaneous/intranodal administration, 196
- Suitability tests, 232
- Superior performance, 7
- Superoxide dismutase (SOD), 155, 233
- Superparamagnetic iron oxide (FeOx), 202
- Superparamagnetic iron oxide nanoparticles (SPIONs), 306, 376, 407, 412
- Superparamagnetism, 15
- Superposition analysis, 110, 114, 115
- Superposition principle, 125
- Supersaturated SMEDDS (S-SMEDDS), 393
- Surface charge, 35
- Surface-decorated nanoparticles, 307
- Surface effects, 12
- Surface engineering, 10
- Surface functionalization, 229
- Surface hydrophobicity, 34
- Surface modification strategies, 326
- Surface-modified NPs, 369
- Surface plasmon resonance (SPR), 14, 211, 221
- Surface tension, 6
- Surfactants, 247, 370
- Surgery, 297
- Sustained drug delivery system, 80
- Synthesized single-walled carbon nanotubes (SWCNTs), 319
- Synthetic (engineered) nanoparticulate materials, 8
- Synthetic polymer NPs, 152
- Systematic clinical research, 65
- Systems-based approach, 94
- T**
- Tablets, 118
- Tacrolimus (lipid nanoparticle), 349, 354
- Targeted carriers, 400
- Targeted delivery, 306, 401
- Targeted drug delivery, 188
- Targeted nanoformulations, 307
- Targeting moieties, 145
- Temozolomide, 154
- Temperature-sensitive products, 406
- Tetrandrine-containing SLNs, 255
- Tetraoctylammonium bromide, 212
- TG-rich lipoproteins, 386
- Theranostic nanomedicine, 299
- Theranostic nanoparticles, 64
active targeting, 146, 152
administration route, 148, 150
application, 146, 152
biological NPs (naturally derived polymers), 152
cages, 147
categorization, 145
classification, 147
clinical use, 146
composition, 148, 149, 151
Cu-CuS, 147
designed, 147
development, 147
diagnosis and therapeutics, 145
drug and gene delivery vehicles, 153–157
in drug delivery, 146
HD, 146
imaging and therapeutic modalities, 150
in vivo capabilities, 146
mesoporous silica, 152
MNPs, 153
in nanomedicine and biomedical applications, 146
nanoshells, 147
nanosizing, 146
nanotechnology, 145
passive targeting, 152
pharmacodynamic efficacy and toxicity, 145
pharmacokinetics, 150

- photodynamic activity, 147
 - physicochemical properties, 146, 148
 - properties, 147
 - renal excretion, 146
 - size and shape, 145, 148
 - surface property, 148
 - synthetic polymer, 152
 - therapeutic
 - chemotherapy, 151
 - gene therapy, 151
 - modality, 148, 149
 - Theranostic NP-based photodynamic therapy, 155
 - Theranostics, 189, 403, 404, 406, 408, 412
 - Therapeutic agents, 300
 - Therapeutic capabilities, 156, 157
 - Therapeutic drugs, 299, 304
 - Therapeutic equivalence, 42
 - Therapeutic FDA-approved nanomedicines, 308
 - Therapeutic modalities, 150
 - Therapeutic molecules, 301–303
 - Thermal energy, 11
 - Thermodynamics, 13, 200
 - Thiolated MNPs, 153
 - Three-compartmental pharmacokinetic models, 56
 - Three-dimensional (3-D) nanoparticulate materials, 10, 11
 - Tight junction (TJ), 387
 - Tilmicosin, 252
 - Tissue/blood concentration ratios, 89
 - Tissue engineering, 42
 - Tissue repair, 32
 - Tissues and organs distribution, 85, 86
 - Titanium oxide nanoparticles (TiO₂ NPs), 63
 - Tmax, 255
 - TNF α assay, 254
 - Topically applied hydrophobic medications, 240
 - Toxicity, 82, 84, 144, 145
 - Toxic material-loaded nanoparticles, 65
 - Toxicokinetics
 - data collection, 110, 115
 - destructive sampling, 110
 - limited sampling data, 112, 116
 - PKMP, 112
 - single blood sample, 110
 - Traditional drug delivery systems, 160
 - Traditional iodine-based X-ray CT molecular probes, 211
 - Transcellular passage, 367
 - Transforming growth factor beta (TGF-b), 376
 - Transgenic species, 42
 - Transmission electron microscopy (TEM), 32, 33, 215, 231
 - Transporter-mediated endocytosis, 369
 - Triblock PLGA-PEG-PLGA polymer, 274
 - Triglycerides (TG), 388, 390
 - Tri-n-octylphosphine oxide (TOPO), 218
 - Trojan horse technology, 367
 - Tumor accumulation of NPs, 327
 - Tumor microenvironment, 307
 - Tumor permeability, 37, 38
 - Tumor-specific targeting, 152
 - Tumor targeting
 - active, 307, 324, 326
 - anticancer drugs, 306
 - defective lymphatic system, 324
 - EPR and hypoxia-like properties, 307
 - inverse targeting, 307
 - nanoformulation, 306
 - passive targeting, 307, 324
 - Tumor vasculature, 298
 - Tumour-induced angiogenesis, 94
 - Tumour microenvironment, 94
 - Tumour-penetrating peptides, 86
 - Tumour targeting, 400
 - Turkevich method, 212
 - Two-compartmental open model with intravenous (IV) injection, 54
 - Two-compartment model (plasma and peripheral), 93
 - Two-compartment open model, 54
 - Two-dimensional (2-D) nanoparticulate materials, 10
 - Two-dimensional (2-D) percolation network, 94–95
 - Two-stage reverse dialysis method, 95
 - Type 2 diabetes mellitus (T2DM), 341
- ## U
- Ultracentrifugations, 34, 45
 - Ultrafiltration, 34, 373
 - Ultrasmall inorganic NPs, 326
 - Ultrasonication, 256, 307
 - Ultrasonography (US), 316
 - Ultrasound (US), 150, 155
 - Ultraviolet spectroscopy (UV spectroscopy), 34
 - Upconversion hollow microtubes (UCHMs), 287
 - Upper respiratory tract, 349
 - Urinary excretion, 109
 - Urine data analysis, 109, 113, 114
 - User-defined differential equation optimization, 135–138
 - User-defined simulation models, 133, 134
 - UV-induced erythema, 254
- ## V
- van der Waals forces, 6, 48
 - Variance-covariance matrix, 121
 - Vascular endothelial growth factor-A (VEGF-A), 38
 - Vascular normalisation, 94
 - Virtual blood, 84
 - Visual diseases, 240
 - Vitreous cavity, 235
 - Volume of distribution (V_d), 60
- ## W
- Wagner-Nelson method, 122, 123
 - Weibull equation, 126, 127
 - Weibull_4 model, 120, 125, 126
 - Welch's correction, 108
 - Well-tempered metadynamics (WTM), 48
 - Whole-body PBPK model, 90, 91

X

- X-ray attenuation, 218, 219
 - X-ray contrast agents, 219
 - X-ray contrast imaging, AuNPs
 - advantages, 217
 - agent designing
 - attenuation coefficient, 218
 - blood circulation time, 218
 - composition properties, 218
 - contrast enhancement, 220
 - functional requirements, 218
 - mass concentration, 219, 220
 - non-toxic, 218
 - size properties, 218, 219
 - sulfur-containing molecules, 218
 - X-rays attenuation, 219
 - in animal, 219
 - circulation time, 217
 - colloidal stability, 217
 - NP-based agents, 217
 - physical properties, 217
 - targeted delivery, 217
- X-ray diffraction (XRD), 232
 - X-ray fluorescence computed tomography (XFCT), 221

X-ray fluorescence imaging (XRF), 221

X-ray imaging technology, AuNPs

- CT, 220
- fluorescence imaging, 220
- MRI, 220
- PAI, 220, 221
- XRF, 221

X-ray photon energy, 219

Y

Yeast cell wall particle systems (YCWPs), 341

YSA-functionalized nanoparticles, 358

Z

Zero-dimensional (0-D), 10

Zero-dimensional (0-D) nanoparticulate materials, 10

Zero-order absorption model, 62

Zeta potential, 34, 214

Zinc-doped iron oxide MNPs, 153

Zwitterion containing exceedingly small
superparamagnetic iron oxide nanoparticles
(ZES-SPIONs), 409, 412